INVESTIGATING PROTEIN- PROTEIN INTERACTIONS IN ORDER TO DEVELOP NOVEL THERAPEUTICS FOR THE TREATMENT OF ALZHEIMER'S DISEASE

Laura Aitken

**A Thesis Submitted for the Degree of PhD
at the
University of St Andrews**

2013

Investigating protein- protein interactions in order to develop novel therapeutics for the treatment of Alzheimer's disease

Laura Aitken
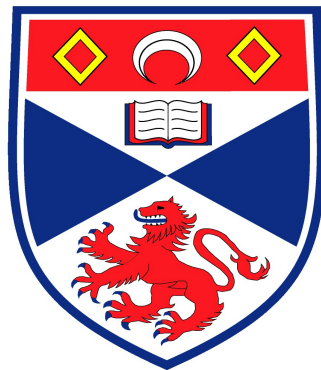
This thesis is submitted in partial fulfilment

for the degree of

Doctor of Philosophy at the University of St Andrews

February 2013

Abstract

Alzheimer's disease (AD) accounts for around two thirds of all dementia cases and an increase in life expectancy of the population has resulted in a substantial increase in dementia cases and with that a rise in AD. AD is a debilitating and ultimately fatal neurodegenerative disorder of the elderly, and despite being identified over a century ago, the current treatments do not treat the underlying causes behind the disease, instead they help to mask the symptoms of the disease and prolong the brain's remaining function. It is therefore vital that an effective, disease modifying treatment for this disease is established as soon as possible.

Soluble intracellular forms of amyloid β (peptide Aβ), a hallmark of AD have been identified and intracellular targets of Aβ are being investigated as potential drug targets for the disease. Two key intracellular, mitochondrial proteins investigated as potential drug targets: amyloid binding alcohol dehydrogenase (ABAD) and cyclophilin D (CypD) are the focus of the work reported in this thesis.

To begin identifying potential inhibitors of the ABAD-Aβ interaction, a two-pronged approach was taken. Firstly, a series of analogues based on a known inhibitor of the interaction were tested using a variety of biophysical assays, for their therapeutic affect on the interaction, and secondly a fragment based screening approach was used to identify new small molecule binding partners of ABAD which could potentially be modified to produced inhibitors of the ABAD-Aβ interaction. Three different CypD constructs have been successfully expressed and purified, and taken into crystal trials. It is hoped that these constructs can be used to significantly aid the progress of identifying any potential inhibitors and binding partners of CypD that may produce therapeutic effects, and in the future could lead to the identification of an effective disease

modifying drug in the treatment of AD. The work reported in this thesis has built upon previously reported findings and the groundwork has also been established for several *in vitro* biophysical assays, these include for example: measuring ABAD enzyme activity, and the novel morphology specific Aβ aggregation assay, which can be used as screening tools to help identify potential inhibitors of these interactions.

Both the ABAD-Aβ interaction, and the blockade of CypD are known to be drug targets in the treatment of AD, and by elucidating the molecular mechanisms behind these interactions, through implementing biophysical assays, this will help in the identification and design of potential new therapeutic agents for the treatment of AD.

Declaration

I, Laura Aitken, hereby certify that this thesis, which is approximately 50,000 words in length, has been written by me, that it is the record of work carried out by me and that it has not been submitted in any previous application for a higher degree.

I was admitted as a research student in October 2008 and as a candidate for the degree of Doctor of Philosophy. in September 2009; the higher study for which this is a record was carried out in the University of St Andrews between 2008 and 2012

Date …………………   Signature of candidate ………………………………….....

I hereby certify that the candidate has fulfilled the conditions of the Resolution and Regulations appropriate for the degree of Doctor of Philosophy in the University of St Andrews and that the candidate is qualified to submit this thesis in application for that degree.

Date …………………   Signature of supervisor …………………………………...

Copyright Declaration

In submitting this thesis to the University of St Andrews I understand that I am giving permission for it to be made available for use in accordance with the regulations of the University Library for the time being in force, subject to any copyright vested in the work not being affected thereby. I also understand that the title and abstract will be published, and that a copy of the work may be made and supplied to any *bona fide* library or research worker, that my thesis will be electronically accessible for personal or research use, and that the library has the right to migrate my thesis into new electronic forms as required to ensure continued access to the thesis. I have obtained any third-party copyright permissions that may be required in order to allow such access and migration.

The following is an agreed request by candidate and supervisor regarding the electronic publication of this thesis:

Embargo on all of both printed copy and electronic copy for the same fixed period of two years on the following grounds: publication would be commercially damaging to the researcher and to the supervisor and the University; publication would preclude future publication.

Date ………………… Signature of candidate ……………………………………

Signature of supervisor ………………………………...

Acknowledgements

There are a lot of people who have made this Ph.D possible, through their help and support, and I would like to thank them at this point.

Firstly, I would like to thank my supervisor Prof Frank Gunn-Moore, for all his guidance, patience and encouragement throughout my Ph.D. He provided endless ideas for new experiments whilst ultimately giving me the freedom to follow up my own ideas, through his confidence in my abilities. I think its safe to say that I probably would not have got to this point without his encouragement and that I definitely could not have chosen a better Ph.D supervisor in that of Frank (a.k.a. Frankie G).

A huge thank you must go to Prof Jim Naismith (University of St Andrews) who allowed me full access to his lab to express and purify proteins. Therefore, without the use of these facilities none of the work described herein would be possible. I would also like to thank the members of his lab group, who adopted me as one of their own, and for all their help and technical advice.

Several aspects of the work reported in thesis were carried out in a number of different laboratories both in the University of St Andrews, and the University of Dundee and several people in particular must be thanked for their assistance with this work; from the University of St Andrews: Dr Catherine Botting (MS), Dr Jesko Koehnke (Protein Purification), Dr Ulrich Schwarz- Linek (ITC), Dr Huanting Liu (Cloning) Dr Stephen McMahon (x-ray crystallography, NMR), Dr Carlos Penedo (Aβ aggregation assay), Steven Quinn (Aβ aggregation assay), Dr Margaret Taylor (TSA), and the late Dr Rupert Russell (TSA). Also, thanks to Dr David Gray (University of Dundee) for his interest in my work, and providing some drug discovery strategy input. Also I would

To all members (past and present) of the Gunn-Moore group, who provided a wealth of knowledge, input and experience, you made my time at St Andrews what it was: enjoyable, fun and interesting in more ways than one. In particular, to Dr Kirsty Muirhead whose studies provided the foundation for this work. Dr Eva Borger for keeping the lab running smoothly, for always having an answer or a suggestion to any questions I had, but also for her friendship throughout my Ph.D. To my great friends Susana Moleirinho, Zoe Allen and Andrew Tilston-Lunel, we always found a way of lifting each other spirits, usually through useful suggestions when things did not quite go to plan, but especially thanks for all the laughs and countless memories, keep going guys your time will come soon!

Of my "BMS friends", I have to particularly thank my sounding board for all discussions and planning of experiments: David Owen. He was also generally good at just keeping me sane, throught the later stages of this Ph.D. But most importantly, my thanks go to Fraser Duthie- the "go to guy" of the BMS. We've been best friends since our undergraduate degree at Dundee, and little did I know that putting in a good word for you to help get you your job in the Naismith group, would benefit me quite so much. A genuinely good guy, you're always on hand and the first person people call when there's a problem in the lab and I am no exception. Without your practical advice and help the protein purification aspects of this project might not have been so successful, or quite so enjoyable! Cheers Fraggle, just for being you!

Finally to my family: we are a small, close-knit bunch, but all of your love and support means the world to me. Most importantly, the two people who got me where I am today: Mum and Dad. I know sometimes you wonder "what I'm going on about, and what I actually do", but I can't tell you how much easier this has been just having you here to listen patiently regardless. Thank you for everything you have selflessly done for me and will undeniably do in the future. I would never have got this far without the continued encouragement, love, self-belief and unconditional support you both give me.

Table of Contents

CHAPTER 3: ELUCIDATING AND IDENTIFYING POTENTIAL SMALL MOLECULE INHIBITORS OF THE ABAD- AB INTERACTION

CHAPTER 4: CYCLOPHILIN D AS A POSSIBLE THERAPEUTIC TARGET IN THE TREATMENT OF ALZHEIMER'S DISEASE.

List of Figures

List of Tables

Abbreviations

ABAD	Amyloid-binding alcohol dehydrogenase
Aβ	Amyloid β peptide
AcAcCoA	S-acetyl coenzyme A
AD	Alzheimer's disease
ADDL	Amyloid derived diffusible ligands
ApoE	Apolipoprotein E
Amp	Ampicillin
ANT	Adenine nucleotide translocase
APP	Amyloid precursor protein
ATP	Adenosine triphosphate
BACE	β- site APP cleavage enzyme
Bis-tris	Bis(2-hydroxyethyl) imino tris (hydroxymethyl) methane
Bp	Base pair
BSA	Bovine serum albumin
cDNA	Complementary DNA
CHANA	Cyclohexenyl amine naphthalene alcohol
C-terminus	Carboxy-terminus
Clu	Clusterin
CoA	Coenzyme-A
COX	Cytochrome C oxidase
CRC	Calcium retention capacity
CsA	Cyclosporin A
CSF	Cerebrospinal fluid
CypD	Cyclophilin D
Da	Mass in daltons
DAPI	4',6-diamidino-2-phenylindole
DMEM	Dulbecco's modifed Eagle's medium
DMSO	Dimethylsulfoxide

DNA	Deoxyribonucleic acid
dNTP	Deoxynucleotide triphosphate
DP	Decoy peptide
DTT	Dithiothreitol
E. coli	*Escherichia coli*
EDTA	Ethylenediaminetetraacetic acid
Ep-1	Endophilin A1
ER	Endoplasmic reticulum
EtOH	Ethanol
ETC	Electron transport chain
FAD	Familial Alzheimer's disease
FCS	Foetal calf serum
Fret	Förster resonance energy transfer
FTD	Frontotemporal dementia
g	Gravitational constant
GFP	Green fluorescent protein
GST	Glutathione S- transferase
HEK-293	Human embryonic kidney cell line
HEPES	4-(2-hydroxyethyl)-1-piperazineethanesulfonic acid
HFIP	1,1,1,3,3,3-hexafluoroisopropanol
His	Histadine
HIV-TAT	Human immunodeficiency virus 1- transactivator
HNE	4-hydroxynonenal
IMM	Inner mitochondrial membrane
IPTG	Isopropyl β-D-1-thiogalactopyranoside
ITC	Isothermal titration calorimetry
JNK	c-Jun-N-terminal kinase
KAN	Kanamycin
k_a	Association rate constant
kb	kilobase
k_d	Dissociation rate constant

K_D	Equilibrium dissociation constant
k	Kilo
LB	Luria-Bertani broth
mAPP	Mutant amyloid precursor protein
MCI	Mild cognitive impairment
MDA	Malondialdehyde
MEM	Minimum essential medium
mRNA	Messenger RNA
MeOH	Methanol
mPTP	Mitochondrial permeability transition pore
MQ	Milli-Q purified water
MS	Mass Spectrometry
Mt	Mutant
MW	Molecular weight
NADH	Nicotinamide adenine dinucleotide hydrate
NFTs	Neurofibrillary tangles
NMDA	N-methyl- D aspartate
NMR	Nuclear magnetic resonance
N-terminus	Amino-terminus
OMM	Outer mitochondrial membrane
PBS	Phosphate buffered saline
PEG	Polyethylene glycol
PET	Positron emission tomography
PIB	Pittsburgh compound B
PICALM	Phosphatidylinositol- binding clathrin assembly lymphoid myeloid
PCR	Polymerase chain reaction
pH	Potential for hydrogen ion concentration
PG	Propylene glycol
Prx-II	Peroxiredoxin-2
PSEN-1 (or 2)	Presenilin-1 (or 2)

PSB	Protein sample buffer
qPCR	Quantitative real time PCR
RNA	Ribonucleic acid
ROS	Reactive oxygen species
rpm	Revolutions per minute
SD	Standard deviation
SEM	Standard error of the mean
SDS	Sodium dodecyl sulfate
SDS PAGE	Sodium dodecyl sulfate polyacrylamide gel electrophoresis
siRNA	Small interference RNA
SK-N-SH	Human neuroblastoma cell line
SOD	Superoxide dismutase
SPR	Surface plasmon resonance
SSA	Super streptavidin sensor
STD	Saturation transfer difference
SyproO	Sypro orange dye
T_m	Unfolding temperature (of protein)
ΔT_m	Change in unfolding temperature
TB	Terrific broth media
TBS	Tris buffered saline
TBS-T	Tris buffered saline with 0.1 % Tween-20
TEV	Tobacco etch virus
Tg	Transgenic
TIM	Translocase of the inner membrane
TOM	Translocase of the outer membrane
Tris	Tris(hydroxymethyl)methylamine
Triton-X100	4-(1,1,3,3-Tetramethylbutyl)phenyl-polyethylene glycol
TSA	Thermal shift analysis
UV	Ultra violet
VDAC	Voltage dependent anion channel

WaterLOGSY	Water ligand optimised gradient spectroscopy
WT	Wild type
X-gal	5-bromo-4-chloro-3-indolyl-galactopyranoside

"……I know three people who have got better after a brain tumour. I haven't heard of anyone who's got better from Alzheimer's. I'm slipping away a bit at a time… and all I can do is watch it happen. It's a physical disease, not some mystic curse; therefore it will fall to a physical cure. There's time to kill the demon before it grows."

Sir Terry Pratchett, OBE (Daily Mail, 2008)

Chapter 1: Introduction

1.1   <u>An overview of Alzheimer's disease</u>

Alzheimer's disease (AD) accounts for around two thirds of all dementia cases and is thought to affect 820,000 people in the UK (Hubbard-Green 2012), 5.4 million people in the US (The Alzheimer's Association 2012), and 36 million people worldwide (Hubbard-Green 2012.) An increase in life expectancy of the population has resulted in a substantial increase in dementia cases and with that a rise in AD. This rise in dementia cases not only provides a huge burden for the social care network, but also has a substantial negative economic impact for society, with the cost of treating dementia presently standing at £23 billion for the UK (Alzheimer's Research UK 2012).

Alzheimer's disease is a debilitating and ultimately fatal neurodegenerative disorder of the elderly. What starts out as minor forgetfulness will progress into the loss of declarative memory and then loss of long-term memories. As a consequence of this, problem-solving abilities, perceptual skills, language and other brain functions are also impaired and gradually decline. Psychiatric and behavioural problems may also occur (Ravetz 1999). The loss of these brain functions then causes social dependence and then death, although the progression time of this disease can vary. It is therefore vital that an effective treatment for this disease is established as soon as possible.

Although this disease was first identified over a century ago, by Alois Alzheimer (Galimberti & Scarpini 2011), the main mechanisms of this disease and indeed the underlying causes, have proved challenging for researchers to ascertain. It is however clear that AD can occur sporadically, often later in a patient's life, or as an inherited disease caused by mutations in genes encoding proteins involved in Aβ turnover. Familial AD is associated with an earlier age of onset (Crouch *et al.* 2008).

1.1.1 <u>**Neuropathology of Alzheimer's disease**</u>

AD is clinically diagnosed by progressive memory loss. It is difficult for clinicians to be absolute on their diagnosis as there are a number of other types of dementia such as fronto-temporal, dementia with Lewy-bodies and vascular dementia (Wong *et al*. 2002; Wilhelmus *et al*. 2011). Furthermore clinical and pathological similarities also occur between Creutzfeldt-Jakob disease (CJD) a prion protein dementia, and AD (Masters *et al*. 1981). A definitive clinical AD diagnosis is only possibly by examining brain tissue after death, therefore the diagnosis is given as probable AD, whereby all other possible diseases have been ruled out. As AD results from the death of neurons, particularly in the hippocampus, frontal and temporal lobes, brain scans are often used in diagnosis to show and monitor brain atrophy and decreased blood flow (Besson *et al*. 1992; Nordberg 2004). An example of the differences between a normal brain and an AD brain is shown in Figure 1.1.
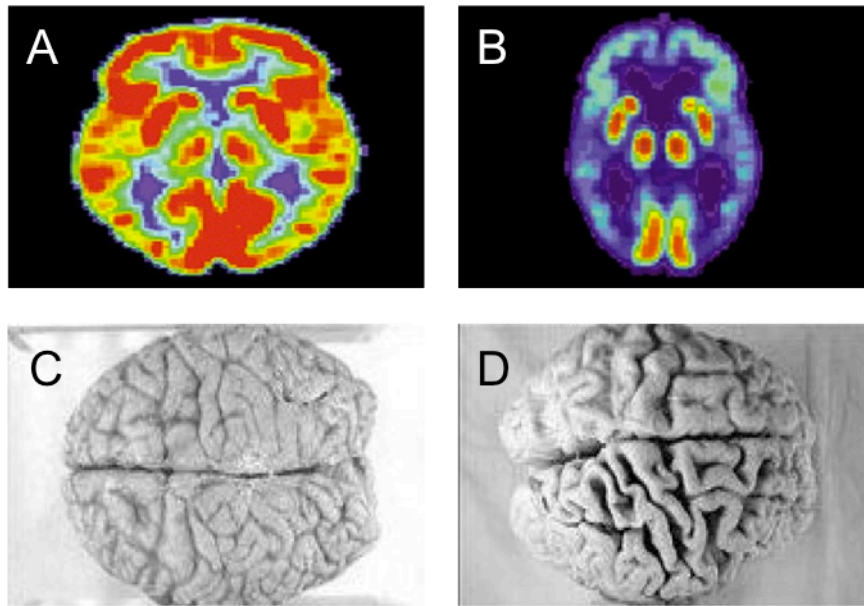
Figure 1.1: The changes observed between a normal brain and an AD brain. A) A normal brain imaged using positron emission topography (PET) depicting changes in blood flow when compared to that of **B)** PET scan of an AD brain. **C)** A normal brain **D)** An AD brain showing brain atrophy. (Image adapted from Mattson 2004).

1.1.2 Possible causes of Alzheimer's disease

The two classic Alzheimer's disease pathological hallmarks are the appearance of extracellular amyloid beta (Aβ) plaques and intracellular neurofibrillary tangles (NFTs) consisting of a hyperphosphorylated protein called tau. However, although originally thought to be one of the major causes of AD, it is now considered that there is no correlation between the number of Aβ plaques and the decline of cognitive function (McLean *et al*. 1999; Lin & Beal 2006). However, there has shown to be correlation between intracellular amyloid and the progression of the disease (Lue *et al*. 1999; McLean *et al*. 1999) and therefore it is undisputed that Aβ is still a major factor in AD and many researchers are now investigating the accumulation of intracellular amyloid,

in particularly within the mitochondria (Caspersen *et al*. 2005). This is described in more detail in section 1.3.

The only cause of AD that can be stated conclusively is in the small population (about 1% of AD sufferers) (van Es & van den Berg 2009) who have familial AD which is caused by an inherited genetic defect. There are several possible mutations which could cause familial AD and interestingly several of the mutations produce increased Aβ levels. These are mutations found in the amyloid precursor protein (APP) gene and the presenilin 1 (PS1) and presenilin 2 (PS2) genes (Bird 2010). Presenilins are components of the γ -secretase complex that, together with β -secretase, processes APP to produce Aβ (summarised in section 1.2.1). It is also known that presenilins are found to be located in a subcompartment of the endoplasmic reticulum (ER), which provides a bridge structure between the ER and the mitochondria called mitochondria-associated ER membranes (MAMs) (Area-Gomez *et al*. 2009). MAMs are responsible for various housekeeping functions including cholesterol, lipid and fatty acid metabolism and Ca^{2+} homeostasis (Hayashi *et al*. 2009), all of these functions have been found to be altered in AD (Canevari *et al*. 2004; Mattson 2004; Hertzel *et al*. 2006; Di Paolo & Kim 2011). This could be explained from γ -secretase activity associated with APP processing being essentially confined to the MAM region (Area-Gomez *et al*. 2009), thus any dysfunction in MAMs could provide a fundamental role in AD pathology.

A number of genetic risk factors for the development of sporadic late-onset AD have now been identified. These include carrying the ε4 allele of the apolipoprotein E (ApoE) gene (Kim *et al*. 2009). ApoE is a plasma protein and is involved in the transport and redistribution of lipids in cells (Mahley & Rall 2000). There are three ApoE isoforms: ε2, ε3 and ε4. The isoform ε2 contains a C158R mutation and ε4 contains a C112R mutation relative to ε3 and it is this ε4 isoform mutation which is elevated in patients

with sporadic AD (Kim *et al.* 2009). Other genetic risk factors for sporadic AD are mutations in the gene encoding the membrane sorting receptor sortilin-1 (Rogaeva *et al.* 2007) and increased levels of the non-proteinogenic amino acid, homocysteine, as well as low serum folate (Ravaglia *et al.* 2005).

More recently *CLU (ApoJ), PICALM* and *CR1* have all been described as genetic risk factors for AD (van Es & van den Berg 2009). The *CLU* gene encodes a multifunctional protein which is a secreted chaperone, when under some stress conditions is also located in the cell cytosol. It has been suggested to be involved in several basic biological events such as cell death, tumour progression, and neurodegenerative disorders (van Es & van den Berg 2009). In animal models of AD, CLU is shown to bind to soluble Aβ and form complexes which are capable of crossing the blood brain barrier. Also in Alzheimer's disease brain, CLU expression is reported to be increased and is shown to be present in amyloid plaques and in the cerebrospinal fluid of AD cases (Harold *et al.* 2009). PICALM (phosphatidylinositol-binding clathrin assembly protein) is ubiquitously expressed in all tissue types but shows a high expression level in neurons. As its name suggests, it is involved in clathrin mediated endocytosis (CME), this is important for the intracellular trafficking of proteins and lipids such as nutrients, growth factors and neurotransmitters (Harold *et al.* 2009). It is thought that PICALM can control the risk of AD through APP processing *via* endocytic pathways resulting in changes in Aβ levels. Cell culture experiments have shown that full length APP is retrieved from the cell surface by CME and inhibition of endocytosis reduces APP internalization and reduces Aβ production and release. Increased synaptic activity is known to lead to the elevated endocytosis of synaptic vesicle proteins and there is evidence to support the theory that increased CME, triggered by increased synaptic activity, drives more APP into endocytotic compartments resulting in an increase of Aβ

production and release (Harold *et al*. 2009). Like CLU, CR1 is shown to have an effect on Aβ clearance (Kok *et al*. 2011). To clarify, these are risk factors and therefore it is not certain that an individual will automatically develop the disease, the risk of developing it are merely increased.

There are also behavioural and environmental risk factors that can increase an individual's chance of developing AD. These include smoking, excessive alcohol consumption, poor diet causing increased mid-life cholesterol levels (Wolozin 2004), head injury (Munoz & Feldman 2000), chronic inflammatory disease (Munoz & Feldman 2000) and many others.

1.1.3 <u>Tau Pathology</u>

The main area of work addressed in this thesis is Aβ interactions, and their role as potential therapeutic targets in AD; however, it is important to include the other main pathology of Alzheimer's disease, hyperphosphorylated tau forming intracellular neurofibrillary tangles (NFTs).

Tau protein belongs to a family of proteins called microtubule- associated proteins (MAPs) and contributes to the correct function of a neuron by promoting tubulin assembly and stabilising microtubules by providing structural support, therefore changes in the amount or structure of tau will affect its ability to carry out this role (Kosik 1993). Tau has the ability to promote tubulin binding, which is controlled by its phosphorylation state, which is normally regulated by the dual action of kinases and phosphatases on the tau molecule (Mandelkow *et al*. 1995) (Shown in Figure 1.2). In AD abnormal phosphorylation of the tau protein not only causes a decrease in tubulin

binding, but also promotes self- polymerisation in the form of NFTs (Iqbal & Grundke-Iqbal 2008).

Human tau is located on the long arm of chromosome 17 at position 17q21 and contains 16 exons. Alternative splicing of exons 2, 3 and 10 result in 6 different tau isoforms that are differentially expressed during brain development (Sergeant *et al*. 2005). The six tau isoforms differ on the contents of three or four tubulin binding domains in the C-terminal region of the protein, or the insertion of one, two or no inserts of 29 amino acids at the N-terminal region of the protein. All isoforms therefore vary in length from between 352 and 441 amino acid residues (Kolarova *et al*. 2012).
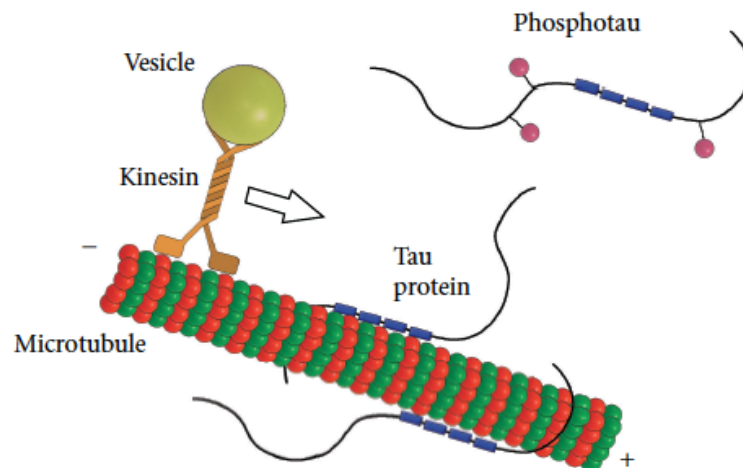
Figure 1.2: The normal function of 441 amino acid tau protein. Tau protein stabilises microtubules through its tubulin binding domains (blue boxes). This function is maintained through the action and presence of kinases and phosphatases. The capability of tau binding to microtubules is regulated by the phosphorylation of tau (pink boxes). Also when tau is present this may inhibit the directed transport of vesicles along microtubules by kinesin (Kolarova *et al*. 2012).

As explained in Figure 1.2, tau binding to microtubules is regulated by the phosphorylation of tau. In a diseased state such as AD, the phosphorylation state is

increased to hyperphosphorylated tau lesions, which causes tau to lose its biological activity. The mechanisms by which this occurs are still widely debated; however post translational modifications appear to be the main cause (Martin *et al.* 2011). These modifications producing hyperphosphorylated tau include acetylation, glycation, ubiquitination, nitration and proteolyic truncations (Kolarova *et al.* 2012).

It has been shown in a genetic model of tau-related neurodegenerative disease in the fruit fly (*Drosophila melanogaster*) that transgenic flies exhibited progressive neurodegeneration, early death, enhanced toxicity of mutant tau, accumulation of abnormal tau, and relative anatomic selectivity, without the NFT formation that is seen in human disease (Wittmann *et al.* 2001). Furthermore, a study in transgenic mice expressing non-mutant human tau isoforms revealed that the presence of tau filaments did not correlate directly with the cell death occurring within individual cells, suggesting that cell death can occur independently of NFT formation (Andorfer *et al.* 2005). Instead they observed that the mechanism of neurodegeneration involved the re-expression of cell-cycle proteins and DNA synthesis, indicating that non-mutant tau pathology and neurodegeneration may be linked *via* abnormal, incomplete cell-cycle re-entry (Andorfer *et al.* 2005). Although the NFTs accumulate in human patients' brains with AD it has been suggested that this is a protective response to the toxic build-up of the hyperphosphorylated tau in order to prolong the lifespan of neurons (Binder *et al.* 2005).

1.1.4 Current treatments for Alzheimer's disease

Currently there is no cure for AD, and the four current drugs that are licensed in the United Kingdom only treat the underlying causes (symptoms) of the disease and slow down its progression. The drugs are used to stabilise and maximise the remaining brain function for as long as possible, but ultimately, a therapeutic effect is only achieved for a short period of time before cognitive decline resumes. The four drugs are described in more detail in Table 1.1

In order to alleviate some of the other symptoms associated with AD such as: depression, anxiety and psychosis, other drugs may also be prescribed in conjunction with the cholinergics. It is worth adding that benefits have also been seen from increasing exercise and having a healthy lifestyle (Wilcox *et al*. 2009).

Table 1.1:Drugs available as a treatment for AD in the UK (Adapted from the Alzheimer's Societry website)

Drug	Brand Name	Manufacturer	Type	Action
Aricept	Donepezil hydrochloride	Pfizer	Acetyl-Cholinesterase Inhibtor	Increases the acetylcholine level and duration of action by inhibiting the cholinesterase enzyme. Used in mild to moderate stages of AD
Reminyl	Galantamine hydrobromide	Shire		
Exelon	Rivastigmine	Novartis		
Ebixa	Memantine	Lundbeck Ltd	NMDA receptor antagonist	Switches off the overactive glutamate receptors of the N-methyl-D-aspartate (NMDA) and thus prevents glutamate toxicity. Due to possible side effects- used in moderate to severe AD

In a normal brain the electrical impulse is transmitted across the synaptic cleft *via* a neurotransmitter, acetylcholine. This is then recycled by acetylcholinesterase. As the levels of acetylcholine are significantly reduced in an AD brain, thus also reducing the impulse activity, the activity and acetylcholine levels are raised by administering patients with AD acetylcholinesterase inhibitors. These will reduce the breakdown or recycling of acetylcholine and therefore increase its concentration at the post-synaptic receptors (Bores *et al.* 1996).

NMDA receptor antagonists are also used in the treatment of AD. In a normal brain, the neurotransmitter glutamate, transmits an impulse *via* the NMDA receptor and is then taken up by glial cells and recycled. In an AD brain, amyloid prevents the glial cells from recycling the glutamate. This increase in glutamate prevents the post-synaptic membrane from firing correctly and produces weakened signals. Treatment with an NMDA receptor antagonist such as memantine prevents a glutamate accumulation and can return the post-synaptic membrane function to normal (Danysz & Parsons 2003).

A topical issue at present is the potential use of immunotherapy in the treatment of AD. Using immunotherapy as a treatment for AD is not a new phenomenon, in fact it was first hypothesised over 13 years ago by Schenk *et al.* using a study in transgenic mice (PDAPP mice) which contain a mutant version of the human amyloid precursor protein (APP) gene (valine717 mutated to phenylalanine) that is associated with an early-onset and aggressive form of AD (Schenk *et al.* 1999). A platelet-derived growth factor promoter is used to increase the brain expression levels of the mutant APP, to exceed the endogenous mouse level of APP by about 4–6 fold. This results in the overproduction of Aβ that deposits plaques in a similar way to that found in human AD

brains. Importantly, several other of the consequent neurodegenerative changes that occur in AD, also develop in PDAPP brains, including the formation of neuritic plaques, astrocytosis, and microgliosis (Schenk *et al*. 1999). Initial findings showed that young PDAPP transgenic mice were immunised with Aβ42, which essentially prevented amyloid deposition; astrocytosis was dramatically reduced, and there was also a reduction in Aβ-induced inflammatory response (Schenk *et al*. 1999). Aβ42 immunisation also appeared to arrest the progression of amyloidosis in older PDAPP mice. Overall, it was shown that the direct Aβ immunisation appeared to increase the clearance of amyloid plaques, and it was therefore suggested that this could be an effective therapeutic for AD. This direct immunisation with synthetic intact Aβ42 stimulates T-cell, B-cell and microglial immune responses, and was an approach used by many groups (including Schenk *et al*. 1999; Games *et al*. 2000). Because this immunotherapy approach had proved to be so effective in reducing amyloid plaques in AD mice model brains and also improving cognitive function, it was taken further into clinical trials. One trial, AN1792, from Elan Pharmaceuticals appeared successful in phase I, however the phase II trial of Aβ42 peptide vaccine was halted because of T cell-mediated meningoencephalitis in 6% of its patients (Orgogozo *et al*. 2003).

Another possible therapeutic immunology approach involves the passive administration of monoclonal antibodies directed against Aβ. As Aβ disorders, are considered conformational diseases, due to the amyloid formation triggering conformational changes in a specific peptide or protein, resulting in its mis-folding, amyloid conformation-specific antibodies that recognize specific amyloid species, eg, fibrils or oligomers, from many types of amyloid proteins have been produced and characterised (Glabe 2004; Sarsoza *et al*. 2009). Britschgi *et al.* demonstrated the presence of sequence independent, oligomeric conformational antibodies in human plasma and

cerebrospinal fluid and although the diversity, and overall function of such endogenous conformational antibodies remain largely uncharacterized, studies have suggested that these antibodies decline with age and advancing AD, suggesting that they may play a neuroprotective role against toxic amyloid oligomers (Britschgi *et al*. 2009).

Although the Aβ immunotherapy approach has proved to be somewhat frustrating due to a lack of clarity on where the broken down amyloid is sequestered to, there are many continued approaches into utilising this field. One such example of a useful tool that has come from an immunology study, is the use of carbon-11-labelled Pittsburgh compound B (^{11}C-PiB) PET, a marker of cortical fibrillar Aβ load *in vivo,* which was used to investigate whether Bapineuzumab, a humanised anti-Aβ monoclonal antibody, would reduce cortical fibrillar Aβ load in patients with AD (Rinne *et al*. 2010). Rinne's findings showed that treatment with Bapineuzumab for 78 weeks reduced cortical ^{11}C-PiB retention compared with both baseline and placebo, therefore concuding that ^{11}C-PiB PET seems to be a useful tool in assessing the effects of potential Alzheimer's disease treatments on cortical fibrillar Aβ load *in vivo*.

It has always been the theory that removal of Aβ plaques would be beneficial to suffers of AD, however it is unclear if the small soluble amyloid can be cleared effectively, and also where it would be sequestered to, therefore the removal and the dissolvation of Aβ plaques may not be the correct therapeutic path. By carrying out this Aβ plaque busting, this could result in the release of more toxic substances. This theory is supported by a follow up study on the initial patients in the Elan Pharmaceutical trial (AN1792), which found that although immunisation with Aβ42 resulted in successful clearance of amyloid plaques in patients with AD, this clearance did not prevent progressive neurodegeneration and 7/8 patients consenting to a *post mortem* had severe end stage dementia before death (Holmes *et al*. 2008).

Another possible therapeutic immunological approach is that of a more recent concept using Tau immunology. In fact there are limited reports published using either active or passive Tau immunotherapy in animal models. Of these publications using active vaccination Rosenmann *et al.* used a tau fragment (379–408) phosphorylated at Ser396 and Ser404 (phosphorylation sites commonly associated with NFT) to vaccinate the P301L mouse model (a mouse model expressing a human tau mutation, capable of developing cognitive decline and motor defects). Later studies on behavioural analysis with these mice showed improved performance after immunisation and this demonstrated that antibodies were able to cross the blood brain barrier and bind to hyperphosphorylated tau (Asuni *et al.* 2007). Further studies also revealed that there was a 40% reduction in NFTs and a 20% increase in microglia (Boimel *et al.* 2010). Although this data appeared to be encouraging, in 2006, Rosenmann *et al.* also reported that full-length tau was encephalitogenic, triggering a severe autoimmune response demonstrating the potential danger of using soluble tau as an immunogen or of antibodies recognising epitopes of full-length tau for passive vaccination (Rosenmann *et al.* 2006). In this study (using mice vaccinated with soluble tau) the mice developed NFT like structures, axonal damage, gliosis, mononuclear infiltrates, and motor phenotypes. An optimal vaccine should therefore aim to target pre-filament tau species (tau oligomers), which form at early stages of NFT development rather than mature, meta-stable NFT (Kayed 2010). Pre-filament specific phosphorylation sites have yet to be conclusively identified due to the complexity of tau aggregation and the overlap between the three stages of NFT development with regard to tau phosphorylation sites (Augustinack *et al.* 2002). This is also harder to target, due to tau phosphorylation being a physiological process that is essential for normal tau function. A passive tau vaccine study using two antibodies that selectively recognize pathological forms of tau reduces

the extent of biochemically detectable tau pathology in two different mouse models, and thus suggests that this translates into a reduction in axonal degeneration, a preservation of motor function and slowing of disease progression in the P301S model of tauopathy (Chai *et al*. 2011). Chai *et al.* make an attempt in predicting the mechanism by which this proposed passive vaccine would work, based on the familiar extracellular Aβ plaque reduction mechanisms. However, they suggest that the mechanism may be more complicated, where antibodies would somehow get access to intracellular tau to block its aggregation or trigger its clearance. As this passive vaccine approach is a relatively new development in the therapeutic field for AD, a complete understanding of the mechanism of action will be important for the generation of better antibodies, with the best combination of epitope, affinity and effector functions, for anti-tau immunotherapy treatment in AD.

Over the past 5 years another area of therapeutical interest is that of the use of methylene blue as a way to slow down the progression of AD by breaking up NFTs (Oz *et al*. 2009). Methylene blue (or Urolene blue) has had many applications throughout its lifetime from an antiseptic dye treating urinary tract infections, to dying jeans blue. In the case of AD, it has been proposed to have many actions including alterations in the cholinergic, serotonergic and glutamatergic neurotransmitter systems, mitochondrial function and upon the formation of amyloid plaques and of neurofibrillary tangles making it a promising candidate for the treatment of AD. A clinical trial of *Rember* (a formulation of methylene blue) was carried out in collaboration between Dr. Wischik (University of Aberdeen) and his spin out company TauRx pharmaceuticals in 2008. Initial results again seemed promising, however the drug was only effective when it dissolved in the stomach, and at the highest dose, of 100mg three times daily, no effect was seen as a result of this, and adverse side effects (at the 100mg dose) were also seen

as the compound dissolved in the intestines resulting in diarrhea in around 30% of the patients (Wischik *et al*. 2008). Wischik *et al.* came under heavy critisim from the Alzheimer's research community for their *Rember* study as no previous data; preclinical, imaging or clinical was published before the drug candidate *Rember* was released and also because there was no proof of efficacy study, as this comes from the phase III trial and the study was halted at phase II.

Therefore given the complexity of the disease, it may be more appropriate to think of future treatments for AD in three categories:

1) The formation or clearance of Aβ/ hyperphosphorylated tau.

2) The protection of specific sensitive targets, these may include ABAD (section 1.4) or CypD (section 1.5), however chemists tend to avoid developing drugs specifically for a protein-protein interaction, as they tend to be notoriously difficult to develop.

3) Support and stabilisation, this would include utilising current drug therapies that already exist to prolong the neuronal networks. Developing a drug is difficult, but developing a drug that must cross the blood- brain barrier is even harder. However, with advances in technologies and increased capabilities these challenges can be overcome.

1.2   Amyloid- β peptide in Alzheimer's disease

1.2.1 Amyloid production by APP cleavage

Amyloid beta (Aβ), which is the principle component of the amyloid plaques, is a small peptide, of 40- 42 amino acids which is derived from the amyloid precursor protein (APP) *via* endoproteolytic cleavage. APP is a transmembrane glycoprotein ubiquitously expressed in the brain. The APP gene is located on chromosome 21 and alternative splicing generates many isoforms of between 365 and 770 amino acids (Goldgaber *et al*. 1987; Kang *et al*. 1987; Matsui *et al*. 2007). The most interesting isoforms are the three major APP mRNA species: APP751 and APP770 contain a Kunitz-type serine protease inhibitor domain (APP-KPI), and APP695 lacking this inhibitor domain (Matsui *et al*. 2007).

APP processing occurs normally in nearly all neuronal and non-neuronal cells following the sequential cleavage of APP by three secretases α, β, and γ. This processing can be divided into two pathways: non-amyloidogenic and the amyloidogenic pathway. The majority of APP is processed *via* the non- amyloidogenic pathway, where APP is firstly cleaved by α-secretase to release non-toxic protein fragments of sAPPα and C83 α-carboxyl- terminal fragments (α-CTPs). Membrane anchored α-CTPs are then subsequently cleaved by γ-secretase to produce the p3 peptide and APP intracellular domain (AICD) (Wilquet & Strooper 2004). In the amyloidogenic pathway, APP is first cleaved at the amino terminus by β-secretase producing sAPPβ and membrane bound C99 (β-CTPs) protein fragments. It is the subsequent cleavage of the C99 fragments, by γ-secretase that produces the toxic Aβ peptide and the position of this cleavage results in peptides of varying lengths (most commonly 40 and 42 amino acids long) (Wilquet & Strooper 2004). The sequential APP cleavage pathways are summarised in Figure 1.3.
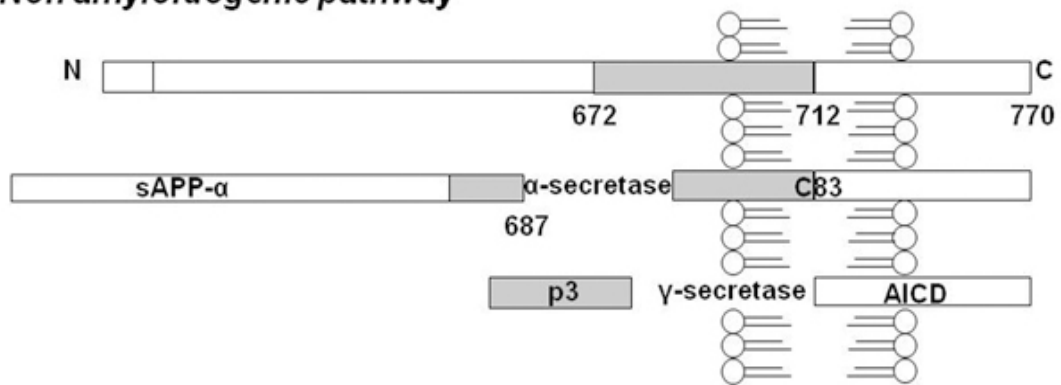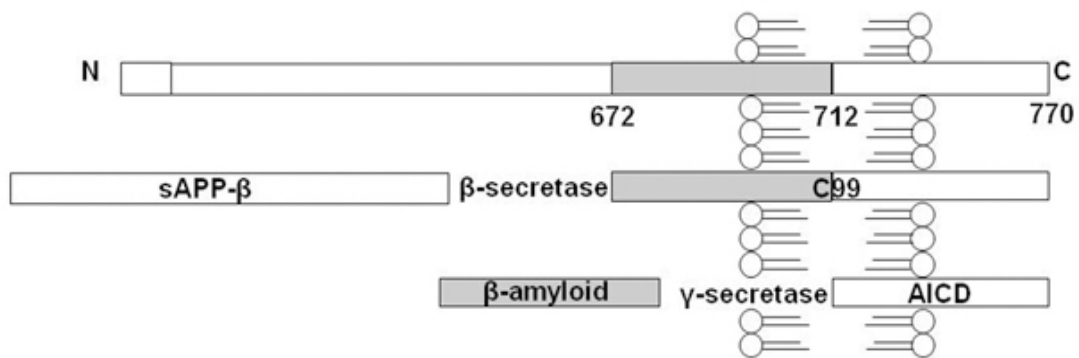
Figure 1.3: The processing of APP in the amyloidogenic and non-amyloidogenic pathways. The majority of APP is processed in the non- amyloidogenic pathway by the sequential cleavage by α-secretase and then γ- secretase to produce non-toxic protein fragments p3 and AICD. In the case of the amyloidogenic pathway APP is sequential cleaved by β-secretase and then γ-sectreatase to produce the toxic fragment Aβ. (Image taken from Stanga 2011)

1.2.2 <u>Forms of amyloid- β</u>

There are several isoforms of Aβ the majority of which are made up of either 40 or 42 amino acids (Aβ40 and Aβ42). Aβ peptides are generated within the cell at different subcellular sites. Aβ40 is only generated in the trans-Golgi network (TGN), whereas Aβ42 is produced in the ER as well as Golgi compartments (Hartmann *et al*. 1997). Although much of the generated Aβ is secreted, there is a significant build-up of Aβ

peptides, which is not readily secreted, thus levels of Aβ42 are shown to be elevated in patients suffering from AD (Gouras *et al*. 2000).

More importantly, these peptides can exist in different aggregation states- from the soluble monomer and oligomers to the insoluble β-sheet amyloid fibrils. It is the many states and isoforms of amyloid that make it difficult for researchers to ascertain amyloid's biological effects and due to its penchant for aggregation, experiments are extremely challenging. The length of the Aβ peptide has a significant impact on its aggregation properties. The Aβ peptide has a hydrophobic C-terminus and a hydrophilic N-terminus. Extending the peptide's length increases the molecules hydrophobicity and causes aggregation at the C-terminus. Therefore the Aβ42 isomer is more likely to aggregate than the Aβ40. It is know that Aβ levels are increased in AD causing insoluble fibrils to form. These fibrils can be made by any species of Aβ, including Aβ40, Aβ42 and Aβ(11-25), and consist of a cross-β sheet structure (Nelson *et al*. 2005). However, fibrillar Aβ is not the only source of toxic Aβ, dimers, trimers, oligomer and protofibrillar structures have also been identified *in vitro* and *in vivo* (Hartley et al. 1999; Walsh et al. 1999). In addition to these protofibrils, it is also possible to synthesise species in a laboratory. One particular species is ADDL (Aβ-derived diffusible ligand), this species is abundant in AD brain, and binds to hippocampal neurons to induce deficits in rodent cognition (Shughrue *et al*. 2010) it is this binding which is believed to result in neuronal deficits, furthermore ADDLs are thought to be a therapeutic drug target in AD simply because Aβ fibrils are intrinsic to AD pathology (Gong *et al*. 2003). However ADDLs were found to be potent neurotoxins, which were able to cause neuronal death at nanomolar concentrations (Lambert *et al*. 1998).

1.2.3 <u>Amyloid cascade hypothesis</u>

In 1992 Hardy and Higgins produced a hypothesis which was thought to explain the underlying cause in a cascade of events that lead to Alzheimer's disease. It was proposed that the clearance imbalance of Aβ and the formation of plaques lead to a signalling cascade causing synaptic dysfunction and neuronal death. Since then this hypothesis has been modified many times, but the hypothesis still remains valid today, with the exception that soluble Aβ oligomers and intraneuronal Aβ instead of amyloid plaques initiate the signalling cascade (Hardy & Higgins 1992). This cascade is summarised in Figure 1.4.
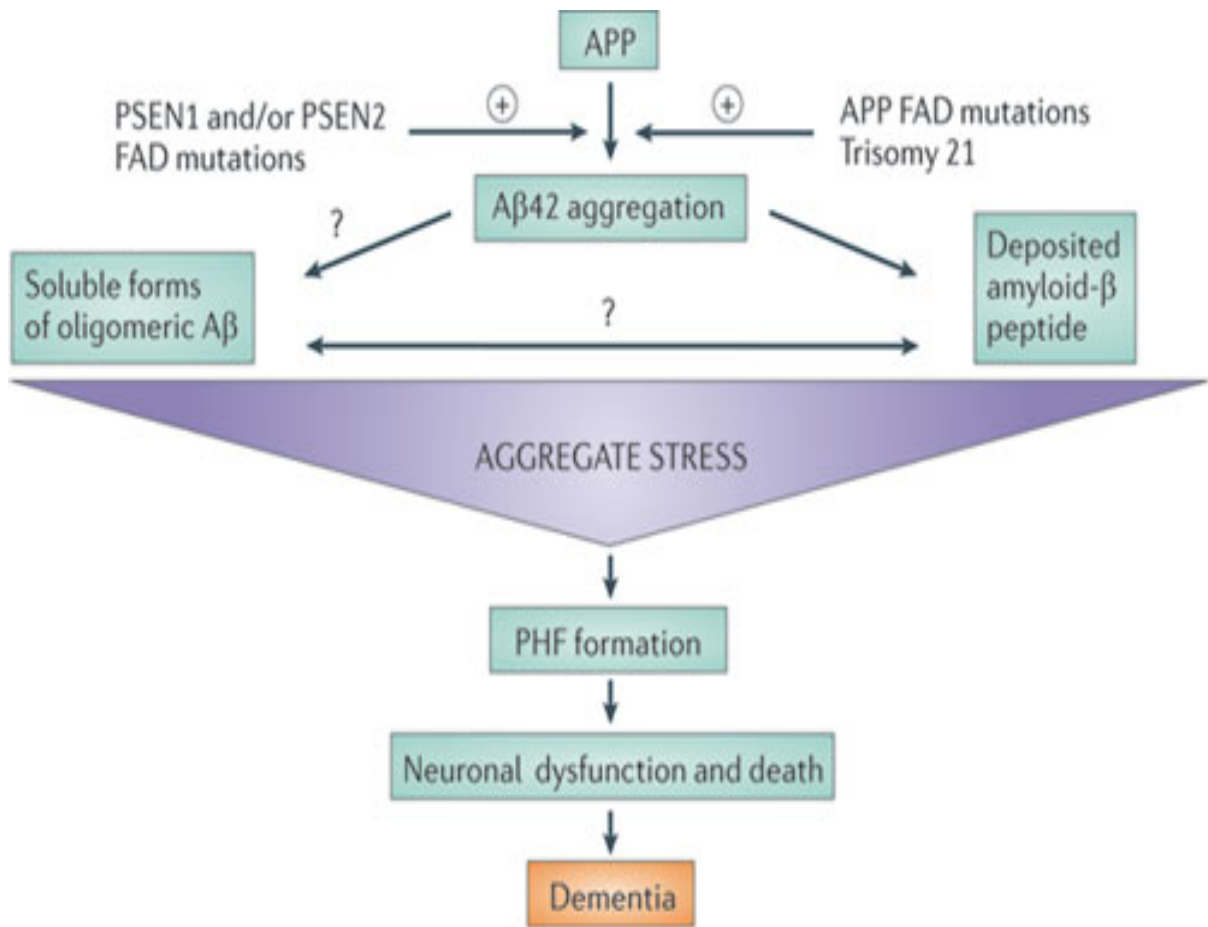
Figure 1.4: The amyloid cascade hypothesis. The amyloid cascade hypothesis suggests that the deposition of the amyloid-β peptide in the brain parenchyma is a crucial step that ultimately leads to Alzheimer's disease. Autosomal dominant mutations that cause early onset familial Alzheimer's disease (FAD) occur in three genes: presenilin 1 (PSEN1), PSEN2 and amyloid precursor protein (APP). In order to cover all forms of aggregation the term aggregate stress has been used to describe the potential mechanisms that may lead to amyloid-β aggregation, the formation of paired helical filaments (PHFs) of tau aggregates and ultimately, resulting in neuronal loss. This hypothesis has been modified over the years and it has become clear that the correlation between dementia or other cognitive alterations and amyloid-β accumulation in the brain in the form of amyloid plaques is not linear, neither in humans nor in mice. The amyloid cascade hypothesis now suggests that synaptotoxicity and neurotoxicity may be mediated by such soluble forms of multimeric amyloid-β peptide species. (Taken from a recent review Karran *et al.* 2011)

1.2.4 **Amyloid-β as a potential drug target**

Given the impact that Aβ has in AD, it is unsurprising that many researchers are investigating Aβ as a possible therapeutic target for new drugs. There are currently three possible approaches that are being investigated:

1) Target the prevention of Aβ formation.

2) Target the clearance issues of Aβ to help remove the build-up.

3) Target the toxic effects and try to diffuse the toxicity using immunotherapy.

Controlling the APP production pathway and inhibiting the β and γ secretases could potentially achieve the prevention of Aβ build up. The role of BACE1 (β-secretase) has been investigated using BACE1 knockout mouse models (BACE1$^{-/-}$), where initial studies suggested that the animals were identical to wild type animals and did not produce detectable Aβ, thus supporting the hypothesis that inhibition of this enzyme could achieve Aβ prevention whilst not affect other pathways (Roberds *et al*. 2001; Luo *et al*. 2003). Later studies indicate that these mice may exhibit schizophrenic like behaviour potentially due to BACE1's role in neuregulin processing, suggesting that other pathways are affected during BACE1 inhibition (Savonenko *et al*. 2008). Several other inhibition strategies targeting BACE1 have been carried out, but to date only one inhibitor CTS-21166 has progressed to a clinical trial (Luo & Yan 2010).

The clearance and neutralisation of Aβ is most specifically related to immunotherapy. Possible vaccines are described in more detail in section 1.1.4.

1.3 Mitochondrial dysfunction and oxidative stress in AD

As outlined in section 1.1 the underlying causes of AD are still unclear, however another possible underlying mechanism of the disease is that of mitochondrial dysfunction and oxidative stress. Mitochondria are the major sites of energy production in all cells, in the form of ATP synthesis. Other functions also include roles in cell signalling, cellular differentiation, cell death, as well as the control of the cell cycle and cell growth. The structure of the mitochondrion is shown in Figure 1.5.
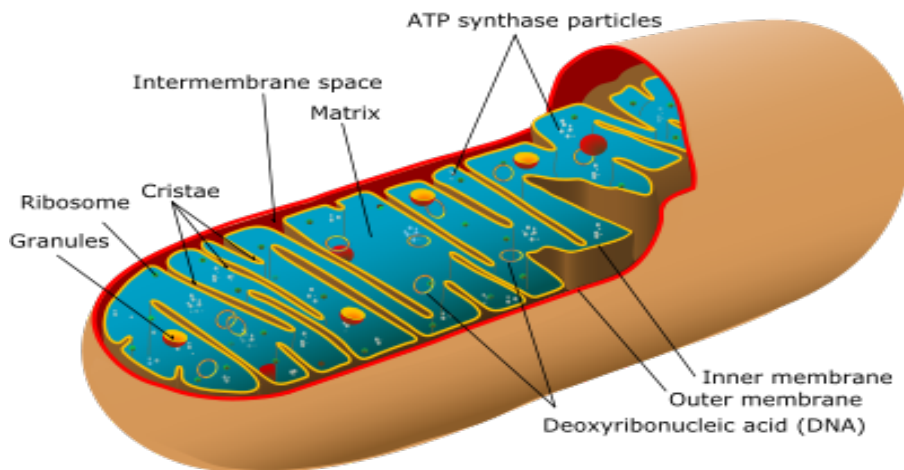
Figure 1.5: Structure of a mitochondrion. The mitochondria consist of two lipid membranes (inner and outer) and it is inside the inner membrane which generates energy (in the form of ATP) using the electron transport chain for oxidative phosphorylation. The outer membrane is permeable allowing substances to move between the cytosol and the inner membrane space. The matrix is an area enclosed by the inner membrane which is principally used to store the components of the citric acid or tricarboxylic acid cycle and β- oxidation.

Evidence to support the theory that mitochondrial dysfunction is involved in AD came from examining *post mortem* brain samples of patients with AD. These samples indicated a decrease in glucose metabolism, therefore showing a decrease in mitochondria function (Mattson 2004). Furthermore a PET study recording how patients with AD responded to performing functional tasks, showed a decline in the cerebral

metabolic rate in the parietal and temporal lobes of patients with AD (Kessler *et al.* 1991). Again this is evidence of a decline in mitochondrial function.

The mitochondrial electron transport system is the largest source of reactive oxygen special (ROS) and hydrogen peroxide (Kowaltowski *et al.* 2009). ROS are damaging to almost all of the contents of cells, especially mitochondria. The brain is particularly susceptible to damage due to ROS and one of the main etiological hypotheses is that free radical oxidative damage in neuronal degeneration occurs in AD (Chauhan & Chauhan 2006).

1.3.1 <u>Mitochondrial dysfunction and Aβ</u>

It has been shown that Aβ peptides are found within the mitochondria of AD brains (Lustbader *et al.* 2004; Caspersen *et al.* 2005; Manczak *et al.* 2006) however it is still not understood if the peptide is produced outside the mitochondria and transported across the membrane, or if Aβ is produced intracellularly, or both.

A study by Peterson in 2005 established that extracellular Aβ can be imported into the mitochondria *via* the translocase of the outer membrane (TOM) complex machinery (Petersen *et al.* 2008). Subsequent import studies revealed that the import is independent of the mitochondria membrane potential and that it solely relies on the transporters TOM20, TOM40 and TOM70. It is important to add that there have also been findings that have shown that the γ-secretase complex components are also found inside the mitochondria, thus allowing potential Aβ production inside the mitochondria (Hansson *et al.* 2004).

Another source of intracellular Aβ entry could be through the amyloid precursor protein (APP). APP carries a dual leader sequence which will either permit targeting to the ER

or to the mitochondria (Lin & Beal 2006). When this leader sequence was mutated, no APP mitochondrial localisation was observed, whereas APP is detected in the mitochondria of diseased brains (Anandatheerthavarada *et al.* 2003; Devi *et al.* 2006; Lin & Beal 2006). Subsequent studies later revealed an association with APP and the mitochondrial import channel in a transmembrane arrested form, resulting in the blockage of the transport channel (Devi *et al.* 2006).

Although Aβ entry mechanisms are still widely debated, what is clear is that once inside the mitochondria, Aβ will bind to many intracellular proteins. These proteins include amyloid binding alcohol dehydrogenase (ABAD) and cyclophilin D (CypD), which are of particular interest in this project and will be discussed in more detail in sections 1.4 and 1.5 respectively.

It is also known that changes in the electron transport chain (ETC) enzyme activities can also result in mitochondrial dysfunction and oxidative stress and therefore, that the electron transport chain is disrupted in AD (Parker Jr *et al.* 1990; Mutisya *et al.* 1994; Parker Jr *et al.* 1994). The ETC results in the formation of ATP via the reduction of oxygen to water in a complex enzymatic system consisting of 5 distinct phases: complex 1 (NADH dehydrogenase), complex 2 (succinate dehydrogenase), complex 3 (ubiquinol–cytochrome-c reductase), complex 4 (cytochrome-c oxidase), and complex 5 (ATP synthase). The ETC studies primarily focus on cytochrome C oxidase (CO), as the decrease in CO activity is the most consistent change seen in ETC enzyme activity where patients have AD. Indeed it has been shown that patients exhibit a 25–30% lower CO level than normal in the cerebral cortex (frontal, parietal, temporal, and occipital) and in the platelets of AD patients (Mutisya *et al.* 1994). More recently, the link between mitochondrial function and CO was supported by the discovery of mutations in CO genes that segregate with late-onset AD (Davis *et al.* 1997). CO is produced by the

combined effect of mitochondrial and nuclear genes however its catalytic centre is formed by three mitochondrial subunits COI- COIII, (Christen 2000). Thus, the assembly and function of ETC enzyme complexes are dependent on the coordinated expression of the genes located in two different informational systems of the cell. Evidence indicates that alterations of gene expression occur in the AD brain (Selkoe 1991) and therefore this may affect the production of the ETC enzymes and thus the ETCs ability to function.

Downstream proteins that are affected by changes in mitochondrial Aβ include endophilin (Ep-1) which becomes up-regulated and causes changes to the cell stress kinase c-Jun N-terminal kinase (JNK), and peroxiredoxin II (Prx-II) which is also up-regulated and could be a potential cell protector by increasing the degradation of peroxides (Yao *et al*. 2007; Ren 2008). Proteomic analysis of brains from transgenic animals engineered to over-express both APP and ABAD (Tg-mAPP/ABAD) identified increased expression of other proteins, hinting at other downstream effects of the interaction of ABAD and Aβ. Expression of Prx-II, an antioxidant enzyme, was found to be increased in mice overexpressing mAPP and in Tg-mAPP/ABAD mice (Yao *et al*. 2007). Transfection of cortical neurons with Prx-II was found to reduce Aβ toxicity, suggesting that its overexpression in AD is playing a protective role (Yao et al. 2007). Interestingly, Prx-II has also been linked with PD, where it was found to be phosphorylated by Cdk5 (cyclin-dependent kinase 5), and hence inactivated in MPTP-induced models of the disease (Qu *et al*. 2007). Similarly, increased phosphorylation of Prx-II was seen in the nigral neurons of human Parkinson's diseased (PD) brains, whereas the overall expression levels of Prx-II remained unchanged. As in AD models, overexpression of Prx-II in the mPTP-induced in vitro and in vivo models of PD was found to protect against neuronal loss (Qu *et al*. 2007). In light of these findings, the

consequences of Prx-II up-regulation in AD, its thought to provide a potential protective role, but this still needs to be investigated in more detail.

Ep-1, a presynaptic protein, also referred to as SH3GL2 (SH3-domain GRB-like 2)], was also identified as being up-regulated in Tg-mAPP/ABAD mice compared with mice expressing ABAD alone and non-transgenic littermates (Ren *et al*. 2008). Further analysis showed that there was up-regulation of Ep-I in the hippocampus and cortex of Tg-mAPP/ABAD mice and in the temporal cortex of human AD brains (Ren *et al*. 2008). Increases in JNK activation have been observed *in vivo* and *in vitro* (Zhu *et al*. 2003; Lagalwar *et al*. 2007) although this had been thought to be solely due to increases in ROS production. Ren *et al*. 2008, showed that an increase in Ep-I expression could increase JNK activity with the subsequent death of primary neuronal cell cultures. However, when neuronal cultures were transfected with truncated Ep-I, lacking its SH3 domain, the activation of JNK by Aβ was blocked and cell viability increased. Therefore it could be hypothesized that the increase in Ep-I expression shown in the AD brain could be another mechanism for the activation of the JNK signalling pathway.

Notably, the reported increases in both Prx-II and Ep-I in AD brains were shown to be directly due to the binding of ABAD and Aβ, as interfering with this binding in living organisms resulted in the expression of these two proteins returning to normal levels (Yao *et al*. 2011).

1.3.2 <u>Oxidative stress and Aβ</u>

Many studies have confirmed that oxidative stress resulting from Aβ occurs in human AD brains (Cutler *et al*. 2004; Chauhan & Chauhan 2006), mouse models (Park *et al*. 2004; Chauhan & Chauhan 2006), and in *in vitro* cell cultures (Chauhan & Chauhan

2006). It is common that ROS will be produced, subsequently producing more damage to cells and there will also be increased cytochrome c oxidase (CO) activity, causing an attempted protective effect in an attempt to minimise damage to cells and their contents (Fukui *et al*. 2007).

Transgenic mouse models expressing the combined London and Swedish mutations of APP have proved a great tool in elucidating the mitochondrial events that are occurring during times of oxidative stress. The mice in these studies developed reduced ATP levels and cytochrome c oxidase activity at a 3 months of age, before any amyloid plaques were visible (Hauptmann *et al*. 2009). It was then observed that after 6 months ROS could be detected (Hauptmann *et al*. 2009). Similarly another study carried out on the triple transgenic AD mouse model (3 x Tg encoding mutations in App, Tau and PS1) showed that after three months the mice exhibited decreased mitochondrial respiration and increased oxidative stress levels (Yao *et al*. 2009).

Several studies have now shown that direct exposure to Aβ significantly impairs functionality of the mitochondrial electron transport chain (ETC) (Crouch *et al*. 2008). The ETC plays a pivitol role in ATP production and its constituent enzyme complexes 1-4 are a major source of ROS generation, particularly when activity of one or more of the enzyme complexes is inhibited.

1.4   Amyloid binding alcohol dehydrogenase

ABAD was first identified as an intracellular receptor for Aβ in 1997 using a yeast two-hybrid screen (Yan *et al*. 1997), and is the most characterised intracellular Aβ binding protein. Other names for this protein are: endoplasmic reticulum amyloid binding protein (ERAB), 3-hydroxyacyl- CoA dehydrogenase type 2 (HADH 2), Short chain L 3-hydroxyacyl-CoA dehydrogenase type 2 (SCHAD) and MHBD. Termed ERAB as it was first identified in the ER, it was later recognised to be localised in the mitochondria and have dehydrogenase activity (Yan *et al*. 1999). ABAD is expressed in all tissue types and it is also expressed in all regions of the brain, and significantly increased in AD brains compared to controls (Yan *et al*. 1997; Yan & Stern 2005). Utilising the cofactor provides an easy measurement of *in vitro* ABAD activity, whereby NAD(H) production/consumption is measured (Muirhead *et al*. 2010).

1.4.1 Functions of amyloid binding alcohol dehydrogenase

ABAD is a member of the dehydrogenase family and shares common features with other members of its family, such as its dependence on the dinucleotide cofactor NAD(H). The features of this multifunctional enzyme include its presence in endoplasmic reticulum and mitochondria, its capacity to bind Aβ and promote Aβ-induced cell stress, and its ability to act on a broad array of substrates, including linear alcohols, 3-hydroxyacyl-CoA derivatives, D-β-hydroxybutyrate, and steroids (Table 1). Moreover, the results in Table 1 indicate the experimentally determined enzymatic parameters for a range of these substrates. As expected, different substrates have different reaction rates with the enzyme, indicating that although ABAD is able to catalyse reactions on a number of different substrates, some have a higher turnover than others (Muirhead *et al*. 2010). It is also shown that widely ranging values for enzyme

activity have been reported for the same substrate, often varying by several orders of magnitude. However, comparisons between values obtained may be complicated due to the range in conditions used during assays used to the potentially wide range of roles that the enzyme is able to perform within the cell (Yan & Stern 2005; Muirhead *et al.* 2010). It is important to note that an enzyme's ability to metabolize a particular substrate *in vitro* does not necessarily guarantee that it performs the same actions *in vivo*.

One function of this protein, is catalysing the reversible reduction of aldehydes and ketones and the oxidation of alcohols using its cofactor NAD(H) (Figure 1.6). It is believed that the primary function of ABAD is energy production and metabolic homeostasis, in particular its involvement in the third step of the β-oxidation of fatty acid in times of a glucose deficiency, utilising its role as an L-3-hydroxyacyl-CoA dehydrogenase (Powell et al. 2000).

ABAD is known to have a role in the degradation pathway of isoleucine. In clinical cases of MHBD (2-methyl-3-hydroxybutyryl-CoA dehydrogenase) deficiency, i.e. deficiency of the enzyme catabolizing the penultimate step in isoleucine degradation, two missense mutations within ABAD were identified in patients presenting with MHBD deficiency; Arg130 was mutated to a cysteine residue in four patients and was found to cause neurological deficits, loss of mental and motor skills and psychomotor retardation, whereas a Leu122 to valine substitution, identified in a single case, presented with only psychomotor retardation (Ofman *et al.* 2003). The mutations were shown to either fully (R130C) or greatly (L122V) inactivate the enzyme. Furthermore, the R130C mutation was also thought to reduce the enzyme's stability, causing the lower protein levels observed in these patients (Ofman *et al.* 2003).

Other suggested functions include the metabolism of hydroxysteroids such as oestradiol (He *et al*. 2001). This is significant if ABAD is metabolizing sex steroids, as it is documented that women are more likely to suffer from AD than men, and that postmenopausal hormone replacement therapy can prove beneficial in delaying the onset of the disease (Tang *et al*. 1996; Fukuzaki *et al*. 2008).

Table 1.2- Experimentally derived activity parameters for ABAD with a range of substrates (Muirhead *et al*. 2010)

SUBSTRATE	CO-FACTOR	SPECIFIC ACTIVITY (μmol min^{-1} mg^{-1})	V_{max} (μmol min^{-1} mg^{-1})	K_m (μM)	K_{cat} (s^{-1})
S-Acetoacetyl- CoA	NADH	-	430 ± 45	68 ± 20	190
	NADH	-	-	89 ± 5.4	37 ± 1.6
	NADH	1.1	-	22.7	-
	NADH	-	-	53 ± 9	11.1 ± 0.7
17β- Oestradiol	NAD$^+$	-	23 ± 3	14 ± 6	10
	NAD$^+$	-	-	15 ± 7	0.00088 ± 0.0012
	NAD$^+$	0.0156 ± 0.0008	-	43 ± 2.1	0.093 ± 0.0028
Dihydroandrosterone	NAD$^+$	0.130 ± 0.0018	-	34 ± 2.4	0.011 ± 0.0013
Androsterone	NAD$^+$	0.0121 ± 0.0009	-	45 ± 9.3	1.0
Ethanol	NAD$^+$	-	2.2 ± 0.4	1210 ± 260	1.9
1- Propanol	NAD$^+$	-	4.2 ± 0.5	272000 ± 62000	0.0060 ± 0.0005
	NAD$^+$	-	-	83200 ± 21000	16
2-Propanol	NAD$^+$	-	36 ± 2	150000 ± 17000	0.0179 ± 0.0008
	NAD$^+$	-	-	156000 ± 18000	0.036 ± 0.0023
	NAD$^+$	-	-	280000 ±33000	-
β-Hydroxybutyrl-CoA	NAD$^+$	65.7	-	9.8	-
	NAD$^+$	-	26.3	134	-
L-β-Hydroxybutyrate	NAD$^+$	-	0.004	1600	-
D-β-Hydroxybutyrate	NAD$^+$	-	0.004	4500	-
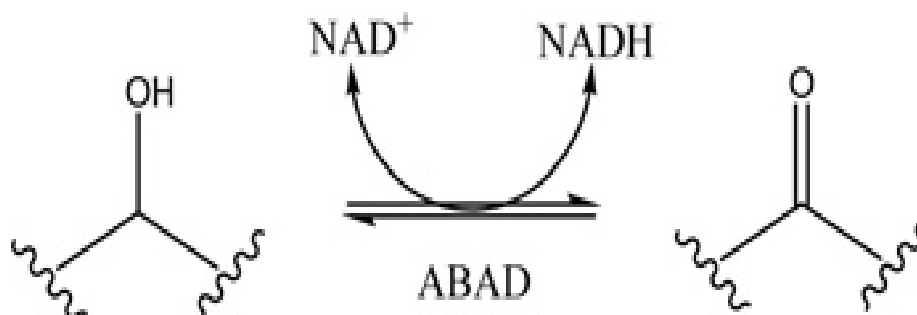
Figure 1.6: The reduction and oxidation of alcohols and ketones by ABAD, using its cofactor NAD(H) (Muirhead *et al.* 2010)

It has been suggested that in the absence of Aβ, ABAD is able to play a cytoprotective role during periods of oxidative stress. For example, in mouse models of ischaemic stress (stroke), ABAD expression was found to be increased in both ABAD overexpressing and non-transgenic mice following 45 minutes of transient middle cerebral artery occlusion (Yan *et al.* 2000). However, the transgenic animals showed fewer effects of the stroke, including fewer neurological deficits and increased ATP levels and were therefore thought to be protected to some degree by the elevated levels of ABAD (Yan *et al.* 2000). Conversely, ABAD levels were shown to be decreased in the ventral midbrain of Parkinson's disease (PD) patients, as well as in the ventral midbrain of MPTP (1-methyl-4- phenyl-1,2,3,6-tetrahydropyridine) treated mice, used as a model of PD. However, MPTP-treated mice overexpressing ABAD were protected against apoptosis and the loss of dopaminergic neurons in this brain region, suggesting that this enzyme can protect against neurodegeneration in times of low Aβ (Tieu *et al.* 2004).

1.4.2 **Structure of amyloid binding alcohol dehydrogenase**

The crystal structure of ABAD is well documented, with several structures of the enzyme published. These include structures in complex with its co-factor NAD+ (Powell *et al*. 2000), a human mutant construct complexed with an inhibitor (Kissinger *et al*. 2004) and the human protein in complex with Aβ (Lustbader *et al*. 2004). From these structures, information on the catalytic mechanism and its interaction with Aβ has been deduced. At present, there are however no crystal structures of ABAD independent from other molecules.

ABAD is found to exist as a homo-tetramer, in both solution and in its crystal form, which is made up of four identical single domain monomers of 27 kDa each. Tetramerization has been shown, by molecular modelling, to stabilise the binding interface region (Marques *et al*. 2008). The conserved catalytic triad of Ser155, Tyr168 and Lys172 is found in the active site of other short chain dehydrogenase reductase enzymes (Kissinger *et al*. 2004; Lustbader *et al*. 2004). Where the mutation of these residues to glycine inactivates the enzyme (Yan *et al*. 1999). In the reduction of a ketone to an alcohol, the hydrogen atom of Tyr168 is thought to co-ordinate to the carbonyl of the ketone substrate, thus increasing the electrophilicity of the carbonyl carbon atom. It is proposed that the ammonium group of Lys172 interacts with the hydroxyl group of Tyr168, increasing the acidity of this residue. The hydride that controls reduction is donated to the activated carbonyl by the NADH cofactor, leading simultaneously, to deprotonation of Tyr168 by the newly formed hydroxyl group. The hydroxyl group of Ser155 is able to form a hydrogen bond with the deprotonated tyrosine, stabilizing the resulting negative charge (Figure 1.7). Structures of rat ABAD with either 3-ketobutyrate or 17β- oestradiol showed that the two substrates bound in

similar positions within the active site (Powell *et al*. 2000). These structures confirm the close proximity of the presumed catalytic triad residues to the substrate molecule.
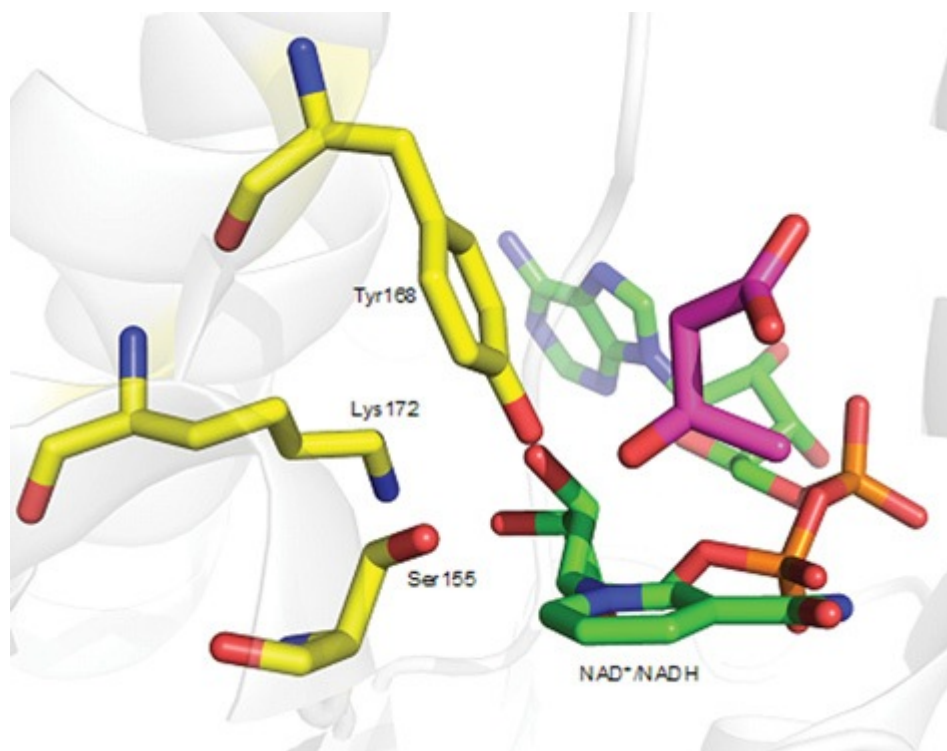
Figure 1.7: The catalytic triad core of ABAD. A PyMol representation of the X-ray crystal structure of rat ABAD bound to its co-factor and an acetoacetic acid substrate. The three conserved active site residues, Ser155, Tyr168 and Lys172 (carbon atoms in yellow), the NAD$^+$/NADH co-factor (carbon atoms in green) and the acetoacetic acid substrate (carbon atoms in magenta) are represented as sticks. It can be seen that the ketone oxygen of the substrate interacts with Tyr168 and is favourably oriented in order to receive or donate a hydride to or from the co-factor. Nitrogen atoms= blue; oxygen atoms=, red; phosphorus atoms= orange (Muirhead *et al*. 2010).

Molecular modelling studies (Marques *et al*. 2008) developed 10 ns MD (molecular docking) simulations of the ABAD tetramer, as well as of the structural units (monomer and dimer) that assemble to form the tetramer. The crystal structure of ABAD in complex with a NAD-inhibitor (Kissinger *et al*. 2004) was used to obtain the starting

structures and the simulations were performed both in the presence and absence of the ligand. In this study they were able to compare the stability of the dimer and monomer with that of the tetramer and to study the effects of the inhibitor binding on the flexibility of the enzyme structure as a whole. The results indicated that the dimer and monomer show a comparable stability with that of tetramer. Some regions of the protein are however more stabilised upon tetramerization as they show no change when exposed to the solvent, whereas dimer and monomer became more flexible. During these studies it was shown that throughout binding of the cofactor and inhibitor ABAD became stabilised, in particular, the substrate- binding loop (Loop D). In the absence of the ligand, this region showed a much higher flexibility and an increase in distance away from the binding cavity. These results show that the ABAD monomer could be used as a model for AD, but it would have its limitations, as the substrate- binding loop is a lot less flexible in the tetramer.

As we do not yet understand ABADs mechanism of action, it is possible that given the similarities of the active site between ABAD and its related enzyme 3-hydroxyacyl-CoA dehydrogenase (HAD), that it may be possible to assume the mechanisms of action are similar (Liu *et al.* 2007). Studies suggest that the reversible oxidation of hydroxyacyl-CoA linked substrates proceed through an essential enolate intermediate, to form 3-ketoacyl- CoA, which can be stabilised by an Asn208 residue or a Ser137 residue (Figure 1.8). When comparing the structures of rat and human ABAD (Powell *et al.* 2000; Lustbader *et al.* 2004) with other HADs, both ABAD molecules were shown to have two inserted residues in the regions of 100-110 and 140-150; therefore, suggesting that although similar this may not be the entire mechanism.

Enolate Intermediate
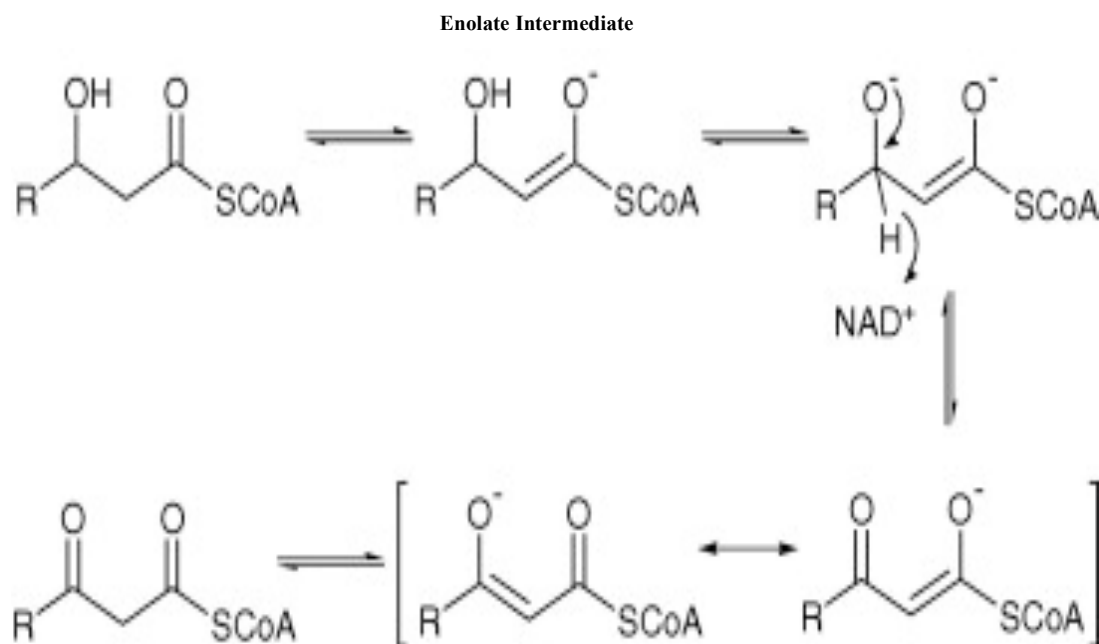
Figure 1.8 : Reversible oxidation of hydroxyacyl CoA to 3-ketoacyl-CoA *via* enolate intermediate stabilised by Asn206 or Ser137 (Liu *et al*. 2007).

1.4.3 The ABAD- Aβ interaction

The initial identification of ABAD as an intracellular binding partner of Aβ was based on a yeast two-hybrid screen (Yan *et al*. 1997), which identified four positive clones (one from human brain and three from HeLa cells), all of which had the same cDNA sequence.

Radio labelled ligand-binding studies confirmed the interaction of ABAD- Aβ and a Kd of 88 nM was determined (Yan *et al*. 1997). Subsequently, a number of techniques have been employed to demonstrate the interaction between ABAD and Aβ, including ELISA (Xie *et al*. 2006), X-ray crystallography (Lustbader *et al*. 2004), surface plasmon resonance (SPR) (Lustbader *et al*. 2004; Yan *et al*. 2007) co-immunoprecipitation (Yan *et al*. 1997; Lustbader *et al*. 2004) and immunocytochemistry followed by confocal microscopy (Lustbader *et al*. 2004). Crucially both Aβ40 and Aβ42 were found to inhibit the activity of purified ABAD

protein, with Ki values of 1.2– 1.6 μM for the reduction of acetoacetyl-CoA (Oppermann *et al*. 1999), 2.6 μM for the oxidation of octanol (Yan *et al*. 1999) and 3.2 μM for the reduction of 17β-oestradiol (Yan *et al*. 1999). Studies by Oppermann *et al* in 1999 showed that residues 13– 22 of Aβ were essential for inhibiting ABAD activity, a region that is also characterized by its fibril-forming properties of residues 16– 20. At cellular level the effects of Aβ can also be observed. Upon the addition of Aβ42 to a neuroblastoma cell line (SK-N-SH cells), the localisation of ABAD appeared to change from the ER and mitochondria to the plasma membrane (Yan *et al*. 1997; Yan *et al*. 1999). The significance of this event has not been explored further, to date.

COS cells, which had been transfected with a DNA plasmid encoding ABAD, exhibited increased Aβ induced cell stress when compared with non-transfected cells, which naturally produce low quantities of endogenous ABAD when exposed to Aβ42 (Yan *et al*. 1999). Similar results were shown in cells overexpressing both ABAD and Aβ, displaying a significant increase in apoptosis than those overexpressing ABAD or Aβ alone (Yan *et al*. 1999). By preparing a catalytically inactive mutant ABAD (mtABAD: containing mutations in the catalytic triad), Yan *et al*. were also able to show that catalytically active ABAD is necessary to cause these effects when exposed to Aβ (Yan *et al*. 1999). COS cells overexpressing the mtABAD/mAPP showed no increase in cytotoxicity when compared with mAPP alone, while those cells transfected with wild type ABAD/mAPP produced an increase in DNA fragmentation compared with mAPP alone. These results demonstrate that the effects produced are not merely down to the loss of ABAD activity due to the presence of Aβ, but that it must result in a change in functionality of the enzyme upon binding.

The toxic effect of overexpressing ABAD together with Aβ has also been confirmed in an AD mouse model. Compared with neurons from non-transgenic mice and mice

overexpressing ABAD or mAPP alone, E18 cortical neurons cultured from Tg-mAPP/ABAD mice were found to exhibit higher levels of hydrogen peroxide, decreased mitochondrial function and increased cell death (Takuma *et al.* 2005). Mitochondrial dysfunction was observed *in vivo* in Tg-mAPP/ABAD mice, which had decreased glucose metabolism and ATP production at 9 months of age (Takuma *et al.* 2005). These mice were also found to have deficits in spatial and temporal memory compared with non-transgenic mice, with impaired performance in the radial-arm water maze as early as 4–5 months of age (Lustbader *et al.* 2004). These results again emphasise that it is the combination of ABAD and Aβ that is necessary for effects to be seen and that these effects occur early in the disease process.

The crystal structure of ABAD in complex with Aβ lends support to the theory that there is a conformation change of the enzyme, distorting the active site upon binding with Aβ (Lustbader *et al.* 2004). Compared with other published ABAD structures (Powell *et al.* 2000; Kissinger *et al.* 2004), the active site and NAD$^+$ binding site were shown to be highly distorted in the presence of Aβ and no bound NAD$^+$ co-factor was observed. Further studies using SPR confirmed binding of ABAD and Aβ at nanomolar concentrations and showed that a conformational change in ABAD occurs upon binding of Aβ (Yan *et al.* 2007). Saturation transfer difference NMR was used to show that the presence of Aβ inhibited the binding of NAD$^+$ to ABAD in a concentration dependent manner (Yan *et al.* 2007). Similarly, the ability of Aβ to bind ABAD was reduced in the presence of NAD$^+$, suggesting that the binding of Aβ and NAD$^+$ to ABAD are competitive (Yan *et al.* 2007). These observations provide strong evidence that Aβ has an influence on the physical structure of ABAD, disrupting its activity.

A proposed consequence of the ABAD-Aβ complex is the cellular accumulation of toxic aldehydes, in particular 4-hydroxynonenal (HNE) and malondialdehyde (MDA),

which have shown to be increased in AD (Sayre *et al*. 1997; Delibas *et al*. 2002). Under normal conditions ABAD would provide a protective effect against the accumulation of these aldehydes, but under the presence of Aβ this protective role is lost (Murakami *et al*. 2009).

From these studies, it has been shown that the interaction of Aβ with ABAD has multiple effects at the molecular, cellular and whole animal level. When Aβ binds to ABAD the overall effect is to inhibit the ABAD enzyme activity. However, the precise molecular mechanisms of how this occurs are yet to be elucidated.

1.4.4 <u>ABAD-Aβ interaction as a potential therapeutic target</u>

It has long been established that the interaction between ABAD and Aβ can lead to harmful effects on cell viability along with subsequent damaging effects on the cognitive performance in transgenic AD mouse models, thus reflecting the importance of these cellular effects on disease progression. Therefore, these studies indicate that the ability to block this interaction could provide a potential target for the treatment of AD.

There is another strong argument for targeting the ABAD- Aβ interaction as a novel therapeutic target in AD. Studies have shown that this interaction has been implicated in the progression of AD, yet there is a huge void in the drugs that are able to act on the underlying mechanisms of the disease.

A "decoy peptide molecule" (DP) encoding ABAD residues 92–120 was found to inhibit the binding of Aβ40 and Aβ42 to ABAD with K_i of 4.9 and 1.7 μM, respectively (Lustbader *et al*. 2004). The ABAD- Aβ inhibition was thought to occur by the decoy peptide binding to Aβ, as these residues correspond to the ABAD binding site. This peptide was later considered as a drug candidate starting point for disrupting the

ABAD- Aβ interaction and developing a novel drug strategy for treating AD. Cellular studies have demonstrated the protective effects of this DP. By making a Tat-DP fusion peptide by the addition of the Tat domain from the human immunodeficiency virus (HIV) this allows the DP to cross cell membranes, where it was found to attenuate Aβ-induced cell toxicity in cultured primary neurons from wild type, Tg ABAD and Tg ABAD/mAPP animals, as shown by reductions in cytochrome c release, production of ROS, DNA fragmentation and LDH release (Lustbader *et al*. 2004). As the DP is so small it would not be considered a suitable drug candidate, so in order to capitalise on its potential to reverse the symptoms seen when ABAD and Aβ interact, it was important to try and increase its half-life and stability. Therefore, a separate study expressed the DP through a larger lentiviral system, fusing the DP to the protein cytosolic thioredoxin-1 (TRX) (Yang *et al*. 2007). This fusion DP, ABAD (92–120)-TRX, was observed to be co-localised with Aβ and, like Tat-DP, was found to significantly decrease Aβ toxicity. Transfected cells exhibited decreased apoptosis, decreased LDH release and increased cell viability in response to Aβ treatment when compared with untransfected cells or those transfected with thioredoxin alone (Yang *et al*. 2007). The benefits of the DP were also observed in animal studies where the DP(93–116), was again fused to the HIV Tat domain containing a mitochondrial targeting sequence (to assemble the peptide in the mitochondria) [Tat-mito-DP(93–116)]. Transgenic mice over expressing mAPP (Tg mAPP) which were treated with Tat-mito-DP(93–116) from the age of 7–10 months were found to have preserved mitochondrial function when compared to animals treated with a peptide encoding the reverse peptide sequence (Tat-mito-RP)(Yao *et al*. 2011). Similarly, 10–11 month old double transgenic mice over-expressing mAPP and mito-DP(92–120) were found to have preserved mitochondrial function when compared with Tg mAPP animals (Yao *et*

al. 2011). The most significant finding was when six-month old Tg mAPP mice were treated with Tat-mito-DP(93–116) or the reverse DP sequence (Tat-mito-RP) by intraperitoneal injection over two weeks. After treatment, western blot analysis of the hippocampus showed elevated Prx-II and Ep-I protein expression levels in untreated Tg mAPP and Tat-mito-RP treated animals, compared with non-Tg controls. Animals treated with Tat-mito-DP showed significant decreases in Prx II and Ep-I protein expression levels compared with Tat-mito RP treated animals, with expression levels comparable to those of non-Tg. Therefore the up-regulated protein biomarkers of AD, Prx-II and Ep-I were found to return to normal basal levels following treatment with the decoy peptide, thus supporting its potential role as a therapeutic agent (Yao *et al.* 2007; Ren *et al.* 2008).

A continuation of these DP studies has revealed that the DP is capable of reversing behavioural symptoms associated with transgenic AD model animals. In 2004 Lustbader *et al.* identified that ten month old Tg mAPP mice showed deficits in the radial-arm water maze test when compared with non-Tg animals. However in 2011 when Yao *et al.* compared Tg mAPP mice which were treated with Tat-mito- DP(93–116) (using intraperitoneal injection for three months from the age of seven months), this resulted in an improvement in spatial learning and memory compared with vehicle-treated animals. Similarly, as an independent method to highlight the significance of this interaction, 10–12 month old transgenic mice over-expressing the decoy peptide [mito-DP(92–120)] and mAPP showed less impairment than Tg mAPP mice (Yao *et al.* 2011). These studies demonstrate that disrupting the ABAD-Aβ interaction can prevent downstream consequences of this interaction, and thus provide support that the ABAD-Aβ complex is a potential therapeutic target for treating AD.

There are some small molecule inhibitors of the ABAD-Aβ complex which have been identified (Inbar & Yang 2006; Xie *et al*. 2006). These compounds are designed from thioflavin T (ThT), the amyloid β-sheet binding dye, and frentizole, an immunosuppressant with a similar structure first identified by an ELISA-based screening assay. ThT and frentizole were shown to be promising inhibitors of the ABAD-Aβ complex with IC_{50} values of 230μM, 200μM respectively, however no *in vitro* activity data is available for these compounds as yet (Inbar & Yang 2006; Xie *et al*. 2006). Due to the ThT action of staining β-sheet structure, it is thought that this is where the ThT would target when inhibiting the compound, therefore being unable to target smaller Aβ monomers. Regardless, these small molecule inhibitors are capable of inhibiting the ABAD-Aβ interaction and provide evidence that small molecule inhibitors of this interaction are a viable approach.

Another approach for drug discovery using this target complex, is to use either crystallography or molecular docking experiments. In 2004, Kissinger *et al*. crystallised human ABAD with its co-factor NAD^+ and a small molecule inhibitor. They designed an inhibitor (AG18051) that could occupy the substrate-binding site and still allow ABAD to form a covalent bond with NAD^+, thus providing a basis for the design of potent, highly specific human ABAD inhibitors which could be used in the treatment of Alzheimer's disease.

This AG18051 inhibitor has been used in further studies, such as Lim *et al.*, who identified that in the presence of AG18051, Aβ-mediated toxicity, metabolic impairment and reduction in estradiol levels are eradicated in SH-SY-5Y neuroblastoma cells (Lim *et al*. 2011), as well as showing as a decrease in ROS levels under Aβ42 toxicity. As estradiol is a hormone and product of ABAD activity, Lim *et al.* also

suggest that as well as using the AG18051 inhibitor in drug development, it may be possible to use estradiol as a marker.

The use of the loop D region in ABAD could also provide a useful drug target, however during crystallography studies the loop D region was unable to be crystallised as it is very flexible (Lustbader *et al*. 2004). The loop D region is shown to be 28 amino acids long, and when adding a target sequence to this, it could prove too large to be a drug like molecule. However as discussed, the exact make up of the loop D region is unknown at present, therefore with further development it may be possible to design a smaller mitochondrial targeting sequence that may help to introduce stability and increase the rigidity of the region.

1.5   <u>Cyclophilin D</u>

Recently, a second major Aβ–protein interaction has been found within mitochondria. Cyclophilin D (CypD), a peptidylprolyl isomerase F, is found in the mitochondrial matrix and translocates to the inner mitochondrial membrane during the opening of the mitochondrial permeability transition pore (mPTP) in times of oxidative stress (Connern & Halestrap 1994). The mPTP plays a central role in both necrotic and apoptotic neuronal cell death. Opening of the mPTP collapses the membrane potential and plausibly amplifies apoptotic mechanisms by releasing proteins with apoptogenic potential from the inner membrane space (Halestrap 2005). The mPTP is thought to involve adenine nucleotide translocase (ANT) in the inner membrane, voltage-dependent ion channel (VDAC) in the outer membrane and CypD in the mitochondrial matrix, although there may also be other components (Halestrap 2005; Leung & Halestrap 2008). CypD associates with ANT and potentially other targets on the inner mitochondrial membrane, contributing to the opening of the mPTP. This association leads to colloidosmotic swelling of the mitochondrial matrix, dissipation of the inner membrane potential (ψm) and/or generation of ROS. Due to these findings, CypD is considered to be part of the mPTP complex as summarized in Figure 1.9.

Oxidative and other cellular stresses promote CypD translocation to the inner membrane (Connern & Halestrap 1994; Nakagawa *et al*. 2005). Other studies provided substantial evidence that a genetic deficiency in CypD protects against $Ca2^+$ and oxidative stress induced cell death (Basso *et al*. 2005). Other CypD functions include providing a pivotal regulatory role in the mPTP opening (Baines *et al*. 2005) and CypD has also been shown to be involved in protein folding (Freeman *et al*. 1996).
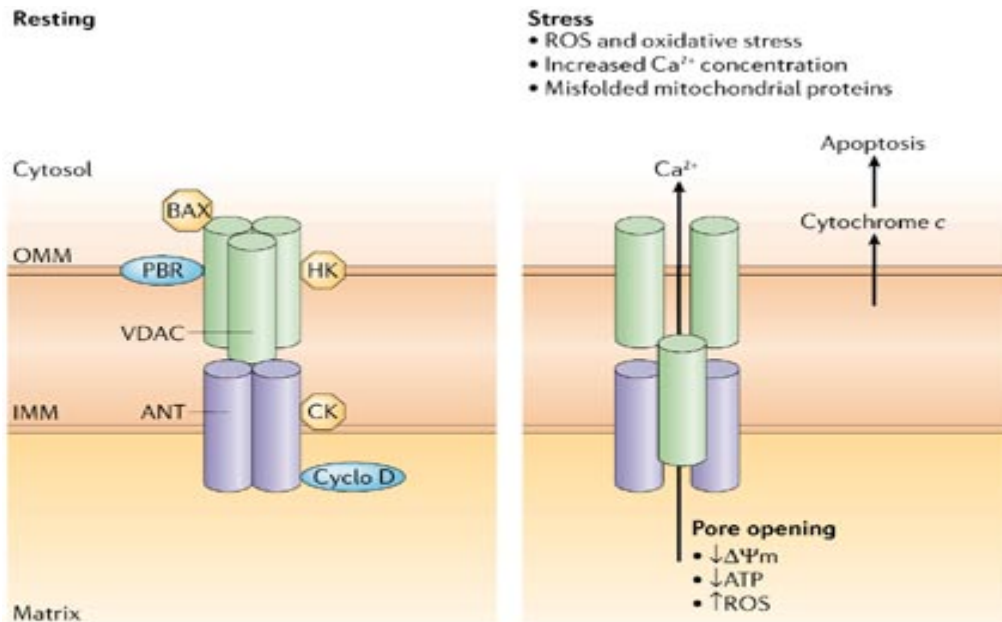
Figure 1.9: Probable components of the mPTP and how the pore differs when under oxidative stress. On the left; a resting mPTP with the components including, ANT (Adenine Nucleotide Translocase), PiC (mitochondrial phosphate carrier) and CypD at the inner mitochondrial membrane (IMM) and VDAC (Voltage Dependent Anion Channel). During times of oxidative or other stresses (as shown on the right of the diagram) pore formation leads to the leakage of H^+ and $Ca2^+$ to the cytosol, disruption of the mitochondrial membrane potential and necrosis. Prolonged or repeated sub-lethal mPTP-formation is thought to cause mitochondrial swelling and rupture of the outer mitochondrial membrane and then finally apoptosis. (BAX= Bcl-2–associated X protein, CK= Creatine Kinase, HK= hexokinase) (Taken from Abou-Sleiman *et al*. 2006)

1.5.1 The CypD- ABAD interaction

As discussed in sections 1.2 and 1.3, the overexpression of ABAD produced a protective effect on cells under metabolic stress. In contrast, overexpression of ABAD in an Aβ rich environment increased Aβ induced neuron toxicity. Yan and Stern reported that ABAD binds CypD (unpublished observation, Yan and Stern, 2004; Ren 2008). Therefore, they hypothesized that CypD may be a contributor to the beneficial effects of ABAD on cellular functions. By anchoring the CypD in the matrix compartment, the molecule is unable to translocate to the inner mitochondrial

membrane, where it could form the mPTP and potentially lead to neuronal death. However, in an Aβ rich environment, the Aβ-ABAD interaction might displace CypD, resulting in its translocation to the inner mitochondrial membrane, thereby leading to mPTP formation (Yan & Stern 2005) This hypothesis is shown in Figure 1.10.
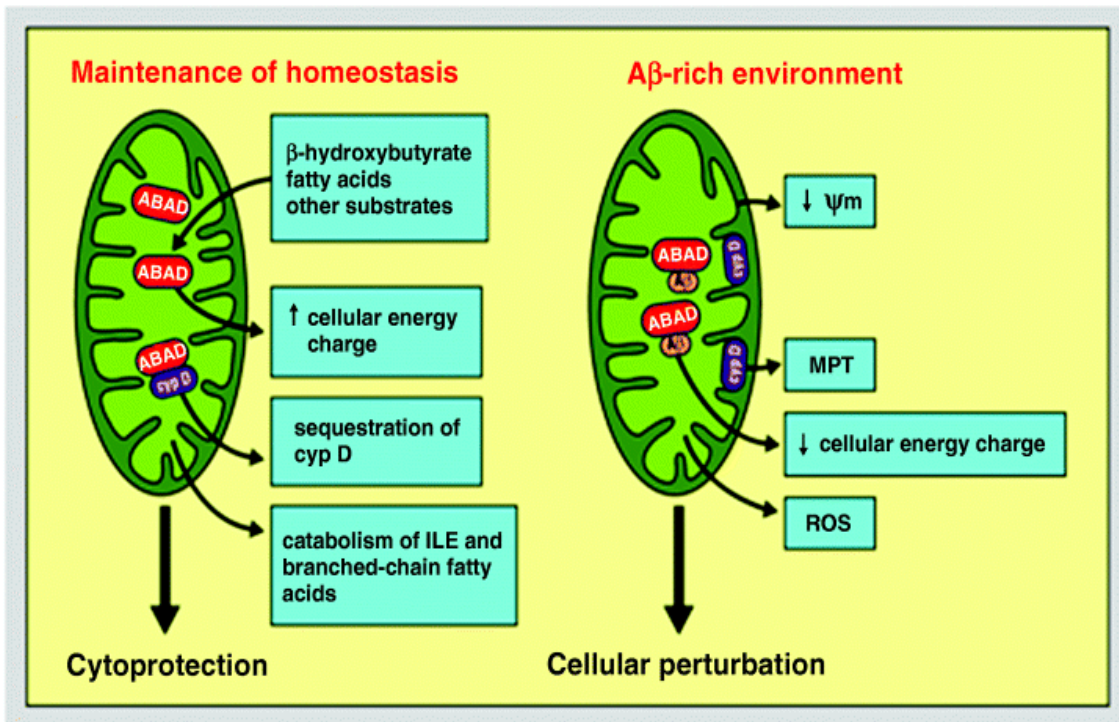
Figure 1.10: Protective effect hypothesis from the possible CypD- ABAD interaction. Under physiological conditions, ABAD-CypD interaction maintains CypD in the mitochondrial matrix, preventing it translocating to the inner membrane of mitochondria. In an Aβ rich environment, ABAD-Aβ interaction displaces CypD, results in its translocation to the inner membrane of mitochondria, which leads to the opening of MPTP and cell death. Ψm= mitochondrial membrane potential, MPT= membrane permeability transition pore. (Taken from Yan & Stern 2005).

The observations that Aβ progressively accumulates in brain mitochondria of AD patients led Du *et al.* to further investigate the mechanism underlying Aβ-mediated mitochondrial dysfunction. In these studies, it was established, by surface plasmon resonance (SPR), that CypD can bind Aβ (Du *et al.* 2008). Elevated CypD levels were

reported in human AD brains, as well as in a mAPP expressing mouse model for AD (Du *et al*. 2008). The Kd for the interaction of CypD and monomerised Aβ40 and Aβ42 was 1.7 μm and 164 nM respectively, whereas interactions with oligomeric Aβ40 and Aβ42 had a Kd of 227 nM and 4 nM, thus indicating that the oligomeric forms of Aβ appear to have a greater affinity for CypD and that Aβ42 has a greater affinity than Aβ40. Co-localization of CypD and Aβ in the mitochondria was also observed by confocal microscopy in the cerebral cortex of both mice overexpressing mAPP and in human AD brains, and immunoprecipation confirmed the enriched presence of CypD–Aβ complexes in AD brains (Du *et al*. 2008).

As with the ABAD and Aβ interaction, at present the exact contact sites of the interaction between CypD and Aβ are unknown, though recent molecular-docking experiments have attempted to produce a model. Singh *et al* also predicted an interaction between ANT and Aβ, which together with CypD has a possible functional impact on the mPTP (Singh *et al*. 2009). It is not known as yet, whether these predictions will prove to be true, as to date, they have not been experimentally tested. The crystal structure of CypD has been published (Schlatter *et al*. 2005; Kajitani *et al*. 2008), but only in the presence of DMSO (Schlatter *et al*. 2005) or CsA (cyclosporin A) an inhibitor of CypD (Kajitani *et al*. 2008). Notably, in both cases a truncated mutant form of CypD was used, starting at Cys29 and containing a single point mutation (K133I). However, at present it is unknown whether these mutated or truncated regions play an important role in the interaction. The crystallographic studies are show in more detail in Figure 1.11.

From the CsA study it was observed that one half of the CsA residues (Sar3-Dal8) are exposed in a solvent region, whereas the other residues (Bmt1, Aba2, Mle9- Mva11) are buried in CypD (Kajitani *et al*. 2008). As CsA is composed of hydrophobic residues it

will therefore interact with CypD *via* hydrophobic contacts. Notably hydrogen bonds are only formed with the nitrogen and oxygen atoms of CsA (Kajitani *et al.* 2008), and all the residues that are in contact with CsA are conserved throughout the human cyclophilins. Residues Ser59, Ser81, Arg82, Ile117, Lys148 and Ser149 which are located near the CsA binding site of CypD are not well conserved in human cyclophilins and are believed to recognise specific ligand proteins (Kajitani *et al.* 2008). Significantly any molecules that are capable of binding to these residues could be considered to be leading compound CypD specific inhibitors (Kajitani *et al.* 2008).
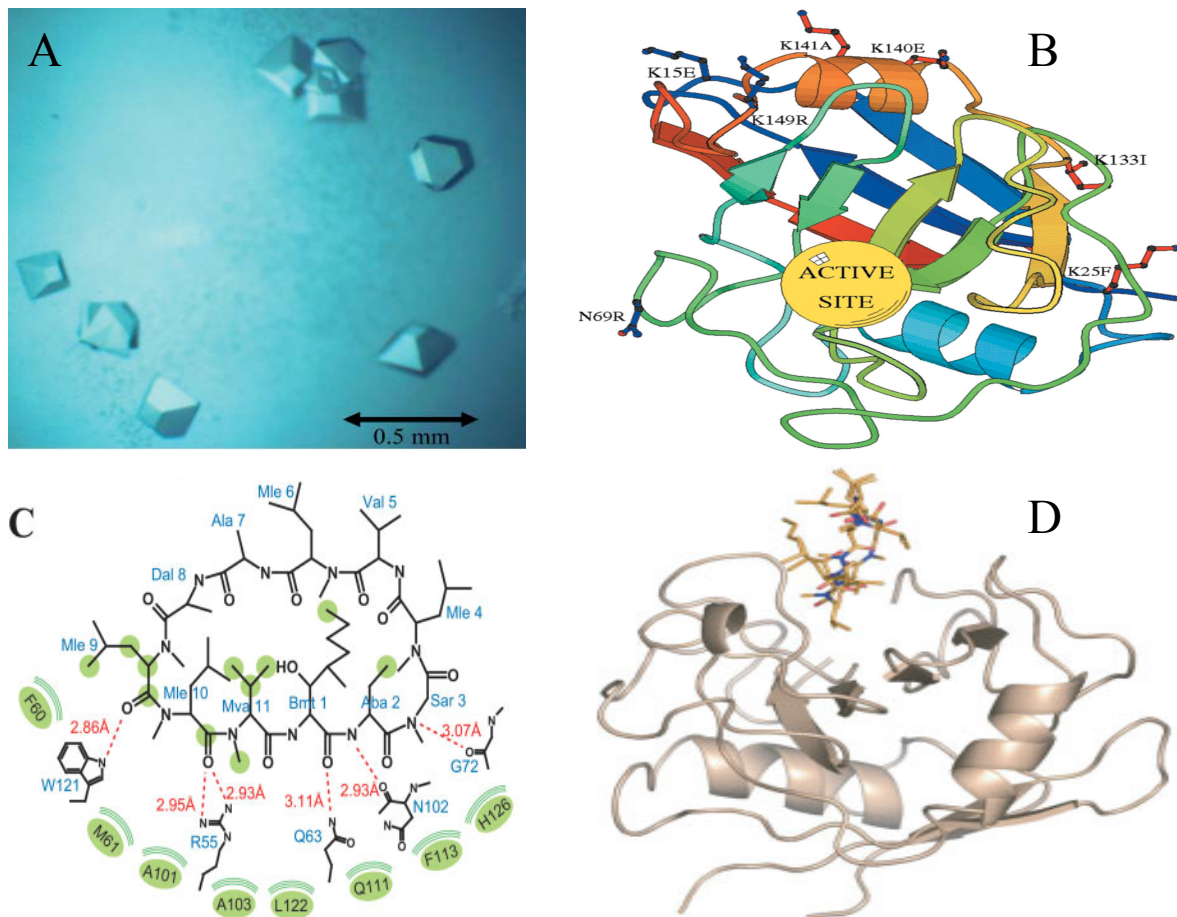
Figure 1.11: Crystal studies that have been carried out on CypD to date: A) ΔCypDK133I Crystals produced by Schlatter *et al*. **B)** A ribbon representation of the ΔCypDK133I mutagenic studies showing the active site region and the various mutations that were made to facilitate crystallisation. Only the K133I construct would facilitate crystallisation and was found to be important in maintaining crystal contacts. Kajitani *et al*. observed that their crystals were composed of two CypD-CsA complexes in an asymmetric unit, one of the two CypD complexes makes no contact with the other complex via Ile133, but Ile133 on the other CypD molecule is directly involved in the intercomplex interaction (Kajitani *et al*. 2008). (A and B taken from Schlatter *et al*. 2005) **C)** Binding geometry of CsA on CypD. Green circles mark the CsA atoms involved in the hydrophobic contact with CypD. The CypD residues in green ellipsoids are involved in the hydrophobic interactions with CsA. The red dotted lines represent hydrogen bonding. This panel was prepared based on a scheme drawn with LIGPLOT.21 Abbreviations of CsA residues: Bmt, (4R)-4[[E)-2-butenyl]-4,N-dimethyl-L-threonine; Aba: L-a-aminobutyric acid, Sar: sarcosine, Mle, N-methyl leucine; Dal, D-alanine; Mva, N-methyl valine. **D)** The structure of CypD (ribbon model) bound with CsA (stick model). (C and D taken from Kajitani *et al*. 2008)

CypD levels of expression are elevated in the aging human brain and in an Aβ-rich environment (Du *et al*. 2008). The reported consequence of the binding of CypD and

Aβ is elevated levels of ROS, which in turn induces mPTP opening and cell death (Du *et al*. 2008; Singh *et al*. 2009). Also, it is believed that this interaction enhances the translocation of CypD from the matrix to the inner mitochondrial membrane where CypD will interact with the mPTP, resulting in its opening (Du *et al*. 2008). This interaction would lead to a build-up of Aβ in the inner mitochondrial membrane, which in itself would cause changes to the mitochondrial membrane potential, leading to cell death (Singh *et al*. 2009). Most of these potential consequences have been determined in studies of CypD-deficient animals (Ppif$^{-/-}$), whereby, the cortical mitochondria, isolated from the AD mouse model lacking CypD, are resistant to both Aβ and Ca^{2+}-induced mitochondrial swelling and opening of the mPTP (Du *et al*. 2008; Du *et al*. 2011). They also display increased calcium buffering capacity and an attenuation of the generation of mitochondrial ROS. Furthermore, CypD-deficient neurons are protected against Aβ and oxidative stress-induced cell death. Importantly, deficiency of CypD greatly improved the learning and memory of a transgenic mAPP expressing AD mouse model (Du *et al*. 2008; Du *et al*. 2011). These animals exhibited increased spatial and memory learning and alleviated Aβ-mediated reduction of long-term potentiation at 12 and 24 months, by which age the mAPP expressing mice are known to display AD like symptoms and synaptic dysfunction (Du *et al*. 2011). Thus the CypD- Aβ dependent activation of the mPTP directly links to the cellular and synaptic perturbation relevant to the pathogenesis of AD (Du *et al*. 2008).

1.5.2 <u>CypD as a potential therapeutic target</u>

The results showing that CypD deficiency is able to ameliorate Aβ toxicity in transgenic animals means that CypD can also be considered as a potential drug target for AD, as it

has for other neurodegenerative disorders (Schinzel *et al*. 2005; Du *et al*. 2008). Indeed, it has been reported that in the presence of CsA, a known immunosuppressant and inhibitor of CypD (Matsuda & Koyasu 2000), there is a decrease in mPTP formation and that a CsA– CypD complex is formed in mitochondria (Nicolli *et al*. 1996). Importantly it was also shown that CsA can inhibit some of the Aβ-induced toxicity (Du *et al*. 2008). Another recent study also indicates that the inhibition of CypD is the basis for its neuroprotective properties in, for example, ischaemia/ reperfusion injury (Mbye *et al*. 2009). However, it has been shown previously that CsA is a highly unspecific, large, bulky compound with poor solubility in water and relatively poor bioavailability (Nicolli *et al*. 1996) limiting the use of CsA as a drug molecule for neurodegenerative disorders.

A recent study produced a new mPTP inhibitor called antamanide, which has been shown to inhibit the mPTP by targeting CypD (Azzolin *et al*. 2011). This new inhibitor is highly selective and completely eliminates all aspects of CypD function, and is also shown to be completely inactive in CypD null mice. The antamanide inhibitor works in a similar fashion to the CsA interaction with CypD, whereby antaminide targets CypD leading to mPTP inhibition and cell protection from other factors causing mPTP opening. Although in its early stages of research these findings have great implications for the comprehension of CypD activity on the permeability transition pore and for the development of novel pore-targeting drugs exploitable as cell death inhibitors, such as in AD. Antamanide is a cyclic peptide produced from the fungus *amanita phalloides*, which again in a similar manner to CsA requires phosphate in order to obtain inhibition (Azzolin *et al*. 2011). The key residues for inhibition are residues 6 and 9 both phenylalanine residues which must be present for inhibition (Azzolin *et al*. 2011). This is represented in Figure 1.12.

A Antamanide (AA)

c(Val-Pro-Pro-Ala-Phe-Phe-Pro-Pro-Phe-Phe)

B

Molecule		1	2	3	4	5	6	7	8	9	10	
AA	c(	Val	Pro	Pro	Ala	Phe	Phe	Pro	Pro	Phe	Phe	)
Tyr⁹-AA	c(	Val	Pro	Pro	Ala	Phe	Phe	Pro	Pro	Tyr	Phe	)
Gly⁹-AA	c(	Val	Pro	Pro	Ala	Phe	Phe	Pro	Pro	Gly	Phe	)
Gly⁶-AA	c(	Val	Pro	Pro	Ala	Phe	Gly	Pro	Pro	Phe	Phe	)
octa-Gly⁹-AA	c(	Val	Pro	Pro	Ala	des	des	Pro	Pro	Gly	Phe	)
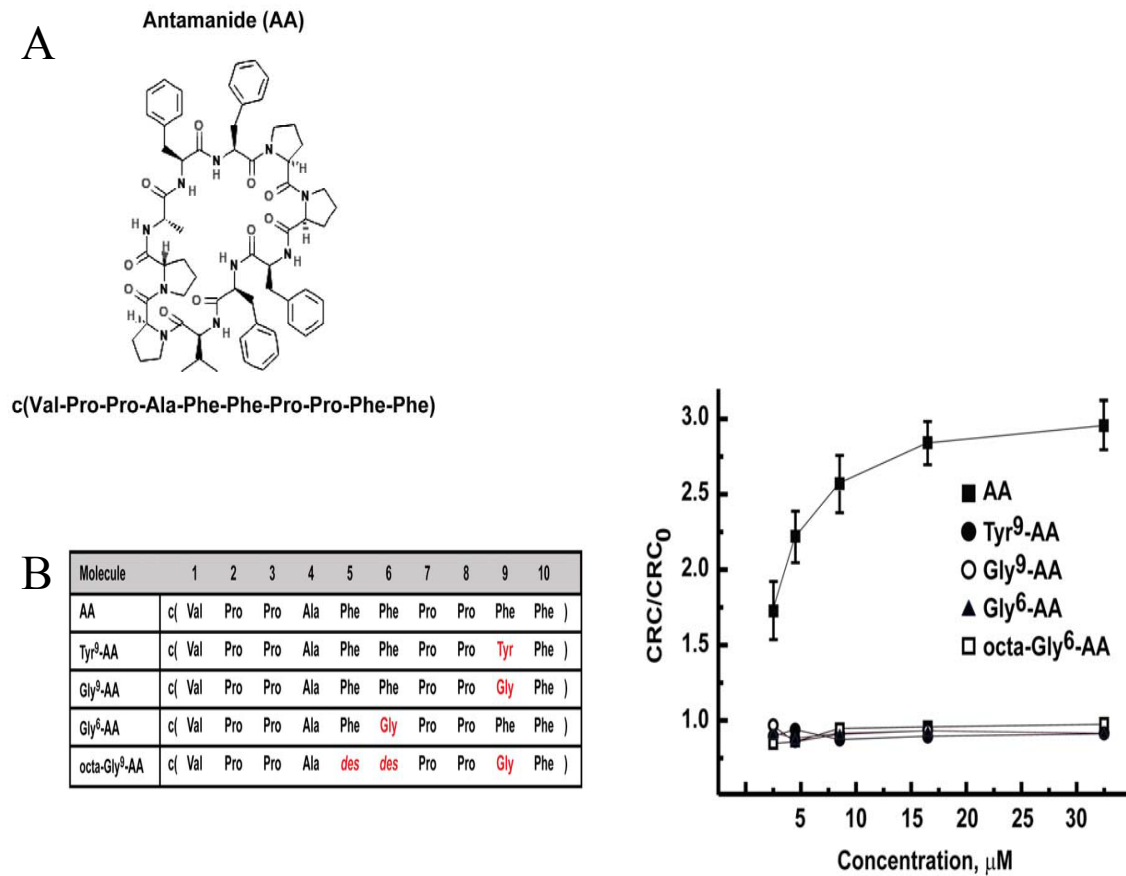
Figure 1.12: Antamanide structure and key residue study: A) The structure of the cyclic peptide Antamanide and the amino acid residue sequence. **B)** The key residues of Antamanide, residue changes are in red. And the effects of these changes are shown in a Ca^{2+} retention capacity test (CRC) whereby the ratio of CRC detected in the presence (CRC) and absence (CRCo) is shown with increasing concentrations of antamanide (Azzolin *et al*. 2011).

Further proof that antamanide exhibits mPTP inhibition has been shown in mouse models by comparing changes in wild type and CypD knock out mice fibroblasts (Azzolin *et al*. 2011). Analysis of fibroblast mitochondria (shown in Figure 1.13) found that under increasing concentrations of antamanide the calcium retention capacity (CRC) ratio was significantly increased when comparing that to a control. However the increase was not as significant as CsA compared with control animals, but these

experiments show that both antamanide and CsA inhibit the mPTP (Azzolin *et al.* 2011).
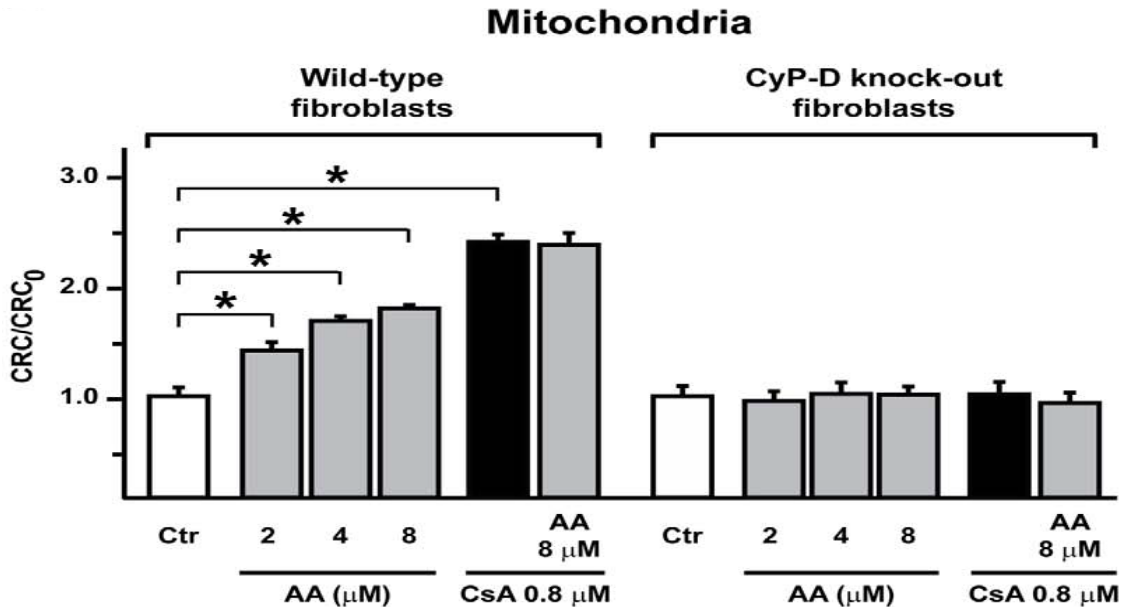
Figure 1.13: The ratio of CRC detected in the presence (CRC) and absence (CRCo) with increasing concentrations of Antamanide (AA) and CsA, in mitochondria from wild type fibroblasts (left) or CypD knock-out fibroblasts (right). Results show a significant (students t-test analysis *: $p<0.01$) increase in the mitochondrial Ca^{2+} uptake when in the presence of either antamanide or CsA when compared to that of the controls. And there is no change in the CypD knock out fibroblasts in the presence of antamanide or CsA compared to untreated mitochondria. These results indicate that both antamanide and CsA inhibit the mPTP (Azzolin *et al.* 2011).

As antamanide works in a similar manner to CsA it is possible to presume the interaction sites may be similar. In the CypD- CsA interaction the binding pocket is formed by a groove where the peptidylprolyl isomerase (PPIase) activity site is located (Kajitani *et al.* 2008). As discussed in section 1.5.2 the CsA is inserted half into the binding cavity by establishing hydrogen and hydrophobic bonds with the CypD amino acids, leaving the exposed residues on the outside of the CypD-CsA complex to be free to interact with other molecules, in particular residues 3-7 on CsA (Waldmeier *et al.*

2003). Antamanide has two residues Phe6 and Phe9 which are vital for inhibition (see Figure 1.14) and it has been suggested that these regions are located inside the binding pocket (Azzolin *et al*. 2011). Crystallography studies of the antamanide and CypD complex would be useful in order to maintain a greater understanding of the other inhibitory affects that antamanide may have. As antamanide is similar in action to CsA it is suggested that other functions could include gene transcription and proliferation, as well as chemotaxis and motility (Azzolin *et al*. 2011). These studies would also allow the development of a more efficacious inhibitor as the small cyclic peptide may provide the basis for a new larger inhibitor (drug like molecule) that may incorporate the CypD binding site more effectively.

Other potential CypD inhibitors that may be used in the treatment of Alzheimer's disease have been developed from quinoxaline in the hope of developing lead molecules to inhibit the mPTP (Guo *et al*. 2005). These studies found four molecules GW2, 5, 6 and 7, that exhibited high inhibitory activity against rat mitochondrial swelling and Ca^{2+} uptake. The studies paid particular focus to GW5 (2,3- (difuran-2-yl)-6-(pyrrolidin-1-yl) carbonylamino quinoxaline) which was the most potent and selective of all the compounds and this indicates that it may be a potential lead like molecule in future drug development (Guo *et al*. 2005). The kinetics of these molecules were investigated using SPR and fluorescent titration techniques, and the inhibitory affects were measured against rat liver Ca^{2+} dependent mitochondria swelling and Ca^{2+} uptake/release. Molecular docking analysis was used to try and identify the interaction at atomic level. Using rat crystal data from the PDB they identified that the GW1-7 compounds are in fact binding in the same pocket as CsA, but due to there smaller size they only occupy a small part of the site (Guo *et al*. 2005). The rat model is highly comparable with the

human CypD model, with a weighted root mean squared distance of 0.6040 and an identity score of 95.7% (Guo *et al*. 2005).
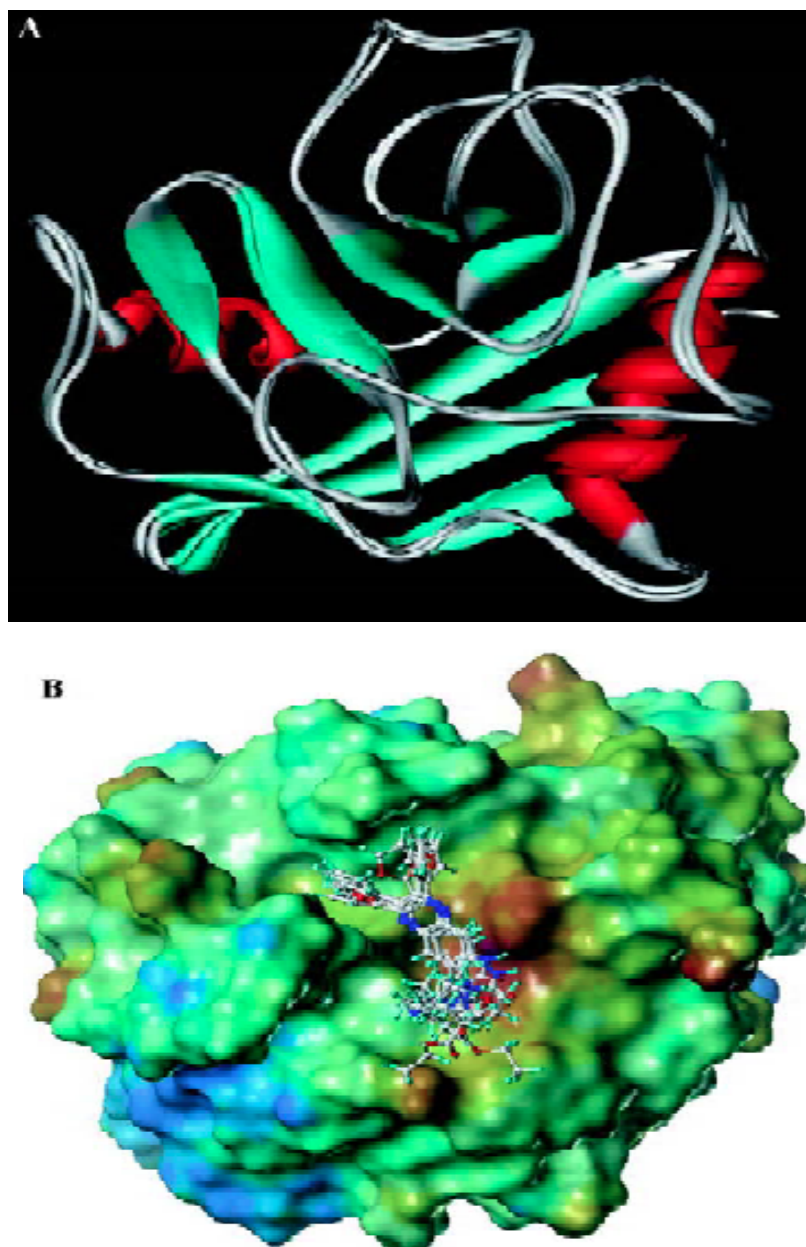
Figure 1.14: Rat and human CypD protein crystal structures: A) The overlapping rat and human CypD models. **B)** GW1-7 in the CypD binding pocket (Guo *et al*. 2005).

1.6   **Project Aims**

The aim of the research described in this thesis was to investigate protein- protein interactions as therapeutic targets in the treatment of AD.

More specifically I investigated; ABAD- Aβ interaction, CypD- Aβ interaction and the potential interaction between CypD- ABAD using various biophysical techniques. These techniques included; principally x-ray crystallography, nuclear magnetic resonance (NMR), thermal shift analysis and isothermal titration calorimetry (ITC). By undertaking the research in this thesis it is hoped that we will gain a better understanding of the thermodynamic properties of each reaction, and establish where the molecules bind and if there are any significant residues or areas of the active site that may be used in future drug design experiments.

Chapter 2: Materials and Methods

2.1 <u>Molecular biology techniques</u>

2.1.1 <u>Culture media</u>

LB Agar (Sigma): 1% (w/v) tryptone, 0.5% (w/v) yeast extract, 0.5% (w/v) NaCl, 1.5% (w/v) agar.

Luria broth (LB; Sigma): 1% (w/v) tryptone, 0.5% (w/v) yeast extract, 0.5% (w/v) NaCl.

Terrific broth (TB; Sigma): 1.2% (w/v) tryptone, 24.5% (w/v) yeast extract, 0.94% (w/v) K_2HPO_4, 0.22% (w/v) KH_2PO_4

Auto-induction media (Invitrogen): An entire Magic Media SoluPouch A placed in 950 mL milliQ water, autoclaved for 20 minutes on the liquid cycle, allowed to cool to 37 °C before selected antibiotic addition and the addition of Magic Media component B. Store at 4°C for up to 1 month.

2.1.2 <u>Polymerase chain reaction</u>

Polymerase chain reaction (PCR) was carried out using a Biometra TPersonal thermocycler (Biometra) in a 50 μL reaction volume containing 50 ng template DNA, 0.2 μM forward and reverse primers (Invitrogen), 20 μM dNTPs (Promega), 2.5 U *Pfu Turbo* DNA polymerase (Agilent technologies) and 10 x cloned *Pfu* DNA polymerase reaction buffer (supplied with the polymerase, Agilent technologies). The thermal cycle profile for the PCR is detailed as in Table 2.1 where annealing temperatures (AT) were determined based on the primers used.

Table 2.1: A thermal cycle profile used during a standard PCR reaction (30 cycles per reaction).

Step	Temperature (°C)	Duration (s)
1	94	180
2	94	30
3	AT	40
4	72	60
5	72	600
6	4	∞

2.1.3 Restriction digests

Restriction digests were performed using restriction enzymes and their appropriate buffers (Promega) on 3–5 μg DNA in a total volume of 50 μL for 4–16 hours. The restriction digest was heat inactivated at 68 °C for 20 min. DNA clean-up was achieved using Wizard PCR and Gel cleanup kit (Promega).

2.1.4 Agarose gels

A 1% (w/v) agarose gel was used to separate DNA fragments larger than 1kb and 2% (w/v) agarose gels were used for DNA fragments smaller than 1kb. 1% (w/v) or 2% (w/v) agarose was melted in TBE buffer (0.45M Tris-borate, 10mM EDTA, pH 8.3; Sigma). Once cooled, a final concentration of 0.5 μg/mL ethidium bromide (Sigma) was added. The gel was left to set for 20 minutes at room temperature in a DNA gel rig (VWR). 6 x agarose gel buffer (50% glycerol, 49.75% TBE, 0.25% bromophenol blue) was added to the samples before DNA was loaded into the wells. Hyperladder I

(Bioline) was run simultaneously to analyse DNA band size. DNA gels were run at 60 V for 1 hour or 72 V for 45 min and bands were visualised under UV light using GeneSnap software (Syngene).

2.1.5 DNA purification by gel electrophoresis

PCR products, DNA fragments and plasmids were separated by their molecular weight using agarose gel electrophoresis (see section 2.1.4). Analytical gels were visualised with a BioRad ChemiDoc XRS+ imager. For preparative gels to isolate DNA fragments generated by PCR or restriction digest, DNA was visualized by a low intensity UV lamp and the appropriate bands excised from the gel using a sterile scalpel. DNA was isolated from the gel band using Wizard PCR and Gel cleanup kit (Promega) according to the manufacturer's instructions.

2.1.6 DNA ligation

Ligations were carried out using 0.5 μL T4 turbo DNA ligase (Promega), 10 x reaction buffer (Promega) according to the manufacturers protocol. 1 μL vector DNA and either 3, 6, 10 μL insert DNA in a total volume of 20 μL were incubated at either 4 °C overnight or at room temperature for 1 h. A control reaction of 1 μL of vector in the absence of DNA insert was also set up.

2.1.7 Making competent cells

E. coli DH5α or BL21 CodonPlus glycerol stocks were used to inoculate a culture whereby a scrape of the glycerol stock was added to 5ml LB medium. *E. coli* bacterial

cells were grown in an orbital incubator at 37 °C, with shaking at 210 rpm for 16 hours. In BL21 innoculations chloramphenicol (35 µg/mL) was added before incubation. After incubation, 0.5ml of overnight cell mixture was placed in fresh 50ml LB medium, and further incubated at 37 °C with shaking at 210 rpm, until the absorbance reading was approximately 0.4, as measured at 600nm (UV1601 Shimadzu Corporation). Cells were harvested by centrifugation (Beckman; J6-MC, rotor 4.2, 3500 rpm, 10 min, 4 °C). The supernatant was removed and the pellet was re- suspended in ice-cold $CaCl_2$ (20 mL, 100 mM), by vortexing. After incubating on ice for 30 min, the cells were centrifuged (J6-MC, rotor 4.2, 1500 rpm, 5 min, 4 °C), the supernatant removed and the pellet re-suspended in ice cold $CaCl_2$ (1 mL, 100 mM). A further incubation on ice for 30 min gave a suspension of competent cells for immediate use or cryogenic storage. For cryogenic storage, competent cells were stored after addition of glycerol (50%, 25 µL) to 100 µL cells. Aliquots were flash-frozen and stored at -80 °C.

2.1.8 Transformation

Ligation mixture (10 µL) or plasmid DNA (1- 5 µL) was added to competent *E. coli* DH5α or BL21 CodonPlus cells and the mixture was incubated on ice for 30 min, before heat-shocking at 42 °C (2 min) and returning to ice (5 min). LB broth (0.5 mL) was added and the culture incubated at 37 °C with shaking at 210 rpm for 1 h. Transformed cells were grown by spreading on LB-agar plates containing the relevant antibiotic (100 µg/mL ampicillin or 50 µg/mL kanamycin) and incubating at 37 °C (16 h). Cultures were grown at two concentrations: 100 µL of transformation culture (low concentration) or 400 µL of transformation culture pelleted by centrifugation for 1 min and resuspended in a small volume (100 µL) of culture medium (high concentration).

2.1.9 <u>Isolation of plasmid DNA from transformed DH5α cells</u>

A single colony from an agar plate (Section 2.1.8) or a glycerol stock scrape was added to 5 mL LB medium, containing the appropriate antibiotic (100 μg/mL ampicillin or 50 μg/mL kanamycin). Transformed *E. coli* DH5α cells were grown 37 °C, with shaking at 210rpm for 16 hours. DNA was purified using a Qiagen Spin Miniprep Kit (Qiagen), according to the manufacturer's instructions. The DNA concentration of purified plasmid was measured at 260nm (Nanodrop Spectrophotometer, Thermo Scientific) and stored at -20 °C. DNA sequencing was performed by DNA Sequencing & Services (MRCPPU, College of Life Sciences, University of Dundee, Scotland, www.dnaseq.co.uk) using Applied Biosystems Big-Dye Ver 3.1 chemistry on an Applied Biosystems model 3730 automated capillary DNA sequencer.

2.1.10 <u>Glycerol stocks</u>

600 μL LB overnight medium containing transformed DH5α cells and 400 μL sterile 50% glycerol were mixed and stored at -80 °C.

2.2   Protein expression and purification

2.2.1 SDS- page gel electrophoresis

SDS- polyacrylamide gel electrophoresis (SDS- PAGE) was carried out using 10, 12, 15, 17 welled NuPAGE Novex, 1 mm, 4–12% Bis-Tris gels (Invitrogen) in 2-(0-morpholino) ethane sulfonic acid (MES) buffer run at a constant voltage (200 V, 120 A, 35 min). Mark12 pre-stained standard (Invitrogen) was used as a molecular weight marker. Gels were then stained with coomassie blue stain (10% acetic acid, 50% methanol, 0.25% W/V coomassie brilliant blue R-250) for 10 min and de-stained in the microwave for 10 min. Gels were imaged on a UVP Gel Doc imager (UVP).

2.2.2 Small scale expression and induction

Plasmid DNA was transformed into *E. coli* BL21 CodonPlus cells as described in section 2.1.8. Overnight cultures comprising the transformed DNA in 5 mL LB broth containing the appropriate antibiotic (100 μg/mL ampicillin or 50 μg/mL kanamycin) were incubated at 37 °C, 210 rpm for 16 h. Overnight cultures (100 μL) were used to inoculate 10 mL fresh LB containing the appropriate antibiotic and were incubated at 37 °C, 210 rpm until an absorbance at 600 nm of ~0.6 was obtained. Protein expression was induced by addition of isopropyl β-D-1-thiogalactopyranoside (IPTG; 1 mM), followed by incubation at 25 °C, 180 rpm for 16 h. Cells were harvested by centrifugation (6000 rpm, 4 °C, 15 min) and the cell pellet stored at -80 °C.

To test for effective induction, 1 mL samples were taken pre- induction and 1, 2, 4 and 16 h post induction. These samples were boiled in equal volumes of protein sample buffer (PSB; 2% (w/v) sodium dodecyl sulfate (SDS), 20% (v/v) glycerol, 20 mM Tris-

HCl, 20 mM ethylenediaminetetraacetic acid (EDTA), 0.24 M β-mercaptoethanol, 1 μg/mL bromophenol blue) for 10 min, and are analysed via SDS- PAGE (section 2.2.1).

2.2.3 Large scale expression

Plasmid DNA was transformed into *E. coli* BL21 CodonPlus cells as described in section 2.1.8. Overnight cultures comprising the transformed DNA in 200 mL LB broth containing the appropriate antibiotic (100 μg/mL ampicillin or 50 μg/mL kanamycin) were incubated at 37 °C, 210 rpm for 16 h. Overnight cultures (10 mL) were used to inoculate 12 x 1 L fresh LB containing the appropriate antibiotic and were incubated at 37 °C, 210rpm until an absorbance at 600 nm of ~0.6 was obtained. Protein expression was induced by addition of IPTG (1 mM), followed by incubation at 25 °C, 180 rpm (16 h). Cells were harvested at 6000 rpm, 4 °C for 15 min (Beckman Avanti J-20XP; JLA 8.1000 rotor), the supernatant was removed and the pellets were stored in 3 L aliquots at -80 °C.

2.2.4 His-TEV ABAD or His-TEV CypD small scale purification

The cell pellets of *E. coli* BL21 containing expressed His-TEV ABAD/ His-TEV CypD protein (see section 2.2.2) were re- suspended for 30 min, 4 °C, in lysis buffer (20 mM NaH$_2$PO$_4$, 30 mM imidazole, 500 mM NaCl, 10% (v/v) glycerol, pH 7.4) with the addition of complete EDTA-free protease inhibitor tablets (Roche), lysozyme (1 mg/mL), DNase (20 μg/mL) and Triton X-100 (0.1% (v/v)). Cells were lysed by sonication (10 s sonication then ice for 1 min, repeated three times) and the lysate was cleared by centrifugation (Sorvall Evolution RC, rotor S5-34 55-34 angle, 20500 rpm, 30 min, 4 °C). Cleared lysate was filtered (0.44 μm membrane; Whatman) then Ni-NTA

His-bind beads (Qiagen; 1 mL) were added to the lysate and were mixed at 4 °C, 1 h. This mixture was then applied to an empty gravity column (GE Healthcare) and the lysate was allowed to drip through. 50 mL of lysis buffer was applied to the column and fractions were collected at 10 mL intervals. 50 mL of elution buffer (20 mM NaH$_2$PO$_4$, 300 mM imidazole, 500 mM NaCl, 10% (v/v) glycerol, pH 7.4) was applied to the column and fractions were collected at 5 mL intervals. SDS- PAGE was used to confirm in which fractions the His-TEV protein was found and these fractions were subsequently pooled. This small scale method was used as an indication of the His-TEV protein solubility, therefore the method did not proceed onto tag cleavage (see section 2.2.5)

2.2.5 His-TEV ABAD large scale purification

Cell pellets *E. coli* BL21 containing His-TEV-ABAD protein (see section 2.2.3) were re-suspended for 30 min, 4 °C, in lysis buffer (20 mM NaH$_2$PO$_4$, 30 mM imidazole, 500 mM NaCl, 10% (v/v) glycerol, pH 7.4) with the addition of complete EDTA-free protease inhibitor tablets (Roche), lysozyme (1 mg/mL), DNase (20 µg/mL) and Triton X-100 (0.1% (v/v)). Cells were lysed by passage through a cell disruptor at 30 kPSI (Constant Systems Ltd) and the lysate was cleared by centrifugation (Sorvall Evolution RC, rotor S5-34 55-34 angle, 20500 rpm, 30 min, 4 °C). Cleared lysate was filtered (0.44 µm membrane; Whatman) then applied to a Ni-NTA (GE Healthcare) column pre-washed with lysis buffer and protein eluted with 300 mM imidazole buffer (20 mM NaH$_2$PO$_4$, 300 mM imidazole, 500 mM NaCl, 10% (v/v) glycerol, pH 7.4). Tobacco etch virus (TEV) protease was added to the protein at a mass-to-mass ratio of 1:10, to cleave the histidine tag and the protein was then dialysed into 20 mM Tris-HCl, 30 mM

imidazole, 500 mM NaCl, 10% (v/v) glycerol, pH 7.4 containing EDTA (1 mM) and DTT (1 mM) to aid solubility. Protein digestion and dialysis was carried out at 4 °C for 16 h. Complete digestion was firstly checked by SDS- PAGE (see section 2.2.1), then fully digested protein was passed over a second Ni-column and the flow-through, containing ABAD, was concentrated using a Vivaspin column (10 kDa MWCO, GE Healthcare) to ~7 mL before final purification using gel filtration to remove the imidazole (Hi-Load 16/60 Superdex 75 prep grade column, GE Healthcare, flow rate 1.5 mL/min). Protein was eluted in gel filtration buffer (10 mM Tris-HCl, 150 mM NaCl, 10% glycerol, pH 7.5) and concentrated (Vivaspin column (10 kDa MWCO, GE Healthcare)) to 10 mg/ml and then 20 mg/ ml. Aliquots (25 μL and 50 μL) were taken for both concentrations and flash frozen in liquid nitrogen before final storage at -80 °C.

2.2.6 ΔCypD^{K133I} purification

Plasmid ΔCypD^{K133I} DNA was transformed into *E. coli* BL21 CodonPlus cells as described in section 2.1.8. ΔCypD^{K133I} was expressed as in section 2.2.3. *E. coli* BL21 containing ΔCypD^{K133I} cell pellets were re-suspended for 30 min, 4 °C, in lysis buffer (100 mM Tris-HCl, 250 mM NaCl, 2 mM EDTA, 2 mM DTT, 10% (v/v) glycerol, pH 7.8) with the addition of complete EDTA-free protease inhibitor tablets (Roche), DNase (20 μg/mL) and Triton X-100 (0.1% (v/v)). Cells were lysed by passage through a cell disruptor at 30 kPSI (Constant Systems Ltd) and the lysate was cleared by centrifugation (Sorvall Evolution RC, rotor S5-34 55-34 angle, 20500 rpm, 30 min, 4 °C). Cleared lysate was filtered (0.44 μm membrane; Whatman) then applied to a Resource S cation exchange column (GE Healthcare), pre-washed with lysis buffer and protein eluted with a step wise gradient of high salt buffer buffer (100 mM Tris-HCl,

1M NaCl, 2 mM EDTA, 2mM DTT, 10% (v/v) glycerol, pH 7.8). The Resource S cation exchange column was washed with lysis buffer and the protein was then again passed through the column to remove further contaminants. The protein was then dialysed into 100 mM Tris-HCl, 250 mM NaCl, 2 mM EDTA, 10% (v/v) glycerol, pH 7.8, where dialysis was carried out at 4 °C for 16 h. The protein was concentrated using a Vivaspin column (3 kDa MWCO, GE Healthcare) to ~7 mL before final purification using gel filtration (Hi-Load 16/60 Superdex 75 prep grade column, GE Healthcare, flow rate 1.5 mL/min). Protein was eluted in gel filtration buffer (50 mM KH_2PO_4, 100 mM NaCl, 2 mM EDTA, 2 mM DTT, pH 7.3) and concentrated (Vivaspin column (10 kDa MWCO, GE Healthcare)) to 25 mg/ ml. Aliquots (25 µL) were taken and flash frozen in liquid nitrogen before final storage at -80 °C.

2.2.7 <u>GST CypD purification with Thrombin cleavage</u>

Plasmid GST CypD (pGEX-4T-1) DNA was transformed into *E. coli* BL21 CodonPlus cells as described in section 2.1.8. GST CypD was expressed as in section 2.2.3. *E. coli* BL21 containing GST CypD cell pellets were re-suspended for 30 min, 4 °C, in lysis buffer (1x PBS, 1 mM DTT, 10% (v/v) glycerol, pH 7.4) with the addition of complete EDTA-free protease inhibitor tablets (Roche), lysozyme (1 mg/mL), DNase (20 µg/mL) and Triton X-100 (0.1% (v/v)). Cells were lysed by passage through a cell disruptor at 30 kPSI (Constant Systems Ltd) and the lysate was cleared by centrifugation (Sorvall Evolution RC, rotor S5-34 55-34 angle, 20500 rpm, 30 min, 4 °C). Cleared lysate was filtered (0.44 µm membrane; Whatman) then applied to a GSTrap FF (GE Healthcare) column pre-washed with lysis buffer and protein eluted with (50 mM Tris-HCl, 10 mM reduced glutathione, 500 mM NaCl, 10% (v/v) glycerol, pH 8.0). Thrombin protease

was added to the protein at a mass-to-mass ratio of 1:10, to cleave the GST tag and the protein was then dialysed into 50 mM Tris-HCl, 150 mM NaCl, 10% (v/v) glycerol, pH 8.0, containing DTT (5 mM) to aid solubility. Protein digestion and dialysis was carried out at 4 °C for 16 h. Complete digestion was firstly checked by SDS- PAGE, this was never observed, therefore the mass: mass ratio of protein: Thrombin was increase to 1:5 and the protein was further dialysed for 6 h. To decrease precipitation the [DTT] was increased to 10 mM. Digestion was found to be incomplete therefore the purification did not proceed further.

2.2.8 PreScission protease purification

Plasmid PreScission protease DNA was transformed into *E. coli* BL21 CodonPlus cells as described in section 2.1.8. PreScission was expressed as in section 2.2.3. *E. coli* BL21 containing PreScission cell pellets were re-suspended for 30 min, 4 °C, in lysis buffer (1x PBS, 1 mM DTT, 10% (v/v) glycerol, pH 7.4). Cells were lysed by passage through a cell disruptor at 30 kPSI (Constant Systems Ltd) and this was repeated to ensure complete lysis. The lysate was cleared by centrifugation (Sorvall Evolution RC, rotor S5-34 55-34 angle, 20500 rpm, 30 min, 4 °C). Cleared lysate was filtered (0.44 μm membrane; Whatman) then applied to a GSTrap FF (GE Healthcare) column pre-washed with lysis buffer and protein eluted with (50 mM Tris-HCl, 10 mM reduced glutathione, 150 mM NaCl, 1 mM DTT, 10% (v/v) glycerol, pH 8.0). PreScission protease was then concentrated (Vivaspin column (10 kDa MWCO, GE Healthcare)) to 1 mg/ml and aliquots (1 mL) were taken, and flash frozen in liquid nitrogen before final storage at -80 °C.

2.2.9 <u>GST CypD purification</u>

Plasmid GST CypD (pGEX-6p-1) DNA was transformed into *E. coli* BL21 CodonPlus cells as described in section 2.1.8. GST CypD was expressed as in section 2.2.3. *E. coli* BL21 containing GST CypD cell pellets were re-suspended for 30 min, 4 °C, in lysis buffer (1x PBS, 1 mM DTT, 10% (v/v) glycerol, pH 7.4) with the addition of complete EDTA-free protease inhibitor tablets (Roche), lysozyme (1 mg/mL), DNase (20 µg/mL) and Triton X-100 (0.1% (v/v)). Cells were lysed by passage through a cell disruptor at 30 kPSI (Constant Systems Ltd) and the lysate was cleared by centrifugation (Sorvall Evolution RC, rotor S5-34 55-34 angle, 20500 rpm, 30 min, 4 °C). Cleared lysate was filtered (0.44 µm membrane; Whatman) then applied to a GSTrap FF (GE Healthcare) column pre-washed with lysis buffer and protein eluted with (50 mM Tris-HCl, 10 mM reduced glutathione, 500 mM NaCl, 10% (v/v) glycerol, pH 8.0). Precision protease was added to the protein at a mass-to-mass ratio of 1:10, to cleave the GST tag and the protein was then dialysed into 50 mM Tris-HCl, 150 mM NaCl, 10% (v/v) glycerol, pH 8.0, containing DTT (5 mM) to aid solubility. Protein digestion and dialysis was carried out at 4 °C for 16 h. Complete digestion was firstly checked by SDS- PAGE (see section 2.2.1), then fully digested protein was passed over a second GSTrap FF column and the flow-through, containing CypD, was concentrated using a Vivaspin column (3 kDa MWCO, GE Healthcare) to ~7 mL before final purification using gel filtration to remove the imidazole (Hi-Load 16/60 Superdex 75 prep grade column, GE Healthcare, flow rate 1.5 mL/min). Protein was eluted in gel filtration buffer (50 mM Tris-HCl, 150 mM NaCl, 5 mM DTT, 10% glycerol, pH 8.0) and concentrated (Vivaspin column (3 kDa MWCO, GE Healthcare)) to 10 mg/ml and then 20 mg/ ml. Aliquots (25 µL and 50 µL) were taken for both concentrations and flash frozen in liquid nitrogen before final storage at -80 °C.

2.2.10 <u>His-TEV CypD purification trials (96 well)</u>

Transformations of His-TEV CypD into 8 different cell lines was carried out as described in section 2.1.8. A 5 mL overnight culture of each cell line containing the His-TEV CypD was set up including ampicillin (100 mg/mL). Ampicillin (100 mg/mL) was added to three different medias (LB, TB and auto induction (AI) media) and a 96 well block (2 mL capacity) was set up as shown in Table 2.2. Each well contains 500 µL media+ ampicillian, and 15 µL of the corresponding overnight culture. The block was incubated at 37 °C, 900 rpm until $Abs_{600\,nm}$ ~0.6 was obtained. The LB and TB containing wells were then induced with 0.4 mg/mL IPTG and the block was incubated at 25 °C, 900 rpm overnight.

After incubation the block was centrifuged at 4600 xg for 40 min, the supernatant removed, and the pellets were lysed *via* two freeze thaw cycles. The pellets were resuspended in 400 µL 50 mM Tris-Hcl, 50 mM sucrose, 1 mM EDTA, pH 8.0 with the addition of 100 mg/mL lysozyme and 2 mg/mL DNase before use, then left at room temperature for 15 min, before adding 400 µL 10 mM Tris-Hcl, 50 mM NaCl, 1 mM EDTA, 10 mM $MgCl_2$, pH 8.0 with the addition of 2 mg/mL DNase before use, before the block was sealed, mixed by inversion and left for a further 15 min at room temperature. The block was centrifuged at 4600 xg for 1 h. In preparation for purification, 100 µL of 50% Ni-NTA beads (diluted with equilibration buffer: 50 mM Tris-HCl, 50 mM NaCl, 10 mM imidazole, pH 8.0; Qiagen) was added to a 96 well filter block. 700 µL equilibration buffer was then passed through the beads by centrifugation for 1 min at 900 xg; the flow through discarded.

Table 2.2: Protein expression set up in 96 well plates. Each row represents a different His-TEV CypD Cell line. Coloured wells represent different media types (yellow LB media; orange TB media; red AI media).

BL21 DE3	**A1**											**A12**
C43 (DE3)	**B1**											**B12**
Rosetta (DE3)	**C1**											**C12**
Origami (DE3)	**D1**											**D12**
Tuner (DE3)	**E1**											**E12**
BL21* (DE3)	**F1**											**F12**
HMS174 (DE3)	**G1**											**G12**
BLR (DE3)	**H1**											**H12**

Once the 1 h spin was complete the supernatant (~ 700 µL) was applied to the Ni- NTA beads and the filter block was centrifuged at 900 x g for 1 min, the flow through was discarded. 700 µL of wash buffer (50 mM Tris-HCl, 300 mM NaCl, 40 mM imidazole, 10% (v/v) glycerol, pH 8.0) was then applied to the beads and the filter block was centrifuged at 900 x g for 1 min, the flow through was discarded and the filter block was placed into a new collection block. 100 µL of elution buffer 20 mM Tris-HCl, 500

mM NaCl, 300 mM imidazole, 10% (v/v) glycerol, pH 8.0 was applied to the beads and the filter block was left to stand at room temperature for 5 min before centrifuging at 900 x g for 1 min.

To analyse for soluble protein fractions 37.5 μL from each well was added to 12.5 μL 4 x SDS free sample loading buffer, and the samples were denatured by boiling at 95 °C for 10 min. Samples were then run on a 96 well 6% E-PAGE gel (Invitrogen) according to manufacturers instructions. Standards and staining were the same as detailed in section 2.2.1.

2.3   *In vitro* assays

2.3.1 Preparation of amyloid β monomers

For the purpose of the work carried out in this thesis, only Aβ42 peptides were used.

Monomerised Aβ peptides were prepared from lyophilised Aβ purchased from Innovagen or GenicBio. 0.1 mg of lyophilised Aβ was dissolved in 1 mL ice- cold hexa-fluoro-isopropanol (HFIP) and left to dissolve for 1 h at room temperature. HFIP was then allowed to evaporate overnight in a fume hood. Samples were dried under a vacuum for 1 h and stored at -20 °C.

For *in vitro* assays, 0.1mg monomerised Aβ aliquots were dissolved in dimethylsulfoxide (DMSO) to a final concentration of 5 mM.

2.3.2 Enzyme activity assay

Assay buffer: 10 mM HEPES, 100 mM NaCl, pH 7.5 (as the buffer is warmed to 30 °C the pH was measured at 30 °C).

S-acetoacetyl-CoA substrate (AcAcCoA): prepared as 9.6 mM stock in assay buffer and stored at -20 °C in 100 μL aliquots. (Diluted to 4.8 mM before use in assay buffer).

Nicotinamide adenine dinucleotide (NAD^+): prepared as 10 mM stock in assay buffer and stored at -20 °C in 200 μL aliquots.

ABAD- Diluted from frozen stock (see section 2.2.5) to a 0.2 mg/mL stock in assay buffer. Due to aggregation and denaturation, this was made fresh; it is not possible to re-freeze this after use.

Frentizole compounds: 1 mg compound dissolved into a 10 mM stock solution with DMSO, then further diluted to a 1 mM working stock with propylene glycol. All dilutions for these compounds were carried out with propylene glycol.

Using a Nunc 96 well plate the enzyme activity assay was set up in the order given in accordance with Table 2.3, whereby after each addition the mixture is thoroughly mixed by pipetting ten times. In order to start the reaction ABAD is added and the initial rate is recorded over the first 30 s using the FLUOstar plate reader (BMG Labtech; parameters λ= 340 nM, T= 30 °C, 0.5 s measuring intervals). Enzyme activity is calculated using, ε= 6220 L/mol/cm for NADH, where the NADH rate of consumption = AcAcCoA rate of reduction. Assays were performed as n= 3, 6, 9 and the error was reported as ± SEM (standard error mean). Controls were set up with no ABAD to test for frentizole compound auto-fluorescence, and with propylene glycol and DMSO to test for assay interference.

Table 2.3: Enzyme activity assay set up:

Solution	Concentration	[Assay]	Volume (µL)
Buffer	-	-	144
AcAcCoA	4.8 mM	120 µM	4
NADH	10 mM	250 µM	4
Frentizole compound	1 mM	25 µM	4
ABAD	0.2 mg/mL	5 µg/mL	4
Total	-	-	160

2.3.3 <u>Isothermal titration calorimetry</u>

Frozen stock solution of ABAD (20 mg/mL; see section 2.2.5) in 10 mM Tris-HCl, 150 mM NaCl, 10% (v/v) glycerol, pH 7.5 (see section 2.2.5). Frozen stock solution of $\Delta CypD^{K133I}$ (25mg/ml) in 50 mM KH_2PO_4, 100 mM NaCl, 2 mM EDTA, 2 mM DTT, pH 7.3 (see section 2.2.6). Cell ($\Delta CypD^{K133I}$) and syringe (ABAD) solutions were prepared in phosphate buffer (10 mM sodium phosphate, pH 7.4), matching protein, ligand and buffer solutions with gel filtration buffer as appropriate. The pH of all solutions was adjusted to pH 7.40 ± 0.01. All solutions were degassed at 20 °C for 15 min before use. Calorimetric titrations were carried out at 25 °C using a VP-ITC instrument (Microcal LLC). The instrument was operated in high feedback mode, applying a reference power of 5 μcal/s and stirring the cell contents at 305 rpm. The cell volume was 1.4 mL and the injector volume was 290 μL. The cell solution contained ABAD (49.3 μM monomer concentration), while the syringe contained 15 mM $\Delta CypD^{K133I}$. The cell and syringe were first washed with buffer (5 times) and degassed buffer (1 times) before filling. The ligand solution was injected into the cell in a series of 20 injections (initial injection 3 μL, subsequent injections 7 μL, injection rate 0.5 μL s-1) every 360 s. In order to account for heat of dilution, the cell solution was then replaced with buffer and the ligand injection repeated. The heat of dilution was then subtracted from the main experiment. Raw data was processed using MicroCal Origin software. Baseline adjustment and integrations were carried out manually.

2.3.4 Thermal shift analysis

Solutions of Frentizole analogue series (10 mM compound stock in DMSO; diluted to 1 mM with propylene glycol) were diluted to 25 mM in propylene glycol. Protein master mix containing ABAD (20 mg/mL; see section 2.2.5) and SYPRO® Orange (1:500, Invitrogen) was prepared. Ninety-six well plates (Greiner) were then prepared by mixing 33.3 μL protein master mix with 10 μL frentizole analogue compound (total volume 100 μL; final [ABAD] 20 μM; [compound] 25 μM; [DMSO] 2.5 %; Assay buffer: 10 mM Tris-HCl, 150 mM NaCl, 10% (v/v) glycerol, pH 7.5). Assays were performed using a Stratagene Mx3005P qPCR machine (Sybr filter, ex. 492 nm, em. 516 nm). Initial temperature was set to 25 °C, increasing in increments of 1 °C every 60 s for 120 cycles (25–85 °C). Readings were taken in triplicate at each temperature point. The negative reciprocal was plotted and the protein unfolding temperature (T_m) taken as the lowest point of the curve obtained. The change in unfolding temperature (ΔT_m) was then calculated as the shift from the T_m when no compound was present. Controls with no compound, no SYPRO® Orange or no ABAD were also run. Monomerised Aβ (see section 2.3.1) was added to the assay at [Aβ final] 50 μM.

2.3.5 Nuclear magnetic resonance

Samples for NMR analysis to analyse ABAD binding partners with the Maybridge fragment library were produced as shown in Table 2.4. ABAD (20 mg/mL; section 2.2.5) was diluted to final assay concentration of 20 μM with assay buffer. 605 Maybridge fragments were divided into 55 fragment cocktails (in eppendorfs) and were kindly provided by Dr Stephen McMahon (University of St Andrews). Assay buffer used was 50 mM Sodium Phosphate (pH 7.5), 10% D_2O.

Table 2.4: NMR sample set up:

Solution	Volume (µL)
Buffer	726
Cocktail	6
ABAD	18
Total	**750**

Samples were loaded into NMR spin tubes and saturated transfer difference and WaterLOGSY experiments were carried out on the 600 MHz triple channel (HXY) wide-bore solid-state NMR spectrometer (with wide-bore magnet, equipped with five (1.3-, 2.5-, and 4-mm) MAS probeheads and one static probehead). Analysis was carried out using the AMIX profiler system where binding of fragments to ABAD was detected by comparing reference spectra for the cocktail eppendorfs with changes in the ABAD- cocktail spectra.

2.3.6 *ForteBio* Octet384 RED Assay

Assay solutions were prepared as follows:

ABAD protein (section 2.2.5) was diluted in assay buffer; 10 mM HEPES, 100 mM NaCl (pH 7.5), to produce a 0.5 mg/mL stock solution. Biotin (2 mg, Thermo Scientific) was reconstituted in water to create a 2 mM stock solution, and then added to ABAD protein in a 1:1 molar ratio. The sample was left to biotinylate at room temperature for 30 minutes. Excess biotin was removed using Zebra desalt spin columns (Thermo Scientific) following the manufacturers instructions.

As described previously in section 2.3.1, 0.1mg monomerised Aβ aliquots were dissolved in DMSO to a final concentration of 5 mM, before further dilution with assay buffer to create a 5 point, 5 fold Aβ gradient, ranging from 22 μM to 35.2 nM.

A stock solution of NADH (1 mM) was prepared using the assay buffer. This solution was then diluted further with assay buffer to create a 5 point, 5 fold Aβ gradient, ranging from 1 mM to 200 μM.

Biotinylated ABAD protein (b-ABAD, 50 mg/mL) was immobilized onto a Super Streptavidin (SSA) biosensor surface (Fortebio) over a period of 10 minutes. The biosensor surface was exposed to the Aβ solution (35.2 μM) for 100 seconds to measure the association of ABAD and Aβ. The sensor was then washed in assay buffer for 100 seconds to measure the dissociation of ABAD and Aβ. This association and dissociation process was repeated four times, with the concentration of Aβ increasing along the gradient each time. The same procedure was then repeated for NADH. Rate constants are then calculated from the binding data, including on-rate (k_a), off-rate (k_d), and equilibrium dissociation constant (K_D).

This procedure can be repeated to measure non specific binding, whereby, the SSA sensor, with ABAD bound, is replaced with an SSA sensor with no ABAD protein bound.

2.3.7 HiLyte Fluor 555 Aβ (Aβ$_{555}$) morphologically specific aggregation assay

Aβ labelled with HiLyte Fluor 555 (Aβ$_{555}$ or Cy3 labelled Aβ) was purchased from Anaspec and monomerised as described in section 2.3.1.

Again the amyloid used in this assay was the full length Aβ42

To obtain HFIP-induced aggregates, pre-treated Aβ$_{555}$ monomers were resuspended in DMSO to a final concentration of 2.5 mg/mL. Aβ peptides were subsequently diluted in Tris-HCl buffer solution (50 mM, pH 7.9) to the final desired concentration and ≤ 4 % HFIP was added to induce aggregation. All aqueous solutions were prepared with deionized water. Incubation of the peptides for 1 h at 4°C with vigorous agitation by continued vortexing results in the progressive formation of Aβ$_{555}$ globular intermediates.

For oligomeric and fibril-like aggregates formed at pH 7.9, HFIP-pre-treated Aβ$_{555}$ monomers were resuspended in DMSO to a final concentration of 2.5 mg/mL and subsequently diluted to 7 μM in 50 mM Tris-HCl buffer (pH 7.9) containing 150 mM NaCl and incubated at 37°C for 24 h as reported previously.

For plaque like structures, pH 6 induced aggregates were created by re-suspending HFIP-pre-treated Aβ$_{555}$ monomers in DMSO to a final concentration of 2.5 mg/mL and subsequently diluting to 7 μM in 50 mM 2-(N-morpholino)ethanesulfonic acid (MES) buffer at pH 6.0. Samples were incubated without agitation at 37°C for 5 hours.

Fluorescence emission spectra from N-terminally labelled Aβ42 aggregates were obtained using a peltier- Varian Eclipse fluorescence spectrophotometer. Cuvettes with a 1 cm path length were used and agitation was achieved with the insertion of magnetic stirring bars. Emission spectra were recorded using excitation wavelengths of 547 nm. Emission scans were taken every 5 minutes, where changes in intensity of the Cy3 dye were monitored. After 4 emission scans and immediately before the 5th scan (25 minutes), ABAD protein was injected into the samples on a 1:1, 1:2, and 1:100 ABAD protein to Aβ$_{555}$ basis. A control sample containing no ABAD protein was also run.

2.4   X-ray crystallography

2.4.1 General techniques

ABAD protein was produced as described in Section 2.2.5, with the His tag removed by TEV protease cleavage.

Commercially available crystallisation screens were used to screen initial conditions of crystallization, such as JCSG+, Classics, JMAC and PEGS (Sigma). A nano-drop crystallization robot Cartesian HoneyBee, Genomic Solutions), as part of the Hamilton-Thermo Rhombix system, was used for preparing 96 well plates. The Hamilton STARline robot was used to prepare optimization screens. All crystal screens used are detailed in Appendix C.

Using 30% (v/v) glycerol in the crystallization buffer, the crystals of target proteins were cryoprotected. A suitable protein crystal was picked out from the drops with a crystal loop and transferred to 5 μL cryoprotectant drop. Then the crystal was mounted onto the X-ray generator at 100K in-house using a Rigaku/MSC MicroMax-007HF rotating anode equipped with a Saturn 944+ CCD detector at wavelength 1.54 Å.

2.4.2 CypD and ABAD co-crystallisation

CypD was prepared as described in section 2.2.6 and section 2.2.9, ABAD was prepared as described as in section 2.2.5. Using various screens (section 2.4.1), 24 well plate crystal trials (hanging drop method) were set up as follows: drop size, 1 μL; 1:1, 1:2 or 2:1 ratio of protein solution: crystallisation buffer; reservoir volume, 400 μL. Plates were incubated at 20 °C.

2.4.2 ABAD and Maybridge fragment co-crystallisation

ABAD was prepared as described in section 2.2.5. Fragments were provided as 2 M stocks in DMSO. Protein solutions were prepared as shown in Table 2. 5. Crystal trials were set up in 96 well plates (sitting drop method) as follows: dropsize, 150 nL; 1:1 ratio of protein solution: crystallisation buffer; reservoir volume, 70 µL. Plates were incubated at 20 °C.

Table 2.5: Protein solutions for ABAD- Maybridge fragment co-crystallography:

	With NADH	**Without NADH**
ABAD	10 mg/mL	10 mg/mL
NADH	5 mM	-
DTT	1 mM	1 mM
Maybridge Fragment	10 mM	10 mM

2.4.3 ABAD crystallography (soaks method)

ABAD was prepared as described in section 2.2.5. Protein solutions were prepared as shown in Table 2. 5. DMSO. Crystal trials were set up (without Maybridge fragment addition) in 96 well plates (sitting drop method) as follows: dropsize, 150 nL; 1:1 ratio of protein solution: crystallisation buffer; reservoir volume, 70 µL. Plates were incubated at 20 °C. Once crystals had grown Maybridge fragments (20 mM, 1 µL) were pipetted onto crushed ABAD crystals and re-examined after 1 h to see if new crystals had formed.

2.4.3 Aβ and ABAD co-crystallisation

Aβ was prepared as described in section 2.3.1 and ABAD was prepared as described as in section 2.2.5. Solutions were prepared as shown in Table 2.5. Using various screens (section 2.4.1), 24 well plate crystal trials (hanging drop method) were set up as follows: drop size, 1 μL; 1:1, 1:2 or 2:1 ratio of protein solution: crystallisation buffer; reservoir volume, 400 μL. Plates were incubated at 20 °C.

Chapter 3: Elucidating and identifying potential small molecule inhibitors of the ABAD- Aβ interaction

3.1 <u>Introduction</u>

Amyloid binding alcohol dehydrogenase (ABAD) is a mitochondrial protein that is the best characterised intracellular Aβ binding protein (Yan *et al*. 1997; Yan *et al*. 1999; Lustbader *et al*. 2004). The features of this multifunctional enzyme include its presence in both the endoplasmic reticulum and the mitochondria, its capacity to bind Aβ and promote Aβ-induced cell stress, and its ability to act on a broad array of substrates. One function of this protein is catalysing the reversible reduction of aldehydes and ketones, and the oxidation of alcohols using its cofactor NAD(H). It is believed that the primary function of ABAD is energy production and metabolic homeostasis, in particular its involvement in the third step of the β-oxidation of fatty acids in times of a glucose deficiency, utilising its role as an L-3-hydroxyacyl-CoA dehydrogenase (Powell et al. 2000). When ABAD binds to Aβ (in the loop D region of ABAD) the overall effect is to inhibit the ABAD enzyme activity. However, the precise molecular mechanisms of how this occurs are yet to be elucidated.

The decrease in ABAD activity upon Aβ binding has been shown and the interaction of ABAD with Aβ has multiple effects at the molecular, cellular and whole animal level (detailed in 1.4.3). Therefore, this indicates that the ability to block this ABAD- Aβ interaction could produce a potentially novel therapeutic target for the treatment of AD.

There has also been the identification of potential inhibitors against this interaction (detailed in 1.4.3 and 1.4.4), this has further emphasised that the targeting of the ABAD- Aβ interaction could produce novel therapeutic target in AD (Kissinger *et al*. 2004; Xie *et al*. 2006). Furthermore, another strong reason for pursuing this approach to aid the treatment of AD is that, as yet, there is still a huge void in the drugs that are able to act on the underlying mechanisms of the disease.

A previous member of the Gunn-Moore Laboratory (Dr Kirsty Muirhead) identified potential small molecule inhibitors of this ABAD-Aβ interaction by carrying out thermal shift analysis (TSA or Thermofluor®), with ABAD protein and the Maybridge fragment library (Muirhead 2011). Potential inhibitor molecules were then classed as 'hit' compounds. Due to the variance observed between biophysical assays and 'hit' compounds obtained, for example, when an identical set of compounds is screened against the same biological target using three different assay formats, the concordance in the number of biologically active compounds or 'hits' obtained from each assay is just 35% (Lipinski & Hopkins 2004). Therefore, it was deemed necessary to re-test and evaluate these compounds using other assay formats. Therefore, in my work, the two main biophysical techniques employed to investigate the ABAD-Aβ interaction and to identify and characterise potential inhibitors of this interaction were x-ray crystallography (described in 4.1.1) and nuclear magnetic resonance (NMR).

3.1.1 The use of fragment screening in drug discovery

Lipinski's influential analysis of the Derwent World Drug Index introduced the concept of 'drug-likeness': whereby orally administered drugs are far more likely to reside in areas of chemical space defined by a limited range of molecular properties. These properties have been defined as Lipinski's 'rule of five' (Lipinski *et al*. 1997). This analysis shows that, historically, 90% of orally absorbed drugs have fewer than five hydrogen-bond donors, less than ten hydrogen-bond acceptors, molecular masses of less than 500 daltons, and cLog P values (a measure of lipophilicity) of less than five. Since this work, various definitions of, and methods to predict, drug-likeness have been proposed (Erlanson *et al*. 2000; Congreve *et al*. 2003; Lipinski 2004; Lundqvist 2005).

However, the consensus is that 'drug-likeness' is defined by a range of molecular properties and features that can differentiate between drugs and non-drugs for such characteristics as oral absorption, aqueous solubility and permeability (Lipinski & Hopkins 2004).

One such proposed method for predicting 'drug likeness' is that of the 'rule of three' (Congreve *et al*. 2003) or the use of a fragment based screening library to aid drug discovery. In these fragment-based approaches, low molecular weight chemical fragments (typically 150-300 daltons) are initially selected and screened on the basis of their ability to bind to the target of interest or to inhibit it in a functional assay (Carr *et al*. 2005). These fragments, which can be considered the building blocks of a more complex lead series, are then combined or optimized into larger compounds that meet or exceed the criteria typically applied to high throughput screen hits (Lipinski's 'rule of 5') (Carr *et al*. 2005). The shrewd rationale behind these fragment-based strategies is that, many drug targets contain distinct areas for binding ligands, substrates, and/or co-factors. A fragment based approach offers the possibility of identifying novel molecules with improved affinity, selectivity, and pharmaceutical properties that are able to sample the chemical space available most efficiently (Erlanson *et al*. 2004; Lipinski & Hopkins 2004). Furthermore, these smaller fragments are less likely to contain moieties that interfere with, or block, a ligand-protein interaction (Erlanson *et al*. 2004).

The Maybridge 'rule of three' fragment library is one of many libraries that can be used to identify potential 'hits' against an interaction. The principle of this library design is that the collection of chemical entries are pharmacophore rich, and all conform to the following criteria: a molecular weight less than 300 daltons, fewer than three hydrogen-bond donors, less than three hydrogen-bond acceptors, cLog P values of less than three, fewer than three rotatable bonds (flexibility index) and a polar surface area of less than

60 Å (Major & Smith 2011). In this chapter of work only 674 fragments, a very small portion of the total Maybridge library, were screened to identify and evaluate potential small molecule inhibitors of the ABAD- Aβ interaction.

3.1.2 <u>NMR screening and hit-validation in drug discovery</u>

One- dimensional nuclear magnetic resonance (NMR) has been developed as a important tool for the characterisation of interactions of small molecule ligands with their corresponding binding protein (Diercks *et al.* 2001; Pellecchia *et al.* 2002; Campos-Olivas 2011). In fact, a significant number of industrial and academic laboratories employ NMR for screening small molecule compound collections for binding to defined macromolecular targets, thus potentially providing initial, low affinity hits for a fragment-based approach in the drug discovery process (Campos-Olivas 2011).

Saturation transfer difference (STD) NMR is a method that allows the study of molecular interactions in solution, and has emerged as one of the most popular ligand-based NMR techniques for the study of protein−ligand interactions (Angulo *et al.* 2008; Xia *et al.* 2010; Viegas *et al.* 2011). The success of this technique is due to the fact that it is focused on the signals of the ligand, without any need of processing NMR information about the macromolecule and indeed only using small quantities of non-labelled macromolecule are required (Xia *et al.* 2010; Viegas *et al.* 2011). The STD-NMR experiment relies on the fact that, for a weak-binding ligand (dissociation constant, K_D, ranging from 10^{-8} mol L^{-1} to 10^{-3} mol L^{-1}), there is an exchange between the bound and the free ligand state (Viegas *et al.* 2011). An STD experiment (shown in Figure 3.1) involves subtracting a spectrum in which the protein was selectively

saturated (on-resonance spectrum) with signal intensities I_{SAT}, from one recorded without protein saturation (off-resonance spectrum), with signal intensities I_0. In the difference spectrum ($I_{STD} = I_0 − I_{SAT}$) only the signals of the ligand(s) that received saturation transfer from the protein, *via* spin diffusion, through the nuclear Overhauser effect will remain (Viegas *et al*. 2011). Other small molecules that may be present, but do not bind to the protein, will not receive any saturation transfer; their signals will be of equal intensity on the on-resonance and the off-resonance spectra and as a consequence, after subtraction no signals will appear in the difference spectrum from the nonbinding small molecule(s). The difference in intensity due to saturation transfer can be quantified ($I_{STD} = I_0 − I_{SAT}$) and constitutes an indication of binding (Viegas *et al*. 2011).
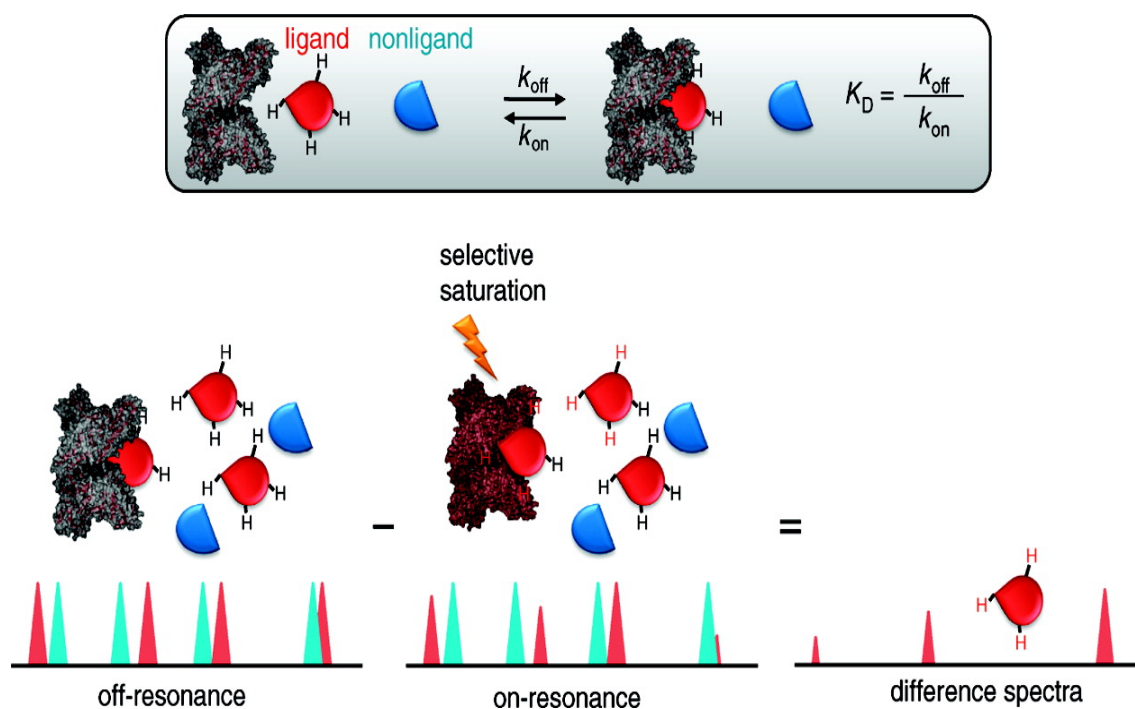
Figure 3.1: Schematic representation of a STD experiment. In a STD experiment, the difference between the signal intensities (I_{SAT}), from a spectrum recorded without protein saturation (off-resonance spectrum), with signal intensities I_0 and a spectrum in which the protein was selectively saturated (on-resonance spectrum) result in a difference spectrum ($I_{STD} = I_0 − I_{SAT}$), where only the signals of the ligand(s) that bind to the protein, and therefore receive saturation transfer from the protein, *via* spin diffusion through the nuclear Overhauser effect are shown (Taken from Viegas *et al.* 2011)**.**

Another type of NMR experiment, which is widely used in fragment based drug discovery, is WaterLOGSY (water- ligand observed *via* gradient spectroscopy). Whereby, this experiment utilizes the large bulk water magnetization to transfer magnetization *via* the protein- ligand complex to the free ligand in a selective manner (shown in Figure 3.2). Furthermore, the resonances of non-binding compounds appear with opposite sign and tend to be weaker than those of the interacting ligands (Dalvit *et al*. 2001; Stockman & Dalvit 2002).
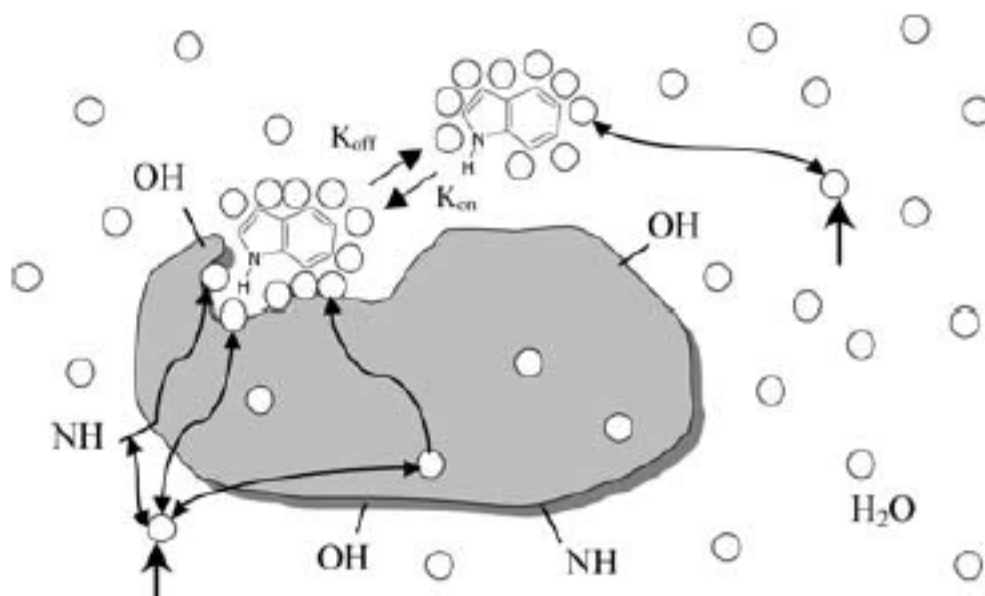
Figure 3.2: Schematic representation of the principle behind a WaterLOGSY NMR experiment. An example of a typical protein- ligand Waterlogsy NMR experiment, whereby, the protein is shown in grey with the buried cavities and the active binding site visible. The ligand is shown in the bound and free states. Excitation of bulk water (circles) is shown with a solid arrow and some of the different magnetization transfer pathways are also shown with double headed arrows (Taken from Dalvit *et al.* 2001).

3.1.3 <u>Thermal shift analysis</u>

Thermal shift analysis (TSA or Thermofluor®) is another biophysical technique used in fragment based drug discovery (Boettcher *et al.* 2010; Kranz & Schalk-Hihi 2011). The principle behind this technique is straightforward, whereby, the unfolding temperature (T_m) of a protein acts as an indicator of protein stability. When the protein is heated in a solution containing fluorescent dye (in this case SYPRO® orange), it becomes denatured and the protein's hydrophobic core structure is exposed. SYPRO® orange can then bind to the exposed hydrophobic region, producing a fluorescence emission. Under normal aqueous conditions the SYPRO® orange dye is quenched therefore, the fluorescence emission can be used to determine the T_m of the protein (shown in Figure 3.3). When a small molecule binding partner is present, the stability of the protein and its ability to unfold will alter as will the T_m. It is therefore possible that this technique can be used as a screening method for small molecule binding partners of proteins (Kranz & Schalk-Hihi 2011). This technique also allows the selectivity of small molecules depending on whether the small molecule stabilises (positive ΔT_m) or destabilises (negative ΔT_m) the protein (Kranz & Schalk-Hihi 2011). For the purpose of this application on the ABAD- Aβ interaction only small molecules with a stabilising effect were considered as 'hit' compound.
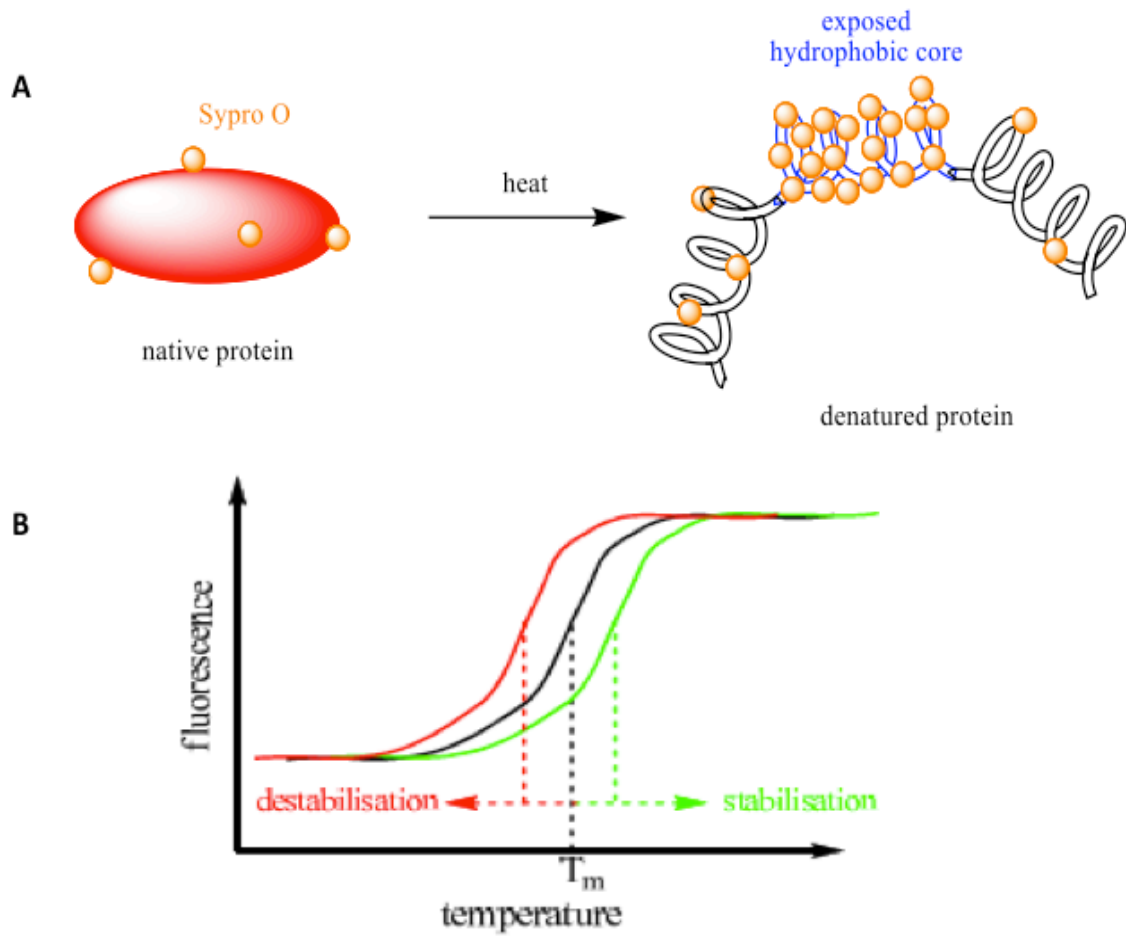
Figure 3.3: Schematic representation of the principle of thermal shift analysis as a measure of protein stability and a method for screening potential small molecule binding partners of proteins. A) Protein and SYPRO® orange dye are mixed in solution, upon heating the protein becomes denatured allowing the dye to bind to the protein's exposed hydrophobic core. This causes a fluorescence emission, from which the unfolding temperature (T_m) can be calculated. **B)** When a small molecule is bound to the protein, this results in a change in T_m, depending on whether the small molecule has a stabilising effect (resulting in a positive ΔT_m, shown in green) or a destabilising effect (resulting in a negative ΔTm, shown in red). Image taken from (Muirhead 2011).

3.2   Chapter aims

Using both x-ray crystallography and nuclear magnetic resonance the aims of this chapter were:

1. To use nuclear magnetic resonance spectroscopy to identify small molecules that are capable of binding to ABAD, and to validate potential 'hit' molecules that had been identified previously using thermal shift analysis, by Dr Kirsty Muirhead (formally FGM laboratory).

2. Subsequently to use x-ray crystallography to obtain a 3-D co-crystal structure of any small molecules bound to ABAD to give a greater understanding of where the key residues of interaction are on the protein, and the chemical space occupied by the molecule.

3. To use x-ray crystallography to gain a clearer crystal structure of the ABAD- Aβ interaction, in which the loop D active site region is no longer distorted.

It was hoped that this chapter of work would ultimately produce small molecules that prevent the ABAD-Aβ interaction. Using the crystallographic information obtained would facilitate future chemical modifications to the molecules, potentially altering them sufficiently to develop 'lead-like' molecules, and eventually transforming them into potential therapeutic agents against Alzheimer's disease.

3.3   ABAD protein production

3.3.1 The pEHis-TEV ABAD construct

To date, there are only three ABAD x-ray crystallography based, published journal articles (Powell *et al*. 2000; Kissinger *et al*. 2004; Lustbader *et al*. 2004). Powell *et al*. used a rat ABAD construct in their studies; however, Kissinger *et al*. and Lustbader *et al*. both used a human ABAD construct in their studies. The most relevant study to this chapter of my thesis was from Lustbader *et al*. who were the first group to crystallise a full length, non- mutated ABAD protein, bound to both Aβ and its co-factor NAD. Although this was a successful crystallisation the highly flexible loop D region (the believed site of the ABAD-Aβ interaction) was distorted and unable to be mapped fully (Lustbader *et al*. 2004). Therefore, it would also be advantageous to be able to produce an ABAD-Aβ co- crystal, where the loop D region is intact and stable allowing a complete interaction structure to be created.

The plasmid construct used in this chapter of work is the pEHis-TEV ABAD (*homo sapien*) plasmid. Figure 3.4 shows the plasmid construct that encodes the ABAD insert within the bacterial expression vector pEHis-TEV(b), the DNA sequence can be found in Appendix A. Of particular note is that this plasmid has a TEV (tobacco etch virus) protease cleavage sight for the removal of the histidine tag.

The ABAD protein sequence can be found in Appendix A.
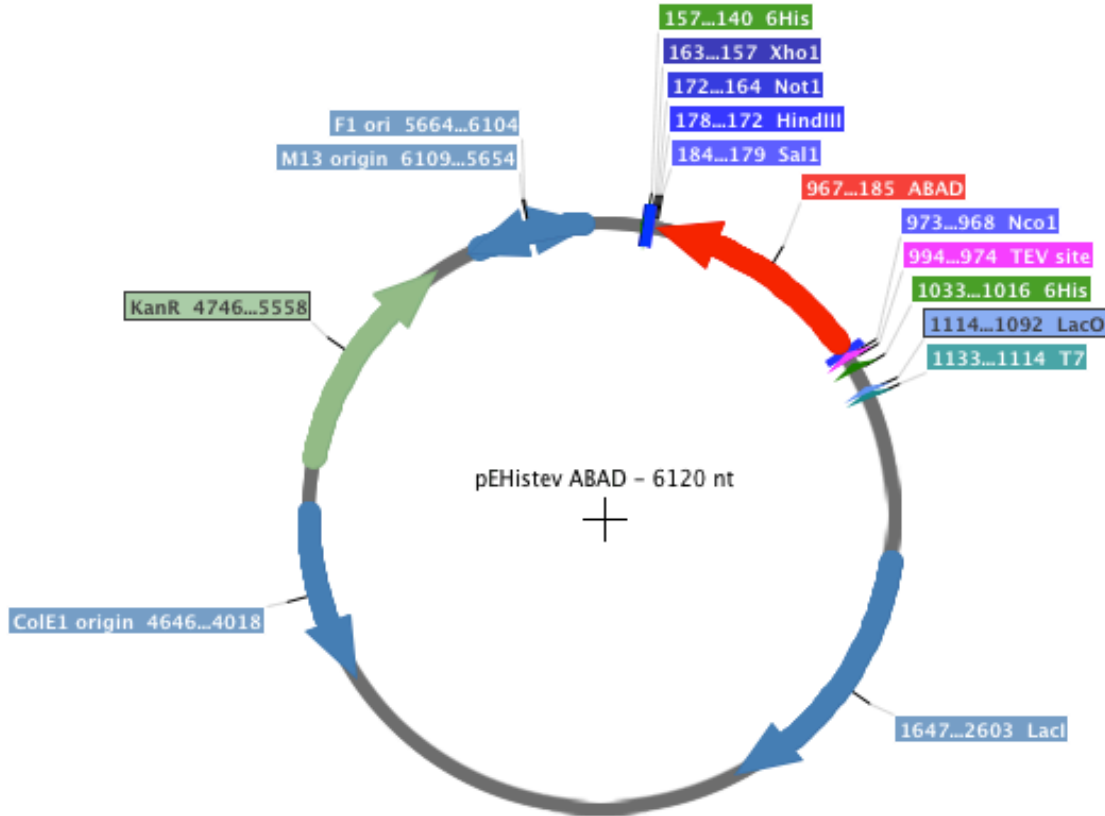
Figure 3.4: Plasmid construct pEHis-TEV ABAD. The ABAD insert (shown in red), located between the *Nco1* and *Sal1* restriction sites in the pEHis-TEV(b) bacterial expression vector. The antibiotic resistance for this construct is kanamycin. The TEV protease cleavage site is shown in pink. (ABAD Protein MW= 27000 Da)

3.3.2 pEHis-TEV ABAD expression and purification

In order to carry out any biophysical techniques it was first necessary to produce and purify ABAD protein. Firstly, the His-TEV ABAD expressing plasmid was transformed into *E.coli* BL21 Codon Plus cells as described in section 2.1.8. As this construct had not been used previously in our laboratory, it was necessary to start with expression trials on a small scale induction test format (section 2.2.4) in order to determine if the expressed protein was soluble and what bacterial growth conditions were optimal for

protein expression. These bacterial expression conditions were found to be growth at 37 °C, 210 rpm for approximately 4 h (or until an absorbance at 600 nm of ~0.6 was obtained), before protein expression was induced by the addition of isopropyl β-D-1-thiogalactopyranoside (IPTG; 1 mM), followed by incubation at 20 °C, 180 rpm for 16 h. Once these tests were complete, large scale expression experiments (section 2.2.3) were then performed before progressing onto a small scale protein purification test (section 2.2.4). As the small scale His-TEV ABAD purification was deemed successful due to the construct being found in the soluble elution fractions (described in 2.2.4) a large scale His-TEV ABAD method development protein purification test was carried out to determine the optimal buffers and TEV protease concentration for purifying His-TEV ABAD protein (described in 2.2.5). Once these conditions were established it was then possible to produce pure untagged ABAD protein. Figure 3.5 summarises the various stages of this His-TEV ABAD purification and the production of pure, untagged protein as indicated by SDS- page gel electrophoresis (section 2.2.1). Overall, the average yield obtained from a 4 L bacterial culture expressing His-TEV ABAD after purification, was in the region of 100 mg. Due to the larger than expected yield, extra care had to be taken during purification in order to avoid saturating the Ni^{2+} columns, and thus maintaining their efficiency.
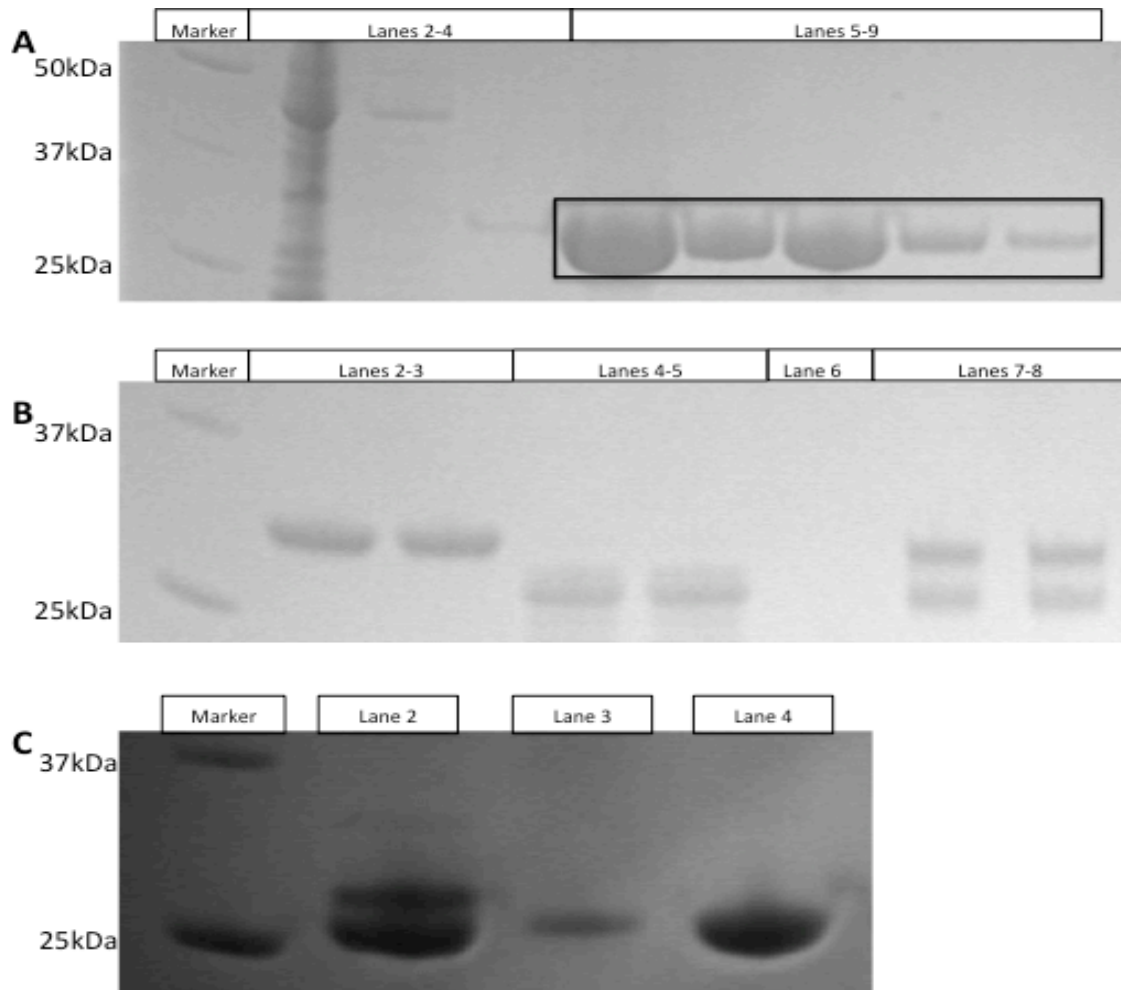
Figure 3.5 ABAD in the protein purification process. A) A gel image taken after electrophoresis showing ABAD containing protein fractions recovered after the first HisTrap column, where histidine tagged ABAD is capable of binding to the columns Ni^{2+} resin whilst impurities pass directly through the column. Lanes 2-4 indicate the impure fractions from the HisTrap column (these lanes exhibit multiple protein bands). Lanes 5-9 indicate purer His-TEV ABAD protein, with one protein band visible at the expected MW for His-TEV ABAD (27 kDa). **B)** A gel image taken after electrophoresis showing His-TEV ABAD before, during and after histidine tag removal. Lanes 2-3 are uncleaved His-TEV ABAD protein (sample taken before the addition of TEV protease). Lanes 7-8 indicate partial cleavage of the histidine tag with 2 protein bands visible (this sample was taken after 1 h of TEV protease cleavage). Lanes 4-5 indicate complete histidine tag removal with a protein band observed at a lower molecular weight than that detected in the uncleaved samples (lanes 2-3). **C)** A gel image taken after electrophoresis showing ABAD containing protein fractions recovered after gel filtration. Lane 2 exhibits two protein bands, indicating impure ABAD protein has been recovered after gel filtration; however, lanes 3 and 4 indicate pure ABAD has been recovered after gel filtration, with a protein band visible at the expected molecular weight. The corresponding fractions from the gel filtration column in lanes 3 and 4 were collected and flash frozen in liquid nitrogen before final storage at 10 and 20 mg/mL, 25 and 50 μL aliquots, -80 °C. The presence of ABAD protein was also confirmed by mass spectrometry.

3.4 <u>NMR as a screening tool to validate small molecule binding partners of ABAD</u>

3.4.1 <u>Previous 'hit' identification of small molecule binding partners of ABAD using TSA</u>

Previous work in the Gunn-Moore laboratory (carried out by Dr Kirsty Muirhead) identified 16 'hit' small molecule binding partners of ABAD by carrying out thermal shift analysis using 674 Maybridge fragment library compounds (Muirhead 2011). Of the 16 fragments Dr Muirhead established 7 fragments were potential inhibitors of the ABAD-Aβ interaction using an enzyme activity assay (described in section 5.3.1). The structures of these fragments are shown in Table 3.1. These findings acted as a foundation for the remainder of the work described in this section of work (3.4.1-3.4.3).

The 674 compounds from the Maybridge fragment library proved to be too large an amount for Dr Muirhead to effectively screen in one pass, in an academic environment. Therefore the thermal shift analysis screening was carried out in systematic waves. Firstly, the entire 674 fragments were screened individually (not in triplicate) and compounds identified as either non- binders ($\Delta T_m < +2°$), or destabilisers ($-\Delta T_m$) were discarded. The remaining 84 compounds were then re-screened in triplicate to allow for any assay errors. This resulted in 16 compounds (Table 3.1), which were classed as 'hit' compounds.

Table 3.1: Maybridge fragment compounds that are binding partners with ABAD, identified using thermal shift analysis. Compound numbers represent their identification within the Maybridge library and compounds highlighted in pink are classified as potential inhibitors of the ABAD- Aβ interaction (Taken from Muirhead 2011).

No.	Name	Structure	No.	Name	Structure
23	2-pyrazinylmethanol		463	methyl 6H-thieno[2,3-b]pyrrole-5-carboxylate	
26	1,3-dimethyl-1H-pyrazol-5-amine		494	ethyl 2-(2-methyl-1,3-thiazol-4-yl)acetate	
39	5-methyl-1,3,4-thiadiazol-2-amine		532	2-(trifluoromethyl) benzamide	
45	tetrahydrothiopyran-4-ylamine		548	1-benzylpiperidin-4-amine	
86	isoxazole-5-carbothioamide		569	(Piperidino-3-pyridinyl)methanol	
94	2,6-dimethyl-benzonitrile		605	N-methyl-N-(3-pyridin-4-ylbenzyl) amine	
268	3-(aminomethyl)-N,N-dimethyltetrahydro-3-thiophenamine		606	N-methyl-N-(3-pyridin-3-ylbenzyl) amine	
390	4-(trifluoromethyl) benzylamine		637	N-methyl-N-[(5-methyl-3-phenylisoxazol-4-yl) methyl]amine	

As these compounds originate from a portion of the Maybridge fragment library, they conform to the 'rule of three' principle. Therefore, as the molecule weights of these compounds are small (below 300 daltons) there is no notable structure- activity relationship (SAR) between the fragments. Due to the variance observed between

biophysical assays and 'hit' compounds obtained, for example, when an identical set of compounds is screened against the same biological target using three different assay formats, the concordance in the number of biologically active compounds or 'hits' obtained from each assay is just 35% (Lipinski & Hopkins 2004), it is therefore important to re-test these potential 'hit' compounds to confirm they are capable of binding to ABAD and elucidate any potential inhibitory effects that they may have.

3.4.2 <u>NMR screening to validate TSA of the Maybridge fragment library</u>

The Maybridge fragment library was adapted by the Prof Jim Naismith group, (University of St Andrews) to allow the library to be screened using two, one dimensional nuclear magnetic resonance (NMR) experiments (saturation transfer difference (STD) and WaterLOGSY) as a method of 'hit' validation. Using these two NMR experiments it was possible to evaluate and confirm the thermal shift analysis results shown in 3.4.1.

The Maybridge fragment library was adapted in such a way that all control spectra (unbound fragments) were individually analysed, and the fragments were then grouped into cocktails of 11 fragments under the stringent condition that each fragment produced a different resonance spectrum. Thus, when the protein was added to the fragments, it was easy to determine which molecule(s) were binding to the protein. All control spectra were then stored in the AMIX profiler analysis software to facilitate straightforward experiments where only protein plus each fragment cocktail is required to be tested. From the 674 Maybridge fragments that were screened by thermal shift analysis, there were 605 fragments that provided sufficiently different resonance

spectra, which could therefore be grouped into 55 fragment cocktails and tested by both STD- NMR and WaterLOGSY NMR (as described in section 2.3.5) to identify potential binding partners of ABAD protein. Purified ABAD protein was diluted with sodium phosphate assay buffer to give a final assay concentration of 20 μM (20 mg/mL as described in section 3.3.2) and added to 55 NMR tubes containing the 605 Maybridge fragment cocktails and 10 % D_2O (as described in section 2.3.5). The 10% D_2O solvent was added to the sample to reduce the spin-spin coupling resulting from the hydrogen bonding between molecules. Since D_2O has a different magnetic dipole moment to hydrogen atoms, the signal produced by D_2O does not contribute to the NMR signal at the hydrogen resonance frequency range.

The NMR analysis (carried out using the AMIX profiler software) for both the STD-NMR and WaterLOGSY-NMR experiments was carried out independently of each other, and then the results were compared to produce a table of fragments, which were categorised as 'hits' in both experiments. Due to the large number of 'hit' fragments identified, the individual STD-NMR 'hits' (89 fragments) and the individual WaterLOGSY- NMR 'hits' (78 fragments) are not presented here. Only the combined 'hits' from both NMR experiments (51 fragments) are shown in Table 3.2.

Table 3.2: Maybridge fragment compounds that were binding partners with ABAD, identified using STD-NMR and WaterLOGSY-NMR. ID numbers represent their unique identifier within the NMR cocktail experimental set-up, alongside their corresponding Maybridge fragment library number.

ID #	Fragment #	ID #	Fragment #
1A6	564	4C4	375
1A11	582	4D1	424
1B2	68	4 E1	217
1C1	94	4F2	113
1C10	501	4G9	441
1C11	185	4G10	136
1D10	221	4H10	111
1F8	151	5A1	390
1G6	172	5A3	97
1G10	533	5A4	123
2A2	555	5B9	496
2A5	168	5C1	356
2H4	99	5C2	43
3A4	345	5D5	142
3A11	381	5F6	160
3B3	542	5F8	358
3B9	320	5G10	134
3C1	413	5H11	155
3C5	489	6A2	139
3D1	133	6B1	148
3D4	409	6C1	213
3 E2	370	6 E1	355
3 E7	523	6F4	176
3F1	492	6H5	96
3F5	347		
3G2	382		
3G10	150		

The next stage of the 'hit' fragment evaluation process was to compare these NMR 'hits' with the previously identified thermal shift analysis 'hits'. On comparison, these two techniques produced very little 'hit' similarity. From the 16 compounds identified by Dr Kirsty Muirhead (Table 3.1) there were only two fragments (fragment numbers 94 and 390) that were also identified as 'hits' from the NMR experiments. On closer inspection of the thermal shift analysis data there were 8 compounds from the NMR experiments, which were also 'hits' in the thermal shift data, but had been discarded

during the thermal shift analysis identification process, possibly due to anomalies in the T_m curves, or because they had not produced a clear result on the first pass screen (described 3.3.1). These 8 'hit' fragments are shown in Figure 3.6.
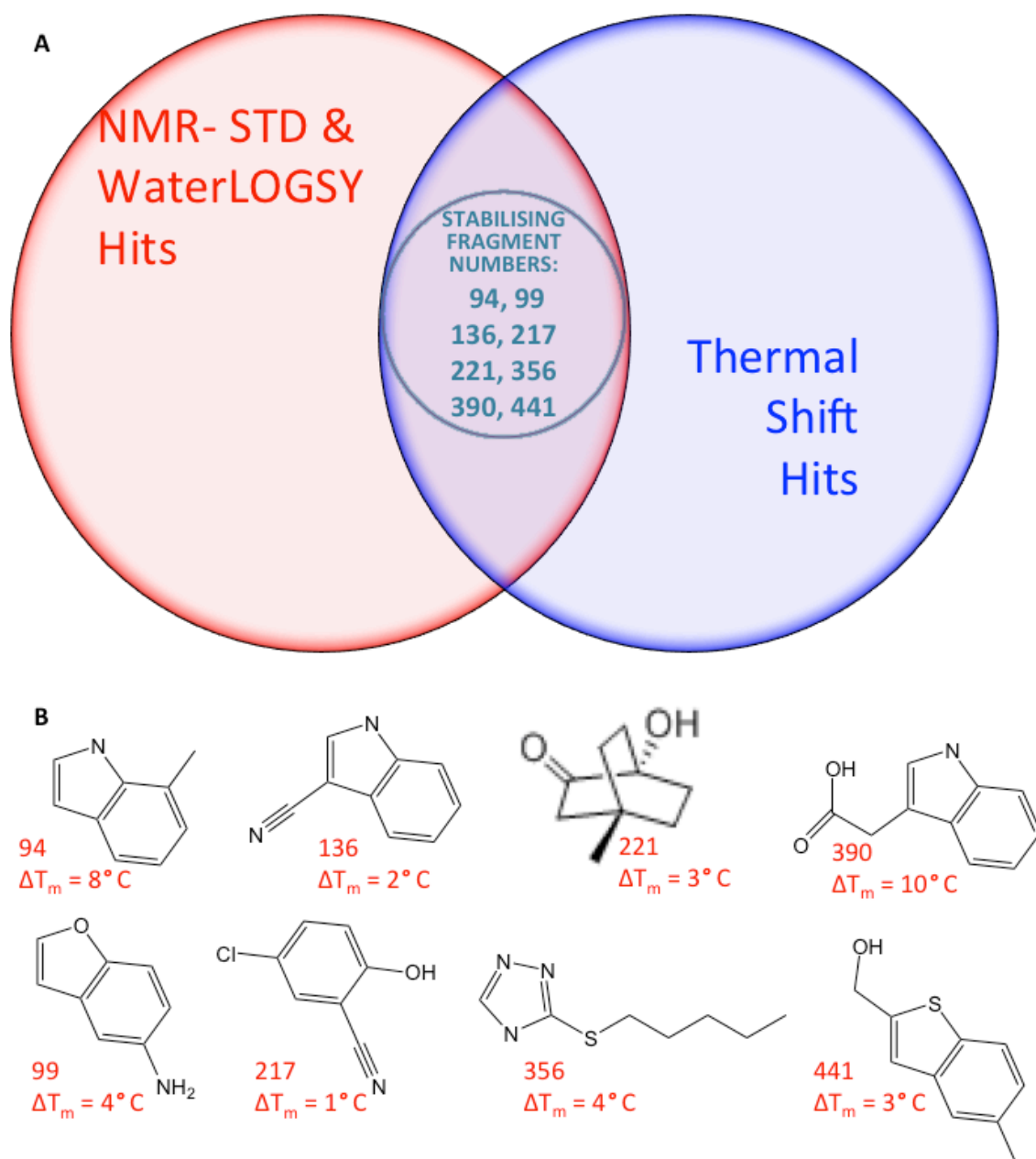
Figure 3.6: Nuclear magnetic screening and thermal shift analysis screening fragment 'hit' comparison. A) Maybridge fragment numbers of the 8 fragments that are 'hits' in both types of NMR experiment (STD-NMR and WaterLOGSY-NMR) and also classified as a stabilising 'hit' fragment in thermal shift analysis. **B)** The molecular structures of the 8 Maybridge fragments that interact with ABAD. Unique Maybridge library numbers for each compound are shown in red, alongside their unfolding temperatures (ΔTm) calculated from the thermal shift analysis. Chemical names of the fragments are detailed as follows: 94: 7-methyl-1H-indole, 99: 1-benzofuran-5-amine, 136: 1H-indole-3-carbonitrile, 217: 5-chloro-2-hydroxybenzonitrile, 221: 4-hydroxy-1-methyl bicyclo[2.2.2]octan-2-one, 358: 2-(3,5-difluorophenyl)acetic acid, 390: 2-(1H-indol-3-yl)acetic acid, 441: 5-Methyl benzo[b]thiophene-2-methanol.

3.4.3 ABAD- Maybridge fragment co-crystallography

In order to investigate these 8 'hit' fragments further, it was necessary to gather more information on how these molecules interact with the ABAD protein. Therefore, x-ray co- crystallography was used to try and obtain a three dimensional structure of the interaction. It was hoped that from these co-crystal trial studies, that the key residues for interaction, on the ABAD protein, could be identified. By elucidating and understanding the mode of binding, then it would become easier to evaluate the fragment's ability to occupy the available chemical space within the ABAD binding site. This structural information is invaluable if the fragments are to progress to chemical modification and onto 'lead- like' compounds (Carvalho *et al*. 2009).

Co-crystallography trials of purified ABAD protein (10 mg/mL; produced as described in section 3.3) and the Maybridge fragment were set up as described in section 2.4.2. The Maybridge fragments were provided as 2 M stocks in DMSO, and were therefore diluted with DMSO to produce a 10 mM stock. It was initially observed that upon contact with the 10 mM Maybridge fragment stocks, that the ABAD protein then appeared to become denatured and precipitate out of solution. It was therefore suggested that the DMSO was facilitating the denaturing of the ABAD protein. To reduce the percentage of DMSO in the crystallographic trial and retain the ABAD protein in solution, the fragments were therefore diluted with water at a 50:50 ratio. All of the fragments demonstrated reduced aqueous solubility when this dilution was carried out with the exception of fragment 94 which appeared to remain in solution and was therefore progressed further into co-crystal trials with the ABAD protein. Several other solvents (for example, 1 x PBS solution, ethanol, isopropanol; all diluted with water) were also tested to try to remove or reduce the percentage of DMSO used in the co-

crystal trials; however in all cases ABAD continued to denature and precipitate out of solution.

In order to try and stabilise the ABAD protein, co-crystallisation trials were next set up in the presence and absence of NAD^+. To date, all published crystal structures of ABAD have contained NAD^+ either bound to the co-crystals, or found within the crystal trial set up conditions (Powell *et al*. 2000; Kissinger *et al*. 2004; Lustbader *et al*. 2004) as this may be necessary for the stabilization of the structure. Conversely, the fragments could be binding to ABAD within the co-factor binding site, and so NAD^+ had been removed in some trials to rule out a competition effect. The co-crystal trials that were set up with ABAD (10 mg/mL) protein and Fragment 94 (10 mM) are shown in Table 3.3. Full details of the exact components of each crystal screen can be found in Appendix C. The nature of the plates used allowed two different tests to be run in parallel using the same reservoir of screen solution. Therefore in a 96 well crystal trial it was possible to test a protein in 192 different conditions.

Table 3.3: Co-crystal trial screen set up for ABAD and Maybridge fragment 94.

Screen Name	Site 1 Compound	Site 2 Compound
JCSG	ABAD + 94	ABAD + 94 + NAD
JMAC	ABAD + 94	ABAD + 94 + NAD
Sto PEG 1	ABAD + 94	ABAD + 94 + NAD
Sto 20	ABAD + 94	ABAD + 94 + NAD
Sto PEG 2	ABAD + 94	ABAD + 94 + NAD

Two possible crystals were identified from these initial trials: in the JCSG screen in site 2, position A11 and also in the Sto PEG 2 screen, site two position F2. The images taken of these two crystals are shown in Figure 3.7; however, these crystals did not achieve any notable diffraction when subjected to x-ray diffraction using the in-house x-ray diffraction equipment at the University of St Andrews (Rigaku/MSC MicroMax-007HF rotating anode equipped with a Saturn 944+ CCD detector).

JCSG- A11 site 2
- 0.1 M potassium thiocyanate
- 30% PEG MME 2000
- 20% PEG 400

Sto PEG 2- F2 site 2
- 28.58% PEG 1.5k
- 0.1 M CHES
- 3.68% Methanol
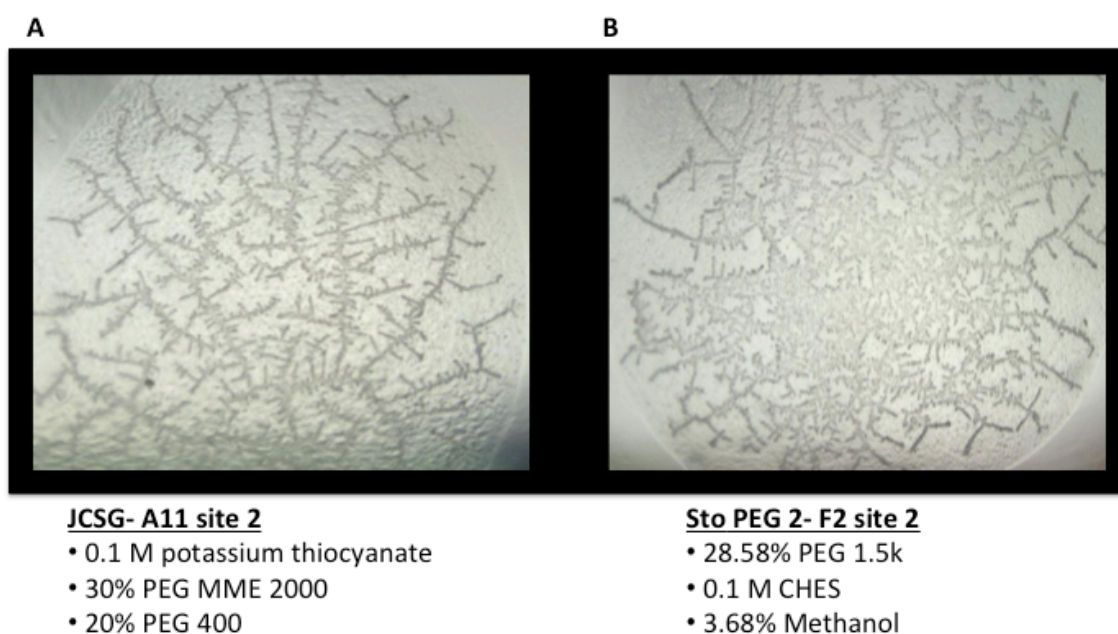
Figure 3.7: Images taken of needle like crystal arrangements obtained from the co-crystallography trials of ABAD and Maybridge fragment number 94. A) An image taken of the needle like crystals obtained from a JCSG crystal screen used to facilitate the co-crystallisation of ABAD and fragment 94. Conditions for reservoir well A11 are detailed under the image. **B)** An image taken of the needle like crystals obtained from the stochastic PEG 2 screen used to facilitate the co-crystallisation of ABAD and fragment 94. Conditions for reservoir well F2 are detailed under the image

Unusually, the crystallography trials that contained ABAD's co-factor NAD^+ did not produce any notable crystals that could have been taken forward into in-house

diffraction trials. This finding was contrary to the literature, as all three previous journal articles had demonstrated ABAD protein crystallography have NAD^+ present within the molecular structure. This could indicate that the crystals found are background precipitation and not needle like ABAD crystal structures. It also suggests that the NAD^+ could be required to stabilise the conformation of ABAD, and also could further suggest that fragment 94 could be competing with the NAD^+ and perhaps interacting with the protein in the NAD^+ binding site.

Therefore, in order to produce crystals that were capable of x-ray diffraction, the crystal conditions from the previously published human ABAD structure papers were used as a template for the screen design (Kissinger *et al*. 2004; Lustbader *et al*. 2004). However, unfortunately despite several attempts, it was not possible to reproduce the crystals that were achieved in these papers for ABAD protein, with bound Maybridge fragment.

Due to the difficulties arising through both the fragment solubility issues, and the ABAD protein becoming denatured and the resulting precipitation causing problems during the co- crystallisation process, it was necessary to provide an alternative method of crystallisation. It was decided to pursue a method where native ABAD protein crystals were grown initially and then the fragments can then be soaked into the protein.

3.4.4 Maybridge fragment soaking of ABAD crystals

In an attempt to make an advancement with the ABAD and Maybridge fragment library and gain further structural information to allow the fragments to progress further along in the drug development pathway, purified native ABAD protein (10 mg/ml) was entered into crystallography trials. These trials were set up as described in section 3.4.3 with the exception that the Maybridge fragment would be added (soaked in) once

diffracting ABAD crystals were obtained. A summary of all the crystal trial screens performed are shown in Table 3.4, full descriptions of the screen conditions can be found in the Appendix C. All crystal plates were set up in a 96 well sitting drop method (section 3.4.3) with 10mg/mL ABAD, 1mM DTT, $\pm$ 5mM NAD$^+$

Table 3.4: ABAD crystal trial screen set up.

Screen Name	Site 1 Compound	Site 2 Compound
JCSG	ABAD	ABAD + NAD
JMAC	ABAD	ABAD + NAD
Sto PEG 1	ABAD	ABAD + NAD
Sto 20	ABAD	ABAD + NAD
Sto PEG 2	ABAD	ABAD + NAD
Sto 19	ABAD	ABAD + NAD
Sto 18	ABAD	ABAD + NAD
Sto Peg 3	ABAD	ABAD + NAD
Sto 17	ABAD	ABAD + NAD
Sto 21	ABAD	ABAD + NAD
Sto 22	ABAD	ABAD + NAD
ABAD Opt 1	ABAD	ABAD + NAD
ABAD Opt 2	ABAD	ABAD + NAD
ABAD Opt 3	ABAD	ABAD + NAD

From the stochastic screens (detailed in Table 3.4), many different types of crystals were observed. By selecting the best-observed crystals, well conditions were examined and varied significantly to produce three optimisation trials (again, full optimisation conditions can be found in Appendix C). One of these conditions proved to be most effective as a basis for crystallography trials: 0.77 M Sodium Citrate (unbuffered), 0.1 M Sodium Citrate (pH 5.5), 0.17 M Magnesium Acetate (From Sto19, well E3, site 2, shown in Figure 3.8). Altering these conditions within a 96 well plate to create an optimised crystal trial (LA opt 1) appeared to be the most successful optimisation crystal trial, with crystal structures appearing to form in nearly all the wells.

Nevertheless, on continuing this forward to in-house x-ray diffraction (Rigaku/MSC MicroMax-007HF rotating anode equipped with a Saturn 944+ CCD detector, University of St Andrews), no notable diffraction was seen in any of the 12 crystals sampled. Another crystal, from each of the 12 crystals sent for in- house diffraction analysis, was re-solubilized in gel filtration buffer (section 3.3.2) and analyzed by SDS-PAGE gel electrophoresis to establish if ABAD protein was detectable in the crystals.
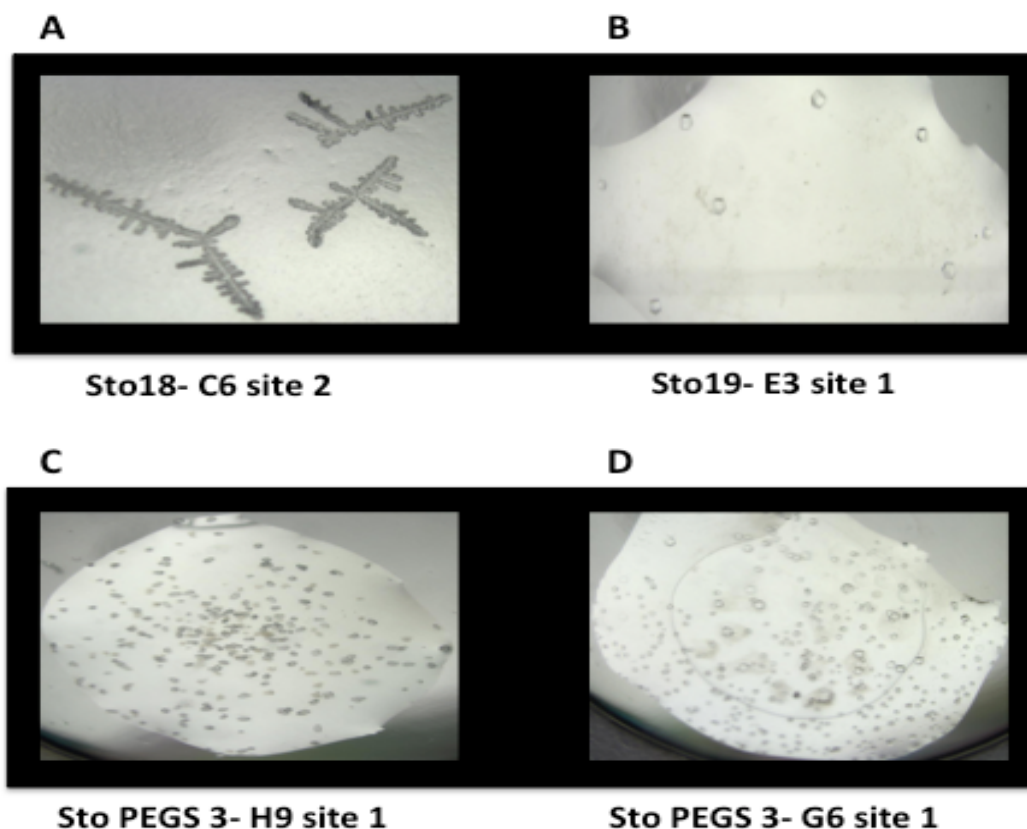
Figure 3.8: Crystal trials with ABAD protein. **A-D)** Needle like crystals obtained from stochastic crystal screen trials. Reservoir well conditions for each crystal are detailed as follows: **A)** Stochastic18- well C6, site 2: 2.41 M Sodium- DL Malate (pH 7.0), 0.1 M Sodium Citrate (pH 4.5), 0.19 M Potassium Nitrate. **B)** Stochastic19- well E3, site 1: 0.77 M Sodium Citrate (unbuffered), 0.1 M Sodium Citrate (pH 5.5), 0.17 M Magnesium Acetate. **C)** Stochastic PEGS 3- well H9 site 1: 12.42% PEG MME 5000), 0.1 M Bis tris (pH 6.0) 0.28 M Magnesium Sulphate. **D)** Stochastic PEGS 3- well G6, site 1: 24.01% PEG 8000, 0.1 M Bicine (pH 8.5), 0.26 M Sodium Potassium Phosphate. B) The conditions from this experiment were used to design a crystal optimisation screen (LA Opt1).

Despite best efforts diffracting ABAD crystals were unable to be produced. X-ray crystallography is a time consume process, with ABAD crystals taking between 7-21 days to grow, however, these trials have provided a basis for future ABAD crystallography investigation studies.

3.5   <u>Conclusion and summary of results</u>

Nuclear magnetic resonance (NMR) spectroscopy was a technique used successfully in this chapter to validate previously identified small molecule binding partners of ABAD. Two types of NMR experiments (saturation transfer difference (STD) and WaterLOGSY) were selected for this purpose. Both NMR experiments were run in parallel against ABAD protein mixed with Maybridge fragments, creating a fast and effective screening method. By applying both NMR experiments this acts as a validation experiment, in itself, as only fragments that displayed a change in their spectrum (signifying ABAD binding occurring) in both the STD-NMR and WaterLOGSY NMR experiments were taken forward and classified as true 'hit' compounds for analysis against the previously obtained results from the thermal shift analysis results.

The NMR analysis revealed 51 'hit' small molecule binding partners of ABAD protein from the Maybridge fragment library. Of these 51 compounds, eight compounds (fragment number 94, 99, 136, 217, 221, 358, 390 and 441) were classified as 'hit' molecules in both thermal shift analysis (TSA) and two NMR experiments. The structures of these fragments are shown in Figure 3.6..

These fragments were then taken forward into co-crystallography trials with purified ABAD protein. Unfortunately, despite several attempts no diffracting crystals were obtained, despite stochastic screening against many conditions and further screen optimisation based on the observed crystal images. It was therefore decided to try and crystallise native ABAD protein, before soaking in the fragment once diffracting ABAD crystals could be achieved and reproduced successfully. Again, despite the many crystallography trials set up, no diffracting ABAD crystals could be achieved. These

crystallography studies do however provide a basis for any future ABAD crystallography trials in excluding and narrowing down many crystallography conditions that were unsuccessful. The conclusion and discussion of these results as well as future perspectives is described further in Chapter 6.

Chapter 4: Cyclophilin D as a possible therapeutic target in the treatment of Alzheimer's disease.

4.1   Introduction

Cyclophilin D is a mitochondrial protein that is known to interact with Aβ (Yao *et al.* 2007; Yan *et al.* 1999; Yan *et al.* 2007). During times of oxidative stress or in the presence of Aβ, this promotes the translocation of CypD to the inner mitochondrial membrane, contributing to the opening of the mPTP and causing cell death. Therefore by preventing the translocation of CypD then this could be beneficial in the treatment of Alzheimer's disease. This hypothesis has already been proven, by inhibiting the CypD-Aβ interaction in the transgenic $_m$APP expressing AD mouse model, and this in turn has been shown to improve cognitive function and recover memory loss (Du *et al.* 2008; Du *et al.* 2011). As this interaction is becoming better understood, the direction of this chapter of my thesis focussed on another potential binding partner of CypD, amyloid binding alcohol dehydrogenase (ABAD), and the difficult task of trying to prove the unpublished hypothesis from Yan and Stern in 2004. This hypothesis suggested that ABAD can bind to CypD and that the ABAD-Aβ interaction may encourage the opening of the mPTP, leading to neuronal death (unpublished observation, Yan and Stern, 2004). In addition, previous work from the Gunn-Moore laboratory has agreed with this hypothesis as it was backed up by FRET (Förster resonance energy transfer) observed between the two proteins (Ren 2008). However as yet, these results have failed to be replicated at the biochemical level.

Therefore, in order to confirm this potential binding partner of CypD it was necessary to elucidate these possible interactions further. There are many biophysical techniques that can be employed to investigate protein- protein interactions, and in this chapter the two techniques, which were used x-ray crystallography and isothermal titration calorimetry (ITC).

4.1.1 <u>X-ray Crystallography</u>

X-ray crystallography is a well-used technique and is considered to be the optimum method for establishing the three dimensional structure of a molecule, by determining the arrangement of atoms within the crystal. The data that is produced from x-ray crystallography includes the size of the atoms, length of the bonds, types of bonds, bond angles and the disorder in the molecule. X-ray crystallography works on the principle that protein crystals will diffract x-rays to produce diffraction wave patterns in the form of the constructive, destructive or partial interference of scattered waves. The diffraction pattern produced obtains the orientation of atoms in space (*via* bond lengths and angles) or the atomic positions within a regular crystal lattice. The process relies on having a crystal which is capable of being mounted on a goniometer and then rotated, whilst being bombarded with x-rays to produce the pattern of reflections (or scattering diffraction pattern). This in itself means that any imperfections or cracks in the crystal will produce poor data (Drenth 2006).

There are certain pitfalls and limitations when carrying out x-ray crystallography, with the main difficulty being that growing suitable crystals capable of diffraction is a time consuming endeavour. Crystals for x-ray diffraction must be pure (homogenous) and perfectly formed, with no twinning (when two crystals are formed in a symmetrical manner they will share crystal lattice points and so this increases the symmetry observed. This observed symmetry does not correlate to the crystal itself and is known as twinning), imperfections or contaminants and they must be relatively small usually about 0.2 mm (Drenth 2006). Flexibility within a molecule (such as in the loop D region of ABAD) also proves problematic when looking to achieve good quality crystals. A further difficulty in protein crystallography is the fragile nature of the crystals themselves. Proteins are irregularly shaped and any change in temperature, pH or

protein concentration will have an effect on the ability to produce diffracting crystals. Also a new protocol for the optimal crystal conditions must be defined for each protein and therefore in order to obtain these unique conditions for each new protein can be very time consuming. This individual protocol *per* protein, also applies to different proteomes and mutations within the protein itself may well require changes to the crystallisation conditions (Drenth 2006).

Once these pitfalls have been overcome the complicated two-dimensional data can be analysed and converted into a three-dimensional data set in the form of electron density maps. The data is then indexed to identify the unit cell dimensions, symmetry and the molecule's space group. After indexing, the data is then integrated to record the Millar index and intensity of each reflection. In order to assess the quality of the data the R-factor can then be calculated, to give an estimate of how many errors there are and the reliability within a data set (Drenth 2006). When analysing the 3-D data, the phase of the wave cannot be calculated and therefore the important structure factor cannot be calculated. Therefore the phase of the wave is estimated using various techniques such as molecular replacement, anomalous x-ray scattering or heavy atom derivatives to solve the phase problem. Once this is complete a structural model can then be built and the refinement process can begin to improve it. This involves building a new electron density map and measuring this against the original map to produce a new R-factor. This could be repeated several times until a molecule's structure is solved and deposited into a crystallographic database such as the Protein Data Bank (PDB) (Drenth 2006).

4.1.2 <u>Isothermal Titration Calorimetry</u>

Isothermal titration calorimetry (ITC) is a biophysical technique that is used to determine the thermodynamic parameters of interactions in solution. ITC works by taking a direct measurement of the heat effect produced during an interaction, i.e. ITC measures the release (exothermic) or absorption (endothermic) of heat. This technique is capable of measuring the binding affinity (K_a) changes in enthalpy (ΔH) and the stoichiometry of two molecules in solution. Using these measurements it is then possibly to calculate the entropy (ΔS) and Gibbs free energy changes (ΔG) (Pierce *et al.* 1999). When used in conjunction with other biophysical techniques, such as structural information gained from x-ray crystallography, ITC can complete the representation of a protein- protein interaction and help to understand the forces that stabilise the folded conformations of proteins (Pierce *et al.* 1999).

During an ITC experiment, a syringe containing one protein solution (ligand) is titrated into a cell containing a solution of the other protein at a constant temperature (Figure 4.1). When the ligand is injected into the cell, the two compounds interact, and heat is released or absorbed in direct proportion to the amount of binding. As the protein in the cell becomes saturated with ligand, the heat signal diminishes until only the background heat of dilution is observed (Pierce *et al.* 1999).

Although ITC has many advantages the major disadvantage it has, which is also similar to other biophysical techniques (Guss & King 2011), such as surface plasmon resonance (SPR), is the high concentration and quality of protein which is required. The sensitivity of the instrument can also be a problem and obtaining a K_d range for low affinity interactions is very difficult (Jecklin *et al.* 2009).
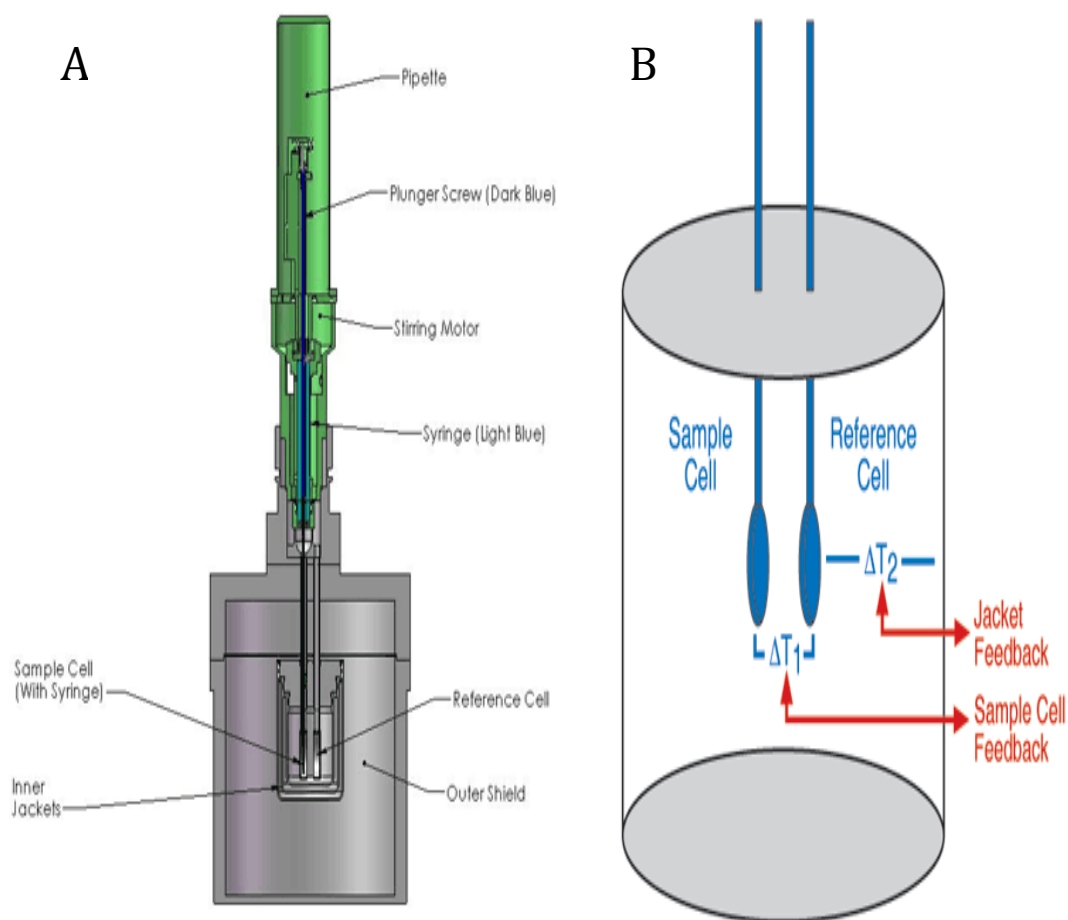
Figure 4.1 ITC experimental set up. A) The cell feedback network which is used to measure and compensate for the heat produced during an interaction. The syringe is rotating during an experiment to facilitate mixing and the plunger is used to inject precise volumes into the cell. **B)** Enhancement of the two coin shaped cells within the machine whereby the thermoelectric device measures changes between the cell sample and the reference cell (ΔT_1) and changes within the reference cell and the jacket (ΔT_2). As the interaction occurs heat is released or absorbed and as ΔT_1 is kept constant, as a baseline, throughout the study the power required to maintain this constant measurement is described as the total heat change resulting from the interaction. (Adapted from GE Healthcare technologies http://www.microcal.com/technology/itc.asp).

4. 2   <u>Chapter aims</u>

Using both x-ray crystallography and isothermal titration calorimetry the ultimate aim of this chapter was to establish whether CypD binds to ABAD and the subsequent parameters for this interaction. In order to achieve these goals, new DNA constructs were prepared in order to attempt to identify the binding site and key residues of the interaction. The general work- flow plan is depicted in Figure 4.2.
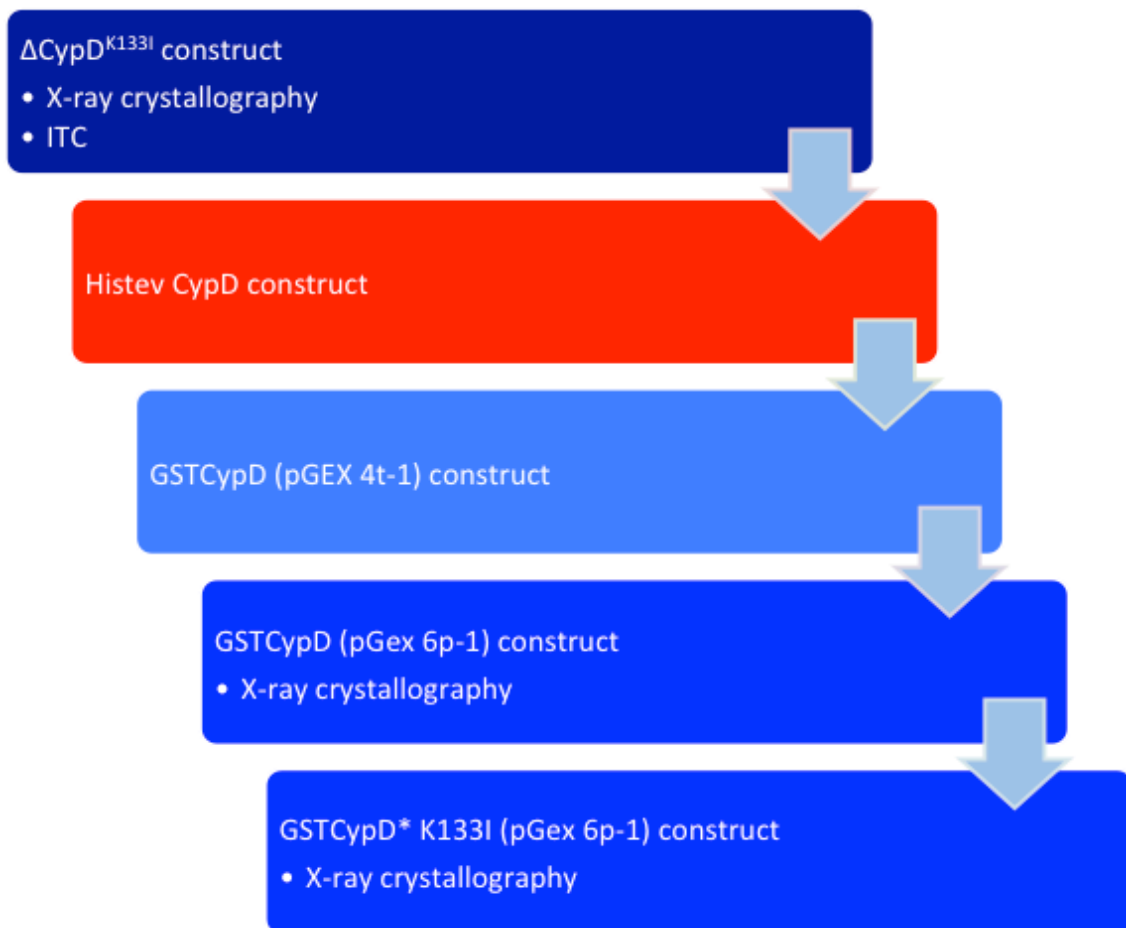
Figure 4.2: Schematic representation of the CypD experiments performed in this chapter. The basis of the work flow program for this chapter, starting with x-ray crystallography and ITC experiments using a truncated, mutated CypD construct, then leading onto utilising several full length CypD studies and biophysical experiments with purified CypD protein.

4.3   Truncated CypD experiments

4.3.1 ΔCypD ^{K133I} background

The only CypD construct which had been previously crystallised successfully to date, was a truncated mutant construct (ΔCypD^{K133I}) which was missing 29 amino acids from its N-terminal region (Schlatter *et al*. 2005; Kajitani *et al*. 2008). This construct was a kind gift from Dr Masahiro Fujihashi (Kajitani Group, Kyoto University, Japan). Figure 4.3 shows the plasmid construct that encodes the truncated mutant CypD (ΔCypD^{K133I}) insert within the bacterial expression vector pET 21a, the DNA sequence can be found in Appendix A. Of particular note is that as well as the truncation of the N terminus, a key residue was mutated at position 133, where a K133I mutation has been inserted into the construct to improve crystallisation (Kajitani *et al*. 2008) (Protein sequences are detailed in Appendix A).
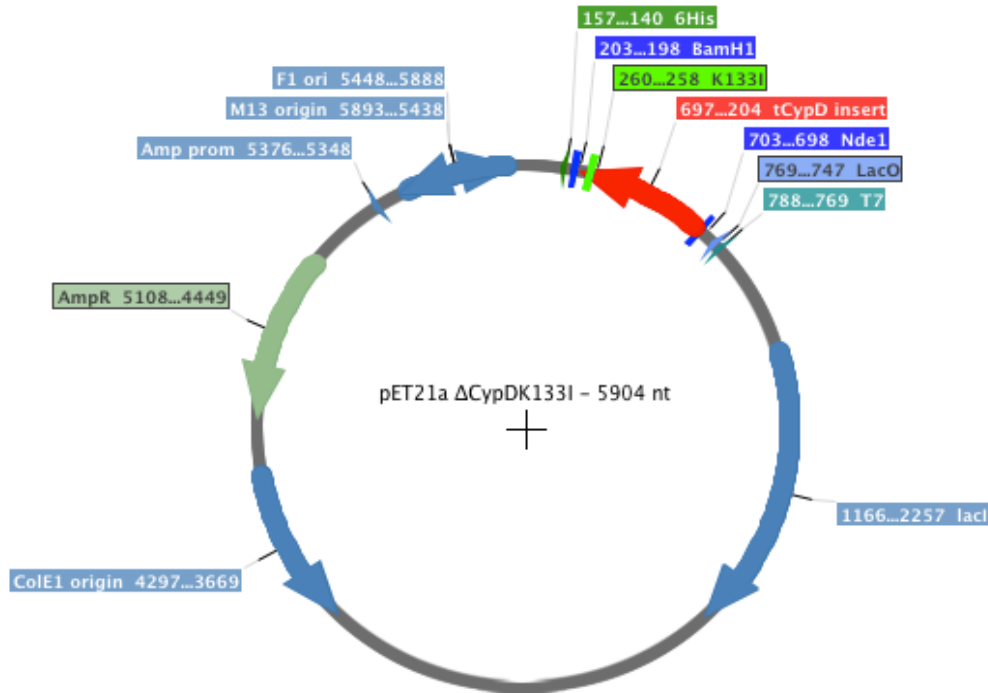
Figure 4.3: Plasmid construct pET21a- ΔCypD^{K133I}. The truncated CypD (ΔCypD^{K133I}, shown in red) insert, located between the *Nde1* and *BamH1* restriction sites in the pET21a bacterial expression vector. The antibiotic resistance for this construct is ampicillin. The K133I mutation is also shown on the ΔCypD^{K133I} insert in green. (ΔCypD^{K133I} protein MW= 17759 Da)

4.3.2 ΔCypD^{K133I} expression and purification

In order to carry out biophysical techniques it was necessary to produce and purify the truncated ΔCypD^{K133I} protein. Firstly, the ΔCypD^{K133I} expressing plasmid was transformed into *E.coli* BL21 Codon Plus cells as described in section 2.1.8. As this construct had not been used previously in our laboratory, it was necessary to start with expression trials on a small scale induction test format (section 2.2.2) in order to determine if the expressed protein was soluble and what bacterial growth conditions were optimal for protein expression. These bacterial expression conditions were found to be growth at 37 °C, 210 rpm for approximately 4 h (or until an absorbance at 600 nm of ~0.6 was obtained), before protein expression was induced by the addition of isopropyl β-D-1-thiogalactopyranoside (IPTG; 1 mM), followed by incubation at 20 °C,

180 rpm for 16 h. Once these tests were complete, large scale expression experiments (section 2.2.3) were then performed before progressing onto protein purification (section 2.2.6). Next after further method development to find the optimal buffers and identify the most efficient columns for purifying the protein completely, the purified truncated CypD protein was produced. Figure 4.4 summarises the various stages of this $\Delta CypD^{K133I}$ purification and the production of pure $\Delta CypD^{K133I}$ protein as indicated by SDS- page gel electrophoresis (section 2.2.1).
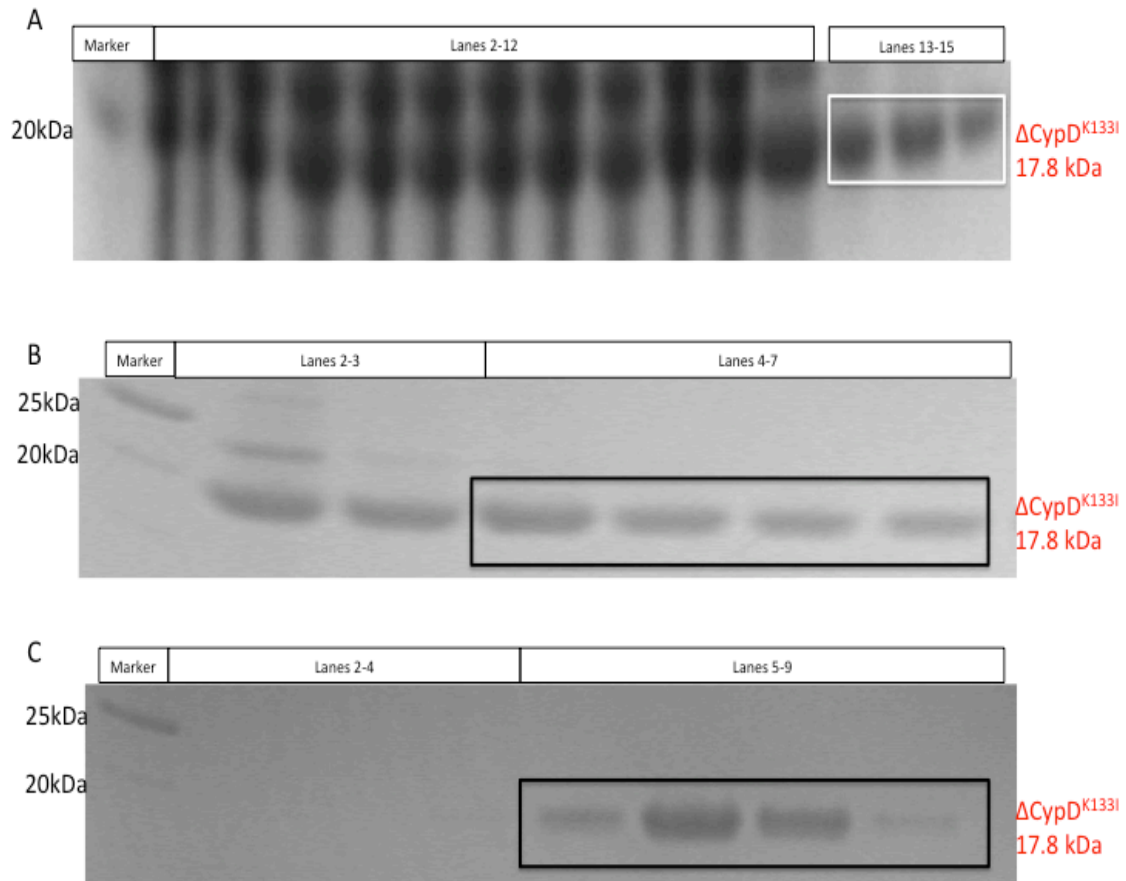
Figure 4.4 ΔCypD^{K133I} in the purification process. A) A gel image taken after electrophoresis showing ΔCypD^{K133I} containing protein fractions recovered after the first cation exchange column. Lanes 2-12 indicate the impure fractions from the cation exchange column (these lanes exhibit multiple protein bands including a protein band at the correct expected molecular weight for ΔCypD^{K133I} at around 17.8 kDa). Lanes 13-15 indicate more pure ΔCypD^{K133I} protein, with one protein band visible at the expected MW for ΔCypD^{K133I}. **B)** A gel image taken after electrophoresis showing ΔCypD^{K133I} containing protein fractions recovered after the second cation exchange column. Lanes 2-3 indicate impure protein fractions, with more than 1 protein band visible, and therefore these samples were discarded. Lanes 4-7 indicate purer ΔCypD^{K133I} containing fractions with a visible protein band at the expected ΔCypD^{K133I} molecular weight. These fractions were pooled and continued the purification process onto dialysis and gel filtration. **C)** A gel image taken after electrophoresis showing ΔCypD^{K133I} containing protein fractions recovered after gel filtration. Lanes 2-4 show no ΔCypD^{K133I} protein has been recovered after gel filtration in the corresponding fractions, however lanes 5-9 indicate pure ΔCypD^{K133I} with a protein band visible at the expected molecular weight. Subsequently these fractions were collected and flash frozen in liquid nitrogen before final storage at 25 mg/mL, 25 μL aliquots, -80 °C. The presence of ΔCypD^{K133I} protein was also confirmed by MALDI-TOF mass spectrometry.

As the ΔCypD^{K133I} protein is in an untagged construct the protein purification was complex and time consuming. In order to achieve pure protein, the purification took approximately 4 days in total, and this created a problem whereby the yield achieved was very low and it was found that the protein often precipitated out from solution. By purifying more than 6 L of bacterial ΔCypD^{K133I} expressing cultures in one run, the purification columns became saturated and were less effective, and so it was necessary to perform multiple purifications. Overall, the average yield obtained from a 6 L bacterial culture expressing ΔCypD^{K133I}, after purification, was in the region of 20- 25 mg.

4.3.3 ΔCypD^{K133I} and ABAD co-crystallography

Despite the low protein yield, I had managed to purify enough protein to investigate whether the truncated CypD protein can bind to ABAD by setting up co-crystallisation protein trials. These were set up as described in section 2.4.2. These trials did successfully produce crystals in various conditions (most notably in 25% Jeffamine and 0.1 M HEPES pH 7.5), which were all capable of diffraction in house using the Rigaku/MSC MicroMax-007HF rotating anode equipped with a Saturn 944+ CCD detector at a wavelength if 1.54 Å. Details of these crystals are shown in Figure 4.5. As the crystal structure of both the human ΔCypD^{K133I} (Schlatter *et al*. 2005; Kajitani *et al*. 2008) and the human ABAD (Lustbader *et al*. 2004) protein had been previously solved, the crystal structure of these potential co-crystals was easy to establish using molecular replacement. Unfortunately the analysis revealed that these potential co-crystals were simply a replication of Schlatter and Kajitani's work in producing only ΔCypD^{K133I} crystals, with no ABAD present. This was also confirmed by SDS-page gel

electrophoresis of a solubilised protein crystal which showed only the presence of the ΔCypD^{K133I} protein and not the ABAD protein (Figure 4.5).
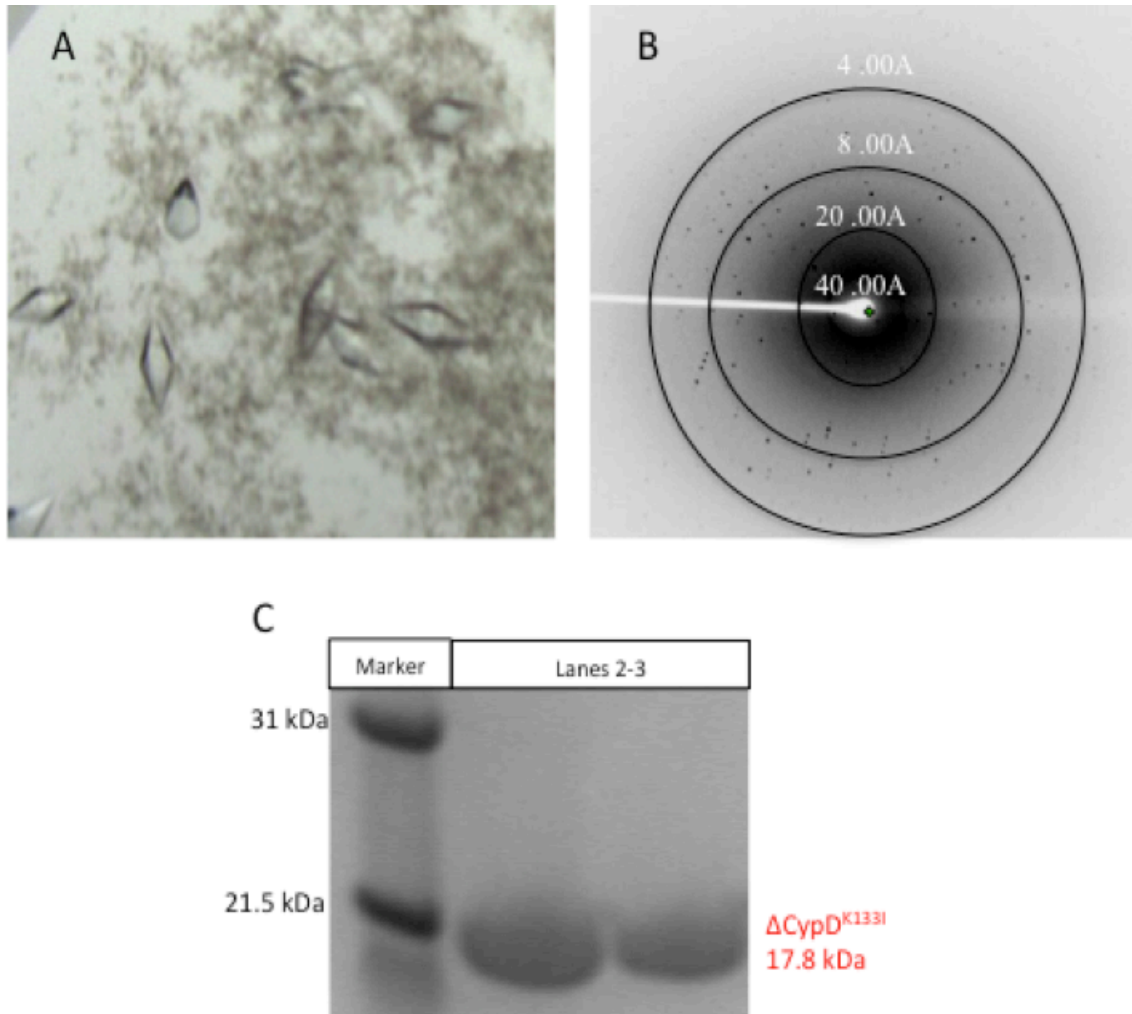
Figure 4.5: ΔCypD^{K133I} protein x-ray crystallography, both individually and in a co-crystallisation attempt with purified ABAD protein. **A)** An image of a ΔCypD^{K133I} protein crystal obtained from a crystallographic trial. **B)** Diffraction pattern of the ΔCypD^{K133I} protein crystal. **C)** A gel image of a taken of re-solubilised co-crystals which confirmed that the crystals obtained are purely ΔCypD^{K133I} crystals, with a protein band being visible around the expected molecular weight of 17.8 kDa and no visible protein band at 27 kDa, the expected molecular weight of ABAD protein. (If these were co-crystals after re-solubilisation, there would have been two protein bands generated at each of the protein's predicted molecular weight). This result was also confirmed by mass spectrometry.

It was therefore hypothesised that the CypD binding site could be in the missing region of the ΔCypD^{K133I} construct, or that the K133I mutation (present in ΔCypD^{K133I} to improve the crystal contacts) was preventing the ABAD from binding.

It was therefore decided to first try a pull down assay using the His-tagged ABAD and ΔCypD^{K133I} using a Ni^{2+}- NTA column to test if the two compounds would bind and could be purified together. This was carried out by first, resuspending a cell pellet of *E.coli* BL21 containing ΔCypD^{K133I} in lysis buffer and a cell pellet of *E.coli* BL21 containing His-TEV ABAD, then incubating both proteins together for 1 h at 4 °C with mixing. This mixture was then lysed and purification was carried out as detailed in section 2.2.5. Unfortunately SDS-page gel electrophoresis revealed, that after the 1st nickel column there were no bands present at the expected MW of 45 kDa (ΔCypDK133I = 17.8 kDa, ABAD=27 kDa, total= 44.8 kDa).

Therefore at this stage, it was unclear whether ΔCypD^{K133I} is capable of binding to ABAD; to investigate this further it was then decided to perform an ITC experiment with the two proteins.

4.3.4 ΔCypD^{K133I} and ABAD Isothermal Titration Calomrimetry

An ITC experiment using the VP-ITC instrument (Microcal LLC) with purified ΔCypD^{K133I} and ABAD protein was set up in accordance with section 2.3.3, to test the binding in the micro molar range. Due to the sensitive nature of ITC experiments, all buffers were prepared and degassed fresh before use to limit the chance of experiencing any temperature changes that are not specific to the reaction. ITC experiments require a large amount of protein therefore in this experiment the limiting factor was the quantity

of purified $\Delta CypD^{K133I}$ protein, so this was placed into the syringe and injected into the cell containing ABAD protein at regular intervals (section 2.3.3).

The raw data was processed using MicroCal Origin software and a baseline and integration adjustments were carried out manually. The results of this ITC experiment confirmed that $\Delta CypD^{K133I}$ appears to be unable to bind ABAD (Figure 4.6).
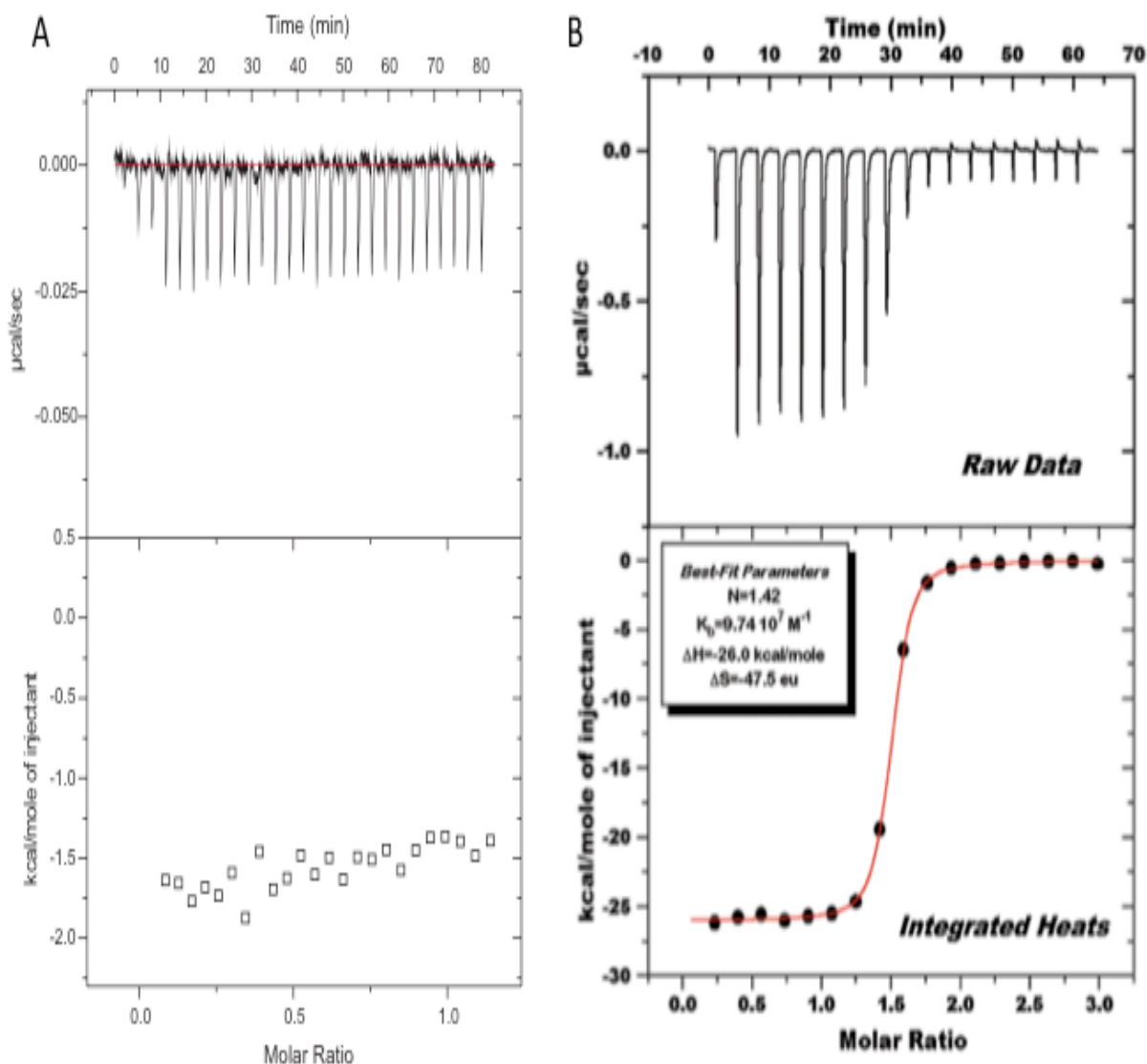
Figure 4.6: ΔCypD^{K133I} and ABAD ITC experiment compared to a typical representative ITC binding result. A) Top half of diagram- ΔCypD^{K133I} protein from the syringe injected into ABAD protein in the ITC cell over a period of 80 minutes. **A) Bottom half of diagram**- integrated heats of the ΔCypD^{K133I} injections into ABAD. As the plotted data does not fit to a sigmoidal curve, this indicates that no binding is occurring. **B) Top half of diagram**- A typical plot for the injection (raw) data from two random interacting proteins. The heat released upon their interaction (ΔH, µcal/sec) is monitored over time. Each peak represents a heat change associated with the injection of a small volume of sample into the ITC reaction cell. As successive amounts of the ligand are titrated into the ITC cell, the quantity of heat absorbed or released is in direct proportion to the amount of binding. As the system reaches saturation, the heat signal diminishes until only heats of dilution are observed **B) Bottom half of diagram**- Typical integrated heat results of two random proteins interacting during an ITC experiment. The sigmoidal nature of the curve is a classic representation of the type of data achieved in an ITC experiment when two proteins interact. The binding curve is analysed with the appropriate binding model to determine K_B, n and ΔH. Where K_B = $1/K_d$. (taken from GE Healthcare technologies: http://www.microcal.com/technology/itc.asp).

4.4   His-TEV CypD experiments

4.4.1 His-TEV CypD background

The results from section 4.3 indicated that the truncated and mutated CypD construct ($\Delta CypD^{K133I}$) was not able to bind or interact with ABAD. One possible reason for this could be due to the fact that the $\Delta CypD^{K133I}$ construct is missing an important N-terminal region, or that the presence of the K133I mutation was preventing the interaction. Therefore, despite previous researchers' experiences and noted observations, it was deemed necessary to use a full length CypD encoding construct to investigate these possibilities. As previously described, most biophysical techniques tend to require a significant amount of purified protein. Therefore, in order to increase the protein yield recovered after purification it was important to use the quickest and simplest purification method possible. In this instance, it was decided to apply a histidine tag to the full-length, non-mutated CypD construct. By using a histidine tag this aids purification by allowing the protein to be purified using a HisTrap column containing Ni^{2+} Sepharose. Proteins with a histidine construct bind onto the nickel sepharose, whilst impurities simply pass through the column. After histidine tag cleavage the column can also be used to separate cleaved protein from the cleaved histidine tag, as the tag will bind to the column and cleaved protein will flow through the column. This method of utilising an affinity purification tag is regarded as one of the easiest method of protein purification (Kobs 2004). This DNA construct was made by Dr Kirsty Muirhead (Formally FGM group) and is shown in Figure 4.7. (The DNA and protein sequence can be found in Appendix A).
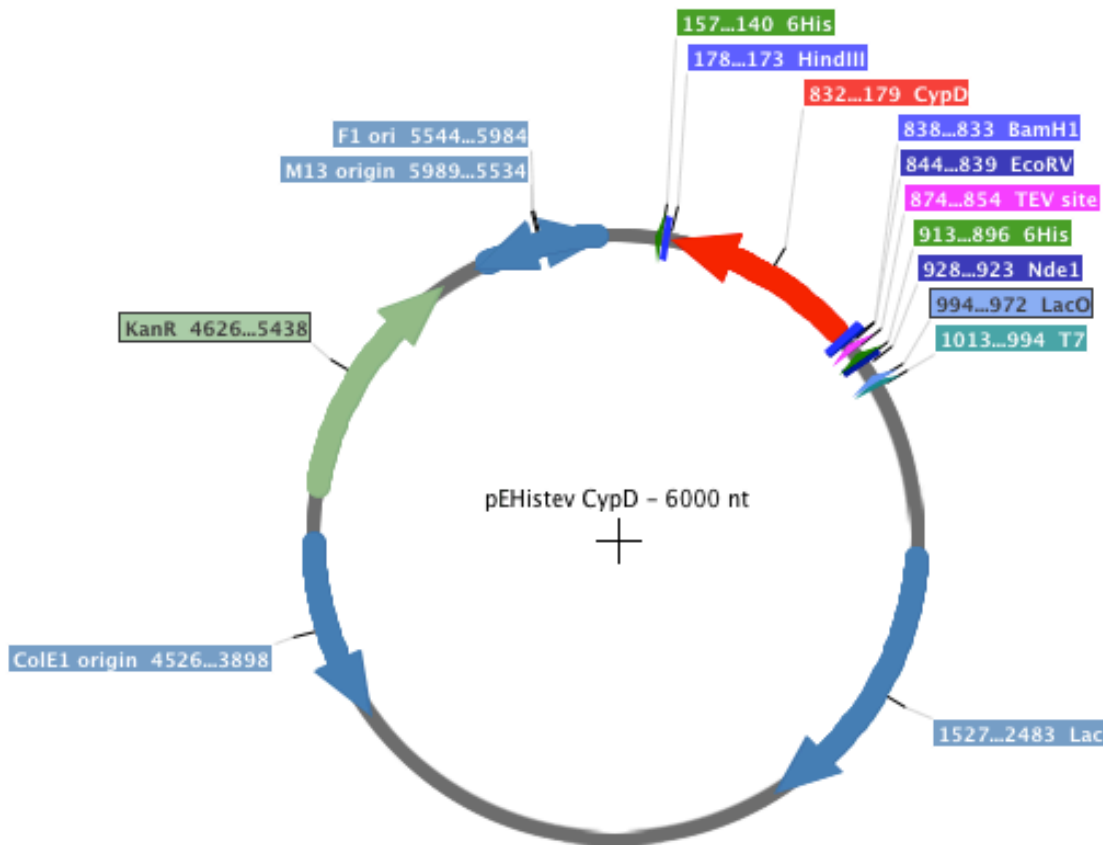
Figure 4.7: pEHis-TEV- CypD. The full length CypD insert (shown in red), is located between the *BamH1* and *Hind III* restriction sites of the bacterial expression vector pEHis-TEV. The antibiotic resistance for this construct is kanamycin. The Histidine tag is shown in green, and the TEV cleavage site for tag removal is shown in pink (MW of purified protein = 23079.3 Da).

4.4.2 His-TEV CypD expression and purification

In order to produce the His-tagged full length CypD protein, the His-TEV CypD expressing plasmid was transformed into *E.coli* BL21 Codon Plus cells as described in section 2.1.8. Again, initial small scale induction tests (section 2.2.2) revealed that the protein appeared to express well: however, when a small scale purification test was carried out (section 2.2.4) the His-TEV CypD protein was found as an insoluble fraction in the resuspended cell pellet instead of being found in the soluble fraction after cell lysis. Therefore, in order to minimise the time spent on method development for this construct, a 96 well block method for testing protein expression and trialling protein

purification was carried out (section 2.2.10). This was a relatively new technique for the laboratory at the time, in fact it had only been performed twice previously, but it was seen as a fast and efficient way of testing protein expression in several bacterial cell lines at the same time.

The use of differing bacterial cultures and media can enhance the expression of bacterially expressed protein. Therefore, the His-TEV CypD protein expression and purification was tested against 8 different bacterial expressing cell lines. The following cell lines were all transformed with the plasmid expressing His-TEV CypD: BL21 (DE3), C43 (DE3), Rosetta (DE3), Origami (DE3), Tuner (DE3), BL21* (DE3), HMS174 (DE3) and BLR (DE3) cells, at the same time as also being tested against three different medias (LB Broth, TB Broth and auto-induction media). This technique is explained in further detail in section 2.2.10, but the 96 well block layout is detailed in Table 4.1. Further details of all bacterial cell lines used in these experiments can be found in Appendix B.

Table 4.1: 96well plate expression set up. Each row represents a different E. coli cell line expressing His-TEV CypD. Coloured wells represent different media types (yellow LB media; orange TB media; red AI media).

BL21 DE3	A1											A12
C43 (DE3)	B1											B12
Rosetta (DE3)	C1											C12
Origami (DE3)	D1											D12
Tuner (DE3)	E1											E12
BL21* (DE3)	F1											F12
HMS174 (DE3)	G1											G12
BLR (DE3)	H1											H12

Two His-TEV CypD protein samples from each transformed bacterial cell line grown in the different media were analysed by SDS-PAGE gel electrophoresis using a 96 well 6% E-PAGE gel (Invitrogen). The two His-TEV CypD samples analysed were the resuspended cell pellet sample and the corresponding elution fraction; in order to test for His-TEV CypD protein in both soluble and insoluble fractions. This method also allowed for all the samples to be run together, on a single 96well gel, with the exception of the BL21 DE3 samples as these had been tested previous. Figure 4.8 shows an image of the gel after electrophoresis, and from this it can be seen that in all the bacterial cell lines, and in all the different media types, the His-TEV CypD protein was found in the insoluble cell pellet fraction, as indicated by a protein band at the expected His-TEV CypD molecular weight of 23 kDa.
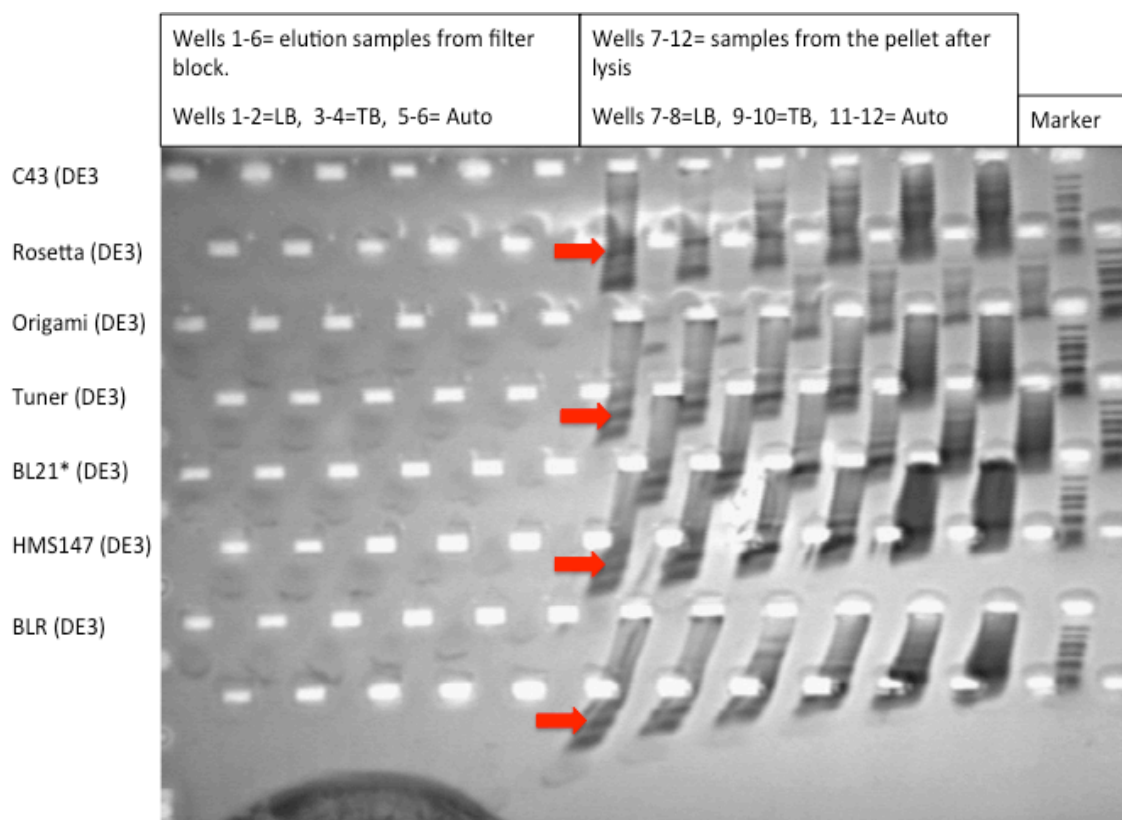
Figure 4.8: A 96 well gel image of *E. coli* cell lines expressing His-TEV CypD protein. An image of a gel taken after the 96 well E-PAGE gel electrophoresis after His-TEV CypD protein purification. Wells 1-6 represent the elution samples for each cell line in various media. Wells 7-12 represent the equivalent sample for each cell line taken from resuspending the corresponding cell pellet collected after lysis. Each row represents a different bacterial expressing cell line. The red arrows indicate the protein band where His-TEV CypD protein is expected to be found (MW=23 kDa), but due to the complex nature of this gel, only the protein band in rows A, C, E and G have been highlighted, even though this protein band was found in rows A-G, wells 6-12. The difficulty in analysing the gel image due to size and skewed running nature was aided by confirming the presence of His-TEV CypD, in the highlighted protein bands, by MALDI-TOF mass spectrometry.

This experiment was repeated a further two times, following the method described in 2.2.10, with the exception that after induction, the incubation temperature was lowered in the first repeat experiment to 20 °C. After the same results were observed during gel electrophoresis analysis, the second repeat experiment used a temperature of 15 °C after induction, with the incubation time being increased to 24 h to obtain sufficient His-TEV

CypD protein expression in such a low temperature. Unfortunately the results obtained from these two experiments were identical to those obtained and shown in Figure 4.8.

In conclusion, despite using a range of different bacterial cell lines and also different induction conditions and media types, the full length His-TEV CypD protein appeared to be insoluble when expressed. It may have been possible to buy in more bacterial expressing cell lines and keep repeating this technique until eventually a soluble expression system was found, but that would have been costly and time consuming.

Also, by introducing another point mutation into the His- TEV CypD sequence this may have changed the conformation sufficiently to allow soluble His-TEV CypD expression and purification, but introducing a different mutation other than the K133I point mutation found in the $\Delta CypD^{K133I}$ construct would have complicated the analysis of this hypothesis further, as a full length non- mutated construct was most needed in order to gain further knowledge about this CypD-ABAD interaction. Therefore it was chosen to abandon work with the His-TEV CypD construct and proceed with another affinity tagged purification method and utilise a different fusion tag to aid purification; a full length glutathione S- transferase tagged (GST) CypD construct.

4.5   GST- tagged CypD experiments

4.5.1 pGEX-4T-1 CypD background

As the His-TEV CypD construct produced insoluble protein, it was necessary to utilise a different affinity tagged CypD protein in order to achieve the purification of a full length CypD protein. A full length GST-fusion CypD construct was therefore obtained from our collator Prof Shi Du Yan (University of Kansas). The full length CypD insert was cloned into the pGEX-4T-1 vector located between the *EcoR1* and *Xho1* restriction sites. This vector contains a thrombin protease cleavage site for GST tag removal. This vector is also ampicillin resistant. (pGEX-4T-1 CypD plasmid map is shown in Figure 4.9 and the DNA sequence can be found in Appendix A).
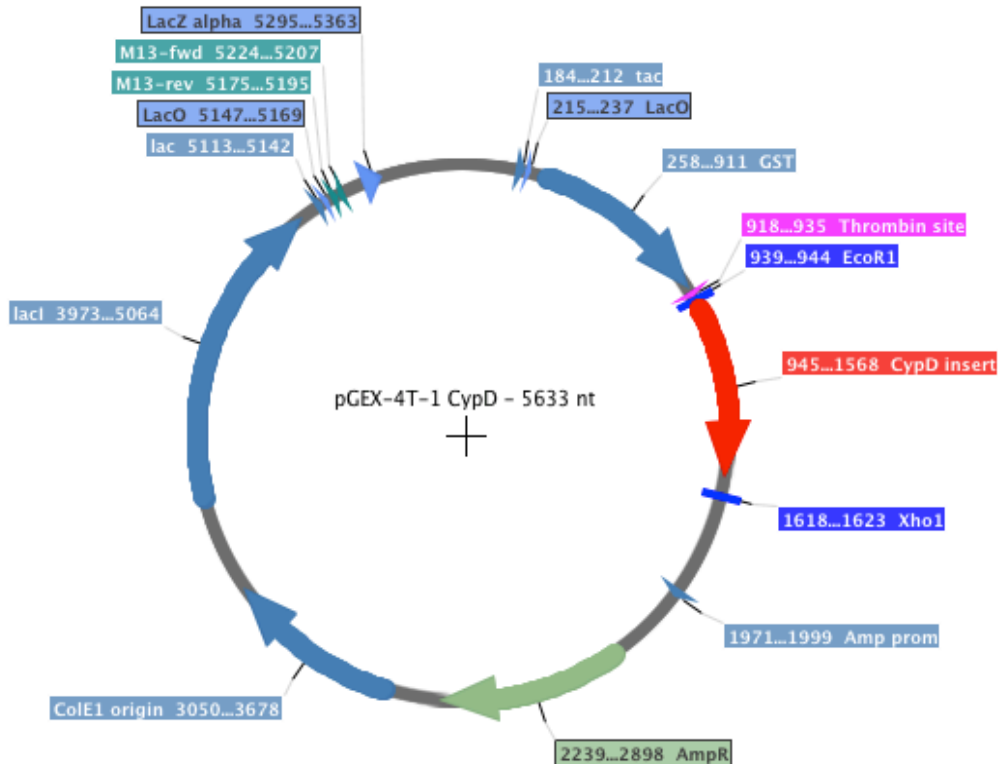
Figure 4.9: pGEX-4T-1 CypD. The full length CypD DNA insert (shown in red) is located between the *EcoR1* and *Xho1* restriction sites of the bacterial expression vector pGEX-4T-1. The antibiotic resistance for this construct is ampicillin. The GST tag is shown in blue and the construct contains a Thrombin cleavage site for GST tag removal which is shown in pink (MW= 49079.3 Da).

4.5.2 pGEX-4T-1 CypD expression and purification

In order to produce full length GST CypD protein, the GST CypD expressing plasmid was transformed into *E.coli* BL21 Codon Plus cells as described in section 2.1.8. Once again initial small scale induction tests (section 2.2.2) revealed that the GST CypD protein appeared to express well. Therefore, a large scale expression study was carried out (section 2.2.3) before proceeding onto GST CypD protein purification as detailed in section 2.2.7. The method for purification was adapted from the GE Healthcare GST protein purification manual, with certain inclusions such as increased concentration of DTT to improve CypD protein solubility.

Upon the addition of the thrombin protease in order to remove the GST tag, the GST tag was still found bound to the protein regardless of how many units of thrombin was added to the protein (gel image after electrophoresis is shown in Figure 4.10). Unfortunately, this finding was also found to be consistent with other co-researchers who had previously used this GST vector: therefore a different vector base, pGEX-6P-1 was selected for use which contains a PreScission protease cleavage site. Due to the large size of the GST tag (26 kDa) it was anticipated that the CypD protein may not fold as efficiently or maintain its conformation throughout protein expression and purification. This theory proved could be correct as it appears that the CypD protein could be folding in a way that prevents thrombin protease from working effectively.
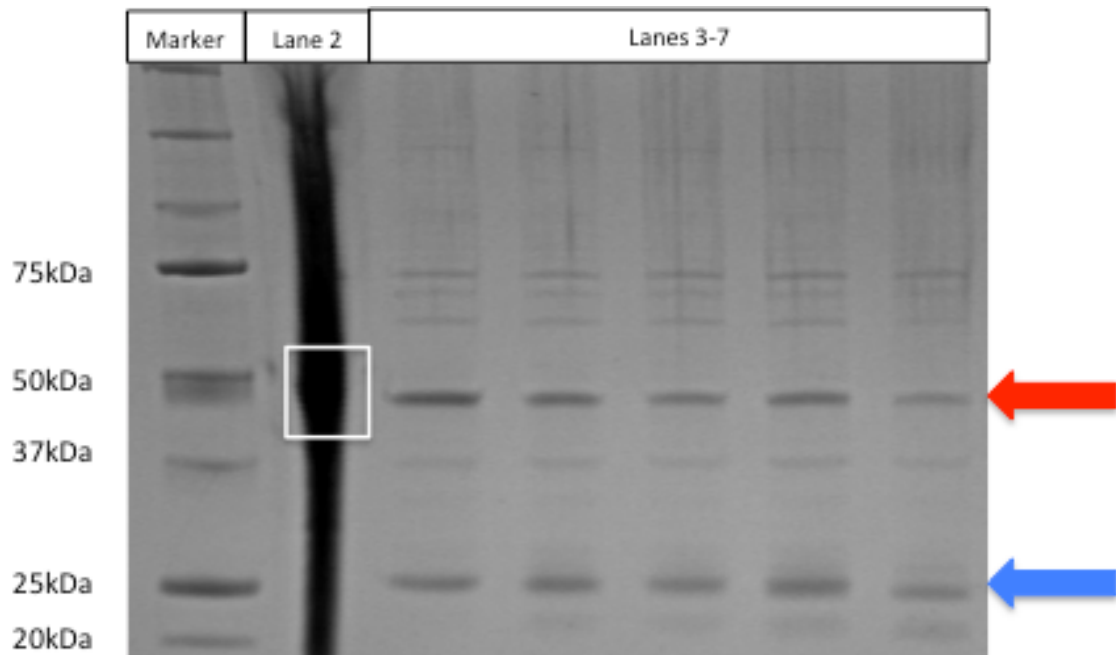
Figure 4.10: SDS-PAGE of the purification of pGEX-4T-1 CypD. Lane 2 is a crude bacterial fraction containing the GST CypD protein recovered after the first step of purification; cell lysis. The white box highlights the position of where the expected molecular weight of GST CypD would appear (49 kDa). Lanes 3-7 are GST CypD protein containing fractions recovered after the thrombin protease cleavage step of purification. The red arrow indicates that the GST CypD complex is still present and makes up the majority of the proteins in the solution. Initially it was thought that the protein band indicated by the blue arrow (in lanes 3-7) was the cleaved CypD protein, however when analysed by mass spectrometry it was found that this protein band was an uncoupled GST monomer. These results are representative of further experiments that were carried out to establish the correct ratio of thrombin: GST CypD protein for cleavage of the GST tag. Subsequently the parameters for the thrombin cleavage of the GST tag on the CypD protein could never be established.

4.5.3 pGEX-6P-1 CypD plasmid creation

An empty pGEX-6P-1 vector and its tag removal protease (PreScission) was a kind gift from Dr Jesko Koehnke (Prof Jim Naismith group, University of St Andrews). In order to create the pGEX-6P-1 CypD construct, both the pGEX-6P-1 vector and pGEX-4T-1 CypD were digested with *EcoR1* and *Xho1* to remove the CypD insert from the pGEX-4T-1 vector and to linearize the vector before ligation (described section 2.1.3). The restriction digest product was then run on a 2% agarose gel for optimal DNA separation

and the full length CypD containing DNA insert was isolated from the gel band as described in sections 2.1.4 and 2.1.5. The isolated CypD DNA was then ligated into the linearized pGEX-6P-1 vector as described in section 2.1.6. This process is shown in Figure 4.11.
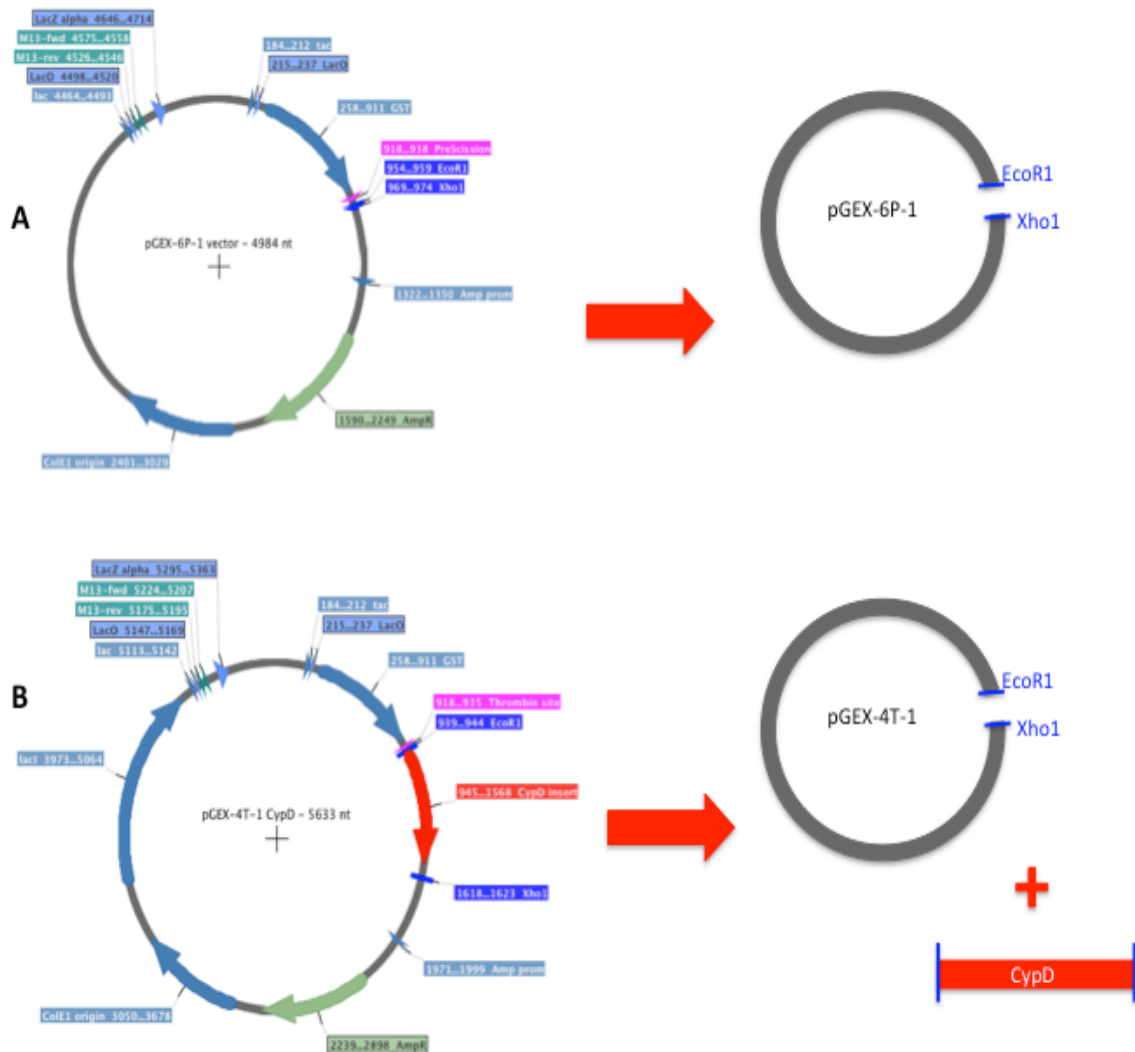
Figure 4.11: pGEX-6P-1 CypD plasmid preparation. **A)** pGEX-6P-1 vector was digested with *EcoR1* and *Xho1* to linearize the vector before ligation. **B)** pGEX-4T-1 CypD was digested with *EcoR1* and *Xho1* to remove the CypD DNA insert. (Continued overleaf)
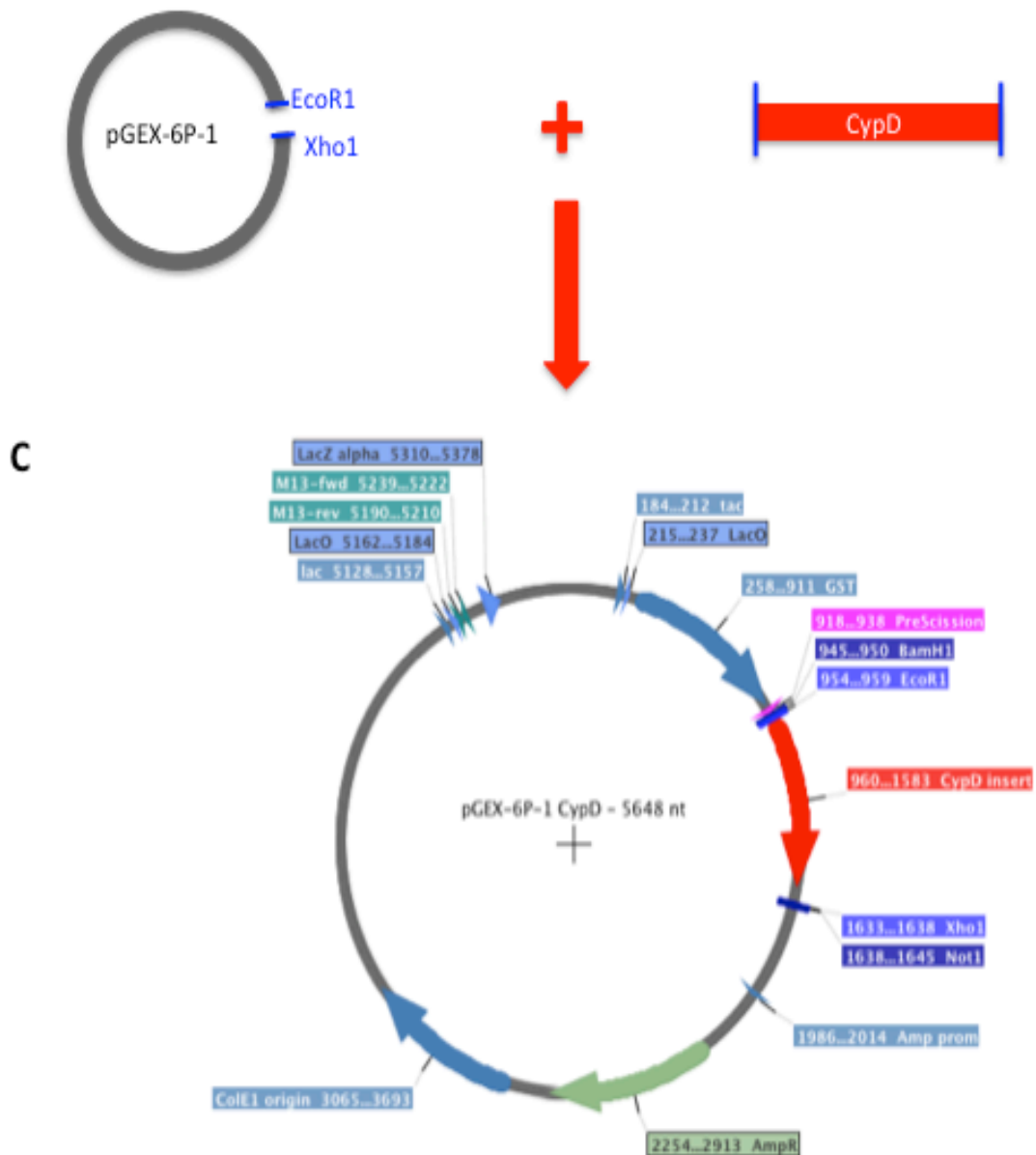
Figure 4.11: pGEX-6P-1 CypD plasmid preparation continued: C) Following gel extraction, the cut pGEX-6P-1 vector **(A)** was ligated with the isolated CypD DNA **(B)** resulting in the pGEX-6P-1 CypD plasmid formation.

4.5.4 pGEX-6P-1 CypD expression and purification

Before pGEX-6P-1 CypD protein could be expressed and purified it was necessary to express and purify a large quantity of PreScission protease in order to be able to cleave

the GST tag. This is a straightforward purification process using a GSTrap column containing glutathione sepharose, which is capable of binding a GST- tagged protein, whilst other impurities will flow through the column. This is described in more detail in section 2.2.8. Mass spectrometry and gel electrophoresis analysis confirmed that only PreScission protease had ben produced (shown in Figure 4.12).

Firstly the pGEX-6P-1 CypD (GST CyD) expressing plasmid was transformed into *E.coli* BL21 Codon Plus cells as described in section 2.1.8. Initial small scale induction (section 2.2.2) revealed that the GST CypD protein appeared to express well. Therefore, a large scale GST CypD expression was carried out (section 2.2.3) proceeding onto purification as detailed in section 2.2.9. Again, the method for purification was adapted from the GE Healthcare GST protein purification manual, with certain inclusions such as the increased concentration of DTT to improve protein solubility and overnight incubation of PreScission protease (with dialysis) to allow complete removal of the GST tag. Following purification, the recovered, pure, full length CypD protein was flash frozen in liquid nitrogen and stored at -80 °C. The yield was slightly lower than anticipated as there appeared to be a large amount of uncoupled GST monomers and dimers produced after lysis, however on average approximately 50 mg of protein was recovered from a 6 L bacterial expression. Due to the small size difference of 3 kDa between GST monomers (26 kDa) and CypD protein (23 kDa) it is difficult to determine which gel band relates to pure protein and which is the GST tag after gel electrophoresis (section 2.2.1), so to be completely sure all bands were confirmed by mass spectrometry analysis before advancing the protein into any other studies. Figure 4.12 summaries the images obtained throughout the purification procedure after gel electrophoresis.
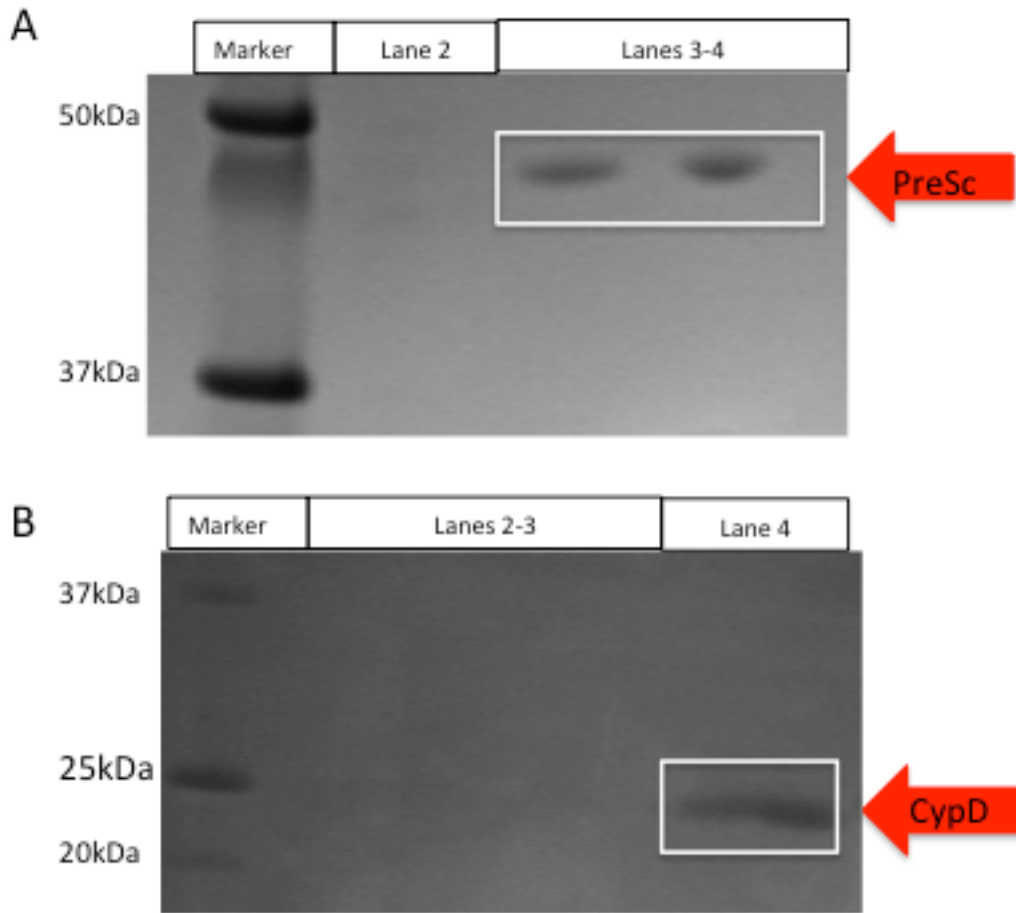
Figure 4.12: Purification of PreScission protease and pGEX-6P-1 CypD A) An image of a gel taken after the protein purification of PreScission protease. Lane 2 is empty, lanes 3 and 4 contain one protein band (indicated by the white box) found at the expected molecular weight of pure PreScission protease (48 kDa). This was confirmed by mass spectrometry before being used in the pGEX-6P-1 CypD purifications for GST tag removal. **B)** A gel image taken after gel electrophoresis, at the end of the CypD protein purification method. Lanes 2 and 3 are empty, lane 4 contains one protein band (indicated by the white box) found at the expected molecular weight of purified full length CypD (MW=23 kDa).

4.5.5 <u>Full- length CypD crystallisation trials</u>

With the success of being able to produce for the first time full length untagged CypD protein, the purified CypD protein (22.5 mg/mL) was used to setup crystal trials as detailed in section 2.4.2. For these trials both native CypD and CypD-ABAD trials were setup in order to see if any crystals could be achieved. Native CypD is a stable protein, however when this was added, in equal molar ratios, to the ABAD protein, precipitation

was observed in some of the wells. This could possibly have been due to differences in storage buffer as ABAD is quite unstable to a change in environment.

Both the CypD alone and co-complex CypD-ABAD trials, carried out in various buffer and precipitant conditions (detailed in Appendix A), failed to produce any good quality crystals that could be taken further into crystal trial optimisation studies or diffraction studies. However this finding may not be surprising, as no full- length CypD construct has been crystallised to date, and only the truncated mutant (ΔCypD^{K133I} construct) has been published. Therefore, as the ΔCypD^{K133I} construct was designed with a K133I mutation in order to improve the contacts made upon crystallisation and to enable the correct protein folding it was deemed logical to produce a full length CypD construct with a matching K133I mutation.

4.6   pGEX-6P-1 CypD^{K133I} construction

4.6.1 pGEX-4T-1 CypD^{K133I} construction

On inspection of the pET-21a ΔCypD^{K133I} plasmid sequence it was found that this plasmid shared two restriction sites (*Nco1* and *Not1*) with the pGEX-4T-1 CypD plasmid around the lysine 133 residue. Therefore 5 µg of both the ΔCypD^{K133I} and pGEX-4T-1 CypD plasmids were digested with *Nco1* and *Not1* (described in section 2.1.3). A 2% agarose gel (section 2.1.4) was used to separate the fragments from the vectors and the DNA was isolated from the gel band as described in section 2.1.5. The 250bp fragment containing the K133I mutation was ligated with the cut pGEX-4T-1 vector as described in section 2.1.6, producing colonies which could then be picked and transformed into DH5α cells (section 2.1.8) and verified by The University of Dundee's sequencing service. This plasmid construction was successful and is outlined in Figure 4.13.
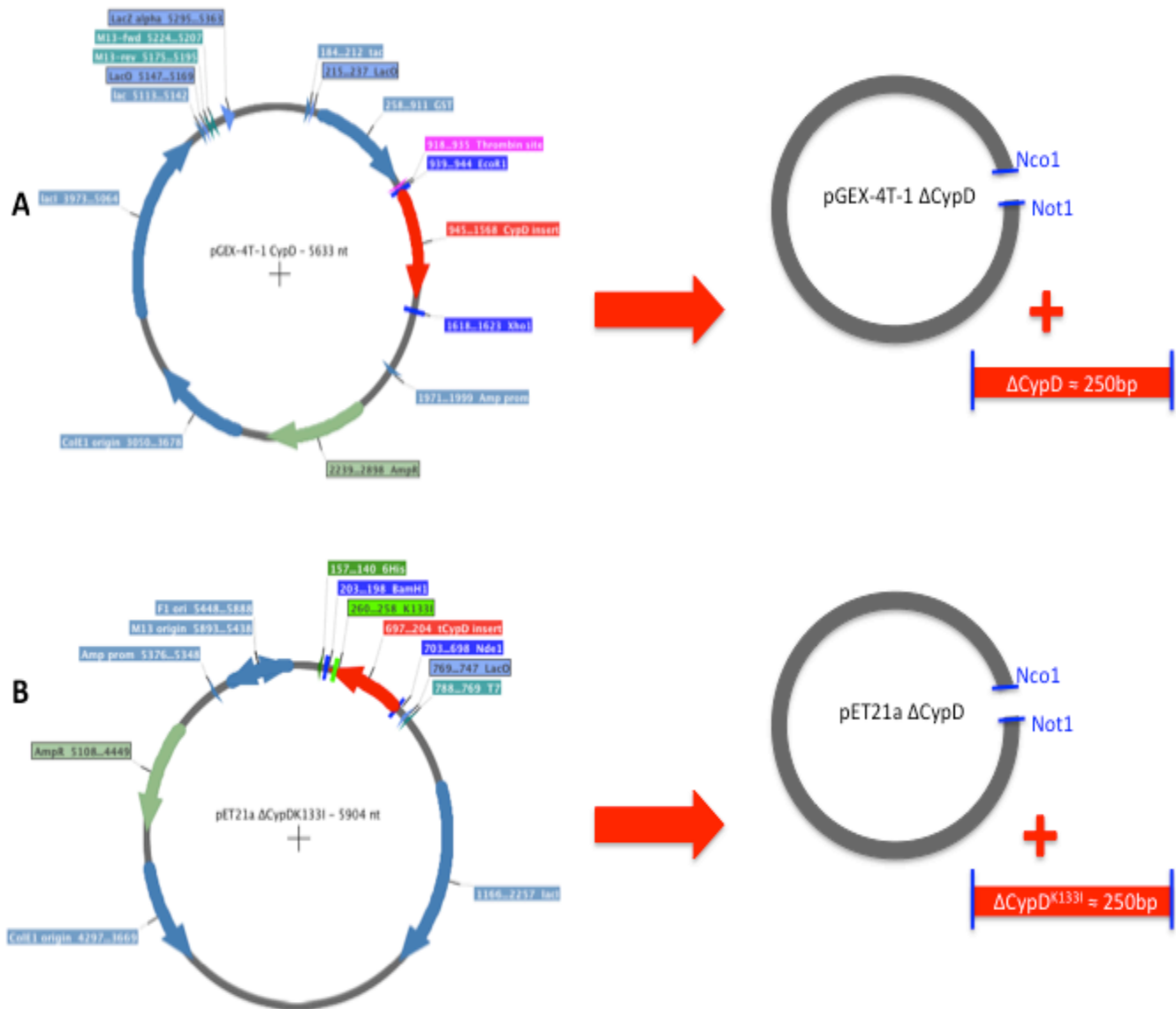
Figure 4.13: Schematic representation of pGEX-4T-1 CypD^{K133I} construction. **A)** pGEX-4T-1 CypD was digested *Nco1* and *Not1*. After separation with gel electrophoresis a gel band indicating the presence of a cut pGEX-4T-1 vector (DNA was then isolated and purified) and another gel band indicating the small piece of digested CypD (which was discarded). **B)** pET-21a ΔCypD^{K133I} was digested with *Nco1* and *Not1*. After separation by electrophoresis, the gel band present at approximately 250 bp was isolated and the DNA was purified, as this was thought to be the DNA insert containing the K133I mutation. (Continued overleaf)
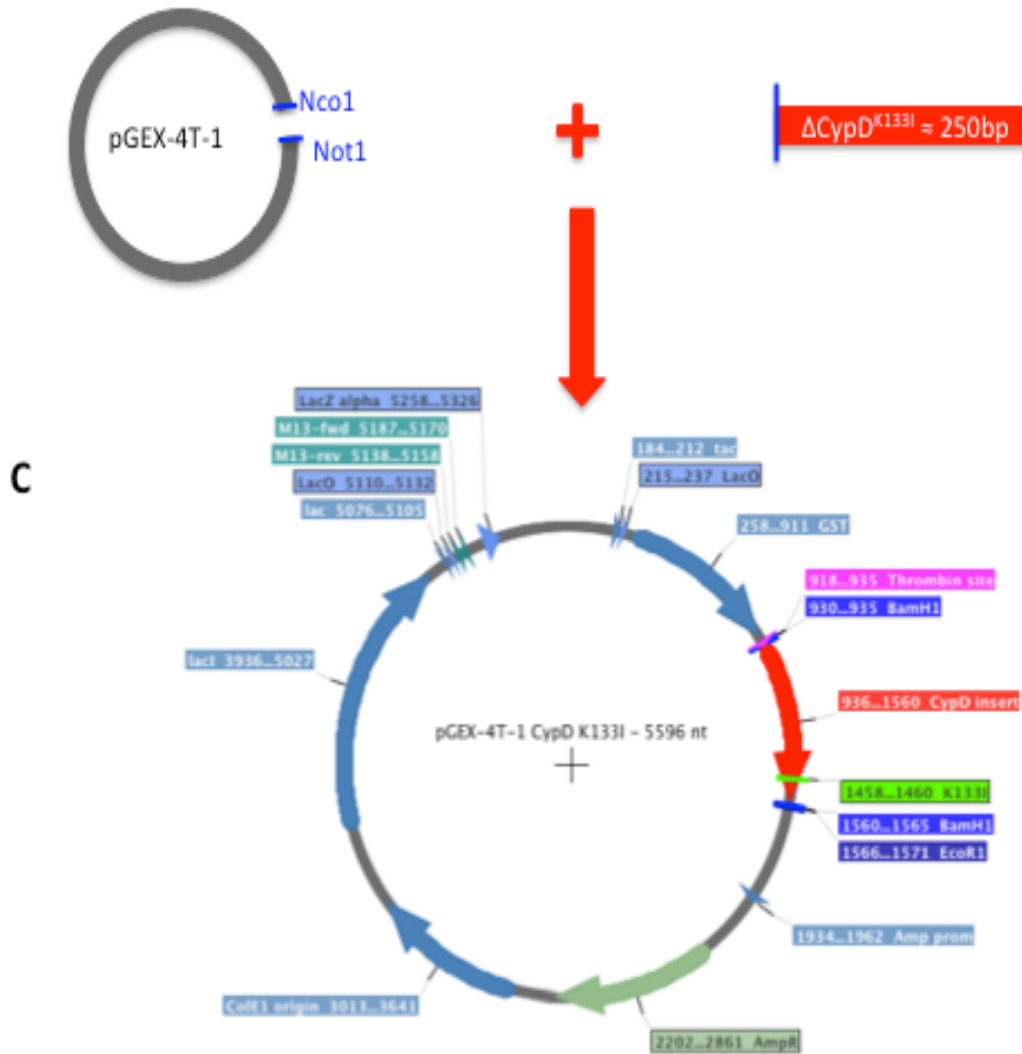
Figure 4.13: Schematic representation of pGEX-4T-1 CypD^{K133I} construction continued. C) pGEX-4T-1 **(A)** and the ΔCypD^{K133I} ≈ 250 bp **(B)** were ligated to form the pGEX-4T-1 CypD^{K133I} vector. This was confirmed by DNA sequencing.

Since thrombin GST tag cleavage is not possible during pGEX-4T-1 CypD protein purification, it was therefore necessary to remove the CypD^{K133I} insert from the pGEX-4T-1 vector and incorporate it into the pGEX-6P-1 vector to produce a pGEX-6P-1 CypD^{K133I}. This expression vector was chosen, as the GST tag removal by PreScission protease was successful in the native pGEX-6P-1 CypD purification (as described in 4.5.4). As pGEX-6P-1 CypD can be purified completely to produce full length CypD protein, it would have been advantageous to use this vector to produce a pGEX-6P-1

CypD^{K133I} plasmid. Unfortunately the restriction sites (*Nco1* and *Not1*), found in the pGEX-4T-1 and pET-21a ΔCypD^{K133I} plasmids, were not shared with the pGEX-6P-1 CypD plasmid; therefore it was not possible to clone this mutation directly into the pGEX-6P-1 CypD plasmid. Site directed mutagenesis was also carried out on the pGEX-6P-1 CypD plasmid, however this also failed to successfully produce a pGEX-6P-1 CypD^{K133I} plasmid.

4.6.2 pGEX-6P-1 CypD^{K133I} construction

Adopting a similar strategy used in section 4.6.1, the pGEX-4T-1 CypD^{K133I} plasmid and the pGEX-6P-1 CypD plasmid were used to produce a pGEX-6P-1 CypD^{K133I} construct (outlined in Figure 4.14). By carrying out a symmetrical restriction digest with *BamH1*, on both plasmids (section 2.1.3) this left a cut, linearized pGEX-6P-1 ΔCypD vector and a 222 bp DNA fragment containing the K133I mutation. High fidelity enzymes (New England Biolabs) were used in these digestions, as the standard Promega enzymes did not give a successful digestion. The DNA band at the expected 222 bp size (separated with gel electrophoresis) was isolated from a 2% agarose gel (section 2.1.4). Before ligation the open pGEX-6P-1 ΔCypD vector was treated with calf intestine alkaline phosphatase to prevent self-ligation. Following ligation (section 2.1.6) colonies were transformed into DH5α cells and the CypD DNA was extracted (section 2.1.8). The CypD DNA was further digested with *Sal1* and *Nco1*. The identification of a gel band at the expected molecular weight after gel electrophoresis was used to indicate if the colony contained the entire CypD^{K133I} insert in the correct orientation. Those colonies that contained a gel band at approximately 620 bp were sent to The University of Dundee's sequencing service for further conformation. This pGEX-6P-1 CypD^{K133I}

plasmid construction was made successfully and gel electrophoresis results are shown in Figure 4.15.
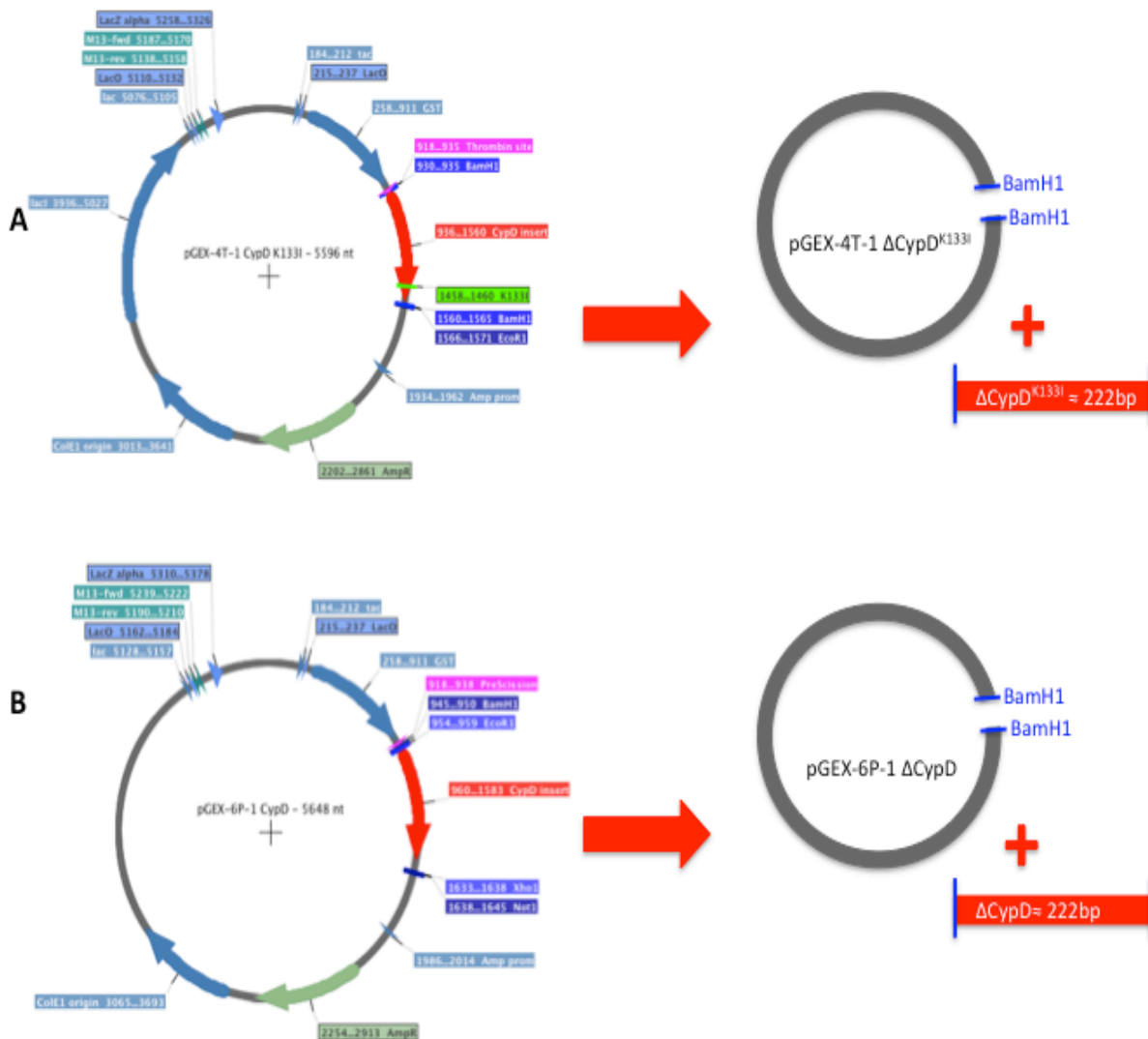
Figure 4.14: Schematic representation of pGEX-6P-1 CypD^{K133I} construction. A) pGEX-4T-1 CypD^{K133I} was digested with *BamH1*. After separation by gel electrophoresis this produced a gel band at approximately 222 bp, which was the expected molecular weight for the cut ΔCypD^{K133I} DNA. B) pGEX-6P-1 CypD was digested with *BamH1*. After separation by gel electrophoresis there were two gel bands present, one at approximately 222 bp and the larger band presumed to be pGEX-6P-1 ΔCypD.
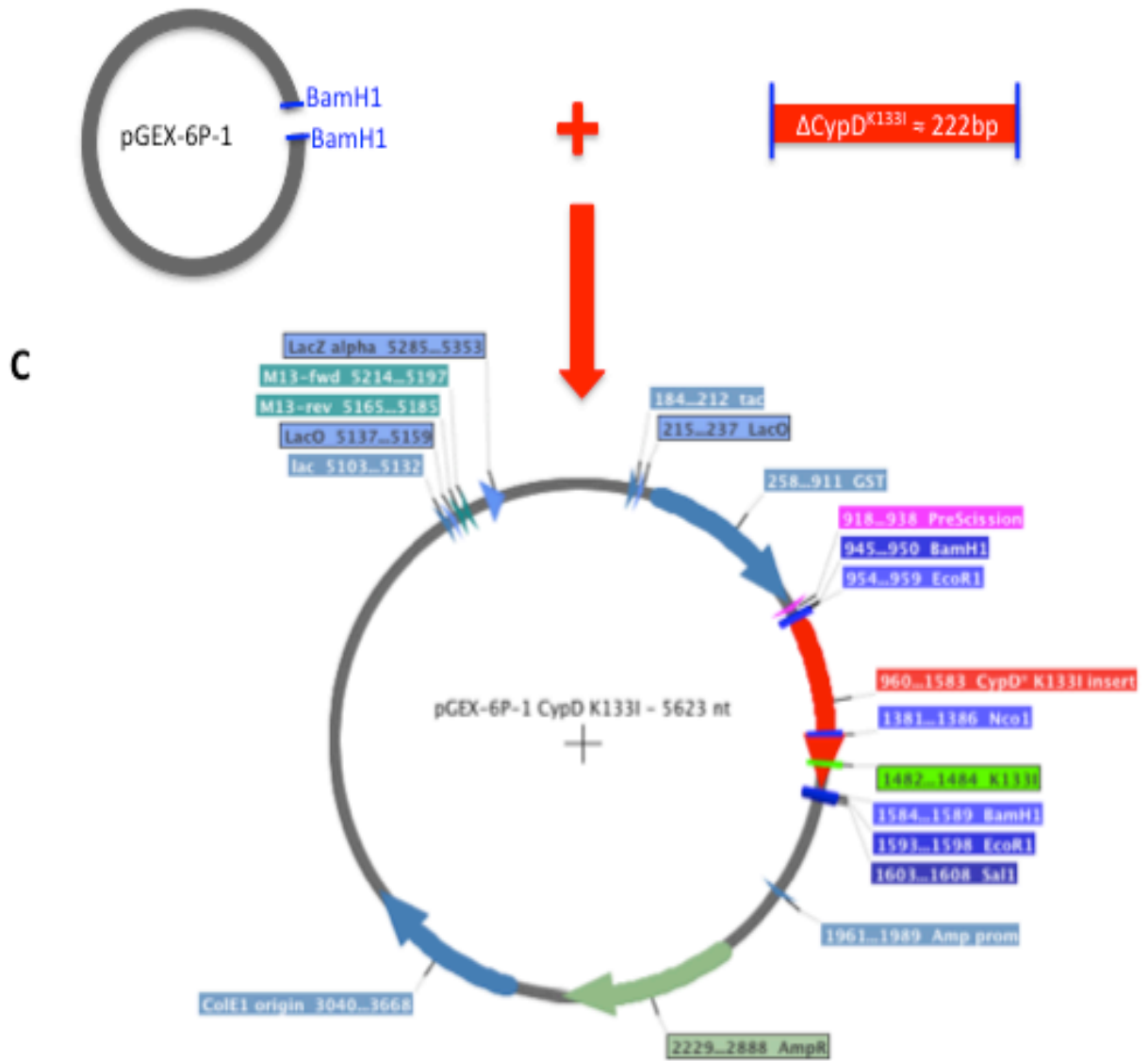
Figure 4.14: Schematic representation of pGEX-6P-1 CypD^{K133I} construction continued: C) Following DNA isolation the extracted pGEX-6P-1 ΔCypD DNA was treated with alkaline phosphatase and then ligated with the ΔCypD^{K133I} DNA. This was firstly confirmed by digestion with *Sal1* and *Nco1* (Figure 4.15) and then subsequently confirmed by DNA sequencing.
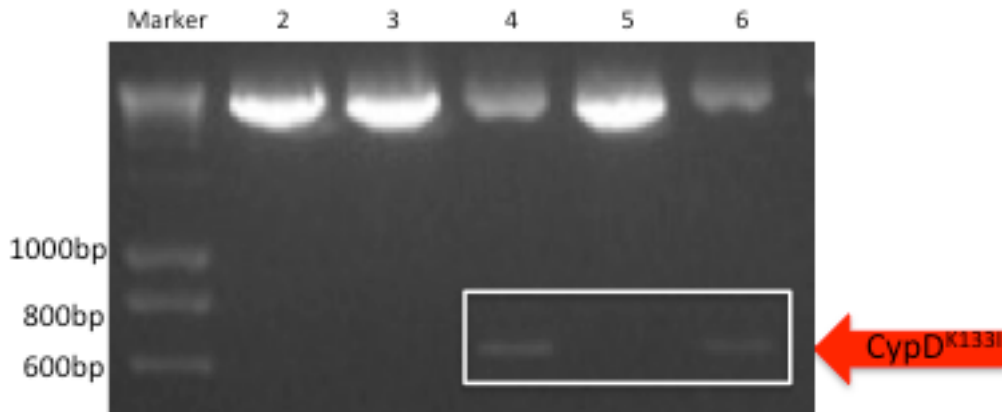
Figure 4.15: Agarose gel of pGEX-6P-1 CypD^{K133I} DNA. Following ligation, colonies were grown and transformed into DH5α cells and new pGEX-6P-1 CypD^{K133I} DNA was isolated from the cells. The DNA from each grown colony was then digested with Sal1 and Nco1 to determine if the plasmid had ligated together effectively and in the correct orientation. Gel electrophoresis was carried out and corresponding colonies that produced a DNA band at 620 bp (highlighted by the white box) were deemed to have successfully incorporated the CypD gene containing a K133I mutation. The DNA obtained from the gel bands in lanes 4 and 6 (at the expected 620 bp size) were confirmed by DNA sequencing as pGEX-6P-1 CypD^{K133I} DNA.

4.6.3 Full length CypD^{K133I} crystallisation trials

Finally having made a pGEX-6P-1 CypD^{K133I} protein construct, it was transformed into E.coli BL21 Codon Plus cells (as described in section 2.1.8), then expressed and the CypD^{K133I} protein purified as described in sections: 2.2.2, 2.2.3, 2.2.8, 2.2.9 and 4.5.4. Only a small amount of CypD^{K133I} protein was recovered. As was also found in pGEX-6P-1 CypD purification, there was evidence of degradation of the protein after cell lysis. However the protein was soluble and the GST tag was cleaved easily by PreScission protease. The overall yield of CypD^{K133I} protein obtained was in the region of 20 mg from a 4 L of bacterial culture. A possible way of reducing the amount of degradation present after cell lysis is to use another method, such as sonication, to disrupt and lyse the cells.

Using CypD^{K133I} purified protein a small number of crystal trials were setup as in section 4.5.5. These trials failed to produce any good quality CypD^{K133I} crystals or CypD^{K133I}- ABAD co-crystals that could be taken further into crystal trial optimisation studies or diffraction studies.

4.7   <u>Conclusion and summary of results</u>

From the experiments presented in this chapter it was established that the truncated mutant CypD protein (ΔCypD^{K133I}) was not shown to bind to ABAD protein in both Isothermal titration calorimetry (ITC) experiments (in the micromolar range) and through co-crystallography trials. From these experiments it was not possible to rule out why the ΔCypD^{K133I} protein did not bind ABAD and there are three possibilities:

1) The K133I mutation present within the ΔCypD^{K133I} construct could be preventing the interaction from occurring.

2) The binding site for the ABAD-CypD interaction is located in the truncated N-terminal region and some of the missing amino acids are required to hold the structure in the correct conformation for an interaction to occur.

3) CypD protein does not bind to ABAD.

Although the co- crystal trials were unsuccessful, it was possible to produce diffracting crystals of the native ΔCypD^{K133I} protein, thus replicating previously published data (Schlatter *et al.* 2005).

In order to try and solve some of these possibilities it was necessary to construct a full-length CypD encoding construct and a full-length CypD encoding construct with the K133I mutation (summaries of all the various CypD encoding constructs used in this chapter are shown in Figure 4.16). Eventually, after a long period of method development and purification issues, two full-length constructs pGEX-6P-1 CypD and pGEX-6P-1 CypD^{K133I} were constructed successfully. These constructs were used to produce protein, that when purified progressed, into crystal trials; however as yet no good quality crystals have been made and therefore they have not progressed onto optimisation and diffraction trials. This is unsurprising as there are no full length CypD

protein constructs that have been crystallised and published to date. The conclusion and discussion of these results as well as future perspectives is described further in Chapter 6.
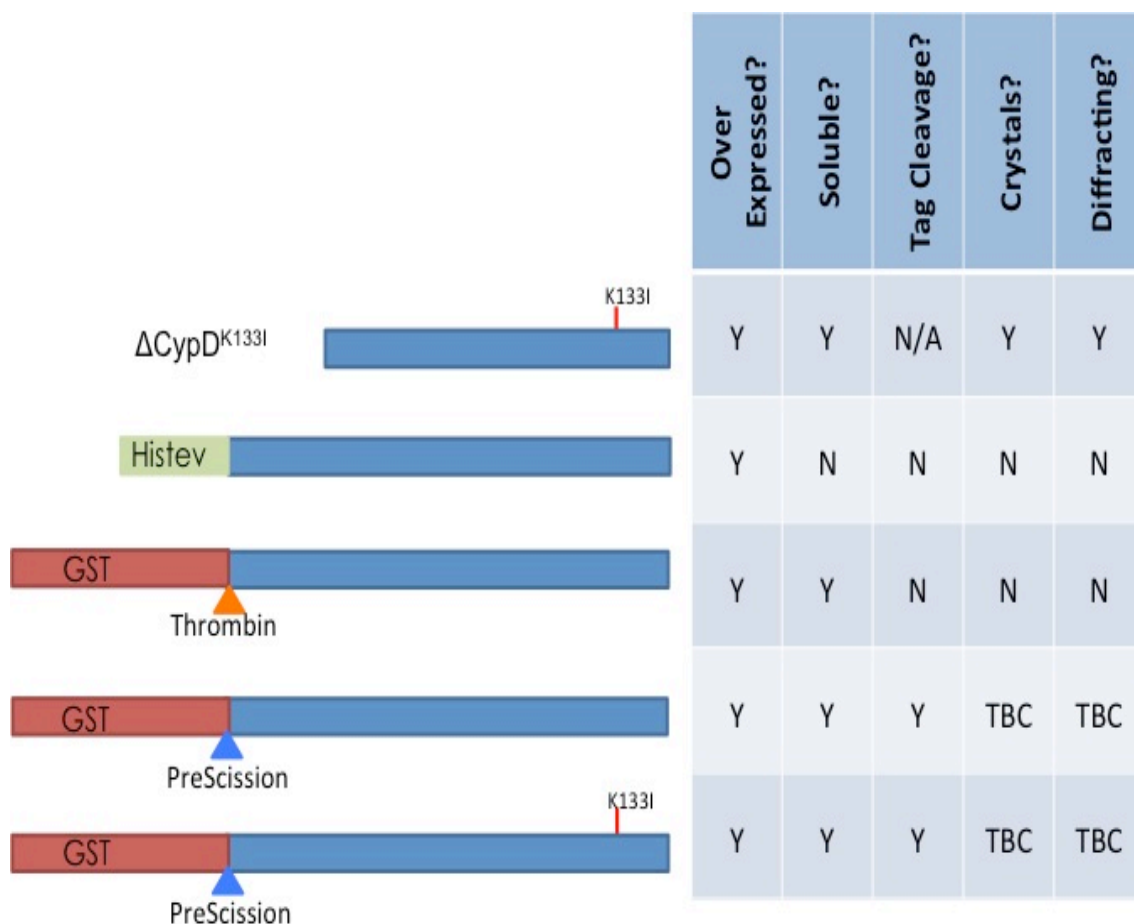
Figure 4.16: The 5 CypD proteins described in chapter 4. **Left)** Represents how the protein is constructed and in particular details the various length, tag and mutation differences between each construct. The blue area represents the CypD region, the tags to aid purification are shown along with their corresponding cleavage sites. If the protein contains the K133I mutation this is also shown. **Right)** Represents the development stages of the protein and how the protein has performed during each phase. (Y= Yes/successful, N= No/unsuccessful, TBC= to be confirmed/on-going work). Protein seqences can be found in Appendix A.

Chapter 5: Assay development for investigating a Frentizole based analogue series as a potential inhibitors of the ABAD- Aβ interaction

5.1   <u>Introduction</u>

It has been established that the interaction between ABAD and Aβ can lead to harmful effects on cell viability along with subsequent damaging effects on the cognitive performance in transgenic AD mouse models, thus reflecting the importance of these cellular effects on disease progression. These studies indicate that the ability to block this interaction could provide a potential target for the treatment of AD (Muirhead *et al.* 2010).

At the cellular level, the decoy peptide (described in 1.4.4) has been used to block the ABAD- Aβ interaction, and this peptide produced a significant decrease in Aβ toxicity, transfected cells exhibited decreased apoptosis, decreased LDH release and increased cell viability in response to Aβ treatment when compared with untransfected cells (Yang *et al.* 2007). These beneficial responses have also been shown in animal models (Yao *et al.* 2011). Specifically, when transgenic mice over- expressing mAPP (Tg mAPP) were treated with the decoy peptide these transgenic mice exhibited a preserved mitochondrial function when compared to untreated animals (Yao *et al.* 2011). Also, two protein biomarkers peroxiredoxin II and endophilin 1, the levels of which are both increased as AD progresses, were found to be significantly reduced in Tg mAPP animals when compared to non- transgenic mice (Yao *et al.* 2011). Behavioural symptoms associated with the transgenic AD animal models have also been reversed with the treatment of the decoy peptide in Tg mAPP mice (Yao *et al.* 2011). Although the decoy peptide is not deemed a suitable drug candidate due to its small size and poor half-life, these studies have shown that inhibiting the ABAD- Aβ interaction has beneficial effects at all levels, and would be a suitable drug target in the treatment of AD.

As previously discussed in section 1.4.4 there have been a variety of potential small molecule inhibitors of the ABAD- Aβ interaction identified, that could help to potentially slow down the progression of AD. Xie *et al.* identified one such inhibitor, frentizole, in 2006. Since then, no further journal articles have been published using frentizole as an inhibitor of the ABAD- Aβ interaction, and recent speculation would suggest that in its present form, the frentizole's immunosuppressant action has more harmful side effects than positive therapeutic effects (Professor Sir Mark Pepys FRS, personal communication). However, using this compound as a starting structure, our collaborator, Dr Kamil Musilek (University of Hradec Kralove, Czech Republic), has designed a series of 28 frentizole analogues, which required further testing to establish if these compounds would inhibit the ABAD- Aβ interaction, and to determine if any of these analogues could be developed further into 'drug like' molecules.

In order to evaluate these analogues, at the molecular level, a series of assays were specifically developed and modified. These assays were:

- The *in vitro* ABAD enzyme activity assay, which utilises ABAD's co-factor (NAD^+) and measures NAD^+ production/ consumption over time.

- A morphology specific single colour fluorescence quenching assay for monitoring Aβ aggregation.

- Thermal shift analysis, of ABAD- Aβ and the analogue series to determine where the analogue is potentially interacting.

- The use of the *Fortebio* Octet RED 384 system to study in real time, the ABAD- Aβ interaction and to detect and analyse the kinetics of potential drug compounds.

5.1.1 <u>A morphology specific single colour fluorescence quenching assay for monitoring Aβ aggregation</u>

The formation of Aβ extracellular plaques is a hallmark for AD, but this is not the only form of amyloid structure present in an AD state. Aβ peptides are capable of aggregating into many forms including: smaller fibril structures (Jan *et al*. 2010), globule like structures (Nichols *et al*. 2005) and more dense plaque like structures (Su & Chang 2001). The many aggregation forms that Aβ can adopt have made it very difficult to produce reproducible results within an assay. However it is now possible to reliably control which Aβ aggregation morphology is prepared so that this hurdle can be overcome.

Aβ aggregates forming a fibrillar morphology which can be promoted with the addition of HFIP (1,1,1,3,3,3-hexafluoro-2-propanol) to the monomerised form of Aβ peptide (Jan *et al*. 2010). Similarly larger Aβ structures adopting a globule like morphology can be promoted with the addition of sodium chloride (NaCl) to monomerised Aβ and this is deemed to be the most physiological type of *in vitro* Aβ aggregation (Nichols *et al*. 2005). By altering the pH of monomerised Aβ to acidic pH 6, this promotes the Aβ aggregation in the form of plaque like structures (Su & Chang 2001). The ability to produce different morphologies and the differences in the structures of these aggregates are illustrated in Figure 5.1.
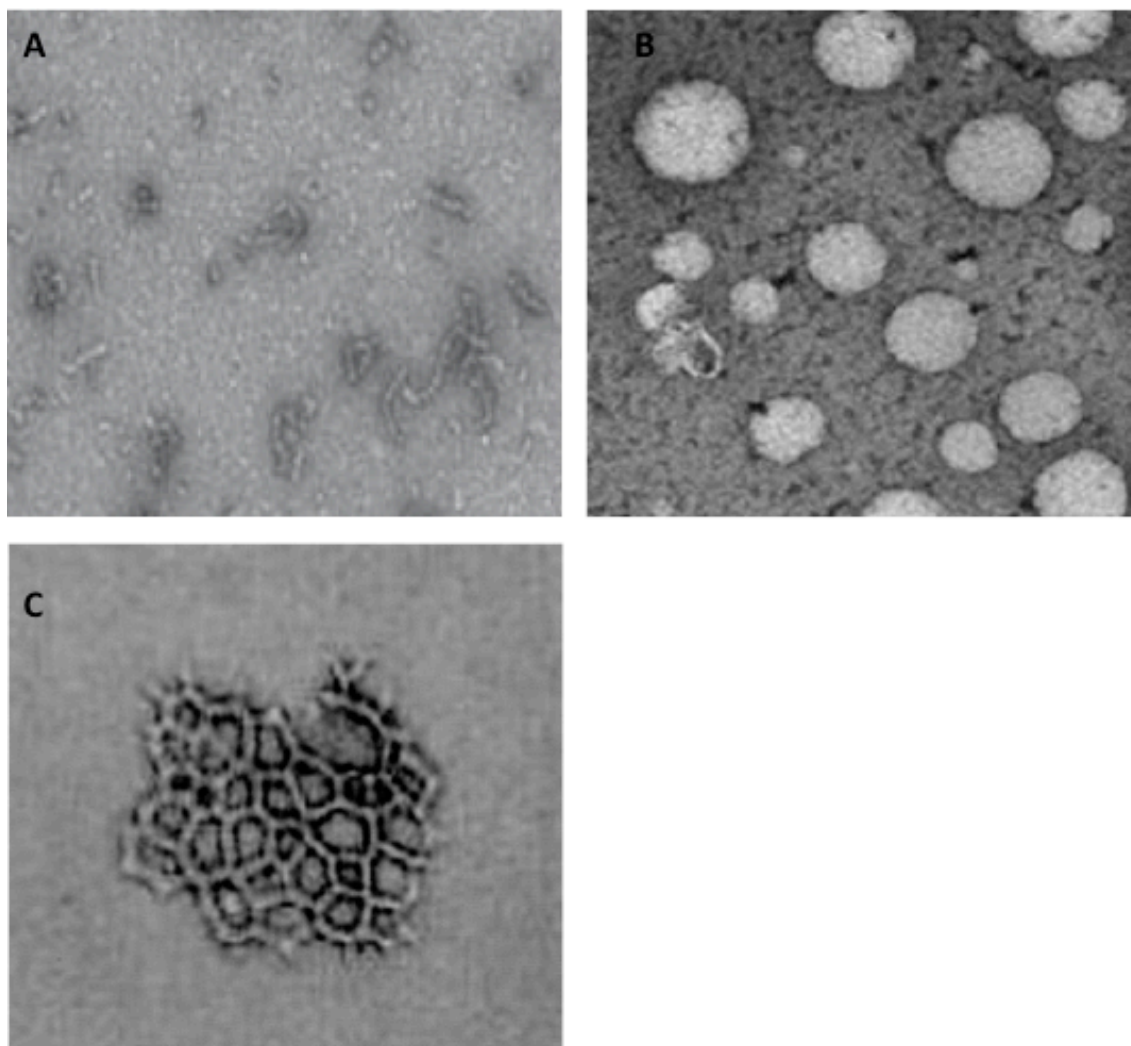
Figure 5.1: Transmission electron microscopy (TEM) images illustrating the ability to induce morphological specific Aβ aggregation from monomerised Aβ. A) Fibril like structures obtained by the addition of 150 mM NaCl in 50 mM Tris-HCl buffer (pH 7.9) to monomerised Aβ (Jan *et al.* 2010). **B)** Globule like structures obtained by the addition of 1.5% (v/v) HFIP to monomerised Aβ (M. R. Nichols *et al.* 2005). **C)** Plaque like structures obtained by altering the pH of the monomerised Aβ to an acidic pH 6 (Y. Su & P.-T. Chang 2001).

To detect Aβ aggregates, small biomarkers such as Congo Red and Thioflavin T (ThT) that specifically bind to the β-sheet structure of amyloid can be used (Maezawa *et al.* 2008). However, both assays are unable to differentiate between Aβ morphological states and are therefore are inadequate not only in the understanding of Aβ aggregation and its link to AD, but also from a therapeutic perspective to search for morphology

specific inhibitors and *in vivo* imaging agents. Subsequently, an alternative approach has been developed using fluorescently tagged Aβ peptides to detect Aβ aggregation in a morphology specific fluorescent quenching manner. This utilises commercially available N-terminal labeled Aβ peptides (labeled with HiLyte Fluor 555 (Aβ$_{555}$)) as a powerful tool to monitor continuously in real-time the Aβ aggregation process and to distinguish between Aβ morphologies (S. Quinn, University of St Andrews, unpublished data).

5.1.2 <u>ABAD enzyme activity assay as an *in vitro* tool for evaluating potential inhibitors of the ABAD-Aβ interaction</u>

One of the most reported methods used to investigate the function of ABAD is by measuring the catalytic activity of the oxidation and reduction of alcohols and ketones (He *et al*. 2001; Oppermann *et al*. 1999; Yan *et al*. 1999). Furthermore, the role of its co-factor NAD$^+$ in these reactions allows the reaction rate to be measured by the production or consumption of NAD$^+$ at 340 nm. (ε= 6220 M^{-1} cm^{-1}) using a UV spectrophotometer (Muirhead 2011). As time increases, the NAD$^+$ absorbance decreases and this change in absorbance over time is proportional to the rate of NAD$^+$ consumption.

In order to analyse the therapeutic effect of any potential inhibitors of the ABAD- Aβ interaction it is important to test directly the ABAD activity. If ABAD and Aβ are interacting then the ABAD activity decreases because the protein is no longer able to function normally. Therefore, by observing changes in the ABAD activity, it may be

possible to assess any potential inhibitors of the interaction (an inhibitor of the ABAD-Aβ interaction would be predicted to show an increase in ABAD activity when compared to the results from ABAD- Aβ tests alone). The nature of this assay, also allows chemically modified compounds to be tested and analysed for their effectiveness in blocking the ABAD- Aβ interaction; as the therapeutic effects increase the ABAD activity would also be expected to rise. Therefore in an inhibitor analogue series, with systematic chemical modifications, it is possible to determine which functional groups are key for achieving the inhibitory effect (structure activity relationship (SAR) analysis) using the ABAD enzyme activity assay.

5.1.3 **Frentizole analogue series**

Frentizole is an non toxic, immunosuppressant drug which is used clinically in a variety of applications including lupus erythematosus and rheumatoid arthritis (Scheetz *et al.* 1977; Xie *et al.* 2006). Xie *et al* established frentizole as a potential inhibitor of the ABAD- Aβ interaction during an ELISA screen of biotinylated ABAD, with Aβ and 50 commercially available chemicals that could potentially disrupt the ABAD- Aβ interaction. The commercially available chemicals were specifically chosen for their structural likeness to Congo red and thioflavin T (two compounds known to bind to amyloid) or their previously reported neuroprotective effects (Xie *et al*. 2006). Frentizole, a benzothiazole urea, was chosen due to its structural similarity to thioflavin T (shown in Figure 5.2).
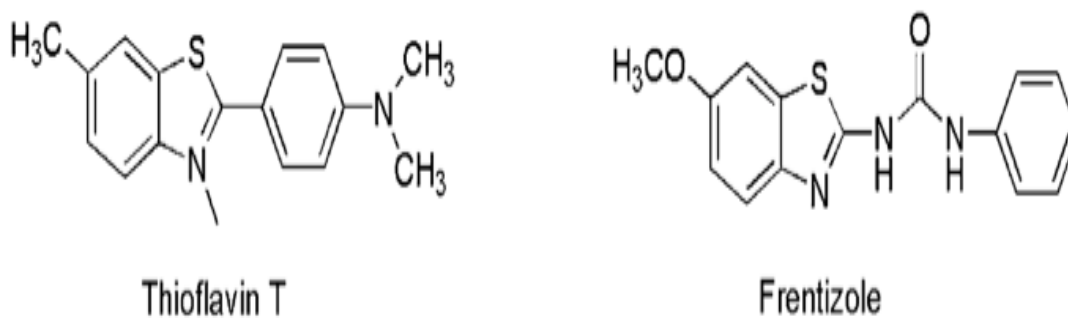
Figure 5.2: The chemical structures of thioflavin T and frentizole

Xie *et al*. reported an initial IC_{50} value= 230 μM for frentizole as an inhibitor of the ABAD- Aβ interaction, this was a slight improvement when compared to thioflavin T which has an IC_{50} value= 200 μM. Therefore, they designed 45 analogues based on frentizole to permit SAR analysis to be carried out. The variations in the analogues were designed to alter the aromatic rings and their linking groups. The SAR analysis revealed that the urea moiety was required for inhibition and that substitutions on the benzothiazole and phenylurea rings dramatically altered compound potency (Xie *et al*. 2006). The substitutions that were favoured on the benzothiazole ring were small electron withdrawing groups, in particularly those compounds containing a chlorine and fluorine in this position were the most potent (Xie *et al*. 2006). Also, the addition of a hydroxyl group in the para position of the phenylurea rings dramatically increased the potency of the compound. The two compounds from the analogue series that proved to be the most potent inhibitors of the ABAD- Aβ interaction (under ELISA screening) were 5h and 5l; both compounds produced an $IC_{50}< 10$ μM. The chemical structure of these compounds is shown in Figure 5.3.
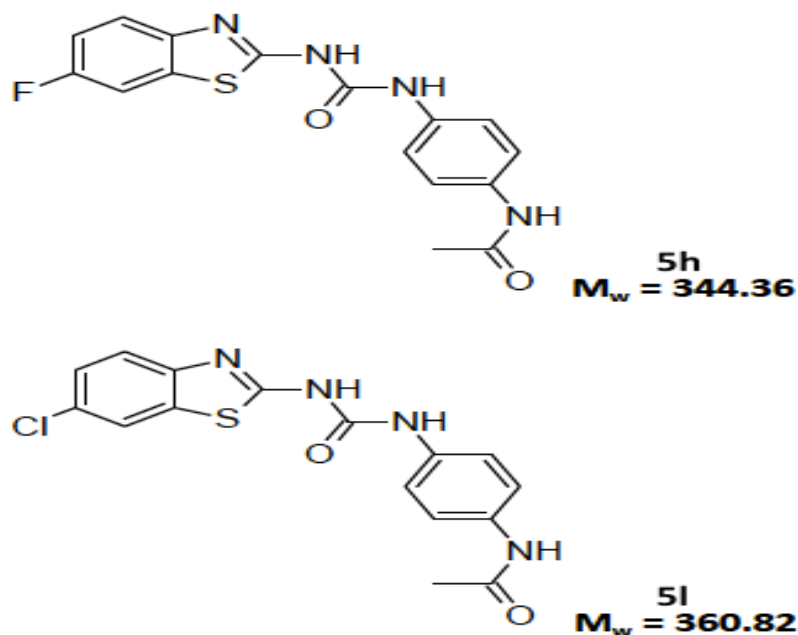
Figure 5.3: The chemical structures of 5h and 5l, two potential inhibitors of the ABAD- Aβ interaction

Since this finding was published in 2006, there have been no further publications regarding the use of frentizole as a potential inhibitor of the ABAD- Aβ interaction, and therefore, a therapeutic agent in the treatment of AD. As suggested in section 5.1.3, speculation would indicate that in its present form, the frentizole's immunosuppressant action has more harmful side effects than positive therapeutic effects when testing progressed into animal models. If this is speculation is to be believed, then that does not mean that frentizole should be discarded as a potential therapeutic in AD. In fact, it would allow the development of a further frentizole analogue series to be synthesised, which would not only be beneficial to optimise the inhibitory effects observed on the ABAD- Aβ interaction, but it would also allow further synthetic modifications which may help to alleviate some of the unwanted side effects.

One such analogue series was designed by Dr Kamil Musilek (University of Hradec Kralove, Czech Republic). Dr Musilek has designed a series of 28 frentizole analogues, which are based on the findings published by Xie *et al*. In this analogue series (K684-K711), the substitutions on the benzothiazole urea ring are adapted from Xie *et al*. with either a fluorine or chlorine electron withdrawing group used. There are several systematic substitutions made on the phenylurea ring and these are shown in Figure 5.4.
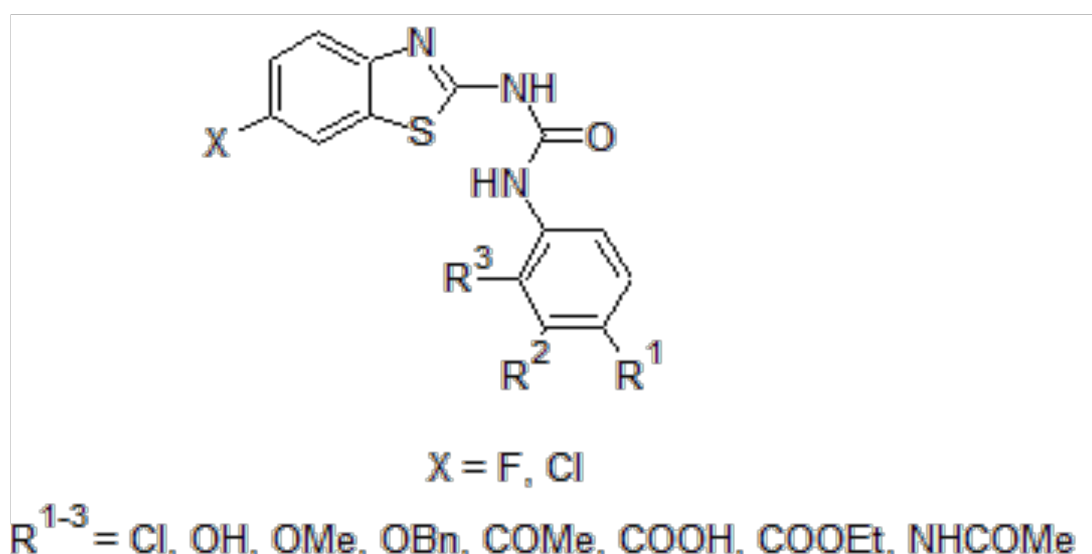
Figure 5.4: Schematic representation of the chemical substitution principle behind the K684- K711 frentizole analogue series. Electron withdrawing groups chlorine and fluorine are substituted at position X in the benzothiazole ring. At positions R1-3 on the phenylurea ring schematic substitutions were used to design new analogues that would allow the series to be series to be scrutinised by SAR analysis.

Chemical structures of the K684- K711 analogue series can be found on pages 175-177 (Figure 5.5). These compounds have been found to be relatively insoluble and indeed must be dissolved in DMSO to create a 10 mM stock solution. Significantly, these 10 mM stock solutions are not capable of being freely diluted in water, or typical laboratory assay buffers and will precipitate from solution rapidly if this is attempted.

The use of propylene glycol (PG (Sigma)) has long been established as a vehicle for water- insoluble drug administration (Bailey 1992; Doenicke *et al.* 1992; Wilson *et al.* 2000). Therefore, by diluting the 10 mM stock solutions with the carrier solution PG, the compounds remain in solution.
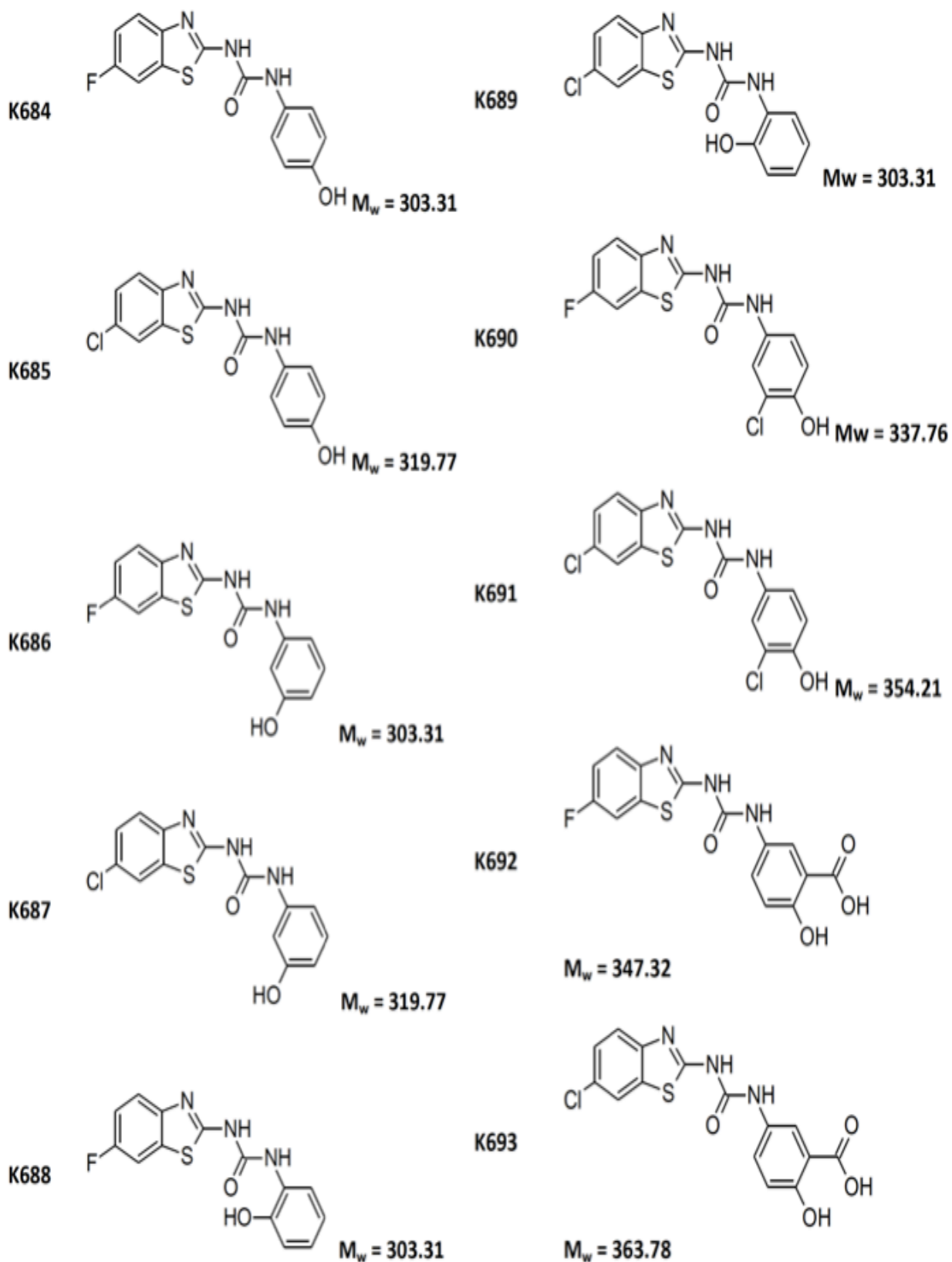
Figure 5.5: Full chemical structures of the K684- K711 frentizole analogue series.
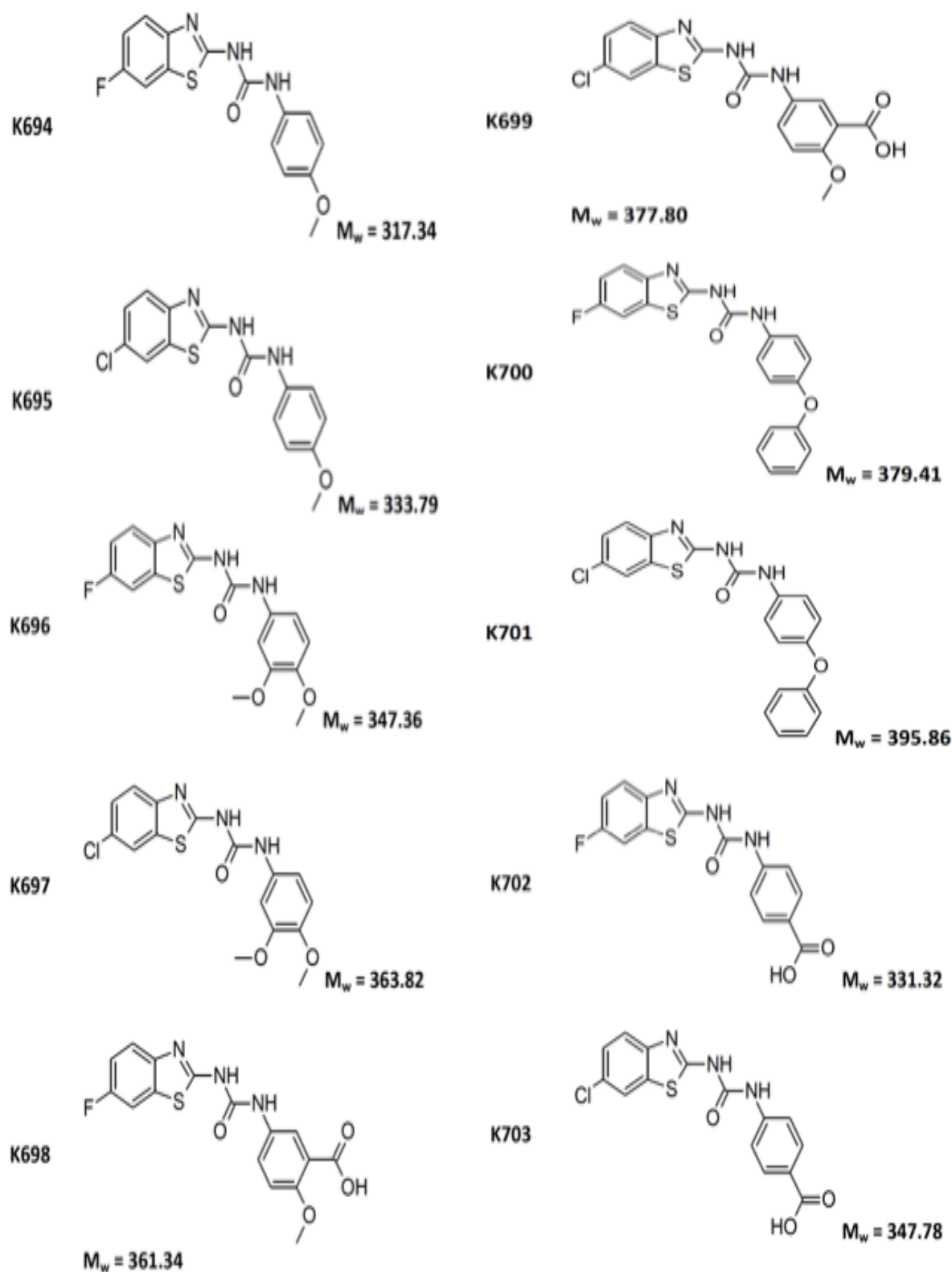
K694 $M_w = 317.34$

K695 $M_w = 333.79$

K696 $M_w = 347.36$

K697 $M_w = 363.82$

K698 $M_w = 361.34$

K699 $M_w = 377.80$

K700 $M_w = 379.41$

K701 $M_w = 395.86$

K702 $M_w = 331.32$

K703 $M_w = 347.78$

Figure 5.5 continued: Full chemical structures of the K684- K711 frentizole analogue series.
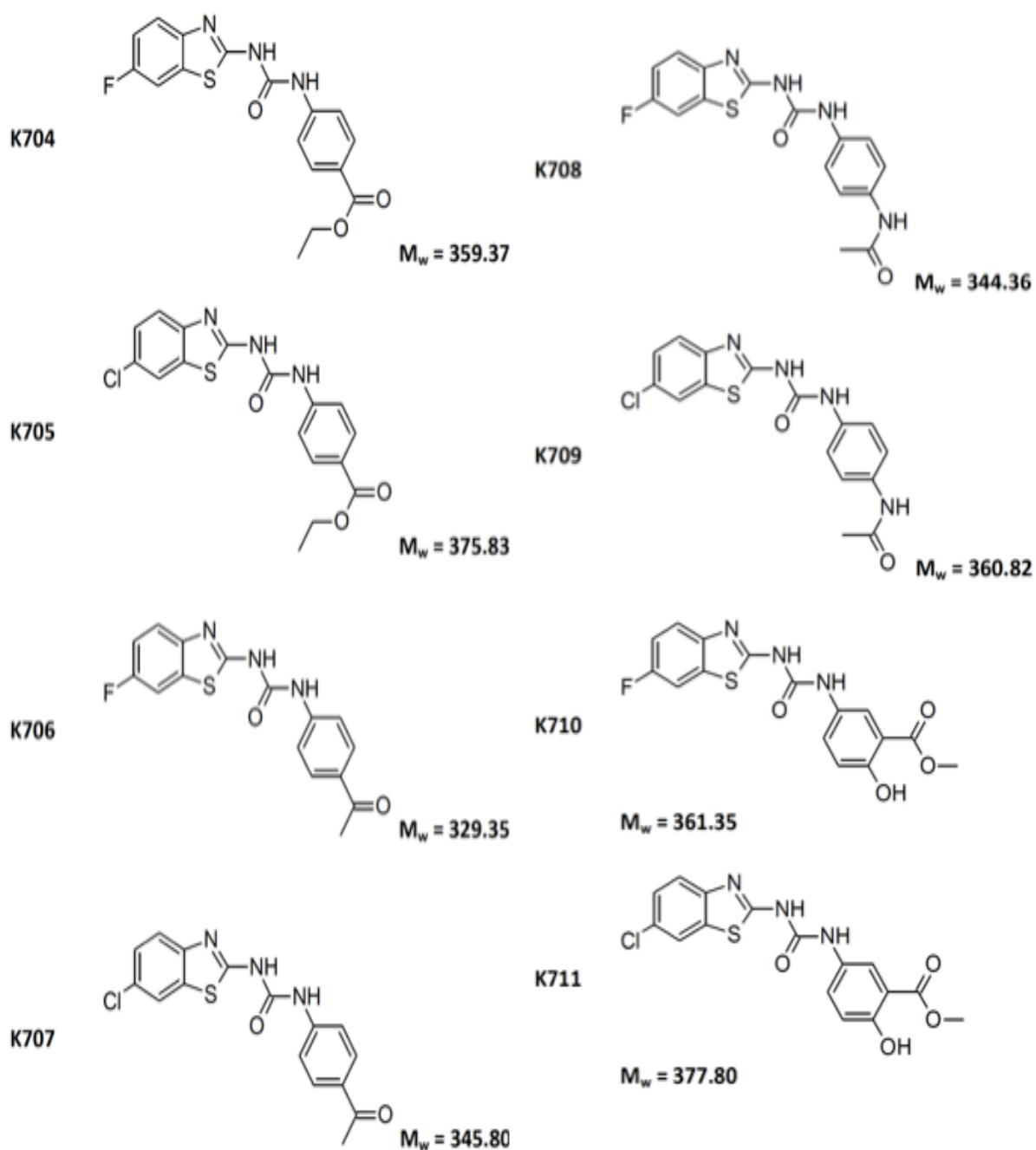
Figure 5.5 continued: Full chemical structures of the K684- K711 frentizole analogue series.

As these compounds are synthetically manufactured, Dr Musilek provided only 20 mg approximately of each analogue. In order to establish assays to investigate the K684-K711 analogue series, the commercially available frentizole (Sigma) was also purchased. As frentizole was the molecular foundation for these analogues, and indeed a published inhibitor of the ABAD- Aβ interaction, this provided a readily available compound that could be used for assay method development, whilst preserving the limited quantity of the analogue series, until such assays were fully functioning. Frentizole was therefore prepared in the same fashion as the K674- K711 analogue series, i.e. frentizole was firstly dissolved as a 10 mM stock solution with DMSO, and then further diluted with propylene glycol (PG).

5.2   Chapter aims

The aims of the work reported in this chapter were three- fold:

Firstly, in order to evaluate the effects of compounds on the ABAD- Aβ interaction, *in vitro* assays were required to monitor the interaction. In particular, the ABAD enzyme activity assay required modification to accurately and reliably measure ABAD activity in the presence of the compounds. In addition, a newly developed, morphology specific single colour fluorescence assay for monitoring Aβ aggregation, also required some initial refinement to ensure that the assay was capable of reliably screening compounds to monitor their effects against Aβ aggregation.

Secondly, once these assays were in place the K684-K711 analogue series could be screened against the various *in vitro* assays to establish which structural modifications are capable of producing the greatest inhibitory effects on the ABAD-Aβ interaction. SAR (structure activity relationship) analysis would then be used to determine if the compounds exhibit any structure- activity relationships.

Finally, other assays that are capable of measuring the direct binding (thermal shift analysis and the Octet RED 384 system) would be employed to attempt to establish the kinetic parameters between the analogue and the ABAD- Aβ interaction.

It was hoped that the work reported in this chapter would provide the groundwork in assay development, which would facilitate the analysis of not only the K684- K711 analogue series, but also any other potential inhibitors of the ABAD-Aβ interaction in the future.

5.3   ABAD enzyme activity assay

5.3.1 ABAD enzyme activity assay method development

As discussed previously in section 5.1.2, it is possible to investigate the catalytic activity (the oxidation and reduction of alcohols and ketones) of ABAD, by measuring the fluorescence emission of ABAD's co-factor (NADH) over time. As time increases, the NADH absorbance decreases, and this change in absorbance over time is proportional to the rate of NAD^+ consumption by the enzyme (Muirhead 2011).

It was anticipated that this activity assay could be used as a fast and effective screening method for analysing the ABAD activity in the presence of the K684- K711 analogue series. The ABAD enzyme activity assay parameters to measure *in vitro* ABAD activity using the FLUOstar plate reader had been previously established (Muirhead 2011). The assay conditions are detailed as follows: S-acetoacetyl-CoA substrate (120 μM), NAD^+ (250 μM), ABAD (5 μg/mL) in assay buffer (50 mM NaH_2PO_4, 300 mM NaCl, pH7.4). The change in absorbance was measured at 340 nM over time (60 s). As the enzyme kinetic parameters had been previously calculated and the substrate concentration had been optimised, these conditions were kept unchanged. However, on closer inspection, the reported assay buffer appeared to cause the ABAD to precipitate out of solution. As any precipitation in the well of the plate could affect reproducibility and result in false positives or negative outcomes, the assay buffer was changed to 10 mM HEPES, 100 mM NaCl, pH 7.5, a buffer in which ABAD is known to be experimentally stable over time (Powell *et al*. 2000). Initial tests to confirm that the enzyme kinetic parameters were similar to that of the ABAD in phosphate buffer were carried out and the specific activity of ABAD in the two buffers was similar (data not shown).

5.3.2 Method development of the ABAD enzyme activity assay in the presence of the K684-K711 analogue series

In order to test the effects of the K684-K711 analogue series on ABAD enzyme activity, 1 mM stocks of the compounds were produced as shown in section 5.1.3. It was anticipated that this activity assay would require further optimisation in order to accurately test the K684-K711 analogue series, due to the nature of the stock compounds.

Firstly, some of the K684-K711 analogue series are coloured. This could potentially produce an auto-fluorescence that could be mistaken for a change in activity. In order to eliminate this likelihood, it was decided that the specific activity of each analogue would be tested in the absence of ABAD to provide an auto-fluorescence result. The average auto-fluorescence for each analogue would then be subtracted from the specific activity recorded in the corresponding ABAD-analogue experiment to give a true specific activity measurement. Colour observations for each analogue are shown in Table 5.1.

Table 5.1 Colour observations of the K684-K711 analogue series

Compound #	MW	10mM stock colour after preparation	1mM stock colour after preparation
K684	303.31	White	Colourless
K685	319.77	White	Colourless
K686	303.31	Grey	Colourless
K687	319.77	Grey	Colourless
K688	303.31	Yellow/Orange	Yellow
K689	303.31	Yellow	Yellow
K690	337.76	Red	Pink
K691	354.21	White	Colourless
K692	347.32	White	White
K693	363.78	White	White
K694	317.34	White	Colourless
K695	333.79	White	Colourless
K696	347.36	White	Colourless
K697	363.82	Yellow	Colourless
K698	361.34	Lilac	White
K699	377.80	Lilac	White
K700	379.41	White	Colourless
K701	395.86	White	Colourless
K702	331.32	White	White
K703	347.78	White	Colourless
K704	359.37	White	White
K705	375.83	White	White
K706	329.35	Yellow	Yellow
K707	345.80	Yellow	Yellow/White
K708	344.36	White	Colourless
K709	360.82	White	Colourless
K710	361.35	White	White
K711	377.80	White	Colourless
Frentizole	299.35	White	Colourless

The ABAD activity assay measures the absorbance of NADH at 340 nM. The K684-K711 analogue series requires the use of the vehicle propylene glycol (PG), to dilute the compounds and avoid precipitation. The PG is a very viscous solution, which could potentially interfere with the assay measurements. It was therefore necessary to measure the specific activity of ABAD in the presence of DMSO diluted with PG, against untreated ABAD, with a control experiment of no ABAD only DMSO and PG used. The assay was set up as described in section 2.3.2 however, in place of the compound, 10% DMSO solution in PG was added. The findings from these experiments (summarised in Table 5.2) suggested that although the average specific activity of ABAD in the presence of DMSO and PG was slightly lower than that of the average

specific activity of untreated ABAD, this was not significant. However, the observed large standard error of the mean, between the replicate samples, suggested that the reproducibility of the assay was highly compromised in the ABAD experiment treated with DMSO and PG.

Table 5.2: Analysis of ABAD in the presence of 10% DMSO in PG. The measured ABAD average specific activity (μmol min-1 mg-1) in the presence of the 10% DMSO and PG was slightly, but not significantly decreased when compared to the average specific activity ABAD with no DMSO or PG. However, the reproducibility of the assay was greatly compromised with large standard error of the mean values produced within the replicates of the ABAD plus DMSO and PG test.

Sample	-dAbs	-dAbs	pathlength	dConc	dConc	dConc (V)	SEM	[ABAD]	specific activity	specific activity	specific activity	SEM
	s^{-1}	min^{-1}	cm	mol L^{-1} min^{-1}	mol L^{-1} min^{-1}	μmol L^{-1} min^{-1}	μmol L^{-1} min^{-1}	mg L^{-1}	mol min^{-1} mg^{-1}	μmol min^{-1} mg^{-1}	μmol min^{-1} mg^{-1}	μmol min^{-1} mg^{-1}
	5.27E-04	0.031645	0.456	1.12E-05				5	2.23E-06	2.2314		
	6.57E-04	0.039410	0.456	1.39E-05				5	2.78E-06	2.7790		
	6.14E-04	0.036847	0.456	1.30E-05				5	2.6E-06	2.5982		
ABAD	5.44E-04	0.032654	0.456	1.15E-05	1.24E-05	12.389	0.640	5	2.3E-06	2.3025	2.4778	0.128
	5.32E-04	0.031913	0.456	1.13E-05				5	2.25E-06	2.2503		
ABAD	7.30E-04	0.043813	0.456	1.54E-05				5	3.09E-06	3.0894		
PG +	6.79E-04	0.040723	0.456	1.44E-05				5	2.87E-06	2.8715		
DMSO	2.35E-04	0.014100	0.456	4.97E-06	1.15E-05	11.507	2.353	5	9.94E-07	0.9942	2.3014	0.471
	1.52E-05	0.000914	0.456	3.22E-07				5	6.45E-08	0.0645		
	2.08E-04	0.012477	0.456	4.40E-06				5	8.8E-07	0.8798		
NO	9.31E-05	0.005587	0.456	1.97E-06				5	3.94E-07	0.3940		
ABAD	6.47E-05	0.003881	0.456	1.37E-06	2.01E-06	2.015	0.865	5	2.74E-07	0.2737	0.4030	0.173

Before testing the specific activity of ABAD in the presence of the K684-K711 analogue series, a random sample of the analogues (K684, K687, K690, K699 and K705) was chosen to test the assay viability. The analogues to be tested were selected because of the varieties in their colour (see table 5.1). During the plate set up, it was noticed that some precipitation formed in the wells of the samples. As the absorbance

reading was set up to measure in the centre spot of the well, any precipitation in this area would produce results with huge discrepancies. Therefore, it was decided to use an orbital scanning method, whereby the absorbance would be measured in a circular fashion around the diameter of the well. By measuring the average specific activity of ABAD in the presence of analogues K684, K687, K690, K699 and K705 the original, absorbance spot method, was compared to the new orbital method. It was therefore possible to establish the best method for accurately measuring NADH absorbance by comparing the standard error of the mean (SEM) between the two trials (Table 5.3). In general the orbital scanning method produced more reliable results with lower SEM.

Table 5.3: Analysis of ABAD (in the presence of frentizole analogues), measured under two conditions (orbital and non-orbital absorbance measurements) to determine the optimum technique for measuring the NAD$^+$ absorbance in the ABAD activity assay. The NAD$^+$ absorbance was measured using an orbital scanning method and a single spot method; by comparing the SEM values produced the two methods could be evaluated. The orbital scanning method was chosen to be used in future ABAD enzyme activity analysis of the K684-K711 analogue series.

	Orbital		No Orbital	
	Specific Activity umol/min/ mg	SEM umol/min/ mg	Specific Activity umol/min/ mg	SEM umol/min/ mg
Control	0.1535	0.1168	0.1374	0.0282
684	1.3467	0.7263	1.6216	0.9260
687	0.5517	0.2001	0.2251	0.1148
690	1.2355	0.6121	1.1331	0.9501
699	0.2658	0.1079	0.4864	0.1819
705	1.3870	0.2288	0.4217	0.1409

5.3.3 ABAD enzyme activity analysis in the presence of the K684-K711 analogue series

Having completed the necessary groundwork for the ABAD enzyme activity assay, it was now possible to evaluate all the K684-K711 analogue series compounds, by measuring the effects they had on ABAD enzyme activity. The assay was carried out as discussed previously in this chapter and also in section 2.3.2. The ABAD enzyme activity was calculated for each compound (with 6 replicates) and the auto-fluorescence of each compound was also measured in order to subtract the mean auto-fluorescence result from the ABAD activity recorded measurement. Figure 5.6 is a graph of average ABAD specific activity (μmol min^{-1} mg^{-1}) for all the K684-K711 analogue series compounds plotted with their average auto-fluorescence (taken as the measurement of ABAD specific activity obtained when no ABAD is present). Control tests for this assay were ABAD in the absence of any compound, and a test with no ABAD and no compound. The ABAD specific activity data, auto-fluorescence data and the recorded ABAD specific activity minus the mean auto-fluorescence data for the K684-K711 analogue series compounds, is shown in Table 5.4. Only the compounds, which appear to increase the ABAD activity, are shown in Table 5.4.
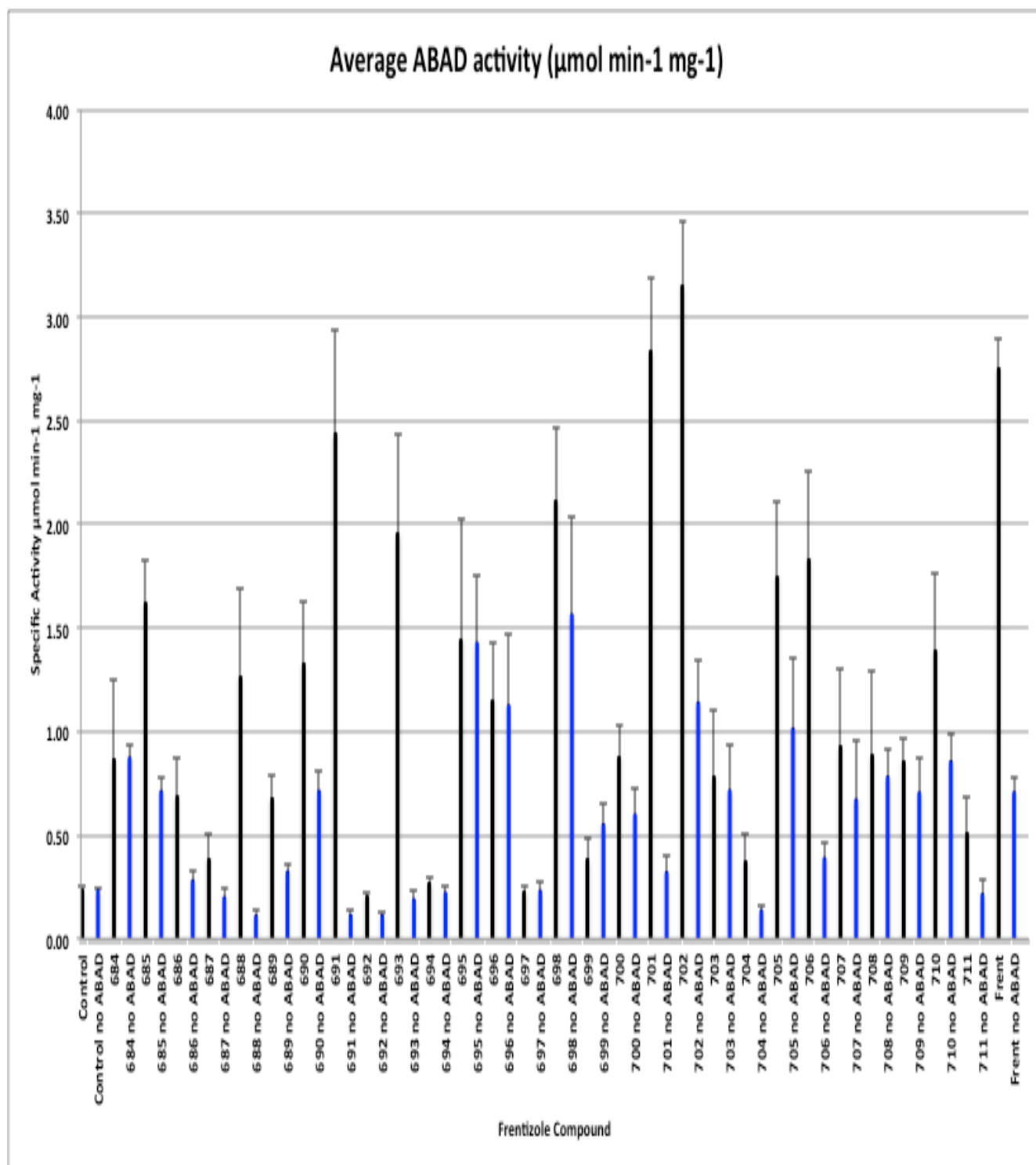
Figure 5.6: Evaluation of the K684-K711 analogue series. The average specific activity of ABAD in the presence of the K684-K711 analogue series (Black columns) and the average auto-fluorescence values for the K684-K711 analogue series taken as the measurement obtained when no ABAD was present (Blue columns). The control sample is described as the observed average ABAD specific activity when no compound is present, and also shown is the control sample where no ABAD and no compound are present. The commercially available compound, frentizole was also tested.

Table 5.4 The ABAD activity auto-fluorescence data and the recorded ABAD specific activity minus the mean auto-fluorescence data for the K684-K711 analogue series compounds.

Analogue #	ABAD specific activity (µmol min-1 mg-1)	auto-fluorescence (µmol min-1 mg-1)	Specific activity-mean auto-fluorescence (µmol min-1 mg-1)	Analogue #	ABAD specific activity (µmol min-1 mg-1)	auto-fluorescence (µmol min-1 mg-1)	Specific activity-mean auto-fluorescence (µmol min-1 mg-1)
685	1.15709	0.50032	0.44926	693	1.72948	0.37239	1.54410
	2.24162	0.83494	1.53379		1.20249	0.27251	1.01711
	1.65903	0.63031	0.95120		0.44147	0.13375	0.25610
	2.10842	0.90533	1.40059		2.15950	0.20004	1.97412
	1.55899	0.83494	0.85116		2.20515	0.08020	2.01978
	0.98337	0.54114	0.27555		3.95968	0.05338	3.77430
686	1.30223	0.41481	1.02558	698	2.81110	2.71668	1.25149
	0.58270	0.10156	0.30605		0.73493	0.48210	-0.82469
	0.32638	0.20646	0.04974		2.40583	0.80639	0.84621
	0.28940	0.37250	0.01275		1.79661	0.25934	0.23699
	1.22589	0.27080	0.94924		3.17663	2.50843	1.61701
	0.40586	0.29377	0.12922		1.74828	2.58475	0.18867
687	0.27564	0.32115	0.08037	701	4.00522	0.34907	3.68845
	0.94058	0.08671	0.74531		2.54878	0.10751	2.23201
	0.43875	0.10255	0.24348		3.57497	0.08942	3.25821
	0.18964	0.32115	-0.00563		1.99268	0.30388	1.67591
	0.31909	0.08542	0.12382		1.76009	0.56867	1.44332
	0.12659	0.25463	-0.06868		3.10500	0.48204	2.78824
688	0.40151	0.25129	0.29521	702	3.56862	1.70831	2.43311
	0.80352	0.05396	0.69722		2.86090	0.48287	1.72539
	3.13547	0.04050	3.02917		1.92489	1.23681	0.78937
	1.75194	0.02514	1.64564		2.76551	0.57194	1.63000
	0.34511	0.11891	0.23881		3.87062	1.62034	2.73511
	1.14508	0.14801	1.03877		3.86838	1.19282	2.73286
689	0.58789	0.41042	0.26810	705	1.84326	0.70996	0.83384
	1.18987	0.42017	0.87008		1.12798	0.15988	0.11856
	0.65957	0.23752	0.33978		1.18984	0.64158	0.18041
	0.43069	0.35135	0.11090		2.86157	0.38587	1.85214
	0.38944	0.34776	0.06965		2.75508	2.07412	1.74565
	0.75800	0.15151	0.43821		0.70338	2.08514	-0.30604
690	0.64834	0.64834	-0.06056	706	2.36175	0.16825	1.97706
	0.63930	0.63930	-0.06960		3.24276	0.28289	2.85807
	1.87307	1.02690	1.16417		2.51859	0.65505	2.13390
	2.21990	0.99775	1.51100		0.86317	0.47062	0.47849
	1.91607	0.46517	1.20717		1.41847	0.20701	1.03379
	0.63178	0.47575	-0.07712		0.56782	0.52430	0.18313
691	3.18183	0.56453	3.07210	Frent	2.51438	0.61493	1.81227
	3.67566	0.08614	3.56593		2.41428	0.60228	1.71217
	0.90953	0.18494	0.79980		3.21393	0.47192	2.51182
	0.85861	0.04352	0.74888		2.85012	0.92440	2.14801
	3.07449	0.10542	2.96477		2.38931	0.93225	1.68720
	2.89156	0.18187	2.78184		3.11909	0.66688	2.41698

The compounds shown in Table 5.4 were subjected to statistical analysis, to determine if any of the observed compounds have significantly increased ABAD activity levels. Column statistics were used to display the SEM accurately and show that despite assay modifications there are still assay reproducibility issues (shown in Table 5.5)

Table 5.5 Statistical analysis on the treated ABAD minus the mean auto fluorescence specific activity values for the K684-K711 analogue series compounds that appear to significantly increase ABAD activity.

	Control	685	686	687	688	689	690	691
Number of values	6	6	6	6	6	6	6	6
Minimum	0.1327	0.2756	0.01275	-0.06868	0.2388	0.06965	-0.07712	0.7489
25% Percentile	0.1763	0.4058	0.04049	-0.02139	0.2811	0.1006	-0.07148	0.7871
Median	0.2331	0.9012	0.2176	0.1021	0.868	0.3039	0.5518	2.873
75% Percentile	0.2944	1.434	0.9683	0.3689	1.992	0.5462	1.283	3.196
Maximum	0.3023	1.534	1.026	0.7453	3.029	0.8701	1.511	3.566
Mean	0.2306	0.9103	0.4121	0.1864	1.157	0.3495	0.6125	2.322
Std. Deviation	0.06452	0.5	0.4576	0.2942	1.054	0.2901	0.7562	1.227
Std. Error	0.02634	0.2041	0.1868	0.1201	0.4303	0.1184	0.3087	0.5009
Lower 95% CI	0.1629	0.3856	-0.06811	-0.1223	0.05133	0.04499	-0.1811	1.035
Upper 95% CI	0.2983	1.435	0.8923	0.4952	2.264	0.6539	1.406	3.61

	693	698	701	702	705	706	Frentizole
Number of values	6	6	6	6	6	6	6
Minimum	0.2561	-0.8247	1.443	0.7894	-0.306	0.1831	1.687
25% Percentile	0.8269	-0.06467	1.618	1.42	0.01241	0.4047	1.706
Median	1.759	0.5416	2.51	2.079	0.5071	1.505	1.98
75% Percentile	2.458	1.343	3.366	2.733	1.772	2.315	2.441
Maximum	3.774	1.617	3.688	2.735	1.852	2.858	2.512
Mean	1.764	0.5526	2.514	2.008	0.7374	1.444	2.048
Std. Deviation	1.186	0.876	0.8873	0.7672	0.9001	1.044	0.3633
Std. Error	0.4841	0.3576	0.3622	0.3132	0.3674	0.4262	0.1483
Lower 95% CI	0.5198	-0.3667	1.583	1.203	-0.2071	0.3484	1.667
Upper 95% CI	3.009	1.472	3.446	2.813	1.682	2.54	2.429

One-way ANOVA, with Dunnet's multiple comparison statistical analysis, was carried out on the ABAD specific activity (recorded after administration of the analogue) minus the mean auto fluorescence produced by the analogue, for the K684-K711 analogue series compounds that appear to significantly increase ABAD enzyme activity activity. From the statistical analysis 5 compounds were shown to significantly increase ABAD enzyme activity: K691, K693, K701, K702 and notably the known inhibitor ABAD-Aβ interaction inhibitor, frentizole. The one-way ANOVA data is displayed in Table 5.6. Data from this one-way ANOVA analysis is shown in graphical form in Figure 5.7.

It is hoped that by identifying these four analogues that they can now be taken forward into further chemical modification trials, to produce another analogue series based on the SAR found between them. This significant finding was slightly marred by the high errors reported from the sample replicates of each analogue run in the activity assay. Although only 5 compounds were shown to significantly increase ABAD activity, it is thought that there may be other analogues in the series, which may produce a greater therapeutic effect, but did not appear significant in the statistical analysis due to these large errors between the sample replicates. These large errors are ultimately caused by make up of the analogues and the buffers used to dissolve them (as discussed in section 5.1.3). It is hoped that by optimising the solubility of the analogues that this may improve the ability to measure the analogues more accurately. This is discussed further in chapter 6.3.

Table 5.6 One-way ANOVA, with Dunnet's multiple comparison statistical analysis, on the treated ABAD protein minus the mean auto fluorescence specific activity values for the K684-K711 analogue series compounds that appear to significantly increase ABAD activity. From the analysis 5 compounds were shown to significantly increase ABAD enzyme activity: K691, K693, K701, K702 and the known inhibitor ABAD-Aβ interaction inhibitor, frentizole.

One-way analysis of variance			
P value	< 0.0001		
P value summary	***		
Are means signif. different? (P < 0.05)	Yes		
Number of groups	15		
F	6.203		
R square	0.5366		
Bartlett's test for equal variances			
Bartlett's statistic (corrected)	43.12		
P value	< 0.0001		
P value summary	***		
Do the variances differ signif. (P < 0.05)	Yes		
ANOVA Table	SS	df	MS
Treatment (between columns)	54.44	14	3.889
Residual (within columns)	47.02	75	0.6269
Total	101.5	89	

Dunnett's Multiple Comparison Test	Mean Diff.	q	Significant? P < 0.05?	Summary	95% CI of diff
Control vs 685	-0.6796	1.487	No	ns	-1.997 to 0.6375
Control vs 686	-0.1815	0.397	No	ns	-1.499 to 1.136
Control vs 687	0.04419	0.09666	No	ns	-1.273 to 1.361
Control vs 688	-0.9268	2.027	No	ns	-2.244 to 0.3903
Control vs 689	-0.1188	0.2599	No	ns	-1.436 to 1.198
Control vs 690	-0.3819	0.8354	No	ns	-1.699 to 0.9353
Control vs 691	-2.092	4.575	Yes	***	-3.409 to -0.7744
Control vs 693	-1.534	3.355	Yes	*	-2.851 to -0.2164
Control vs 698	-0.322	0.7043	No	ns	-1.639 to 0.9952
Control vs 701	-2.284	4.996	Yes	***	-3.601 to -0.9666
Control vs 702	-1.777	3.887	Yes	**	-3.094 to -0.4598
Control vs 705	-0.5068	1.109	No	ns	-1.824 to 0.8104
Control vs 706	-1.213	2.654	No	ns	-2.531 to 0.1037
Control vs Frentizole	-1.817	3.976	Yes	**	-3.135 to -0.5003
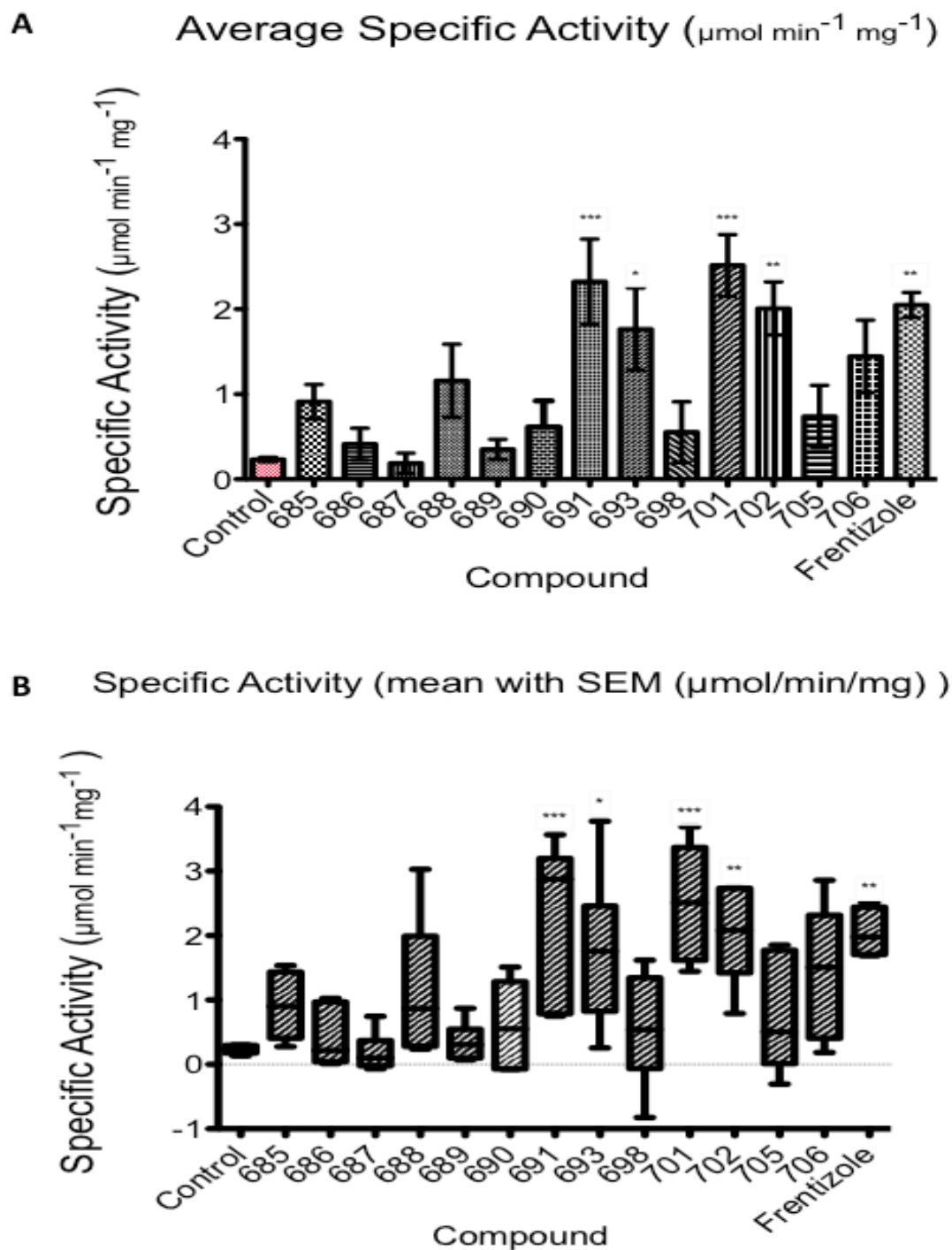
Figure 5.7: One way ANOVA statistic analysis carried out on K684-K711 analogue series to analyse if the compound significantly increased ABAD enzyme activity. A) ABAD average specific activity (μmol min^{-1} mg^{-1}) in the presence of K684-K711 analogue series. **B)** Box plot analysis of the ABAD specific activity values plotted with the standard error mean to determine the range between the replicates. From the one way ANOVA analysis compounds K691, K693 K701, K702 and frentizole are found to have significantly increased ABAD activity.

5.4 Thermal shift analysis of the K684-711 analogue series as potential inhibitors of the ABAD- Aβ interaction

Thermal shift analysis (TSA), (previously described in section 3.1.3) can be used as an initial screening method to identify binding partners of proteins. However, it is a technique that can also be implemented to establish inhibitors of protein interactions and therefore to categorise their inhibitory effects on the binding of proteins, by monitoring the change in a protein's unfolding temperature (ΔT_m) which occurs upon inhibitor binding. It was therefore anticipated that it should be possible to also use this technique to measure the effects of the K684- K711 analogue series, as potential inhibitors of the ABAD- Aβ interaction.

Since the assay parameters for measuring small molecule binding partners to prevent the ABAD- Aβ interaction had already been established (Muirhead 2011), it was only necessary to determine if the DMSO and/or propylene glycol (PG), present to solubilise the K684- K711 analogue series, would have any negative affects on the assay. There are many negative effects that this buffer could produce, these include for example: the DMSO or PG may interact with the dye to mask any ΔTm produced during the assay, or that the ΔT_m could not be measured due to the viscosity of the PG.

The dissociation curve of the control test samples (Figure 5.8) plots the negative reciprocal of fluorescence as a function of temperature. The ΔT_m therefore occurs at the lowest point on the curve (Muirhead 2011). The control test conditions were: 30 μM ABAD, 1 x SYPRO® orange dye, 2.5% (v/v) DMSO, 2.5 % (v/v) PG. The assay was carried out as described in section 2.3.4, and the observed baseline ΔT_m was performed at 45°C for all replicates.
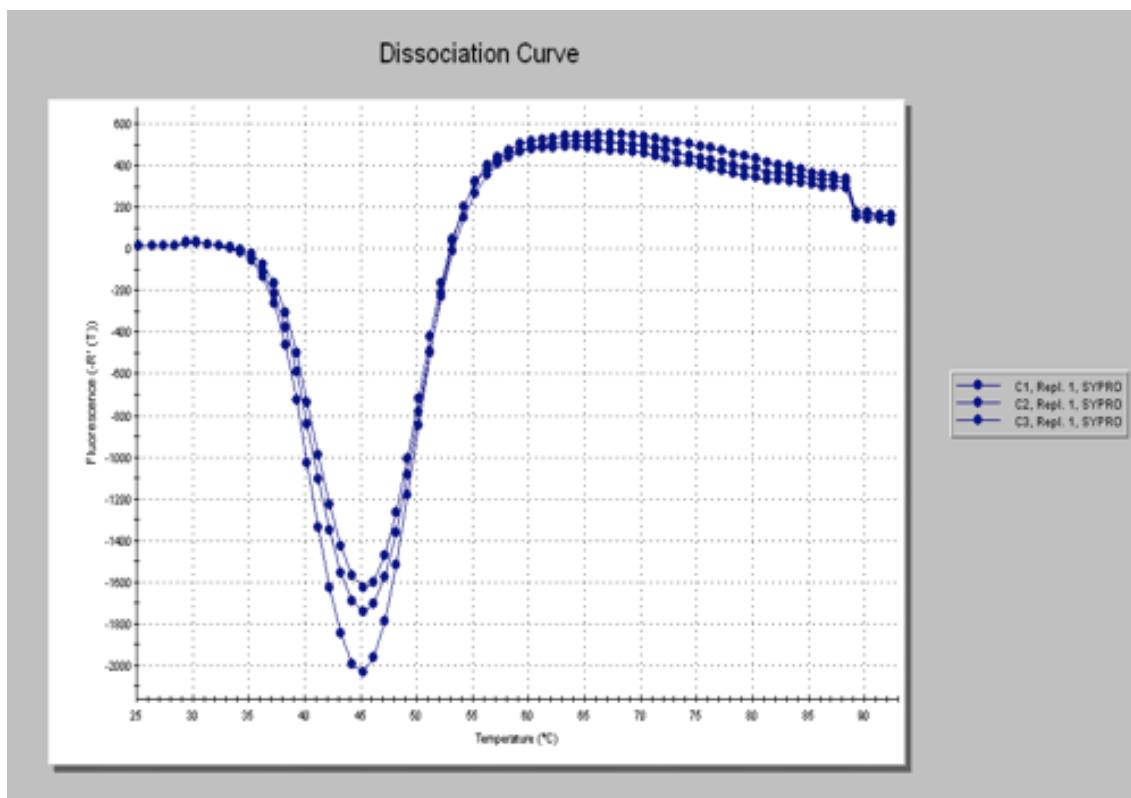
Figure 5.8: Thermal shift analysis control sample dissociation curve, showing the unfolding temperature (T_m) of native ABAD protein. This assay was carried out in triplicate, and each sample produced a T_m of 45 °C (as observed at the lowest point on the dissociation curve). It was also observed that although the triplicates unfold at the same temperature, there was a slight difference in the fluorescence output within the samples. The TSA assay control sample contains: ABAD protein (30 μM), 1 x SYPRO® orange dye, 2.5% (v/v) DMSO, 2.5% (v/v) PG.

Since the control test proved that the presence of DMSO and PG were not significantly interfering with the TSA, frentizole (prepared as described in section 5.1.3) was then analysed to assess the thermal shift assay's capability to be used as a screening tool to measure the K684- K711 analogue series. A frentizole concentration of 25 μM was chosen, in order to maintain the same concentration used in the other *in vitro* assays. Figure 5.13 illustrates the dissociation curve of ABAD protein in the presence of frentizole.
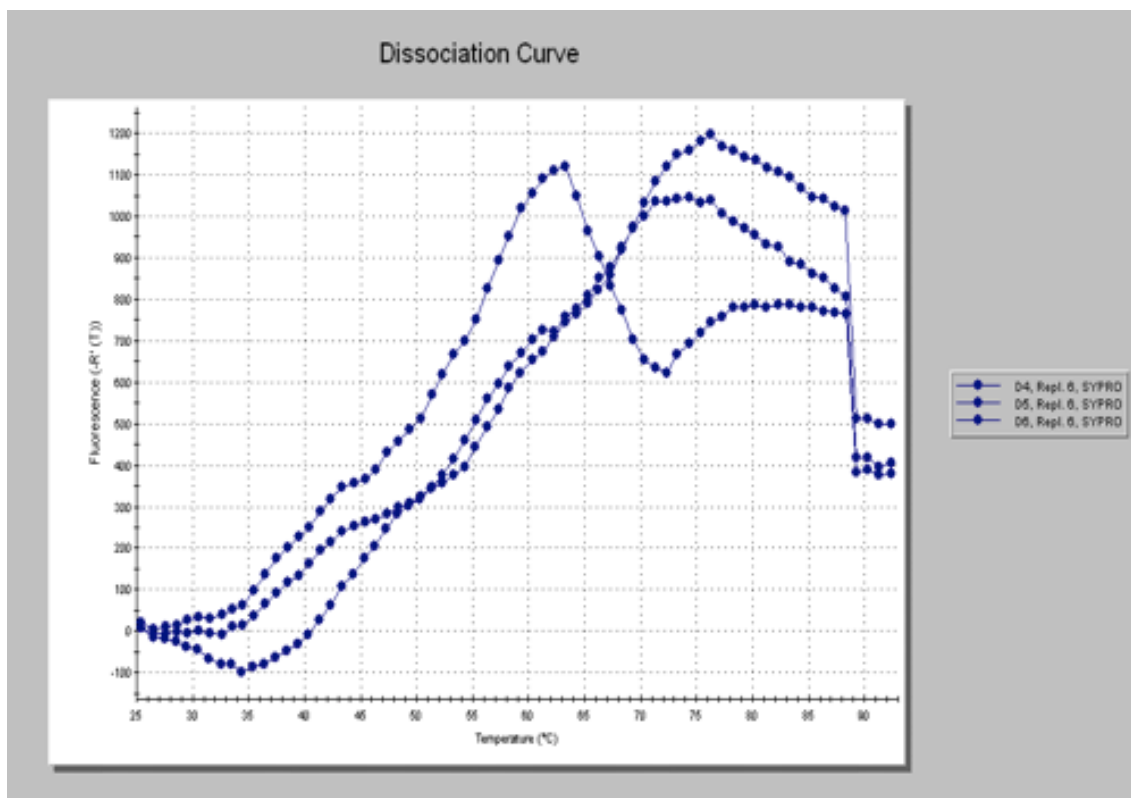
Figure 5.9: The dissociation curve of ABAD protein in the presence of frentizole. The assay conditions for this experiment were: ABAD protein (30 μM), 1 x SYPRO® orange dye, 25 μM frentizole.

Unfortunately, Figure 5.9 shows that the frentizole molecule had an effect on the ABAD protein; however, it was not possible to use TSA to measure this effect, because the dissociation curve that was produced was distorted and the reproducibility between the triplicates was greatly diminished. Therefore, in order to determine if these findings corresponded to the whole of the K684- K711 analogue series, or if these findings were purely associated with frentizole, compound K711 was selected to replace the frentizole compound. The dissociation curve of ABAD protein in the presence of compound K711 is shown in Figure 5.10.
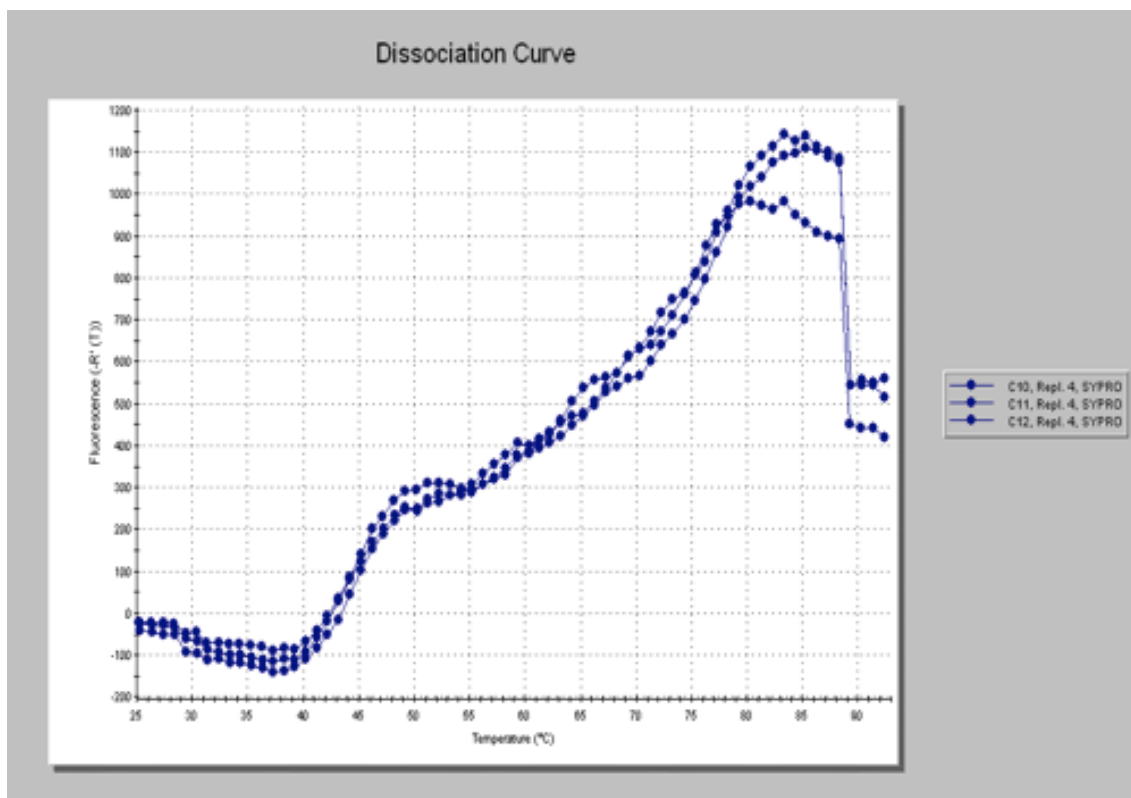
Figure 5.10: The dissociation curve of ABAD protein in the presence of compound K711. The assay conditions for this experiment were: ABAD protein (30 μM), 1 x SYPRO® orange dye, 25 μM K711.

Again, unfortunately, when comparing the dissociation curves of both frentizole (Figure 5.9) and compound K711 (Figure 5.10) the results are very similar. Both compounds produced an effect on the ABAD protein; however, in both cases this effect could not be measured using TSA because the dissociation curves were distorted. It was therefore decided that these findings were probably representative of the whole of the K684-K711 analogue series, and so no further TSA work should be carried out with this series of compounds until more about the interaction is known.

5.5   A direct binding assay to establish the kinetic parameters of the K684-K711 analogue series as potential inhibitors of the ABAD- Aβ interaction

The *Fortebio®* Octet RED 384 system is a biomolecular interactions platform that is capable of determining and evaluating the affinity of small molecule binding to a therapeutic target. The fast, label- free analysis of the association and dissociation of a small molecule with the target protein of interest, results in the determination of kinetic constants including the association rate constant (k_a), dissociation rate constant (k_d), and equilibrium dissociation constant (K_D) (Myszka 2004). It was therefore deemed appropriate to use the Octet RED 384 system to test the K684-K711 analogue series against the ABAD-Aβ interaction.

In a typical Octet RED 384 small molecule binding experiment, a biotinylated protein target (in this instance; biotinylated ABAD protein (b-ABAD)) is immobilized onto a Super Streptavidin (SSA) biosensor surface, and this surface is exposed to a solution of the small molecule (in this instance; one of the K684-K711 analogues) in a microplate well. The association of the small molecule to the target protein on the biosensor is measured over time. The biosensor is moved to a well containing buffer to monitor the dissociation of the small molecule from the target protein. Rate constants are then calculated from the binding data, including on-rate (k_a), off-rate (k_d), and equilibrium dissociation constant (K_D). This assay process, and the data expected from a typical small molecule binding experiment is shown in Figure 5.11.
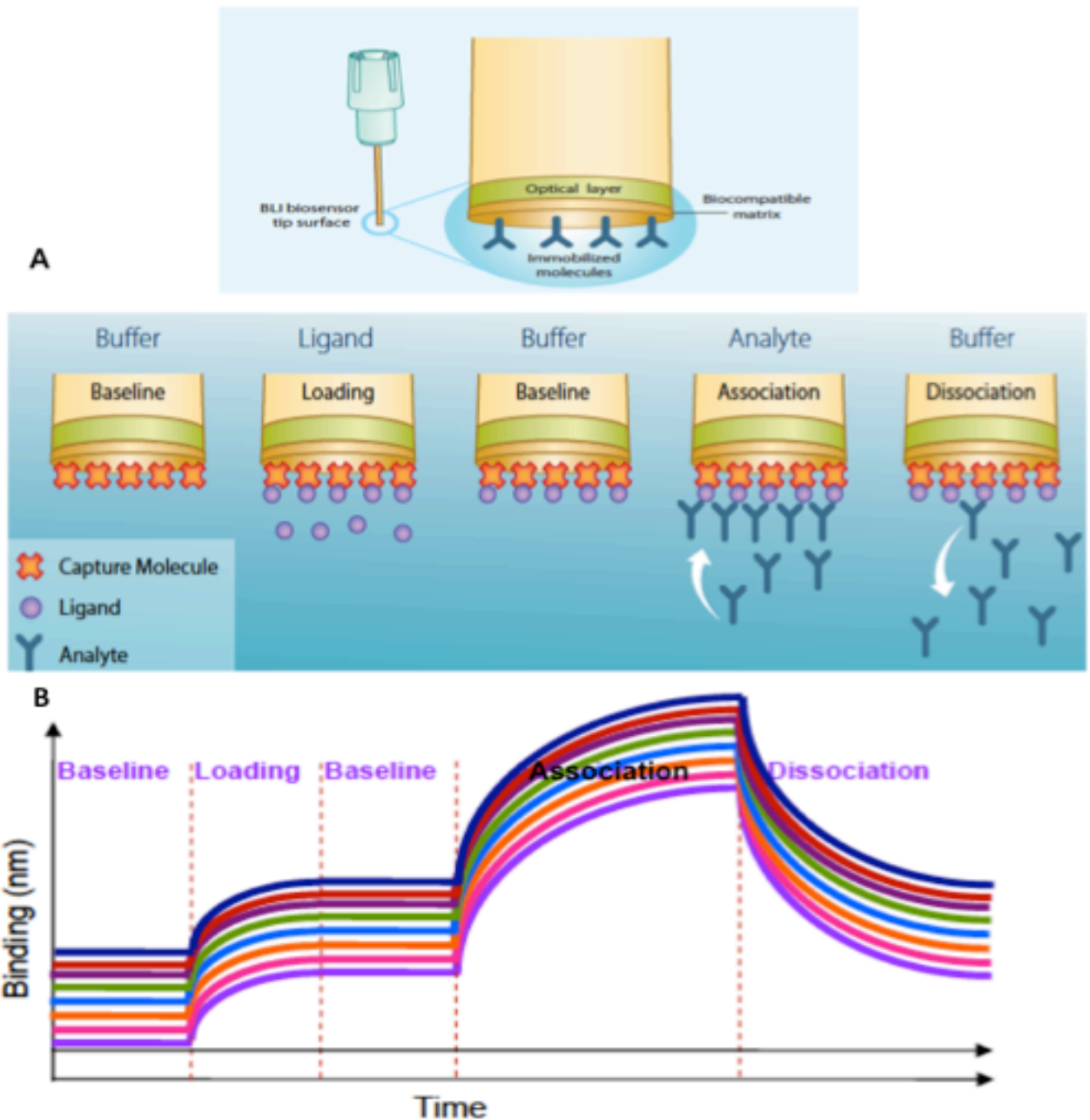
Figure 5.11: A typical small molecule binding experiment using the Octet RED 384 system and the sensorgram and data achieved from the experiment. A) A typical assay is divided into 5 sections 1) a baseline buffer is achieved 2) The biotinylated protein is loaded onto the SSA sensor. The more detailed view of the BLI biosensor (shown at top of diagram **A)** shows that the instrument contains an optical layer, that emits white light down the biosensor, collects the light and then emits it back 3) After the protein is loaded a further baseline is made to confirm the protein has bound successfully to the SSA sensor. 4) The association of a small molecule. 5) The dissociation of the small molecule. **B)** A typical sensorgram reported after a small molecule binding assay. The curves shown are representative of a typical small molecule binding experiment, where the various colours would depict the use of a dilution series to test the effect of a small molecule and the target protein (Images from Fortebio® Octet literature).

The b-ABAD protein was produced as described in section 2.3.6. As the Octet RED 384 system is a relatively new technique in the drug discovery field, primary testing of the b-ABAD protein with Aβ and also with its co-factor NAD^+ was first used to confirm that the b-ABAD protein is functioning normally, and is still capable of binding known ABAD protein interacting molecules. Again frentizole was used as a test compound in order to validate the assay, before the K684-K711 analogue series were tested. This work was carried out in collaboration with Dr David Robinson (University of Dundee).

The findings of the initial experiment to test the ability of b-ABAD protein to bind Aβ are shown in Figure 5.12. The nature of the sensogram suggests that the ABAD protein has become saturated with biotin and so indicating that the biotin tag has bound to multiple sites on the protein. This potentially translates into the b-ABAD protein attaching too quickly to the SSA and, more significantly, this indicates that the b-ABAD protein may have attached itself in a conformation that will not allow any binding of additional small molecules to occur.
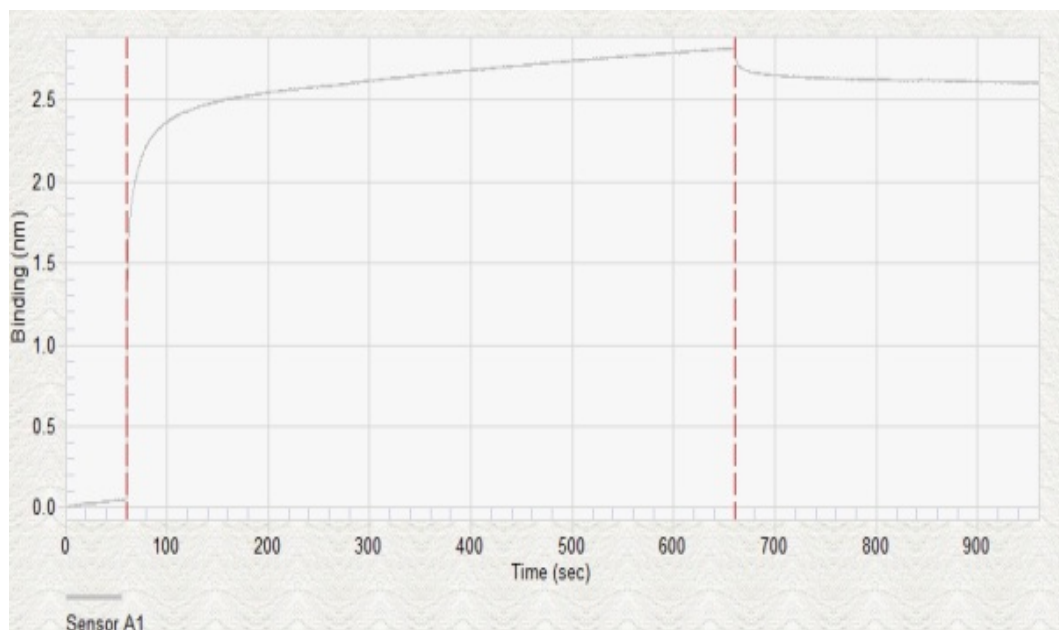
Figure 5.12: Sensorgram for the loading of b-ABAD protein onto the SSA biosensor in the Octet RED 384 system. Biotinylated ABAD (b-ABAD) protein at 50 μg/ml binds to SSA biosensor. It was observed that the sensorgram saturated rapidly in the first 200 seconds, suggesting biotin molecules were bound to multiple sites on the protein.

As the b-ABAD protein had been frozen after biotinylation, it was thought that this may have had an effect on the b-ABAD protein conformation. Therefore fresh b-ABAD protein was prepared before use in the assay. The previous experiment was then repeated to determine if the fresh b-ABAD protein would attach itself at the correct rate and conformation. Following the biotinylation of ABAD protein, the standard biotin assay buffer (10 mM HEPES, 100 mM NaCl, pH 7.5), was exchanged to enable the ABAD protein to return to the buffer that the protein had been previously found to be most stable in (10 mM Tris-HCl, 150 mM NaCl, pH7.5), in the hope that this would also aid with the correct attachment to the SSA sensor. Fortunately, these modifications were favourable and the b-ABAD protein attached itself to the SSA biosensor in the correct manner (shown in Figure 5.13).
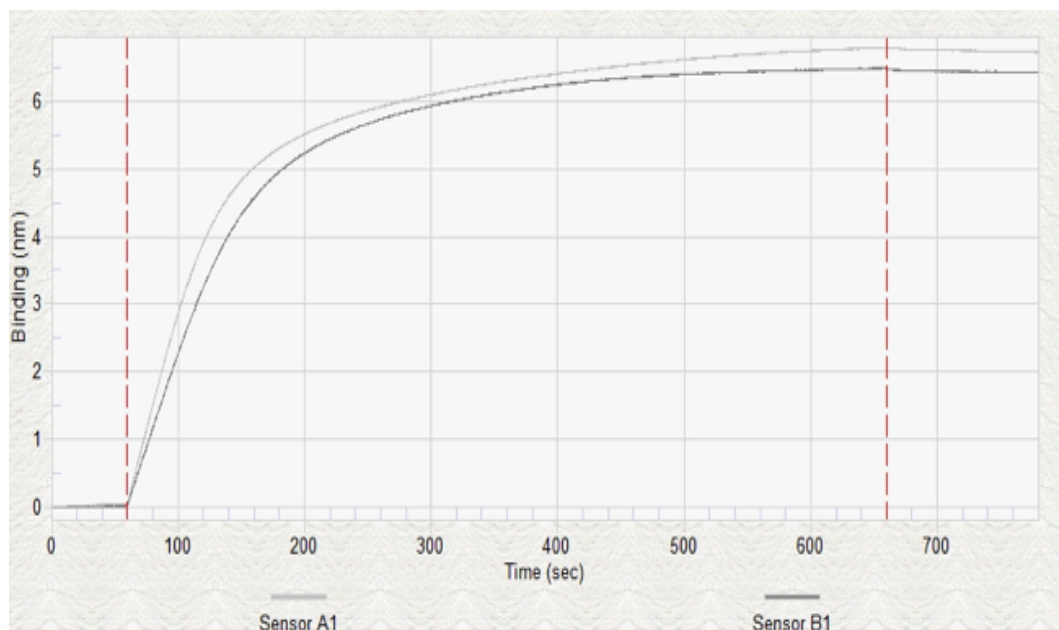
Figure 5.13: Sensorgram for the repeated loading of b-ABAD protein onto the SSA biosensor in the Octet RED 384 system with both Tris and HEPES sample buffers. Biotinylated ABAD (b-ABAD) protein at 50ug/ml bound to the SSA biosensor in both the HEPES sample buffer (biosensor A1) and the Tris-HCl sample buffer (biosensor B1). It was observed that b-ABAD protein bound equally to the SSA biosensor in both sample buffers, and at an optimal response level of 6- 7 nM. The sample buffers used were: 10 mM HEPES, 100 mM NaCl, pH 7.5 and 10 mM Tris-HCl, 150 mM NaCl, pH7.5.

Despite the b-ABAD protein attaching rapidly to the SSA it was necessary to determine if Aβ could bind to the immobilised b-ABAD protein. A 5 point, 5 fold dilution series of Aβ was used to study the binding of Aβ and b-ABAD protein. A second blank SSA biosensor with no immobilised b-ABAD protein was used to determine if any non-specific binding was occurring. It was possible that non- specific binding could occur between Aβ and the SSA biosensor containing the immobilised b-ABAD protein, because when the b-ABAD protein attaches itself to the biosensor it does not encompass the entire biosensor area; therefore allowing space for Aβ to attach directly to the SSA biosensor. It is a vital to establish if there is any non- specific binding between Aβ and the SSA sensor, because Aβ is a very sticky molecule, prone to aggregation, and any non- specific binding between the SSA biosensor containing immobilised b-ABAD

protein would result in a false positive reading. The sensorgrams for this experiment are shown in Figure 5.14.
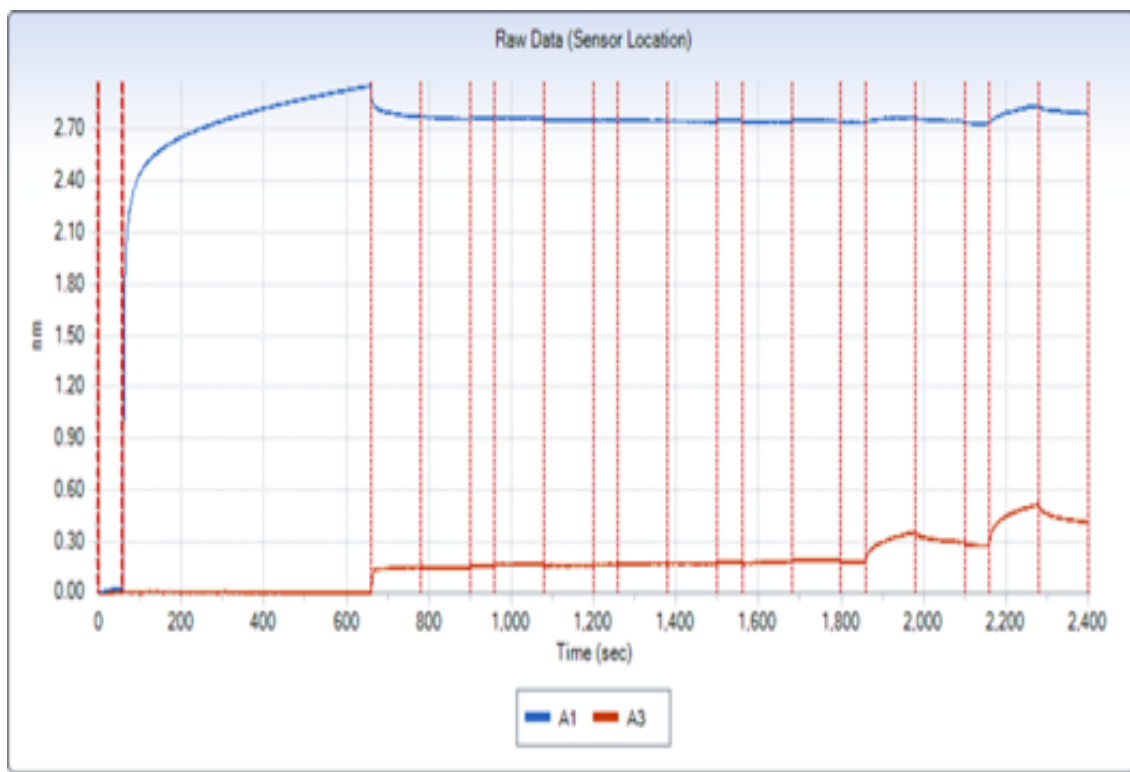
Figure 5.14: Sensorgram for b-ABAD protein and Aβ binding experiments. The biosensor shown by the blue line is the SSA biosensor with immobilised b-ABAD protein (A1). The red line shows the blank control SSA biosensor with no protein present (A3). A high level of non- specific binding was observed between the Aβ and the control SSA sensor.

In order to reduce the non- specific binding observed between the control SSA biosensor and Aβ, it was important to try to find a suitable inhibitor of Aβ binding. As albumin has been reported to prevent Aβ internalisation in neurons (Vega *et al.* 2009), 0.1% (v/v) BSA (bovine serum albumin) was added to the sample buffer, and the experiment was repeated. This addition proved to be successful in preventing the non-

specific binding of Aβ to the control SSA sensor, however it also completely abolished the Aβ- b-ABAD protein binding (shown in Figure 5.15).
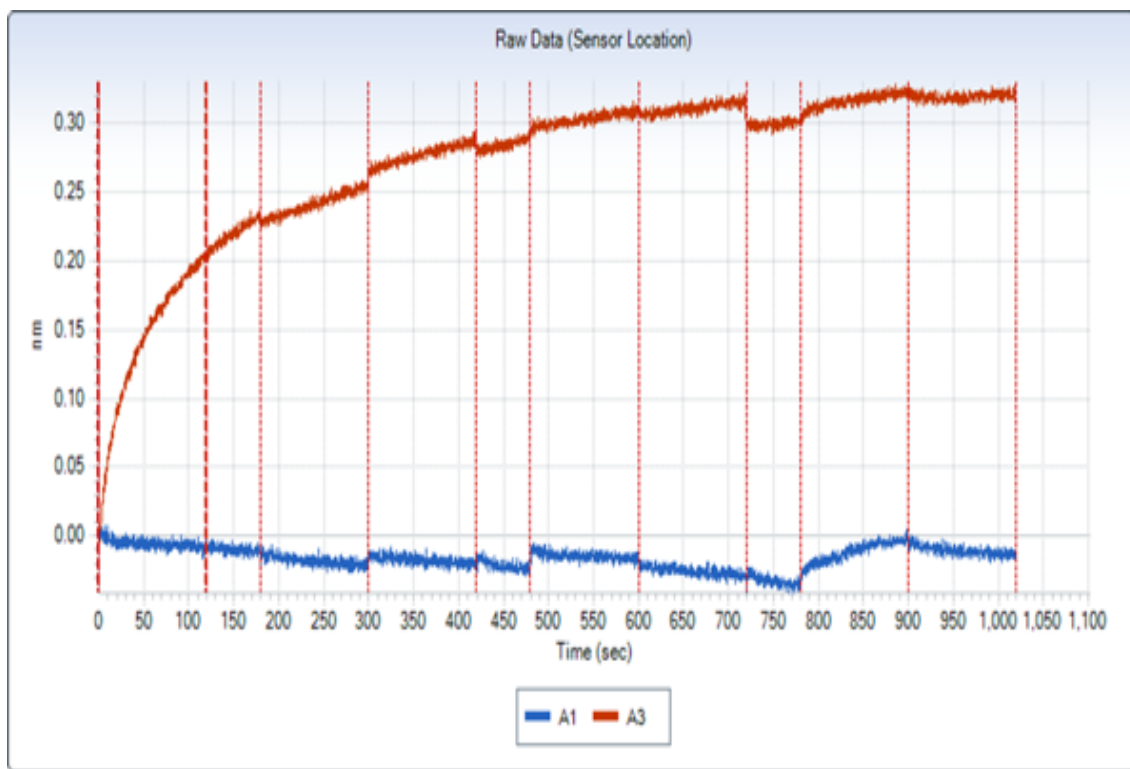
Figure 5.15: Sensorgram for the repeat b-ABAD protein and Aβ binding experiments with the addition of 0.1% (v/v) BSA. The biosensor shown by the blue line is the SSA biosensor with immobilised b-ABAD (A1). The red line shows the blank control SSA biosensor with no protein present (A3). A decreased level of non- specific binding was observed between the Aβ and the control SSA sensor. However, no binding of Aβ was observed on the immobilised b-ABAD protein.

As no binding was observed between the b-ABAD protein and the Aβ peptide, it is possible that by biotinylating the ABAD protein, the enzyme has become inactivated. Therefore, the *in vitro* enzyme activity assay (section 5.3) was used to confirm if b-ABAD protein was still biologically active. The activity assay was performed as described in section 2.3.2 (in 6 replicate experiments), where the effects of samples labelled with b-ABAD protein were compared against unlabelled ABAD protein and the

control experiment where no ABAD protein was present. The specific activity data (μmol min^{-1} mg^{-1}) from this experiment (shown in Table 5.7) revealed that the b-ABAD protein did indeed have 47% less activity than that of unlabelled ABAD protein. However, the b-ABAD protein was still deemed to be biologically active as the specific activity was 35% more when compared to the control sample with no ABAD present.

Table 5.7: Analysis of labelled b-ABAD protein, to determine if the enzyme is still active after biotin labelling. b-ABAD protein, non- labelled ABAD protein and no ABAD present control experiments, were tested with the FLUOstar plate reader to detect changes in enzyme activity, and to therefore determine if the b-ABAD protein was still active following biotinylation. The average specific activity (μmol min-1 mg-1) of b-ABAD protein was 47% less than the unlabelled ABAD protein with the average specific activity of the enzyme falling to 0.156 μmol min-1 mg-1 compared to the average specific activity of unlabelled ABAD protein measured at 0.2923 μmol min-1 mg-1. However, the b-ABAD protein was still deemed to be active as the b-ABAD protein average specific activity was 35 % higher than that of the average specific activity (0.1157 μmol min-1 mg-1) of the control experiment where no ABAD was present.

Sample	Well	-dAbs s^{-1}	-dAbs min^{-1}	pathlength cm	dConc mol L^{-1} min^{-1}	dConc mol L^{-1} min^{-1}	dConc (V) μmol L^{-1} min^{-1}	SEM μmol L^{-1} min^{-1}	[ABAD] mg/L	specific activity mol/min/ mg	specific activity μmol/min/ mg	specific activity μmol/min/ mg	SEM μmol/min/ mg
Non-labelled ABAD	A1	1.02E-04	0.006109	0.456	2.15E-06	2.01E-06	2.007	0.264	5	4.31E-07	0.4307	0.2923	0.058
	A2	1.12E-04	0.00673	0.456	2.37E-06				5	4.75E-07	0.4746		
	A3	7.07E-05	0.00424	0.456	1.49E-06				5	2.99E-07	0.2990		
	A4	3.22E-05	0.001933	0.456	6.82E-07	9.16E-07	0.916	0.222	5	1.36E-07	0.1363		
	A5	6.43E-05	0.003858	0.456	1.36E-06				5	2.72E-07	0.2721		
	A6	3.34E-05	0.002004	0.456	7.07E-07				5	1.41E-07	0.1413		
BIOTIN ABAD	B1	3.87E-05	0.002319	0.456	8.18E-07	7.88E-07	0.788	0.149	5	1.64E-07	0.1636	0.1560	0.041
	B2	2.44E-05	0.001465	0.456	5.16E-07				5	1.03E-07	0.1033		
	B3	4.87E-05	0.002923	0.456	1.03E-06				5	2.06E-07	0.2061		
	B4	3.57E-05	0.002144	0.456	7.56E-07	7.72E-07	0.772	0.431	5	1.51E-07	0.1512		
	B5	7.22E-05	0.00433	0.456	1.53E-06				5	3.05E-07	0.3053		
	B6	1.56E-06	9.33E-05	0.456	3.29E-08				5	6.58E-09	0.0066		
Control no ABAD	C1	3.82E-05	0.002292	0.456	8.08E-07	1.06E-06	1.056	0.136	10	8.08E-08	0.0808	0.1157	0.008
	C2	5.12E-05	0.003071	0.456	1.08E-06				10	1.08E-07	0.1083		
	C3	6.03E-05	0.00362	0.456	1.28E-06				10	1.28E-07	0.1276		
	C4	6.49E-05	0.003896	0.456	1.37E-06				10	1.37E-07	0.1374		
	C5	5.96E-05	0.003575	0.456	1.26E-06				10	1.26E-07	0.1260		
	C6	5.38E-05	0.00323	0.456	1.14E-06	1.26E-06	1.258	0.068	10	1.14E-07	0.1139		

As the b-ABAD protein was still found to be active after biotinylation, and since there is very little published data on the use of frentizole as a potential inhibitor of the ABAD- Aβ interaction (Xie *et al*. 2006), it was decided to proceed further with this assay, but to remove the Aβ binding component of the experiment. By removing the Aβ peptide, the assay was no longer a small molecule inhibitor screen, but instead became an indicator purely of small molecule binding to ABAD. This type of experiment is still extremely useful, and if successful would provide vital information that could then be used in the structural development of future ABAD protein activity promoters and also ABAD-Aβ interaction inhibitors for the treatment of AD.

Therefore, two further experiments were designed to test the ability of b-ABAD protein to bind its co-factor NAD^+ and known ABAD-Aβ inhibitor, frentizole. In these experiments 6 point, 5 fold serial dilutions were used to obtain a top concentration of 100 μM NAD^+ and 10 μM frentizole. Unfortunately results showed that neither compound was capable of binding to the immobilised b-ABAD protein. Sensorgrams for these experiments are shown in (Figure 5.16).

Despite the improvements made by applying freshly b-ABAD protein to the SSA biosensors, no binding of NAD^+ or frentizole was observed on the sensorgrams. The most likely reason for this could be that the surface immobilisation of ABAD protein renders the protein inactive, possibly due to the orientation of ABAD on the biosensor surface, hindering access to the active site. Another possible explanation for the lack of b-ABAD protein binding, is that in order to biotinylate the protein, lysine residues are targeted, and there is a lysine residue (Lys 172) present in ABAD's active site region which may have become biotinylated, thus preventing any other molecules from entering the active site. Also if this lysine has become biotinylated, then it may have

immobilised itself to the SSA biosensor and orchestrated an orientation that leaves the active site inaccessible to any potential binding partners.
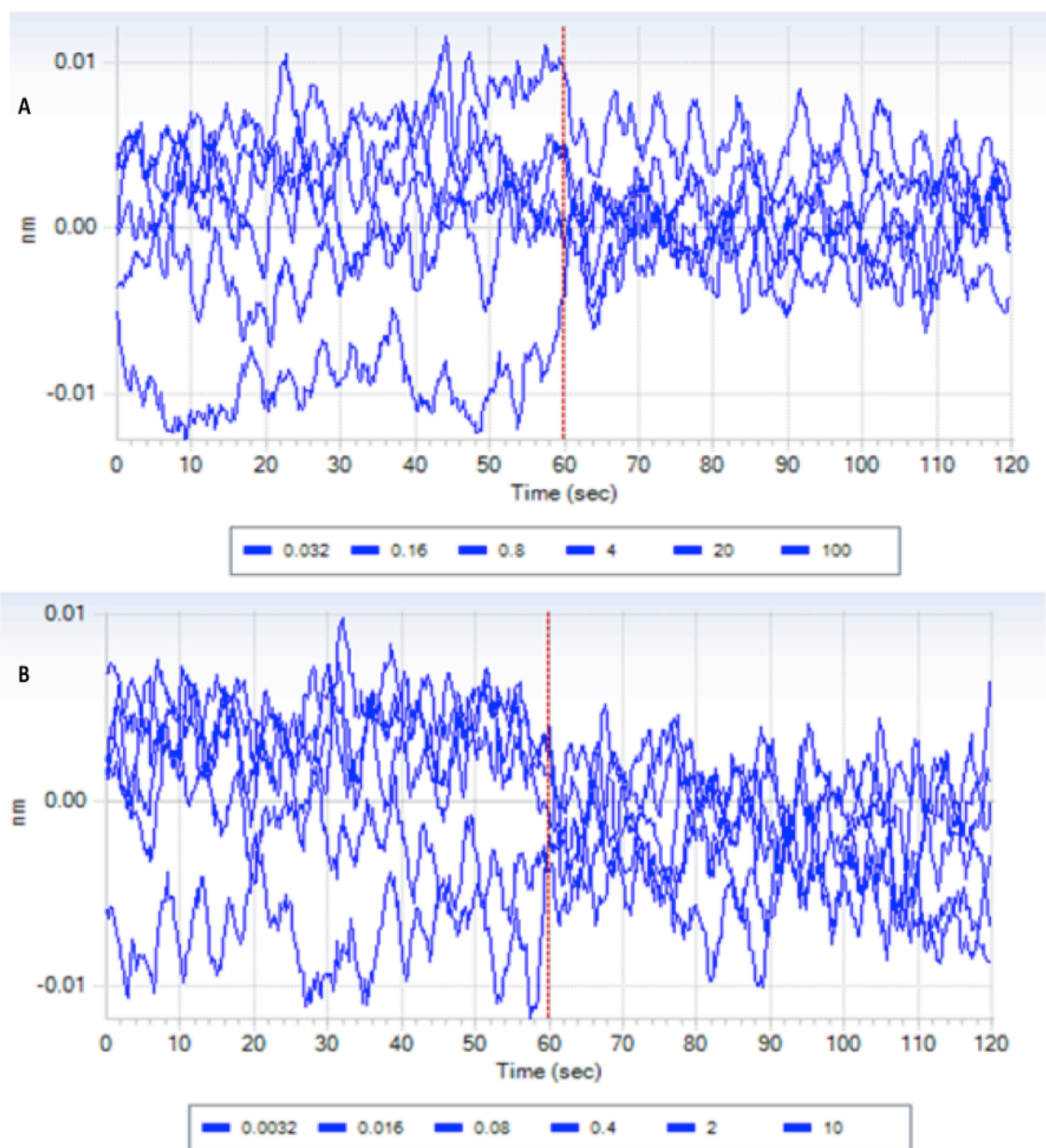
Figure 5.16: Expanded sensorgrams for the small molecule binding of NAD^{+} and frentizole with immobilised b-ABAD protein. In both **A)** (NAD^{+}) and **B)** (frentizole) the sensorgrams have been expanded around the 0 nM baseline, indicating that in both cases there is no binding observed between the compounds and immobilised b-ABAD protein.

5.6 <u>A morphology specific Aβ aggregation assay which can be used as a screening tool for evaluating potential ABAD-Aβ inhibitors</u>

As described previously in section 5.1.1, it has been found that there are biomarkers that are capable of detecting Aβ aggregation (Congo red, Thioflavin T) (Maezawa *et al.* 2008). However, these compounds are not able to recognise the various aggregation states that ABAD can adopt. A morphology specific Aβ assay would aid in finding Aβ morphology specific inhibitors and *in vivo* imaging agents. In this instance, the morphology specific assay could be used to screen potential inhibitors of the ABAD-Aβ interaction and to assess if the potential inhibitors have different effects on the ABAD-Aβ interaction in the various Aβ morphology conditions. This morphology sensitive quenching assay works on the principle of measuring in real time changes that occur in the fluorescence emission of the N-terminally Cy3 labelled Aβ aggregates, and where differences in the fluorescence quenching during the Aβ growth process indicate either inhibition or promotion of Aβ aggregation.

Our collaborator Dr J.Carlos Penedo and his group (University of St Andrews), had previously developed such an assay. However, their assay had never been used to measure any potential Aβ interactions, or possible inhibitors of the interactions previously. Therefore, before any potential inhibitors of the ABAD-Aβ interaction could be screened the assay required to be validated for the purpose of measuring how ABAD and Aβ interact under the various morphology changes. Thus, it was first necessary to determine how changes in ABAD concentration affected Aβ aggregation in all three aggregation conditions (HFIP induced aggregation, NaCl induced aggregation and pH6 induced aggregation).

First the HiLyte Fluor 555 (Aβ$_{555}$) was monomerised as described in section 2.3.1 and then treated to form the various morphological states as described in section 2.3.7. For each type of aggregate 4 experiments were carried out (as described in section 2.3.7), where the ABAD was then added to the Aβ aggregates in a peptide to ABAD ratio of 1:1, 2:1 and 100:1 and a control experiment where no ABAD was added to the Aβ aggregates. Fluorescence quenching data obtained during the Aβ growth pattern for each of the induced aggregation conditions, with the addition of ABAD (in varying concentrations) is used to determine the effect of the ABAD on Aβ aggregation and is shown in Figures 5.17-5.19.
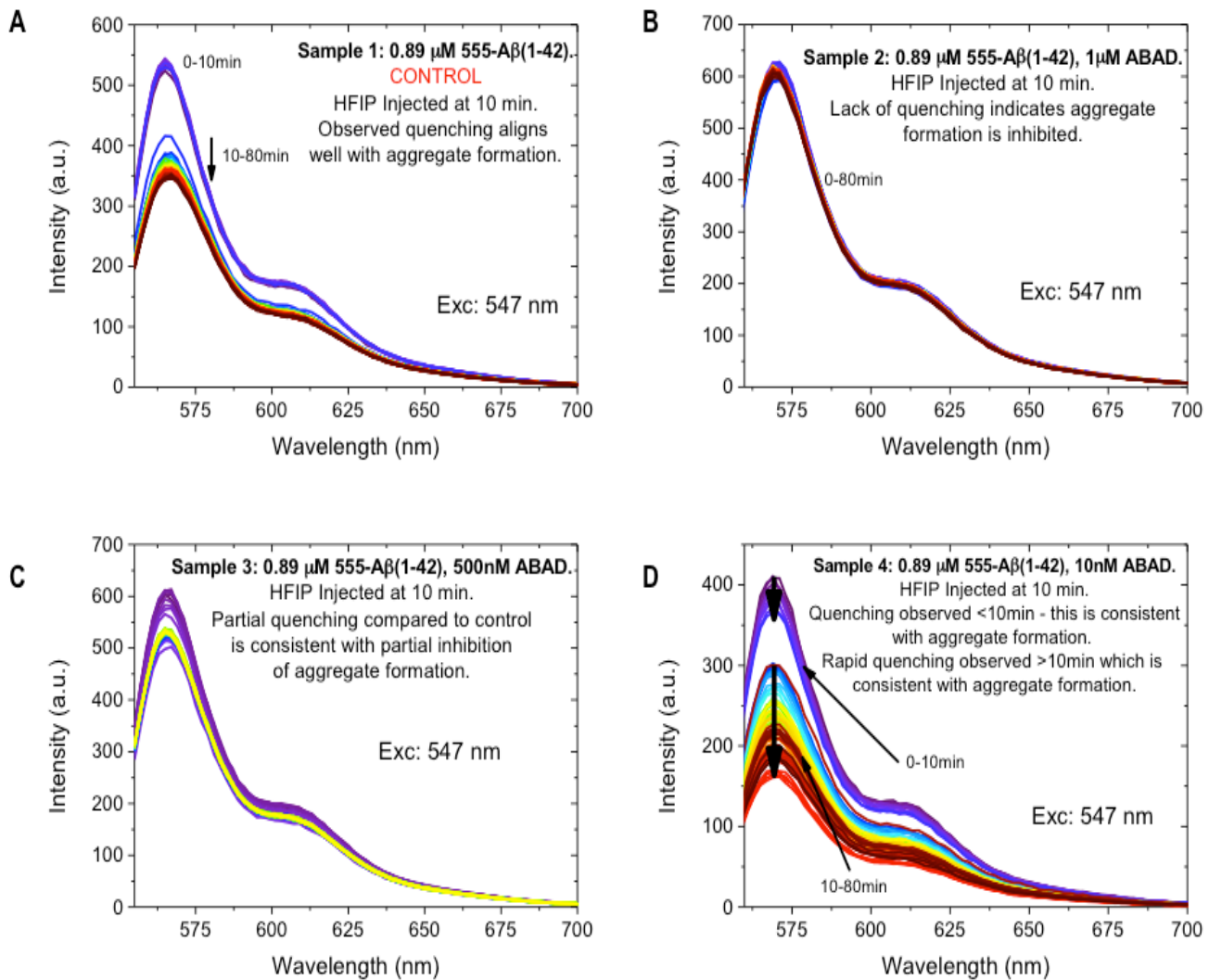
Figure 5.17: Fluorescence quenching of HFIP induced Aβ aggregation, with the addition of different concentrations of ABAD protein, to monitor its effects in fibril like aggregation conditions. **A)** Control sample test 0.89 μM Aβ$_{555}$: no ABAD present, after the HFIP injection, Aβ continues to form aggregates over 80 minutes with a 30% quenching of Cy3 dye. **B)** 0.89 μM Aβ$_{555}$: 1 μM ABAD, after ABAD injection there is no observed quenching of the Cy3 dye. This is consistent with the Aβ aggregation being completely inhibited. **C)** 0.89 μM Aβ$_{555}$: 500 nM ABAD, after ABAD injection there is a partial quenching of the Cy3 dye observed at around 15%. This is consistent with the partial inhibition of Aβ aggregation. **D)** 0.89 μM Aβ$_{555}$: 10 nM ABAD, after ABAD injection there is a 30% quenching of the Cy3 dye observed, similar to that of the control sample. This is consistent with the promotion of Aβ aggregation
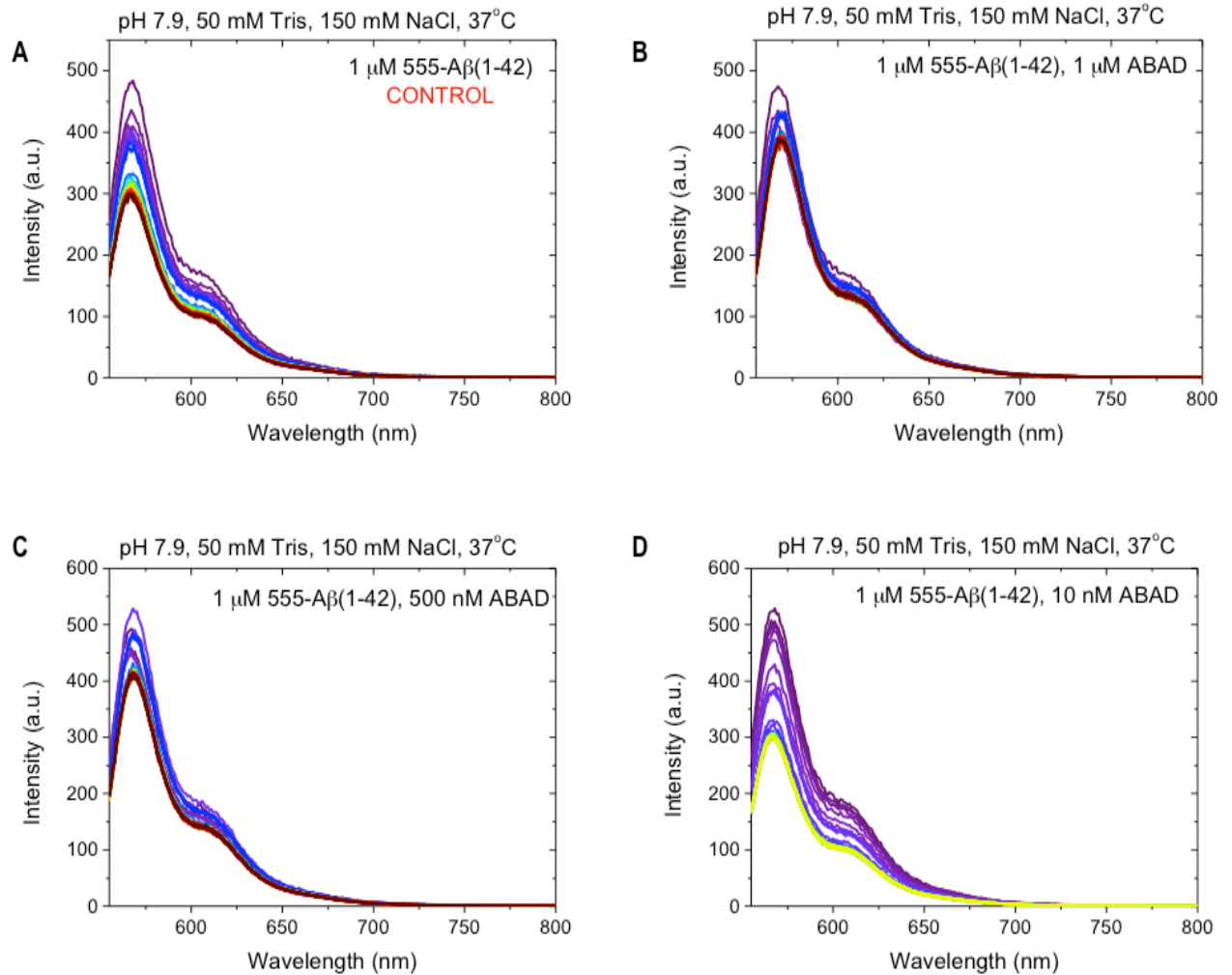
Figure 5.18: Fluorescence quenching of NaCl induced Aβ aggregation, with the addition of different concentrations of ABAD protein, to monitor its effects in globular like aggregation conditions. A) Control sample test 0.89 μM Aβ$_{555}$: no ABAD present, Aβ continues to form aggregates over 80 minutes with an observed quenching of approximately 30%. **B)** 0.89 μM Aβ$_{555}$: 1 μM ABAD, after ABAD injection (20minutes into assay) there is no quenching of Cy3 dye observed. This is consistent with the Aβ aggregation being completely inhibited. **C)** 0.89 μM Aβ$_{555}$: 500 nM ABAD, after ABAD injection there is a partial quenching of Cy3 dye observed at approximately 5%. This is consistent with the partial inhibition of Aβ aggregation. **D)** 0.89 μM Aβ$_{555}$: 10 nM ABAD, after ABAD injection there is a 35% quenching of Cy3 dye observed, similar to that of the control sample. This is consistent with the promotion of Aβ aggregation.
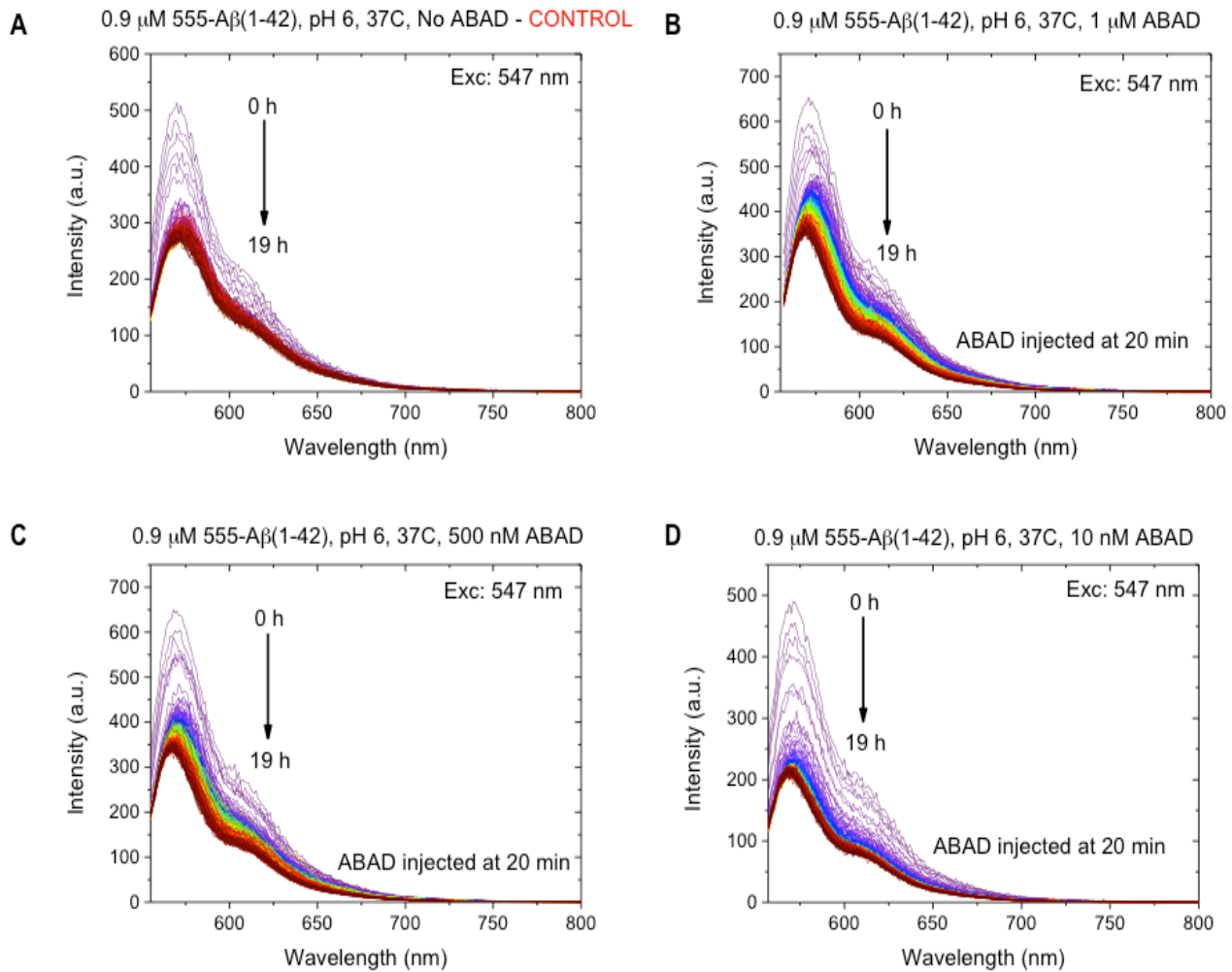
Figure 5.19: Fluorescence quenching of pH6 induced Aβ aggregation, with the addition of different concentrations of ABAD protein, to monitor its effects in plaque like aggregation conditions. A) Control sample test 0.89 μM Aβ$_{555}$: no ABAD present, Aβ continues to form aggregates over 19 h with an observed 30% quenching. **B)** 0.89 μM Aβ$_{555}$: 1 μM ABAD, after ABAD injection, there is an observed 30% quenching of Cy3 dye. This is consistent with the control sample. **C)** 0.89 μM Aβ$_{555}$: 500 nM ABAD, after ABAD injection there is observed quenching of the Cy3 dye of approximately 35%. This is consistent with the promotion of Aβ aggregation. **D)** 0.89 μM Aβ$_{555}$: 10 nM ABAD, after ABAD injection there is observed 40% quenching of the Cy3 dye. This is consistent with the promotion of Aβ aggregation.

The ABAD produced similar effects in both the HFIP (globular structures) and NaCl (fibril structures) induced aggregation conditions, where the addition of 1 μM ABAD appeared to prevent the aggregation of Aβ: the addition of 500 nM ABAD appeared to partially inhibit the Aβ aggregation and the addition of 10 nM ABAD appeared to

promote the aggregation of Aβ. In the acidic pH6 conditions (plaque like structures) the addition of ABAD appeared to promote the aggregation of Aβ in all ABAD concentrations (Figure 5.20).
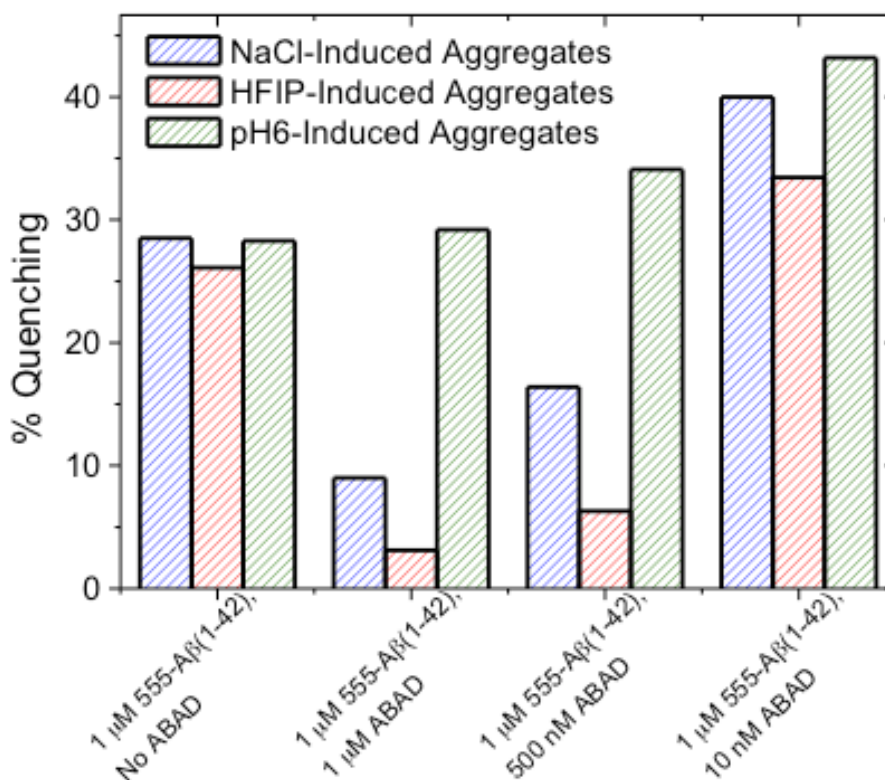
Figure 5.20: The percentage quenching of Cy3 dye, in three different induced Aβ aggregation conditions, treated with three ABAD concentrations. The change in ABAD concentration produced similar results in both the HFIP and NaCl induced aggregation conditions; the addition of 1 μM ABAD and 500 nM ABAD inhibited the Aβ aggregation and the addition of 10 nM ABAD promoted the Aβ aggregation. At pH6 (plaque like structures) the addition of ABAD appeared to promote the aggregation in all ABAD concentrations.

Having determined how varying concentrations of the ABAD protein effect the Aβ aggregation, it was now possible to progress this assay to evaluate potential inhibitors of the ABAD-Aβ interaction.

As described previously in section 5.1.3 the known inhibitor frentizole could be used for any method development tests and so to determine if the compounds could be screened using this assay. Due to the nature of the K684-K711 analogue series and the solubility issues previously described, it was important to determine if the assay buffer was going to interfere with the Cy3 dye and therefore prevent the compounds from being screened, or whether the compounds themselves were going to interact with the Cy3 dye and cause a quench in Cy3 emission. Fortunately, the buffer had no effect on the fluorescence emission of the Cy3 dye over the aggregation timescale. Similarly, although frentizole did initially quench the Cy3 dye (by approximately 1%) thereafter there was no observed effect on the fluorescence emission of the Cy3 dye (shown in Figure 5.21).
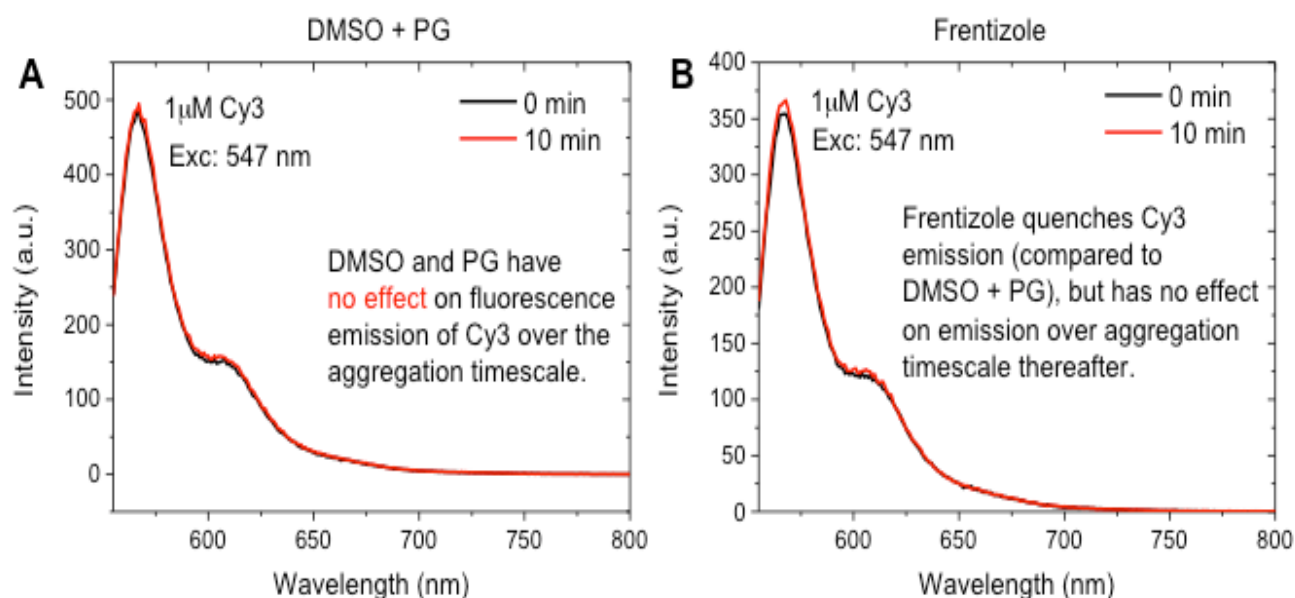
Figure 5.21: The fluorescence emission spectrum of Cy3 dye in the presence of analogue buffer (DMSO and PG) and frentizole. A) The addition of DMSO and PG causes no change to the fluorescence emission spectrum of Cy3. **B)** The addition of frentizole initially quenched the Cy3 dye (by approximately 1%) thereafter there was no observed effect on the fluorescence emission of the Cy3 dye.

Further assay validation was required before the full K684-K711 analogue series could be analysed. However due to time constraints, it was not possible to evaluate this Aβ aggregation assay as a screening method for the K684-K711 compounds. However, the groundwork has now been established for this assay, and it is hoped that in the near future, that the work reported in this chapter will play a vital role in utilising this technique as a screening method to help validate potential ABAD-Aβ inhibitors (further discussion carried out in Chapter 6.3).

5.7   Conclusion and summary of results

In summary, the specific activity of ABAD in the presence of the K684-K711 analogue series was measured and having subtracted the compound's auto-fluorescence from the obtained results, the data was analysed using a one-way ANOVA analysis with Dunnet's mulitiple comparison correction. The ABAD enzyme activity analysis produced 5 compounds which were shown to significantly increase ABAD activity. It is also worth noting that all the K684-K711 analogues produced an increase in ABAD activity, however the variation between the replicates of each compound in the assay was great, therefore influencing the statistical analysis results.

It has been shown that a novel morphology sensitive fluorescence assay for amyloid aggregation can be used to measure potential inhibitors of the ABAD-Aβ interaction. Due to time constraints it has not been possible to measure the effects that the K684-K711 analogue series have on Aβ aggregation, using this assay.

Unfortunately, it was shown that due to the composition of the K684-K711 analogue series, and the solubility issues caused by their organic synthesis, the thermal shift analysis technique and the direct binding assay (Octet RED 384 system) could not be used to investigate the kinetic parameters of the K684- K711 analogue series inhibition against the ABAD-Aβ interaction.

The conclusion and discussion of these results as well as future perspectives is described further in Chapter 6.

Chapter 6: Conclusions, discussion and future directions

The work described in this thesis has laid the foundations for targeting two key interactions as a strategy for the treatment of Alzheimer's disease. This research focused on two main aspects: firstly, the identification and development of new inhibitors of the ABAD- Aβ interaction in the treatment of Alzheimer's disease, and establishing biophysical assays which could potentially be used as screening methods to test these inhibitors. And secondly, investigating CypD as a potential therapeutic target in Alzheimer's disease.

6.1 <u>Elucidating and identifying potential small molecule inhibitors of the ABAD- Aβ interaction</u>

Previous work in the Gunn- Moore laboratory (carried out by Dr Kirsty Muirhead) identified 16 'hit' small molecule binding partners of ABAD by carrying out thermal shift analysis (TSA) using 674 Maybridge fragment library compounds (Muirhead 2011). This Maybridge fragment library was adapted by Prof Jim Naismith group (University of St Andrews) to allow it to be screened using two, one dimensional nuclear magnetic resonance (NMR) experiments (saturation transfer difference and WaterLOGSY) as a method of 'hit' validation. Using these two NMR experiments it was therefore possible to evaluate and confirm the thermal shift analysis results. These NMR experiments were run in parallel against the ABAD protein mixed with Maybridge fragments, creating a fast and reliable screening method. Only Maybridge fragments that were 'hits' in both NMR experiments were taken forward and classified as true 'hit' compounds when validated against the TSA results.

The NMR analysis was highly successful and revealed 51 'hit' small molecule binding partners of ABAD protein from the Maybridge fragment library. Of these 51

compounds, eight compounds (fragment numbers: 94,99, 136, 217, 221, 358, 390 and 441) were classified as 'hit molecules in both TSA and the two NMR experiments. Having effectively been identified from three different experiments, these compounds were then considered to be molecules which could eventually be potential inhibitors of the Aβ interaction. The structures of these fragments are shown in Figure 6.1.
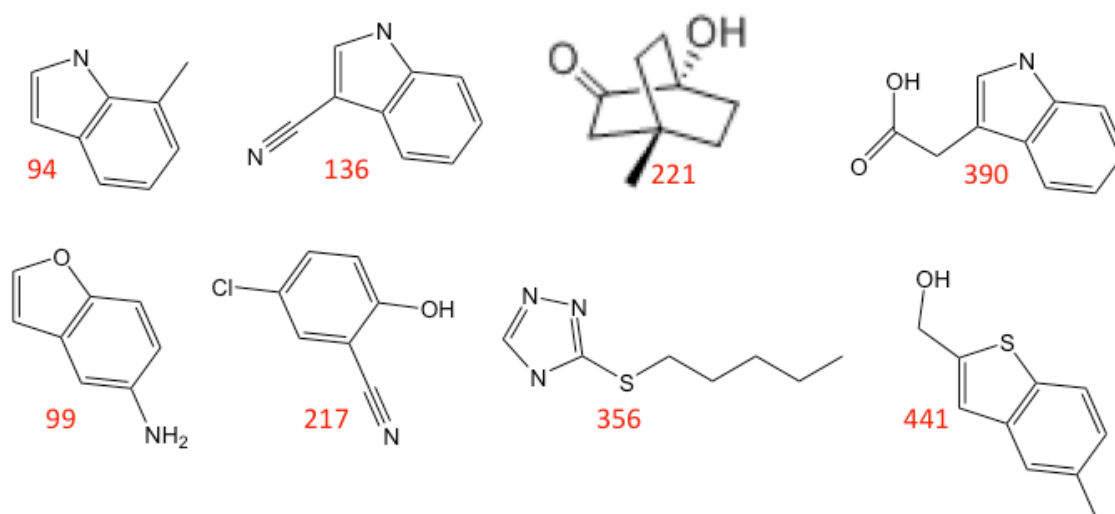
Figure 6.1: Molecular structure of the eight Maybridge fragments identified as ABAD binding partners in both TSA and NMR analysis. These fragments have been classified as 'hit' compounds having been shown to bind to ABAD in both thermal shift analysis (TSA) and two NMR experiments. The Maybridge fragment library identifier numbers are shown in red (Chemical names of the fragments are detailed in Figure 3.6).

The variations observed between the compounds that are capable of binding to ABAD protein in the TSA assay and in the NMR experiments were quite large. This is normal in fragment based screening and emphasises the need to validate 'hit' compounds in more than one biophysical assay (Erlanson *et al.* 2004; Carr *et al.* 2005; Hajduk & Greer 2007). One suggestion for the variation in 'hit' compounds observed between assays could be explained by the size of the fragments. A fragment of molecular weight less than 300 daltons, does not effectively occupy the chemical space available in the

ABAD binding site, and could therefore appear as a positive 'hit' molecule in one assay condition, but may not adopt the same conformation and enter the binding site in the same fashion, within another assay and therefore produce a negative result indicating that no binding is observed.

Future work using these 'hit' compounds would consist of firstly investigating the kinetic parameters of their interactions with ABAD. This could be through the use of isothermal titration calorimetry, surface plasmon resonance or utilising the *Fortebio* Octet RED 384 system. By measuring their effects against ABAD with the enzyme activity assay this would also allow the compounds to be ranked in order of how significantly they increase ABAD activity.

As the compounds were tested in the presence of Aβ in the TSA, their ability to bind to ABAD in the presence of Aβ is not impaired. However, by applying the morphology sensitive aggregation assay to measure how the compounds effect Aβ aggregation induced by various aggregation conditions this will provide further information on the compounds ability to potentially inhibit the ABAD-Aβ interaction.

As these 'hit' molecules are taken from the Maybridge fragment library and conform to the 'rule of three', the compounds are particularly small and are likely to be weak (millimolar) binding partners of ABAD protein, and thus would require future chemical modifications to grow the molecules to produce a more complex lead series of compounds. By establishing the kinetic parameters of the fragments' interactions with ABAD and their effects against Aβ aggregation, this will allow the selection of key fragments which produce the greatest therapeutic effect to be taken on chemical modification. This modification could possibly take two forms, whereby compounds could either be grouped and combined as 'building blocks' to produce larger molecules

that would effectively sample the available ABAD binding site, or compounds would be analysed by a structural activity relationship (SAR) approach would be used. Using SAR analysis is only usually considered in a larger fragment screen where many compounds have been identified and could possibly be ranked in a structurally similar manner, however, it may be considered in this instance as three of the compounds have an indole group, with two other compounds contain the structurally similar benzofuran and benzothiophene groups. These structurally related groups could potentially form the basis for a chemical modification study that could determine the key groups involved in the fragment- ABAD interaction.

Ultimately however, key structural information is required to progress these compounds further down the drug discovery pipeline. Irrespective of numerous attempts, and by exhausting many stochastic screens to test many crystallisation conditions, no ABAD-fragment diffracting co-crystals could be produced. Three optimisation trials were set up using the best crystals produced as a basis for the screen, however, it was not possible to obtain diffracting ABAD-fragment co-crystals from these screens either. It was thought that this issue could be resolved by first crystallising native ABAD protein and soaking in the fragment once diffracting, reproducible ABAD crystals were achieved, however, this method of crystallisation also failed as it was found to be impossible to crystallise ABAD by itself. This is supported by the three published ABAD structure papers, which have all crystallised ABAD in the presence of another molecule (Powell *et al*. 2000; Kissinger *et al*. 2004; Lustbader *et al*. 2004).

A significant reason for the ABAD-fragment co-crystallography failing could have been the use of DMSO to dissolve the fragment compounds. Throughout my extensive experiments with ABAD protein it was observed that ABAD can be quite unstable, and will precipitate rapidly in a buffer that does not contain DTT, or glycerol. It is also

important to limit the concentration of DMSO used in the assay, as it was observed that ABAD precipitates rapidly in the presence of this solvent.

The most successful conditions that proved to be the most effective for the native ABAD protein crystallography, were 0.77 M sodium citrate (unbuffered), 0.1 M sodium citrate (pH 5.5), 0.17 M magnesium acetate (From Sto19, well E3, site 2, shown in Figure 3.8). By altering or broadening these conditions this could prove to be an effective foundation for any future crystallographic work with ABAD.

6.2   Cyclophilin D as a possible therapeutic target in the treatment of Alzheimer's disease

In comparison to the on-going research being carried out on the ABAD-Aβ interaction, relatively little study is currently being carried out to investigate the use of CypD as a therapeutic target in AD. During times of oxidative stress, or in the presence of Aβ, this promotes the translocation of CypD to the inner mitochondrial membrane contributing to the opening of the mPTP, triggering apoptosis and necrosis. By targeting CypD and preventing this translocation this could be beneficial in AD (Du *et al*. 2008; Du *et al*. 2011). The CypD protein studies presented in this work were not to investigate the CypD-Aβ interaction, but were to investigate another potential binding partner of CypD protein: ABAD protein, and the difficult task of trying validate the unpublished data experimental data from Dr Yimin Ren (formally of the Gunn-Moore group) who observed that CypD is capable of binding to ABAD using FRET (Förster resonance energy transfer) analysis. In order to confirm ABAD as a potential CypD binding partner it was necessary to use biophysical techniques to elucidate these possible interactions further. Two techniques specifically employed to investigate the CypD-ABAD interaction were x-ray crystallography and isothermal titration calorimetry (ITC).

The only CypD construct which had been previously crystallised successfully to date was a truncated mutant construct ($\Delta CypD^{K133I}$) which was missing 29 amino acids from its N-terminal region (Schlatter *et al*. 2005; Kajitani *et al*. 2008). This construct was a kind gift from the Fujihashi group (Kyoto University, Tokyo) and it was believed that as this construct had been crystallised previously, that it would be straightforward to firstly purify and then crystallise, however this was not the case.

The $\Delta CypD^{K133I}$ construct is an untagged protein, which requires a more stringent purification method in order to remove all the contaminants. It was a lengthy protein purification process, which lasted approximately 4 days (double that of a His-tagged protein), and provided very little protein. The lack of pure CypD protein produced is most likely due to the length of the purification process, and that the protein was observed to become unstable and precipitate out of the purification buffer solution.

Nevertheless, pure, soluble $\Delta CypD^{K133I}$ protein was produced and taken forward into co-crystallographic trials with the ABAD protein, where diffracting crystals were achieved. However, once these crystals were re-solublised, they were found to only contain native $\Delta CypD^{K133I}$ protein without any bound ABAD protein (this was also confirmed by solving the crystal structure by molecular replacement).

The $\Delta CypD^{K133I}$ construct was established by Schlatter *et al*. in 2005, who developed this construct by direct surface engineering, where many mutations were added to the surface of the truncated CypD construct, to determine which mutation proved to be the most effective in conferring crystallisability on the protein. By introducing mutations on a protein these can increase the stability of the crystal, improve the solubility and reduce the entropic barrier of crystallisation by reducing flexible loops and surface entropy reduction (Trevino *et al*. 2007). Unfortunately by introducing mutations in the protein it may also render its function inactive and leave it incapable of interacting with other molecules. In this instance this could be a plausible reason as to why $\Delta CypD^{K133I}$ does not appear to interact with ABAD. It could also be possible that the binding site for the ABAD- CypD interaction is located in the truncated N-terminal region, or that this truncated region contains key amino acids that are required to hold the structure in the correct conformation for an interaction to occur. As this construct has been co-

crystallised previously with a known inhibitor cyclosporine A (Kajitani *et al*. 2008), it also seems plausible that contrary to previously observed results, the ABAD protein may not be a binding partner of CypD. This theory was also supported by an isothermal titration calorimetry experiment (ITC), which again did not show the ΔCypD^{K133I} protein binding to ABAD protein in the micromolar range. Due to the small yield of pure ΔCypD^{K133I} protein obtained after purification, and the large amount of protein that an ITC experiment requires it was not possible to investigate if ΔCypD^{K133I} protein was capable of binding ABAD protein in the weaker millimolar range. This would be a good origin for any ΔCypD^{K133I} protein experiments that may take place in the future as it could potentially provide the solution that ΔCypD^{K133I} protein does bind ABAD protein, but that it is a very weak protein interaction, or possibly a transient interaction in nature.

As it was not possible to rule out why ΔCypD^{K133I} protein did not bind ABAD protein, it was vital to establish if the ABAD protein was capable of binding to full length CypD protein. Eventually after a long period of method development involving several full length CypD constructs inserted in various purification vectors two full length GST-tagged CypD constructs were produced (pGEX-6P-1 CypD and pGEX-6P-1 CypD^{K133I}) that included a full length CypD construct containing the K133I mutation present in the truncated mutant CypD construct. These constructs were made utilising a GST fusion purification system, with a PreScission protease tag cleavage site. This system should have resulted in a large yield of pure CypD protein, however the recovery rate was much lower than anticipated at an average 50 mg. A possible reason for this could be that a large number of uncoupled GST monomers and dimers are produced after lysis. Changing the cell lysis method, perhaps to alternating between small sonication bursts and freezing, rather than the cell disrupter method currently in use may possibly reduce this degradation.

These DNA constructs were used to produce protein, that when purified, progressed into crystal trials; however as yet no good quality crystals have been made, and have therefore not progressed into any optimisation and diffraction trials. This is unsurprising as no full length CypD construct has been crystallised and published to date. This however is believed to be the first full length untagged CypD protein to be purified successfully and used in any biophysical assay. It is believed that previous reported studies have not cleaved the GST tag from the protein before terminating the purification (Du *et al*. 2008). As the GST tag is larger than the size of the CypD protein (26 kDa compared to 23 kDa, respectively), this could have a significant negative effect in the folding of the protein, and in the conformations which the protein is capable of adopting. But also, by retaining the GST tag, this may hold the protein in a conformation which not only keeps the CypD protein stable, but may also facilitate its ability to bind another protein.

Further studies are therefore required to establish if CypD protein is capable of binding to ABAD protein. In light of the many failed crystallography trials that were set up, not only for investigating the CypD-ABAD interaction, but also investigating the ABAD-Aβ interaction, it would be sensible to adopt another biophysical technique strategy when trying to learn more about these interaction. The use of the *Fortebio* Octet RED 384 system would be ideal to use in this instance. The three CypD constructs could be biotinylated and bound to the SSA sensor, before ABAD protein was applied to establish if the two proteins could bind.

6.3 Assay development for investigating a frentizole based analogue series as potential inhibitors of the ABAD-Aβ interaction

In 2006, it was established that frentizole, an immunosuppressant drug, was an inhibitor of the ABAD-Aβ interaction (Xie *et al.* 2006). Very little was known about how this compound disrupts the ABAD-Aβ interaction, simply because the identification was made by being structurally similar to an ELISA based screening assay and no further publications have succeeded it. However, Xie *et al.* did show that by modifying the compound to produce a novel benzothiazole urea moiety as a backbone for the compound, this resulted in a 30-fold increase in potency. This therefore established that by designing an analogue series based on frentizole that it was possible to increase potency and improve the therapeutic effect achieved. In theory, this may also reduce the immunosuppressive action which frentizole currently has. Research speculation has suggested that no further publications have been produced using this compound as an inhibitor of the ABAD-Aβ interaction due to its adverse immunosuppressive side effects (Prof Sir Mark Pepys FRS, personal communication).

Dr Kamil Musilek (University of Hradec Kralove, Czech Republic) designed a series of 28 frentizole based analogues which required further testing to establish if these compounds would inhibit the ABAD-Aβ interaction, and also if any of these analogues could be developed further into 'drug like' molecules. In order to evaluate these compounds at the molecular level, several assays were optimised and specifically developed for this purpose.

The K684-K711 analogue series compounds proved to be a very difficult set of compounds to work with when developing reproducible assays to test their therapeutic

effects on the ABAD- Aβ interaction. The compounds were found to be insoluble in all buffers except DMSO and propylene glycol (PG), thus when optimising biophysical assays to measure their effects on the ABAD-Aβ interaction care was taken to reduce the overall percentage of DMSO within the assay to its lowest possible concentration as ABAD appears to denature and precipitate rapidly in this buffer (previously described in section 6.1). This in itself proved problematic, as only 20 mg of each synthesised analogue was provided, it was often difficult to maintain a high enough concentration of the compound to see a therapeutic effect in the assay, with a small enough percentage of DMSO present so that the ABAD protein remained active and could be measured effectively. The PG, although a useful vehicle in this scenario for reducing the concentration of DMSO, is a very viscous solution, which in turn could interfere with any fluorescent or absorbance measurements. Some of the compounds in the analogue series are also coloured, which may increase the auto-fluorescence values observed in an assay of that nature (Table 5.1). It is because of the reasons described above that the thermal shift analysis assay was unable to be used to measure the effects of the K684-K711 analogue series as potential inhibitors of the ABAD- Aβ interaction.

In order to improve the solubility issues of the K684-K711 analogue series, it may be possible to prepare the analogues as hydrochloride salts (substances currently used in medications to improve water and acid solubility), guanidines (could be used to prepare compounds containing an amine group) and carboxylic salts (could be used to prepare those compounds with a carboxyl group (–COOH), thus making the compound more polar with both hydrogen bond donors and acceptors) (Stahl 2008). In this instance, guanidines may not be the best option taken if the compounds were to be re-synthesised, because although they could improve the solubility issues of the K684-K711 analogue

series; guanidinium salts are a very powerful protein denaturant so may not allow the ABAD protein to remain active during the assay.

The *Fortebio* Octet RED 384 assay could not be used to measure the effects of the K684-K711 analogue series on the ABAD-Aβ interaction, but for different reasons than those discussed above. In order to measure small molecule binding, this assay relies on the immobilisation of a biotinylated protein (b-ABAD) onto a superstreptavidin (SSA) sensor. When ABAD protein was biotinylated the ABAD specific enzyme activity fell by 47% in comparison to unlabelled ABAD. However, the b-ABAD was still active as its enzyme activity levels were still 35% higher than when compared to a control sample with no ABAD present. This suggests that the surface immobilisation of ABAD renders the protein inactive. The absence of b-ABAD binding to its co-factor NAD^+ binding that it could possible that the biotin could be altering the ABAD conformation sufficiently to inhibit access to the binding site.

Also, this assay failed because the Aβ peptide was capable of binding non- specifically to the SSA sensor. Therefore if any binding was observed, then it would not have been possible to determine whether the Aβ peptide was binding to the sensor, or to the b-ABAD. It may be possible to revisit this assay at a later date and try immobilising biotinylated Aβ (b-Aβ) to the SSA sensor and then add the ABAD with the analogue series to see if the kinetic parameters of the interactions can be established this way, however, due to its sticky nature it seems unlikely that once the b-Aβ is bound onto the sensor, that any interaction it makes could be easily dissociated.

The enzyme activity assay approach was used to measure the catalytic activity of ABAD, in the presence of the K684-K711 analogue series, as a measurement of its function. The principles of this assay involved measuring the reduction of S-

Acetoacetyl- CoA by monitoring the absorbance of its co-factor NAD^+ at 340 nM over time (60 s). Again, this assay required substantial evaluation and development (potentially due to the solubility issues within the K684-K711 analogue series), but eventually it was possible to screen this series to determine their effects on ABAD activity.

All of the K684-K711 compounds were found to increase ABAD activity, although the difficulty in accurately measuring the absorbance due to the compound solubility issues (as discussed in this chapter) and being able to reliably reproduce the data was hard to achieve and the variation between sample replicates was quite large. However after the analogues were subjected to statistic analysis using a one- way ANOVA test with Dunnet's multiple comparison, four of the analogues (K691, K693, K701 and K703) were shown to significantly increase ABAD activity. The structures of these four analogues are shown in Figure 6.2.
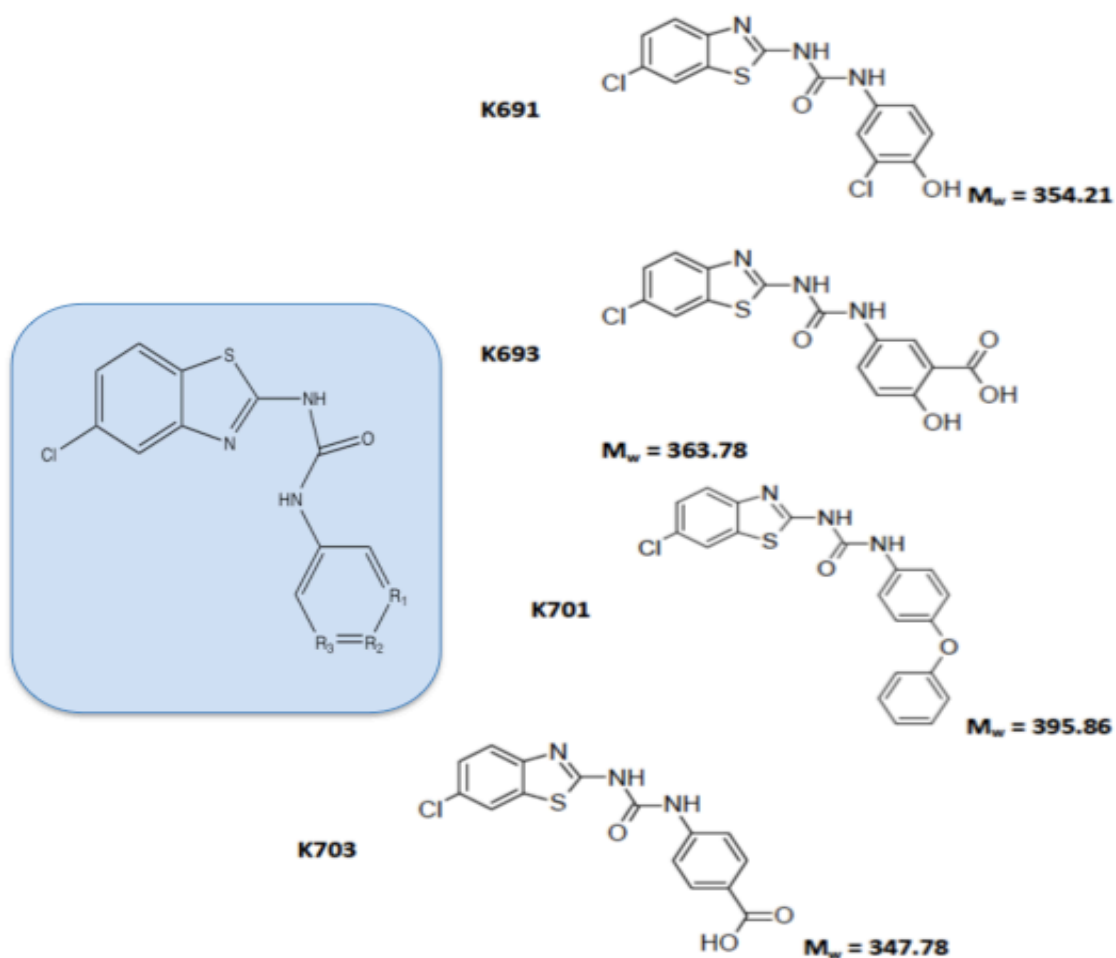
Figure 6.2: The chemical structures of 4 compounds from the K684-K711 analogue series, which were found to significantly increase ABAD activity. On the right of the figure are the four compounds that were found to have significantly increased ABAD activity after statistical analysis with a one way ANOVA test with Dunnet's multiple comparison. Blue box: indicates the basic design for the analogue series modifications, with changes applied to the R_{1-3} groups and to the chlorine atom are altered in a stepwise fashion.

This series of analogues was designed in order to determine where the key functional groups were found within the basic benzothiazole urea backbone. A chlorine molecule appears to be the important electron withdrawing group favoured on the benzothiazole urea ring as this is consistently found in the structure of all four analogues. The hydroxyl group in the para position of the phenylurea ring is also quite conserved and is present in two analogues (K691 and K693) and the oxidised form of the hydroxyl

group; the carboxylic acid is found in the para position of compound K703. Future direction on this area of work may be the synthesis of another analogue series, based on these findings, which would focus on designing compounds that conform with the benzothiazole urea backbone, and contain a chlorine atom in the benziothiazole ring, and a hydroxyl, or a carboxylic acid group located in the para position of the phenylurea ring. Nevertheless, due to the variation between sample replicates within one compound, there may be other analogues in the K684-K711 analogue series which produce a greater increase in ABAD activity, but have not been found to significantly increase the results because of this variation. It is therefore vital, that any future work on these compounds will either address these solubility issues, or measure the analogues again in a different biophysical assay to validate these results.

The novel morphology sensitive Aβ aggregation assay is one method that could be used as a screening tool to validate the ABAD activity analysis findings for the K684-K711 analogue series. This Aβ aggregation assay would be capable of measuring the analogues' ability to inhibit Aβ aggregation and thus its potential to become an inhibitor of the ABAD-Aβ interaction. The principle of this assay is to measure, in real time, changes that occur in the fluorescence emission of the N-terminally labelled Cy3 Aβ aggregates, and where differences in the fluorescence quenching during the Aβ growth process, indicate either promotion or inhibition of Aβ aggregation. The changes to the Aβ growth process are also carried out under three different induced Aβ aggregation conditions to mimic some of the more common Aβ morphologies that are found within cells: HFIP induced Aβ aggregation (to produce globular like structures), NaCl induced aggregation conditions (fibril like structures) and pH6 induced Aβ aggregation conditions (large plaque like structures).

The method development for this novel morphologically sensitive assay revealed that when ABAD is present in both 1:1 Aβ peptide to ABAD protein ratios and 2:1 Aβ peptide to ABAD ratios in HFIP induced and NaCl induced Aβ aggregation conditions, there is no quenching of the Cy3 dye and this indicates that the Aβ aggregation is inhibited. Conversely, when the ABAD protein is present in low concentrations at an Aβ peptide to ABAD ratio of 100:1, in both HFIP and NaCl induced aggregation conditions, the Cy3 dye is quenched by approximately 30%, indicating that the ABAD protein is promoting aggregation. In the acidic pH 6 inducing conditions the ABAD protein appears to promote aggregation at all Aβ peptide to ABAD protein ratios. To some extent, this is consistent with what would occur inside the brain, as the pH 6 induced Aβ aggregation conditions produce plaque like molecules, it is unlikely that the ABAD would have any effect on these aggregates as plaques are found extracellularly and ABAD is a mitochondrial protein. It is therefore more important to focus on the HFIP and the NaCl induced Aβ aggregation conditions for the purpose of this work, as they are more physiologically relevant. However a further use of this assay, in the future, would be to identify other potential Aβ binding compounds that may be morphology specific and bind only to one aggregation condition, and this is where the analysis of all three Aβ aggregation conditions would be useful.

Unfortunately due to time constraints it was not possible to evaluate the K684-K711 analogue series as potential inhibitors of the ABAD-Aβ interaction during the timeframe for the work presented in this thesis. This initial assay advancement has produced a screening tool for an otherwise troublesome set of compounds to reliably measure their effects on the ABAD-Aβ interaction in biophysical assays. It is also hoped that this assay may be used to investigate the Maybridge fragments that have been identified as potential inhibitors of the ABAD-Aβ interaction.

6.4 The overall outlook for targeting the ABAD-Aβ interaction and CypD as potential therapeutic targets in Alzheimer's disease.

The results reported in this work have laid the foundations for investigating two key interactions in Alzheimer's disease. The groundwork has also been established for biophysical assays, which can be used as screening tools to help identify potential inhibitors of these interactions. Both the ABAD-Aβ interaction, and the blockade of CypD are known to be drug targets in the treatment of AD, and by elucidating the molecular mechanisms behind these interactions, through implementing biophysical assays, this will help in the identification and design of potential new therapeutic agents for the treatment of Alzheimer's disease.

With the number of AD cases rising yearly, due to an aging population, this places a great burden on the healthcare system, and the supporting charity foundations, to provide adequate care for AD sufferers. The root of this problem is that the current treatments do not treat the underlying causes behind the disease, instead they help to mask the symptoms of the disease and prolong the brains remaining function. The drug development process is long and costly (as shown in Figure 6.3), but by focussing research into developing treatments for the causative rather than the symptomatic pathway this could lead to new breakthroughs in the treatment of this debilitating disease.
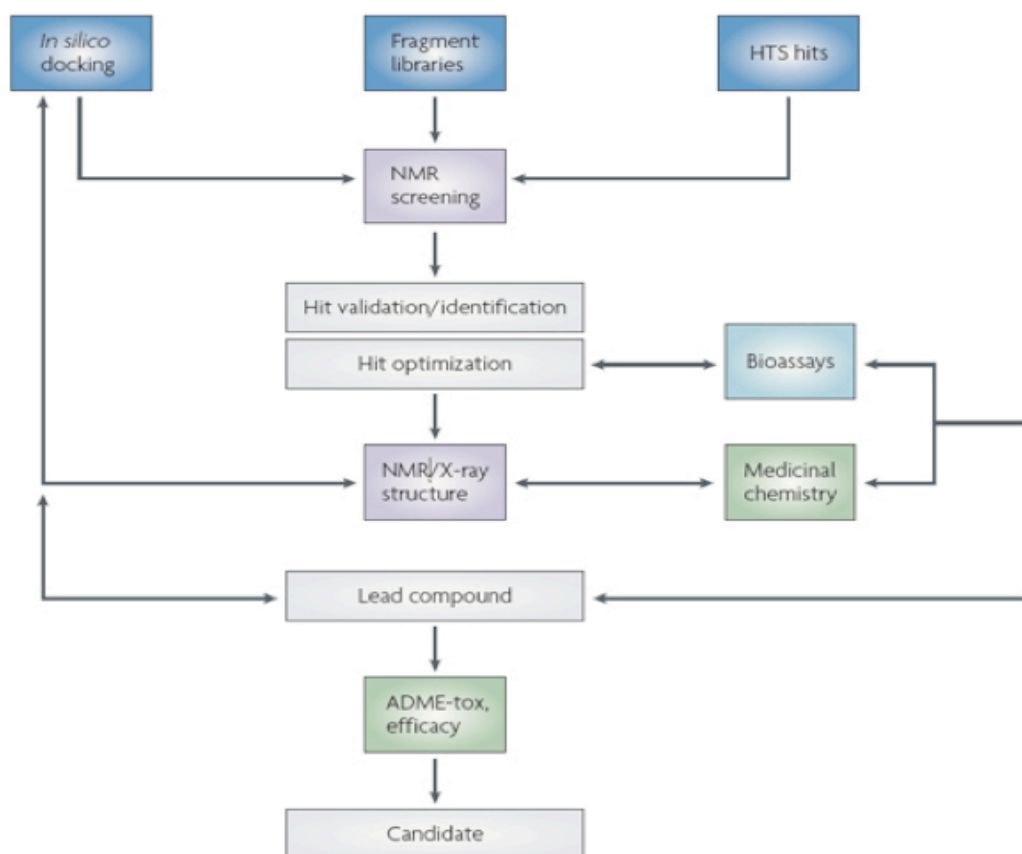
Figure 6.2: A schematic of a drug discovery work program, undertaken to ultimately develop a drug candidate. This is the schematic work flow program detailing the drug discovery process, and highlighting the complex nature of the many techniques that are used to validate and elucidate an eventual drug candidate.

Following the investigations herein, into further understanding the ABAD-Aβ interaction, and the two-pronged approach to identifying and developing potential inhibitors to disrupt this interaction, this work has built upon previously reported findings and the results from the work reported here represent budding advances towards the development of novel therapeutics against the ABAD-Aβ interaction for the treatment of AD.

Although the targeting of CypD as a novel therapeutic in AD, is lagging slightly behind the ABAD-Aβ interaction on the drug discovery work program, it did eventually

produced some promising results, in that, three different constructs have been successfully expressed and purified, and taken into crystal trials. The substantial biophysical assay development carried out when investigating the ABAD-Aβ interaction will also aid significantly in the progress of identifying any potential inhibitors and binding partners of CypD that may produce therapeutic effects, and in the future could lead to the identification of an effective disease modifying drug in the treatment of AD.

References

Abou-Sleiman, P.M., Muqit, M.M.K., Wood, N.W., 2006. Expanding insights of mitochondrial dysfunction in Parkinson's disease. *Nat Rev Neurosci,* 7, 207–219.

Aitken, L, Gunn-Moore, F.J, 2012. ABAD or a good approach to Alzheimer's disease drug discovery? *Biotech International Magazine,* 24, 13–16.

Alzheimer, Scotland. 2011. Drugs - Reminyl/galantamine/Razadyne URL: http://www.alzscot.org/pages/info/reminyl.htm

Alzheimer, Scotland, 2011. Drugs: Aricept/donepezil hydrochloride URL: http://www.alzscot.org/pages/info/aricept.htm

Alzheimer, Scotland. 2011 Drugs: Exelon/rivastigmine URL: http://www.alzscot.org/pages/info/exelon.htm

Alzheimer's Research UK, 2012. Defeating Dementia 2012.

Anandatheerthavarada, H.K., Biswas, G., Mullick, J., Sepuri, N.B.V., Otvos, L., Pain, D., Avadhani, N.G., 1999. Dual targeting of cytochrome P4502B1 to endoplasmic reticulum and mitochondria involves a novel signal activation by cyclic AMP-dependent phosphorylation at Ser128. *EMBO J* 18, 5494–5504.

Andorfer, C., Acker, C.M., Kress, Y., Hof, P.R., Duff, K., Davies, P., 2005. Cell-cycle reentry and cell death in transgenic mice expressing nonmutant human tau isoforms. *J. Neurosci.* 25, 5446–5454.

Angulo, J., Díaz, I., Reina, J.J., Tabarani, G., Fieschi, F., Rojo, J., Nieto, P.M., 2008. Saturation Transfer Difference (STD) NMR Spectroscopy Characterization of Dual Binding Mode of a Mannose Disaccharide to DC-SIGN. *ChemBioChem,* 9, 2225–2227.

Area-Gomez, E., De Groof, A.J.C., Boldogh, I., Bird, T.D., Gibson, G.E., Koehler, C.M., Yu, W.H., Duff, K.E., Yaffe, M.P., Pon, L.A., Schon, E.A., 2009. Presenilins Are Enriched in Endoplasmic Reticulum Membranes Associated with Mitochondria. *Am J Pathol,* 175, 1810–1816.

Asuni, A.A., Boutajangout, A., Quartermain, D., Sigurdsson, E.M., 2007. Immunotherapy Targeting Pathological Tau Conformers in a Tangle Mouse Model Reduces Brain Pathology with Associated Functional Improvements. *J. Neurosci.* 27, 9115–9129.

Augustinack, J.C., Schneider, A., Mandelkow, E.-M., Hyman, B.T., 2002. Specific tau phosphorylation sites correlate with severity of neuronal cytopathology in Alzheimer's disease. *Acta Neuropathol,* 103, 26–35.

Azzolin, L., Antolini, N., Calderan, A., Ruzza, P., Sciacovelli, M., Marin, O., Mammi, S., Bernardi, P., Rasola, A., 2011. Antamanide, a Derivative of Amanita phalloides, Is a Novel Inhibitor of the Mitochondrial Permeability Transition Pore. *PLoS One,* 6, 1.

Bailey, D.N., 1992. Propylene glycol as a vehicle for percutaneous absorption of therapeutic agents. *J. Anal. Toxicol*. 16, 97–98.

Baines, C.P., Kaiser, R.A., Purcell, N.H., Blair, N.S., Osinska, H., Hambleton, M.A., Brunskill, E.W., Sayen, M.R., Gottlieb, R.A., Dorn, G.W., Robbins, J., Molkentin, J.D., 2005a. Loss of cyclophilin D reveals a critical role for mitochondrial permeability transition in cell death. *Nature*, 434, 658–662.

Besson, J.A., Crawford, J.R., Evans, N.T., Gemmell, H.G., Roeda, D., 1992. PET imaging in Alzheimer's disease. *J. R. Soc. Med*. 85, 231–234.

Binder, L.I., Guillozet-Bongaarts, A.L., Garcia-Sierra, F., Berry, R.W., 2005. Tau, tangles, and Alzheimer's disease. *Biochim. Biophys. Acta,* 1739, 216–223.

Bird, T., 2010. Early-Onset Familial Alzheimer Disease - GeneReviews - NCBI Bookshelf. URL http://www.ncbi.nlm.nih.gov/books/NBK1236/

Boettcher, A., Ruedisser, S., Erbel, P., Vinzenz, D., Schiering, N., Hassiepen, U., Rigollier, P., Mayr, L.M., Woelcke, J., 2010. Fragment-Based Screening by Biochemical Assays Systematic Feasibility Studies with Trypsin and MMP12. *J. Biomol. Screen*, 15, 1029–1041.

Boimel, M., Grigoriadis, N., Lourbopoulos, A., Haber, E., Abramsky, O., Rosenmann, H., 2010. Efficacy and safety of immunization with phosphorylated tau against neurofibrillary tangles in mice. *Exp. Neurol*. 224, 472–485.

Bores, G.M., Huger, F.P., Petko, W., Mutlib, A.E., Camacho, F., Rush, D.K., Selk, D.E., Wolf, V., Kosley, R.W., Davis, L., Vargas, H.M., 1996. Pharmacological evaluation of novel Alzheimer's disease therapeutics: acetylcholinesterase inhibitors related to galanthamine. *Journal of Pharmacology and Experimental Therapeutics*, 277, 728 –738.

Borger, E., Aitken, L., Du, H., Zhang, W., Gunn-Moore, F.J., Yan, S., 2013. Is Amyloid binding alcohol dehydrogenase a drug target for treating Alzheimer's disease? *Curr. Alz. Res*. 1, 21-29

Borger, E., Aitken, L., Muirhead, K.E.A., Allen, Z.E., Ainge, J.A., Conway, S.J., Gunn-Moore, F.J., 2011. Mitochondrial β-amyloid in Alzheimer's disease. *Biochem. Soc. Trans*. 39, 868–873

Britschgi, M., Olin, C.E., Johns, H.T., Takeda-Uchimura, Y., LeMieux, M.C., Rufibach, K., Rajadas, J., Zhang, H., Tomooka, B., Robinson, W.H., Clark, C.M., Fagan, A.M., Galasko, D.R., Holtzman, D.M., Jutel, M., Kaye, J.A., Lemere, C.A., Leszek, J., Li, G., Peskind, E.R., Quinn, J.F., Yesavage, J.A., Ghiso, J.A., Wyss-Coray, T., 2009. Neuroprotective Natural Antibodies to Assemblies of Amyloidogenic Peptides Decrease with Normal Aging and Advancing Alzheimer's Disease. *PNAS*. 106, 12145-12150.

Campos-Olivas, R., 2011. NMR screening and hit validation in fragment based drug discovery. *Curr. Top Med. Chem*. 11, 43–67.

Canevari, L., Abramov, A.Y., Duchen, M.R., 2004. Toxicity of amyloid beta peptide: tales of calcium, mitochondria, and oxidative stress. *Neurochem. Res*. 29, 637–650.

Carvalho, A.L., Trincão, J., Romão, M.J., 2009. X-ray crystallography in drug discovery. *Methods Mol. Biol.* 572, 31–56.

Caspersen, C., Wang, N., Yao, J., Sosunov, A., Chen, X., Lustbader, J.W., Xu, H.W., Stern, D., McKhann, G., Yan, S.D., 2005. Mitochondrial Abeta: a potential focal point for neuronal metabolic dysfunction in Alzheimer's disease. *FASEB J*, 19, 2040–2041.

Chai, X., Wu, S., Murray, T.K., Kinley, R., Cella, C.V., Sims, H., Buckner, N., Hanmer, J., Davies, P., O'Neill, M.J., Hutton, M.L., Citron, M., 2011. Passive Immunization with Anti-Tau Antibodies in Two Transgenic Models: Reduction of Tau Pathology and Delay of Disease Progression. *J. Biol. Chem*, 286, 34457-34467.

Chang, L., Karin, M., 2001. Mammalian MAP kinase signalling cascades. *Nature*, 410, 37–40.

Chauhan, V., Chauhan, A., 2006. Oxidative stress in Alzheimer's disease. *Pathophysiology*, 13, 195–208.

Christen, Y., 2000. Oxidative Stress and Alzheimer Disease. *Am J. Clin. Nutr*. 71, 621–629.

Congreve, M., Carr, R., Murray, C., Jhoti, H., 2003. A "Rule of Three" for fragment-based lead discovery? *Drug Discovery Today*, 8, 876–877.

Connern, C.P., Halestrap, A.P., 1996. Chaotropic agents and increased matrix volume enhance binding of mitochondrial cyclophilin to the inner mitochondrial membrane and sensitize the mitochondrial permeability transition to [Ca2+]. *Biochemistry*, 35, 8172–8180.

Crouch, P.J., Harding, S.M.E., White, A.R., Camakaris, J., Bush, A.I., Masters, C.L., 2008. Mechanisms of A[beta] mediated neurodegeneration in Alzheimer's disease. *Int. J. Biochem. Cell Biol*, 40, 181–198.

Cumming, R.C., Dargusch, R., Fischer, W.H., Schubert, D., 2007. Increase in Expression Levels and Resistance to Sulfhydryl Oxidation of Peroxiredoxin Isoforms in Amyloid β-Resistant Nerve Cells. *J. Biol. Chem*. 282, 30523 – 30534.

Cutler, R.G., Kelly, J., Storie, K., Pedersen, W.A., Tammara, A., Hatanpaa, K., Troncoso, J.C., Mattson, M.P., 2004. Involvement of oxidative stress-induced abnormalities in ceramide and cholesterol metabolism in brain aging and Alzheimer's disease. *PNAS*, 101, 2070 –2075.

Dalvit, C., Fogliatto, G., Stewart, A., Veronesi, M., Stockman, B., 2001. WaterLOGSY as a method for primary NMR screening: practical aspects and range of applicability. *J. Biomol. NMR*, 21, 349–359.

Danysz, W., Parsons, C.G., 2003. The NMDA receptor antagonist memantine as a symptomatological and neuroprotective treatment for Alzheimer's disease: preclinical evidence. *International Journal of Geriatric Psychiatry*, 18, S23–S32.

Davis, R.E., Miller, S., Herrnstadt, C., Ghosh, S.S., Fahy, E., Shinobu, L.A., Galasko, D., Thal, L.J., Beal, M.F., Howell, N., Parker, W.D., 1997. Mutations in Mitochondrial Cytochrome C Oxidase Genes Segregate with Late-Onset Alzheimer Disease. *PNAS*, 94, 4526–4531.

Delibas, N., Ozcankaya, R., Altuntas, I., 2002. Clinical importance of erythrocyte malondialdehyde levels as a marker for cognitive deterioration in patients with dementia of Alzheimer type: a repeated study in 5-year interval. *Clin. Biochem.* 35, 137–141.

Devi, L., Prabhu, B.M., Galati, D.F., Avadhani, N.G., Anandatheerthavarada, H.K., 2006. Accumulation of Amyloid Precursor Protein in the Mitochondrial Import Channels of Human Alzheimer's Disease Brain Is Associated with Mitochondrial Dysfunction. *J. Neurosci.* 26, 9057 –9068.

Di Paolo, G., Kim, T.-W., 2011a. Linking lipids to Alzheimer's disease: cholesterol and beyond. *Nat. Rev. Neurosci.* 12, 284–296.

Diercks, T., Coles, M., Kessler, H., 2001. Applications of NMR in drug discovery. *Current Opinion in Chemical Biology*, 5, 285–291.

Doenicke, A., Nebauer, A.E., Hoernecke, R., Mayer, M., Roizen, M.F., 1992. Osmolalities of propylene glycol-containing drug formulations for parenteral use. Should propylene glycol be used as a solvent? *Anesth. Analg.* 75, 431–435.

Drenth, J., 2006. Principles of Protein X-ray Crystallography, 3rd edition. ed. Springer.

Du, H., Guo, L., Fang, F., Chen, D., Sosunov, A.A., McKhann, G.M., Yan, Y., Wang, C., Zhang, H., Molkentin, J.D., Gunn-Moore, F.J., Vonsattel, J.P., Arancio, O., Chen, J.X., Yan, S.D., 2008. Cyclophilin D deficiency attenuates mitochondrial and neuronal perturbation and ameliorates learning and memory in Alzheimer's disease. *Nat Med*. 14, 1097–1105.

Du, H., Guo, L., Zhang, W., Rydzewska, M., Yan, S., 2011. Cyclophilin D deficiency improves mitochondrial function and learning/memory in aging Alzheimer disease mouse model. *Neurobiol. Aging*, 32, 398–406.

Du Yan, S., Shi, Y., Zhu, A., Fu, J., Zhu, H., Zhu, Y., Gibson, L., Stern, E., Collison, K., Al-Mohanna, F., Ogawa, S., Roher, A., Clarke, S.G., Stern, D.M., 1999. Role of ERAB/l-3-Hydroxyacyl-coenzyme A Dehydrogenase Type II Activity in Aβ-induced Cytotoxicity. *J. Biol. Chem*. 274, 2145 –215.6.

Du Yan, S., Zhu, Y., Stern, E.D., Hwang, Y.C., Hori, O., Ogawa, S., Frosch, M.P., Connolly, E.S., McTaggert, R., Pinsky, D.J., Clarke, S., Stern, D.M., Ramasamy, R., 2000. Amyloid β-Peptide-binding Alcohol Dehydrogenase Is a Component of the Cellular Response to Nutritional Stress. *J. Biol. Chem*. 275, 27100 –27109.

Erlanson, D.A., Braisted, A.C., Raphael, D.R., Randal, M., Stroud, R.M., Gordon, E.M., Wells, J.A., 2000. Site-directed ligand discovery. *PNAS*. 97, 9367–9372.

Erlanson, D.A., McDowell, R.S., O'Brien, T., 2004. Fragment-based drug discovery. *J. Med. Chem*. 47, 3463–3482.

Freeman, B.C., Toft, D.O., Morimoto, R.I., 1996. Molecular Chaperone Machines: Chaperone Activities of the Cyclophilin Cyp-40 and the Steroid Aporeceptor-Associated Protein p23. *Science*, 274, 1718 –1720.

Fukui, H., Diaz, F., Garcia, S., Moraes, C.T., 2007a. Cytochrome c oxidase deficiency in neurons decreases both oxidative stress and amyloid formation in a mouse model of Alzheimer's disease. *PNAS*. 104, 14163–14168.

Fukuzaki, E., Takuma, K., Funatsu, Y., Himeno, Y., Kitahara, Y., Gu, B., Mizoguchi, H., Ibi, D., Koike, K., Inoue, M., Yan, S.D., Yamada, K., 2008. Ovariectomy increases neuronal amyloid-beta binding alcohol dehydrogenase level in the mouse hippocampus. *Neurochem. Int*, 52, 1358–1364.

Galimberti, D., Scarpini, E., 2012. Progress in Alzheimer's disease. *J. Neurol*. 259, 201–211.

Games, D., Bard, F., Grajeda, H., Guido, T., Khan, K., Soriano, F., Vasquez, N., Wehner, N., Johnson-Wood, K., Yednock, T., Seubert, P., Schenk, D., 2000. Prevention and reduction of AD-type pathology in PDAPP mice immunized with A beta 1-42. *Ann. Sci*. 920, 274–284.

Gibson, G.E., Starkov, A., Blass, J.P., Ratan, R.R., Beal, M.F., 2010. Cause and Consequence: Mitochondrial Dysfunction Initiates and Propagates Neuronal Dysfunction, Neuronal Death and Behavioral Abnormalities in Age Associated Neurodegenerative Diseases. *Biochim. Biophys. Acta*, 1802, 122–134.

Glabe, C.G., 2004. Conformation-dependent antibodies target diseases of protein misfolding. *Trends in Biochemical Sciences*, 29, 542–547.

Golde, T.E., 2003. Alzheimer disease therapy: Can the amyloid cascade be halted? *J. Clin. Invest*. 111, 11–18.

Gong, Y., Chang, L., Viola, K.L., Lacor, P.N., Lambert, M.P., Finch, C.E., Krafft, G.A., Klein, W.L., 2003. Alzheimer's disease-affected brain: Presence of oligomeric Aβ ligands (ADDLs) suggests a molecular basis for reversible memory loss. *PNAS*, 100, 10417–10422.

Gouras, G.K., Tsai, J., Naslund, J., Vincent, B., Edgar, M., Checler, F., Greenfield, J.P., Haroutunian, V., Buxbaum, J.D., Xu, H., Greengard, P., Relkin, N.R., 2000a. Intraneuronal Aβ42 Accumulation in Human Brain. *Am J Pathol*, 156, 15–20.

Gunn-Moore, F.J., Tavaré, J.M., 1998. Apoptosis of cerebellar granule cells induced by serum withdrawal, glutamate or beta-amyloid, is independent of Jun kinase or p38 mitogen activated protein kinase activation. *Neurosci. Lett*, 250, 53–56.

Guo, H., Wang, F., Yu, K., Chen, J., Bai, D., Chen, K., Shen, X., Jiang, H., 2005. Novel cyclophilin D inhibitors derived from quinoxaline exhibit highly inhibitory activity against rat mitochondrial swelling and Ca2+ uptake/ release. *Acta Pharmacol. Sin*. 26, 1201–1211.

Guss, J.M., King, G.F., 2011. Macromolecular Structure Determination: Comparison of Crystallography and NMR.

Haass, C., Selkoe, D.J., 1993. Cellular processing of beta-amyloid precursor protein and the genesis of amyloid beta-peptide. *Cell*, 75, 1039–1042.

Hajduk, P.J., Greer, J., 2007. A decade of fragment-based drug design: strategic advances and lessons learned. *Nat. Rev. Drug Discov*. 6, 211–219.

Halestrap, A., 2005. Biochemistry: A pore way to die. *Nature*, 434, 578–579.

Halestrap, A.P., 2006. Calcium, mitochondria and reperfusion injury: a pore way to die. *Biochem. Soc. Trans*, 34, 232–237.

Halestrap, A.P., Connern, C.P., Griffiths, E.J., Kerr, P.M., 1997. Cyclosporin A binding to mitochondrial cyclophilin inhibits the permeability transition pore and protects hearts from ischaemia/reperfusion injury. *Mol. Cell. Biochem*, 174, 167–172.

Hansson, C.A., Frykman, S., Farmery, M.R., Tjernberg, L.O., Nilsberth, C., Pursglove, S.E., Ito, A., Winblad, B., Cowburn, R.F., Thyberg, J., Ankarcrona, M., 2004. Nicastrin, Presenilin, APH-1, and PEN-2 Form Active γ-Secretase Complexes in Mitochondria. *J. Biol. Chem*. 279, 51654 –51660.

Hansson Petersen, C.A., Alikhani, N., Behbahani, H., Wiehager, B., Pavlov, P.F., Alafuzoff, I., Leinonen, V., Ito, A., Winblad, B., Glaser, E., Ankarcrona, M., 2008. The amyloid β-peptide is imported into mitochondria via the TOM import machinery and localized to mitochondrial cristae. *PNAS*, 105, 13145 –13150.

Hardy, J.A., Higgins, G.A., 1992. Alzheimer's disease: the amyloid cascade hypothesis. *Science*, 256, 184–185.

Harold, D., Abraham, R., Hollingworth, P., Sims, R., Gerrish, A., et al., 2009. Genome-wide association study identifies variants at CLU and PICALM associated with Alzheimer's disease, and shows evidence for additional susceptibility genes. *Nat. Genet*. 41, 1088–1093.

Hartley, D.M., Walsh, D.M., Ye, C.P., Diehl, T., Vasquez, S., Vassilev, P.M., Teplow, D.B., Selkoe, D.J., 1999. Protofibrillar intermediates of amyloid beta-protein induce acute electrophysiological changes and progressive neurotoxicity in cortical neurons. *J. Neurosci*. 19, 8876–8884.

Hartmann, T., Bieger, S.C., Bruhl, B., Tienari, P.J., Ida, N., Allsop, D., Roberts, G.W., Masters, C.L., Dotti, C.G., Unsicker, K., Beyreuther, K., 1997b. Distinct sites of intracellular production for Alzheimer's disease A[beta]40/42 amyloid peptides. *Nat. Med*. 3, 1016–1020.

Hayashi, T., Rizzuto, R., Hajnoczky, G., Su, T.-P., 2009. MAM: more than just a housekeeper. *Trends Cell. Biol*. 19, 81–88.

He, X., Cooley, K., Chung, C.H.Y., Dashti, N., Tang, J., 2007. Apolipoprotein Receptor 2 and X11α/β Mediate Apolipoprotein E-Induced Endocytosis of Amyloid-β Precursor Protein and β-Secretase, Leading to Amyloid-β Production. *J. Neurosci*. 27, 4052 –4060.

He, X., Merz, G., Yang, Y., Mehta, P., Schulz, H., Yang, S., 2001. Characterization and localization of human type10 17β-hydroxysteroid dehydrogenase. *Eu. J. Biochem*. 268, 4899–4907.

Hertzel, A.V., Smith, L.A., Berg, A.H., Cline, G.W., Shulman, G.I., Scherer, P.E., Bernlohr, D.A., 2006. Lipid metabolism and adipokine levels in fatty acid-binding protein null and transgenic mice. *Am. J. Phys. - Endocrinology And Metabolism*, 290, E814 –E823.

Holmes, C., Boche, D., Wilkinson, D., Yadegarfar, G., Hopkins, V., Bayer, A., Jones, R.W., Bullock, R., Love, S., Neal, J.W., Zotova, E., Nicoll, J.A.R., 2008. Long-term effects of Abeta42 immunisation in Alzheimer's disease: follow-up of a randomised, placebo-controlled phase I trial. *Lancet*, 372, 216–223.

Hubbard-Green, T., 2012. Alzheimer's Society Demography. URL: http://alzheimers.org.uk/site/scripts/documents_info.php?documentID=412.

Inbar, P., Yang, J., 2006. Inhibiting protein-amyloid interactions with small molecules: a surface chemistry approach. *Bioorg. Med. Chem. Lett*. 16, 1076–1079.

Iqbal, K., Grundke-Iqbal, I., 2008. Alzheimer neurofibrillary degeneration: significance, etiopathogenesis, therapeutics and prevention. *J. Cell. Mol. Med*. 12, 38–55.

Jan, A., Hartley, D.M., Lashuel, H.A., 2010. Preparation and characterization of toxic Aβ aggregates for structural and functional studies in Alzheimer's disease research. *Nature Protocols*, 5, 1186–1209.

Jecklin, M.C., Schauer, S., Dumelin, C.E., Zenobi, R., 2009. Label-free determination of protein-ligand binding constants using mass spectrometry and validation using surface plasmon resonance and isothermal titration calorimetry. *J. Mol. Recognit*. 22, 319–329.

Kadowaki, H., Nishitoh, H., Urano, F., Sadamitsu, C., Matsuzawa, A., Takeda, K., Masutani, H., Yodoi, J., Urano, Y., Nagano, T., Ichijo, H., 2005. Amyloid [beta] induces neuronal cell death through ROS-mediated ASK1 activation. *Cell Death Differ*. 12, 19–24.

Kaether, C., Haass, C., 2004. A lipid boundary separates APP and secretases and limits amyloid beta-peptide generation. *J. Cell. Biol*. 167, 809–812.

Kajitani, K., Fujihashi, M., Kobayashi, Y., Shimizu, S., Tsujimoto, Y., Miki, K., 2008. Crystal structure of human cyclophilin D in complex with its inhibitor, cyclosporin A at 0.96Å resolution. *Proteins: Structure, Function, and Bioinformatics*, 70, 1635–1639.

Karbowski, M., Jeong, S.-Y., Youle, R.J., 2004. Endophilin B1 is required for the maintenance of mitochondrial morphology. *J. Cell. Biol*, 166, 1027–1039.

Kayed, R., Head, E., Thompson, J.L., McIntire, T.M., Milton, S.C., Cotman, C.W., Glabe, C.G., 2003. Common Structure of Soluble Amyloid Oligomers Implies Common Mechanism of Pathogenesis. *Science*, 300, 486 –489

Keil, U., Bonert, A., Marques, C.A., Scherping, I., Weyermann, J., Strosznajder, J.B., Müller-Spahn, F., Haass, C., Czech, C., Pradier, L., Müller, W.E., Eckert, A., 2004. Amyloid beta-induced changes in nitric oxide production and mitochondrial activity lead to apoptosis. *J. Biol. Chem*, 279, 50310–50320.

Kessler, J., Herholz, K., Grond, M., Heiss, W.D., 1991. Impaired metabolic activation in Alzheimer's disease: a PET study during continuous visual recognition. *Neuropsychologia*, 29, 229–243.

Kissinger, C.R., Rejto, P.A., Pelletier, L.A., Thomson, J.A., Showalter, R.E., Abreo, M.A., Agree, C.S., Margosiak, S., Meng, J.J., Aust, R.M., Vanderpool, D., Li, B., Tempczyk-Russell, A., Villafranca, J.E., 2004. Crystal Structure of Human ABAD/HSD10 with a Bound Inhibitor: Implications for Design of Alzheimer's Disease Therapeutics. *J. Mol. Biol*. 342, 943–952.

Klein, W.L., 2002. A[beta] toxicity in Alzheimer's disease: globular oligomers (ADDLs) as new vaccine and drug targets. *Neurochem. I*. 41, 345–352.

Kobs, G., 2004. Finding the right protein purification system. *Cell Notes*, 4.

Krapfenbauer, K., Engidawork, E., Cairns, N., Fountoulakis, M., Lubec, G., 2003. Aberrant expression of peroxiredoxin subtypes in neurodegenerative disorders. *Brain Res*, 967, 152–160.

Kuhla, B., Boeck, K., Lüth, H.-J., Schmidt, A., Weigle, B., Schmitz, M., Ogunlade, V., Münch, G., Arendt, T., 2006. Age-dependent changes of glyoxalase I expression in human brain. *Neurobiol. Aging*, 27, 815–822.

LaFerla, F.M., Green, K.N., Oddo, S., 2007. Intracellular amyloid-[beta] in Alzheimer's disease. *Nat Rev Neurosci*, 8, 499–509.

Leung, A.W.C., Halestrap, A.P., 2008. Recent progress in elucidating the molecular mechanism of the mitochondrial permeability transition pore. *Biochim. Biophys. Acta*, 1777, 946–952.

Lim, Y.-A., Grimm, A., Giese, M., Mensah-Nyagan, A.G., Villafranca, J.E., Ittner, L.M., Eckert, A., Götz, J., 2011. Inhibition of the Mitochondrial Enzyme ABAD Restores the Amyloid-β-Mediated Deregulation of Estradiol. *PLoS One*, 6, e28887.

Lin, M.T., Beal, M.F., 2006. Mitochondrial dysfunction and oxidative stress in neurodegenerative diseases. *Nature*, 443, 787–795.

Lipinski, C., Hopkins, A., 2004. Navigating chemical space for biology and medicine. *Nature*, 432, 855–861.

Lipinski, C.A., 2004. Lead- and drug-like compounds: the rule-of-five revolution. *Drug Discovery Today: Technologies*, 1, 337–341.

Lipinski, C.A., Lombardo, F., Dominy, B.W., Feeney, P.J., 1997. Experimental and computational approaches to estimate solubility and permeability in drug discovery and development settings. *Advanced Drug Delivery Reviews*, 23, 3–25.

Liu, X., Deng, G., Chu, X., Li, N., Wu, L., Li, D., 2007. Formation of an enolate intermediate is required for the reaction catalyzed by 3-hydroxyacyl-CoA dehydrogenase. *Bioorg. Med. Chem. Lett.* 17, 3187–3190.

Lue, L.F., Kuo, Y.M., Roher, A.E., Brachova, L., Shen, Y., Sue, L., Beach, T., Kurth, J.H., Rydel, R.E., Rogers, J., 1999. Soluble amyloid beta peptide concentration as a predictor of synaptic change in Alzheimer's disease. *Am. J. Pathol.* 155, 853–862.

Lundqvist, T., 2005. The devil is still in the details--driving early drug discovery forward with biophysical experimental methods. *Curr Opin Drug Discov Devel*, 8, 513–519.

Luo, X., Yan, R., 2010. Inhibition of BACE1 for therapeutic usein Alzheimer's disease. *Int J Clin Exp Pathol*, 3, 618–628.

Luo, Y., Bolon, B., Damore, M.A., Fitzpatrick, D., Liu, H., Zhang, J., Yan, Q., Vassar, R., Citron, M., 2003. BACE1 (β-secretase) knockout mice do not acquire compensatory gene expression changes or develop neural lesions over time. *Neurobiology of Disease*, 14, 81–88.

Lustbader, J.W., Cirilli, M., Lin, C., Xu, H.W., Takuma, K., Wang, N., Caspersen, C., Chen, X., Pollak, S., Chaney, M., Trinchese, F., Liu, S., Gunn-Moore, F., Lue, L.-F., Walker, D.G., Kuppusamy, P., Zewier, Z.L., Arancio, O., Stern, D., Yan, S.S., Wu, H., 2004. ABAD Directly Links Aß to Mitochondrial Toxicity in Alzheimer's Disease. *Science*, 304, 448–452.

Luvisetto, S., Basso, E., Petronilli, V., Bernardi, P., Forte, M., 2008. Enhancement of anxiety, facilitation of avoidance behavior, and occurrence of adult-onset obesity in mice lacking mitochondrial cyclophilin D. *Neuroscience*, 155, 585–596.

Maezawa, I., Hong, H.-S., Liu, R., Wu, C.-Y., Cheng, R.H., Kung, M.-P., Kung, H.F., Lam, K.S., Oddo, S., LaFerla, F.M., Jin, L.-W., 2008. Congo red and thioflavin-T analogs detect Aβ oligomers. *J Neurochem*, 104, 457–468.

Mahley, R.W., Rall, S.C., 2000. APOLIPOPROTEIN E: Far More Than a Lipid Transport Protein. *Annual Review of Genomics and Human Genetics*, 1, 507–537.

Major, L.L., Smith, T.K., 2011. Screening the MayBridge Rule of 3 Fragment Library for Compounds That Interact with the Trypanosoma brucei myo-Inositol-3-Phosphate Synthase and/or Show Trypanocidal Activity. *Mol. Biol. Int*. 2011, 389364.

Manczak, M., Anekonda, T.S., Henson, E., Park, B.S., Quinn, J., Reddy, P.H., 2006. Mitochondria are a direct site of Aβ accumulation in Alzheimer's disease neurons: implications for free radical generation and oxidative damage in disease progression. *Hum. Mol Genet.* 15, 1437 –1449.

Mandelkow, E.M., Biernat, J., Drewes, G., Gustke, N., Trinczek, B., Mandelkow, E., 1995. Tau domains, phosphorylation, and interactions with microtubules. *Neurobiol. Aging*, 16, 355–363.

Marques, A.T., Fernandes, P.A., Ramos, M.J., 2008. Molecular dynamics simulations of the amyloid-beta binding alcohol dehydrogenase (ABAD) enzyme. *Bioorg. Med. Chem*. 16, 9511–9518.

Martin, L., Latypova, X., Terro, F., 2011. Post-translational modifications of tau protein: implications for Alzheimer's disease. *Neurochem. Int*. 58, 458–471.

Masters, C.L., Gajdusek, D.C., Gibbs, C.J., Jr, 1981. The familial occurrence of Creutzfeldt-Jakob disease and Alzheimer's disease. *Brain*, 104, 535–558.

Matsuda, S., Koyasu, S., 2000. Mechanisms of action of cyclosporine. *Immunopharmacology*, 47, 119–125.

Matsui, T., Ingelsson, M., Fukumoto, H., Ramasamy, K., Kowa, H., Frosch, M.P., Irizarry, M.C., Hyman, B.T., 2007b. Expression of APP pathway mRNAs and proteins in Alzheimer's disease. *Brain Research*, 1161, 116–123.

Mattson, M.P., 2004. Pathways towards and away from Alzheimer's disease. *Nature*, 430, 631–639.

Mbye, L.H.A.N., Singh, I.N., Carrico, K.M., Saatman, K.E., Hall, E.D., 2009. Comparative neuroprotective effects of cyclosporin A and NIM811, a nonimmunosuppressive cyclosporin A analog, following traumatic brain injury. *J. Cereb. Blood Flow Metab*. 29, 87–97.

McLean, C.A., Cherny, R.A., Fraser, F.W., Fuller, S.J., Smith, M.J., Beyreuther, K., Bush, A.I., Masters, C.L., 1999. Soluble pool of Abeta amyloid as a determinant of severity of neurodegeneration in Alzheimer's disease. *Ann. Neurol*. 46, 860–866.

Milton, N.G.N., 2002. Anandamide and noladin ether prevent neurotoxicity of the human amyloid-[beta] peptide. *Neurosci Lett*. 332, 127–130.

Molina, H., Bunkenborg, J., Reddy, G.H., Muthusamy, B., Scheel, P.J., Pandey, A., 2005. A proteomic analysis of human hemodialysis fluid. *Mol. Cell Proteomics*, 4, 637–650.

Moreira, P.I., Santos, M.S., Seiça, R., Oliveira, C.R., 2007. Brain mitochondrial dysfunction as a link between Alzheimer's disease and diabetes. *J. Neurol. Sci*, 257, 206–214.

Muirhead, K.E.A., 2011. An investigation of the ABAD-Aβ interaction as a potential therapeutic target for the treatment of Alzheimer's disease (Thesis). University of St Andrews, URL: http://research-repository.st-andrews.ac.uk/handle/10023/2228

Muirhead, K.E.A., Borger, E., Aitken, L., Conway, S.J., Gunn-Moore, F.J., 2010a. The consequences of mitochondrial amyloid β-peptide in Alzheimer's disease. *Biochem. J*. 426, 255–270.

Muirhead, K.E.A., Froemming, M., Li, X., Musilek, K., Conway, S.J., Sames, D., Gunn-Moore, F.J., 2010b. (-)-CHANA, a fluorogenic probe for detecting amyloid binding alcohol dehydrogenase HSD10 activity in living cells. *ACS Chem. Biol*. 5, 1105–1114.

Munoz, D.G., Feldman, H., 2000. Causes of Alzheimer's disease. *Canadian Medical Association Journal*, 162, 65 –72.

Murakami, Y., Ohsawa, I., Kasahara, T., Ohta, S., 2009. Cytoprotective role of mitochondrial amyloid β peptide-binding alcohol dehydrogenase against a cytotoxic aldehyde. *Neurobiol. Aging*, 30, 325–329.

Mutisya, E.M., Bowling, A.C., Beal, M.F., 1994. Cortical cytochrome oxidase activity is reduced in Alzheimer's disease. *J. Neurochem*. 63, 2179–2184.

Myszka, D.G., 2004. Analysis of small-molecule interactions using Biacore S51 technology. *Anal. Biochem*. 329, 316–323.

Nagele, R.., D'Andrea, M.., Anderson, W.., Wang, H.-Y., 2002. Intracellular accumulation of β-amyloid1–42 in neurons is facilitated by the α7 nicotinic acetylcholine receptor in Alzheimer's disease. *Neuroscience*, 110, 199–211.

Nakagawa, T., Shimizu, S., Watanabe, T., Yamaguchi, O., Otsu, K., Yamagata, H., Inohara, H., Kubo, T., Tsujimoto, Y., 2005. Cyclophilin D-dependent mitochondrial permeability transition regulates some necrotic but not apoptotic cell death. *Nature*, 434, 652–658.

Nelson, R., Sawaya, M.R., Balbirnie, M., Madsen, A., Riekel, C., Grothe, R., Eisenberg, D., 2005. Structure of the cross-β spine of amyloid-like fibrils. *Nature*, 435, 773–778.

Nichols, M.R., Moss, M.A., Reed, D.K., Cratic-McDaniel, S., Hoh, J.H., Rosenberry, T.L., 2005. Amyloid-{beta} Protofibrils Differ from Amyloid-{beta} Aggregates Induced in Dilute Hexafluoroisopropanol in Stability and Morphology. *J. Biol. Chem*. 280, 2471–2480.

Nicolli, A., Basso, E., Petronilli, V., Wenger, R.M., Bernardi, P., 1996. Interactions of cyclophilin with the mitochondrial inner membrane and regulation of the permeability transition pore, and cyclosporin A-sensitive channel. *J. Biol. Chem.* 271, 2185–2192.

Nordberg, A., 2004. PET imaging of amyloid in Alzheimer's disease. *The Lancet Neurology*, 3, 519–527.

Ofman, R., Ruiter, J.P.N., Feenstra, M., Duran, M., Poll-The, B.T., Zschocke, J., Ensenauer, R., Lehnert, W., Sass, J.O., Sperl, W., Wanders, R.J.A., 2003. 2-Methyl-3-hydroxybutyryl-CoA dehydrogenase deficiency is caused by mutations in the HADH2 gene. *Am. J. Hum. Genet*, 72, 1300–1307.

Oppermann, U.C.T., Salim, S., Tjernberg, L.O., Terenius, L., Jörnvall, H., 1999. Binding of amyloid [beta]-peptide to mitochondrial hydroxyacyl-CoA dehydrogenase (ERAB): regulation of an SDR enzyme activity with implications for apoptosis in Alzheimer's disease. *FEBS Letters*, 451, 238–242.

Orgogozo, J.-M., Gilman, S., Dartigues, J.-F., Laurent, B., Puel, M., Kirby, L.C., Jouanny, P., Dubois, B., Eisner, L., Flitman, S., Michel, B.F., Boada, M., Frank, A., Hock, C., 2003. Subacute meningoencephalitis in a subset of patients with AD after Abeta42 immunization. *Neurology*, 61, 46–54.

Oz, M., Lorke, D.E., Petroianu, G.A., 2009. Methylene blue and Alzheimer's disease. *Biochem. Pharmacol.* 78, 927–932.

Park, L., Anrather, J., Forster, C., Kazama, K., Carlson, G.A., Iadecola, C., 2004. A[beta]-Induced Vascular Oxidative Stress and Attenuation of Functional Hyperemia in Mouse Somatosensory Cortex. *J Cereb Blood Flow Metab*, 24, 334–342.

Parker, W.D., Jr, Filley, C.M., Parks, J.K., 1990. Cytochrome oxidase deficiency in Alzheimer's disease. *Neurology*, 40, 1302–1303.

Parker, W.D., Jr, Parks, J., Filley, C.M., Kleinschmidt-DeMasters, B.K., 1994. Electron transport chain defects in Alzheimer's disease brain. *Neurology*, 44, 1090–1096.

Pellecchia, M., Sem, D.S., Wuthrich, K., 2002. NMR in drug discovery. *Nat Rev Drug Discov*, 1, 211–219.

Pierce, M.M., Raman, C.S., Nall, B.T., 1999. Isothermal Titration Calorimetry of Protein-Protein Interactions. *Methods* 19, 213–221.

Powell, A.., Read, J.., Banfield, M.., Gunn-Moore, F., Yan, S.., Lustbader, J., Stern, A.., Stern, D.., Brady, R.., 2000. Recognition of structurally diverse substrates by type II 3-hydroxyacyl-CoA dehydrogenase (HADH II)/Amyloid-[beta] binding alcohol dehydrogenase (ABAD). *J Mol Biol*, 303, 311–327.

Qu, D., Rashidian, J., Mount, M.P., Aleyasin, H., Parsanejad, M., Lira, A., Haque, E., Zhang, Y., Callaghan, S., Daigle, M., Rousseaux, M.W.C., Slack, R.S., Albert, P.R., Vincent, I., Woulfe, J.M., Park, D.S., 2007. Role of Cdk5-mediated phosphorylation of Prx2 in MPTP toxicity and Parkinson's disease. *Neuron*, 55, 37–52.

Ravaglia, G., Forti, P., Maioli, F., Martelli, M., Servadei, L., Brunetti, N., Porcellini, E., Licastro, F., 2005. Homocysteine and folate as risk factors for dementia and Alzheimer disease. *The American Journal of Clinical Nutrition*, 82, 636 –643.

Ravetz, R., 1999. Psychiatric disorders associated with Alzheimer's disease. JAOA: *Journal of the American Osteopathic Association*, 99, 13S

Reddy, P.H., 2009. Amyloid beta, mitochondrial structural and functional dynamics in Alzheimer's disease. *Experimental Neurology*, 218, 286–292.

Reddy, P.H., McWeeney, S., Park, B.S., Manczak, M., Gutala, R.V., Partovi, D., Jung, Y., Yau, V., Searles, R., Mori, M., Quinn, J., 2004. Gene expression profiles of transcripts in amyloid precursor protein transgenic mice: up-regulation of mitochondrial metabolism and apoptotic genes is an early cellular change in Alzheimer's disease. *Hum. Mol. Genet*, 13, 1225 –1240.

Ren, Y., 2008. Consequences of the interaction of amyloid beta with amyloid binding alcohol dehydrogenase and the receptor for advanced glycation end products (Thesis). University of St Andrews, URL: http://research-repository.st-andrews.ac.uk/handle/10023/503

Ren, Y., Xu, H.W., Davey, F., Taylor, M., Aiton, J., Coote, P., Fang, F., Yao, J., Chen, D., Chen, J.X., Yan, S.D., Gunn-Moore, F.J., 2008. Endophilin I Expression Is Increased in the Brains of Alzheimer Disease Patients. *J. Biol. Chem*. 283, 5685 –5691.

Rinne, J.O., Brooks, D.J., Rossor, M.N., Fox, N.C., Bullock, R., Klunk, W.E., Mathis, C.A., Blennow, K., Barakos, J., Okello, A.A., De LIano, S.R.M., Liu, E., Koller, M., Gregg, K.M., Schenk, D., Black, R., Grundman, M., 2010. 11C-PiB PET assessment of change in fibrillar amyloid-β load in patients with Alzheimer's disease treated with bapineuzumab: a phase 2, double-blind, placebo-controlled, ascending-dose study. *The Lancet Neurology*, 9, 363–372.

Roberds, S.L., Anderson, J., Basi, G., Bienkowski, M.J., Branstetter, D.G., Chen, K.S., Freedman, S., Frigon, N.L., Games, D., Hu, K., Johnson-Wood, K., Kappenman, K.E., Kawabe, T.T., Kola, I., Kuehn, R., Lee, M., Liu, W., Motter, R., Nichols, N.F., Power, M., Robertson, D.W., Schenk, D., Schoor, M., Shopp, G.M., Shuck, M.E., Sinha, S., Svensson, K.A., Tatsuno, G., Tintrup, H., Wijsman, J., Wright, S., McConlogue, L., 2001. BACE knockout mice are healthy despite lacking the primary β-secretase activity in brain: implications for Alzheimer's disease therapeutics. *Hum. Mol. Genet*. 10, 1317–1324.

Rogaeva, E., Meng, Y., Lee, J.H., Gu, Y., Kawarai, T., Zou, F., Katayama, T., Baldwin, C.T., Cheng, R., Hasegawa, H., Chen, F., Shibata, N., Lunetta, K.L., Pardossi-Piquard, R., Bohm, C., Wakutani, Y., Cupples, L.A., Cuenco, K.T., Green, R.C., Pinessi, L., Rainero, I., Sorbi, S., Bruni, A., Duara, R., Friedland, R.P., Inzelberg, R., Hampe, W., Bujo, H., Song, Y., Andersen, O., Willnow, T.E., Graff-Radford, N., Petersen, R., Dickson, D., Der, S.D., Fraser, P.E., Schmitt-Ulms, G., Younkin, S., Mayeux, R., Farrer, L.A., St George-Hyslop, P., 2007. The neuronal sortilin-related receptor SORL1 is genetically associated with Alzheimer's Disease. *Nat. Genet*. 39, 168–177.

Rosenmann, H., Grigoriadis, N., Karussis, D., Boimel, M., Touloumi, O., Ovadia, H., Abramsky, O., 2006. Tauopathy-like abnormalities and neurologic deficits in mice immunized with neuronal tau protein. *Arch. Neurol*. 63, 1459–1467.

Sarsoza, F., Saing, T., Kayed, R., Dahlin, R., Dick, M., Broadwater-Hollifield, C., Mobley, S., Lott, I., Doran, E., Gillen, D., Anderson-Bergman, C., Cribbs, D.H., Glabe, C., Head, E., 2009. A fibril-specific, conformation-dependent antibody recognizes a subset of Aβ plaques in Alzheimer disease, Down syndrome and Tg2576 transgenic mouse brain. *Acta Neuropathol.* 118, 505–517.

Savonenko, A.V., Melnikova, T., Laird, F.M., Stewart, K.-A., Price, D.L., Wong, P.C., 2008. Alteration of BACE1-dependent NRG1/ErbB4 signaling and schizophrenia-like phenotypes in BACE1-null mice. *PNAS*, 105, 5585–5590.

Sayre, L.M., Zelasko, D.A., Harris, P.L.R., Perry, G., Salomon, R.G., Smith, M.A., 1997. 4-Hydroxynonenal-Derived Advanced Lipid Peroxidation End Products Are Increased in Alzheimer's Disease. *J. Neurochem*. 68, 2092–2097.

Scheetz ME, I.I., Carlson, D.G., Schinitsky, M.R., 1977. Frentizole, a novel immunosuppressive, and azathioprine: their comparative effects on host resistance to Pseudomonas aeruginosa, Candida albicans, herpes simplex virus, and influenza (Ann Arbor) virus. *Infect. Immun*. 15, 145–148.

Schenk, D., Barbour, R., Dunn, W., Gordon, G., Grajeda, H., Guido, T., Hu, K., Huang, J., Johnson-Wood, K., Khan, K., Kholodenko, D., Lee, M., Liao, Z., Lieberburg, I., Motter, R., Mutter, L., Soriano, F., Shopp, G., Vasquez, N., Vandevert, C., Walker, S., Wogulis, M., Yednock, T., Games, D., Seubert, P., 1999. Immunization with amyloid-beta attenuates Alzheimer-disease-like pathology in the PDAPP mouse. *Nature,* 400, 173–177.

Schinzel, A.C., Takeuchi, O., Huang, Z., Fisher, J.K., Zhou, Z., Rubens, J., Hetz, C., Danial, N.N., Moskowitz, M.A., Korsmeyer, S.J., 2005. Cyclophilin D is a component of mitochondrial permeability transition and mediates neuronal cell death after focal cerebral ischemia. *PNAS*, 102, 12005–12010.

Schlatter, D., Thoma, R., Küng, E., Stihle, M., Müller, F., Borroni, E., Cesura, A., Hennig, M., 2005. Crystal engineering yields crystals of cyclophilin D diffracting to 1.7 A resolution. *Acta Crystallogr. D Biol. Crystallogr*. 61, 513–519.

Selkoe, D.J., 2001. Alzheimer's Disease: Genes, Proteins, and Therapy. *Physiological Reviews*, 81, 741 –766.

Selkoe, D.J., Walsh, D.M., Abeta Oligomers - a decade of discovery. *J. Neurochem.* 101, 1172–1184.

Sergeant, N., Delacourte, A., Buée, L., 2005. Tau protein as a differential biomarker of tauopathies. *Biochim. Biophys. Acta*, 1739, 179–197.

Shughrue, P.J., Acton, P.J., Breese, R.S., Zhao, W.-Q., Chen-Dodson, E., Hepler, R.W., Wolfe, A.L., Matthews, M., Heidecker, G.J., Joyce, J.G., Villarreal, S.A., Kinney, G.G., 2010. Anti-ADDL antibodies differentially block oligomer binding to hippocampal neurons. *Neurobiol. Aging*, 31, 189–202.

Singh, P., Suman, S., Chandna, S., Das, T.K., 2009. Possible role of amyloid-beta, adenine nucleotide translocase and cyclophilin-D interaction in mitochondrial dysfunction of Alzheimer's disease. *Bioinformation*, 3, 440–445.

Stahl, P.H., 2008. Handbook of Pharmaceutical Salts, 2nd ed. Wiley-VCH.

Stanga, S., 2011. Unfolded p53 in the pathogenesis of Alzheimer's disease. *Aging*, 9, 545-554.

Stockman, B., Dalvit, C., 2002. NMR screening techniques in drug discovery and drug design. *Progress in Nuclear Magnetic Resonance Spectroscopy*, 41, 187–231.

Su, Y., Chang, P.-T., 2001. Acidic pH promotes the formation of toxic fibrils from β-amyloid peptide. *Brain Research*, 893, 287–291.

Takuma, K., Yao, J., Huang, J., Xu, H., Chen, X., Luddy, J., Trillat, A.-C., Stern, D.M., Arancio, O., Yan, S.S., 2005. ABAD enhances Aβ-induced cell stress via mitochondrial dysfunction. *FASEB J.* 04–2582fje.

Tang, M.-X., Jacobs, D., Stern, Y., Marder, K., Schofield, P., Gurland, B., Andrews, H., Mayeux, R., 1996. Effect of oestrogen during menopause on risk and age at onset of Alzheimer's disease. *The Lancet*, 348, 429–432.

The Alzheimer's Association, 2012. Alzheimer's disease facts and figures. *Alzheimer's and Dementia*, 8, 131–168.

Tieu, K., Perier, C., Vila, M., Caspersen, C., Zhang, H.-P., Teismann, P., Jackson-Lewis, V., Stern, D.M., Yan, S.D., Przedborski, S., 2004. L-3-hydroxyacyl-CoA dehydrogenase II protects in a model of Parkinson's disease. *Ann. Neurol.* 56, 51–60.

Trevino, S.R., Scholtz, J.M., Pace, C.N., 2007. Amino acid contribution to protein solubility: Asp, Glu, and Ser contribute more favorably than the other hydrophilic amino acids in RNase Sa. *J. Mol. Biol.* 366, 449–460.

Van Es, M.A., Van den Berg, L.H., 2009. Alzheimer/'s disease beyond APOE. *Nat. Genet.* 41, 1047–1048.

Vega, I.E., Traverso, E.E., Ferrer-Acosta, Y., Matos, E., Colon, M., Gonzalez, J., Dickson, D., Hutton, M., Lewis, J., Yen, S.H., 2008. A novel calcium-binding protein is associated with tau proteins in tauopathy. *J. Neurochem*, 106, 96–106.

Viegas, A., Manso, J., Nobrega, F.L., Cabrita, E.J., 2011. Saturation-Transfer Difference (STD) NMR: A Simple and Fast Method for Ligand Screening and Characterization of Protein Binding. *J. Chem. Educ*. 88, 990–994.

Waldmeier, P.C., Zimmermann, K., Qian, T., Tintelnot-Blomley, M., Lemasters, J.J., 2003. Cyclophilin D as a drug target. *Curr. Med. Chem*. 10, 1485–1506.

Walsh, D.M., Hartley, D.M., Kusumoto, Y., Fezoui, Y., Condron, M.M., Lomakin, A., Benedek, G.B., Selkoe, D.J., Teplow, D.B., 1999. Amyloid beta-protein fibrillogenesis. Structure and biological activity of protofibrillar intermediates. *J. Biol. Chem*. 274, 25945–25952.

Wilcox, S., Sharkey, J.R., Mathews, A.E., Laditka, J.N., Laditka, S.B., Logsdon, R.G., Sahyoun, N., Robare, J.F., Liu, R., 2009. Perceptions and Beliefs About the Role of Physical Activity and Nutrition on Brain Health in Older Adults. *The Gerontologist*, 49, S61–S71.

Wilhelmus, M.M.M., Van der Pol, S.M.A., Jansen, Q., Witte, M.E., Van der Valk, P., Rozemuller, A.J.M., Drukarch, B., De Vries, H.E., Van Horssen, J., 2011. Association of Parkinson disease-related protein PINK1 with Alzheimer disease and multiple sclerosis brain lesions. *Free Radical Biology and Medicine*, 50, 469–476.

Wilquet, V., Strooper, B.D., 2004. Amyloid-beta precursor protein processing in neurodegeneration. *Current Opinion in Neurobiology*, 14, 582–588.

Wilson, K.C., Reardon, C., Farber, H.W., 2000. Propylene Glycol Toxicity in a Patient Receiving Intravenous Diazepam. *New England Journal of Medicine*, 343, 815–815.

Wischik, C.M., Bentham, P., Wischik, D.J., Seng, K.M., 2008. Tau aggregation inhibitor (TAI) therapy with rember[TM] arrests disease progression in mild and moderate Alzheimer's disease over 50 weeks. *Alzheimer's and Dementia*, 4, T167.

Wittmann, C.W., Wszolek, M.F., Shulman, J.M., Salvaterra, P.M., Lewis, J., Hutton, M., Feany, M.B., 2001. Tauopathy in Drosophila: neurodegeneration without neurofibrillary tangles. *Science*, 293, 711–714.

Wolozin, B., 2004. Cholesterol and the Biology of Alzheimer's Disease. *Neuron* 41, 7–10.

Wong, P.C., Cai, H., Borchelt, D.R., Price, D.L., 2002. Genetically engineered mouse models of neurodegenerative diseases. *Nat. Neurosci*. 5, 633–639.

Xia, Y., Zhu, Q., Jun, K., Wang, J., Gao, X., 2010. Clean STD-NMR spectrum for improved detection of ligand-protein interactions at low concentration of protein. *Magnetic Resonance in Chemistry*, 48, 918–924.

Xie, Y., Deng, S., Chen, Z., Yan, S., Landry, D.W., 2006. Identification of small-molecule inhibitors of the A[beta]-ABAD interaction. *Bioorganic & Medicinal Chemistry Letters*, 16, 4657–4660.

Yan, S.D., Roher, A., Chaney, M., Zlokovic, B., Schmidt, A.M., Stern, D., 2000. Cellular cofactors potentiating induction of stress and cytotoxicity by amyloid [beta]-peptide. *Biochimica et Biophysica Acta- Molecular Basis of Disease*, 1502, 145–157.

Yan, S.D., Stern, D.M., 2005. Mitochondrial dysfunction and Alzheimer's disease: role of amyloid-β peptide alcohol dehydrogenase (ABAD). *International Journal of Experimental Pathology*, 86, 161–171.

Yan, Y., Liu, Y., Sorci, M., Belfort, G., Lustbader, J.W., Yan, S.S., Wang, C., 2007. Surface Plasmon Resonance and Nuclear Magnetic Resonance Studies of ABAD−Aβ Interaction. *Biochemistry*, 46, 1724–1731.

Yan, Y., Wang, C., 2006. A[beta]42 is More Rigid than A[beta]40 at the C Terminus: Implications for A[beta] Aggregation and Toxicity. *J. Mol. Biol.* 364, 853–862.

Yang, X., Yang, Y., Wu, J., Zhu, J., 2007. Stable expression of a novel fusion peptide of thioredoxin-1 and ABAD-inhibiting peptide protects PC12 cells from intracellular amyloid-beta. *J. Mol. Neurosci.* 33, 180–188.

Yao, J., Du, H., Yan, S., Fang, F., Wang, C., Lue, L.-F., Guo, L., Chen, D., Stern, D.M., Gunn Moore, F.J., Xi Chen, J., Arancio, O., Yan, S.S., 2011. Inhibition of Amyloid-β (Aβ) Peptide-Binding Alcohol Dehydrogenase-Aβ Interaction Reduces Aβ Accumulation and Improves Mitochondrial Function in a Mouse Model of Alzheimer's Disease. *J. Neurosci.* 31, 2313 –2320.

Yao, J., Irwin, R.W., Zhao, L., Nilsen, J., Hamilton, R.T., Brinton, R.D., 2009. Mitochondrial bioenergetic deficit precedes Alzheimer's pathology in female mouse model of Alzheimer's disease. *PNAS*, 106, 14670–14675.

Yao, J., Taylor, M., Davey, F., Ren, Y., Aiton, J., Coote, P., Fang, F., Chen, J.X., Yan, S.D., Gunn-Moore, F.J., 2007. Interaction of amyloid binding alcohol dehydrogenase/Abeta mediates up-regulation of peroxiredoxin II in the brains of Alzheimer's disease patients and a transgenic Alzheimer's disease mouse model. *Mol. Cell. Neurosci.* 35, 377–382.

Zhu, X., Ogawa, O., Wang, Y., Perry, G., Smith, M.A., 2003. JKK1, an upstream activator of JNK/SAPK, is activated in Alzheimer's disease. *J. Neurochem.* 85, 87–93.

Appendices

Appendix A: Sequences and plasmid maps

A.1: Human ABAD DNA Sequence

Accession number: NM_001037811.2

Gene Sequence:

```
atccccatcc cgtggagtgg ccggcgacaa gatggcagca gcgtgtcgga
gcgtgaaggg cctggtggcg gtaataaccg gaggagcctc gggcctgggc
ctggccacgg cggagcgact tgtggggcag ggagcctctg ctgtgcttct
ggacctgccc aactcgggtg gggaggccca agccaagaag ttaggaaaca
actgcgtttt cgccccagcc gacgtgacct ctgagaagga tgtgcaaaca
gctctggctc tagcaaaagg aaagtttggc cgtgtggatg tagctgtcaa
ctgtgcaggc atcgcggtgg ctagcaagac gtacaactta aagaagggcc
agacccatac cttggaagac ttccagcgag ttcttgatgt gaatctcatg
ggcaccttca atgtgatccg cctggtggct ggtgagatgg gccagaatga
accagaccag ggaggccaac gtggggtcat catcaacact gccagtgtgg
ctgccttcga gggtcaggtt ggacaagctg catactctgc ttccaagggg
ggaatagtgg gcatgacact gcccattgct cgggatctgg ctcccatagg
tctgtttggc accccactgc tgaccagcct cccagagaaa gtgtgcaact
tcttggccag ccaagtgccc ttccctagcc gactgggtga ccctgctgag
tatgctcacc tcgtacaggc catcatcgag aacccattcc tcaatggaga
ggtcatccgg ctggatgggg ccattcgtat gcagccttga agggagaagg
cagagaaaac acacgctcct ctgcccttcc tttccctggg gtactactct
ccagcttggg aggaagccca gtagccattt tgtaactgcc taccagtcgc
cctctgtgcc taataaagtc tcttttctc acagag
```

A.2: Human ABAD Protein Sequence

```
M A A A C R S V K G L V A V I T G G A S G L G L A T A
E R L V G Q G A S A V L L D L P N S G G E A Q A K K L
G N N C V F A P A D V T S E K D V Q T A L A L A K G K
F G R V D V A V N C A G I A V A S K T Y N L K K G Q T
H T L E D F Q R V L D V N L M G T F N V I R L V A G E
M G Q N E P D Q G G Q R G V I I N T A S V A A F E G Q
V G Q A A Y S A S K G G I V G M T L P I A R D L A P I
G I R V M T I A P G L F G T P L L T S L P E K V C N F
L A S Q V P F P S R L G D P A E Y A H L V Q A I I E N
P F L N G E V I R L D G A I R M Q P
```
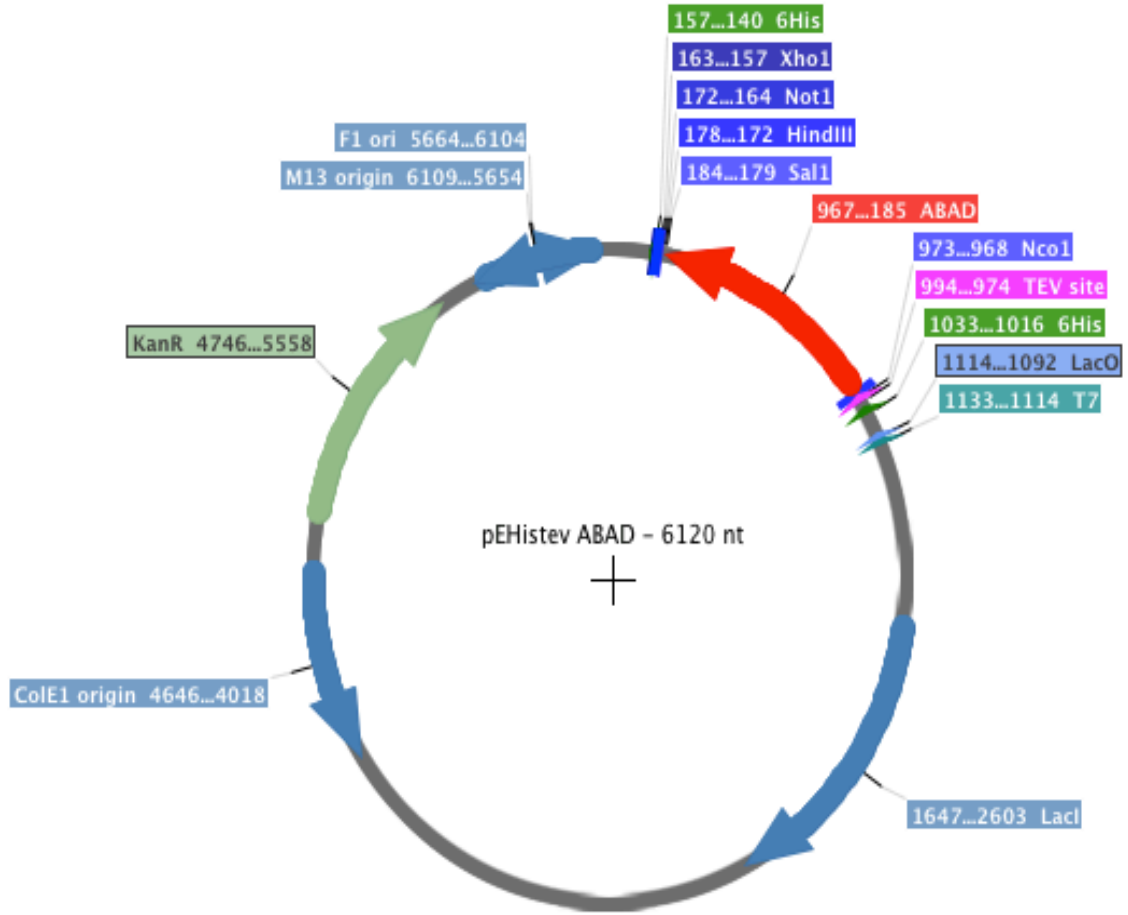
Features :

Nco1 : [973 : 968 - CCW]
Xho1 : [163 : 157 - CCW]
ABAD : [967 : 185 - CCW]
Sal1 : [184 : 179 - CCW]
HindIII : [178 : 173 - CCW]
Not1 : [172 : 165 - CCW]
T7 : [1133 : 1114 - CCW]
ColE1 origin : [4646 : 4018 - CCW]
F1 origin : [5664 : 6104 - CW]
M13 origin : [6109 : 5654 - CCW]
LacO : [1114 : 1092 - CCW]
LacI : [1647 : 2603 - CW]
KanR : [4746 : 5558 - CW]
6His : [1033 : 1016 - CCW]
6His : [157 : 140 - CCW]
TEV site : [994 : 974 - CCW]

A.3: **ΔCypD^{K133I} DNA Sequence**

Accession Number: NM_005038

ΔCypD^{K133I} sequence: (495 bp)

```
gggaacccgc tcgtgtacct ggacgtggac gccaacggga agccgctcgg
ccgcgtggtg ctggagctga aggcagatgt cgtcccaaag acagctgaga
acttcagagc cctgtgcact ggtgagaagg cttcggcta caaaggctcc
accttccaca gggtgatccc ttccttcatg tgccaggcgg gcgacttcac
caaccacaat ggcacaggcg ggaagtccat ctacggaagc cgctttcctg
acgagaactt tacactgaag cacgtggggc caggtgtcct gtccatggct
aatgctggtc ctaacaccaa cggctcccag ttcttcatct gcaccataaa
gacagactgg ttggatggca agcatgttgt gttcggtcac gtcaaagagg
gcatggacgt cgtgaagaaa atagaatctt tcggctctaa gagtgggagg
acatccaaga agattgtcat cacagactgt ggccagttga gctaa
```


A.4: **ΔCypD^{K133I} DNA Sequence**


```
M L A L R C G S R W L G L L S V P R S V P L R L P A A R A C

S K G S G D P S S S S S G N P L V Y L D V D A N G K P L G

R V V L E L K A D V V P K T A E N F R A L C T G E K G F G Y

K G S T F H R V I P S F M C Q A G D F T N H N G T G G K S I

Y G S R F P D E N F T L K H V G P G V L S M A N A G P N T N

G S Q F F I C T I K T D W L D G K H V V F G H V K E G M D V

V K K I E S F G S K S G R T S K K I V I T D C G Q L S
```

pET21a ΔCypD K133I – 5904 nt
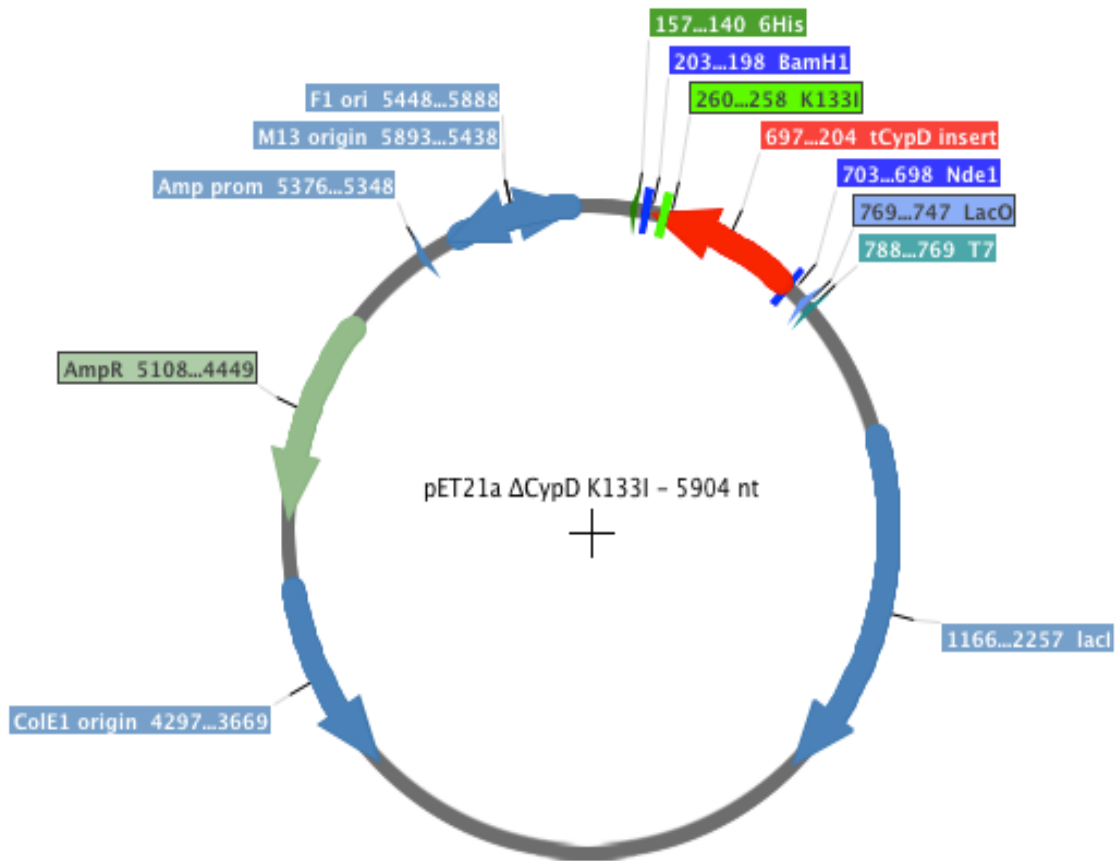
Features:

BamH1 : [203 : 198 - CCW]

Nde1 : [703 : 698 - CCW]

tCypD insert : [697 : 204 - CCW]

T7 : [788 : 769 - CCW]

ColE1 origin : [4297 : 3669 - CCW]

F1 origin : [5448 : 5888 - CW]

M13 origin : [5893 : 5438 - CCW]

LacO : [769 : 747 - CCW]

AmpR : [5108 : 4449 - CCW]

Amp prom : [5376 : 5348 - CCW]

lacI : [1166 : 2257 - CW]

6His : [157 : 140 - CCW]

K133I : [260 : 258 - CCW]

A.5: Full length CypD DNA Sequence

Accession Number: NM_005038

Gene Sequence:

```
1 ggccggtcag cgtcgctgcc ggtctccggc ggagacggac tctggagttt
gggcggcccg ggcggccact aggtactctg atattccgta ctaaacacgt
ctgcaagtca agatgtcgca cccgtccccc caagccaagc cctccaaccc
cagtaaccct cgagtcttct ttgacgtgga catcggaggg gagcgagttg
gtcgaattgt cttagaattg tttgcagata tcgtacccaa aactgcggaa
aattttcgtg cactgtgtac aggagaaaaa ggcattggac acacgactgg
gaaacctctc catttcaaag gatgcccttt tcatcgaatt attaagaaat
ttatgattca gggtggagac ttctcaaatc agaatgggac aggtggagaa
agtatttatg gtgaaaaatt tgaagatgaa aatttccatt acaagcatga
tcgggagggt ttactgagca tggcaaatgc aggccgcaac acaaacggtt
ctcagttttt tatcacaaca gttccaactc ctcatttgga tgggaaacat
gtggtgtttg gccaagtaat taaaggaata ggagtggcaa ggatattgga
aaatgtggaa gtgaaaggtg aaaaacctgc taaattgtgc gttattgcag
aatgtggaga attgaaggaa ggagatgacg ggggaatatt cccaaaagat
ggctctggcg acagtcatcc agatttccct gaggatgcgg atatagattt
aaaagatgta gataaaattt tattaataac agaagactta aaaaacattg
gaaatacttt tttcaaatcc cagaactggg agatggctat taaaaaatat
gcagaagttt taagatacgt ggacagttca aaggctgtta ttgagacagc
agatagagcc aagctgcaac ctatagcttt aagctgtgta ctgaatattg
gtgcttgtaa actgaagatg tcaaattggc agggagcaat tgacagttgt
ttagaggctc ttgaactaga cccatcaaat accaaagcat gtaccgcag
agctcaagga tggcaaggat taaaagaata tgatcaagca ttggctgatc
ttaagaaagc tcagggggata gcaccagaag ataaagctat ccaggcagaa
ttgctgaaag tcaaacaaaa gataaaggca cagaagata aagagaaggc
agtatatgca aaaatgtttg cttagaaagg attcagtttt gcttattgtg
tgttgattgt ataaatgcaa taagaaatg taaaggtttt tgtctatgaa
tatgatccct aatgtgtttc ttttgacacc ttagttcctt actgtttaca
gtttaggagt actgataggg gttcatgctt aataaacatg tcacaataca
gtaagtaaag tggttttgtt tgtttctttg agatggagtc ttgctctgtc
acccaggctg gagtgcggtg cgcaatctc ggctcactgc atcctctgcc
tcccgggttc aagcaattct cctgcctcag cttcccaagt agctgggatt
acaggcacgt gccaccacgc ccagctaatt tttgtatttt tagtagagat
ggggtttcac catattggtc acgtcacgtt ggtcttgaac tcctgacctt
gtgatccacc ccgccttggc ctcccaaagt gctgggatta caggtgtgag
ccaccgtgcc cggccaagta aaatgttttt taaaatggtt atgtgcatta
ttcataaaaa ataatggtgt ccagtctttt taaacttgta aagacacatc
ttattgaata aagagatgag agcttaagtt tgtaaaaaaa aaaaaaaaa
```

A.6: Full length CypD Protein Sequence

```
M L A L R C G S R W L G L L S V P R S V P L R L P A A R A C

S K G S G D P S S S S S G N P L V Y L D V D A N G K P L G

R V V L E L K A D V V P K T A E N F R A L C T G E K G F G Y

K G S T F H R V I P S F M C Q A G D F T N H N G T G G K S I

Y G S R F P D E N F T L K H V G P G V L S M A N A G P N T N

G S Q F F I C T I K T D W L D G K H V V F G H V K E G M D V

V K K I E S F G S K S G R T S K K I V I T D C G Q L S
```

A.7: Primers for CypD construction

Sequence	Primer Name
CGTCATTGAGGGCATGGACG	tCypD-F
CGTCCATGCCCTCAATGACG	tCypD-R
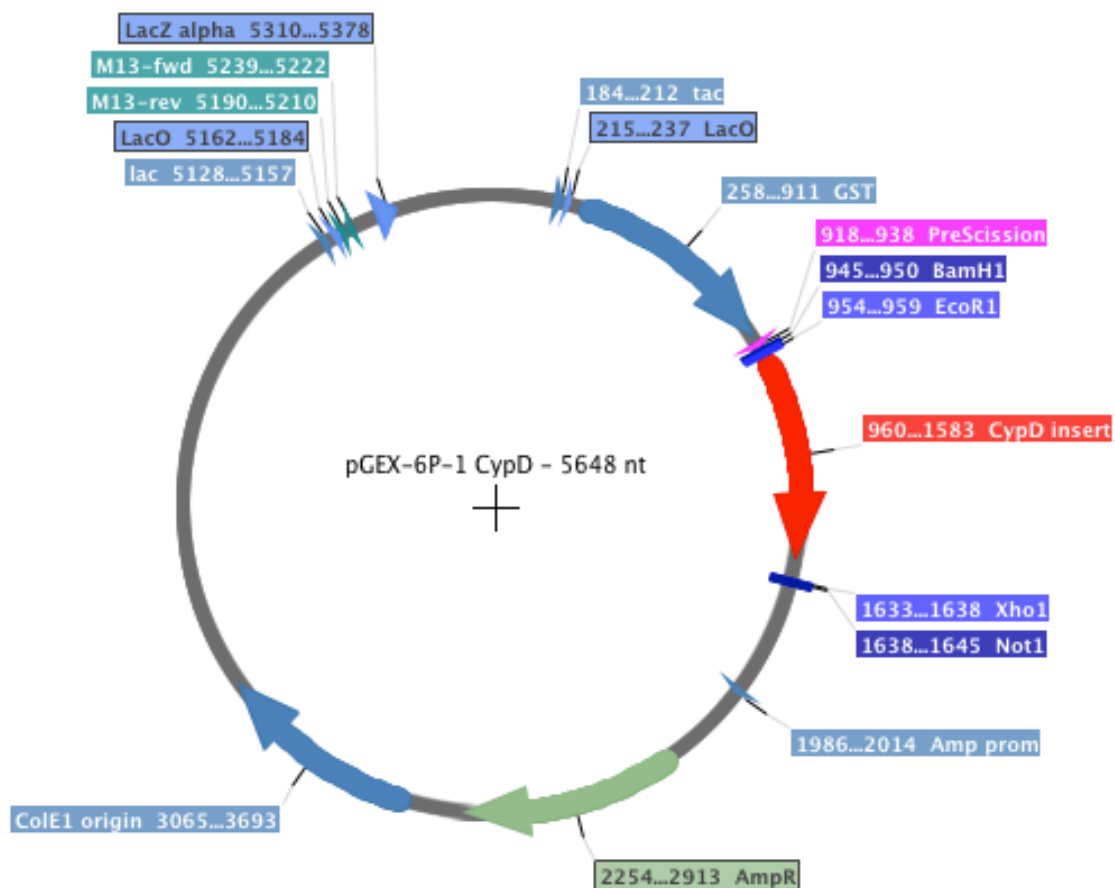
Features:

CypD insert	: [960 : 1583 - CW]	GST	: [258 : 911 - CW]
Xho1	: [1633 : 1638 - CW]	Amp prom	: [1986 : 2014 - CW]
Not1	: [1638 : 1645 - CW]	lac	: [5128 : 5157 - CW]
BamH1	: [945 : 950 - CW]	tac	: [184 : 212 - CW]
EcoR1	: [954 : 959 - CW]	PreScission	: [918 : 938 - CW]
M13-fwd	: [5239 : 5222 - CCW]	M13-rev	: [5190 : 5210 - CW]
ColE1 origin	: [3065 : 3693 - CW]	LacO	: [215 : 237 - CW]
LacZ alpha	: [5310 : 5378 - CW]	LacO	: [5162 : 5184 - CW]
AmpR	: [2254 : 2913 - CW]		

pGEX-6P-1 CypD K133I – 5623 nt
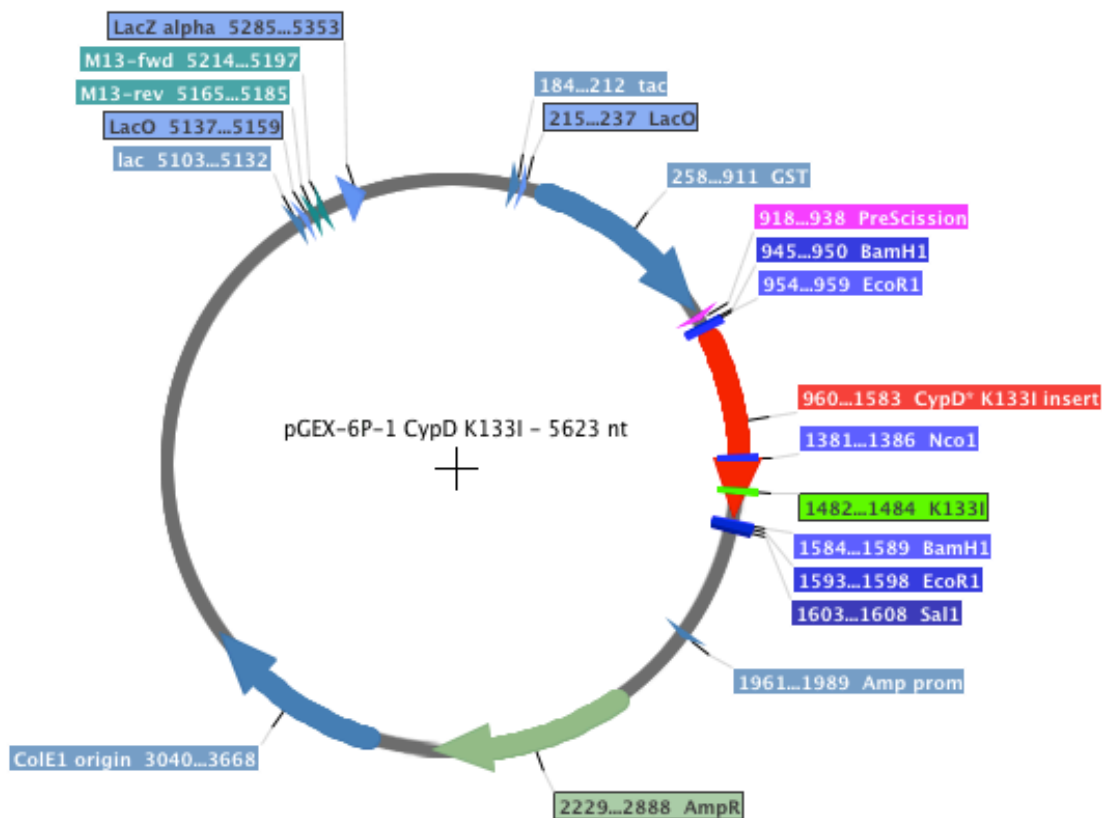
Features:

CypD insert	: [960 : 1583 - CW]	K133I	: [1482 : 1484 - CW]
Xho1	: [1633 : 1638 - CW]	Amp prom	: [1986 : 2014 - CW]
Not1	: [1638 : 1645 - CW]	lac	: [5128 : 5157 - CW]
BamH1	: [945 : 950 - CW]	tac	: [184 : 212 - CW]
EcoR1	: [954 : 959 - CW]	PreScission	: [918 : 938 - CW]
M13-fwd	: [5239 : 5222 - CCW]	M13-rev	: [5190 : 5210 - CW]
ColE1 origin	: [3065 : 3693 - CW]	LacO	: [215 : 237 - CW]
LacZ alpha	: [5310 : 5378 - CW]	LacO	: [5162 : 5184 - CW]
AmpR	: [2254 : 2913 - CW]	GST	: [258 : 911 - CW]

Appendix B: Bacterial cell line descriptions

BL21 (DE3)

- Genotype- F⁻ *ompT hsdS*$_B$ (r$_B$⁻m$_B$⁻) *gal dcm* (DE3)
- BL21 strains are most widely used hosts for protein expression from pET recombinants.
- Are deficient of both lon and ompT proteases.
- DE3= host is lysogen λDE3 therefore carries a chromosomal copy of the T7 RNA polymerase gene under control of the lacUV5 promoter.
- Induction by IPTG.
- Can potentially have leaky expression of T7 polymerase, which leads to the production of potentially toxic proteins.

BL21*™ (DE3)

- Genotype- F⁻ *ompT hsdS*$_B$ (r$_B$⁻m$_B$⁻) *gal dcm rne131* (DE3)
- DE3= host is lysogen λDE3 therefore carries a chromosomal copy of the T7 RNA polymerase gene under control of the lacUV5 promoter.
- Induction by IPTG
- Mutated *rne 131* gene which encodes a truncated RNase E enzyme that lacks the ability to degrade mRNA resulting in increase mRNA stability.
- Deficient in both lon and ompT proteases.
- Due to increase in stability of mRNAs, higher basal expression of heterogenous genes is noted in BL21* than other BL21 strains. Especially in low copy number pET (T7 based) plasmids.

C43 (DE3)

- Genotype- F⁻*ompT gal hsd*S$_B$ (r$_B$⁻m$_B$⁻) *dcm lon* (DE3)
- Two uncharacterised mutations- could be helping to avoid uncoupling of transcription and translation and also affecting the folding and insertion into bacterial membrane.
- From parental BL21 (DE3) strain

- DE3= host is lysogen λDE3 therefore carries a chromosomal copy of the T7 RNA polymerase gene under control of the lacUV5 promoter.
- Induction by IPTG.
- Effective for toxic and membrane proteins.

BLR (DE3)

- Gentotype- F⁻ *ompT hsdS*$_B$ (r$_B^-$m$_B^-$) *gal dcm* (DE3) Δ(*srl-recA*)*306*::Tn*10* (Tet^R)
- recA⁻ derivative of BL21 strain that improves plasmid monomer yields and may help to stabilise the target plasmids containing repetitive sequences (tandem repeats) or whose products may cause the loss of the DE3 prophage.
- DE3= host is lysogen λDE3 therefore carries a chromosomal copy of the T7 RNA polymerase gene under control of the lacUV5 promoter.
- Induction by IPTG
- Deficient in both lon and ompT proteases.

HMS174 (DE3)

- Genotype- F⁻ *recA1 hsdR* (r$_{K12}^-$m$_{K12}^+$) (DE3) (Rif^R)
- recA mutation in a K-12 background.
- Like BLR may help to stabilise certain target genes whose products lose the DE3 prophage.
- Rif resistant (rifampin). RIF kills bacteria by binding to RNA polymerase and blocking the elongation of the RNA transcript when it becomes 2 or 3 nucleotides in length. Bacteria develop resistance to RIF at a high frequency.

Rosetta™ (DE3)

- Genotype- F⁻ *ompT hsdS*$_B$ (r$_B^-$m$_B^-$) *gal dcm* (DE3) pRARE^2 (Cam^R)
- BL21 derivatives designed to enhance the expression of eukaryotic proteins that contain proteins rarely used in *E. coli*. Rosetta strain supplies tRNAs for codons

AUA, AGG, AGA, CUA, CCC and GGA on a compatible chloramphenicol-resistant plasmid pRARE to provide "universal" translation, where translation would be otherwise limited by the codon usage of *E.coli*.

Tuner™ (DE3)

- Genotype- F⁻ *ompT hsdS*$_B$ (r$_B$⁻m$_B$⁻) *gal dcm lacY1* (DE3)
- *lacZY* deletion mutants of BL21 strain which enable adjustable levels of protein expression throughout all cells in a culture.
- *lac* permease (*lacY*) mutation allows uniform entry of IPTG into all cells in the population allowing IPTG induction to occur at a true concentration-dependent fashion that is exceptionally uniform throughout the culture.
- By adjusting the IPTG concentration this means that expression can be regulated easily. A lower expression level may enhance the solubility and activity of the target protein.
- Deficient in both lon and ompT proteases

ORAGAMI (DE3)

- Genotype- Δ*(ara–leu)7697* Δ*lacX74* Δ*phoA PvuII phoR araD139 ahpC galE galK rpsLF'*[*lac*⁺ *lacI*^{q} *pro*] (DE3) *gor522*::Tn*10 trxB* (*Kan*^{R}, *Str*^{R}, *Tet*^{R})[4]
- K12 derivative that has mutations in both the thioreductase (*trxB*) and the glutathione reductase (*gor*) genes. These mutations greatly enhance disulfide bond formation in the cytoplasm.
- Compatible with Amp resistant plasmids.
- Leu auxotroph

Appendix C: Crystallography Screens

Screen layout using The Hamilton STARline robot

	i	ii	iii	Iv	v	vi	vii	viii	ix	x	xi	xii
A	1	9	17	25	33	41	49	57	65	73	81	89
B	2	10	18	26	34	42	50	58	66	74	82	90
C	3	11	19	27	35	43	51	59	67	75	83	91
D	4	12	20	28	36	44	52	60	68	76	84	92
E	5	13	21	29	37	45	53	61	69	77	85	93
F	6	14	22	30	38	46	54	62	70	78	86	94
G	7	15	23	31	39	47	55	63	71	79	87	95
H	8	16	24	32	40	48	56	64	72	80	88	96

All 96 well crystal screens are laid out in this manner when using the Hamilton STARline robot. Subsequent screens described in this appendix are detailed by their sample number, which then by using this table it is possible to find the corresponding well number for the crystal condition.

StoPEG 1:

	Precipitant	%	Buffer	Conc (M)	Stock Conc (M)	Salt	Conc (M)	Additive	%
1	PEG10k	20.58	HEPES	0.1	8	Am-Acetate	0.08	-	0
2	PEGMME5k	21.44	BICINE	0.1	9.5	K-Thiocyanate	0.19	-	0
3	PEG8k	18.95	Na-Cacod	0.1	6.5	K-Nitrate	0.07	-	0
4	PEG6k	19.29	Tris-Chloride	0.1	8	K-Thiocyanate	0.25	-	0
5	PEGMME5k	17.77	Na-Acetate	0.1	5	Na-Bromide	0.1	DMSO	3.06
6	PEG4k	20.29	MOPS	0.1	7	Mg-Formate	0.11	-	0
7	PEGMME5k	20.64	BICINE	0.1	8.5	-	0	BME	5.72
8	PEG8k	12.6	HEPES	0.1	8	K-Chloride	0.19	-	0
9	PEG400	34.19	MOPS	0.1	6.5	Ca-Acetate	0.12	BOG	0.02
10	PEGMME550	37.52	CHES	0.1	9	Mg-Acetate	0.23	-	0
11	PEG8k	12.66	MOPS	0.1	6.5	Ca-Chloride	0.14	-	0
12	PEG400	46.79	-	0	0	Zn-Chloride	0.11	-	0
13	PEG10k	19.3	Na-Citrate	0.1	5.5	Na-Chloride	0.18	-	0
14	PEGMME2k	20.02	Na-Cacod	0.1	7	Na-Acetate	0.14	-	0
15	PEG400	50.02	BICINE	0.1	8.5	Am-Sulfate	0.09	PEG400	1.56
16	PEGMME2k	22.07	Na-Cacod	0.1	7	Zn-Acetate	0.11	-	0
17	PEG1.5k	25.96	MES	0.1	6	Na-K-Tartrate	0.07	BOG	0.04
18	PEG6k	16.22	Na-Citrate	0.1	4.5	Mg-Formate	0.04	-	0
19	PEG3350	24.04	MES	0.1	6	Am-Sulfate	0.3	-	0
20	PEG6k	18	Na-Acetate	0.1	5	Zn-Chloride	0.07	LDAO	0.09
21	PEG4k	23.35	BisTris	0.1	6	Mg-Sulfate	0.07	-	0
22	PEG8k	24.63	BICINE	0.1	8.5	Na-Citrate	0.12	LDAO	0.05
23	PEGMME550	29.77	Na-Acetate	0.1	5	Ca-Acetate	0.12	-	0
24	PEG3350	33.69	BICINE	0.1	9.5	Am-Tartrate	0.03	-	0

25	PEGMME5k	27.65	Na-Citrate	0.1	5	-	0	-	0
26	PEG1.5k	35.93	Na-Citrate	0.1	4.5	Na-Chloride	0.25	PEGMME350	0.56
27	PEGMME550	45.62	CHES	0.1	9.5	Am-Phosphate	0.09	-	0
28	PEGMME2k	31.4	Na-Citrate	0.1	5.5	Na-Acetate	0.08	-	0
29	PEG8k	22.28	Na-Citrate	0.1	5	-	0	-	0
30	PEG10k	11.01	CHES	0.1	9	K-Chloride	0.24	EDTA	8.55
31	PEG1.5k	28.28	BICINE	0.1	9.5	Na-K-Tartrate	0.13	-	0
32	PEG4k	29.75	Na-Citrate	0.1	5	-	0	-	0
33	PEGMME5k	16.88	BICINE	0.1	9	Mg-Chloride	0.11	-	0
34	PEG3350	30.84	BisTris	0.1	6.5	Ca-Chloride	0.03	-	0
35	PEGMME550	23.63	Na-Cacod	0.1	7	Na-K-Phosphate	0.12	Ethglycol	2.99
36	PEG400	54.24	Tris-Chloride	0.1	8.5	-	0	EDTA	9.04
37	PEGMME2k	23.27	BICINE	0.1	8.5	Am-Tartrate	0.1	Methanol	3.6
38	PEG1.5k	32.21	MES	0.1	6	-	0	-	0
39	PEG3350	32.84	MOPS	0.1	7	Am-Citrate	0.11	-	0
40	PEGMME2k	21.32	BICINE	0.1	9.5	Mg-Chloride	0.05	LDAO	0.09
41	PEG1.5k	40.13	Na-Acetate	0.1	5.5	Na-Citrate	0.13	-	0
42	PEGMME5k	25.1	-	0	0	Ca-Chloride	0.11	-	0
43	PEGMME550	37.73	HEPES	0.1	7.5	Mg-Chloride	0.12	-	0
44	PEG8k	22.73	-	0	0	K-Nitrate	0.1	MPD	2.41
45	PEG10k	13.13	Tris-Chloride	0.1	7.5	-	0	Ethglycol	1.08
46	PEG4k	18.03	Na-Acetate	0.1	4.5	-	0	Butanediol	2.79
47	PEG3350	15.59	MOPS	0.1	7	-	0	-	0
48	PEG4k	14.02	Na-Acetate	0.1	5.5	-	0	-	0

49	PEG6k	20.75	MES	0.1	6	-	0	-	0
50	PEG8k	15.15	Tris-Chloride	0.1	8.5	Na-Acetate	0.04	-	0
51	PEG1.5k	31.05	-	0	0	Na-K-Phosphate	0.25	Dioxane	3.83
52	PEG8k	13.11	MES	0.1	6.5	Li-Chloride	0.1	-	0
53	PEG400	44.73	MOPS	0.1	6.5	Am-Tartrate	0.11	-	0
54	PEG8k	27.66	Na-Citrate	0.1	5	-	0	-	0
55	PEGMME5k	19.49	CHES	0.1	9.5	Am-Citrate	0.1	-	0
56	PEG10k	14.68	CHES	0.1	9.5	-	0	Hexanediol	2.46
57	PEG6k	12.51	MES	0.1	6	Am-Acetate	0.12	-	0
58	PEG400	44.9	Tris-Chloride	0.1	7.5	Ca-Acetate	0.13	Methanol	2.44
59	PEGMME2k	39.87	BisTris	0.1	6	K-Chloride	0.17	-	0
60	PEG10k	13.18	HEPES	0.1	7.5	-	0	-	0
61	PEG4k	15.59	Na-Citrate	0.1	5	Li-Sulfate	0.16	PEG400	3.39
62	PEG1.5k	30.78	-	0	0	Zn-Chloride	0.09	-	0
63	PEG6k	16.58	Na-Acetate	0.1	5.5	Li-Chloride	0.2	-	0
64	PEG4k	20.22	HEPES	0.1	8	Li-Sulfate	0.12	-	0
65	PEG1.5k	24.31	Tris-Chloride	0.1	7.5	-	0	-	0
66	PEG3350	33.83	Na-Acetate	0.1	4.5	-	0	-	0
67	PEGMME2k	32.33	Tris-Chloride	0.1	7.5	Zn-Chloride	0.14	-	0
68	PEG10k	19.58	Tris-Chloride	0.1	8	Na-K-Tartrate	0.14	-	0
69	PEGMME2k	19.42	-	0	0	Ca-Chloride	0.14	-	0
70	PEG400	54.58	HEPES	0.1	8	NONE	0	-	0
71	PEGMME550	40.72	Na-Acetate	0.1	4.5	Li-Chloride	0.21	-	0
72	PEGMME2k	25.94	HEPES	0.1	8	Zn-Acetate	0.08	-	0

73	PEG10k	12.22	BICINE	0.1	8.5	NONE	0	Glycerol	2.07
74	PEG3350	25.18	MOPS	0.1	7	Mg-Sulfate	0.15	PEGDME250	3.47
75	PEG8k	26.34	-	0	0	Am-Citrate	0.09	-	0
76	PEGMME2k	25.81	Na-Citrate	0.1	5.5	-	0	-	0
77	PEG4k	28	Tris-Chloride	0.1	8	Na-K-Tartrate	0.08	-	0
78	PEGMME550	45.42	Tris-Chloride	0.1	8.5	Ca-Chloride	0.04	-	0
79	PEGMME2k	28.52	MES	0.1	6.5	-	0	-	0
80	PEG6k	12.41	BICINE	0.1	9	-	0	-	0
81	PEG400	32.32	BICINE	0.1	9	Na-Bromide	0.06	Dioxane	1.73
82	PEG8k	16.13	MOPS	0.1	7	Ca-Chloride	0.05	-	0
83	PEG3350	18.09	BICINE	0.1	9	-	0	-	0
84	PEGMME550	22.83	BICINE	0.1	9	K-Chloride	0.21	-	0
85	PEG1.5k	29.58	CHES	0.1	9.5	Mg-Sulfate	0.24	BOG	0.07
86	PEG6k	20.47	Tris-Chloride	0.1	7.5	-	0	-	0
87	PEG8k	19.51	HEPES	0.1	8	-	0	-	0
88	PEG6k	24.43	Na-Citrate	0.1	5.5	Am-Phosphate	0.06	-	0
89	PEGMME550	45.33	Na-Acetate	0.1	5	Mg-Sulfate	0.18	-	0
90	PEGMME5k	19.33	Na-Acetate	0.1	5.5	K-Thiocyanate	0.26	PEGDME250	2.99
91	PEG6k	22.82	Na-Citrate	0.1	4.5	Mg-Acetate	0.06	Butanediol	0.47
92	PEG10k	17.88	Na-Citrate	0.1	4.5	Na-Bromide	0.06	-	0
93	PEGMME550	21.24	-	0	0	Mg-Chloride	0.15	-	0
94	PEG400	25.87	BICINE	0.1	9	Am-Sulfate	0.22	-	0
95	PEG6k	27.53	-	0	0	Li-Chloride	0.14	-	0
96	PEG8k	25.89	Na-Acetate	0.1	5.5	Zn-Acetate	0.1	-	0

StoPEG 2:

	Precipitant	%	Buffer	Conc (M)	Stock Conc (M)	Salt	Conc (M)	Additive	%
1	PEGMME5k	22.84	-	0	0	Zn-Chloride	0.15	-	0
2	PEG10k	11	MES	0.1	6.5	-	0	EDTA	5.1
3	PEG1.5k	27.31	BICINE	0.1	8.5	Mg-Formate	0.15	-	0
4	PEG4k	27.56	BICINE	0.1	8.5	Na-K-Phosphate	0.15	-	0
5	PEGMME550	44.55	BisTris	0.1	6.5	Li-Chloride	0.18	-	0
6	PEGMME2k	30.53	-	0	0	Zn-Acetate	0.12	-	0
7	PEG6k	13.88	Na-Acetate	0.1	5	Li-Chloride	0.22	-	0
8	PEG400	48.46	CHES	0.1	9.5	Mg-Acetate	0.27	-	0
9	PEGMME550	41.15	CHES	0.1	9.5	Am-Sulfate	0.19	-	0
10	PEG4k	26.19	-	0	0	Li-Sulfate	0.24	Ethglycol	2.56
11	PEG10k	15.9	MES	0.1	6	Ca-Acetate	0.04	-	0
12	PEG8k	27.8	BisTris	0.1	6	-	0	-	0
13	PEGMME5k	14.47	Tris-Chloride	0.1	8.5	Zn-Acetate	0.09	-	0
14	PEG1.5k	28.58	CHES	0.1	9	-	0	Methanol	3.68
15	PEG3350	18.71	MOPS	0.1	7	-	0	-	0
16	PEG1.5k	36.32	Na-Acetate	0.1	4.5	Ca-Chloride	0.1	-	0
17	PEGMME550	32.66	Tris-Chloride	0.1	7.5	Mg-Chloride	0.19	-	0
18	PEG6k	23.4	CHES	0.1	9	Na-Bromide	0.22	CHAPS	0.1
19	PEGMME550	35.12	MOPS	0.1	7	Am-Phosphate	0.14	-	0
20	PEG6k	23.42	BICINE	0.1	8.5	K-Thiocyanate	0.29	BOG	0.05
21	PEG10k	14.72	Na-Citrate	0.1	5	-	0	-	0
22	PEG6k	27.15	MOPS	0.1	7	K-Nitrate	0.13	-	0
23	PEGMME5k	14.55	BICINE	0.1	9	-	0	-	0
24	PEG4k	20.58	BisTris	0.1	6.5	Am-Tartrate	0.03	-	0

25	PEG400	24.82	Na-Citrate	0.1	5.5	-	0	-	0
26	PEGMME2k	28	Tris-Chloride	0.1	7.5	Am-Phosphate	0.15	-	0
27	PEG4k	16.96	Na-Acetate	0.1	4.5	Zn-Acetate	0.04	-	0
28	PEG3350	24.27	CHES	0.1	9	K-Thiocyanate	0.18	Methanol	2.95
29	PEG8k	22.1	Na-Acetate	0.1	4.5	-	0	MPD	2.46
30	PEG10k	14.17	Na-Cacod	0.1	6.5	Mg-Acetate	0.06	DMSO	2.44
31	PEG6k	21.09	Tris-Chloride	0.1	8	Na-Acetate	0.06	PEG400	0.85
32	PEG8k	15.11	BICINE	0.1	9.5	Mg-Formate	0.05	-	0
33	PEG8k	16.23	Na-Acetate	0.1	5	Mg-Acetate	0.1	Glycerol	3.6
34	PEG3350	28.41	-	0	0	Mg-Sulfate	0.18	-	0
35	PEGMME550	46.05	Na-Citrate	0.1	4.5	-	0	-	0
36	PEGMME2k	34.19	Na-Cacod	0.1	7	-	0	PEGDME250	3.45
37	PEG10k	13.64	-	0	0	Mg-Acetate	0.09	PEG400	2.48
38	PEG4k	23.22	Tris-Chloride	0.1	8.5	Mg-Sulfate	0.22	-	0
39	PEG8k	15.8	BICINE	0.1	9	Mg-Sulfate	0.23	-	0
40	PEG8k	22.76	BICINE	0.1	8.5	-	0	-	0
41	PEGMME550	23.84	-	0	0	Na-Chloride	0.17	-	0
42	PEG400	34.24	-	0	0	K-Chloride	0.29	-	0
43	PEG3350	33.32	BICINE	0.1	9	-	0	-	0
44	PEGMME2k	39.36	Tris-Chloride	0.1	8	-	0	-	0
45	PEGMME5k	24.06	Na-Citrate	0.1	5.5	-	0	-	0
46	PEGMME2k	39.83	MOPS	0.1	7	Na-Citrate	0.07	-	0
47	PEG3350	29.57	Tris-Chloride	0.1	8.5	Am-Acetate	0.06	-	0
48	PEGMME550	46.52	BisTris	0.1	6	Am-Phosphate	0.15	-	0

49	PEGMME5k	15.21	HEPES	0.1	8	-	0	-	0
50	PEG1.5k	28.51	Tris-Chloride	0.1	7.5	Ca-Acetate	0.04	-	0
51	PEG6k	26.38	Tris-Chloride	0.1	8.5	Ca-Acetate	0.07	-	0
52	PEGMME2k	20.27	Tris-Chloride	0.1	7.5	-	0	EDTA	3
53	PEG400	50.85	HEPES	0.1	7.5	Li-Chloride	0.29	-	0
54	PEGMME2k	39.4	MES	0.1	6.5	Zn-Chloride	0.1	-	0
55	PEG3350	22.74	CHES	0.1	9.5	Mg-Chloride	0.07	-	0
56	PEG8k	14.92	-	0	0	-	0	-	0
57	PEG400	33.81	Na-Citrate	0.1	5	Na-K-Tartrate	0.12	-	0
58	PEG4k	16.48	BICINE	0.1	9.5	Am-Tartrate	0.13	-	0
59	PEG1.5k	22.34	Na-Acetate	0.1	5.5	Zn-Acetate	0.09	MPD	1.75
60	PEG10k	13.5	Na-Citrate	0.1	4.5	-	0	-	0
61	PEG4k	25.47	BICINE	0.1	9.5	Am-Citrate	0.08	PEGMME350	0.95
62	PEG10k	18.89	Na-Cacod	0.1	7	Ca-Chloride	0.12	DMSO	1.07
63	PEGMME2k	26.02	Tris-Chloride	0.1	7.5	Mg-Formate	0.04	-	0
64	PEG3350	18.44	Na-Acetate	0.1	5.5	Am-Acetate	0.1	EDTA	3.76
65	PEG400	40.48	Na-Cacod	0.1	7	Am-Citrate	0.07	-	0
66	PEG8k	16.57	BisTris	0.1	6.5	-	0	-	0
67	PEG3350	15.59	Na-Acetate	0.1	4.5	Mg-Sulfate	0.29	Hexanediol	2.19
68	PEG400	44.69	HEPES	0.1	8	Na-Chloride	0.15	-	0
69	PEGMME550	41.38	BICINE	0.1	9	-	0	-	0
70	PEG1.5k	35.74	Na-Citrate	0.1	5.5	Na-Bromide	0.11	-	0
71	PEGMME2k	22.5	MOPS	0.1	7	Na-Acetate	0.1	-	0
72	PEG1.5k	39.19	MES	0.1	6.5	Mg-Sulfate	0.28	-	0

73	PEGMME5k	25.92	NONE	0	0	Na-K-Phosphate	0.21	-	0
74	PEG1.5k	20.72	HEPES	0.1	8	Na-Acetate	0.06	LDAO	0.03
75	PEG400	46.14	BICINE	0.1	9.5	Na-Citrate	0.15	-	0
76	PEGMME2k	32.03	BICINE	0.1	8.5	-	0	-	0
77	PEG6k	21.04	Na-Acetate	0.1	5	K-Thiocyanate	0.18	CHAPS	0.08
78	PEG8k	13.84	Na-Acetate	0.1	4.5	Ca-Chloride	0.1	-	0
79	PEG400	52.35	Na-Citrate	0.1	4.5	Na-Acetate	0.11	-	0
80	PEGMME2k	26.43	Tris-Chloride	0.1	7.5	Ca-Chloride	0.06	Hexanediol	0.68
81	PEG4k	27.07	BisTris	0.1	6	K-Chloride	0.18	BOG	0.02
82	PEG10k	16.18	Na-Cacod	0.1	7	Am-Sulfate	0.28	BME	2.73
83	PEG8k	16.53	Na-Cacod	0.1	6.5	Li-Chloride	0.25	-	0
84	PEG4k	26.89	HEPES	0.1	8	Na-K-Tartrate	0.09	-	0
85	PEGMME550	32.77	Tris-Chloride	0.1	8.5	Am-Citrate	0.04	Ethglycol	0.61
86	PEG6k	19.24	MES	0.1	6	Ca-Acetate	0.07	-	0
87	PEG400	28.08	CHES	0.1	9.5	-	0	-	0
88	PEG8k	12.53	Na-Citrate	0.1	5	Na-K-Phosphate	0.14	BME	6.6
89	PEG400	34.17	Tris-Chloride	0.1	8	Mg-Chloride	0.11	Ethglycol	0.41
90	PEG3350	19.86	MES	0.1	6	Zn-Acetate	0.07	-	0
91	PEG10k	15.71	Na-Citrate	0.1	5	K-Nitrate	0.29	-	0
92	PEGMME2k	20.13	Na-Acetate	0.1	5.5	K-Nitrate	0.16	-	0
93	PEG400	51.12	HEPES	0.1	7.5	Mg-Formate	0.04	-	0
94	PEGMME2k	38.36	MOPS	0.1	6.5	Mg-Sulfate	0.27	-	0
95	PEGMME5k	16.68	-	0	0	-	0	-	0
96	PEG4k	23.73	MOPS	0.1	6.5	Na-Acetate	0.07	-	0

StoPEG 3:

	Precipitant	%	Buffer	Conc (M)	Stock Conc (M)	Salt	Conc (M)	Additive	%
1	PEG6k	15.56	BisTris	0.1	6.5	Zn-Chloride	0.08	-	0
2	PEG3350	34.07	BICINE	0.1	9.5	Mg-Acetate	0.08	-	0
3	PEGMME5k	14.04	Na-Acetate	0.1	5.5	Ca-Chloride	0.04	-	0
4	PEG1.5k	36.52	-	0	0	-	0	BOG	0.06
5	PEGMME550	37.36	BICINE	0.1	9	-	0	-	0
6	PEG10k	17.7	Na-Citrate	0.1	5	Am-Sulfate	0.09	PEG400	1.8
7	PEGMME550	35.13	MES	0.1	6	Li-Chloride	0.28	-	0
8	PEG8k	15.01	-	0	0	Mg-Sulfate	0.22	-	0
9	PEG1.5k	32.14	CHES	0.1	9.5	-	0	EDTA	6.68
10	PEG8k	22	-	0	0	-	0	-	0
11	PEG10k	17.53	Na-Citrate	0.1	4.5	K-Chloride	0.15	Glycerol	1.51
12	PEGMME550	26.64	Na-Citrate	0.1	5	Am-Acetate	0.08	-	0
13	PEG1.5k	24.76	Tris-Chloride	0.1	8	K-Chloride	0.3	-	0
14	PEG3350	20.26	Tris-Chloride	0.1	7.5	Zn-Acetate	0.12	-	0
15	PEG4k	27.89	MES	0.1	6.5	-	0	-	0
16	PEGMME2k	27.89	Tris-Chloride	0.1	8	-	0	-	0
17	PEG6k	20.68	Na-Citrate	0.1	5	Am-Citrate	0.06	PEGMME350	2.47
18	PEG8k	23.21	Tris-Chloride	0.1	7.5	-	0	-	0
19	PEGMME550	42.96	BisTris	0.1	6	Li-Sulfate	0.09	-	0
20	PEGMME2k	38.7	BICINE	0.1	9.5	-	0	-	0
21	PEGMME550	39.89	MES	0.1	6	-	0	-	0
22	PEG10k	17.42	HEPES	0.1	7.5	-	0	-	0
23	PEG4k	17.68	Na-Acetate	0.1	4.5	Zn-Acetate	0.06	LDAO	0.08
24	PEGMME2k	22.08	Na-Acetate	0.1	5.5	K-Thiocyanate	0.28	-	0

25	PEG400	25.19	Na-Citrate	0.1	4.5	Na-Bromide	0.29	-	0
26	PEG4k	23.49	CHES	0.1	9	Li-Chloride	0.3	-	0
27	PEG400	48.75	BICINE	0.1	8.5	Na-Bromide	0.21	-	0
28	PEGMME5k	12.17	MOPS	0.1	7	-	0	Methanol	1
29	PEG400	52.24	HEPES	0.1	7.5	Ca-Chloride	0.08	-	0
30	PEG1.5k	26.96	HEPES	0.1	8	Na-K-Tartrate	0.09	EDTA	2.87
31	PEGMME550	36.98	Na-Acetate	0.1	5.5	Am-Acetate	0.06	-	0
32	PEG8k	23.74	-	0	0	-	0	-	0
33	PEGMME550	32.68	MOPS	0.1	7	K-Chloride	0.06	-	0
34	PEG6k	19.83	MOPS	0.1	7	K-Chloride	0.26	-	0
35	PEG400	38.5	Na-Citrate	0.1	4.5	-	0	-	0
36	PEG8k	14.39	Na-Cacod	0.1	6.5	-	0	-	0
37	PEG1.5k	41.65	HEPES	0.1	7.5	Na-Acetate	0.15	-	0
38	PEGMME5k	19.99	MOPS	0.1	6.5	Am-Phosphate	0.11	Dioxane	1.38
39	PEG6k	14.72	Na-Acetate	0.1	5.5	Ca-Acetate	0.12	-	0
40	PEG3350	22.49	Na-Citrate	0.1	5.5	Am-Citrate	0.06	-	0
41	PEG4k	30.88	Tris-Chloride	0.1	7.5	-	0	-	0
42	PEGMME5k	22.75	BICINE	0.1	9.5	-	0	-	0
43	PEG10k	11.17	NONE	0	0	Na-Chloride	0.28	Hexanediol	3.19
44	PEG1.5k	40.01	BICINE	0.1	8.5	Ca-Acetate	0.04	-	0
45	PEGMME5k	22.06	MES	0.1	6	Ca-Acetate	0.1	Hexanediol	1.92
46	PEG10k	16.14	-	0	0	K-Nitrate	0.25	-	0
47	PEG8k	24.01	BICINE	0.1	8.5	Na-K-Phosphate	0.26	-	0
48	PEGMME550	44.2	CHES	0.1	9	Am-Tartrate	0.15	-	0

49	PEG1.5k	33.68	Tris-Chloride	0.1	8	-	0	-	0
50	PEG8k	16.85	Na-Cacod	0.1	7	Mg-Chloride	0.16	-	0
51	PEG3350	19.59	Na-Citrate	0.1	5.5	Na-Citrate	0.06	BOG	0.07
52	PEG400	29.94	MES	0.1	6.5	Zn-Acetate	0.04	-	0
53	PEG3350	27.57	MES	0.1	6.5	Na-Acetate	0.12	-	0
54	PEGMME2k	25.96	MES	0.1	6	Zn-Acetate	0.07	-	0
55	PEG4k	30.59	Na-Citrate	0.1	5	Mg-Acetate	0.08	BME	1.48
56	PEGMME5k	25.11	-	0	0	Zn-Chloride	0.08	-	0
57	PEGMME2k	24.38	MOPS	0.1	7	K-Nitrate	0.12	CHAPS	0.02
58	PEG3350	22.76	BICINE	0.1	8.5	-	0	PEGDME250	2.9
59	PEG4k	30.77	Na-Citrate	0.1	4.5	Li-Sulfate	0.14	-	0
60	PEG400	28.5	Na-Citrate	0.1	5.5	Na-K-Phosphate	0.26	-	0
61	PEG4k	23.58	-	0	0	Zn-Chloride	0.06	-	0
62	PEG8k	20.84	Na-Cacod	0.1	7	Na-Bromide	0.12	PEGMME350	1.2
63	PEGMME2k	38.87	NONE	0	0	Li-Chloride	0.18	-	0
64	PEGMME5k	13.85	HEPES	0.1	8	Am-Phosphate	0.2	-	0
65	PEG10k	10.55	Tris-Chloride	0.1	8.5	K-Thiocyanate	0.08	-	0
66	PEG1.5k	21.34	Na-Acetate	0.1	5	K-Nitrate	0.2	-	0
67	PEG4k	13.54	Tris-Chloride	0.1	8.5	Am-Citrate	0.05	-	0
68	PEG400	31.17	Tris-Chloride	0.1	8	Am-Acetate	0.1	-	0
69	PEG4k	25.3	Na-Citrate	0.1	5.5	Am-Phosphate	0.2	MPD	0.78
70	PEG10k	15.04	Tris-Chloride	0.1	8.5	Mg-Sulfate	0.29	-	0
71	PEG6k	27.23	-	0	0	Mg-Formate	0.15	-	0
72	PEGMME5k	12.42	BisTris	0.1	6	Mg-Sulfate	0.28	-	0

73	PEG400	29.56	-	0	0	Na-Acetate	0.14	-	0
74	PEGMME550	32.77	BICINE	0.1	9	Na-K-Tartrate	0.05	-	0
75	PEG3350	17.94	CHES	0.1	9.5	Mg-Chloride	0.24	-	0
76	PEG1.5k	40.16	-	0	0	Am-Tartrate	0.13	-	0
77	PEGMME2k	23.76	BICINE	0.1	9.5	Mg-Formate	0.07	Butanediol	1.56
78	PEG3350	33.19	MOPS	0.1	7	Ca-Chloride	0.12	-	0
79	PEGMME5k	15.22	Na-Citrate	0.1	5	-	0	-	0
80	PEG3350	16.87	Na-Acetate	0.1	5.5	Na-Chloride	0.13	-	0
81	PEG1.5k	39.99	BICINE	0.1	9	Am-Acetate	0.08	-	0
82	PEGMME5k	12.49	HEPES	0.1	7.5	Am-Phosphate	0.23	-	0
83	PEG400	40.27	Tris-Chloride	0.1	8	Ca-Chloride	0.05	-	0
84	PEG6k	14.5	HEPES	0.1	7.5	K-Thiocyanate	0.09	-	0
85	PEG8k	19.36	Tris-Chloride	0.1	8.5	-	0	BME	5
86	PEG400	39.62	BICINE	0.1	8.5	Mg-Formate	0.08	-	0
87	PEG4k	24.19	Na-Acetate	0.1	5	Mg-Chloride	0.25	-	0
88	PEG10k	11.53	MOPS	0.1	7	Li-Sulfate	0.09	DMSO	0.56
89	PEG3350	18.29	MOPS	0.1	6.5	Li-Sulfate	0.22	-	0
90	PEGMME2k	33.71	Na-Cacod	0.1	7	K-Thiocyanate	0.18	-	0
91	PEGMME550	48.57	HEPES	0.1	8	Mg-Chloride	0.13	DMSO	1.69
92	PEGMME5k	22.51	Na-Acetate	0.1	4.5	Ca-Chloride	0.13	-	0
93	PEG10k	20.06	Na-Citrate	0.1	4.5	-	0	-	0
94	PEGMME5k	18.97	Na-Acetate	0.1	4.5	Na-K-Phosphate	0.15	EDTA	1.79
95	PEG6k	17.9	CHES	0.1	9	Na-Chloride	0.18	-	0
96	PEG400	33.63	Na-Acetate	0.1	5.5	-	0	-	0

Stochastic 17:

	Precipitant	%	Buffer	Conc (M)	Stock Conc (M)	Salt	Conc (M)	Additive	%
1	PEGMME550	31.16	Na-Cacod	0.1	7	NONE	0	NONE	0
2	Na-Formate	2	Na-Acetate	0.1	5	Am-Phosphate	0.07	NONE	0
3	PEGMME2k	30.73	MES	0.1	6	NONE	0	NONE	0
4	PEG400	42.04	BisTris	0.1	6	Am-Phosphate	0.26	NONE	0
5	PEG1.5k	29.11	Na-Acetate	0.1	4.5	Ca-Acetate	0.05	PEGDME250	0.76
6	PEGMME5k	27.17	Na-Cacod	0.1	7	Ca-Chloride	0.14	NONE	0
7	PEG4k	22.87	BisTris	0.1	6.5	Zn-Chloride	0.12	BME	7.69
8	Na-Citrate	1.06	BICINE	0.1	9	Mg-Acetate	0.22	NONE	0
9	PEGMME2k	27.2	CHES	0.1	9.5	Am-Phosphate	0.16	NONE	0
10	Na-Citrate	0.81	NONE	0	0	Mg-Sulfate	0.29	NONE	0
11	Na-Malate	1.99	NONE	0	0	Na-K-Tartrate	0.03	DMSO	2.62
12	PEG1.5k	25.25	BICINE	0.1	8.5	Na-Citrate	0.14	NONE	0
13	Na-Tartrate	0.87	BisTris	0.1	6	NONE	0	PEG400	2.77
14	Mg-Sulfate	1.33	Tris-Chloride	0.1	8	NONE	0	NONE	0
15	Na-Tartrate	1.36	Na-Citrate	0.1	4.5	Am-Phosphate	0.23	NONE	0
16	Isopropanol	10.72	NONE	0	0	Am-Citrate	0.12	NONE	0
17	Na-Tartrate	0.99	NONE	0	0	NONE	0	NONE	0
18	MPD	50.55	Tris-Chloride	0.1	8.5	NONE	0	PEGMME350	2.52
19	PEGMME550	33.77	HEPES	0.1	8	Am-Citrate	0.12	NONE	0
20	PEG400	42.72	Tris-Chloride	0.1	8	Zn-Acetate	0.04	NONE	0
21	Na-Chloride	2.72	Na-Acetate	0.1	5.5	Zn-Acetate	0.05	BOG	0.03
22	PEG400	50.15	Na-Citrate	0.1	5	NONE	0	NONE	0
23	PEGMME550	43.96	CHES	0.1	9	NONE	0	BOG	0.05
24	PEG10k	9.09	BisTris	0.1	6	Zn-Acetate	0.09	CHAPS	0.08

25	PEG10k	19.97	NONE	0	0	Am-Tartrate	0.12	NONE	0
26	Ethanol	6.86	NONE	0	0	Na-Bromide	0.21	NONE	0
27	PEG6k	23.33	HEPES	0.1	7.5	Zn-Chloride	0.1	NONE	0
28	PEGMME5k	17.22	NONE	0	0	Na-K-Tartrate	0.11	NONE	0
29	PEG1.5k	29.43	Na-Citrate	0.1	4.5	Mg-Acetate	0.09	NONE	0
30	Na-Malonate	1.69	MOPS	0.1	7	Na-Chloride	0.21	NONE	0
31	Am-Phosphate	2.34	Tris-Chloride	0.1	7.5	Na-K-Tartrate	0.09	NONE	0
32	PEG1.5k	33.09	MES	0.1	6	Li-Chloride	0.15	NONE	0
33	PEG4k	18.49	Na-Citrate	0.1	5.5	Li-Sulfate	0.21	NONE	0
34	Na-K-Phosphate	2.39	Na-Acetate	0.1	5.5	Na-K-Phosphate	0.15	NONE	0
35	PEG4k	28.02	HEPES	0.1	7.5	NONE	0	NONE	0
36	PEG10k	19.28	HEPES	0.1	7.5	Na-Acetate	0.07	NONE	0
37	PEGMME2k	29.7	BICINE	0.1	9.5	Mg-Acetate	0.23	NONE	0
38	Na-Citrate	0.75	MOPS	0.1	7	Li-Chloride	0.14	NONE	0
39	Na-Acetate	2.38	Tris-Chloride	0.1	8	NONE	0	NONE	0
40	PEG8k	19.88	CHES	0.1	9	NONE	0	NONE	0
41	Na-Malonate	2.63	BisTris	0.1	6	Na-Chloride	0.24	NONE	0
42	PEGMME2k	32.2	HEPES	0.1	7.5	NONE	0	NONE	0
43	PEG3350	23.08	Tris-Chloride	0.1	8	Zn-Acetate	0.05	MPD	0.96
44	PEG8k	16.21	HEPES	0.1	8	Am-Acetate	0.05	NONE	0
45	Na-K-Phosphate	2.19	Na-Cacod	0.1	7	NONE	0	NONE	0
46	Na-Citrate	0.91	Na-Citrate	0.1	5.5	Li-Chloride	0.06	NONE	0
47	PEG3350	29.44	Tris-Chloride	0.1	7.5	Zn-Chloride	0.14	NONE	0
48	PEG8k	18.37	Na-Acetate	0.1	5	K-Chloride	0.06	NONE	0

49	Na-Formate	1.86	MOPS	0.1	6.5	Am-Sulfate	0.17	NONE	0
50	Mg-Sulfate	1.44	CHES	0.1	9.5	Na-Acetate	0.14	NONE	0
51	PEG3350	34.73	MES	0.1	6	Na-Chloride	0.21	PEGDME250	1.23
52	Isopropanol	15.21	CHES	0.1	9.5	K-Nitrate	0.29	NONE	0
53	PEG4k	15.42	NONE	0	0	Am-Citrate	0.09	NONE	0
54	Am-Sulfate	1.77	Na-Cacod	0.1	6.5	Mg-Sulfate	0.21	NONE	0
55	Na-Malate	2.31	BisTris	0.1	6.5	NONE	0	EDTA	2.24
56	PEGMME5k	21.34	BICINE	0.1	9.5	NONE	0	NONE	0
57	PEG3350	33.97	BisTris	0.1	6	Ca-Acetate	0.06	NONE	0
58	Isopropanol	19.61	Na-Acetate	0.1	5	Ca-Acetate	0.1	Glycerol	2.4
59	Ethanol	15.61	Na-Acetate	0.1	5.5	Mg-Chloride	0.28	NONE	0
60	PEG6k	18.3	Na-Citrate	0.1	5.5	Na-Citrate	0.1	NONE	0
61	Na-Formate	2.24	BICINE	0.1	9.5	Mg-Formate	0.05	NONE	0
62	Ethanol	14.2	Na-Cacod	0.1	6.5	Am-Sulfate	0.18	Dioxane	1.93
63	PEG3350	28.82	NONE	0	0	NONE	0	Butanediol	1.21
64	PEG8k	12.28	Na-Acetate	0.1	4.5	Am-Sulfate	0.23	NONE	0
65	PEG3350	31.35	Na-Citrate	0.1	5	Mg-Sulfate	0.18	NONE	0
66	PEGMME5k	12.86	MES	0.1	6.5	Mg-Acetate	0.12	MPD	1.07
67	Am-Phosphate	1.91	Na-Acetate	0.1	4.5	Am-Tartrate	0.04	LDAO	0.05
68	PEG10k	13.29	BICINE	0.1	9.5	Mg-Sulfate	0.11	NONE	0
69	Na-Formate	2.79	Na-Citrate	0.1	4.5	Am-Tartrate	0.09	NONE	0
70	Am-Phosphate	2.19	BICINE	0.1	8.5	NONE	0	NONE	0
71	PEGMME550	39.83	Tris-Chloride	0.1	8.5	K-Thiocyanate	0.29	NONE	0
72	PEG6k	23.07	BICINE	0.1	9.5	Mg-Formate	0.05	NONE	0

73	Na-Chloride	2.29	NONE	0	0	Na-Chloride	0.19	NONE	0
74	Na-Acetate	1.62	Na-Cacod	0.1	6.5	Li-Chloride	0.17	Glycerol	2.84
75	Na-K-Phosphate	1.79	Tris-Chloride	0.1	8.5	Na-K-Phosphate	0.24	NONE	0
76	PEG400	33.83	Na-Acetate	0.1	4.5	NONE	0	NONE	0
77	Na-Tartrate	1.28	Na-Citrate	0.1	4.5	Na-K-Phosphate	0.13	NONE	0
78	PEGMME550	34.6	BisTris	0.1	6.5	Na-Chloride	0.23	NONE	0
79	PEG400	45.98	Tris-Chloride	0.1	7.5	NONE	0	NONE	0
80	PEG6k	15.85	MES	0.1	6.5	Na-Bromide	0.06	Hexanediol	2.67
81	Na-Acetate	2.04	Tris-Chloride	0.1	8.5	Ca-Acetate	0.09	NONE	0
82	PEG400	38.33	Na-Cacod	0.1	7	Am-Phosphate	0.15	BME	8.17
83	Na-Citrate	0.92	HEPES	0.1	7.5	Na-Bromide	0.06	NONE	0
84	Am-Phosphate	2.32	Na-Citrate	0.1	5	Na-K-Phosphate	0.17	NONE	0
85	PEG10k	18.46	BICINE	0.1	9	Mg-Acetate	0.18	NONE	0
86	PEGMME2k	32.3	BICINE	0.1	9	Li-Sulfate	0.13	Methanol	1.83
87	PEG4k	20.66	Na-Acetate	0.1	5.5	NONE	0	NONE	0
88	Na-Malonate	2.28	Na-Cacod	0.1	7	Na-Bromide	0.26	PEG400	3.12
89	PEG3350	18.86	MOPS	0.1	7	Am-Phosphate	0.19	NONE	0
90	Na-K-Phosphate	2.75	Tris-Chloride	0.1	8.5	NONE	0	NONE	0
91	MPD	24.57	Tris-Chloride	0.1	8	Am-Acetate	0.05	NONE	0
92	Am-Sulfate	2.19	BisTris	0.1	6	Mg-Chloride	0.3	Glycerol	2.11
93	PEG8k	25.24	NONE	0	0	Ca-Chloride	0.15	NONE	0
94	PEGMME5k	15.87	NONE	0	0	Na-K-Phosphate	0.19	NONE	0
95	Na-Acetate	1.58	BICINE	0.1	8.5	Na-Chloride	0.08	NONE	0
96	PEGMME550	33.36	CHES	0.1	9	Am-Sulfate	0.24	NONE	0

Stochastic 18:

	Precipitant	%	Buffer	Conc (M)	Stock Conc (M)	Salt	Conc (M)	Additive	%
1	PEG8k	27.84	NONE	0	0	Zn-Chloride	0.03	NONE	0
2	PEG6k	26.4	HEPES	0.1	7.5	Ca-Acetate	0.09	Ethglycol	1.91
3	PEGMME5k	19.98	Tris-Chloride	0.1	8	Na-Chloride	0.06	NONE	0
4	Na-Citrate	1.01	Na-Citrate	0.1	5	NONE	0	NONE	0
5	PEG10k	16.25	Na-Cacod	0.1	7	Na-K-Phosphate	0.05	NONE	0
6	PEG1.5k	38.87	NONE	0	0	Zn-Acetate	0.08	NONE	0
7	PEG400	52.81	HEPES	0.1	7.5	Na-Bromide	0.09	Methanol	0.44
8	PEGMME5k	22.47	MES	0.1	6	Zn-Acetate	0.08	Methanol	0.89
9	PEG3350	25.45	NONE	0	0	Zn-Chloride	0.03	NONE	0
10	PEGMME2k	31.76	Tris-Chloride	0.1	8.5	Ca-Acetate	0.09	NONE	0
11	Na-Formate	1.79	Na-Citrate	0.1	5.5	Mg-Sulfate	0.28	NONE	0
12	Na-Chloride	2.26	Na-Acetate	0.1	5	K-Thiocyanate	0.11	PEGMME350	3.52
13	PEG6k	27.24	CHES	0.1	9.5	Na-Chloride	0.29	NONE	0
14	Na-Malonate	2.78	Tris-Chloride	0.1	8	NONE	0	NONE	0
15	MPD	51.62	BICINE	0.1	9	NONE	0	NONE	0
16	PEGMME2k	24.54	NONE	0	0	Na-K-Tartrate	0.09	NONE	0
17	Na-Acetate	2.7	MOPS	0.1	6.5	Na-Acetate	0.08	NONE	0
18	Ethanol	20.03	Na-Citrate	0.1	5	Li-Chloride	0.16	PEG400	1.62
19	PEG4k	13.94	BICINE	0.1	8.5	NONE	0	PEGDME250	2.48
20	Am-Phosphate	2.27	MES	0.1	6.5	NONE	0	Butanediol	1.71
21	Isopropanol	12.81	Tris-Chloride	0.1	8.5	Ca-Chloride	0.11	NONE	0
22	Na-Malate	2	Tris-Chloride	0.1	7.5	NONE	0	NONE	0
23	Na-Citrate	0.86	Na-Acetate	0.1	5.5	NONE	0	NONE	0
24	PEGMME550	43.98	BICINE	0.1	9	Am-Citrate	0.13	NONE	0

25	PEG10k	11.6	BICINE	0.1	9.5	Am-Tartrate	0.04	NONE	0
26	Na-K-Phosphate	1.8	NONE	0	0	Am-Phosphate	0.2	NONE	0
27	Mg-Sulfate	1.37	Na-Acetate	0.1	5	Na-Citrate	0.09	NONE	0
28	Na-Malate	2.1	MOPS	0.1	6.5	NONE	0	PEG400	2.4
29	PEG3350	28.21	MOPS	0.1	7	Na-Citrate	0.07	NONE	0
30	Na-Tartrate	1.11	NONE	0	0	Am-Citrate	0.13	BME	3.7
31	PEGMME5k	18.13	Na-Acetate	0.1	4.5	Ca-Chloride	0.1	LDAO	0.06
32	PEG1.5k	34.84	MES	0.1	6	Li-Sulfate	0.25	NONE	0
33	PEG4k	17.06	NONE	0	0	Zn-Chloride	0.09	NONE	0
34	Mg-Sulfate	1.07	BICINE	0.1	9	NONE	0	NONE	0
35	PEG400	39.6	CHES	0.1	9	Li-Sulfate	0.29	PEG400	2.69
36	Na-Malonate	2.42	BICINE	0.1	9.5	NONE	0	NONE	0
37	PEG4k	28.98	Na-Acetate	0.1	5.5	Na-K-Phosphate	0.05	NONE	0
38	PEGMME550	34.75	Na-Acetate	0.1	5.5	Ca-Acetate	0.03	NONE	0
39	Na-Malonate	2.13	Na-Citrate	0.1	5	K-Thiocyanate	0.22	NONE	0
40	Na-Malate	2.15	MOPS	0.1	7	NONE	0	NONE	0
41	Na-K-Phosphate	1.75	Na-Cacod	0.1	6.5	Na-K-Phosphate	0.17	NONE	0
42	Am-Sulfate	1.93	BICINE	0.1	8.5	NONE	0	NONE	0
43	Na-Malate	2.41	Na-Citrate	0.1	4.5	K-Nitrate	0.19	NONE	0
44	Am-Phosphate	1.71	Tris-Chloride	0.1	7.5	K-Chloride	0.29	NONE	0
45	PEG1.5k	30.77	Na-Citrate	0.1	4.5	NONE	0	CHAPS	0.08
46	PEG10k	16.23	Tris-Chloride	0.1	8	Zn-Acetate	0.05	NONE	0
47	PEG3350	34.51	MOPS	0.1	6.5	Na-K-Tartrate	0.09	NONE	0
48	MPD	53.86	NONE	0	0	Am-Sulfate	0.15	DMSO	3.03

49	Ethanol	19.97	Tris-Chloride	0.1	8	Mg-Acetate	0.18	BOG	0.08
50	PEG10k	16.62	MES	0.1	6	NONE	0	Dioxane	1.27
51	PEG3350	26.98	BisTris	0.1	6	Zn-Acetate	0.08	CHAPS	0.05
52	Am-Sulfate	2.45	BICINE	0.1	9	K-Nitrate	0.23	PEGMME350	0.86
53	MPD	39.45	CHES	0.1	9	NONE	0	NONE	0
54	Na-Malonate	2.44	Na-Cacod	0.1	7	Am-Tartrate	0.13	NONE	0
55	PEG6k	26.52	Tris-Chloride	0.1	8.5	Am-Citrate	0.1	NONE	0
56	PEGMME5k	20.23	MES	0.1	6	Mg-Formate	0.1	NONE	0
57	Na-Citrate	1.06	MES	0.1	6.5	Mg-Sulfate	0.29	Hexanediol	2.19
58	PEGMME5k	20.48	MOPS	0.1	7	NONE	0	NONE	0
59	PEG400	51.34	BICINE	0.1	8.5	Na-Chloride	0.11	NONE	0
60	PEGMME2k	22	Na-Acetate	0.1	5.5	NONE	0	NONE	0
61	Na-Malonate	2.65	Tris-Chloride	0.1	8.5	K-Chloride	0.1	NONE	0
62	PEGMME2k	34.75	NONE	0	0	Na-Bromide	0.17	NONE	0
63	PEG6k	19.04	Na-Acetate	0.1	5	Li-Chloride	0.11	NONE	0
64	Na-Malate	2.1	CHES	0.1	9.5	Am-Sulfate	0.17	NONE	0
65	PEG4k	27.08	Na-Citrate	0.1	5	NONE	0	LDAO	0.01
66	PEG8k	24.25	Tris-Chloride	0.1	8	Am-Phosphate	0.05	NONE	0
67	Am-Sulfate	1.62	Na-Citrate	0.1	5	Am-Acetate	0.14	Glycerol	2.93
68	Na-Chloride	3.38	BisTris	0.1	6	Ca-Acetate	0.08	NONE	0
69	MPD	52.95	Na-Acetate	0.1	4.5	K-Thiocyanate	0.28	PEGDME250	1.26
70	PEGMME2k	31.82	Na-Citrate	0.1	5.5	Am-Acetate	0.1	PEGMME350	2.65
71	PEG400	25.46	Na-Acetate	0.1	4.5	K-Nitrate	0.24	NONE	0
72	Am-Phosphate	1.95	Na-Citrate	0.1	4.5	K-Chloride	0.07	Ethglycol	3.23

73	PEGMME550	37.95	Na-Citrate	0.1	5.5	Li-Sulfate	0.26	LDAO	0.08
74	PEG1.5k	37.75	MOPS	0.1	7	K-Chloride	0.19	EDTA	6.29
75	PEGMME550	21.61	HEPES	0.1	8	Mg-Chloride	0.07	NONE	0
76	Am-Phosphate	2.21	Na-Cacod	0.1	7	Am-Acetate	0.1	NONE	0
77	Na-Acetate	2.44	Tris-Chloride	0.1	7.5	K-Thiocyanate	0.11	NONE	0
78	PEGMME5k	18.71	CHES	0.1	9	Am-Phosphate	0.27	NONE	0
79	Na-Formate	2.5	Na-Cacod	0.1	7	NONE	0	NONE	0
80	PEG8k	19.65	BICINE	0.1	9.5	NONE	0	NONE	0
81	Na-Acetate	1.95	BisTris	0.1	6.5	NONE	0	NONE	0
82	Na-Malate	1.96	Na-Cacod	0.1	7	Am-Phosphate	0.09	NONE	0
83	PEG400	25.33	Tris-Chloride	0.1	8.5	Mg-Acetate	0.17	NONE	0
84	Am-Phosphate	1.71	Na-Citrate	0.1	5.5	Na-Acetate	0.1	NONE	0
85	Mg-Sulfate	1.65	Tris-Chloride	0.1	7.5	Mg-Chloride	0.16	NONE	0
86	PEG6k	23.54	Tris-Chloride	0.1	7.5	NONE	0	NONE	0
87	PEG8k	22.8	BisTris	0.1	6.5	NONE	0	NONE	0
88	PEG10k	11.2	BICINE	0.1	9.5	Na-Bromide	0.11	NONE	0
89	Na-Chloride	2.39	MOPS	0.1	6.5	Ca-Chloride	0.07	NONE	0
90	PEGMME5k	15.48	Tris-Chloride	0.1	8	Am-Phosphate	0.13	NONE	0
91	Na-K-Phosphate	1.82	HEPES	0.1	8	NONE	0	NONE	0
92	PEG1.5k	30.26	Na-Citrate	0.1	4.5	Am-Sulfate	0.2	NONE	0
93	Na-Citrate	0.71	CHES	0.1	9	Na-Chloride	0.23	NONE	0
94	Na-Chloride	2.71	HEPES	0.1	8	Ca-Chloride	0.08	NONE	0
95	Na-Malonate	2.23	HEPES	0.1	7.5	K-Chloride	0.3	NONE	0
96	PEG1.5k	29.79	Na-Acetate	0.1	5.5	NONE	0	NONE	0

Stochastic 19:

	Precipitant	%	Buffer	Conc (M)	Stock Conc (M)	Salt	Conc (M)	Additive	%
1	PEG400	30.7	MES	0.1	6	Na-Chloride	0.25	NONE	0
2	Na-Chloride	2.8	BisTris	0.1	6	Zn-Chloride	0.09	NONE	0
3	PEG1.5k	27.57	NONE	0	0	Ca-Chloride	0.14	NONE	0
4	Na-Malonate	1.86	Na-Acetate	0.1	5	Am-Sulfate	0.18	NONE	0
5	PEG400	40.17	Na-Citrate	0.1	5.5	Li-Sulfate	0.1	NONE	0
6	Na-K-Phosphate	2.73	BICINE	0.1	9.5	Na-K-Tartrate	0.07	NONE	0
7	Isopropanol	9.89	HEPES	0.1	8	Ca-Chloride	0.13	NONE	0
8	Mg-Sulfate	1.43	Tris-Chloride	0.1	8	NONE	0	NONE	0
9	PEG1.5k	21.79	Tris-Chloride	0.1	8.5	K-Chloride	0.2	NONE	0
10	Na-K-Phosphate	2.71	HEPES	0.1	8	NONE	0	NONE	0
11	Isopropanol	6.9	Na-Citrate	0.1	4.5	Mg-Chloride	0.11	NONE	0
12	Ethanol	9.18	BisTris	0.1	6	Zn-Chloride	0.14	PEGMME350	3.22
13	Na-Acetate	2.76	HEPES	0.1	7.5	Li-Chloride	0.07	NONE	0
14	MPD	35.21	CHES	0.1	9.5	Am-Citrate	0.14	NONE	0
15	Na-Malate	2.1	Na-Citrate	0.1	4.5	NONE	0	DMSO	2.4
16	PEG6k	16.89	MOPS	0.1	7	Na-K-Tartrate	0.12	NONE	0
17	PEG1.5k	35.16	Tris-Chloride	0.1	7.5	Zn-Chloride	0.03	NONE	0
18	PEG8k	20.93	Na-Cacod	0.1	6.5	Zn-Acetate	0.09	NONE	0
19	PEG4k	16.24	MES	0.1	6	NONE	0	NONE	0
20	Na-Malonate	2.06	BICINE	0.1	9	K-Thiocyanate	0.28	NONE	0
21	Na-Citrate	0.77	Na-Citrate	0.1	5.5	Mg-Acetate	0.17	NONE	0
22	PEGMME2k	36.82	Na-Cacod	0.1	7	Mg-Chloride	0.09	NONE	0
23	PEGMME550	28.8	CHES	0.1	9	NONE	0	LDAO	0.03
24	PEGMME5k	24.8	Na-Cacod	0.1	7	Na-Citrate	0.13	NONE	0

25	PEGMME550	38.79	MES	0.1	6.5	Mg-Formate	0.11	Butanediol	3.59
26	PEG6k	23.59	BisTris	0.1	6	Mg-Acetate	0.12	NONE	0
27	PEG10k	11.67	MOPS	0.1	6.5	Am-Tartrate	0.04	NONE	0
28	Na-K-Phosphate	1.7	NONE	0	0	Na-Bromide	0.2	Hexanediol	1.32
29	PEG4k	17.94	NONE	0	0	Am-Phosphate	0.15	NONE	0
30	Na-Citrate	1	BisTris	0.1	6.5	NONE	0	NONE	0
31	PEGMME550	31.69	BisTris	0.1	6	Am-Tartrate	0.05	Dioxane	3.24
32	Na-Malonate	2.38	Na-Citrate	0.1	5	NONE	0	NONE	0
33	PEG6k	15.1	Na-Citrate	0.1	4.5	Am-Acetate	0.03	PEG400	0.44
34	PEG4k	30.26	Na-Citrate	0.1	4.5	Mg-Chloride	0.26	NONE	0
35	Ethanol	10.53	Na-Citrate	0.1	5	NONE	0	NONE	0
36	Na-Malate	1.63	BisTris	0.1	6.5	Am-Citrate	0.08	MPD	3.05
37	PEG400	50.05	Tris-Chloride	0.1	8	NONE	0	NONE	0
38	PEGMME2k	38.14	Tris-Chloride	0.1	7.5	NONE	0	NONE	0
39	PEG8k	12.66	BisTris	0.1	6.5	Na-K-Phosphate	0.1	Ethglycol	1.3
40	Am-Phosphate	2.16	HEPES	0.1	8	Na-Citrate	0.04	NONE	0
41	Na-Formate	2.14	HEPES	0.1	7.5	NONE	0	NONE	0
42	PEG400	53.24	Na-Acetate	0.1	4.5	Zn-Acetate	0.06	NONE	0
43	Am-Phosphate	2.46	Na-Citrate	0.1	5.5	NONE	0	Glycerol	2
44	PEG8k	13.15	HEPES	0.1	8	Li-Chloride	0.27	NONE	0
45	Am-Sulfate	2.49	Na-Citrate	0.1	4.5	K-Nitrate	0.13	DMSO	2.17
46	PEGMME5k	24.93	Na-Cacod	0.1	7	Zn-Acetate	0.08	NONE	0
47	PEGMME550	40.49	BisTris	0.1	6.5	Ca-Acetate	0.1	NONE	0
48	PEG8k	15.71	Na-Acetate	0.1	5.5	Ca-Chloride	0.11	NONE	0

49	Na-Acetate	1.68	BICINE	0.1	8.5	Am-Tartrate	0.13	NONE	0
50	Na-Formate	2.09	NONE	0	0	Ca-Chloride	0.04	NONE	0
51	PEG400	51.72	MES	0.1	6.5	NONE	0	PEGDME250	2.53
52	PEGMME5k	24.92	MOPS	0.1	7	Mg-Sulfate	0.17	NONE	0
53	PEGMME550	37.38	BICINE	0.1	8.5	Zn-Acetate	0.09	PEG400	3.49
54	PEG3350	17.55	CHES	0.1	9	K-Nitrate	0.21	NONE	0
55	Mg-Sulfate	1.71	BICINE	0.1	9.5	NONE	0	NONE	0
56	Am-Phosphate	1.85	Na-Acetate	0.1	5	Na-Bromide	0.05	Ethglycol	3.5
57	Mg-Sulfate	1.01	MES	0.1	6	NONE	0	NONE	0
58	Am-Sulfate	1.69	Tris-Chloride	0.1	7.5	Mg-Acetate	0.1	NONE	0
59	PEG6k	23.13	MES	0.1	6	Ca-Acetate	0.05	NONE	0
60	PEG10k	20.29	Na-Citrate	0.1	4.5	NONE	0	NONE	0
61	Isopropanol	7.95	BisTris	0.1	6	Na-K-Phosphate	0.12	CHAPS	0.02
62	Na-Acetate	1.99	NONE	0	0	Mg-Sulfate	0.19	NONE	0
63	PEG1.5k	25.99	Na-Acetate	0.1	4.5	Na-Chloride	0.07	NONE	0
64	Na-Malate	1.81	Na-Acetate	0.1	4.5	NONE	0	BME	7.47
65	Am-Phosphate	2.38	Na-Citrate	0.1	5	NONE	0	NONE	0
66	Ethanol	14.05	Na-Acetate	0.1	5	Zn-Chloride	0.12	BME	6.39
67	PEG3350	32.03	Na-Acetate	0.1	5.5	Li-Chloride	0.15	NONE	0
68	PEGMME5k	14.19	CHES	0.1	9.5	Li-Sulfate	0.23	Methanol	2.56
69	Na-Malonate	2.25	HEPES	0.1	8	NONE	0	BOG	0.02
70	PEG3350	33.28	NONE	0	0	NONE	0	NONE	0
71	Ethanol	19.56	HEPES	0.1	7.5	NONE	0	NONE	0
72	Isopropanol	10.67	BICINE	0.1	9	NONE	0	EDTA	4.93

73	PEG6k	20.5	BisTris	0.1	6.5	Na-K-Tartrate	0.03	NONE	0
74	PEG1.5k	28.66	Na-Citrate	0.1	5	K-Thiocyanate	0.11	NONE	0
75	Na-Citrate	1.01	BICINE	0.1	8.5	Am-Phosphate	0.1	PEGDME250	1.43
76	PEGMME550	22.93	Tris-Chloride	0.1	8	Na-K-Phosphate	0.15	NONE	0
77	Am-Sulfate	2.36	Na-Citrate	0.1	5.5	Am-Phosphate	0.21	NONE	0
78	PEGMME550	31.34	BICINE	0.1	9	Am-Phosphate	0.17	NONE	0
79	Na-Malate	1.95	CHES	0.1	9.5	Na-Chloride	0.16	NONE	0
80	PEG3350	24.2	BICINE	0.1	8.5	Am-Acetate	0.1	NONE	0
81	PEG400	46.17	BICINE	0.1	9.5	Am-Citrate	0.11	NONE	0
82	PEG8k	15.6	Na-Citrate	0.1	5.5	NONE	0	Methanol	0.51
83	Na-Acetate	1.48	Na-Acetate	0.1	5.5	K-Thiocyanate	0.24	LDAO	0.05
84	Na-K-Phosphate	2.03	HEPES	0.1	7.5	Na-Acetate	0.07	MPD	3
85	PEG4k	15.24	NONE	0	0	Mg-Formate	0.05	NONE	0
86	Na-Chloride	3.05	Tris-Chloride	0.1	8.5	NONE	0	NONE	0
87	PEG10k	13.69	Na-Acetate	0.1	5	Li-Sulfate	0.23	Dioxane	1.28
88	PEG8k	15.81	HEPES	0.1	7.5	Am-Sulfate	0.26	BOG	0.04
89	Na-Tartrate	0.95	Na-Acetate	0.1	5	Am-Sulfate	0.17	NONE	0
90	MPD	47.24	NONE	0	0	NONE	0	NONE	0
91	PEG10k	12.48	CHES	0.1	9	Li-Sulfate	0.08	NONE	0
92	Na-Formate	2.02	MOPS	0.1	7	Ca-Acetate	0.06	NONE	0
93	Mg-Sulfate	1.5	NONE	0	0	Mg-Formate	0.08	NONE	0
94	PEGMME2k	39.05	Na-Citrate	0.1	5	Na-K-Phosphate	0.26	NONE	0
95	Ethanol	15.98	Tris-Chloride	0.1	8.5	Li-Sulfate	0.06	NONE	0
96	PEG8k	15.79	Na-Citrate	0.1	5.5	Li-Chloride	0.1	BME	2.32

Stochastic 20:

	Precipitant	%	Buffer	Conc (M)	Stock Conc (M)	Salt	Conc (M)	Additive	%
1	Na-Acetate	2.43	NONE	0	0	Zn-Acetate	0.11	LDAO	0.06
2	Isopropanol	14.69	Na-Acetate	0.1	5.5	Mg-Acetate	0.29	NONE	0
3	PEG3350	28.76	MES	0.1	6	Ca-Chloride	0.04	NONE	0
4	PEG4k	23.4	BICINE	0.1	9	Am-Acetate	0.15	MPD	0.99
5	PEGMME2k	22.78	MES	0.1	6	Li-Sulfate	0.13	NONE	0
6	Am-Sulfate	2.46	Na-Acetate	0.1	5	Na-K-Tartrate	0.07	NONE	0
7	Am-Phosphate	1.69	Na-Acetate	0.1	5.5	Am-Citrate	0.08	NONE	0
8	Am-Phosphate	2.34	CHES	0.1	9.5	Am-Phosphate	0.11	NONE	0
9	Na-Malate	2.29	BICINE	0.1	9	Na-Chloride	0.24	NONE	0
10	Na-Acetate	2.22	MES	0.1	6.5	Ca-Acetate	0.11	NONE	0
11	PEG3350	18.02	Na-Acetate	0.1	5	Zn-Chloride	0.05	NONE	0
12	Na-Chloride	2.73	MES	0.1	6	Ca-Chloride	0.13	NONE	0
13	Na-Citrate	0.65	Na-Citrate	0.1	5.5	Na-Bromide	0.06	NONE	0
14	PEG4k	15.79	BisTris	0.1	6	Mg-Sulfate	0.07	PEG400	2.02
15	Mg-Sulfate	1.13	Na-Acetate	0.1	5	Mg-Sulfate	0.2	CHAPS	0.05
16	PEG8k	24.81	BisTris	0.1	6.5	Mg-Formate	0.07	NONE	0
17	PEGMME550	27.85	BICINE	0.1	9.5	NONE	0	NONE	0
18	Na-Tartrate	1	Na-Citrate	0.1	5	Na-Citrate	0.04	NONE	0
19	Na-Malate	2.2	BICINE	0.1	8.5	NONE	0	NONE	0
20	PEG8k	23.16	NONE	0	0	Zn-Acetate	0.08	NONE	0
21	PEG6k	12.74	BICINE	0.1	8.5	Na-Acetate	0.05	NONE	0
22	Na-Acetate	2.28	NONE	0	0	Li-Chloride	0.16	NONE	0
23	PEG4k	27.96	CHES	0.1	9	NONE	0	NONE	0
24	PEGMME2k	36.65	Na-Citrate	0.1	5.5	Na-Citrate	0.03	NONE	0
25	PEG10k	18.27	CHES	0.1	9	Na-Citrate	0.07	NONE	0

26	Na-K-Phosphate	2.69	HEPES	0.1	7.5	NONE	0	CHAPS	0.05
27	PEGMME5k	25.6	BisTris	0.1	6	NONE	0	Butanediol	1.31
28	PEGMME2k	35.07	Na-Acetate	0.1	5	K-Chloride	0.17	DMSO	0.85
29	PEG6k	25.87	Na-Cacod	0.1	6.5	Li-Sulfate	0.08	NONE	0
30	PEGMME2k	22.61	Na-Acetate	0.1	4.5	Li-Sulfate	0.25	NONE	0
31	Na-Malonate	2.54	BICINE	0.1	9.5	Na-K-Tartrate	0.07	NONE	0
32	PEGMME5k	14.84	Na-Acetate	0.1	5.5	Li-Chloride	0.07	NONE	0
33	Na-Chloride	3.23	Tris-Chloride	0.1	7.5	Am-Citrate	0.14	NONE	0
34	PEGMME550	24.48	MOPS	0.1	7	Am-Phosphate	0.24	NONE	0
35	Mg-Sulfate	1.71	HEPES	0.1	8	K-Nitrate	0.18	NONE	0
36	Ethanol	19.37	BICINE	0.1	9.5	Mg-Chloride	0.29	NONE	0
37	PEGMME2k	34.16	Tris-Chloride	0.1	7.5	NONE	0	NONE	0
38	PEG3350	21.72	Na-Acetate	0.1	5	Zn-Acetate	0.11	NONE	0
39	Na-Formate	1.61	Na-Citrate	0.1	4.5	NONE	0	NONE	0
40	Am-Phosphate	2.69	BisTris	0.1	6	Am-Sulfate	0.08	NONE	0
41	PEGMME550	32	MOPS	0.1	7	Na-K-Phosphate	0.27	Glycerol	2.81
42	MPD	53.13	MOPS	0.1	7	NONE	0	Methanol	0.8
43	PEGMME5k	18.43	Na-Citrate	0.1	4.5	NONE	0	PEGMME350	2.41
44	Na-Malate	2.34	Na-Cacod	0.1	7	NONE	0	NONE	0
45	PEGMME5k	16.9	MOPS	0.1	6.5	Zn-Acetate	0.08	NONE	0
46	Na-Formate	2.07	MES	0.1	6	Na-Bromide	0.05	NONE	0
47	Na-Malate	2.06	CHES	0.1	9.5	NONE	0	NONE	0
48	PEG1.5k	32.29	CHES	0.1	9.5	Na-Bromide	0.08	Ethglycol	0.43

49	PEG8k	12.79	NONE	0	0	Ca-Acetate	0.1	NONE	0
50	PEG6k	18.59	BICINE	0.1	8.5	Am-Tartrate	0.04	NONE	0
51	PEG400	31.76	Tris-Chloride	0.1	8.5	NONE	0	NONE	0
52	PEGMME550	41	Tris-Chloride	0.1	8.5	Mg-Acetate	0.14	NONE	0
53	PEG4k	14.78	HEPES	0.1	8	Am-Citrate	0.04	LDAO	0.01
54	Am-Sulfate	2.2	BisTris	0.1	6.5	NONE	0	NONE	0
55	PEG3350	32.17	BisTris	0.1	6.5	Na-Chloride	0.09	BME	7.84
56	Isopropanol	11.97	Na-Acetate	0.1	5	NONE	0	NONE	0
57	Na-Citrate	0.72	HEPES	0.1	7.5	Mg-Formate	0.04	Ethglycol	2.91
58	Na-K-Phosphate	1.88	HEPES	0.1	7.5	Am-Phosphate	0.24	PEGDME250	3.99
59	Na-Tartrate	1.39	Na-Acetate	0.1	4.5	NONE	0	NONE	0
60	Isopropanol	16.29	NONE	0	0	NONE	0	NONE	0
61	PEG4k	14.16	Na-Cacod	0.1	6.5	Zn-Acetate	0.04	NONE	0
62	PEG4k	21.75	Na-Acetate	0.1	4.5	Li-Chloride	0.08	NONE	0
63	Na-Citrate	1.11	HEPES	0.1	7.5	Na-Citrate	0.07	NONE	0
64	Na-K-Phosphate	2.02	MOPS	0.1	7	Na-Bromide	0.22	NONE	0
65	Na-Formate	1.8	BisTris	0.1	6	Am-Tartrate	0.13	NONE	0
66	Mg-Sulfate	1.44	CHES	0.1	9	Mg-Acetate	0.2	NONE	0
67	PEG3350	20.46	BICINE	0.1	9.5	K-Thiocyanate	0.14	NONE	0
68	PEG6k	19.61	MES	0.1	6	Am-Acetate	0.11	NONE	0
69	Na-Citrate	0.99	NONE	0	0	Na-Acetate	0.11	NONE	0
70	PEG10k	11.28	NONE	0	0	NONE	0	NONE	0
71	Ethanol	5.25	Na-Cacod	0.1	6.5	Mg-Chloride	0.13	NONE	0
72	PEG1.5k	23.21	BICINE	0.1	9	Mg-Formate	0.05	BME	4.61

73	Na-K-Phosphate	2.67	Na-Citrate	0.1	5.5	K-Nitrate	0.06	NONE	0
74	PEGMME5k	14.69	Na-Cacod	0.1	7	Ca-Acetate	0.07	NONE	0
75	Na-Chloride	3.17	Tris-Chloride	0.1	8.5	Na-Chloride	0.09	NONE	0
76	PEGMME550	47.31	Na-Citrate	0.1	5.5	NONE	0	Hexanediol	3.65
77	Isopropanol	17.35	NONE	0	0	Na-K-Tartrate	0.1	NONE	0
78	PEG10k	9.3	BICINE	0.1	8.5	Li-Sulfate	0.26	NONE	0
79	PEGMME5k	25.06	Na-Cacod	0.1	7	Am-Tartrate	0.09	NONE	0
80	PEGMME550	35.97	Tris-Chloride	0.1	8	Mg-Acetate	0.18	NONE	0
81	PEG400	38.26	CHES	0.1	9	Na-Bromide	0.13	NONE	0
82	Na-Malonate	1.89	Na-Acetate	0.1	5.5	NONE	0	NONE	0
83	Na-Tartrate	0.9	BICINE	0.1	8.5	Na-K-Phosphate	0.05	NONE	0
84	Na-Chloride	2.83	Tris-Chloride	0.1	8.5	Zn-Acetate	0.1	NONE	0
85	Na-Citrate	0.9	Tris-Chloride	0.1	8.5	Mg-Chloride	0.27	NONE	0
86	PEG1.5k	31.41	BisTris	0.1	6	Ca-Chloride	0.06	NONE	0
87	Ethanol	9.25	HEPES	0.1	7.5	Am-Sulfate	0.13	BOG	0.03
88	PEG4k	20.77	Tris-Chloride	0.1	8	K-Chloride	0.14	NONE	0
89	Na-Malate	2.24	Na-Acetate	0.1	4.5	NONE	0	EDTA	4.35
90	PEG10k	18.97	HEPES	0.1	8	NONE	0	NONE	0
91	PEGMME2k	31.99	NONE	0	0	Zn-Chloride	0.06	Hexanediol	3.45
92	PEG1.5k	20.74	Na-Acetate	0.1	5.5	Na-Chloride	0.29	NONE	0
93	Na-Citrate	0.89	Na-Citrate	0.1	5	Am-Acetate	0.12	NONE	0
94	PEG400	29.8	CHES	0.1	9.5	NONE	0	NONE	0
95	PEG3350	20.37	HEPES	0.1	8	Na-Chloride	0.26	NONE	0
96	Na-Tartrate	1.05	Na-Cacod	0.1	7	Am-Citrate	0.13	DMSO	3.42

Stochastic 21:

	Precipitant	%	Buffer	Conc (M)	Stock Conc (M)	Salt	Conc (M)	Additive	%
1	PEG10k	13.14	MOPS	0.1	6.5	Li-Sulfate	0.26	NONE	0
2	PEG6k	23.19	BICINE	0.1	9	NONE	0	PEGDME250	2.05
3	PEG8k	16.52	Na-Cacodylate	0.1	6.5	NONE	0	NONE	0
4	Na-Tartrate	0.95	Na-Cacodylate	0.1	7	K-Chloride	0.13	NONE	0
5	Na-Malate	2.13	BICINE	0.1	8.5	Am-Acetate	0.1	NONE	0
6	PEG8k	27.31	MES	0.1	6.5	Na-Acetate	0.11	NONE	0
7	MPD	43.53	Na-Cacod	0.1	7	NONE	0	NONE	0
8	PEG4k	16.09	CHES	0.1	9	Na-Citrate	0.05	DMSO	2.51
9	PEG6k	20.17	Na-Citrate	0.1	5.5	Am-Tartrate	0.11	NONE	0
10	PEG3350	20.82	MOPS	0.1	7	NONE	0	CHAPS	0.13
11	Na-Tartrate	0.89	Na-Acetate	0.1	5	K-Nitrate	0.09	NONE	0
12	Am-Sulfate	2.47	BICINE	0.1	9.5	Mg-Chloride	0.21	NONE	0
13	PEGMME2k	24.77	MOPS	0.1	7	Am-Tartrate	0.07	NONE	0
14	PEG1.5k	33.49	BICINE	0.1	9	Mg-Chloride	0.1	NONE	0
15	PEG6k	24.19	Na-Citrate	0.1	5	NONE	0	NONE	0
16	PEGMME550	26	BisTris	0.1	6.5	NONE	0	NONE	0
17	PEGMME5k	24.16	MOPS	0.1	6.5	Zn-Sulfate	0.09	NONE	0
18	PEGMME550	26.05	Na-Cacod	0.1	6.5	Na-K-Tartrate	0.12	LDAO	0.18
19	Na-K-Phosphate	1.88	CHES	0.1	9.5	Am-Citrate	0.11	NONE	0
20	Na-Acetate	1.5	NONE	0	0	Mg-Sulfate	0.3	BOG	0.15
21	Na-Tartrate	1.18	NONE	0	0	NONE	0	NONE	0
22	PEG8k	23.75	CHES	0.1	9	Am-Phosphate	0.2	NONE	0
23	PEG10k	10.64	NONE	0	0	Mg-Acetate	0.05	NONE	0

24	Na-Chloride	3.24	BICINE	0.1	9.5	Na-Chloride	0.19	NONE	0
25	PEGMME550	26.05	MES	0.1	6	Zn-Sulfate	0.14	NONE	0
26	Na-K-Phosphate	2.18	NONE	0	0	K-Nitrate	0.19	EDTA	8.28
27	PEG400	30.62	Tris-Chloride	0.1	8	Am-Phosphate	0.27	PEGMME350	2.17
28	Na-Acetate	1.24	BICINE	0.1	9	Am-Citrate	0.14	NONE	0
29	Am-Sulfate	2.45	Tris-Chloride	0.1	8	Mg-Acetate	0.29	NONE	0
30	PEG8k	21.47	MES	0.1	6	NONE	0	Glycerol	1.74
31	PEG4k	16.01	CHES	0.1	9	Zn-Sulfate	0.03	PEGDME250	0.7
32	Isopropanol	10.06	Na-Acetate	0.1	5.5	NONE	0	NONE	0
33	PEG6k	26.93	NONE	0	0	NONE	0	NONE	0
34	Isopropanol	20.46	MES	0.1	6	Li-Sulfate	0.26	NONE	0
35	MPD	31.64	BisTris	0.1	6	NONE	0	NONE	0
36	Na-Acetate	1.48	BisTris	0.1	6	Ca-Acetate	0.08	NONE	0
37	Na-K-Phosphate	2.71	Tris-Chloride	0.1	8	NONE	0	BOG	0.18
38	PEGMME5k	27.47	Na-Cacod	0.1	7	Na-Bromide	0.21	LDAO	0.1
39	Isopropanol	12.88	BICINE	0.1	9	Ca-Chloride	0.09	NONE	0
40	PEG400	38.31	MOPS	0.1	7	Mg-Acetate	0.3	NONE	0
41	PEG8k	17.2	MOPS	0.1	6.5	Am-Sulfate	0.26	NONE	0
42	Na-Formate	2.36	Na-Citrate	0.1	5.5	Am-Sulfate	0.16	NONE	0
43	PEG4k	18.78	Tris-Chloride	0.1	7.5	Am-Citrate	0.08	NONE	0
44	Na-Formate	2.28	Na-Cacod	0.1	7	Na-Chloride	0.2	NONE	0
45	Am-Phosphate	1.73	Na-Citrate	0.1	5.5	K-Chloride	0.12	NONE	0
46	PEG4k	29.61	Na-Acetate	0.1	5.5	Mg-Sulfate	0.24	NONE	0
47	Ethanol	8.85	MES	0.1	6	Na-Acetate	0.03	NONE	0
48	Na-Acetate	1.72	Tris-Chloride	0.1	8.5	Na-Acetate	0.09	NONE	0

48	Na-Acetate	1.72	Tris-Chloride	0.1	8.5	Na-Acetate	0.09	NONE	0
49	Na-Formate	1.94	Na-Cacod	0.1	6.5	Na-K-Phosphate	0.22	NONE	0
50	Na-Formate	2.37	Na-Citrate	0.1	5	Am-Sulfate	0.08	NONE	0
51	PEG4k	26.75	Tris-Chloride	0.1	7.5	Na-Bromide	0.14	NONE	0
52	Mg-Sulfate	1.54	Tris-Chloride	0.1	8.5	Zn-Acetate	0.03	BOG	0.06
53	PEGMME550	33.55	BisTris	0.1	6	NONE	0	NONE	0
54	PEG1.5k	26.68	BICINE	0.1	8.5	Am-Tartrate	0.06	NONE	0
55	Na-Malate	1.94	MES	0.1	6	Am-Phosphate	0.14	NONE	0
56	PEG1.5k	30.47	MOPS	0.1	7	Am-Citrate	0.12	Butanediol	1.31
57	PEG1.5k	19.31	BICINE	0.1	9.5	Mg-Acetate	0.07	NONE	0
58	Am-Sulfate	2.31	MES	0.1	6	NONE	0	NONE	0
59	PEGMME5k	20.78	Na-Acetate	0.1	5	Mg-Acetate	0.25	NONE	0
60	PEG3350	28.52	Na-Citrate	0.1	5	Na-Sulfate	0.09	NONE	0
61	PEG8k	15.5	NONE	0	0	Mg-Sulfate	0.23	LDAO	0.03
62	Na-Acetate	2.73	BICINE	0.1	9	Mg-Sulfate	0.26	NONE	0
63	Isopropanol	12.55	Na-Acetate	0.1	5	NONE	0	CHAPS	0.07
64	PEG400	36.95	HEPES	0.1	7.5	Ca-Chloride	0.04	NONE	0
65	Na-Malonate	1.77	CHES	0.1	9	NONE	0	NONE	0
66	Na-Chloride	2.59	Tris-Chloride	0.1	8	Am-Citrate	0.03	NONE	0
67	PEG10k	19.9	Tris-Chloride	0.1	8	Li-Chloride	0.17	NONE	0
68	Isopropanol	5.83	MOPS	0.1	7	NONE	0	NONE	0
69	Am-Sulfate	1.43	Na-Acetate	0.1	5.5	K-Nitrate	0.13	Glycerol	3.58
70	Am-Sulfate	1.41	BisTris	0.1	6	Am-Acetate	0.13	BOG	0.02
71	Isopropanol	11.62	Na-Citrate	0.1	5.5	NONE	0	PEGDME250	2.84
72	Na-Citrate	1.11	CHES	0.1	9	Na-Citrate	0.05	NONE	0

73	MPD	30.77	MES	0.1	6	Na-Acetate	0.03	DMSO	1.98
74	Na-Acetate	1.85	CHES	0.1	9.5	Am-Sulfate	0.09	NONE	0
75	Na-Citrate	1.09	MES	0.1	6	Am-Tartrate	0.09	NONE	0
76	Isopropanol	13.48	MOPS	0.1	7	Mg-Acetate	0.25	NONE	0
77	PEG1.5k	28.8	CHES	0.1	9.5	Na-Bromide	0.29	BOG	0.1
78	Na-Citrate	1.1	Tris-Chloride	0.1	8	Na-Citrate	0.05	CHAPS	0.14
79	Isopropanol	18.7	MOPS	0.1	7	NONE	0	NONE	0
80	PEGMME5k	15.65	CHES	0.1	9.5	Na-Acetate	0.09	NONE	0
81	Na-Acetate	2.29	BICINE	0.1	9	Ca-Acetate	0.06	NONE	0
82	PEG8k	22.45	HEPES	0.1	8	NONE	0	NONE	0
83	PEG6k	23.04	Na-Acetate	0.1	5	K-Nitrate	0.09	BME	2.32
84	PEG8k	16.23	Na-Acetate	0.1	5.5	Mg-Sulfate	0.12	NONE	0
85	Na-Tartrate	1.07	Tris-Chloride	0.1	8.5	Na-Chloride	0.05	NONE	0
86	PEG400	55.52	HEPES	0.1	7.5	Mg-Chloride	0.25	NONE	0
87	Isopropanol	8.66	HEPES	0.1	8	NONE	0	NONE	0
88	Na-Acetate	2.46	CHES	0.1	9.5	Am-Acetate	0.09	NONE	0
89	PEGMME2k	20.49	MOPS	0.1	7	Am-Acetate	0.13	NONE	0
90	Mg-Sulfate	1.12	NONE	0	0	NONE	0	Ethglycol	0.56
91	Na-K-Phosphate	2.5	Na-Citrate	0.1	5.5	K-Chloride	0.23	NONE	0
92	PEGMME550	36.99	Na-Acetate	0.1	4.5	Na-Chloride	0.29	NONE	0
93	PEG4k	30.96	Na-Acetate	0.1	4.5	Li-Sulfate	0.11	NONE	0
94	MPD	41.39	NONE	0	0	Ca-Chloride	0.08	NONE	0
95	PEG1.5k	40.21	BICINE	0.1	8.5	Na-K-Tartrate	0.07	NONE	0
96	Isopropanol	14.3	Na-Citrate	0.1	5.5	K-Nitrate	0.13	PEGDME250	0.49

Stochastic 22:

	Precipitant	%	Buffer	Conc (M)	Stock Conc (M)	Salt	Conc (M)	Additive	%
1	Na-Malate	2.07	HEPES	0.1	7.5	NONE	0	NONE	0
2	PEG6k	18.41	MOPS	0.1	6.5	Ca-Acetate	0.08	PEG400	3.19
3	Na-Malonate	1.61	Tris-Chloride	0.1	8	Am-Citrate	0.06	NONE	0
4	MPD	41.63	Tris-Chloride	0.1	7.5	Na-Acetate	0.04	NONE	0
5	PEG1.5k	26.8	Na-Cacod	0.1	7	Zn-Chloride	0.06	LDAO	0.14
6	Na-Malate	1.52	BisTris	0.1	6.5	Na-K-Phosphate	0.29	BOG	0.07
7	Mg-Sulfate	1.56	Tris-Chloride	0.1	8.5	Na-Sulfate	0.12	NONE	0
8	PEG6k	21.94	Tris-Chloride	0.1	8	Na-Chloride	0.06	NONE	0
9	PEG4k	29.83	BICINE	0.1	8.5	Na-Citrate	0.05	NONE	0
10	Ethanol	14.96	MES	0.1	6	Mg-Formate	0.12	NONE	0
11	PEG4k	21.37	BICINE	0.1	8.5	K-Chloride	0.09	NONE	0
12	Na-Citrate	0.86	BICINE	0.1	9	NONE	0	NONE	0
13	PEG400	54.34	Na-Cacod	0.1	7	Li-Sulfate	0.09	NONE	0
14	Isopropanol	10.38	NONE	0	0	Na-Bromide	0.23	NONE	0
15	Na-Malate	1.64	NONE	0	0	NONE	0	NONE	0
16	Na-Acetate	2.59	BisTris	0.1	6	NONE	0	PEGMME350	1.62
17	PEGMME2k	39.74	CHES	0.1	9	Ca-Chloride	0.09	NONE	0
18	Isopropanol	13.86	Na-Acetate	0.1	5.5	K-Chloride	0.13	NONE	0
19	PEG3350	17.06	Na-Acetate	0.1	5.5	K-Chloride	0.23	NONE	0
20	Mg-Sulfate	1.58	HEPES	0.1	8	Mg-Chloride	0.08	NONE	0
21	PEGMME2k	25.33	Tris-Chloride	0.1	8.5	Na-Chloride	0.23	EDTA	7.24
22	Na-Formate	2.54	NONE	0	0	Na-Citrate	0.05	NONE	0
23	PEGMME550	33.78	MOPS	0.1	6.5	Mg-Sulfate	0.19	NONE	0

| 24 | PEG400 | 31.99 | BICINE | 0.1 | 9.5 | Na-Sulfate | 0.28 | DMSO | 1.28 |

25	Na-Acetate	1.83	MOPS	0.1	7	Ca-Acetate	0.07	NONE	0
26	Na-Malonate	2.67	MES	0.1	6.5	Na-K-Tartrate	0.1	NONE	0
27	PEGMME5k	18.95	Na-Cacod	0.1	6.5	Na-Bromide	0.27	NONE	0
28	Na-Citrate	0.95	HEPES	0.1	8	Na-Bromide	0.18	NONE	0
29	PEG8k	20.8	BICINE	0.1	9	Am-Acetate	0.08	NONE	0
30	PEG3350	20.82	Na-Cacod	0.1	7	Na-Acetate	0.1	NONE	0
31	Na-Formate	2.79	NONE	0	0	NONE	0	NONE	0
32	MPD	36.59	BisTris	0.1	6	Am-Sulfate	0.26	Ethglycol	1.74
33	PEG400	34.58	Tris-Chloride	0.1	8	Na-K-Tartrate	0.13	NONE	0
34	Na-Formate	2.7	Tris-Chloride	0.1	7.5	Am-Sulfate	0.28	Dioxane	2.65
35	Isopropanol	8.67	Na-Cacod	0.1	7	NONE	0	Hexanediol	2.92
36	Na-Acetate	1.8	MOPS	0.1	6.5	Li-Sulfate	0.07	NONE	0
37	Na-Malonate	2.31	Na-Acetate	0.1	5.5	NONE	0	BME	7.83
38	PEG4k	23.59	CHES	0.1	9	NONE	0	NONE	0
39	PEG3350	30.06	Na-Cacod	0.1	7	NONE	0	NONE	0
40	PEGMME550	37.95	Na-Citrate	0.1	5	Na-Citrate	0.1	PEG400	2.3
41	PEG4k	26.55	Na-Citrate	0.1	5	Am-Sulfate	0.09	BOG	0.08
42	PEG10k	17.9	CHES	0.1	9.5	Na-K-Tartrate	0.07	PEGDME250	3.18
43	PEG10k	18.25	Na-Acetate	0.1	5	Na-Bromide	0.21	LDAO	0.2
44	PEGMME550	30.86	Na-Cacod	0.1	7	Am-Sulfate	0.25	NONE	0
45	Na-Malate	2.25	Na-Acetate	0.1	4.5	K-Nitrate	0.08	NONE	0
46	PEGMME2k	30.4	NONE	0	0	Am-Phosphate	0.13	NONE	0
47	PEG1.5k	19.94	Tris-Chloride	0.1	8	Na-K-Phosphate	0.06	NONE	0
48	Mg-Sulfate	1.01	CHES	0.1	9	Na-Bromide	0.1	NONE	0

49	MPD	52.88	BisTris	0.1	6	Na-Acetate	0.11	NONE	0
50	Ethanol	12.03	BisTris	0.1	6	Na-Chloride	0.13	CHAPS	0.12
51	Na-Citrate	0.61	Na-Citrate	0.1	4.5	Na-K-Phosphate	0.14	PEGMME350	2.37
52	Am-Phosphate	1.92	MES	0.1	6.5	Am-Acetate	0.04	NONE	0
53	PEG10k	18.76	Tris-Chloride	0.1	8.5	Na-K-Phosphate	0.06	BOG	0.03
54	PEGMME5k	22.06	MES	0.1	6	Am-Phosphate	0.28	NONE	0
55	PEG6k	15.14	NONE	0	0	NONE	0	NONE	0
56	Na-K-Phosphate	2.5	BisTris	0.1	6	NONE	0	NONE	0
57	PEGMME550	27.32	BICINE	0.1	9	Na-K-Tartrate	0.14	NONE	0
58	PEG400	29.87	Tris-Chloride	0.1	8.5	Zn-Acetate	0.08	NONE	0
59	Na-K-Phosphate	2.61	NONE	0	0	NONE	0	NONE	0
60	PEGMME2k	23.29	Na-Citrate	0.1	4.5	K-Nitrate	0.17	NONE	0
61	Na-K-Phosphate	2.19	Na-Citrate	0.1	5	NONE	0	NONE	0
62	PEG1.5k	18.45	BisTris	0.1	6	Li-Chloride	0.23	NONE	0
63	PEG1.5k	31.89	Tris-Chloride	0.1	8.5	NONE	0	Hexanediol	1.89
64	PEG4k	17.92	Na-Cacod	0.1	7	Li-Chloride	0.23	Butanediol	3.63
65	Na-Acetate	1.88	Na-Citrate	0.1	5	NONE	0	NONE	0
66	PEG1.5k	30.85	MOPS	0.1	6.5	Am-Phosphate	0.15	PEGDME250	2.03
67	PEG3350	17.71	NONE	0	0	Na-Chloride	0.15	NONE	0
68	Na-Chloride	2.16	NONE	0	0	Mg-Chloride	0.18	NONE	0
69	PEG10k	20.22	BICINE	0.1	8.5	NONE	0	Butanediol	2.84
70	Isopropanol	6.34	BisTris	0.1	6	Na-Bromide	0.21	NONE	0
71	Am-Sulfate	1.44	NONE	0	0	Am-Citrate	0.05	NONE	0
72	Am-Sulfate	2.32	CHES	0.1	9.5	NONE	0	BME	5.97

73	PEG10k	9.74	Na-Acetate	0.1	5.5	Am-Tartrate	0.15	Hexanediol	1.74
74	Na-Citrate	0.77	Na-Citrate	0.1	5.5	Na-Citrate	0.11	Glycerol	1.4
75	Na-Formate	1.86	Na-Acetate	0.1	5.5	Na-K-Phosphate	0.21	NONE	0
76	Na-Acetate	1.31	BICINE	0.1	8.5	NONE	0	NONE	0
77	PEG10k	20.42	NONE	0	0	Na-Chloride	0.06	NONE	0
78	Isopropanol	16.37	Na-Citrate	0.1	5	Am-Phosphate	0.14	NONE	0
79	PEG8k	13.49	Na-Acetate	0.1	5.5	Li-Sulfate	0.14	NONE	0
80	Isopropanol	10.27	Na-Acetate	0.1	5.5	Mg-Formate	0.07	NONE	0
81	Na-Formate	2.32	CHES	0.1	9.5	NONE	0	NONE	0
82	PEG4k	14.01	Tris-Chloride	0.1	7.5	Na-Sulfate	0.16	NONE	0
83	Am-Phosphate	1.87	Na-Acetate	0.1	4.5	Am-Citrate	0.11	NONE	0
84	PEG400	55.67	Na-Acetate	0.1	5	Am-Acetate	0.03	NONE	0
85	Isopropanol	9.44	Na-Citrate	0.1	5	Mg-Chloride	0.12	NONE	0
86	Na-Tartrate	1.05	BisTris	0.1	6	NONE	0	NONE	0
87	Na-Malonate	2.41	BICINE	0.1	8.5	Na-K-Tartrate	0.1	NONE	0
88	PEG6k	25	BICINE	0.1	8.5	Na-Chloride	0.09	NONE	0
89	PEGMME2k	24.15	Na-Acetate	0.1	5.5	NONE	0	NONE	0
90	Na-Acetate	2.54	BICINE	0.1	8.5	NONE	0	NONE	0
91	PEGMME2k	29.45	Na-Acetate	0.1	4.5	Am-Phosphate	0.22	CHAPS	0.16
92	PEG400	53.79	Na-Citrate	0.1	4.5	Li-Chloride	0.15	NONE	0
93	Isopropanol	9.81	Na-Citrate	0.1	5.5	NONE	0	NONE	0
94	Na-Formate	2.32	HEPES	0.1	7.5	Ca-Chloride	0.03	NONE	0
95	PEG4k	15.8	NONE	0	0	Zn-Chloride	0.07	NONE	0
96	Mg-Sulfate	1.09	MOPS	0.1	7	Li-Sulfate	0.23	NONE	0

JCSG and JMAC:

These screens were purchased from Molecular Dimensions and were used as detailed in the manufactures guidelines.

ABAD Opt 1 Screen:

This screen was set up based on Stochastic screen 19, using Sodium Citrate (unbuffered) as the precipitant, with varying buffers of sodium citrate pH 4.5/ 5/ 5.5, and Sodium Acetate pH 4.6/ 5. The salts used in this screen were: Magnesium Acetate, Magnesium Formate and Magnesium Chloride. No additives were added to this screen.

ABAD Opt 2 Screen:

This screen was optimized from StoPEGS 3, and so is set up partially under the same conditions with slight modifications to the use of additive BOG (2%). The main condition used to generate this screen was 24.01% PEG 8000, 0.1 M Bicine (pH 8.5), 0.26 M Sodium Potassium Phosphate.

ABAD Opt 3 Screen:

This screen was set up to optimize conitions taken from Stochastic screen 22. The main conditions used were Buffer: BisTris (1M, pH 6/7), PEGMME 2000/5000 was the altered precipitant and salts used were Lithium Sulphate, Magnesium Sulphate and Magnesium Acetate

No additives were added to this screen.

Appendix D: Publications

REVIEW ARTICLE
The consequences of mitochondrial amyloid β-peptide in Alzheimer's disease

Kirsty E. A. MUIRHEAD*[1,2], Eva BORGER*[2], Laura AITKEN*, Stuart J. CONWAY† and Frank J. GUNN-MOORE*[1]

*School of Biology, Bute Medical Building, University of St Andrews, Westburn Lane, St Andrews, Fife KY16 9TS, U.K., and †Department of Chemistry, Chemistry Research Laboratory, University of Oxford, Mansfield Road, Oxford OX1 3TA, U.K.

The Aβ (amyloid-β peptide) has long been associated with Alzheimer's disease, originally in the form of extracellular plaques. However, in the present paper we review the growing evidence for the role of soluble intracellular Aβ in the disease progression, with particular reference to Aβ found within the mitochondria. Once inside the cell, Aβ is able to interact with a number of targets, including the mitochondrial proteins ABAD (amyloid-binding alcohol dehydrogenase) and CypD (cyclophilin D), which is a component of the mitochondrial permeability transition pore. Interference with the normal functions of these proteins results in disruption of cell homoeostasis and ultimately cell death. The present review explores the possible mechanisms by which cell death occurs, considering the evidence presented on a molecular, cellular and *in vivo* level.

Key words: Alzheimer's disease, amyloid-binding alcohol dehydrogenase (ABAD), cyclophilin D (CypD), intracellular amyloid-β peptide (Aβ), mitochondrial dysfunction, mitochondrial permeability transition pore.

INTRODUCTION

AD (Alzheimer's disease) is the most common neurodegenerative disease of the elderly. AD is clinically characterized by progressive loss of declarative memory, which in turn impairs functions such as memory, language, perceptual skills, attention, orientation and problem-solving abilities. The loss of these brain functions eventually results in the patient's complete social dependence and inevitable death. The main feature of the disease progression is extensive death of neurons, starting in the entorhinal cortex and hippocampus, before proceeding to other parts of the brain cortex and subcortical grey matter. It is in these brain regions where extracellular amyloid plaques, mainly consisting of Aβ (amyloid-β peptide), and intracellular neurofibrillary tangles, caused by aggregation of the hyper-phosphorylated microtubule-associated protein tau, are found [1]. Since the first description of the disease by Alois Alzheimer in the early 20th century, much work has been done to identify the molecular basis of the disease [2,3]. It is now clear that AD can either occur sporadically or be an inherited disease caused by mutations in genes encoding proteins involved in Aβ turnover. Sporadic AD occurs later in life, generally after the age of 65, whereas familial AD tends to have an earlier age of onset.

Aβ is produced from the transmembrane APP (amyloid precursor protein) by the sequential actions of the aspartate proteases β- and γ-secretase [4]. β-Secretase sheds the N-terminal domain of APP, leaving a 99-residue fragment in the membrane. This fragment is further cleaved by γ-secretase at one of several sites within the transmembrane region to produce the Aβ peptide and the AICD (APP intracellular domain), which is released into the cytosol. The exact location of the γ-secretase cleavage determines the final size of the Aβ peptide, which is most commonly either 40 or 42 residues long, producing Aβ-(1–40) or Aβ-(1–42), respectively. An alternative non-amyloidogenic cleavage pathway exists in which α-secretase cleaves inside the Aβ region of APP thus preventing production of the Aβ peptide [4]. The mutations observed in familial (hereditary) AD generally occur in one of the components of the amyloidogenic pathway (i.e. APP, β-secretase or γ-secretase) and lead to the increased production of Aβ, especially the more aggregation prone Aβ-(1–42) [5,6]. In contrast, tau-pathology results in the formation of intracellular neurofibrillary tangles and is considered by some to be a process associated with the later stages of AD caused directly or indirectly by the amyloid pathology [7,8].

A number of risk factors for the development of sporadic late-onset AD have been identified. These include carrying the ε4 allele of the *ApoE* (apolipoprotein E) gene [9] (recently reviewed in [10]), mutations in the gene encoding the membrane sorting receptor sortilin-1 [11,12] and increased levels of the non-proteinogenic amino acid homocysteine [13,14]. It has been
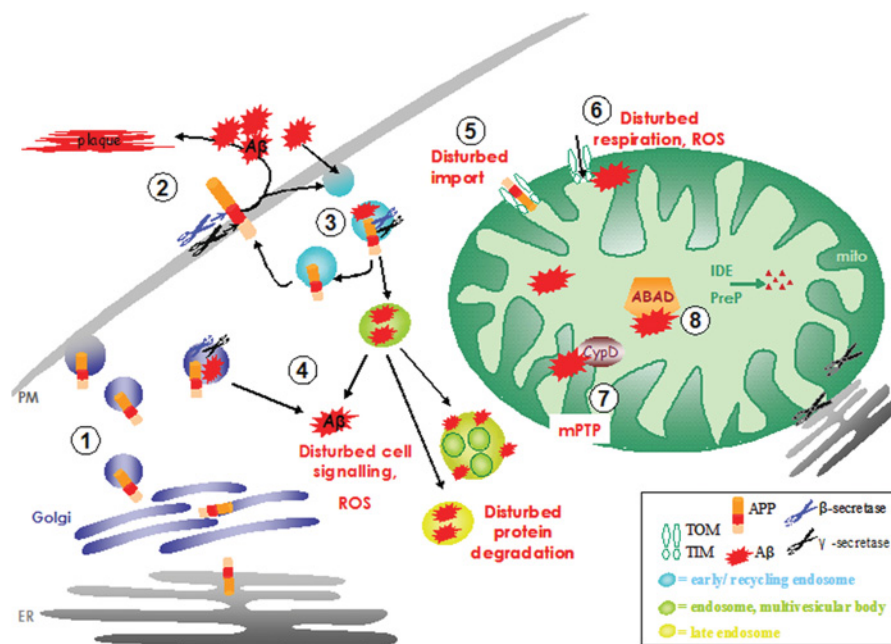
Figure 1   APP and Aβ inside the cell

During protein synthesis, the APP is targeted to the ER and transported to the plasma membrane (PM) by vesicular transport through the Golgi apparatus (1). Amyloidogenic processing of APP by the β- and γ-secretases at the plasma membrane produces the Aβ peptide. This cleavage has also been found to take place prior to exocytosis in the *trans*-Golgi network. Aβ can aggregate extracellularly forming extracellular plaques, which are one of the hallmarks of AD (2). APP undergoes endocytosis and is normally recycled to the plasma membrane via recycling endosomes. Aβ peptides can also enter the cell by endocytosis, but can also be produced from APP by β- and γ-secretase cleavage in endosomes. Accumulation of Aβ in endosomes, multivesicular bodies and lysosomes disturbs the protein degradation machinery (3). Aβ can also compromise the integrity of endosomes and lysosomes and can be found in the cytosol, probably due to leakage out of these compartments, disturbing cell signalling and causing oxidative stress by interaction with cytosolic proteins (4). Owing to its chimaeric targeting sequence, APP can also be transported to mitochondria (mito) where it interacts with TOM and TIM (translocase of the inner membrane) proteins, disturbing mitochondrial protein import (5). Aβ can be imported into the mitochondria via the mitochondrial import machinery, where it has been found associated with the inner mitochondrial membrane, disrupting processes of mitochondrial respiration and causing ROS (6). At the inner mitochondrial membrane, Aβ can interact with CypD, which is involved in the formation of the mPTP (7). In the mitochondrial matrix, Aβ has been found to interact with the ABAD inhibiting its actions. Mitochondrial peptidases have been found to be able to degrade Aβ in the mitochondrial matrix and possibly the intermembrane space (8).

suggested that these factors are indirectly associated with an increased production of Aβ in neuronal cells. Very recently two new genes, *CLU* [clusterin, also known as ApoJ (apolipoprotein J)] and *PICALM* (phosphatidylinositol-binding clathrin assembly lymphoid-myeloid leukaemia gene), have been linked to AD [15]. However, the detailed mechanisms and intracellular processes resulting in the development of sporadic AD remain unclear.

There have been many excellent reviews of Aβ production and the different forms and structures of this unusual peptide [4,16–18]. Most of these reports have predominately been concerned with extracellular production and accumulation of Aβ and with how understanding this process is important in the prevention of plaque formation as a potential therapy. In the present paper we will discuss recent findings and implications of the accumulation of Aβ inside cells. Recently it has been realized that the presence of extracellular amyloid plaques is not a good indicator of disease state and that increased levels of intracellular Aβ, predominantly Aβ-(1–42), more accurately reflects the stage of neurodegeneration [6,19]. As a result of this finding, a hypothesis describing a 'mitochondrial spiral' of neurodegeneration in AD has been proposed [20] and subsequently much experimental work has substantiated the idea that mitochondria play a crucial part in the disease progression [21,22]. The importance of this new approach has been highlighted by the limited success of vaccination trials against Aβ [23]. Although they have been shown to clear extracellular Aβ, by their nature these approaches do not clear the intracellular Aβ.

The present article summarizes the current understanding of the intracellular location of Aβ and reviews the evidence for its existence in mitochondria. We discuss how intracellular Aβ might exert its neurotoxic function, with a focus on its known intracellular binding partners. In particular, we will present recent evidence for the interaction of Aβ with two mitochondrial proteins, ABAD (amyloid-binding alcohol dehydrogenase) and CypD (cyclophilin D), both of which have been implicated in AD. The structure and function of ABAD and the consequences of its interaction with Aβ are discussed. Finally, we address how characterizing the interaction of Aβ with ABAD and CypD has highlighted potential therapeutic targets for the treatment of AD.

SOURCE OF INTRACELLULAR Aβ

The presence of APP and Aβ peptides within neuronal and non-neuronal cells has been reported by numerous researchers (reviewed in [19], see Figure 1). Aβ immunoreactivity has been located to the secretory pathways and cytosol of both neuronal and non-neuronal cells [24,25], the outer membrane of multivesicular bodies of cultured neurons [26,27], endosomes and lysosomes [28,29] and the mitochondria of neuronal cell cultures and in both the murine and human brain [30,31]. In all cases, the most studied sites of Aβ production are within membranes, such as in the plasma membrane [2,32], the secretory pathway [33] and in the endosomal compartment [34,35], where APP and all components of the cleavage machinery have been found. However, due to the orientation of APP and the secretases, it has been more difficult to explain the presence of Aβ peptides in the cytosol. Aβ can integrate into lipid membranes at high

concentrations [36], possibly leading to the observed loss of the integrity of endosomes and lysosomes in the cell; subsequently Aβ can then leak out of these compartments [24]. This possibility is substantiated by the known membrane-disordering capabilities of Aβ [37,38]. However, the mechanism that regulates the traffic of Aβ in and through membranes, as well as its subsequent significance for AD, still remains obscure.

SPECIES OF INTRACELLULAR Aβ

Studies on human brains revealed that the majority of intracellular Aβ comprises the 42-residue peptide Aβ-(1–42) [39,40]. Immunohistochemical studies have shown that the levels of intracellular immunoreactivity against Aβ-(1–42) are reduced in more advanced stages of AD when plaque burden and cognitive dysfunction become more prominent, pointing towards a role for Aβ-(1–42) in the early stages of the disease [39]. Accordingly, comparison of the effects of Aβ-(1–42) and Aβ-(1–40) in several studies has revealed that the activation of intracellular signalling events and ROS (reactive oxygen species) production is more pronounced with Aβ-(1–42) or when APP^m (mutant APP), which produces higher levels of Aβ-(1–42), is expressed [41,42].

It appears that the detectable form of intracellular Aβ reflects the state of neuropathology. In post-mortem human AD brains, intracellular Aβ has mainly been described as aggregates in the cell soma and perinuclear region, which do not stain with Congo Red or other β-sheet-selective stains [39]. Zhang et al. [41] have tested the toxicity of Aβ-(1–42) in different aggregation states when microinjected into the cytosol. They found that the non-fibrillized (monomers, dimers and oligomers) and fibrillized Aβ-(1–42) are both toxic to neurons, whereas Aβ-(1–40) fibrils or non-fibrillized peptides do not cause neuronal cell death. Again, this result suggests that Aβ monomers and oligomers can be neurotoxic before intracellular fibrils are formed.

Park et al. [43] have shown that there is accumulation of GFP (green fluorescent protein)-tagged Aβ and the APP-C99 fragment in undefined perinuclear aggregates in both H4 neuroglioma cells and HEK (human embryonic kidney)-293 cells. They correlated the formation of these aggregates with the recruitment and attenuation of the proteosome and with apoptotic cell death. These findings agree with the results of a study by Bückig et al. [25], who observed perinuclear accumulation of Aβ which co-localized with ubiquitin in CHO (Chinese-hamster ovary) K1 cells. Yoon et al. [44] not only detected GFP-tagged Aβ in perinuclear aggregates following transfection into H4 neuroglioma cells, but also found SOD1 (superoxide dismutase 1) associated with the aggregates, which they reported to interact selectively with Aβ. Taken together, these results suggest a defined pathological role for monomers or low-number oligomers of Aβ inside the cell, whereas the observed perinuclear Aβ aggregates might be indicative of later stages of neurotoxicity.

MITOCHONDRIAL Aβ

Mitochondrial Aβ was first described in detail by Lustbader et al. in 2004 [45]. The study also confirmed the interaction of Aβ with ABAD and showed, by immunoelectron microscopy, that the proteins co-localize inside mitochondria from the human AD brain. Subsequently, Caspersen et al. [46] also confirmed that Aβ accumulates in the mitochondria of APP^m-expressing transgenic mice and in brains from AD patients, but to a lesser extent in non-transgenic mice and brains from non-demented subjects. Using immunoelectron microscopy and Western blot analysis, they detected Aβ-(1–42) and Aβ-(1–40) in AD-affected brain mitochondria co-localizing with the mitochondrial matrix

chaperone Hsp60 (heat shock protein 60), although Aβ-(1–42) appeared to be the more abundant form [46]. Although it was shown that Aβ peptides were in close proximity to Hsp60 by immunoelectron microscopy, the protease-protection assay on whole mitochondria used in the study did not discriminate between the matrix compartment and the intermembrane space or the inner mitochondrial membrane [46]. Hence, the possibility of an association with the inner mitochondrial membrane, which has been found by other researchers using digitonin-treated mitochondrial preparations [47] or mitoplasts produced by osmotic shock [48], could not be ruled out. However, an inner mitochondrial membrane location seems to be incompatible with the interaction of Aβ with ABAD, which is located in the mitochondrial matrix [45]. Thus it is currently unclear whether Aβ accumulates inside the mitochondrial matrix in the AD-affected brain or whether it is found exclusively in the membrane compartment.

A possible reason why Aβ has not been detected in the mitochondrial matrix might be its rapid degradation by mitochondrial proteases, such as PreP (prolyl endopeptidase). PreP is a thiol-sensitive metalloprotease that resides in the mitochondrial matrix fraction and is able to rapidly degrade different forms of Aβ [49]. Its sensitivity to oxidative inactivation has been demonstrated *in vitro* [49], but so far deregulation or dysfunction of PreP in AD have not been reported.

Another Aβ-degrading enzyme, IDE (insulin-degrading enzyme), has been genetically linked to AD since 1998 [50,51]. Like PreP, IDE is an intra- and extracellular metalloprotease belonging to the pitrilysin family of peptidases [49]. Inside cells, IDE is located in the cytosol and the mitochondria, where it degrades mitochondrial-targeting sequences cleaved by the mitochondrial processing peptidase [52]. The relevance of IDE for AD was confirmed by the finding that IDE and Aβ can interact *in vitro* to form complexes that are stable to denaturing conditions, in both rat and human AD-affected brains [53]. Moreover, nitrosative stress was recently reported to compromise its enzyme activity in a non-competitive manner by S-nitrosylation of essential cysteine residues [54]. This post-translational modification has emerged as an important factor in neurodegenerative processes [55,56]. It is probable that IDE is able to degrade Aβ inside mitochondria and that it is affected by oxidative and nitrosative stress brought about by higher levels of Aβ during AD pathology. The possible compensatory increase of IDE protein levels in AD-affected brain regions seen in a transgenic mouse model [50] supports these ideas. The up-regulation of this protein, which was only observed after the occurrence of plaque pathology in an AD mouse model, and an up-regulation of the peptidase neprilysin [50], suggests that its contribution to very early events in disease pathogenesis is not significant. Nevertheless, mis-sorting or malfunction of IDE have to be taken into account as potential risk factors for the progression of AD [57,58] or other neurodegenerative diseases. Further investigation into the control of sorting and function of intracellular IDE will shed light on this aspect of AD and elucidate at which stage IDE is involved in the disease progression. In summary, it is possible that Aβ in the mitochondrial matrix has not been detected due to its rapid degradation.

HOW IS Aβ TRANSPORTED/PRODUCED INSIDE MITOCHONDRIA?

The origin of mitochondrial Aβ is still a matter of debate. There is experimental evidence for both the local production and/or the import of Aβ from the cytosol as possible explanations for its occurrence.

Localized Aβ synthesis

APP is targeted to mitochondria in cell-culture systems and in human brain due to its chimaeric N-terminal targeting sequence which causes the peptide to translocate to the ER (endoplasmic reticulum) and mitochondria [30,47]. In earlier studies, Anandatheerthavarada et al. [59] demonstrated that sorting of other proteins with chimaeric targeting sequences, to either the ER or mitochondria, can be regulated by phosphorylation, but no such phosphorylation has been described for the N-terminus of APP. Co-staining, immunoblotting and immunoprecipitation experiments only detected APP in a transmembrane-arrested form, in contact with the mitochondrial translocases of the outer and inner membrane [30]; APP was found in an N-in C-out orientation spanning the mitochondrial intermembrane space with a C-terminal 73 kDa fragment facing the cytosol, and the transport arrest was associated with mitochondrial dysfunction [47]. The authors therefore proposed that the acidic domain, spanning amino acids 220–290 of APP-695, would hinder transfer [30]. A correlation between the amount of membrane-arrested APP and the presence of the ApoE ε4 allele in AD patients has been observed [47].

The components of the γ-secretase complex [nicastrin, presenilin, APH-1 (anterior pharynx-defective homologue 1) and PEN-2 (presenilin-enhancer 2 homologue)] have been detected in mitochondria [60]. Dual targeting of nicastrin was proposed, based on its amino acid sequence, and its targeting to mitochondria was demonstrated by immunoelectron microscopy. The other components of the γ-secretase complex were also shown to be present in mitochondria by electron microscopy [60]. In summary, the components necessary for the production of Aβ in mitochondria, except the β-secretase, have been detected locally. However, it has also been reported that the topology of APP detected in mitochondria, with the Aβ region located in the intermembrane space [30], would not be suitable for cleavage by the γ-secretase complex, which is an intramembrane cleaving protease [32,61].

Interestingly, another enzyme, HtrA2 (HtrA serine peptidase 2), has been found to act on APP in the mitochondrial intermembrane space and sheds the N-terminal portion of the protein. HtrA2 is a serine protease which was known to interact with Aβ and APP-C100 fragments in cell cultures [62]. This protease is able to cleave APP at amino acid 534 and produces a 161-residue long C-terminal fragment, which includes the Aβ region of APP, which is released into the cytosol of APP-transfected cells [63]. The significance of this cleavage for APP metabolism and Aβ processing is not yet clear; it might represent a mechanism to clear membrane-arrested APP from the mitochondria, as indicated by the authors [63]. However, despite this C-terminal domain cleavage, the N-terminal part of APP, with the acidic domain, would still be arrested in the inner mitochondrial membrane, disturbing mitochondrial protein transport and metabolism [30]. The role of the two fragments and their impact on mitochondrial and cellular metabolism still remains to be elucidated.

Given the topological problems of Aβ production in the mitochondrial membrane, one possible mechanism by which it could accumulate is via cleavage in MAMs (mitochondria-associated membranes). These membrane compartments represent close contact points between the ER and mitochondria [64], where lipids and membrane proteins are thought to be exchanged directly between the organelles [65]. Presenilin 1 and 2 have been detected in this compartment [66], so it is possible that APP can be cleaved while residing in the ER membrane and that Aβ would subsequently be transported into mitochondria [48]. Another possibility is the transfer of APP or β-site-cleaved APP from the ER to the mitochondrial outer membrane, alongside lipids that are also transferred through MAMs [65]. The APP could subsequently be cleaved by the γ-secretase in the mitochondrial membrane [60,66], releasing Aβ on the mitochondrial side. The mitochondrial proteins DLP1 (dynamin-like protein, also known as Drp1) and Mfn1/2 (mitofusin 1/2) are known to be involved in mitochondrial fission and fusion [67]. These proteins are thought to modulate the ER–mitochondrial functional link at MAMs [67] and have been reported to be down-regulated in an AD cell-culture model [68] and in post-mortem human AD brains [68]. This down-regulation was shown by immunohistochemistry to result in the redistribution of mitochondria away from axons to the cell soma in human AD hippocampus and to negatively affect dendritic spine formation in primary mouse hippocampal neurons [68]. Further investigations are clearly needed to address whether Aβ can be produced in the mitochondrial membrane, whether cleavage might take place in the MAM compartment and what the resulting implications are for AD.

Direct import of Aβ

Aβ itself can be imported into mitochondria via the translocase system and is consequently found within the mitochondrial cristae associated with the inner mitochondrial membrane [48]. Hansson Petersen et al. [48] demonstrated mitochondrial localization of Aβ in mitochondrial preparations from in vivo human brain biopsies from non-demented patients. Significantly, this result indicates that Aβ is indeed present in mitochondria of the non-demented human brain, albeit at lower levels. Subsequent import studies on a human neuroblastoma cell line further revealed that Aβ can be imported into mitochondria from outside the cell and that import is independent of the mitochondrial membrane potential and involves the TOM (translocase of outer mitochondrial membrane) transporters TOM20, TOM40 and TOM70 [48].

Recent genetic studies on AD and non-demented human brain samples revealed another interesting link between the mitochondrial import machinery and AD [69,70]. In these studies, SNPs (single nucleotide polymorphisms) in the TOM40 gene on chromosome 19, which is directly proximal to the ApoE gene, were linked to an increased risk for AD. In an initial study looking at SNP haplotypes, the polymorphisms were not linked to a risk of AD independently from the ApoE ε4 allele [70]. However, in a later study comparing diplotypes of these polymorphisms, one of these SNPs was found to contribute to a significantly increased risk for AD [69]. Bekris et al. [71] also observed that these SNPs were associated with the level of ApoE in the cerebrospinal fluid. It is therefore possible that a SNP in the TOM40 gene might play a role in increasing the risk of developing AD, and further research is needed to clarify if this represents an independent risk factor and how this risk is realized at the molecular level.

BINDING OF Aβ TO INTRACELLULAR PROTEINS

Having established that Aβ is present within cells, it is of interest to consider its resulting intracellular action. The build-up of Aβ within cells has been found to affect the expression or activation of several signalling proteins within cells, such as the stress kinases of the JNK (c-jun N-terminal kinase) pathway [72], NF-κB (nuclear factor-κB) [73], the Ca^{2+}-dependent metalloprotease calpain [74], the pro-apoptotic Bcl-2 protein family member Bim (Bcl-2-interacting mediator of cell death) [75], Akt/PI3K (phosphoinositide 3-kinase) [76] and CREB (cAMP-response-element-binding protein) [77]. Intracellular Aβ has also been found to impair cellular metabolism by disturbing mitochondrial

respiration [46,78]. Some of the intracellular effects, for example the activation of the p65 subunit of NF-κB, are indirect and are believed to be a result of the production of ROS [73]. Other studies suggest direct interactions of mono- or oligomeric Aβ with intracellular proteins. These specific interactions are probably critical events in AD (see below); they might represent early steps in the development of this disorder.

PDK (phosphoinositide-dependent kinase)

In a recent study, Lee et al. [76] investigated the effect of Aβ on the expression and activity of PDK and its target, Akt, both *in vitro* and *in vivo*. Involvement of the PDK/Akt kinase pathway in AD had been suggested previously, when it was observed that Akt expression levels were reduced in APP^m-expressing cell cultures and in lymphoblast cells from familial AD patients [79]. Additionally, it was known that overexpression of Akt in PC12 cell cultures attenuated the apoptotic effect of extracellular Aβ [80]. Evidence also existed that the PI3K/Akt kinase pathway can regulate levels of IDE [81], which might play a role in the degradation of Aβ inside mitochondria [52] and in the extracellular space [51], as described above.

Lee at al. [76] found decreased activation of Akt in human AD brain compared with control aged brain when they assessed the level of PDK-mediated phosphorylation. The *in vitro* activity of Akt from Aβ-expressing myotube or neuroblastoma cell cultures on a GSK (glycogen synthase kinase)-3 fusion protein was selectively reduced when compared with controls. PDK-dependent activation of Akt kinase activity *in vitro* was also diminished in the presence of Aβ. However, no direct binding studies with PDK, Akt and Aβ have been performed. Co-immunoprecipitation experiments have demonstrated the increased association of Aβ with Akt and PDK by Western blotting. However, dissociation of Akt from PDK was observed in preparations from AD-affected brain. The authors concluded that Aβ selectively interferes with the interaction between PDK and Akt, and therefore, Akt phosphorylation [76]. A detailed description of the interaction between Aβ, PDK and Akt on the biochemical level has so far not been provided, but this will be an important step in understanding its molecular causes and consequences. It is clear that Akt inhibition would inevitably result in a lack of pro-survival signalling in the cell and contribute to neurodegeneration. However, the question remains whether these processes are specific for late stages of AD or also occur in early phases of the disease.

SOD1

Yoon et al. [44] have demonstrated an interaction between Aβ and Cu–Zn SOD1 in a human neuroglioma cell line by co-immunoprecipitaion and co-localization. This interaction resulted in the inhibition of *in vitro* SOD1 catalytic activity and this effect was even stronger with a G93A mutant of SOD1 [44], which is implicated in familial cases of amyotrophic lateral sclerosis [81a]. At the same time, proteins involved in other neurodegenerative diseases, such as α-synuclein or its fragment NAC (non-Aβ component of AD amyloid) did not co-immunoprecipitate with SOD1. Co-localization studies revealed that GFP-tagged Aβ and SOD1 are eventually found in aggregates in the perinuclear region of cells [44]. Similar Aβ aggregates have recently been reported to attenuate the actions of the proteasome and lead to mitochondrially induced apoptosis in neuronal cells [63]. It is logical to conclude that inhibition of a key antioxidant enzyme in the cell will also lead to increased oxidative stress in the cell, which is

known to cause neurodegeneration and memory deficits [82,83]. However, at present, there has been no evidence for a direct *in vivo* interaction of Aβ with SOD1. Despite this, the significance of SOD1 in AD is supported by an earlier study, which showed that the β-site cleavage enzyme BACE1 (β-site APP-cleaving enzyme 1) is able to bind Cu^{2+} and interact with CCS (Cu^{2+} chaperone of SOD1) in cell cultures and normal rat brain. The authors suggested that BACE1 levels could therefore control SOD1 activity by competing for the limited pool of CCS in cells [84]. Additionally, these findings link an enzyme involved in Aβ production with SOD1 both *in vitro* and *in vivo*, and support the view that SOD1 could play an active role in the pathogenesis of AD.

It is also important to note that the manganese-dependent mitochondrial superoxide dismutase, SOD2, has been implicated in AD. Li et al. [85] found elevated Aβ levels and an increased plaque burden in APP^m-expressing mice when they lacked one allele of the *SOD2* gene. Two recent studies have also shown that overexpression of SOD2 reduces oxidative stress and memory deficits in a transgenic mouse model for AD [86,87]. However, no direct interaction between Aβ and Mn–SOD2 has been reported.

Catalase

Another protein that was reported to directly interact with Aβ peptides is the hydrogen peroxide-degrading enzyme, catalase. There is *in vitro* evidence for an interaction between isolated catalase and biotinylated Aβ, which inhibits the catalase's enzymatic activity [88,89]. Milton [88] characterized the binding of Aβ to catalase and found that Aβ-(1–42) and Aβ-(25–35) bound to catalase with a K_d of 3.3 ± 0.02 nM, whereas Aβ-(12–28) did not bind. The author suggested that the inhibition of catalase activity was caused by oxidation of the enzyme, as the effect of Aβ could be relieved in the presence of ethanol or NADPH [88]. Moreover, the cytotoxic effect of extracellular Aβ was enhanced when catalase was inhibited by 3-aminotriazole. [90]. Applying an antisense peptide approach, Milton et al. [91] later identified that amino acids 400–409 of the human catalase protein can interact with Aβ. When testing the Aβ-binding affinity of a peptide representing this region, a K_d of 1.2 ± 0.1 nM was determined, which is similar to the K_d identified for binding of Aβ to catalase. The peptide was also able to protect from some of the adverse effects of Aβ on a myeloma cell line [91]. Despite these results, it is not clear whether inhibition of catalase by Aβ is relevant for physiological and pathological processes in AD. Notably these studies used concentrations of up to 20 μM Aβ and the aggregation state of the different amyloid peptides is undefined. This concentration is important, as it is known that different Aβ states (i.e. monomers, oligomers or fibrils) can have different effects on cells and this also turns out to be true for different concentrations of Aβ [73,77]. It would be interesting to see whether catalase also interacts with Aβ peptides in a cellular environment and at lower concentrations and if binding of Aβ to antioxidant proteins, like SOD and catalase, turns out to be a common theme.

ABAD

To date, the most characterized intracellular Aβ-binding protein has been ABAD. ABAD was first identified as an Aβ-binding protein in 1997 using a yeast two-hybrid screen [92] and later, in a separate study, as the human analogue of a newly discovered bovine hydroxyacyl-CoA dehydrogenase type II [93]. As ABAD was originally identified within the ER [92,94], it was initially termed ERAB (ER-associated amyloid-binding protein) [92]. However, it was identified later within mitochondria [92,94–96] and it has been suggested that the distribution of ABAD in
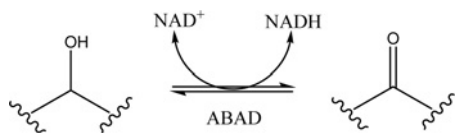
Scheme 1   Reduction and oxidation of alcohols and ketones by ABAD

cells may be cell-line-dependent [96]. ABAD is also known by a number of other names, including SCHAD (human brain short chain L-3-hydroxyacyl-CoA dehydrogenase) [97,98], HSD10 (17β-hydroxysteroid dehydrogenase) [99,100] and HADH II (human hydroxyacyl-CoA dehydrogenase type II) [101,102]. This protein is expressed in all tissue types, particularly in the heart and liver, and was also found to be expressed in all regions of the brain [92].

Structure and function of ABAD

ABAD is a multifunctional enzyme catalysing the reduction of aldehydes and ketones and oxidation of alcohols (Scheme 1) and as such it is known to act on a broad range of structurally diverse substrates, including simple alcohols [97,101,102], steroids [95], hydroxysteroids [95,97,101] and 3-hydroxyacetyl-CoA derivatives, such as acetoacetyl-CoA [95,101,102] and D-β-hydroxybutyrate [101].

Table 1 lists the experimentally determined enzymatic parameters for a range of these substrates. Unsurprisingly, different substrates have different reaction rates with the enzyme, indicating that although ABAD is able to catalyse reactions on a number of different substrates, some have a higher turnover than others. It can also be seen that widely ranging values for enzyme activity have been reported for the same substrate, often varying by several orders of magnitude. However, comparisons between values obtained may be complicated due to the range in conditions used during assays used to study activity. Despite this, the results are still an indication of the potentially wide range of roles that the enzyme is able to perform within the cell. It is, however, important to note that an enzyme's ability to metabolize a particular substrate *in vitro* does not necessarily guarantee that it does so in an *in vivo* environment. Given the mitochondrial location of ABAD, one of its main functions is thought to be in energy production and metabolic homoeostasis, notably the third step of β-oxidation of fatty acids, utilizing its function as an L-3-hydroxyacyl-CoA dehydrogenase [93,102]. This role may be especially important in glucose-deficient environments, where other energy sources become more significant. For example, it has been found that the overexpression of ABAD in COS cells increases the ability of the cell to utilize ketones, such as D-β-hydroxybutyrate, in the absence of other energy sources [103]. Similarly, transgenic mice overexpressing ABAD showed increased utilization of D-β-hydroxybutyrate compared with non-transgenic animals, indicating their better adaptability to metabolic challenges [103].

A proposed alternative role to energy homoeostasis is in the metabolism of hydroxysteroids, such as oestradiol [95]. The role of ABAD in metabolizing sex steroids could be significant, as it is documented that women are more likely to suffer from AD than men [104], and that postmenopausal hormone replacement therapy can prove beneficial in delaying the onset of the disease [105]. ABAD has also been shown to oxidize steroid modulators of the GABA$_A$ receptor (GABA is γ-aminobutyric acid) to give inactive metabolites, and as such it has been suggested that these compounds are better substrates for ABAD than the sex steroids [106] (see Table 1).

ABAD is known to play a role in the degradation pathway of isoleucine. In clinical cases of MHBD (2-methyl-3-hydroxybutyryl-CoA dehydrogenase) deficiency, i.e. deficiency of the enzyme catabolizing the penultimate step in isoleucine degradation, two missense mutations within ABAD were identified in patients presenting with MHBD deficiency; Arg[130] was mutated to a cysteine residue in four patients and was found to cause neurological deficits, loss of mental and motor skills and psychomotor retardation, whereas a Leu[122] to valine substitution, identified in a single case, presented with only psychomotor retardation [107]. The mutations were shown to either fully (R130C) or greatly (L122V) inactivate the enzyme; in addition, the R130C mutation was also thought to reduce the enzyme's stability, causing the lower protein levels observed in these patients [107].

It has been proposed that in the absence of Aβ, ABAD is able to play a cytoprotective role during periods of stress. For example, in mouse models of ischaemic stress (stroke), ABAD expression was found to be increased in both ABAD-overexpressing and non-transgenic mice following 45 minutes of transient middle cerebral artery occlusion. However, the transgenic animals showed fewer effects of the stroke, including fewer neurological deficits and increased ATP levels [103] and were hence thought to be protected to some degree by the elevated levels of ABAD. Conversely, ABAD levels were shown to be decreased in the ventral midbrain of PD (Parkinson's disease) patients, as well as in the ventral midbrain of MPTP (1-methyl-4-phenyl-1,2,3,6-tetrahydropyridine)-treated mice, used as a model of PD. However, MPTP-treated mice overexpressing ABAD were protected against apoptosis and the loss of dopaminergic neurons in this brain region, suggesting that this enzyme can protect against neurodegeneration [108].
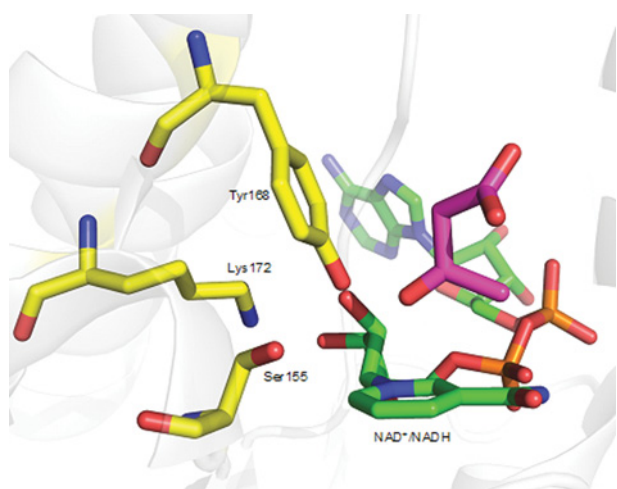
The crystal structure of ABAD is well documented, with several structures of the enzyme published. These include structures in complex with its co-factor NAD$^+$ [102], a human mutant version complexed with an inhibitor [99] and the human protein in complex with Aβ [45]. From these structures, information on the catalytic mechanism and its interaction with Aβ has been deduced.

ABAD was found to form a homotetramer, both in solution and in the crystal form, which was made up of four identical single domain monomers of 27 kDa each. Tetramerization has been shown, by molecular modelling, to stabilize the binding interface region [109]. The conserved catalytic triad of Ser[155], Tyr[168] and Lys[172] is also found in the active site of other short-chain dehydrogenase reductase enzymes [45,99]; mutation of these residues to glycine inactivates the enzyme [101]. In the reduction of a ketone to an alcohol, the hydrogen atom of Tyr[168] is thought to co-ordinate to the carbonyl of the ketone substrate, increasing the electrophilicity of the carbonyl carbon atom. It is proposed that the ammonium group of Lys[172] interacts with the hydroxy group of Tyr[168], increasing the acidity of this residue. The hydride that effects reduction is donated to the activated carbonyl by the NADH co-factor, leading, simultaneously, to deprotonation of Tyr[168] by the newly formed hydroxy group. The hydroxy group of Ser[155] is able to form a hydrogen bond with the deprotonated tyrosine, stabilizing the resulting negative charge (Figure 2).

Structures of rat ABAD with either 3-ketobutyrate or 17β-oestradiol showed that the two substrates bound in similar positions within the active site [102]. These structures confirm the close proximity of the presumed catalytic residues to the substrate molecule. Liu et al. [110] have investigated the mechanism of the related enzyme HAD (3-hydroxyacyl-CoA dehydrogenase) using fluorinated substrates and have determined that the oxidation of hydroxyacyl-CoA-linked substrates proceeds through an enolate

Table 1   Experimentally derived enzyme activity parameters for ABAD with a range of substrates

Results are means $\pm$ S.D.; -, not determined.

Substrate	Reference	Co-factor	Specific activity (μmol $\cdot$ min^{-1} $\cdot$ mg^{-1})	V_{max} (μmol $\cdot$ min^{-1} $\cdot$ mg^{-1})	K_m (μM)	k_{cat} (s^{-1})
S-Acetoacetyl-CoA	[101]	NADH	-	430 ± 45	68 ± 20	190
	[93]	NADH	-	-	89 ± 5.4	37 ± 1.6
	[94]	NADH	1.1	-	22.7	-
	[102]	NADH	-	-	53 ± 9	11.1 ± 0.7
17β-Oestradiol	[101]	NAD$^+$	-	23 ± 3	14 ± 6	10
	[102]	NAD$^+$	-	-	15 ± 7	0.00088 ± 0.0012
	[95]	NAD$^+$	0.0156 ± 0.0008	-	43 ± 2.1	0.011 ± 0.0002
Dihydroandrosterone	[95]	NAD$^+$	0.130 ± 0.0018	-	34 ± 2.4	0.093 ± 0.0028
Androsterone	[95]	NAD$^+$	0.0121 ± 0.0009	-	45 ± 9.3	0.011 ± 0.0013
Ethanol	[101]	NAD$^+$	-	2.2 ± 0.4	1210 ± 260	1.0
1-Propanol	[101]	NAD$^+$	-	4.2 ± 0.5	272000 ± 62000	1.9
	[102]	NAD$^+$	-	-	83200 ± 21100	0.0060 ± 0.0005
2-Propanol	[101]	NAD$^+$	-	36 ± 2	150000 ± 17000	16
	[102]	NAD$^+$	-	-	156000 ± 18000	0.0179 ± 0.0008
	[97]	NAD$^+$	-	-	280000 ± 33000	0.036 ± 0.0023
β-Hydroxybutyryl-CoA	[94]	NAD$^+$	65.7	-	9.8	-
	[103]	NAD$^+$	-	26.3	134	-
L-β-Hydroxybutyrate	[103]	NAD$^+$	-	0.004	1600	-
D-β-Hydroxybutyrate	[103]	NAD$^+$	-	0.004	4500	-

Figure 2   Representation of the catalytic core of ABAD

A PyMol representation of the X-ray crystal structure of rat ABAD bound to its co-factor and an acetoacetic acid substrate. The three conserved active site residues, Ser[155], Tyr[168] and Lys[172] (carbon atoms in yellow), the NAD$^+$/NADH co-factor (carbon atoms in green) and the acetoacetic acid substrate (carbon atoms in magenta) are represented as sticks. It can be seen that the ketone oxygen of the substrate interacts with Tyr[168] and is favourably oriented in order to receive or donate a hydride to or from the co-factor. Nitrogen atoms, blue; oxygen atoms, red; phosphorus atoms, orange.

intermediate, stabilized by Asn[208] and Ser[137], and that this enolate formation is essential for the reaction to occur. Given the similarity of the active-site residues, it is possible that oxidation of similar substrates by ABAD might occur through a similar mechanism.

The crystal structure of rat ABAD indicated the presence of an 'active-site loop' from residues 202–220, which encloses the active site in the presence of substrate, preventing further access by solvent molecules. Thr[208] of this loop would therefore be able to form a strong hydrogen bond with the substrate [102]. Molecular modelling suggested that this loop is in an open conformation in the absence of substrates, whereas the presence of NAD$^+$ induces the conformational change to a 'closed' position [109].

Compared with other HAD type I short-chain enzymes, both rat [102] and human [45] ABAD were found to have two significant insertions between residues 100–110 and 140–150. A model of the expected binding of a CoA-linked substrate to the active site suggests an interaction between the negatively charged phosphate groups of CoA and a group of positively charged residues within the 100–110 region (namely Lys[99], His[102], Lys[104] and Lys[105]) [99,102]. CoA-linked substrates were found to be more efficiently oxidized than their non-CoA analogues [102]. The region connecting the proposed CoA-binding site and the active site is lined with hydrophobic residues, which is consistent with the binding of aliphatic chains. In contrast, few interactions were observed outside the active site with 17β-oestradiol as the substrate [102], corroborating the idea that sex steroids are not the main substrates for ABAD.

ABAD–Aβ interaction

The initial identification of ABAD as an intracellular binding partner of Aβ was based on a yeast two-hybrid screen [92], which identified four positive clones (one from human brain and three from HeLa cells), all of which had the same cDNA sequence. Radiolabelled ligand-binding studies confirmed the interaction of ABAD and Aβ and a K_d of 88 nM was determined [92]. Subsequently, a number of techniques have been employed to demonstrate the interaction between ABAD and Aβ, including ELISA [111], crystallography [45], SPR (surface plasmon resonance) [45,112], co-immunoprecipitation [45,92, 95] and immunocytochemistry followed by confocal microscopy [45].

Both Aβ-(1–40) and Aβ-(1–42) were found to inhibit the activity of purified ABAD, with K_i values of 1.2–1.6 μM for the reduction of acetoacetyl-CoA, [94,101], 2.6 μM for the oxidation of octanol [101] and 3.2 μM for the reduction of 17β-oestradiol [101]. Studies by Oppermann et al. [94] showed that residues 13–22 of Aβ were critical for inhibiting ABAD activity, a region that is also characterized by its fibril-forming properties (residues 16–20). It is interesting to note that inhibition of ABAD requires micromolar concentrations of Aβ, whereas binding has been shown to occur in the nanomolar range [92,112]. This result implies that Aβ monomers alone are not sufficient to induce

inhibition. Perhaps further aggregation of Aβ is necessary to alter the conformation of the enzyme to an extent that its active site is distorted or, more simply, that an aggregation of Aβ on the surface sterically hinders access of substrate to the active site.

The crystal structure of ABAD in complex with Aβ lends support to the first hypothesis that the enzyme shape is distorted upon binding to Aβ [45]. Compared with other published ABAD structures [99,102], the active site and NAD$^+$-binding site were shown to be highly distorted in the presence of Aβ and no bound NAD$^+$ co-factor was seen. Further studies using SPR confirmed binding of ABAD and Aβ at nanomolar concentrations and showed that a conformational change in ABAD occurs upon binding of Aβ [112]. Saturation transfer difference NMR was used to show that the presence of Aβ inhibited the binding of NAD$^+$ to ABAD in a concentration-dependent manner. Similarly, the ability of Aβ to bind ABAD was reduced in the presence of NAD$^+$, suggesting that the binding of Aβ and NAD$^+$ to ABAD are competing [112]. These observations provide strong evidence that Aβ has an influence on the physical structure of ABAD, disrupting its activity.

Although no electron density for Aβ was observed in the ABAD–Aβ crystal, SDS/PAGE confirmed its presence in the complex, indicating that the Aβ present within the crystal is in a disordered state. The region comprising residues 100–110 was also highly disordered [45], despite it being well ordered in other known structures [99,102]. These observations led to the hypothesis that this region, referred to as loop D, may be the binding site for Aβ. It is possible that the lack of order in the Aβ component of the complex is either due to high levels of flexibility within the amino acid chain of Aβ or due to a disordered aggregation of the peptide, which would fit with the aggregation hypothesis. Mutagenesis studies showed that replacing residues within the loop D region prevented the binding of Aβ to ABAD. In particular, two groups of residues were highlighted as being significant: the first group consisted of Ser[98], Lys[99], Thr[100] and Tyr[101], and the second of Thr[108], His[109] and Thr[110]. Point mutations to replace these residues with alanine residues, either individually or in combination, resulted in the loss of ABAD–Aβ binding [45]. The activity of related enzymes, such as the bacterial 3β/17β dehydrogenase and type I HADH, which have a similar mechanism, but do not contain the insertion of loop D seen in ABAD, is unaffected by Aβ [94], again providing support for this region of the enzyme being the Aβ-binding region. In addition, the energetics of the binding between ABAD and Aβ were broken down into their enthalpic and entropic components, revealing a large increase in entropy upon binding, overcoming an unfavourable enthalpy change. Yan et al. [112] proposed that this large increase in entropy is probably due to the displacement of highly ordered water molecules from the protein surface upon binding of Aβ to ABAD.

The interaction between ABAD and Aβ has also been demonstrated *in vivo* using a number of techniques. Analysis of human cerebral cortex samples using immunoprecipitation revealed the enrichment of the ABAD–Aβ complex in AD brains, and similar results were seen in mitochondria isolated from the cerebral cortex of mice APP^m-expressing or Tg-APP^m/ABAD (transgenic expression of both APP^m and ABAD) mice [45]. These results indicate that the interaction of ABAD and Aβ does occur in physiologically relevant environments. Immunocytochemistry was also used to show co-localization of ABAD and Aβ and to verify the localization of ABAD in mitochondria by co-localization with VDAC (voltage-dependent anion channel) [45].

In addition to the direct interaction between ABAD and Aβ, it has been shown that Aβ can influence the expression of ABAD. Indeed, transgenic mice overexpressing APP^m, including

the triple transgenic model (expressing AD-linked mutations in APP, presenilin 1 and tau), show increased ABAD expression in the hippocampus when compared with non-transgenic littermates [113,114]. This increased expression has also been observed in human AD brains, where comparison with age-matched controls revealed elevated expression of ABAD in the temporal lobes of AD brains, which was localized to neuronal cells [92]. Significantly, when not associated with elevated Aβ, overexpression of ABAD can have a positive outcome with regard to other stresses (see above) [103,108]. However, under conditions when both ABAD and Aβ are elevated the consequences of their interaction are numerous and occur at the molecular, cellular and *in vivo* levels.

Consequences of ABAD–Aβ interaction

At the molecular level, as described above, the binding of Aβ causes the inhibition of ABAD activity. However, overexpressing a catalytically inactive form of ABAD in the presence of Aβ does not enhance cytotoxicity in cell cultures compared with Aβ alone [101]. This observation indicates that these cellular effects are not simply based on the inactivation of ABAD, but are due to other downstream effects mediated by the active enzyme once bound with Aβ. This view is supported by the observed discrepancies in the binding constants of Aβ and ABAD (in the nanomolar range) and the K_i values determined for the inhibition of ABAD by Aβ (in the micromolar range) [101].

Another direct effect on the enzyme was reported when the localization of ABAD was seen to change in the presence of Aβ. Under normal conditions, ABAD was observed both in the ER and in mitochondria. However, in the presence of Aβ (which was either applied externally or produced from a transfected APP plasmid), redistribution from the ER to the inner surface of the plasma membrane was reported [92,101].

At the cellular level, it has been shown that overexpression of ABAD in the presence of elevated Aβ has deleterious effects on cell function and survival. Aβ was found to suppress the reduction of MTT (dimethylthiazolyl diphenyltetrazolium) bromide and increase DNA fragmentation and apoptosis in the neuroblastoma SK-N-SH cell line, and these effects were minimized by the addition of anti-ABAD antibodies [92]. Apoptosis and DNA fragmentation were greatly enhanced in COS cells co-transfected with plasmids expressing Aβ and ABAD [92], or APP^m and ABAD [101], compared with those transfected with Aβ or ABAD alone. Conversely, this enhancement of toxicity was not seen in cells transfected with mutant (inactive) ABAD in the presence of Aβ, despite Aβ having a similar binding affinity for the mutant and wild-type forms (K_d of 64.5 nM and 38.9 nM respectively) [101]. Again, these results indicate that it is the combination of increased ABAD activity and Aβ expression that is necessary for toxicity.

It has been suggested that the interaction of ABAD with Aβ may induce a toxic effect through the build-up of toxic aldehydes. Increases in both HNE (4-hydroxynonenal) and MDA (malondialdehyde) have been correlated with AD [115,116] and a cytoprotective action of ABAD against these toxic aldehydes has been demonstrated [117]. SH-SY5Y cells transfected with ABAD and then treated with HNE for 24 hours showed an improved survival compared with control cells. Similarly, HeLa cells transfected with ABAD were able to catabolize HNE better than control cells, an effect lost in the presence of Aβ-(1–42) [117]. However, neuroblastoma cell cultures overexpressing both ABAD and APP (either wild-type or APP^m forms) were found to exhibit enhanced production of MDA and HNE, compared with those expressing ABAD or APP^m alone. Transfection with mutant (inactive) ABAD and APP^m together did not produce this response

[101]. It has therefore been proposed that a native function of ABAD may be to remove toxic aldehydes such as HNE and MDA and that this function is impaired in the presence of Aβ, resulting in the disruption of normal cellular processes [117].

The toxic effect of overexpressing ABAD together with Aβ has also been confirmed in an AD mouse model. Compared with neurons from non-transgenic mice and mice overexpressing ABAD or APP[m] alone, E18 cortical neurons cultured from Tg-APP[m]/ABAD mice were found to exhibit higher levels of hydrogen peroxide, decreased mitochondrial function and increased cell death [118]. Mitochondrial dysfunction was observed *in vivo* in Tg-APP[m]/ABAD mice, which had decreased glucose utilization and ATP production at 9 months of age [118]. These mice were also found to have deficits in spatial and temporal memory compared with non-transgenic mice, with impaired performance in the radial-arm water maze as early as 4–5 months of age [45]. These results again emphasize that it is the combination of ABAD and Aβ that is necessary for effects to be seen and that these effects occur early in the disease process.

Proteomic analysis of brains from Tg-APP[m]/ABAD mice has identified increased expression of other proteins, hinting at other downstream effects of the interaction of ABAD and Aβ. Expression of Prx-II (peroxiredoxin II), an antioxidant enzyme, was found to be increased in mice overexpressing APP[m] and in Tg-APP[m]/ABAD mice. Further analysis of Tg-APP[m]/ABAD mice brains and human AD brains by Western blotting and immunocytochemistry showed increased expression of Prx-II in the cerebral cortex. Transfection of cortical neurons with Prx-II was found to reduce Aβ toxicity, suggesting that its overexpression in AD is playing a protective role [119]. Interestingly, Prx-II has also been linked with PD, where it was found to be phosphorylated by Cdk5 (cyclin-dependent kinase 5), and hence inactivated in MPTP-induced models of the disease [120]. Similarly, increased phosphorylation of Prx-II was seen in the nigral neurons of human PD brains, whereas the overall expression levels of Prx-II remained unchanged. As in AD models, overexpression of Prx-II in the MPTP-induced *in vitro* and *in vivo* models of PD was found to protect against neuronal loss [120]. In light of these findings, the consequences of Prx-II up-regulation in AD, its association with ABAD and potential protective role still need to be investigated in more detail.

A second protein, Ep-I [endophilin I, also referred to as SH3GL2 (SH3-domain GRB-like 2)], was also identified as being up-regulated in Tg-APP[m]/ABAD mice compared with mice expressing ABAD alone and non-transgenic littermates. Further analysis showed that there was up-regulation of Ep-I in the hippocampus and cortex of Tg-APP[m]/ABAD mice and in the temporal cortex of human AD brains [121]. Ep-I is a presynaptic protein known for its involvement in synaptic vesicle biogenesis [122] and it has previously been shown that its expression could also activate JNK [123]. Increases in JNK activation have been observed in AD patients [124] and AD mouse models [72], as well as in Aβ-expressing cell culture models [125–127], although this had been thought to be solely due to increases in ROS production. Ren et al. [121] showed that an increase in Ep-I expression could increase JNK activity with the subsequent death of primary neuronal cell cultures. However, when neuronal cultures were transfected with truncated Ep-I, lacking its SH3 domain, the activation of JNK by Aβ was blocked and cell viability increased [121]. Thus the increase in Ep-I expression shown in the AD brain could be another mechanism for the activation of the JNK signalling pathway. Notably, the reported increases in both Prx-II and Ep-I were shown to be directly due to the binding of ABAD and Aβ, as interfering with this binding in living organisms resulted in the expression of these two proteins returning to

normal (see below), therefore emphasizing the importance of this interaction *in vivo*.

From these studies, it can be seen that the interaction of Aβ with ABAD has multiple effects at the molecular, cellular and whole animal level. Indeed, when Aβ binds to ABAD the net effect is to inhibit the ABAD enzyme activity. However, the precise molecular mechanisms of how this occurs are yet to be deciphered; what is known is that in the living brain this results in the activation of genes which in AD appear to shift the balance of events, with increasing Prx-II expression promoting neuronal survival and increasing Ep-I expression promoting neuronal death.

CypD

Recently, a second major Aβ–protein interaction has been found within mitochondria. CypD, a peptidylprolyl isomerase F, is found in the mitochondrial matrix and translocates to the inner mitochondrial membrane during the opening of the mPTP (mitochondrial permeability transition pore) in times of oxidative stress [128]. There are many excellent reviews on the mPTP [129,130], but in brief, the mPTP plays a central role in both necrotic and apoptotic neuronal cell death. Opening of the mPTP collapses the membrane potential and possibly amplifies apoptotic mechanisms by releasing proteins with apoptogenic potential from the inner membrane space [131]. The mPTP is thought to involve, at least, ANT (adenine nucleotide translocase) in the inner membrane, VDAC in the outer membrane (although note that recent studies have suggested the involvement of the mitochondrial phosphate carrier [129,132]) and CypD in the mitochondrial matrix [129,131]. CypD associates with ANT and potentially other targets on the inner mitochondrial membrane, contributing to the opening of the mPTP. This association leads to colloidosmotic swelling of the mitochondrial matrix, dissipation of the inner membrane potential ($\Delta\psi_m$) and/or generation of ROS. Therefore CypD is considered to be part of the mPTP complex as summarized in Figure 3. Oxidative and other cellular stresses promote CypD translocation to the inner membrane [128,133,134] and other studies provided substantial evidence that a genetic deficiency in CypD protects against Ca^{2+}- and oxidative stress-induced cell death [135,136]. In addition to providing a pivotal regulatory role in the mPTP opening [137], CypD has also been shown to be involved in protein folding [138,139].

CypD–Aβ interaction

The observations that Aβ progressively accumulates in brain mitochondria of AD patients led Du et al. [140] to further investigate the mechanism underlying Aβ-mediated mitochondrial dysfunction. In these studies, it was established by SPR that CypD can bind Aβ [140]. Elevated CypD levels were reported in human AD brains, as well as in an APP[m]-expressing mouse model for AD [140]. The K_d for the interaction of CypD and monomeric Aβ-(1–40) and Aβ-(1–42) was 1.7 μm and 164 nM respectively, whereas interactions with oligomeric Aβ-(1–40) and Aβ-(1–42) had a K_d of 227 nM and 4 nM, thus indicating that the oligomeric forms of Aβ appear to have a greater affinity for CypD and that Aβ-(1–42) has a greater affinity than Aβ-(1–40). Co-localization of CypD and Aβ in the mitochondria was also observed by confocal microscopy in the cerebral cortex of both mice overexpressing APP[m] and in human AD brains, and immunoprecipitation confirmed the enriched presence of CypD–Aβ complexes in AD brains [140].

As with the ABAD and Aβ interaction, at present the exact contact sites of the interaction between CypD and Aβ are unknown, though recent molecular-docking experiments have
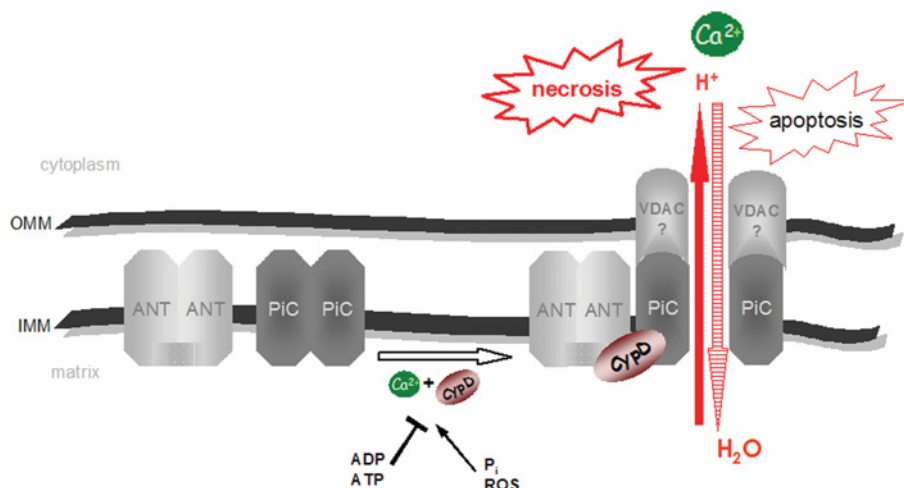
Figure 3   Components of the mPTP

Probable components of the pore include ANT, PiC (mitochondrial phosphate carrier) and CypD at the inner mitochondrial membrane (IMM) together with Ca^{2+} and a pore-forming component, e.g. VDAC, in the outer mitochondrial membrane (OMM). High concentrations of phosphates as well as ROS promote mPTP formation, whereas high levels of ADP or ATP inhibit mPTP formation. Pore formation leads to the leakage of H^+ and Ca^{2+} to the cytosol, disruption of the mitochondrial membrane potential and necrosis. Prolonged or repeated sub-lethal mPTP-formation is thought to cause mitochondrial swelling, rupture of the outer mitochondrial membrane and apoptosis.

attempted to produce a model [141]. Singh et al. [141] also predicted an interaction between ANT and Aβ, which together with that of CypD has a possible functional impact on the mPTP [141]. Whether these predictions prove true will only be known when they are experimentally tested. To date, the crystal structure of CypD has been published [142,143], but only in the presence of DMSO [143] or CsA (cyclosporin A), an inhibitor of CypD [142]. Notably, in both cases a truncated mutant form of CypD was used, starting at Cys^{29} and containing a single point mutation (with Lys^{133} replaced by an isoleucine residue). However, at present it is unknown whether these regions are an important region for the interaction.

Consequences of CypD–Aβ interaction

CypD levels of expression are elevated in the aging human brain and in an Aβ-rich environment [140]. The reported consequence of the binding of CypD and Aβ is elevated levels of ROS, which in turn induces mPTP opening and cell death [140,141]. Additionally it is thought that this interaction enhances the translocation of CypD from the matrix to the inner mitochondrial membrane where CypD will interact with the mPTP, resulting in its opening [140]. The interaction would lead to a build-up of Aβ in the inner mitochondrial membrane, which in itself can cause changes in the mitochondrial membrane potential, leading to cell death [141].

Much of these potential consequences of the interaction of Aβ and CypD have been determined in studies of CypD-deficient animals (Ppif$^{-/-}$). Notably, the cortical mitochondria isolated from a AD mouse model lacking CypD are resistant to both Aβ and Ca^{2+}-induced mitochondrial swelling and opening of the mPTP, and display an increased calcium buffering capacity and an attenuation of the generation of mitochondrial ROS. Furthermore, CypD-deficient neurons are protected against Aβ- and oxidative stress-induced cell death. Importantly, deficiency of CypD greatly improved the learning and memory of a transgenic APP^m-expressing AD mouse model [140,144]. These animals exhibited increased spatial and memory learning and alleviated

Aβ-mediated reduction of long-term potentiation at 12 [140] and 24 months, by which age the APP^m-expressing mice are known to display AD-like symptoms and synaptic dysfunction [144]. Thus the CypD/Aβ-dependent activation of the mPTP directly links to the cellular and synaptic perturbation relevant to the pathogenesis of AD [140].

ARE INTRACELLULAR Aβ-BINDING SITES POSSIBLE THERAPEUTIC TARGETS IN ALZHEIMER'S DISEASE?

Having described a number of intracellular binding partners for Aβ, there is the obvious question of whether these sites are relevant for therapeutic intervention in AD. At present there is evidence that both ABAD and CypD are potential drug target sites.

ABAD as a therapeutic target

It has been established that the interaction between ABAD and Aβ can lead to harmful effects on cell viability along with subsequent deleterious effects on the cognitive performance in transgenic AD mouse models, thus reflecting the importance of these cellular effects on disease progression. Therefore these studies indicate that the ability to block this interaction could provide a potential target for the treatment of AD.

Mutagenesis studies have shown that ABAD contains two groups of residues that are particularly important for the binding of Aβ (i.e. the Ser^{98}, Lys^{99}, Thr^{100} and Tyr^{101} group and the Thr^{108}, His^{109} and Thr^{110} group; both are found in Loop D as described above). It was further reported the development of a 'decoy peptide', ABAD-DP, which spanned these important amino acids (residues 92–120), prevented the binding of Aβ to ABAD [45]. The use of this region as a discrete synthetic peptide in competitive SPR-binding studies was able to prevent the binding of Aβ to ABAD at micromolar concentrations, with a K_i of 4.9 and 1.7 μM for Aβ-(1–40) and Aβ-(1–42) respectively, and also attenuated

cytotoxicity of Aβ towards primary neurons in a cell-based assay [45].

Notably, the same region of ABAD had been independently identified previously using an antisense peptide approach [91]. In this approach the antisense DNA strand was translated to give the antisense peptide sequence, which was believed to contain complementary binding surfaces to the peptide produced from the coding DNA strand. This antisense sequence was then compared with the Aβ sequence in order to reveal potential Aβ-binding sites. As a result, a region similar to Aβ residues 16–20 was identified within ABAD residues 99–108, which contained a Leu-Val-Phe-Phe motif. This region of ABAD, again synthesized as a discrete peptide, was found to bind biotinylated Aβ in an ELISA binding-assay with a K_d of 107 nM and to increase the level of neuronal cell survival in the presence of Aβ [91]. This K_d value is in the same range as the K_d value observed by Yan et al. [92] for the interaction of Aβ with the whole enzyme (88 nM) but is much lower than the K_i observed for the inhibition of the ABAD–Aβ interaction found by Lustbader et al. [45], supporting the hypothesis mentioned previously that oligomeric forms of Aβ are the species interacting with and inhibiting the enzyme.

An effect of the ABAD-DP was also observed in cell culture models. Addition of the Tat domain from HIV allowed the peptide to cross cell membranes, where it was shown to be effective at protecting cultured primary neurons (from wild-type, ABAD-expressing and Tg-ABAD/APP^m animals) from Aβ-mediated toxicity. Mitochondrial stress resulting from Aβ treatment was alleviated, as shown by reductions in cytochrome c release, the production of ROS, DNA fragmentation and LDH (lactate dehydrogenase) release [45]. A major problem with testing the effects of the small ABAD-DP in cellular systems is its rapid degradation by peptidases. In order to stabilize the peptide, in a separate study it was therefore fused with TRX (thioredoxin I), to give the ABAD-(92–120)–TRX peptide, and introduced into PC12 cells using a lentiviral system. There the fusion peptide was still found to protect cells against Aβ-induced toxicity [145]. Moreover, TRX is a scavenger of ROS and known to assist with protein folding and stability [146,147], and so it was also noted to complement the decoy peptide's protective activity, probably by scavenging ROS produced as a result of Aβ toxicity. ABAD-(92–120)-TRX-transfected cells exhibited decreased apoptosis, decreased LDH release and increased cell viability in response to Aβ or hydrogen peroxide treatment compared with untransfected cells or those transfected with TRX alone [145].

The decoy peptide has also been effective in whole animal studies. Expression levels of protein biomarkers known to be elevated in AD brains, such as Prx-II [119] and Ep-I [121], have also shown a response to the disruption of the ABAD–Aβ interaction using the decoy peptide. In these studies, a peptide spanning residues 93–116 of ABAD was again modified, this time to contain a Tat sequence for transport across the cell membrane, along with a mitochondrial-targeting sequence to direct the peptide to the site of ABAD–Aβ complexes in the mitochondria. This Tat-mito-DP-(93–116) peptide was introduced into transgenic APP^m-expressing mice by intraperitoneal injection, resulting in systemic application of the peptide. Transgenic APP^m mice were shown to have increased Prx-II in the hippocampus, whereas mice treated with Tat-mito-DP showed a significant reduction in Prx-II, comparable with the level seen in non-transgenic mice [119]. Similarly, Tg-APP^m/ABAD mice, which exhibit elevated Ep-I expression compared with wild-type littermates, showed a significant reduction in Ep-I, which returned to basal levels [121]. Therefore this indicated that disrupting the ABAD–Aβ interaction can prevent further downstream effects seen in this AD mouse model. It has been shown that by using these additional peptide sequences the decoy peptide can enter the brain and as such it can be used to reverse biochemical symptoms in mouse models of AD. Transgenic mice expressing both APP^m and the decoy peptide ABAD-(91–119), as well as transgenic APP^m-expressing mice systemically treated with the decoy peptide by intraperitoneal injection, showed improvements in the radial-arm water maze test compared with untreated transgenic APP^m-expressing mice [148].

Taken together, these experimental results consistently underline the therapeutic value of interrupting the ABAD–Aβ interaction. However, whereas small peptides have been shown to inhibit the ABAD–Aβ interaction, the nature of peptides limits their application as drugs due to their low bioavailability and instability. There is therefore a need to develop alternative small molecule inhibitors of the ABAD–Aβ interaction. This has been initiated and screening of a commercially available fragment library consisting of compounds that interact with Aβ or have neuroprotective properties resulted in the development of a series of benzothiole urea compounds, which are capable of inhibiting the interaction at micromolar concentrations, as shown by ELISA [111]. However, further studies into the cellular effects of these compounds and their pharmacological properties will be required for the development of new treatment strategies for AD.

CypD as a therapeutic target

The results showing that CypD deficiency is able to ameliorate Aβ toxicity in transgenic animals means that CypD can also be considered as a potential drug target for AD, as it has for other neurodegenerative disorders [140,149,150]. Indeed, it has been reported that in the presence of CsA, a known immunosuppressant and inhibitor of CypD [151], there is a decrease in mPTP formation and that a CsA–CypD complex is formed in mitochondria [152]. More directly it was shown that CsA can block some of the Aβ-induced toxicity [140]. Another recent study also indicates that inhibition of CypD is the basis for its neuroprotective properties in, for example, ischaemia/reperfusion injury [150]. However, it has been noted previously that CsA is a large, bulky compound with poor solubility in water and relatively poor bioavailability, especially in the brain [153], limiting the use of CsA as a drug molecule for neurodegenerative disorders. It also has to be taken into account that CsA exerts its function via several intracellular routes in addition to the inhibition of CypD [154]. Specifically, in the cytoplasm CsA binds to a complex of CypA (cyclophilin A) and calcineurin and thus blocks the peptidyl prolyl isomerase activity of CypA as well as the calcineurin phosphatase activity [155]. It was also noted that CypA can activate peroxiredoxins [156] and CsA could therefore influence cellular peroxide levels. CsA also blocks the JNK and p38 stress kinase signalling pathways, independently from its inhibition of calcineurin signalling [157]. CsA has also been found to inhibit Ca^{2+} entry into mitochondria by inhibition of the Ca^{2+}-uniporter in the mitochondrial inner membrane [158].

Considering these multilayered intracellular effects of CsA and that it is currently used as an immunosuppressant, which in itself would not be beneficial for a disease of the elderly, more research is required to decipher the intracellular effects of CsA. There is also a need for the identification of new modulators of mPTP formation in order to clarify under what circumstances each of them can act neuroprotectively, and at which stage their administration might be useful in neurodegenerative diseases like AD.
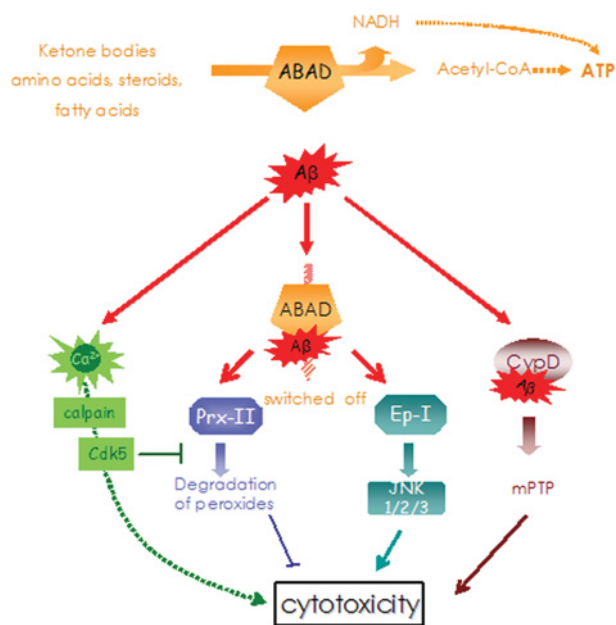
Figure 4   Summary of the consequences of intracellular Aβ accumulation

ABAD is involved in metabolism under normal conditions. In AD, intracellular Aβ increases and leads to the up-regulation of ABAD and CypD, as well as increases in intracellular Ca^{2+} levels. Binding of Aβ to ABAD inhibits its enzymatic activity and this interaction leads to the up-regulation of Prx-II and Ep-I. Prx-II is an antioxidant protein that can protect cells from cytotoxicity through the degradation of peroxides. Ep-I can activate JNK 1, 2 or 3 within the cell. This is associated with mitochondrial dysfunction and cell death. CypD is involved in the opening of the mPTP together with mitochondrial Ca^{2+}, which is involved in mechanisms of necrotic and apoptotic cell death. Among other processes, intracellular Ca^{2+} can activate Ca^{2+}-dependent kinases like calpain and, via the activation of the Cdk5, this could lead to the inhibition of Prx-II by its phosphorylation on Thr[89].

CONCLUSIONS

In conclusion, many studies have identified numerous receptor proteins that can bind to extracellular Aβ in all its different forms of both size and aggregation state. However, it is becoming increasingly clear that before this build-up of extracellular Aβ there are events that are occurring within cells. Of those described in the present review, we have concentrated on two molecules which have both been proven to bind directly to Aβ in the AD brain, both of which are centred on the action of the mitochondria. These studies have resulted in the identification of new signalling events that are occurring both potentially in the early stages of the disease and all the way through to its final stages (Figure 4). Therefore it could be envisioned that modulators that interfere with the interactions of Aβ with either CypD or ABAD could be potential therapeutic targets of the disease; however this will require imaginative new approaches. Recent possibilities could include the use of new mitochondrial-targeting compounds [159] or the use of novel compounds that prevent the mitochondrial uptake of Aβ in neuronal cells [160]. What is certain is that there are still many undiscovered events that are occurring due to the rise of intracellular Aβ levels, whether that is the Aβ-(1–40) or Aβ-(1–42) form, and the actual aggregation states at a particular binding site are still largely unknown. As such, new knowledge on these critical topics will result in the identification of potential new drug targets. Although the development of selective drugs for these targets may at first appear to be difficult, it is unlikely that it will prove intractable, and ingenious solutions to these problems will arise.

REFERENCES

1   Braak, H., Braak, E. and Bohl, J. (1993) Staging of Alzheimer-related cortical destruction. Eur. Neurol. **33**, 403–408
2   Mattson, M. P. (2004) Pathways towards and away from Alzheimer's disease. Nature **430**, 631–639
3   Crouch, P. J. and Harding, S.-M. E. (2008) Mechanisms of Aβ-mediated neurodegeneration in Alzheimer's disease. Int. J. Biochem. Cell Biol. **40**, 181–198
4   Haass, C. and Selkoe, D. J. (1993) Cellular processing of β-amyloid precursor protein and the genesis of amyloid β-peptide. Cell **75**, 1039–1042
5   Suzuki, N., Cheung, T. T., Cai, X. D., Odaka, A., Otvos, Jr, L., Eckman, C., Golde, T. E. and Younkin, S. G. (1994) An increased percentage of long amyloid β protein secreted by familial amyloid β protein precursor (β APP717) mutants. Science **264**, 1336–1340
6   Haass, C., Lemere, C. A., Capell, A., Citron, M., Seubert, P., Schenk, D., Lannfelt, L. and Selkoe, D. J. (1995) The Swedish mutation causes early-onset Alzheimer's disease by β-secretase cleavage within the secretory pathway. Nat. Med. **1**, 1291–1296
7   Crawford, F., Freeman, M., Town, T., Fallin, D., Gold, M., Duara, R. and Mullan, M. (1999) No genetic association between polymorphisms in the *Tau* gene and Alzheimer's disease in clinic- or population-based samples. Neurosci. Lett. **266**, 193–196
8   Blurton-Jones, M. and Laferla, F. (2006) Pathways by which Aβ facilitates tau pathology. Curr. Alzheimer Res. **3**, 437–448.
9   Saunders, A. M., Strittmatter, W. J., Schmechel, D., George-Hyslop, P. H., Pericak-Vance, M. A., Joo, S. H., Rosi, B. L., Gusella, J. F., Crapper-MacLachlan, D. R., Alberts, M. J. et al. (1993) Association of apolipoprotein E allele ε4 with late-onset familial and sporadic Alzheimer's disease. Neurology **43**, 1467–1472
10 Kim, J. and Basak, J. M. (2009) The role of apolipoprotein E in Alzheimer's disease. Neuron **63**, 287–303
11 Rogaeva, E., Meng, Y., Lee, J. H., Gu, Y., Kawarai, T., Zou, F., Katayama, T., Baldwin, C. T., Cheng, R., Hasegawa, H. et al. (2007) The neuronal sortilin-related receptor SORL1 is genetically associated with Alzheimer disease. Nat. Genet. **39**, 168–177
12 Zhao, Y., Cui, J. G. and Lukiw, W. J. (2007) Reduction of sortilin-1 in Alzheimer hippocampus and in cytokine-stressed human brain cells. Neuroreport **18**, 1187–1191
13 Seshadri, S., Beiser, A., Selhub, J., Jacques, P. F., Rosenberg, I. H., D'Agostino, R. B., Wilson, P. W. and Wolf, P. A. (2002) Plasma homocysteine as a risk factor for dementia and Alzheimer's disease. N. Engl. J. Med. **346**, 476–483
14 Pacheco-Quinto, J., Rodriguez de Turco, E. B., DeRosa, S., Howard, A., Cruz-Sanchez, F., Sambamurti, K., Refolo, L., Petanceska, S. and Pappolla, M. A. (2006) Hyperhomocysteinemic Alzheimer's mouse model of amyloidosis shows increased brain amyloid β peptide levels. Neurobiol. Dis. **22**, 651–656
15 Harold, D., Abraham, R., Hollingworth, P., Sims, R., Gerrish, A., Hamshere, M. L., Pahwa, J. S., Moskvina, V., Dowzell, K., Williams, A. et al. (2009) Genome-wide association study identifies variants at CLU and PICALM associated with Alzheimer's disease. Nat. Genet. **41**, 1088–1093
16 Selkoe, D. J., Yamazaki, T., Citron, M., Podlisny, M. B., Koo, E. H., Teplow, D. B. and Haass, C. (1996) The role of APP processing and trafficking pathways in the formation of amyloid β-Protein. Ann. N.Y. Acad. Sci. **777**, 57–64
17 Finder, V. H. and Glockshuber, R. (2007) Amyloid-β aggregation. Neurodegener. Dis. **4**, 13–27
18 Walsh, D. M. and Selkoe, D. J. (2007) Aβ oligomers: a decade of discovery. J. Neurochem. **101**, 1172–1184
19 LaFerla, F. M., Green, K. N. and Oddo, S. (2007) Intracellular amyloid-β in Alzheimer's disease. Nat. Rev. Neurosci. **8**, 499–509
20 Blass, J. P. (2000) The mitochondrial spiral: an adequate cause of dementia in the Alzheimer's syndrome. Ann. N.Y. Acad. Sci. **924**, 170–183
21 Lin, M. T. and Beal, M. F. (2006) Mitochondrial dysfunction and oxidative stress in neurodegenerative diseases. Nature **443**, 787–795
22 Chen, J. X. and Yan, S. D. (2007) Amyloid-β-induced mitochondrial dysfunction. J. Alzheimers Dis. **12**, 177–184
23 Brody, D. L. and Holtzman, D. M. (2008) Active and passive immunotherapy for neurodegenerative disorders. Annu. Rev. Neurosci. **31**, 175–193

24 Yang, A. J., Chandswangbhuvana, D., Margol, L. and Glabe, C. G. (1998) Loss of endosomal/lysosomal membrane impermeability is an early event in amyloid Aβ1–42 pathogenesis. J. Neurosci. Res. **52**, 691–698

25 Bückig, A., Tikkanen, R., Herzog, V. and Schmitz, A. (2002) Cytosolic and nuclear aggregation of the amyloid β-peptide following its expression in the endoplasmic reticulum. Histochem. Cell. Biol. **118**, 353–360

26 Takahashi, R. H., Milner, T. A., Li, F., Nam, E. E., Edgar, M. A., Yamaguchi, H., Beal, M. F., Xu, H., Greengard, P. and Gouras, G. K. (2002) Intraneuronal alzheimer Aβ42 accumulates in multivesicular bodies and is associated with synaptic pathology. Am. J. Pathol. **161**, 1869–1879

27 Almeida, C. G., Takahashi, R. H. and Gouras, G. K. (2006) β-Amyloid accumulation impairs multivesicular body sorting by inhibiting the ubiquitin-proteasome system. J. Neurosci. **26**, 4277–4288

28 Haass, C., Koo, E. H., Mellon, A., Hung, A. Y. and Selkoe, D. J. (1992) Targeting of cell-surface β-amyloid precursor protein to lysosomes: alternative processing into amyloid-bearing fragments. Nature **357**, 500–503

29 Andersen, O. M., Reiche, J., Schmidt, V., Gotthardt, M., Spoelgen, R., Behlke, J., von Arnim, C. A., Breiderhoff, T., Jansen, P., Wu, X. et al. (2005) Neuronal sorting protein-related receptor sorLA/LR11 regulates processing of the amyloid precursor protein. Proc. Natl. Acad. Sci. U.S.A. **102**, 13461–13466

30 Anandatheerthavarada, H. K., Biswas, G., Robin, M. A. and Avadhani, N. G. (2003) Mitochondrial targeting and a novel transmembrane arrest of Alzheimer's amyloid precursor protein impairs mitochondrial function in neuronal cells. J. Cell. Biol **161**, 41–54

31 Keil, U., Bonert, A., Marques, C. A., Scherping, I., Weyermann, J., Strosznajder, J. B., Müller-Spahn, F., Haass, C., Czech, C., Pradier, L. et al. (2004) Amyloid β-induced changes in nitric oxide production and mitochondrial activity lead to apoptosis. J. Biol. Chem. **279**, 50310–50320

32 Haass, C. and Steiner, H. (2002) Alzheimer disease γ-secretase: a complex story of GxGD-type presenilin proteases. Trends Cell Biol. **12**, 556–562

33 Khvotchev, M. and Sudhof, T. C. (2004) Proteolytic processing of amyloid-β precursor protein by secretases does not require cell surface transport. J. Biol. Chem. **279**, 47101–47108

34 Mathews, P. M., Jiang, Y., Schmidt, S. D., Grbovic, O. M., Mercken, M. and Nixon, R. A. (2002) Calpain activity regulates the cell surface distribution of amyloid precursor protein. Inhibition of calpains enhances endosomal generation of β-cleaved C-terminal APP fragments. J. Biol. Chem. **277**, 36415–36424

35 Yamazaki, T., Koo, E. H. and Selkoe, D. J. (1996) Trafficking of cell-surface amyloid β-protein precursor. II: Endocytosis, recycling and lysosomal targeting detected by immunolocalization. J. Cell Sci. **109**, 999–1008

36 Arispe, N., Rojas, E. and Pollard, H. B. (1993) Alzheimer disease amyloid β protein forms calcium channels in bilayer membranes: blockade by tromethamine and aluminum. Proc. Natl. Acad. Sci. U.S.A. **90**, 567–571

37 Eckert, G. P., Wood, W. G. and Muller, W. E. (2001) Effects of aging and β-amyloid on the properties of brain synaptic and mitochondrial membranes. J. Neural. Transm. **108**, 1051–1064

38 Kremer, J. J., Sklansky, D. J. and Murphy, R. M. (2001) Profile of changes in lipid bilayer structure caused by β-amyloid peptide. Biochemistry **40**, 8563–8571

39 Gouras, G. K., Tsai, J., Naslund, J., Vincent, B., Edgar, M., Checler, F., Greenfield, J. P., Haroutunian, V., Buxbaum, J. D., Xu, H. et al. (2000) Intraneuronal Aβ42 accumulation in human brain. Am. J. Pathol. **156**, 15–20

40 Nagele, R. G., D'Andrea, M. R., Anderson, W. J. and Wang, H. Y. (2002) Intracellular accumulation of β-amyloid1–42 in neurons is facilitated by the α7 nicotinic acetylcholine receptor in Alzheimer's disease. Neuroscience **110**, 199–211

41 Zhang, Y., McLaughlin, R., Goodyer, C. and LeBlanc, A. (2002) Selective cytotoxicity of intracellular amyloid β peptide1–42 through p53 and Bax in cultured primary human neurons. J. Cell Biol. **156**, 519–529

42 Kuperstein, F. and Yavin, E. (2002) ERK activation and nuclear translocation in amyloid-β peptide- and iron-stressed neuronal cell cultures. Eur. J. Neurosci. **16**, 44–54

43 Park, H. J., Kim, S. S., Kang, S. and Rhim, H. (2009) Intracellular Aβ and C99 aggregates induce mitochondria-dependent cell death in human neuroglioma H4 cells through recruitment of the 20S proteasome subunits. Brain Res. **1273**, 1–8

44 Yoon, E. J., Park, H. J., Kim, G. Y., Cho, H. M., Choi, J. H., Park, H. Y., Jang, J. Y., Rhim, H. S. and Kang, S. M. (2009) Intracellular amyloid β interacts with SOD1 and impairs the enzymatic activity of SOD1: implications for the pathogenesis of amyotrophic lateral sclerosis. Exp. Mol. Med. **41**, 611–617

45 Lustbader, J. W., Cirilli, M., Lin, C., Xu, H. W., Takuma, K., Wang, N., Caspersen, C., Chen, X., Pollak, S., Chaney, M. et al. (2004) ABAD directly links Aβ to mitochondrial toxicity in Alzheimer's disease. Science **304**, 448–452

46 Caspersen, C., Wang, N., Yao, J., Sosunov, A., Chen, X., Lustbader, J. W., Xu, H. W., Stern, D., McKhann, G. and Yan, S. D. (2005) Mitochondrial Aβ: a potential focal point for neuronal metabolic dysfunction in Alzheimer's disease. FASEB J. **19**, 2040–2041

47 Devi, L., Prabhu, B. M., Galati, D. F., Avadhani, N. G. and Anandatheerthavarada, H. K. (2006) Accumulation of amyloid precursor protein in the mitochondrial import channels of human Alzheimer's disease brain is associated with mitochondrial dysfunction. J. Neurosci. **26**, 9057–9068

48 Hansson Petersen, C. A., Alikhani, N., Behbahani, H., Wiehager, B., Pavlov, P. F., Alafuzoff, I., Leinonen, V., Ito, A., Winblad, B., Glaser, E. and Ankarcrona, M. (2008) The amyloid β-peptide is imported into mitochondria via the TOM import machinery and localized to mitochondrial cristae. Proc. Natl. Acad. Sci. U.S.A. **105**, 13145–13150

49 Falkevall, A., Alikhani, N., Bhushan, S., Pavlov, P. F., Busch, K., Johnson, K. A., Eneqvist, T., Tjernberg, L., Ankarcrona, M. and Glaser, E. (2006) Degradation of the amyloid β-protein by the novel mitochondrial peptidasome, PreP. J. Biol. Chem. **281**, 29096–29104

50 Vepsalainen, S., Hiltunen, M., Helisalmi, S., Wang, J., van Groen, T., Tanila, H. and Soininen, H. (2008) Increased expression of Aβ-degrading enzyme IDE in the cortex of transgenic mice with Alzheimer's disease-like neuropathology. Neurosci. Lett. **438**, 216–220

51 Qiu, W. Q., Walsh, D. M., Ye, Z., Vekrellis, K., Zhang, J., Podlisny, M. B., Rosner, M. R., Safavi, A., Hersh, L. B. and Selkoe, D. J. (1998) Insulin-degrading enzyme regulates extracellular levels of amyloid β-protein by degradation. J. Biol. Chem. **273**, 32730–32738

52 Leissring, M. A., Farris, W., Wu, X., Christodoulou, D. C., Haigis, M. C., Guarente, L. and Selkoe, D. J. (2004) Alternative translation initiation generates a novel isoform of insulin-degrading enzyme targeted to mitochondria. Biochem. J. **383**, 439–446

53 Llovera, R. E., de Tullio, M., Alonso, L. G., Leissring, M. A., Kaufman, S. B., Roher, A. E., de Prat Gay, G., Morelli, L. and Castano, E. M. (2008) The catalytic domain of insulin-degrading enzyme forms a denaturant-resistant complex with amyloid β peptide: implications for Alzheimer disease pathogenesis. J. Biol. Chem. **283**, 17039–17048

54 Cordes, C. M., Bennett, R. G., Siford, G. L. and Hamel, F. G. (2009) Nitric oxide inhibits insulin-degrading enzyme activity and function through S-nitrosylation. Biochem. Pharmacol. **77**, 1064–1073

55 Uehara, T., Nakamura, T., Yao, D., Shi, Z. Q., Gu, Z., Ma, Y., Masliah, E., Nomura, Y. and Lipton, S. A. (2006) S-nitrosylated protein-disulphide isomerase links protein misfolding to neurodegeneration. Nature **441**, 513–517

56 Cho, D. H., Nakamura, T., Fang, J., Cieplak, P., Godzik, A., Gu, Z. and Lipton, S. A. (2009) S-nitrosylation of Drp1 mediates β-amyloid-related mitochondrial fission and neuronal injury. Science **324**, 102–105

57 Vepsalainen, S., Parkinson, M., Helisalmi, S., Mannermaa, A., Soininen, H., Tanzi, R. E., Bertram, L. and Hiltunen, M. (2007) Insulin-degrading enzyme is genetically associated with Alzheimer's disease in the Finnish population. J. Med. Genet. **44**, 606–608

58 Kim, M., Hersh, L. B., Leissring, M. A., Ingelsson, M., Matsui, T., Farris, W., Lu, A., Hyman, B. T., Selkoe, D. J., Bertram, L. and Tanzi, R. E. (2007) Decreased catalytic activity of the insulin-degrading enzyme in chromosome 10-linked Alzheimer disease families. J. Biol. Chem. **282**, 7825–7832

59 Anandatheerthavarada, H. K., Biswas, G., Mullick, J., Sepuri, N. B., Otvos, L., Pain, D. and Avadhani, N. G. (1999) Dual targeting of cytochrome P4502B1 to endoplasmic reticulum and mitochondria involves a novel signal activation by cyclic AMP-dependent phosphorylation at Ser128. EMBO. J. **18**, 5494–5504

60 Hansson, C. A., Frykman, S., Farmery, M. R., Tjernberg, L. O., Nilsberth, C., Pursglove, S. E., Ito, A., Winblad, B., Cowburn, R. F., Thyberg, J. and Ankarcrona, M. (2004) Nicastrin, presenilin, APH-1, and PEN-2 form active γ-secretase complexes in mitochondria. J. Biol. Chem. **279**, 51654–51660

61 Wolfe, M. S. and Kopan, R. (2004) Intramembrane proteolysis: theme and variations. Science **305**, 1119–1123

62 Park, H. J., Seong, Y. M., Choi, J. Y., Kang, S. and Rhim, H. (2004) Alzheimer's disease-associated amyloid β interacts with the human serine protease HtrA2/Omi. Neurosci. Lett. **357**, 63–67

63 Park, H. J., Kim, S. S., Seong, Y. M., Kim, K. H., Goo, H. G., Yoon, E. J., Min, D. S., Kang, S. and Rhim, H. (2006) β-Amyloid precursor protein is a direct cleavage target of HtrA2 serine protease: implications for the physiological function of HtrA2 in the mitochondria. J. Biol. Chem. **281**, 34277–34287

64 Rusiñol, A. E., Cui, Z., Chen, M. H. and Vance, J. E. (1994) A unique mitochondria-associated membrane fraction from rat liver has a high capacity for lipid synthesis and contains pre-Golgi secretory proteins including nascent lipoproteins. J. Biol. Chem. **269**, 27494–27502

65 Stone, S. J., Levin, M. C., Zhou, P., Han, J., Walther, T. C. and Farese, R. V. (2009) The endoplasmic reticulum enzyme DGAT2 is found in mitochondria-associated membranes and has a mitochondrial targeting signal that promotes its association with mitochondria. J. Biol. Chem. **284**, 5352–5361

66 Area-Gomez, E., de Groof, A. J., Boldogh, I., Bird, T. D., Gibson, G. E., Koehler, C. M., Yu, W. H., Duff, K. E., Yaffe, M. P., Pon, L. A. and Schon, E. A. (2009) Presenilins are enriched in endoplasmic reticulum membranes associated with mitochondria. Am. J. Pathol. **175**, 1810–1816

67   Giorgi, C., De Stefani, D., Bononi, A., Rizzuto, R. and Pinton, P. (2009) Structural and functional link between the mitochondrial network and the endoplasmic reticulum. Int. J. Biochem. Cell Biol. **41**, 1817–1827

68   Wang, X., Su, B., Lee, H.-g., Li, X., Perry, G., Smith, M. A. and Zhu, X. (2009) Impaired balance of mitochondrial fission and fusion in Alzheimer's disease. J. Neurosci. **29**, 9090–9103

69   Bekris, L. M., Galloway, N. M., Montine, T. J., Schellenberg, G. D. and Yu, C.-E. (2009) APOE mRNA and protein expression in postmortem brain are modulated by an extended haplotype structure, Am. J. Med. Genet. B Neuropsychiatr. Genet., doi:10.1002/ajmg.b.30993

70   Yu, C. E., Seltman, H., Peskind, E. R., Galloway, N., Zhou, P. X., Rosenthal, E., Wijsman, E. M., Tsuang, D. W., Devlin, B. and Schellenberg, G. D. (2007) Comprehensive analysis of APOE and selected proximate markers for late-onset Alzheimer's disease: patterns of linkage disequilibrium and disease/marker association. Genomics **89**, 655–665

71   Bekris, L. M., Millard, S. P., Galloway, N. M., Vuletic, S., Albers, J. J., Li, G., Galasko, D. R., DeCarli, C., Farlow, M. R., Clark, C. M. et al. (2008) Multiple SNPs within and surrounding the apolipoprotein E gene influence cerebrospinal fluid apolipoprotein E protein levels. J. Alzheimers Dis. **13**, 255–266

72   Shoji, M., Iwakami, N., Takeuchi, S., Waragai, M., Suzuki, M., Kanazawa, I., Lippa, C. F., Ono, S. and Okazawa, H. (2000) JNK activation is associated with intracellular β-amyloid accumulation. Brain Res. Mol. Brain Res. **85**, 221–233

73   Kaltschmidt, B., Uherek, M., Volk, B., Baeuerle, P. A. and Kaltschmidt, C. (1997) Transcription factor NF-κB is activated in primary neurons by amyloid β peptides and in neurons surrounding early plaques from patients with Alzheimer disease. Proc. Natl. Acad. Sci. U.S.A. **94**, 2642–2647

74   Kuwako, K.-I., Nishimura, I., Uetsuki, T., Saido, T. C. and Yoshikawa, K. (2002) Activation of calpain in cultured neurons overexpressing Alzheimer amyloid precursor protein. Brain Res. Mol. Brain Res. **107**, 166–175

75   Biswas, S. C., Shi, Y., Vonsattel, J. P., Leung, C. L., Troy, C. M. and Greene, L. A. (2007) Bim is elevated in Alzheimer's disease neurons and is required for β-amyloid-induced neuronal apoptosis. J. Neurosci. **27**, 893–900

76   Lee, H.-K., Kumar, P., Fu, Q., Rosen, K. M. and Querfurth, H. W. (2009) The Insulin/Akt signaling pathway is targeted by intracellular β-amyloid. Mol. Biol. Cell **20**, 1533–1544

77   Arvanitis, D. N., Ducatenzeiler, A., Ou, J. N., Grodstein, E., Andrews, S. D., Tendulkar, S. R., Ribeiro-da-Silva, A., Szyf, M. and Cuello, A. C. (2007) High intracellular concentrations of amyloid-β block nuclear translocation of phosphorylated CREB. J. Neurochem. **103**, 216–228

78   Yan, S. D. and Stern, D. M. (2005) Mitochondrial dysfunction and Alzheimer's disease: role of amyloid-β peptide alcohol dehydrogenase (ABAD). Int. J. Exp. Pathol. **86**, 161–171

79   Ryder, J., Su, Y. and Ni, B. (2004) Akt/GSK3β serine/threonine kinases: evidence for a signalling pathway mediated by familial Alzheimer's disease mutations. Cell Signal. **16**, 187–200

80   Martin, D., Salinas, M., Lopez-Valdaliso, R., Serrano, E., Recuero, M. and Cuadrado, A. (2001) Effect of the Alzheimer amyloid fragment Aβ(25–35) on Akt/PKB kinase and survival of PC12 cells. J. Neurochem. **78**, 1000–1008

81   Zhao, L., Teter, B., Morihara, T., Lim, G. P., Ambegaokar, S. S., Ubeda, O. J., Frautschy, S. A. and Cole, G. M. (2004) Insulin-degrading enzyme as a downstream target of insulin receptor signaling cascade: implications for Alzheimer's disease intervention. J. Neurosci. **24**, 11120–11126

81a Deng, H. X., Hentati, A., Tainer, J. A. Iqbal, Z., Cayabyab, A., Hung, W. Y. Getzoff, E. D., Hu, P., Herzfeldt, B., Roos, R. P. et al. (1993) Amyotrophic lateral sclerosis and structural defects in Cu,Zn superoxide dismutase. Science **261**, 1047–1051

82   Butterfield, D. A., Drake, J., Pocernich, C. and Castegna, A. (2001) Evidence of oxidative damage in Alzheimer's disease brain: central role for amyloid β-peptide. Trends Mol. Med. **7**, 548–554

83   Liu, J., Head, E., Gharib, A. M., Yuan, W., Ingersoll, R. T., Hagen, T. M., Cotman, C. W. and Ames, B. N. (2002) Memory loss in old rats is associated with brain mitochondrial decay and RNA/DNA oxidation: partial reversal by feeding acetyl-L-carnitine and/or R-α-lipoic acid. Proc. Natl. Acad. Sci. U.S.A. **99**, 2356–2361

84   Angeletti, B., Waldron, K. J., Freeman, K. B., Bawagan, H., Hussain, I., Miller, C. C., Lau, K. F., Tennant, M. E., Dennison, C., Robinson, N. J. and Dingwall, C. (2005) BACE1 cytoplasmic domain interacts with the copper chaperone for superoxide dismutase-1 and binds copper. J. Biol. Chem. **280**, 17930–17937

85   Li, F., Calingasan, N. Y., Yu, F., Mauck, W. M., Toidze, M., Almeida, C. G., Takahashi, R. H., Carlson, G. A., Beal, M. F., Lin, M. T. and Gouras, G. K. (2004) Increased plaque burden in brains of APP mutant MnSOD heterozygous knockout mice. J. Neurochem. **89**, 1308–1312

86   Dumont, M., Wille, E., Stack, C., Calingasan, N. Y., Beal, M. F. and Lin, M. T. (2009) Reduction of oxidative stress, amyloid deposition, and memory deficit by manganese superoxide dismutase overexpression in a transgenic mouse model of Alzheimer's disease. FASEB J. **23**, 2459–2466

87   Massaad, C. A., Washington, T. M., Pautler, R. G. and Klann, E. (2009) Overexpression of SOD-2 reduces hippocampal superoxide and prevents memory deficits in a mouse model of Alzheimer's disease. Proc. Natl. Acad. Sci. U.S.A. **106**, 13576–13581

88   Milton, N. G. (1999) Amyloid-β binds catalase with high affinity and inhibits hydrogen peroxide breakdown. Biochem. J. **344**, 293–296

89   Milton, N. G. and Harris, J. R. (2009) Polymorphism of amyloid-β fibrils and its effects on human erythrocyte catalase binding. Micron **40**, 800–810

90   Milton, N. G. N. (2001) Inhibition of catalase activity with 3-amino-triazole enhances the cytotoxicity of the Alzheimer's amyloid-β Peptide. Neurotoxicology **22**, 767–774

91   Milton, N. G. N., Mayor, N. P. and Rawlinson, J. (2001) Identification of amyloid-β binding sites using an antisense peptide approach. Neuroreport **12**, 2561–2566

92   Yan, S. D., Fu, J., Soto, C., Chen, X., Zhu, H., Al-Mohanna, F., Collison, K., Zhu, A., Stern, E., Saido, T. et al. (1997) An intracellular protein that binds amyloid-β peptide and mediates neurotoxicity in Alzheimer's disease. Nature **389**, 689–695

93   He, X.-Y., Schulz, H. and Yang, S.-Y. (1998) A human brain L-3-hydroxyacyl-coenzyme A dehydrogenase is identical to an amyloid β-peptide-binding protein involved in Alzheimer's disease. J. Biol. Chem. **273**, 10741–10746

94   Oppermann, U. C. T., Salim, S., Tjernberg, L. O., Terenius, L. and Jornvall, H. (1999) Binding of amyloid β-peptide to mitochondrial hydroxyacyl-CoA dehydrogenase (ERAB): regulation of an SDR enzyme activity with implications for apoptosis in Alzheimer's disease. FEBS Lett. **451**, 238–242

95   He, X.-Y., Merz, G., Mehta, P., Schulz, H. and Yang, S.-Y. (1999) Human brain short chain L-3-hydroxyacyl coenzyme A dehydrogenase is a single-domain multifunctional enzyme: characterization of a novel 17-β-hydroxysteroid dehydrogenase. J. Biol. Chem. **274**, 15014–15019

96   Frackowiak, J., Mazur-Kolecka, B., Kaczmarski, W. and Dickson, D. (2001) Deposition of Alzheimer's vascular amyloid-β is associated with decreased expression of brain L-3-hydroxyacyl-coenzyme A dehydrogenase (ERAB). Brain. Res. **907**, 44–53

97   He, X. Y., Yang, Y. Z., Schulz, H. and Yang, S. Y. (2000) Intrinsic alcohol dehydrogenase and hydroxysteroid dehydrogenase activities of human mitochondrial short-chain L-3-hydroxyacyl-CoA dehydrogenase. Biochem. J. **345**, 139–143

98   Yang, S.-Y., He, X.-Y. and Schulz, H. (2005) 3-Hydroxyacyl-CoA dehydrogenase and short chain 3-hydroxyacyl-CoA dehydrogenase in human health and disease. FEBS J. **272**, 4874–4883

99   Kissinger, C. R., Rejto, P. A., Pelletier, L. A., Thomson, J. A., Showalter, R. E., Abreo, M. A., Agree, C. S., Margosiak, S., Meng, J. J., Aust, R. M. et al. (2004) Crystal structure of human ABAD/HSD10 with a bound inhibitor: implications for design of Alzheimer's disease therapeutics. J. Mol. Biol. **342**, 943–952

100 Froemming, M. K. and Sames, D. (2007) Harnessing functional plasticity of enzymes: a fluorogenic probe for imaging 17β-HSD10 dehydrogenase, an enzyme involved in Alzheimer's and Parkinson's diseases. J. Am. Chem. Soc. **129**, 14518–14522

101 Yan, S. D., Shi, Y., Zhu, A., Fu, J., Zhu, H., Zhu, Y., Gibson, L., Stern, E., Collison, K., Al-Mohanna, F. et al. (1999) Role of ERAB/L-3-hydroxyacyl-coenzyme A dehydrogenase type II activity in Aβ-induced cytotoxicity. J. Biol. Chem. **274**, 2145–2156

102 Powell, A. J., Read, J. A., Banfield, M. J., Gunn-Moore, F., Yan, S. D., Lustbader, J., Stern, A. R., Stern, D. M. and Brady, R. L. (2000) Recognition of structurally diverse substrates by type II 3-hydroxyacyl-CoA dehydrogenase (HADH II)/amyloid-β binding alcohol dehydrogenase (ABAD). J. Molec. Biol. **303**, 311–327

103 Du Yan, S., Zhu, Y., Stern, E. D., Hwang, Y. C., Hori, O., Ogawa, S., Frosch, M. P., Connolly, Jr., E. S., McTaggert, R., Pinsky, D. J. et al. (2000) Amyloid β-peptide-binding alcohol dehydrogenase is a component of the cellular response to nutritional stress. J. Biol. Chem. **275**, 27100–27109

104 McGonigal, G., Thomas, B., McQuade, C., Starr, J. M., MacLennan, W. J. and Whalley, L. J. (1993) Epidemiology of Alzheimer's presenile dementia in Scotland, 1974–88. Br. Med. J. **306**, 680–683

105 Tang, M.-X., Jacobs, D., Stern, Y., Marder, K., Schofield, P., Gurland, B., Andrews, H. and Mayeux, R. (1996) Effect of oestrogen during menopause on risk and age at onset of Alzheimer's disease. Lancet **348**, 429–432

106 He, X.-Y., Wegiel, J., Yang, Y.-Z., Pullarkat, R., Schulz, H. and Yang, S.-Y. (2005) Type 10 17β-hydroxysteroid dehydrogenase catalyzing the oxidation of steroid modulators of γ-aminobutyric acid type A receptors. Mol. Cell. Endocrinol. **229**, 111–117

107 Ofman, R., Ruiter, J. P., Feenstra, M., Duran, M., Poll-The, B. T., Zschocke, J., Ensenauer, R., Lehnert, W., Sass, J. O., Sperl, W. and Wanders, R. J. (2003) 2-Methyl-3-hydroxybutyryl-CoA dehydrogenase deficiency is caused by mutations in the HADH2 gene. Am. J. Hum. Genet. **72**, 1300–1307

108 Tieu, K., Perier, C., Vila, M., Caspersen, C., Zhang, H. P., Teismann, P., Jackson-Lewis, V., Stern, D. M., Yan, S. D. and Przedborski, S. (2004) 3-hydroxyacyl-CoA dehydrogenase II protects in a model of Parkinson's disease. Ann. Neurol. **56**, 51–60

109 Marques, A. T., Fernandes, P. A. and Ramos, M. J. (2008) Molecular dynamics simulations of the amyloid-β binding alcohol dehydrogenase (ABAD) enzyme. Bioorg. Med. Chem. **16**, 9511–9518

110 Liu, X., Deng, G., Chu, X., Li, N., Wu, L. and Li, D. (2007) Formation of an enolate intermediate is required for the reaction catalyzed by 3-hydroxyacyl-CoA dehydrogenase. Bioorg. Med. Chem. Lett. **17**, 3187–3190

111 Xie, Y., Deng, S., Chen, Z., Yan, S. and Landry, D. W. (2006) Identification of small-molecule inhibitors of the A-β-ABAD interaction. Bioorg. Med. Chem. Lett. **16**, 4657–4660

112 Yan, Y., Liu, Y., Sorci, M., Belfort, G., Lustbader, J. W., Yan, S. S. and Wang, C. (2007) Surface plasmon resonance and nuclear magnetic resonance studies of ABAD–Aβ interaction. Biochemistry **46**, 1724–1731

113 He, X.-Y., Wen, G.-Y., Merz, G., Lin, D., Yang, Y.-Z., Mehta, P., Schulz, H. and Yang, S.-Y. (2002) Abundant type 10 17β-hydroxysteroid dehydrogenase in the hippocampus of mouse Alzheimer's disease model. Brain Res. Mol. Brain Res. **99**, 46–53

114 Yao, J., Irwin, R. W., Zhao, L., Nilsen, J., Hamilton, R. T. and Brinton, R. D. (2009) Mitochondrial bioenergetic deficit precedes Alzheimer's pathology in female mouse model of Alzheimer's disease. Proc. Natl. Acad. Sci. U.S.A. **106**, 14670–14675

115 Sayre, L. M., Zelasko, D. A., Harris, P. L., Perry, G., Salomon, R. G. and Smith, M. A. (1997) 4-Hydroxynonenal-derived advanced lipid peroxidation end products are increased in Alzheimer's disease. J. Neurochem. **68**, 2092–2097

116 Delibas, N., Ozcankaya, R. and Altuntas, I. (2002) Clinical importance of erythrocyte malondialdehyde levels as a marker for cognitive deterioration in patients with dementia of Alzheimer type: a repeated study in 5-year interval. Clin. Biochem. **35**, 137–141

117 Murakami, Y., Ohsawa, I., Kasahara, T. and Ohta, S. (2009) Cytoprotective role of mitochondrial amyloid β peptide-binding alcohol dehydrogenase against a cytotoxic aldehyde. Neurobiol. Aging **30**, 325–329

118 Takuma, K., Yao, J., Huang, J., Xu, H., Chen, X., Luddy, J., Trillat, A. C., Stern, D. M., Arancio, O. and Yan, S. S. (2005) ABAD enhances Aβ-induced cell stress via mitochondrial dysfunction. FASEB J. **19**, 597–598

119 Yao, J., Taylor, M., Davey, F., Ren, Y., Aiton, J., Coote, P., Fang, F., Chen, J. X., Yan, S. D. and Gunn-Moore, F. J. (2007) Interaction of amyloid binding alcohol dehydrogenase/Aβ mediates up-regulation of peroxiredoxin II in the brains of Alzheimer's disease patients and a transgenic Alzheimer's disease mouse model. Mol. Cell Neurosci. **35**, 377–382

120 Qu, D., Rashidian, J., Mount, M. P., Aleyasin, H., Parsanejad, M., Lira, A., Haque, E., Zhang, Y., Callaghan, S., Daigle, M. et al. (2007) Role of Cdk5-mediated phosphorylation of Prx2 in MPTP toxicity and Parkinson's disease. Neuron **55**, 37–52

121 Ren, Y., Xu, H. W., Davey, F., Taylor, M., Aiton, J., Coote, P., Fang, F., Yao, J., Chen, D., Chen, J. X. et al. (2008) Endophilin I expression is increased in the brains of Alzheimer disease patients. J. Biol. Chem. **283**, 5685–5691

122 Schmidt, A., Wolde, M., Thiele, C., Fest, W., Kratzin, H., Podtelejnikov, A. V., Witke, W., Huttner, W. B. and Soling, H. D. (1999) Endophilin I mediates synaptic vesicle formation by transfer of arachidonate to lysophosphatidic acid. Nature **401**, 133–141

123 Ramjaun, A. R., Angers, A., Legendre-Guillemin, V., Tong, X.-K. and McPherson, P. S. (2001) Endophilin regulates JNK activation through its interaction with the germinal center kinase-like kinase. J. Biol. Chem. **276**, 28913–28919

124 Lagalwar, S., Guillozet-Bongaarts, A. L., Berry, R. W. and Binder, L. I. (2006) Formation of phospho-SAPK/JNK granules in the hippocampus is an early event in Alzheimer disease. J. Neuropathol. Exp. Neurol. **65**, 455–464

125 Marques, C. A., Keil, U., Bonert, A., Steiner, B., Haass, C., Muller, W. E. and Eckert, A. (2003) Neurotoxic mechanisms caused by the Alzheimer's disease-linked Swedish amyloid precursor protein mutation: oxidative stress, caspases, and the JNK pathway. J. Biol. Chem. **278**, 28294–28302

126 Troy, C. M., Rabacchi, S. A., Xu, Z., Maroney, A. C., Connors, T. J., Shelanski, M. L. and Greene, L. A. (2001) β-Amyloid-induced neuronal apoptosis requires c-Jun N-terminal kinase activation. J. Neurochem. **77**, 157–164

127 Smith, W. W., Norton, D. D., Gorospe, M., Jiang, H., Nemoto, S., Holbrook, N. J., Finkel, T. and Kusiak, J. W. (2005) Phosphorylation of p66Shc and forkhead proteins mediates Aβ toxicity. J. Cell Biol. **169**, 331–339

128 Connern, C. P. and Halestrap, A. P. (1994) Recruitment of mitochondrial cyclophilin to the mitochondrial inner membrane under conditions of oxidative stress that enhance the opening of a calcium-sensitive non-specific channel. Biochem. J. **302**, 321–324

129 Leung, A. W. and Halestrap, A. P. (2008) Recent progress in elucidating the molecular mechanism of the mitochondrial permeability transition pore. Biochim. Biophys. Acta **1777**, 946–952

130 Halestrap, A. P. (2009) What is the mitochondrial permeability transition pore? J. Mol. Cell. Cardiol. **46**, 821–831

131 Halestrap, A. (2005) Biochemistry: a pore way to die. Nature **434**, 578–579

132 Basso, E., Petronilli, V., Forte, M. A. and Bernardi, P. (2008) Phosphate is essential for inhibition of the mitochondrial permeability transition pore by cyclosporin A and by cyclophilin D ablation. J. Biol. Chem. **283**, 26307–26311

133 Halestrap, A. P., Woodfield, K.-Y. and Connern, C. P. (1997) Oxidative stress, thiol reagents, and membrane potential modulate the mitochondrial permeability transition by affecting nucleotide binding to the adenine nucleotide translocase. J. Biol. Chem. **272**, 3346–3354

134 Nakagawa, T., Shimizu, S., Watanabe, T., Yamaguchi, O., Otsu, K., Yamagata, H., Inohara, H., Kubo, T. and Tsujimoto, Y. (2005) Cyclophilin D-dependent mitochondrial permeability transition regulates some necrotic but not apoptotic cell death. Nature **434**, 652–658

135 Basso, E., Fante, L., Fowlkes, J., Petronilli, V., Forte, M. A. and Bernardi, P. (2005) Properties of the permeability transition pore in mitochondria devoid of cyclophilin D. J. Biol. Chem. **280**, 18558–18561

136 Schinzel, A. C., Takeuchi, O., Huang, Z., Fisher, J. K., Zhou, Z., Rubens, J., Hetz, C., Danial, N. N., Moskowitz, M. A. and Korsmeyer, S. J. (2005) Cyclophilin D is a component of mitochondrial permeability transition and mediates neuronal cell death after focal cerebral ischemia. Proc. Natl. Acad. Sci. U.S.A. **102**, 12005–12010

137 Baines, C. P., Kaiser, R. A., Purcell, N. H., Blair, N. S., Osinska, H., Hambleton, M. A., Brunskill, E. W., Sayen, M. R., Gottlieb, R. A., Dorn, G. W. et al. (2005) Loss of cyclophilin D reveals a critical role for mitochondrial permeability transition in cell death. Nature **434**, 658–662

138 Schiene-Fischer, C. and Yu, C. (2001) Receptor accessory folding helper enzymes: the functional role of peptidyl prolyl cis/trans isomerases. FEBS Lett. **495**, 1–6

139 Freeman, B. C., Toft, D. O. and Morimoto, R. I. (1996) Molecular chaperone machines: chaperone activities of the cyclophilin Cyp-40 and the steroid aporeceptor-associated protein p23. Science **274**, 1718–1720

140 Du, H., Guo, L., Fang, F., Chen, D., Sosunov, A. A., McKhann, G. M., Yan, Y., Wang, C., Zhang, H., Molkentin, J. D. et al. (2008) Cyclophilin D deficiency attenuates mitochondrial and neuronal perturbation and ameliorates learning and memory in Alzheimer's disease. Nat. Med. **14**, 1097–1105

141 Singh, P., Suman, S., Chandna, S. and Das, T. K. (2009) Possible role of amyloid-β, adenine nucleotide translocase and cyclophilin-D interaction in mitochondrial dysfunction of Alzheimer's disease. Bioinformation **3**, 440–445

142 Kajitani, K. and Fujihashi, M. (2008) Crystal structure of human cyclophilin D in complex with its inhibitor, cyclosporin A at 0.96-Å resolution. Proteins **70**, 1635–1639.

143 Schlatter, D., Thoma, R., Küng, E. Stihle, M., Müller, F., Borroni, E., Cesura, A. and Henning, M. (2005) Crystal engineering yields crystals of cyclophilin D diffracting to 1.7 Å resolution. Acta Crystallogr. D Biol. Crystallogr. **61** 513–519

144 Du, H., Guo, L., Zhang, W., Rydzewska, M. and Yan, S. (2009) Cyclophilin D deficiency improves mitochondrial function and learning/memory in aging Alzheimer disease mouse model, Neurobiol. Aging., doi:10.1016/j.neurobiolaging.2009.03.003

145 Yang, X., Yang, Y., Wu, J. and Zhu, J. (2007) Stable expression of a novel fusion peptide of thioredoxin-1 and ABAD-inhibiting peptide protects PC12 cells from intracellular amyloid-β. J. Mol. Neurosci. **33**, 180–188

146 Berndt, C., Lillig, C. H. and Holmgren, A. (2008) Thioredoxins and glutaredoxins as facilitators of protein folding. Biochim. Biophys. Acta **1783**, 641–650

147 Lillig, C. H. and Holmgren, A. (2007) Thioredoxin and related molecules: from biology to health and disease. Antioxid. Redox Signal. **9**, 25–47

148 Yao, J., Mei, L., Luddy, J., Chen, X., Stern, D., Arancio, O. and Yan, S. D. (2004) Antagonizing ABAD–Aβ interaction maintains mitochondrial and neuronal function in an Aβ rich environment: studies in neuronal cultures and transgenic mice, Neuroscience 2004 Meeting, San Diego, CA, 23–27 October 2004, Abstract 716. 11

149 Morota, S., Månsson, R., Hansson, M. J., Kasuya, K., Shimazu, M., Hasegawa, E., Yanagi, S. Omi, A., Uchino and H., Elmér E. (2009) Evaluation of putative inhibitors of mitochondrial permeability transition for brain disorders: specificity vs. toxicity. Exp. Neurol. **218**, 353–362

150 Mbye, L. H., Singh, I. N., Carrico, K. M., Saatman, K. E. and Hall, E. D. (2008) Comparative neuroprotective effects of cyclosporin A and NIM811, a nonimmunosuppressive cyclosporin A analog, following traumatic brain injury. J. Cereb. Blood Flow Metab. **29**, 87–97

151 Matsuda, S. and Koyasu, S. (2000) Mechanisms of action of cyclosporine. Immunopharmacology **47**, 119–125

152 Nicolli, A., Basso, E., Petronilli, V., Wenger, R. M. and Bernardi, P. (1996) Interactions of cyclophilin with the mitochondrial inner membrane and regulation of the permeability transition pore, a cyclosporin A-sensitive channel. J. Biol. Chem. **271**, 2185–2192

153 Uchino, H., Elmér, E., Uchino, K., Li, P.-A., He, Q.-P., Smith, M.-L. and Siesjö, B. K. (1998) Amelioration by cyclosporin A of brain damage in transient forebrain ischemia in the rat. Brain Res. **812**, 216–226

154 Matsuda, S., Moriguchi, T., Koyasu, S. and Nishida, E. (1998) T lymphocyte activation signals for interleukin-2 production involve activation of MKK6-p38 and MKK7-SAPK/JNK signaling pathways sensitive to cyclosporin A. J. Biol. Chem. **273**, 12378–12382

155   Liu, J., Farmer, Jr, J. D., Lane, W. S., Friedman, J., Weissman, I. and Schreiber, S. L. (1991) Calcineurin is a common target of cyclophilin-cyclosporin A and FKBP–FK506 complexes. Cell **66**, 807–815

156   Lee, S. P., Hwang, Y. S., Kim, Y. J., Kwon, K.-S., Kim, H. J., Kim, K. and Chae, H. Z. (2001) Cyclophilin A binds to peroxiredoxins and activates its peroxidase activity. J. Biol. Chem. **276**, 29826–29832

157   Matsuda, S., Shibasaki, F., Takehana, K., Mori, H., Nishida, E. and Koyasu, S. (2000) Two distinct action mechanisms of immunophilin-ligand complexes for the blockade of T-cell activation. EMBO Rep. **1**, 428–434

158   Montero, M., Lobaton, C. D., Moreno, A. and Alvarez, J. (2002) A novel regulatory mechanism of the mitochondrial Ca^{2+} uniporter revealed by the p38 mitogen-activated protein kinase inhibitor SB202190. FASEB J. **16**, 1955–1957

159   Horton, K. L., Stewart, K. M., Fonseca, S. B., Guo, Q. and Kelley, S. O. (2008) Mitochondria-penetrating peptides. Chem. Biol. **15**, 375–382

160   Tillement, L., Lecanu, L., Yao, W., Greeson, J. and Papadopoulos, V. (2006) The spirostenol (22R, 25R)-20α-spirost-5-en-3β-yl hexanoate blocks mitochondrial uptake of Aβ in neuronal cells and prevents Aβ-induced impairment of mitochondrial function. Steroids **71**, 725–735

Mitochondrial β-amyloid in Alzheimer's disease

Eva Borger*, Laura Aitken*, Kirsty E.A. Muirhead*, Zoe E. Allen*, James A. Ainge†, Stuart J. Conway‡ and Frank J. Gunn-Moore*[1]

*School of Biology, Biological and Medical Sciences Building, University of St Andrews, North Haugh, St Andrews, Fife KY16 9TF, U.K., †School of Psychology, St. Mary's College, University of St Andrews, South Street, St Andrews, Fife KY16 9JP, U.K., and ‡Department of Chemistry, Chemistry Research Laboratory, University of Oxford, Mansfield Road, Oxford OX1 3TA, U.K.

Abstract

It is well established that the intracellular accumulation of Aβ (amyloid β-peptide) is associated with AD (Alzheimer's disease) and that this accumulation is toxic to neurons. The precise mechanism by which this toxicity occurs is not well understood; however, identifying the causes of this toxicity is an essential step towards developing treatments for AD. One intracellular location where the accumulation of Aβ can have a major effect is within mitochondria, where mitochondrial proteins have been identified that act as binding sites for Aβ, and when binding occurs, a toxic response results. At one of these identified sites, an enzyme known as ABAD (amyloid-binding alcohol dehydrogenase), we have identified changes in gene expression in the brain cortex, following Aβ accumulation within mitochondria. Specifically, we have identified two proteins that are up-regulated not only in the brains of transgenic animal models of AD but also in those of human sufferers. The increased expression of these proteins demonstrates the complex and counteracting pathways that are activated in AD. Previous studies have identified approximate contact sites between ABAD and Aβ; on basis of these observations, we have shown that by using a modified peptide approach it is possible to reverse the expression of these two proteins in living transgenic animals and also to recover mitochondrial and behavioural deficits. This indicates that the ABAD–Aβ interaction is potentially an interesting target for therapeutic intervention. To explore this further we used a fluorescing substrate mimic to measure the activity of ABAD within living cells, and in addition we have identified chemical fragments that bind to ABAD, using a thermal shift assay.

Introduction

A link between mitochondrial dysfunction and neurodegenerative conditions, such as AD (Alzheimer's disease), has long been suggested to exist. Observations of altered cerebral blood flow and bioenergetic deficits in dementia patients, made using positron electron tomography [1,2], initiated research into the function of mitochondria in neurodegeneration as they are central to cellular energy metabolism. Evidence of the pivotal role of metabolic pathways and free-radical turnover in mitochondria in normal aging and neurodegenerative diseases has since accumulated [3,4]. For example, Parker et al. detected reduced cytochrome c oxidase activity in platelets [5] and the brains of AD patients [6], whereas Sayre et al. found increased levels of 4-HNE (4-hydroxynonenal), a product of lipid peroxidation, in AD brain tissue in comparison with controls [7]. Due to the proximity of mitochondrial DNA to ROS

(reactive oxygen species), which are naturally produced in the electron transport chain, this DNA is thought to accumulate mutations over time, which can lead to increasing mitochondrial dysfunction and increased production of ROS with age [8–10]. Key mitochondrial enzymes that are affected by AD include cytochrome c oxidase [5,11], the pyruvate dehydrogenase complex, α-ketoglutarate dehydrogenase and isocitrate dehydrogenase [12,13].

Lustbader et al. [14] used immunoelectron microscopy to show that mitochondrial Aβ (amyloid β-peptide) (both the 1–40 and 1–42 forms) localizes inside the mitochondria of Tg-mAPP [mAPP (mutant amyloid precursor protein)-overexpressing transgenic] animals and, significantly, the human AD brain. A further study showed that Aβ accumulation in the mitochondria from Tg-mAPP mice and the cerebral cortex of human AD brains is significantly higher than that in non-transgenic mice and non-AD brains [15]. More recent studies indicate that mitochondrial dysfunction and the accumulation of mitochondrial Aβ [and ABAD (amyloid-binding alcohol dehydrogenase): see below] can be observed in the early stages of AD in other commonly used transgenic animal strains, including the popular triple transgenic mouse model (human APP_{SWE}, Tau_{P301L} and $PS1_{M146V}$ [16]).

The origin of this mitochondrial Aβ is still under debate and there is experimental evidence of the local production (e.g. the presence of the γ-secretase complex within mitochondria) and/or the import of Aβ from the

cytosol via the TOM (translocase of outer mitochondrial membrane) [17–19]. In addition to the ongoing efforts to determine how Aβ occurs within mitochondria, the other key question regards the action of Aβ once it is located within mitochondria. The addition of Aβ to cell cultures induces the dysfunction of mitochondrial respiration, ATP depletion and production of ROS [20,21]; the exposure of isolated mitochondria to Aβ reduces complex IV activity [22] and induces the formation of the permeability transition pore, which is linked to cell death [23]. In addition to these organelle-level changes, in the last decade attention has been increasingly focused on two mitochondrial proteins, ABAD (amyloid binding alcohol dehydrogenase) and CypD (cyclophilin D), both of which appear able to mediate the toxicity of the Aβ peptide. The binding of both proteins to Aβ (both the 1–40 and 1–42 forms) has been demonstrated at nanomolar Aβ concentrations, and Aβ accumulation within cells is known to result in an increase in the expression of both these proteins [23–25].

CypD

CypD, a peptidylprolyl isomerase F, is found in the mitochondrial matrix and it translocates to the inner mitochondrial membrane during times of oxidative stress where it is thought to play a role in the opening of the mPTP (mitochondrial permeability transition pore) [26]. CypD is considered to be a part of the mPTP as it associates with ANT (adenine nucleotide translocase) and possibly other factors, such as the VDAC (voltage-dependent anion channel) and the PiC (mitochondrial phosphate carrier), to contribute to the opening of the pore [27]. Using a variety of methods such as immunoprecipitation, co-localization and SPR (surface plasmon resonance) assays it was shown that CypD can bind to Aβ at nanomolar concentrations of Aβ. However, no direct contact sites have yet been identified [23]. Du et al. [23] also reported that under Aβ-rich conditions in the aging brain, CypD expression levels are increased and coincide with increased levels of ROS production. Further studies using Tg-mAPP mice deficient in the gene encoding CypD, revealed that the interaction of CypD with Aβ can result in cellular stress and cell death [23,25]. Notably, neurons derived from CypD-deficient animals are resistant to Aβ-induced opening of the mPTP and are thus protected against Aβ- and oxidative stress-induced cell death. These animals also exhibited significantly improved learning and memory functions in comparison with transgenic mAPP mice with normal expression of CypD [25].

ABAD

ABAD is the most characterized intracellular Aβ-binding protein and it was first identified in 1997 using a yeast two-hybrid screen [24]. It was originally identified within the ER (endoplasmic reticulum) and was termed ERAB (ER-associated amyloid-binding protein) [24]; however, later studies confirmed its presence inside mitochondria [28]. The action of this enzyme is primarily to catalyse the reduction

of aldehydes and ketones or the reverse reaction of oxidation from alcohols for energy production. As described in more detail by Muirhead et al. [29] ABAD acts on a range of substrates, indicating the variety of functions it can have within the cell. This variety of potential substrates correlates with the finding that ABAD appears to act as a molecular switch. In the presence of low levels of Aβ, ABAD can exhibit neuroprotective effects, and its increased expression is protective in animal models of Parkinsonism [30] and metabolic stress [31]; however, as Aβ levels rise, it appears that ABAD loses its ability to protect and that it enhances Aβ toxicity [32]. X-ray crystallography studies of human and rat ABAD have provided a clear representation of the catalytic core of ABAD and enabled the identification of key residues involved in substrate binding and interaction with Aβ [33]. However, the precise identity of the residues involved in the Aβ–ABAD interaction could not be identified by means of crystallography, since loop D, the region that is thought to bind Aβ, was disordered in the structure [14]. Interaction with Aβ not only inhibits ABAD's enzyme function (though notably only at micromolar concentrations) [28,34], but also causes severe mitochondrial dysfunction and cellular toxicity [14,32], which cannot be attributed to a loss of enzyme function alone. Proteomics studies on mice overexpressing ABAD and mAPP revealed that in the living brain the ABAD–Aβ interaction also affects the expression of proteins. Proteins that were specifically identified were Ep-1 (endophilin-1) [35] and Prdx-2 (peroxiredoxin-2) [36], both of which were found to be more abundant in human AD brains in comparison with controls [35,36]. To date, the link between these two proteins and mitochondrial dysfunction remains unclear. However, evidence exists that increased levels of Ep-1 can cause the activation of JNK (c-Jun-N-terminal kinase) [35,37]. JNK is a stress kinase that has been linked to Aβ production in neuronal cells [38,39], whose action is associated with the early stages of AD [40]. Conversely, Prdx-2 is an antioxidant protein and an increase in its expression can protect against Aβ-induced toxicity [36]. Thus the increased expression of these two proteins typifies competing pathways that are activated in an AD afflicted brain.

Another important metabolic function located in mitochondria is Ca^{2+} homoeostasis. Evidence of disturbed Ca^{2+} homoeostasis [41] and alterations in Ca^{2+} regulated proteins, especially the neuronal proteinase calpain and its targets, has been detected in human AD brains, in human cortical neuron cultures *in vitro* [42,43] and in transgenic mice [44]. Interestingly, a link between the calpain-regulated Cdk5 (cyclin-dependent kinase 5) and Prdx-2 inactivation by phosphorylation has been discovered in a model of Parkinson's disease [45]. In addition, Cdk5 had been earlier identified as a candidate kinase for the mediation of neuronal toxicity in AD [46–48]. The relevance of this pathway to Prdx-2 function in AD has not been investigated so far. Our own studies indicate that the phosphorylation of Thr^{89} in Prdx-2 can regulate the observed protection against Aβ-induced toxicity (E. Borger, unpublished work). More

recently a novel Ca^{2+}-binding protein, EFHD 2 (EF-hand domain containing protein 2; swiprosin 1) was also linked to one of the hallmarks of AD [49]. EFHD 2 is associated with hyperphosphorylated tau protein in a mouse tauopathy model and in human AD brains to a greater degree than it is in control tissues [49]. Additionally, it was reported that protein levels of EFHD 2 were found to have increased in AD cases in comparison with those in controls [49], and our own studies suggest that this is also the case in the Tg-mAPP mouse model, which does not develop tauopathy (E. Borger, unpublished work). The function of EFHD 2 in neuronal cells is still unknown, but its association with two of AD hallmarks points towards its potential importance in AD pathology.

Taken together, research on human dementia patients and studies using animal as well as *in vitro* models for AD have shown that all key functions of mitochondria are affected in AD. A detrimental link between impaired brain energy metabolism, ROS production and disturbed Ca^{2+} homoeostasis has also been established in the case of other neuropathological conditions such as delirium, ischaemia and hypoglycaemia. Consequently, Blass [50,51] and Lin and Beal [52] have proposed the role of a downward 'mitochondrial spiral' in the development of neurodegenerative diseases, in particularly with regard to AD.

Therapeutic targets and development of assays

The proposed binding site of Aβ on ABAD, 'loop D', was identified through a range of complimentary techniques including X-ray crystallography and mutagenesis studies [14]. It has been shown that a synthetic peptide consisting of residues 92–120, which forms this loop, can be used as a DP (decoy peptide), which competes with ABAD as a partner that binds to Aβ. Using SPR, it was shown that this DP was able to prevent the binding of Aβ to ABAD [14]. The same region of ABAD, identified independently through an antisense peptide approach, was found to bind biotinylated Aβ with a K_d (dissociation constant) of 107 nM, using ELISA [53]. Cellular studies of the DP effects, using a Tat-DP fusion peptide to allow the peptide to cross the cell membrane, found that the application of the peptide protected neurons (from wild-type, Tg-ABAD and Tg-ABAD/mAPP mice) against Aβ-induced toxicity [14]. Similarly, the introduction of DP-TRX (thioredoxin 1; an enzyme introduced here in order to stabilize the peptide) into cell cultures using a lentiviral approach, revealed that DP-TRX-transfected cells showed decreased apoptosis, decreased LDH (lactate dehydrogenase) release and increased cell viability after treatment with Aβ in comparison with controls [54]. Compelling evidence of the effectiveness of the peptide was provided by *in vivo* studies in transgenic animals, where a fusion peptide consisting of amino acids 93–116 of loop D with a Tat sequence and a mitochondrial-targeting sequence [Tat-mito-DP(93–116)] was found to alter levels of AD biomarker proteins Prdx-2 and Ep-1 [35,36]. Intraperitoneal injection of Tat-mito-DP(93–116) into Tg-mAPP mice resulted in a reduction in

Prdx-2 levels in these mice to levels that were comparable with those in non-transgenic mice [36]. Similarly, Ep-1 levels were elevated in double transgenic ABAD/mAPP mice and were found to return to basal levels when the mice were treated with Tat-mito-DP(93–116) [35]. In addition, behavioural studies revealed that treatment with the DP improved short-term memory performance in transgenic AD mouse models. Recently, Yao et al. demonstrated that double transgenic mAPP/Tat-mito-DP(91–119) mice as well as mAPP mice when systemically treated with the DP, showed significant improvement in the radial-arm water maze test of short-term memory performance in comparison with untreated mAPP mice [55].

In order to develop therapeutic compounds that target the Aβ–ABAD interaction, a robust method for monitoring the activity of the desired drug target is required. The use of purified ABAD protein to measure enzyme activity *in vitro* is well documented [29]. Utilizing the absorption of NADH at 340 nm, the rate of reduction in substrate can be measured by means of spectroscopy. Recently, we and our collaborators developed a cell-based assay that enables the study of ABAD activity in intact living cells. The assay uses a fluorescent ABAD substrate mimic, CHANA (cyclo-hexenyl amine naphthalene alcohol), which is based on the endogenous ABAD substrate oestradiol. CHANA is a non-fluorescent substrate under assay conditions, whereas the reaction product, CHANK (cyclohexenyl amine naphthalene ketone) fluoresces in non-aqueous environments, e.g. in cell membranes [56]. Due to these different photochemical properties, the selective detection of the accumulation of CHANK is possible. Thus the conversion of CHANA to CHANK, and hence ABAD activity, can be monitored by means of fluorescence microscopy. This novel approach has recently been improved upon by the means of synthesis of the individual stereoisomers of CHANA. (−)-CHANA was found to be selectively metabolized by ABAD, whereas (+)-CHANA showed a much higher level of background oxidation by other cellular dehydrogenases [57]. Thus, using (−)-CHANA, we have laid the foundations for a cell-based assay monitoring of ABAD activity. When using (−)-CHANA, metabolism was seen to be substantially diminished in cells treated with a known ABAD inhibitor, AG18051 [33]. Importantly, it was also demonstrated that Aβ can inhibit ABAD activity in living cells. Upon addition of 22 μM Aβ(1–42), HEK-293 cells (human embryonic kidney cells) were shown to exhibit a significant decrease in (−)-CHANA metabolism of approximately 20%. It is hoped that further development of this system will provide a robust cell-based assay for use in the identification of potential modulators of ABAD function [57].

The future

AD is a complex disease, and likewise it becomes more and more apparent that the toxicity of the Aβ peptide is also a complex process. Indeed, although many approaches to explain AD pathology have centred on extracellular Aβ, there

Figure 1 | Consequences of mitochondrial Aβ

APP (amyloid precursor protein) can be transported to mitochondria, where it interacts with TOM and TIM (translocase of the inner membrane), disturbing mitochondrial protein import (1). Aβ can be imported into mitochondria via TIM and TOM and is found associated with the inner mitochondrial membrane, disrupting mitochondrial respiration and leading to an excess production of ROS (2). Aβ has been found to interact with ABAD in the mitochondrial matrix, inhibiting enzyme activity (3). The Aβ–ABAD interaction also leads to an up-regulation of AD biomarkers Ep-1 (4) and Prdx-2 (5). At the inner mitochondrial membrane, Aβ can interact with CypD, which is involved in the formation of mPTP and Ca^{2+}-release from mitochondria (6). Aβ can be found in the cytosol, disturbing cell signalling, protein degradation and causing ROS production, which leads to an increase in cytosolic Ca^{2+} (7). Ca^{2+}-mediated Cdk5 activation has been found to inhibit Prdx-2's antioxidant function.
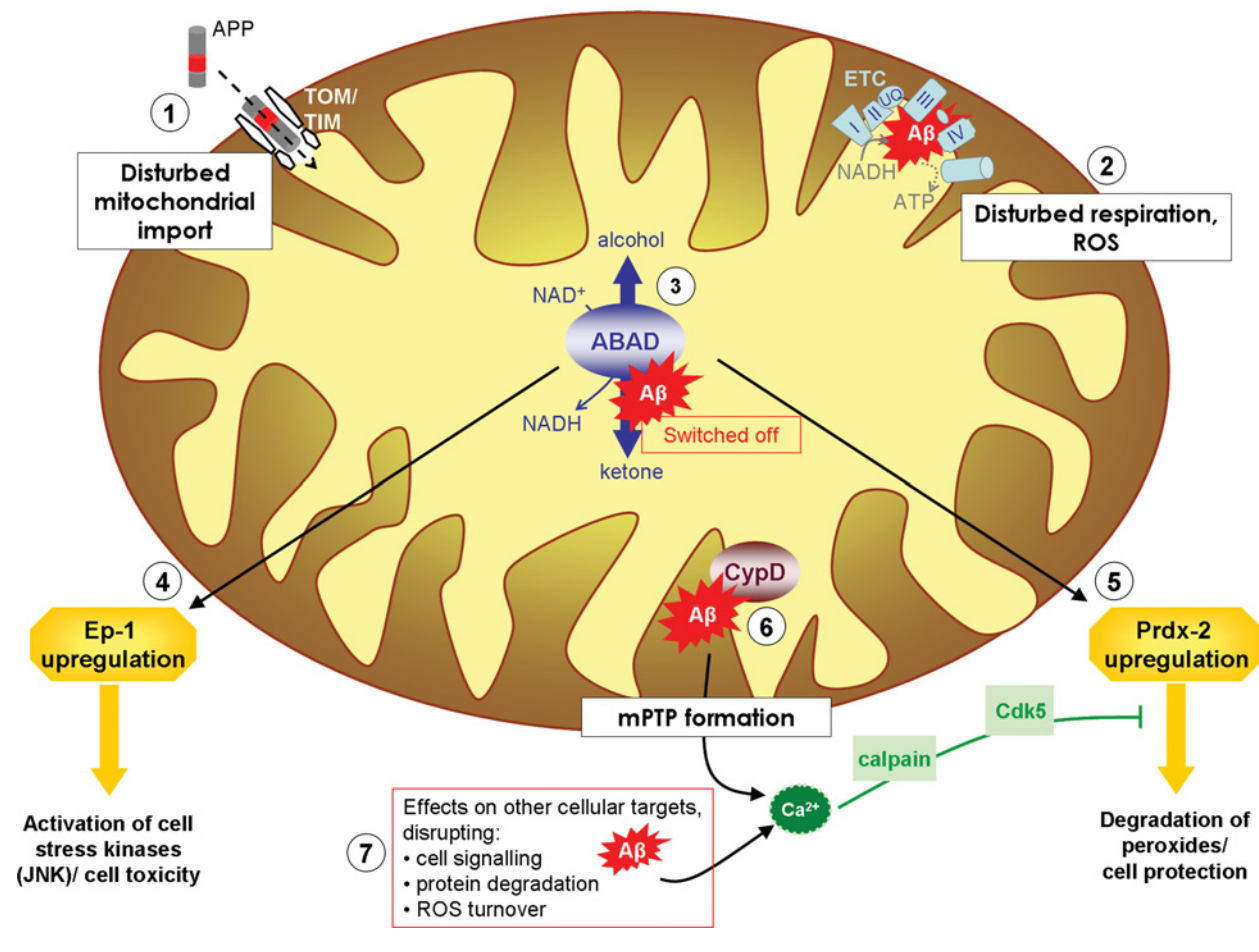
has been lesser focus on the involvement of intracellular species of Aβ. Our studies with our collaborators have focused on these events (summarized in Figure 1). They suggest that the one-drug and one-target approaches for the treatment of AD are unlikely to constitute an effective strategy of treatment of AD. Consequently, the treatment of this disease will probably require a three-pronged approach, targeting, for example: (i) the formation/clearance of Aβ and that of hyperphosphorylated tau; (ii) the support and stabilization of the remaining neuronal networks; and (iii) protection of potential sensitive intracellular targets. The integrity and function of mitochondria is one such sensitive intracellular target, and though ABAD and CypD are not classical drug targets they are important players in the sequence of events resulting in mitochondrial dysfunction. Therefore future approaches for the treatment of AD will greatly benefit from an understanding of their involvement in AD.

Funding

References

1 Foster, N.L., Chase, T.N., Fedio, P., Patronas, N.J., Brooks, R.A. and Di Chiro, G. (1983) Alzheimer's disease: focal cortical changes shown by positron emission tomography. Neurology **33**, 961–965

2 Duara, R., Grady, C., Haxby, J., Sundaram, M., Cutler, N.R., Heston, L., Moore, A., Schlageter, N., Larson, S. and Rapoport, S.I. (1986) Positron emission tomography in Alzheimer's disease. Neurology **36**, 879–887

3 Beal, M.F. (1995) Aging, energy, and oxidative stress in neurodegenerative diseases. Ann. Neurol. **38**, 357–366

4 Bowling, A.C. and Beal, M.F. (1995) Bioenergetic and oxidative stress in neurodegenerative diseases. Life Sci. **56**, 1151–1171

5 Parker, Jr, W.D., Mahr, N.J., Filley, C.M., Parks, J.K., Hughes, D., Young, D.A. and Cullum, C.M. (1994) Reduced platelet cytochrome *c* oxidase activity in Alzheimer's disease. Neurology **44**, 1086–1090

6 Parker, Jr, W.D., Parks, J., Filley, C.M. and Kleinschmidt-DeMasters, B.K. (1994) Electron transport chain defects in Alzheimer's disease brain. Neurology **44**, 1090–1096

7 Sayre, L.M., Zelasko, D.A., Harris, P.L.R, Perry, G., Salomon, R.G. and Smith, M.A. (1997) 4-Hydroxynonenal-derived advanced lipid peroxidation end products are increased in Alzheimer's disease. J. Neurochem. **68**, 2092–2097

8 Richter, C., Park, J.W. and Ames, B.N. (1988) Normal oxidative damage to mitochondrial and nuclear DNA is extensive. Proc. Natl. Acad. Sci. U.S.A. **85**, 6465–6467

9 Beal, M.F. (2005) Mitochondria take center stage in aging and neurodegeneration. Ann. Neurol. **58**, 495–505

10 Liu, J., Head, E., Gharib, A.M., Yuan, W., Ingersoll, R.T., Hagen, T.M., Cotman, C.W. and Ames, B.N. (2002) Memory loss in old rats is associated with brain mitochondrial decay and RNA/DNA oxidation: partial reversal by feeding acetyl-L-carnitine and/or *R-α*-lipoic acid. Proc. Natl. Acad. Sci. U.S.A. **99**, 2356–2361

11 Cottrell, D.A., Blakely, E.L., Johnson, M.A., Ince, P.G. and Turnbull, D.M. (2001) Mitochondrial enzyme-deficient hippocampal neurons and choroidal cells in AD. Neurology **57**, 260–264

12 Bubber, P., Haroutunian, V., Fisch, G., Blass, J.P. and Gibson, G.E. (2005) Mitochondrial abnormalities in Alzheimer brain: mechanistic implications. Ann. Neurol. **57**, 695–703

13 Gibson, G.E., Park, L.C., Zhang, H., Sorbi, S. and Calingasan, N.Y. (1999) Oxidative stress and a key metabolic enzyme in Alzheimer brains, cultured cells, and an animal model of chronic oxidative deficits. Ann. N.Y. Acad. Sci. **893**, 79–94

14 Lustbader, J.W., Cirilli, M., Lin, C., Xu, H.W., Takuma, K., Wang, N., Caspersen, C., Chen, X., Pollak, S., Chaney, M. et al. (2004) ABAD directly links Aβ to mitochondrial toxicity in Alzheimer's disease. Science **304**, 448–452

15 Caspersen, C., Wang, N., Yao, J., Sosunov, A., Chen, X., Lustbader, J.W., Wei Xu, H., Stern, D., McKhann, G. and Yan, S.D. (2005) Mitochondrial Aβ: a potential focal point for neuronal metabolic dysfunction in Alzheimer's disease. FASEB J. **19**, 2040–2041

16 Yao, J., Irwin, R.W., Zhao, L., Nilsen, J., Hamilton, R.T. and Brinton, R.D. (2009) Mitochondrial bioenergetic deficit precedes Alzheimer's pathology in female mouse model of Alzheimer's disease. Proc. Natl. Acad. Sci. U.S.A. **106**, 14670–14675

17 Anandatheerthavarada, H.K., Biswas, G., Robin, M.A. and Avadhani, N.G. (2003) Mitochondrial targeting and a novel transmembrane arrest of Alzheimer's amyloid precursor protein impairs mitochondrial function in neuronal cells. J. Cell Biol. **161**, 41–54

18 Devi, L., Prabhu, B.M., Galati, D.F., Avadhani, N.G. and Anandatheerthavarada, H.K. (2006) Accumulation of amyloid precursor protein in the mitochondrial import channels of human Alzheimer's disease brain is associated with mitochondrial dysfunction. J. Neurosci. **26**, 9057–9068

19 Hansson Petersen, C.A., Alikhani, N., Behbahani, H., Wiehager, B., Pavlov, P.F., Alafuzoff, I., Leinonen, V., Ito, A., Winblad, B., Glaser, E. and Ankarcrona, M. (2008) The amyloid β-peptide is imported into mitochondria via the TOM import machinery and localized to mitochondrial cristae. Proc. Natl. Acad. Sci. U.S.A. **105**, 13145–13150

20 Casley, C.S., Land, J.M., Sharpe, M.A., Clark, J.B., Duchen, M.R. and Canevari, L. (2002) β-Amyloid fragment 25–35 causes mitochondrial dysfunction in primary cortical neurons. Neurobiol. Dis. **10**, 258–267

21 Chen, J.X. and Yan, S.D. (2007) Amyloid-β-induced mitochondrial dysfunction. J. Alzheimer's Dis. **12**, 177–184

22 Canevari, L., Clark, J.B. and Bates, T.E. (1999) β-Amyloid fragment 25–35 selectively decreases complex IV activity in isolated mitochondria. FEBS Lett. **457**, 131–134

23 Du, H., Guo, L., Fang, F., Chen, D., Sosunov, A.A., McKhann, G.M., Yan, Y., Wang, C., Zhang, H., Molkentin, J.D. et al. (2008) Cyclophilin D deficiency attenuates mitochondrial and neuronal perturbation and ameliorates learning and memory in Alzheimer's disease. Nat. Med. **14**, 1097–1105

24 Yan, S.D., Fu, J., Soto, C., Chen, X., Zhu, H., Al-Mohanna, F., Collison, K., Zhu, A., Stern, E., Saido, T. et al. (1997) An intracellular protein that binds amyloid-β peptide and mediates neurotoxicity in Alzheimer's disease. Nature **389**, 689–695

25 Du, H., Guo, L., Zhang, W., Rydzewska, M. and Yan, S. (2011) Cyclophilin D deficiency improves mitochondrial function and learning/memory in aging Alzheimer disease mouse model. Neurobiol. Aging **32**, 398–406

26 Connern, C.P. and Halestrap, A.P. (1994) Recruitment of mitochondrial cyclophilin to the mitochondrial inner membrane under conditions of oxidative stress that enhance the opening of a calcium-sensitive non-specific channel. Biochem. J. **302**, 321–324

27 Crompton, M., Virji, S. and Ward, J.M. (1998) Cyclophilin-D binds strongly to complexes of the voltage-dependent anion channel and the adenine nucleotide translocase to form the permeability transition pore. Eur. J. Biochem. **258**, 729–735

28 Oppermann, U.C., Salim, S., Tjernberg, L.O., Terenius, L. and Jornvall, H. (1999) Binding of amyloid β-peptide to mitochondrial hydroxyacyl-CoA dehydrogenase (ERAB): regulation of an SDR enzyme activity with implications for apoptosis in Alzheimer's disease. FEBS Lett. **451**, 238–242

29 Muirhead, K.E.A., Borger, E., Aitken, L., Conway, S.J. and Gunn-Moore, F.J. (2010) The consequences of mitochondrial amyloid β-peptide in Alzheimer's disease. Biochem. J. **426**, 255–270

30 Tieu, K., Perier, C., Vila, M., Caspersen, C., Zhang, H.-P., Teismann, P., Jackson-Lewis, V., Stern, D.M., Yan, S.D. and Przedborski, S. (2004) L-3-hydroxyacyl-CoA dehydrogenase II protects in a model of Parkinson's disease. Ann. Neurol. **56**, 51–60

31 Yan, S.D., Zhu, Y., Stern, E.D., Hwang, Y.C., Hori, O., Ogawa, S., Frosch, M.P., Connolly, Jr, E.S., McTaggert, R., Pinsky, D.J. et al. (2000) Amyloid β-peptide-binding alcohol dehydrogenase is a component of the cellular response to nutritional stress. J. Biol. Chem. **275**, 27100–27109

32 Takuma, K., Yao, J., Huang, J., Xu, H., Chen, X., Luddy, J., Trillat, A.C., Stern, D.M., Arancio, O. and Yan, S.S. (2005) ABAD enhances Aβ-induced cell stress via mitochondrial dysfunction. FASEB J. **19**, 597–598

33 Kissinger, C.R., Rejto, P.A., Pelletier, L.A., Thomson, J.A., Showalter, R.E., Abreo, M.A., Agree, C.S., Margosiak, S., Meng, J.J., Aust, R.M. et al. (2004) Crystal structure of human ABAD/HSD10 with a bound inhibitor: implications for design of Alzheimer's disease therapeutics. J. Mol. Biol. **342**, 943–952

34 Yan, S.D., Shi, Y., Zhu, A., Fu, J., Zhu, H., Zhu, Y., Gibson, L., Stern, E., Collison, K., Al-Mohanna, F. et al. (1999) Role of ERAB/L-3-hydroxyacyl-coenzyme a dehydrogenase type II activity in Aβ-induced cytotoxicity. J. Biol. Chem. **274**, 2145–2156

35 Ren, Y., Xu, H.W., Davey, F., Taylor, M., Aiton, J., Coote, P., Fang, F., Yao, J., Chen, D., Chen, J.X. et al. (2008) Endophilin I expression is increased in the brains of Alzheimer disease patients. J. Biol. Chem. **283**, 5685–5691

36 Yao, J., Taylor, M., Davey, F., Ren, Y., Aiton, J., Coote, P., Fang, F., Chen, J.X., Yan, S.D. and Gunn-Moore, F.J. (2007) Interaction of amyloid binding alcohol dehydrogenase/Aβ mediates up-regulation of peroxiredoxin II in the brains of Alzheimer's disease patients and a transgenic Alzheimer's disease mouse model. Mol. Cell. Neurosci. **35**, 377–382

37 Ramjaun, A.R., Angers, A., Legendre-Guillemin, V., Tong, X.-K. and McPherson, P.S. (2001) Endophilin regulates JNK activation through its interaction with the germinal center kinase-like kinase. J. Biol. Chem. **276**, 28913–28919

38 Colombo, A., Bastone, A., Ploia, C., Sclip, A., Salmona, M., Forloni, G. and Borsello, T. (2009) JNK regulates APP cleavage and degradation in a model of Alzheimer's disease. Neurobiol. Dis. **33**, 518–525

39 Tamagno, E., Parola, M., Bardini, P., Piccini, A., Borghi, R., Guglielmotto, M., Santoro, G., Davit, A., Danni, O., Smith, M.A. et al. (2005) β-Site APP cleaving enzyme up-regulation induced by 4-hydroxynonenal is mediated by stress-activated protein kinases pathways. J. Neurochem. **92**, 628–636

40 Lagalwar, S., Guillozet-Bongaarts, A.L., Berry, R.W. and Binder, L.I. (2006) Formation of phospho-SAPK/JNK granules in the hippocampus is an early event in Alzheimer disease. J. Neuropathol. Exp. Neurol. **65**, 455–464

41 Mattson, M.P., Cheng, B., Davis, D., Bryant, K., Lieberburg, I. and Rydel, R.E. (1992) β-Amyloid peptides destabilize calcium homeostasis and render human cortical neurons vulnerable to excitotoxicity. J. Neurosci. **12**, 376–389

42 Kuwako, K.-I., Nishimura, I., Uetsuki, T., Saido, T.C. and Yoshikawa, K. (2002) Activation of calpain in cultured neurons overexpressing Alzheimer amyloid precursor protein. Mol. Brain Res. **107**, 166–175

43 Saito, K., Elce, J.S., Hamos, J.E. and Nixon, R.A. (1993) Widespread activation of calcium-activated neutral proteinase (calpain) in the brain in Alzheimer disease: a potential molecular basis for neuronal degeneration. Proc. Natl. Acad. Sci. U.S.A. **90**, 2628–2632

44 Liang, B., Duan, B.-Y., Zhou, X.-P., Gong, J.-X. and Luo, Z.-G. (2010) Calpain activation promotes BACE1 expression, amyloid precursor protein processing, and amyloid plaque formation in a transgenic mouse model of Alzheimer disease. J. Biol. Chem. **285**, 27737–27744

45 Qu, D., Rashidian, J., Mount, M.P., Aleyasin, H., Parsanejad, M., Lira, A., Haque, E., Zhang, Y., Callaghan, S., Daigle, M. et al. (2007) Role of Cdk5-mediated phosphorylation of Prx2 in MPTP toxicity and Parkinson's disease. Neuron **55**, 37–52

46 Cole, A.R., Noble, W., van Aalten, L., Plattner, F., Meimaridou, R., Hogan, D., Taylor, M., LaFrancois, J., Gunn-Moore, F., Verkhratsky, A. et al. (2007) Collapsin response mediator protein-2 hyperphosphorylation is an early event in Alzheimer's disease progression. J. Neurochem. **103**, 1132–1144

47 Cruz, J.C., Kim, D., Moy, L.Y., Dobbin, M.M., Sun, X., Bronson, R.T. and Tsai, L.-H. (2006) p25/cyclin-dependent kinase 5 induces production and intraneuronal accumulation of amyloid β *in vivo*. J. Neurosci. **26**, 10536–10541

48 Smith, P.D., Crocker, S.J., Jackson-Lewis, V., Jordan-Sciutto, K.L., Hayley, S., Mount, M.P., O'Hare, M.J., Callaghan, S., Slack, R.S., Przedborski, S. et al. (2003) Cyclin-dependent kinase 5 is a mediator of dopaminergic neuron loss in a mouse model of Parkinson's disease. Proc. Natl. Acad. Sci. U.S.A. **100**, 13650–13655

49 Vega, I.E., Traverso, E.E., Ferrer-Acosta, Y., Matos, E., Colon, M., Gonzalez, J., Dickson, D., Hutton, M., Lewis, J. and Yen, S.H. (2008) A novel calcium-binding protein is associated with tau proteins in tauopathy. J. Neurochem. **106**, 96–106

50 Blass, J.P. (2000) The mitochondrial spiral: an adequate cause of dementia in the Alzheimer's syndrome. Ann. N.Y. Acad. Sci. **924**, 170–183

51 Blass, J.P. (2001) Brain metabolism and brain disease: is metabolic deficiency the proximate cause of Alzheimer dementia? J. Neurosci. Res. **66**, 851–856

52 Lin, M.T. and Beal, M.F. (2006) Mitochondrial dysfunction and oxidative stress in neurodegenerative diseases. Nature **443**, 787–795

53 Milton, N.G., Mayor, N.P. and Rawlinson, J. (2001) Identification of amyloid-β binding sites using an antisense peptide approach. NeuroReport **12**, 2561–2566

54 Yang, X., Yang, Y., Wu, J. and Zhu, J. (2007) Stable expression of a novel fusion peptide of thioredoxin-1 and ABAD-inhibiting peptide protects PC12 cells from intracellular amyloid-β. J. Mol. Neurosci. **33**, 180–188

55 Yao, J., Du, H., Yan, S., Fang, F., Wang, C., Lue, L.-F., Guo, L., Chen, D., Stern, D., Gunn-Moore, F.J. et al. (2011) Inhibition of ABAD–Aβ interaction reduces Aβ accumulation and improves mitochondrial function in a mouse model of Alzheimer's disease. J. Neurosci. **31**, 2313–2320

56 Froemming, M.K. and Sames, D. (2007) Harnessing functional plasticity of enzymes: a fluorogenic probe for imaging 17β-HSD10 dehydrogenase, an enzyme involved in Alzheimer's and Parkinson's diseases. J. Am. Chem. Soc. **129**, 14518–14522

57 Muirhead, K.E.A., Froemming, M., Li, X., Musilek, K., Conway, S.J., Sames, D. and Gunn-Moore, F.J. (2010) (−)-CHANA, a fluorogenic probe for detecting amyloid binding alcohol dehydrogenase HSD10 activity in living cells. ACS Chem. Biol. **5**, 1105–1114

Is Amyloid binding alcohol dehydrogenase a drug target for treating Alzheimer's disease?

Eva Borger[*], Laura Aitken[*], Heng Du[#], Wenshen Zhang[$], Frank J Gunn-Moore[*], and Shirley Shi Du Yan[#@]

[*]School of Biology, Medical and Biological Sciences Building, North Haugh, University of St Andrews, Scotland UK KY16 9TF

[#]Higuchi Bioscience Center and Pharmacology & Toxicology, School of Pharmacy, University of Kansas, Lawrence, KS66047, USA

[$]State Key Laboratory of Earth Surface Process and Resource Ecology, Center for Natural Medicine Engineering, The Ministry of Education of China, Beijing Normal University, Beijing 100875

[@]Corresponding author:

Shirley ShiDu Yan

Departments of Pharmacology and Toxicology and Higuchi Bioscience Center, University of Kansas, Lawrence, KS 66047, USA; e-mail: shidu@ku.edu，phone: 785-864-3637

Abstract

Current strategies for the treatment of Alzheimer's disease (AD) involve tackling the formation or clearance of the amyloid-beta peptide (Aβ) and/or hyper-phosphorylated tau, or the support and stabilization of the remaining neuronal networks. However, as we gain a clearer idea of the large number of molecular mechanisms at work in this disease, it is becoming clearer that the treatment of AD should take a combined approach of dealing with several aspects of the pathology. The concept that we also need to protect specific sensitive targets within the cell should also be considered. In particular the role of protecting the function of a specific mitochondrial protein, amyloid binding alcohol dehydrogenase (ABAD), will be the focus of this review. Mitochondrial dysfunction is a well-recognized fact in the progression of AD, though until recently the mechanisms involved could only be loosely labeled as changes in 'metabolism'. The discovery that Aβ can be present within the mitochondria and specifically bind to ABAD, has opened up a new area of AD research. Here we review the evidence that the prevention of Aβ binding to ABAD is a drug target for the treatment of AD.

Introduction

The past decade has seen many advances in dementia research towards the development of new innovative therapies for Alzheimer's disease (AD). However, these efforts have yet to lead to a major breakthrough in AD treatment. The AD research community still debates the relative significance of tau and amyloid-beta (Aβ) pathologies in the progression of this disease and with regard to the latter whether this is intracellular or extracellular [1]. There is also debate concerning the relative importance of "nature and nurture" with regard to active research programs using genome wide analysis to identify genetic risk factors versus changes in lifestyle [2]. The truth is likely to be a combination of all of these events. What is therefore clear is that a future treatment for AD will not consist of a one-drug therapy, but will include a combination of different approaches.

Despite the best efforts of the pharmaceutical industry, some in the science community are now seeking a radical rethink in how drugs to treat this disease will be developed. In particular, many new and recent attempts can become thwarted in the early stages of development when trying to solve all the technical issues of target-based drug design in one go [3]. Instead, methods such as lead-oriented synthesis of new compounds have recently been suggested as more promising alternative routes [4]. This is accompanied by an increasing number of authors stressing the importance of understanding the detailed molecular mechanism of action of a potential new drug and of using appropriate phenotypic assays in its validation and design [5]. It could be argued that we are only starting to understand the molecular changes that are occurring within neurons in AD. However, we would predict that future treatments will consist of targeting three aspects:

i) The formation or clearance of Aβ and/or hyper-phosphorylated tau; though debate rages on whether dismantling a protein aggregate would be a good thing, and as yet targeting the production or synthesis of these toxic proteins has proven to be difficult [6-8] .

ii) The support and stabilization of the remaining neuronal networks. This includes the current drug therapies such as cholinesterase inhibitors and memantine [9].

iii) The protection of specific sensitive targets. By identifying the particularly important sensitive targets in AD, it may be possible to protect them against the toxicities of Aβ and/or tau.

It is in regard to this last point which provides the setting of this review and in particular leads to the role of protecting a specific mitochondrial protein (amyloid-binding alcohol dehydrogenase (ABAD)) as an example of how the new criteria of drug-design can be applied.

Mitochondrial dysfunction is a well-recognized fact in the progression of AD, though until recently the mechanisms involved could be loosely labeled as changes in 'metabolism' [10]. It is now apparent that there are subtle and complex molecular factors at work in mitochondria and of particular importance is the fact that the observed mitochondrial damage is potentially reversible, as has been shown in various animal models [11-13]. It is also now known that not all mitochondria are created equal and as such synaptic mitochondria have been found to be more vulnerable to the stresses associated with AD pathology [14-18].

The function of mitochondria is to create energy and provide homeostasis and so energy production and metabolism have been known for many years to be defective in AD pathology [10, 19]. Changes in mitochondrial enzymes involved in the electron transport chain and citric acid cycle have been previously noted by many groups [9, 20-22] and as such these observations fit with the idea of mitochondrial dysfunction and oxidative stress as central aspects of AD pathogenesis [23]. Accordingly, clinicians have used the metabolism of glucose as a particular useful method of detecting specific metabolic changes in the brains of AD patients [24, 25]. In addition, although administration of simple antioxidants, such as vitamin E, in the management of AD has so far been unsuccessful [26], the development and application of mitochondria-targeted antioxidant compounds has emerged as a promising approach for the treatment of neurodegenerative diseases [13, 27]. However, until recently what has not been so clear are the molecular mechanisms causing mitochondrial damage.

Recent research efforts have introduced the concept that the accumulation of Aβ inside the cells and specifically in mitochondria might be a likely explanation for the observed mitochondrial damage in AD (reviewed in [28]). The accumulation of intracellular Aβ (of both Aβ(1-40) and Aβ(1-42)) has been shown several times [29-37] and indeed, unlike extracellular plaques, has been shown to correlate with the disease progression [38, 39]. In 2004, it was published that Aβ could be found inside mitochondria in both animal models and significantly also in human AD sufferers [34]. This therefore begs the question what is the intra-mitochondrial Aβ doing? At present two molecular binding targets for Aβ have been identified within mitochondria, namely ABAD and cyclophilin D [15, 40]. What is particularly significant about these two proteins, is that both show an increase in expression

4

levels in AD and at the same time have been shown to bind Aβ with nanomolar affinity [34, 37]. This is in contrast to the changes observed in other mitochondrial proteins involved in metabolism which have been found to have reduced expression levels and activity in AD and for which a specific interaction with Aβ has not been described.

Amyloid binding alcohol dehydrogenase

It was the identification of an intracellular protein *via* originally a yeast two hybrid screen for Aβ binding molecules, that opened up a new area of mitochondria focused AD research [41]. From this initial screen the mitochondrial protein ABAD has subsequently been shown to bind Aβ *via* a plethora of different techniques ranging from biophysical approaches (NMR, SPR) through to immunoprecipitation experiments from both AD transgenic mice and human AD brains [34, 42, 43], where ABAD expression levels have also been found to be up-regulated [41]. Initial studies indicated that the binding of Aβ could occur at nanomolar affinity; however, it was not until micromolar levels of Aβ were reached, that changes in ABAD activity were also observed [44, 45]. ABAD contains a Rossman fold [46] for the binding of nucleotides and it has been shown to be able to catalyze, with the help of $NAD^+/NADH$, the reduction of aldehydes and ketones and oxidation of alcohols for energy production utilizing different substrates. As reviewed by Muirhead et *al.* [47], these substrates range from simple alcohols and amino acid metabolites [48] through to fatty acid metabolites and steroids [28]. Of interest, deficient turnover of one of these substrates, isoleucine, due to inherited point mutations in ABAD, is associated with neurological abnormalities [48].

ABAD activity can be manipulated in two ways, under conditions of stress (it increases) [49] or in the presence of Aβ (it decreases) [34, 50]. With regard to the latter, the change in activity due to the binding of Aβ to ABAD has been previously presented as a rather digital response, that is, as Aβ binds to ABAD it switches its activity off with respect to a number of simple substrates [44, 45]. However, recent data from our laboratories suggests that this rather digital view may be an over simplification (FGM, unpublished data). An up-regulation of ABAD has been suggested to have protective effects in models of Parkinsonism [51] and metabolic stress [49]. However, in AD models, it has been shown that the presence of active ABAD [34, 52], but not an inactive mutant of the enzyme [45], can in fact enhance mitochondrial dysfunction and oxidative stress *in vitro* [34, 41] and *in vivo* [34, 52] (Figure 1). Moreover, studies have now identified additional consequences of Aβ binding to ABAD in living organisms. Specifically, there are a number of genes that are switched on and appear

5

to be controlled by the binding of Aβ to ABAD. Examples include the antioxidant protein peroxiredoxin-2 [53] and the presynaptic endocytic protein endophilin-1 (also referred to as endophilin A1) [54], both of which have been found to be up-regulated in the human AD brain as well [53, 54]. Other proteins have also been shown to be increased such as creatine kinase B, and heat shock protein 70 (FGM and SDY unpublished data) both of which have now been linked by other groups to AD progression [55-57]. The ability to control the expression of an array of other proteins could suggest that it is not a simple question of switching off activity, but potentially that the binding of Aβ to ABAD causes the enzyme to change its ability to utilize certain substrates, which in turn would affect other proteins directly or indirectly. It has been challenging to pin point the exact *in vivo* substrates of ABAD in the brain, though our recent work suggests that there are indeed subtle changes in lipid metabolism in response to altered ABAD activity in cells (FGM and SDY unpublished data).

Consequences of ABAD and Aβ binding.

A number of molecular and cellular changes occur after ABAD and Aβ interact within the mitochondria [28], but as mentioned above, in living organisms it can result in protein expression changes in the brain. The two best described proteins, peroxiredoxin-2 and endophilin-1, are examples of the complexity of the biochemical pathways that become activated in AD and both can be linked to synaptic activity (Figure 1).

Peroxiredoxin-2 is known to be an antioxidant protein, which has the ability to prevent Aβ induced toxicity [53]. Its expression has also been shown to be elevated in both transgenic AD animals and the *post-mortem* human brain [53]. Peroxiredoxin-2 has further been linked to the mechanisms at work in the parkinsonian brain [58-60]. However, it would appear that it is not a simple question of just elevated levels of this protein, as it has been shown that there is a critical residue that can be phosphorylated (Thr^{89}) which would lead to the inactivation of the enzyme's activity [59]. This is thought to be the case in the parkinsonian brain [59], but it remains to be seen whether this is the case in the AD brain, too. Indeed, one of the kinases known to phosphorylate this residue in peroxiredoxin-2 is CDK5 [59], which in turn has been shown to have elevated levels of activity in the AD brain [61, 62], thus suggesting peroxiredoxin-2 may indeed be phosphorylated and therefore inactivated in AD. In addition, peroxiredoxin-2 activity can also be controlled directly by

6

oxidation [63], for example induced by the administration of the dopaminergic toxin 6-hydroxydopamine [58] or S-nitrosylation [60]. Therefore it appears that the actual state of post-translational modification of this protein in the brain affected by Parkinson's disease or AD, may be an important aspect.

The second protein that has been shown to be elevated in the AD brain in response to ABAD binding to Aβ is endophilin-1. This is a member of a family of proteins which together have an expanding number of functions, ranging from synaptic vesicle endocytosis, mitochondrial function and receptor trafficking [64]. Specifically, this family of proteins was predicted to be involved in neurodegenerative diseases [65] prior to them now being shown to be involved in AD [54], Parkinson's disease [66], spinocerebellar ataxia 2 [67], and Huntington's disease [64]. In the case of AD, it was the family member endophilin-1 that has been directly shown to be involved. Initially, it was shown that increased levels of endophilin-1 can be linked to increased activation levels of the stress kinase c-Jun N-terminal kinase (JNK) in both HEK293 cells [68] and primary cortical neurons [54] and increased JNK-activity has been known to be a feature of AD pathology [69]. The activation by endophilin-1 occurs potentially through a germinal center like kinase (GLK)-mediated pathway [68]. GLK is part of the germinal center kinases family and their activation is thought to be *via* the binding of SH2/SH3 adapter binding proteins which are associated with membranes [70]. Endophilin-1 fulfills both of these criteria by affecting lipid membrane curvature for synaptic vesicle formation and by containing a C-terminal SH3 domain [65]. With this in mind, it is interesting to note that endophilin-1 as well as peroxiredoxin-2 have been identified in the same vesicle complexes as the scaffold protein Sunday driver/JNK-interacting protein 3 (JIP3) by immunoprecipitation studies on synaptosomes from the mouse cortex [71]. The recruitment and activation of GLK can lead to the activation of the MAP3K, MEKK1 [72]. Previous findings indicated that MEKK1 interacts with inactive MKK4 to form a MEKK1-MKK4 complex. Active MEKK1 can phosphorylate and activate MKK4 (and/or MKK7), resulting in its dissociation from the complex. The free and active MKK4 then specifically interacts with JNK. Once activated, JNK can translocate to the nucleus or other target sites to phosphorylate downstream effectors, thereby affecting important aspects of neuronal function such as neurite outgrowth, mitochondrial function, synaptic plasticity and apoptosis (all reviewed in [69]). This suggests that through recruiting GLK *via* its SH3-domain, endophilin-1 might be able to co-localize important components of the JNK-signaling cascade and facilitate its activation. This might further be influenced by the

presence of peroxiredoxin-2 [71], which has also been implicated in the activation of JNK-signaling in a cancer cell model [73].

However, it is possible that endophilin-1 may have another direct effect on synaptic signaling as it can lead to the increased probability of glutamate release [74]. This implies that an elevated level of endophilin-1 at the synapse can interfere with normal neurotransmitter signaling. Indeed, it is possible to speculate that an increase in endophilin-1 may have different effects in different locations, as endophilin-1 has been found both in the pre-synaptic neuron [75-77] but also the post-synaptic density [78], where it has recently been given a role in dendritic development [79]. In either case, the relative presence or absence of other signaling molecules will determine which pathways endophilin-1 can influence inside the cell. In addition, the function of endophilin-1 has also been found to be affected by local levels of calcium [80], which are known to be disturbed in AD [81]. This coupled with the recent discovery that pre-synaptic mitochondria expressing ABAD and Aβ are more sensitive than their soma compatriots [14] implies, that spatial localization of these events could be of paramount importance as they may also influence endophilin-1 function through altered ABAD activity affecting lipid metabolism or mitochondrial dysfunction and calcium homeostasis. Therefore, the interaction of ABAD and Aβ within mitochondria is able to elevate endophilin-1 protein [54] and mRNA expression levels (Yan, unpublished results). How this occurs is unknown, but it is likely to have far-reaching consequences for synaptic function (Figure 2).

Evidence that ABAD is a drug target.

The specific up-regulation of ABAD in human AD and interaction with Aβ [34, 41] which caused mitochondrial dysfunction [52] and other cellular effects also present in the human AD brain [53, 54], suggested that the ABAD-Aβ interaction might be a potential drug target. Using the knowledge gained from understanding how ABAD and Aβ bind to each other, a series of publications have now further validated this view. The crystal structure of ABAD with Aβ bound produced an insight into their interaction. Unfortunately, the exact contact sites could not be established due to distortion of the crystal structure in this area [34], but it was found that a region called loop D encompassing residues 92 to 120 was the region of ABAD that could bind Aβ and this could be confirmed by various biophysical experiments [34, 82]. However, the most convincing data that this interaction was significant, came from

the ability of a peptide based on the sequence of this region to work as a decoy *in vivo* (Figure 2). Initial experiments showed that modifying the decoy peptide by addition of peptide sequences from the cell-membrane transduction domain of the human immunodeficiency virus-1 (HIV-1) tat protein [83, 84], enabled the ABAD decoy peptides (ABAD-DP) to cross cell membranes and prevent Aβ toxicity in neuronal cultures [34, 85]. Others showed that linking this peptide region with thioredoxin 1 and then expressing the chimeric protein in cell cultures, also protected against Aβ toxicity [85]. It was then the ability of using modified decoy peptides in living organisms that introduced the fascinating possibility that the ABAD and Aβ interaction could be a drug target. Adding a mitochondrial targeting sequence to the decoy peptide facilitated its localization in mitochondria after intraperitoneal injection and transport through the blood brain barrier. It was then possible to show in 6 month old transgenic animals expressing elevated levels of ABAD and Aβ, that the observed increases in the expression levels of peroxiredoxin-2 and endophilin-1, could be reversed [53, 54]. Even more significant was the finding that using the same approach, it was possible to reverse the behavioral changes in these animals as well [11]. Another important aspect of these studies was, that the reversal of behavioral changes could be achieved by both purified peptide injected intraperitoneally and also in a transgenic animal model expressing the ABAD region 92-120 [11]. This approach also showed an additional potentially protectiveeffect as the level of mitochondrial Aβ was reduced in the treated animals which correlated with an increase in the Aβ-degrading enzyme PreP (presequence peptidase) [11].

Therefore, in keeping with the requirements for a suitable drug target ("ligandability" and "druggability") recently reviewed by Hann *et al* [86], it has been shown by both biochemical and physiological determinates that preventing Aβ binding to ABAD can be achieved (ligandability) and has a significant positive effect (druggability). However the question remains whether it is possible to design drugs around such a complex target.

Approaches: blood brain barriers, cellular assays and peptides

As indicated above, ABAD is a sensitive site in AD that can be protected from its interaction with Aβ, which could be beneficial in AD treatment. Classically, protein-protein interactions have been avoided as therapeutic targets because of perceived difficulties in developing compounds [87]. To overcome the perceived problems, then it is necessary to be imaginative.

For example, crossing the blood brain barrier is a perennial problem when dealing with small molecules; however, the studies above have shown that intraperitoneally injected peptides are capable of crossing the blood brain barrier and targeting the correct site in animal models [11, 53, 54]. Other recent imaginative work has shown that other approaches can have the same capability. A study in mice revealed, that modified retroviruses showed an increased efficiency of gaining access to the central nervous system when mannitol was peritoneally injected before intravenous administration of the viruses [88]. Another recent breakthrough has been the use of targeted exosomes, again injected intravenously, which allowed biological relevant compounds (in this case siRNA) encapsulated in these membranes, to be successfully delivered into the brain [89]. Therefore there may be new horizons for getting compounds across the blood brain barrier.

For good reasons, the development of small molecules as drugs is the standard method in academia [3]. However, coupled to this approach has been the classical method of devising a high throughput *in vitro* enzyme assay, but this approach has recently been one of the pitfalls for the pharmaceutical industry, and so there has been a push to develop more cell based phenotypic assays [5]. For ABAD and Aβ the ability of the tested compounds to prevent this interaction has been monitored at the cellular level by measuring the protection provided by them in terms of for example preserving mitochondrial integrity, cytochrome C release and respiration [12, 34, 85]. More direct methods may also be possible with the advent of the first generation of ABAD targeted substrate mimics such as the fluorogenic cyclohexenylamine naphthalene alcohol (CHANA)-(-) [47, 90], which, under specific conditions, could be used to measure the prevention of Aβ induced inhibition of ABAD activity in living cells as a read out for compound testing.

Use of the loop D of ABAD has proven to be successful as described above, but in drug terms a 40 amino acid peptide (20 amino acids from ABAD, approximately 20 amino acids from targeting sequences) would be thought of as too large a molecule to become a drug. However, it could be thought of as a template. At present the minimal size of the loop D ABAD and its constituent parts that provide protection is not known. In addition, it might be possible to design smaller mitochondrial targeting peptides [91], and also modify the amino acids as simple peptide isosteres and heterocyclic peptide isosteres to increase rigidity of the peptidomimetic, or the use of cyclic peptides which increase cellular stability. Indeed, there are examples of modified peptides that have been produced to act on mitochondrial proteins such as antamanide, a 10 amino acid cyclic peptide that targets cyclophilin D [92].

10

However, small molecule compounds that prevent Aβ binding to ABAD can also be considered as possible. For example, frentizole was identified by an ELISA-based screening assay, as a novel inhibitor of the ABAD-Aβ interaction, and was subsequently modified with the production of a novel benzothiazole urea, resulting in a 30-fold improvement in potency [42]. This compound was found to have potential undesirable immunosuppressive qualities [42]; however, this approach indicated that it might be possible to develop pharmacologically active and medically useful compounds targeting ABAD. Fragment-based drug discovery has been a popular strategy for this used in academia as well as pharmaceutical industry [3]. Two commonly employed screening technologies in this field are thermal shift analysis and saturated transfer difference NMR spectroscopy [93-95], which can identify compounds with millimolar affinity for the target. By grouping compounds, for example using structure activity relation (SAR) analysis, improved affinities for the target can then be achieved [93, 96]. Alternatively, fragments can also be combined, in order to effectively sample the available chemical space as proposed by Hann et al. [86].

Thus, though the ABAD-Aβ interaction is not a classical site for drug therapy, the biology dictates that this interaction may be a future target (Figure 3). At the very least, the work that was inspired from the original yeast two hybrid screen has shown that it is possible to identify not just new drug targets but also novel biological pathways and events that occur in neurodegenerative diseases such as AD.

Conclusion

Multiple lines of evidence indicate that mitochondrial dysfunction is an early pathological feature of AD. Aβ can directly and indirectly interfere with mitochondria by affecting mitochondrial energy metabolism, oxidative stress, calcium homeostasis and mitochondrial dynamics in axons and the synapse, eventually leading to neuronal injury and cognitive impairment. Therefore, the mitochondria are a very important target in the pathogenesis of AD. Given the role of ABAD in Aβ-induced synaptic pathology, the development of small molecules that inhibit the interaction of ABAD with Aβ, as outlined in this review, is a novel innovative therapeutic strategy for the management of AD.

References

1. Gravitz, L. (2011). Drugs: a tangled web of targets. Nature *475*, S9-11.
2. Deweerdt, S. (2011). Prevention: activity is the best medicine. Nature *475*, S16-17.
3. Frearson, J.A., and Collie, I.T. (2009). HTS and hit finding in academia – from chemical genomics to drug discovery. Drug Discovery Today *14*, 1150-1158.
4. Nadin, A., Hattotuwagama, C., and Churcher, I. (2012). Lead-Oriented Synthesis: A New Opportunity for Synthetic Chemistry. Angewandte Chemie International Edition *51*, 1114-1122.
5. Swinney, D.C., and Anthony, J. (2011). How were new medicines discovered?
6. Brody, D.L., and Holtzman, D.M. (2008). Active and Passive Immunotherapy for Neurodegenerative Disorders. Annu. Rev. Neurosci. *31*, 175-193.
7. Citron, M. (2004). Strategies for disease modification in Alzheimer's disease. Nat Rev Neurosci *5*, 677-685.
8. Citron, M. (2004). Beta-secretase inhibition for the treatment of Alzheimer's disease--promise and challenge. Trends Pharmacol Sci *25*, 92-97.
9. Palmer, A.M. (2011). Neuroprotective therapeutics for Alzheimer's disease: progress and prospects. Trends Pharmacol Sci *32*, 141-147.
10. Beal, M.F. (1995). Aging, energy, and oxidative stress in neurodegenerative diseases. Ann Neurol *38*, 357-366.
11. Yao, J., Du, H., Yan, S., Fang, F., Wang, C., Lue, L.F., Guo, L., Chen, D., Stern, D.M., Gunn Moore, F.J., et al. (2011). Inhibition of amyloid-beta (Abeta) peptide-binding alcohol dehydrogenase-Abeta interaction reduces Abeta accumulation and improves mitochondrial function in a mouse model of Alzheimer's disease. J Neurosci *31*, 2313-2320.
12. Yao, J., Mei, L., Luddy, J., Chen, X., Stern, D., Arancio, O., and Yan, S.D. (2004). Antagonizing ABAD–Aβ interaction maintains mitochondrial and neuronal function in an Aβ rich environment: Studies in neuronal cultures and transgenic mice. In Neuroscience 2004 Meeting, S.f. Neuroscience, ed. (San Diego, California, USA), p. Program No 716.711.
13. Manczak, M., Mao, P., Calkins, M.J., Cornea, A., Reddy, A.P., Murphy, M.P., Szeto, H.H., Park, B., and Reddy, P.H. (2010). Mitochondria-targeted antioxidants protect against amyloid-beta toxicity in Alzheimer's disease neurons. J Alzheimers Dis. *20*, S609-631.
14. Du, H., Guo, L., Yan, S., Sosunov, A.A., McKhann, G.M., and Yan, S.S. (2010). Early deficits in synaptic mitochondria in an Alzheimer's disease mouse model. Proc Natl Acad Sci U S A *107*, 18670-18675.
15. Du, H., and Yan, S.S. (2010). Mitochondrial permeability transition pore in Alzheimer's disease: cyclophilin D and amyloid beta. Biochim Biophys Acta *1802*, 198-204.
16. Calkins, M.J., Manczak, M., Mao, P., Shirendeb, U., and Reddy, P.H. (2011). Impaired mitochondrial biogenesis, defective axonal transport of mitochondria, abnormal mitochondrial dynamics and synaptic degeneration in a mouse model of Alzheimer's disease. Hum Mol Genet *20*, 4515-4529.

17. Du, H., Guo, L., and Yan, S.S. (2012). Synaptic mitochondrial pathology in Alzheimer's disease. Antioxid Redox Signal *16*, 1467-1475.
18. Brown, M.R., Sullivan, P.G., and Geddes, J.W. (2006). Synaptic mitochondria are more susceptible to Ca2+overload than nonsynaptic mitochondria. J Biol Chem *281*, 11658-11668.
19. Bowling, A.C., and Beal, M.F. (1995). Bioenergetic and oxidative stress in neurodegenerative diseases. Life Sci *56*, 1151-1171.
20. Gibson, G.E., Park, L.C., Zhang, H., Sorbi, S., and Calingasan, N.Y. (1999). Oxidative stress and a key metabolic enzyme in Alzheimer brains, cultured cells, and an animal model of chronic oxidative deficits. Ann N Y Acad Sci *893*, 79-94.
21. Cottrell, D.A., Blakely, E.L., Johnson, M.A., Ince, P.G., and Turnbull, D.M. (2001). Mitochondrial enzyme-deficient hippocampal neurons and choroidal cells in AD. Neurology *57*, 260-264.
22. Bubber, P., Haroutunian, V., Fisch, G., Blass, J.P., and Gibson, G.E. (2005). Mitochondrial abnormalities in Alzheimer brain: mechanistic implications. Ann Neurol *57*, 695-703.
23. Beal, M.F. (2005). Mitochondria take center stage in aging and neurodegeneration. Ann Neurol *58*, 495-505.
24. Duara, R., Grady, C., Haxby, J., Sundaram, M., Cutler, N.R., Heston, L., Moore, A., Schlageter, N., Larson, S., and Rapoport, S.I. (1986). Positron emission tomography in Alzheimer's disease. Neurology *36*, 879-887.
25. McKhann, G.M., Knopman, D.S., Chertkow, H., Hyman, B.T., Jack, C.R., Jr., Kawas, C.H., Klunk, W.E., Koroshetz, W.J., Manly, J.J., Mayeux, R., et al. (2011). The diagnosis of dementia due to Alzheimer's disease: recommendations from the National Institute on Aging-Alzheimer's Association workgroups on diagnostic guidelines for Alzheimer's disease. Alzheimers Dement *7*, 263-269.
26. Vina, J., Lloret, A., Giraldo, E., Badia, M.C., and Alonso, M.D. (2011). Antioxidant pathways in Alzheimer's disease: possibilities of intervention. Curr Pharm Des. *17*, 3861-3864.
27. Szeto, H.H. (2008). Development of mitochondria-targeted aromatic-cationic peptides for neurodegenerative diseases. Ann N Y Acad Sci. *1147*, 112-121.
28. Muirhead, K.E.A., Borger, E., Aitken, L., Conway, S.J., and Gunn-Moore, F.J. (2010). The consequences of mitochondrial amyloid β-peptide in Alzheimer's disease. Biochemical Journal *426*, 255-270.
29. Haass, C., Lemere, C.A., Capell, A., Citron, M., Seubert, P., Schenk, D., Lannfelt, L., and Selkoe, D.J. (1995). The Swedish mutation causes early-onset Alzheimer's disease by beta-secretase cleavage within the secretory pathway. Nat. Med. *1*, 1291-1296.
30. Yang, A.J., Chandswangbhuvana, D., Margol, L., and Glabe, C.G. (1998). Loss of endosomal/lysosomal membrane impermeability is an early event in amyloid Abeta1-42 pathogenesis. J Neurosci Res *52*, 691-698.
31. Buckig, A., Tikkanen, R., Herzog, V., and Schmitz, A. (2002). Cytosolic and nuclear aggregation of the amyloid beta-peptide following its expression in the endoplasmic reticulum. Histochem Cell Biol *118*, 353-360.
32. Takahashi, R.H., Milner, T.A., Li, F., Nam, E.E., Edgar, M.A., Yamaguchi, H., Beal, M.F., Xu, H., Greengard, P., and Gouras, G.K. (2002). Intraneuronal Alzheimer abeta42 accumulates in multivesicular bodies and is associated with synaptic pathology. Am J Pathol *161*, 1869-1879.
33. Keil, U., Bonert, A., Marques, C.A., Scherping, I., Weyermann, J., Strosznajder, J.B., Muller-Spahn, F., Haass, C., Czech, C., Pradier, L., et al. (2004). Amyloid beta-

13

induced changes in nitric oxide production and mitochondrial activity lead to apoptosis. J Biol Chem *279*, 50310-50320.

34. Lustbader, J.W., Cirilli, M., Lin, C., Xu, H.W., Takuma, K., Wang, N., Caspersen, C., Chen, X., Pollak, S., Chaney, M., et al. (2004). ABAD directly links Abeta to mitochondrial toxicity in Alzheimer's disease. Science *304*, 448-452.

35. Martin, B.L., Schrader-Fischer, G., Busciglio, J., Duke, M., Paganetti, P., and Yankner, B.A. (1995). Intracellular accumulation of beta-amyloid in cells expressing the Swedish mutant amyloid precursor protein. J Biol Chem *270*, 26727-26730.

36. Caspersen, C., Wang, N., Yao, J., Sosunov, A., Chen, X., Lustbader, J.W., Xu, H.W., Stern, D., McKhann, G., and Yan, S.D. (2005). Mitochondrial Abeta: a potential focal point for neuronal metabolic dysfunction in Alzheimer's disease. Faseb J *19*, 2040-2041.

37. Du, H., Guo, L., Fang, F., Chen, D., Sosunov, A.A., McKhann, G.M., Yan, Y., Wang, C., Zhang, H., Molkentin, J.D., et al. (2008). Cyclophilin D deficiency attenuates mitochondrial and neuronal perturbation and ameliorates learning and memory in Alzheimer's disease. Nat Med *14*, 1097-1105.

38. Gouras, G.K., Tsai, J., Naslund, J., Vincent, B., Edgar, M., Checler, F., Greenfield, J.P., Haroutunian, V., Buxbaum, J.D., Xu, H., et al. (2000). Intraneuronal Abeta42 accumulation in human brain. Am J Pathol *156*, 15-20.

39. Gyure, K.A., Durham, R., Stewart, W.F., Smialek, J.E., and Troncoso, J.C. (2001). Intraneuronal abeta-amyloid precedes development of amyloid plaques in Down syndrome. Arch Pathol Lab Med *125*, 489-492.

40. Giorgio, V., Soriano, M.E., Basso, E., Bisetto, E., Lippe, G., Forte, M.A., and Bernardi, P. (2010). Cyclophilin D in mitochondrial pathophysiology. Biochimica et Biophysica Acta (BBA) - Bioenergetics *1797*, 1113-1118.

41. Yan, S.D., Fu, J., Soto, C., Chen, X., Zhu, H., Al-Mohanna, F., Collison, K., Zhu, A., Stern, E., Saido, T., et al. (1997). An intracellular protein that binds amyloid-beta peptide and mediates neurotoxicity in Alzheimer's disease. Nature *389*, 689-695.

42. Xie, Y., Deng, S., Chen, Z., Yan, S., and Landry, D.W. (2006). Identification of small-molecule inhibitors of the A-ß-ABAD interaction. Bioorg. Med. Chem. Lett. *16*, 4657-4660.

43. Yan, Y., Liu, Y., Sorci, M., Belfort, G., Lustbader, J.W., Yan, S.S., and Wang, C. (2007). Surface plasmon resonance and nuclear magnetic resonance studies of ABAD-Abeta interaction. Biochemistry *46*, 1724-1731.

44. Oppermann, U.C., Salim, S., Tjernberg, L.O., Terenius, L., and Jornvall, H. (1999). Binding of amyloid beta-peptide to mitochondrial hydroxyacyl-CoA dehydrogenase (ERAB): regulation of an SDR enzyme activity with implications for apoptosis in Alzheimer's disease. FEBS Lett *451*, 238-242.

45. Yan, S.D., Shi, Y., Zhu, A., Fu, J., Zhu, H., Zhu, Y., Gibson, L., Stern, E., Collison, K., Al-Mohanna, F., et al. (1999). Role of ERAB/L-3-Hydroxyacyl-coenzyme A Dehydrogenase Type II Activity in Aß-induced Cytotoxicity. J. Biol. Chem. *274*, 2145-2156.

46. Powell, A.J., Read, J.A., Banfield, M.J., Gunn-Moore, F., Yan, S.D., Lustbader, J., Stern, A.R., Stern, D.M., and Brady, R.L. (2000). Recognition of structurally diverse substrates by type II 3-hydroxyacyl-CoA dehydrogenase (HADH II)/amyloid-beta binding alcohol dehydrogenase (ABAD). J Mol Biol *303*, 311-327.

47. Muirhead, K.E.A., Froemming, M., Li, X., Musilek, K., Conway, S.J., Sames, D., and Gunn-Moore, F.J. (2010). (−)-CHANA, a Fluorogenic Probe for Detecting Amyloid Binding Alcohol Dehydrogenase HSD10 Activity in Living Cells. ACS Chemical Biology *5*, 1105-1114.

14

48. Ofman, R., Jos Ruiter, P.N., Feenstra, M., Duran, M., Bwee Poll-The, T., Zschocke, J., Ensenauer, R., Lehnert, W., Sass, J.O., Sperl, W., et al. (2003). 2-Methyl-3-Hydroxybutyryl-CoA Dehydrogenase Deficiency Is Caused by Mutations in the HADH2 Gene. Am. J. Hum. Genet. *72*, 1300-1307.

49. Yan, S.D., Zhu, Y., Stern, E.D., Hwang, Y.C., Hori, O., Ogawa, S., Frosch, M.P., Connolly, E.S., Jr., McTaggert, R., Pinsky, D.J., et al. (2000). Amyloid beta -Peptide-binding Alcohol Dehydrogenase Is a Component of the Cellular Response to Nutritional Stress. J. Biol. Chem. *275*, 27100-27109.

50. He, X.-Y., Wen, G.-Y., Merz, G., Lin, D., Yang, Y.-Z., Mehta, P., Schulz, H., and Yang, S.-Y. (2002). Abundant type 10 17[beta]-hydroxysteroid dehydrogenase in the hippocampus of mouse Alzheimer's disease model. Brain Res. Mol. Brain Res. *99*, 46-53.

51. Tieu, K., Perier, C., Vila, M., Caspersen, C., Zhang, H.-P., Teismann, P., Jackson-Lewis, V., Stern, D.M., Yan, S.D., and Przedborski, S. (2004). L3-hydroxyacyl-CoA dehydrogenase II protects in a model of Parkinson's disease. Annals of Neurology *56*, 51-60.

52. Takuma, K., Yao, J., Huang, J., Xu, H., Chen, X., Luddy, J., Trillat, A.C., Stern, D.M., Arancio, O., and Yan, S.S. (2005). ABAD enhances Abeta-induced cell stress via mitochondrial dysfunction. Faseb J *19*, 597-598.

53. Yao, J., Taylor, M., Davey, F., Ren, Y., Aiton, J., Coote, P., Fang, F., Chen, J.X., Yan, S.D., and Gunn-Moore, F.J. (2007). Interaction of amyloid binding alcohol dehydrogenase/Abeta mediates up-regulation of peroxiredoxin II in the brains of Alzheimer's disease patients and a transgenic Alzheimer's disease mouse model. Mol Cell Neurosci *35*, 377-382.

54. Ren, Y., Xu, H.W., Davey, F., Taylor, M., Aiton, J., Coote, P., Fang, F., Yao, J., Chen, D., Chen, J.X., et al. (2008). Endophilin I expression is increased in the brains of Alzheimer disease patients. J Biol Chem *283*, 5685-5691.

55. Aksenov, M.Y., Aksenova, M.V., Butterfield, D.A., Geddes, J.W., and Markesbery, W.R. (2001). Protein oxidation in the brain in Alzheimer's disease. Neuroscience *103*, 373-383.

56. Castegna, A., Aksenov, M., Aksenova, M., Thongboonkerd, V., Klein, J.B., Pierce, W.M., Booze, R., Markesbery, W.R., and Butterfield, D.A. (2002). Proteomic identification of oxidatively modified proteins in Alzheimer's disease brain. Part I: creatine kinase BB, glutamine synthase, and ubiquitin carboxy-terminal hydrolase L-1. Free Radic Biol Med *33*, 562-571.

57. Di Domenico, F., Sultana, R., Tiu, G.F., Scheff, N.N., Perluigi, M., Cini, C., and Butterfield, D.A. (2010). Protein levels of heat shock proteins 27, 32, 60, 70, 90 and thioredoxin-1 in amnestic mild cognitive impairment: An investigation on the role of cellular stress response in the progression of Alzheimer disease. Brain Research *1333*, 72-81.

58. Hu, X., Weng, Z., Chu, C.T., Zhang, L., Cao, G., Gao, Y., Signore, A., Zhu, J., Hastings, T., Greenamyre, J.T., et al. (2011). Peroxiredoxin-2 Protects against 6-Hydroxydopamine-Induced Dopaminergic Neurodegeneration via Attenuation of the Apoptosis Signal-Regulating Kinase (ASK1) Signaling Cascade. J. Neurosci. *31*, 247-261.

59. Qu, D., Rashidian, J., Mount, M.P., Aleyasin, H., Parsanejad, M., Lira, A., Haque, E., Zhang, Y., Callaghan, S., Daigle, M., et al. (2007). Role of Cdk5-Mediated Phosphorylation of Prx2 in MPTP Toxicity and Parkinson's Disease. Neuron *55*, 37-52.

60.   Fang, J., Nakamura, T., Cho, D.H., Gu, Z., and Lipton, S.A. (2007). S-nitrosylation of peroxiredoxin 2 promotes oxidative stress-induced neuronal cell death in Parkinson's disease. Proc Natl Acad Sci U S A *104*, 18742-18747.

61.   Pei, J.-J., Grundke-Iqbal, I., Iqbal, K., Bogdanovic, N., Winblad, B., and Cowburn, R.F. (1998). Accumulation of cyclin-dependent kinase 5 (cdk5) in neurons with early stages of Alzheimer's disease neurofibrillary degeneration. Brain Research *797*, 267-277.

62.   Swatton, J.E., Sellers, L.A., Faull, R.L.M., Holland, A., Iritani, S., and Bahn, S. (2004). Increased MAP kinase activity in Alzheimer's and Down syndrome but not in schizophrenia human brain. European Journal of Neuroscience *19*, 2711-2719.

63.   Wood, Z.A., Schroder, E., Robin Harris, J., and Poole, L.B. (2003). Structure, mechanism and regulation of peroxiredoxins. Trends in Biochemical Sciences *28*, 32-40.

64.   Kjaerulff, O., Brodin, L., and Jung, A. (2010). The Structure and Function of Endophilin Proteins. Cell Biochem Biophys.

65.   Reutens, A.T., and Glenn Begley, C. (2002). Endophilin-1: a multifunctional protein. The International Journal of Biochemistry & Cell Biology *34*, 1173-1177.

66.   Trempe, J.F., Chen, C.X., Grenier, K., Camacho, E.M., Kozlov, G., McPherson, P.S., Gehring, K., and Fon, E.A. (2009). SH3 domains from a subset of BAR proteins define a Ubl-binding domain and implicate parkin in synaptic ubiquitination. Mol Cell *36*, 1034-1047.

67.   Nonis, D., Schmidt, M.H., van de Loo, S., Eich, F., Dikic, I., Nowock, J., and Auburger, G. (2008). Ataxin-2 associates with the endocytosis complex and affects EGF receptor trafficking. Cell Signal *20*, 1725-1739.

68.   Ramjaun, A.R., Angers, A., Legendre-Guillemin, V., Tong, X.-K., and McPherson, P.S. (2001). Endophilin Regulates JNK Activation through Its Interaction with the Germinal Center Kinase-like Kinase. J. Biol. Chem. *276*, 28913-28919.

69.   Mehan, S., Meena, H., Sharma, D., and Sankhla, R. (2011). JNK: a stress-activated protein kinase therapeutic strategies and involvement in Alzheimer's and various neurodegenerative abnormalities. Journal of molecular neuroscience : MN *43*, 376-390.

70.   Kyriakis, J.M. (1999). Signaling by the germinal center kinase family of protein kinases. J Biol Chem *274*, 5259-5262.

71.   Abe, N., Almenar-Queralt, A., Lillo, C., Shen, Z., Lozach, J., Briggs, S.P., Williams, D.S., Goldstein, L.S.B., and Cavalli, V. (2009). Sunday Driver Interacts with Two Distinct Classes of Axonal Organelles. Journal of Biological Chemistry *284*, 34628-34639.

72.   Diener, K., Wang, X.S., Chen, C., Meyer, C.F., Keesler, G., Zukowski, M., Tan, T.H., and Yao, Z. (1997). Activation of the c-Jun N-terminal kinase pathway by a novel protein kinase related to human germinal center kinase. Proc Natl Acad Sci U S A *94*, 9687-9692.

73.   Lee, K.W., Lee, D.J., Lee, J.Y., Kang, D.H., Kwon, J., and Kang, S.W. (2011). Peroxiredoxin II restrains DNA damage-induced death in cancer cells by positively regulating JNK-dependent DNA repair. J Biol Chem. *286*, 8394-8404. Epub 2010 Dec 8399.

74.   Weston, Matthew C., Nehring, Ralf B., Wojcik, Sonja M., and Rosenmund, C. (2011). Interplay between VGLUT Isoforms and Endophilin A1 Regulates Neurotransmitter Release and Short-Term Plasticity. Neuron *69*, 1147-1159.
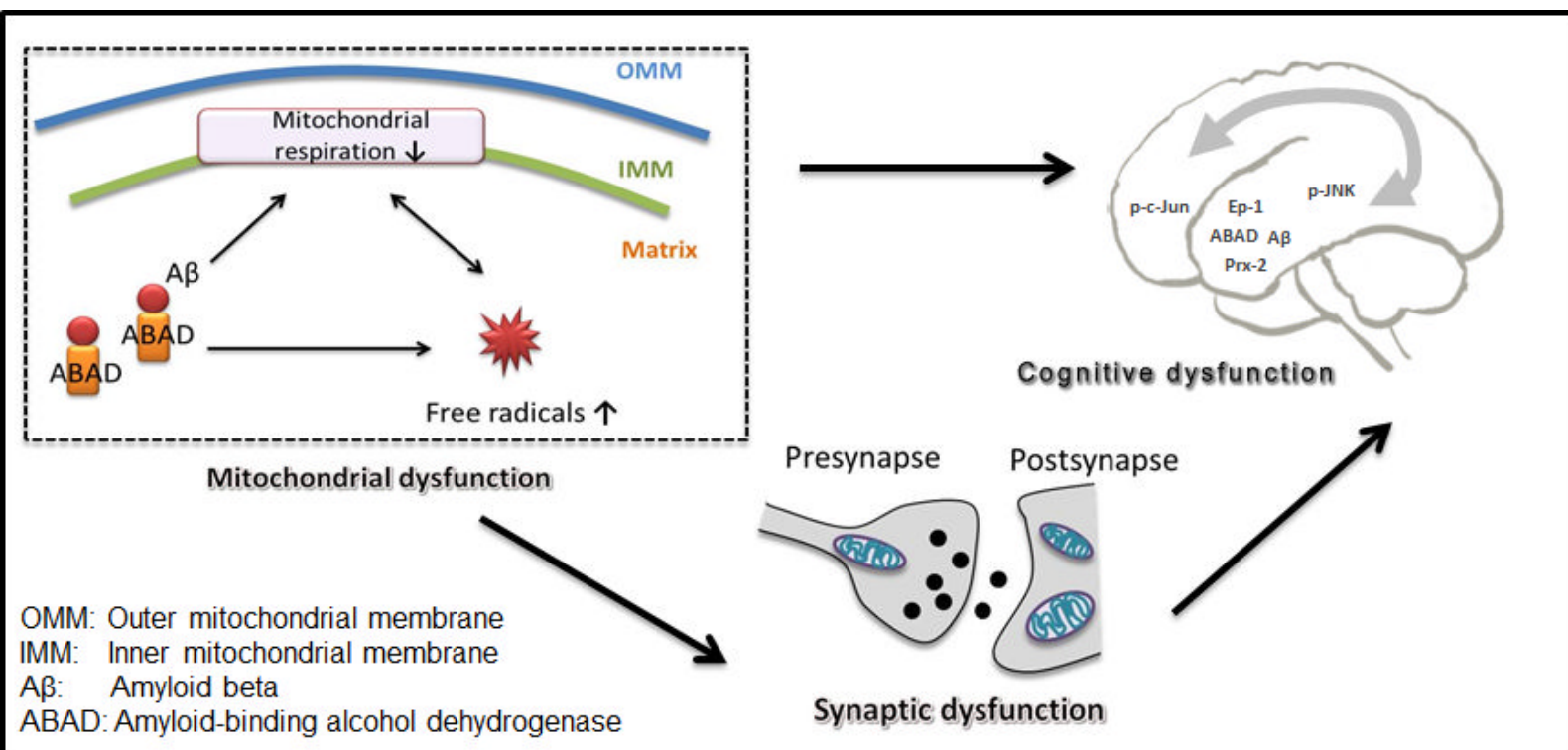
75. Micheva, K.D., Kay, B.K., and McPherson, P.S. (1997). Synaptojanin Forms Two Separate Complexes in the Nerve Terminal. Journal of Biological Chemistry *272*, 27239-27245.

76. Ringstad, N., Nemoto, Y., and De Camilli, P. (2001). Differential Expression of Endophilin 1 and 2 Dimers at Central Nervous System Synapses. Journal of Biological Chemistry *276*, 40424-40430.

77. Schuske, K.R., Richmond, J.E., Matthies, D.S., Davis, W.S., Runz, S., Rube, D.A., van der Bliek, A.M., and Jorgensen, E.M. (2003). Endophilin is required for synaptic vesicle endocytosis by localizing synaptojanin. Neuron *40*, 749-762.

78. Bayes, A., van de Lagemaat, L.N., Collins, M.O., Croning, M.D.R., Whittle, I.R., Choudhary, J.S., and Grant, S.G.N. (2011). Characterization of the proteome, diseases and evolution of the human postsynaptic density. Nat Neurosci *14*, 19-21.

79. Fu, X., Yang, Y., Xu, C., Niu, Y., Chen, T., Zhou, Q., and Liu, J.-J. (2011). Retrolinkin cooperates with endophilin A1 to mediate BDNF-TrkB early endocytic trafficking and signaling from early endosomes. Molecular Biology of the Cell.

80. Chen, Y., Deng, L., Maeno-Hikichi, Y., Lai, M., Chang, S., Chen, G., and Zhang, J.F. (2003). Formation of an endophilin-Ca2+ channel complex is critical for clathrin-mediated synaptic vesicle endocytosis. Cell *115*, 37-48.

81. Berridge, M.J. (2010). Calcium hypothesis of Alzheimer's disease. Pflugers Arch *459*, 441-449.

82. Milton, N.G., Mayor, N.P., and Rawlinson, J. (2001). Identification of amyloid-beta binding sites using an antisense peptide approach. Neuroreport *12*, 2561-2566.

83. Aarts, M., Liu, Y., Liu, L., Besshoh, S., Arundine, M., Gurd, J.W., Wang, Y.T., Salter, M.W., and Tymianski, M. (2002). Treatment of ischemic brain damage by perturbing NMDA receptor- PSD-95 protein interactions. Science *298*, 846-850.

84. Cao, G., Pei, W., Ge, H., Liang, Q., Luo, Y., Sharp, F.R., Lu, A., Ran, R., Graham, S.H., and Chen, J. (2002). In Vivo Delivery of a Bcl-xL Fusion Protein Containing the TAT Protein Transduction Domain Protects against Ischemic Brain Injury and Neuronal Apoptosis. J Neurosci *22*, 5423-5431.

85. Yang, X., Yang, Y., Wu, J., and Zhu, J. (2007). Stable expression of a novel fusion peptide of thioredoxin-1 and ABAD-inhibiting peptide protects PC12 cells from intracellular amyloid-ß. J. Mol. Neurosci. *33*, 180-188.

86. Hann, M.M., and Keserü, G.M. (2012). Finding the sweet spot: the role of nature and nurture in medicinal chemistry.

87. Y., J.B.G.G.G.N.G.M.T.S.P.P.J.A.V.K.K.K. (2009). Protein Based Drug Discovery. International Journal of Drug Discovery *1*, 40-51.

88. Louboutin, J.P., Chekmasova, A.A., Marusich, E., Chowdhury, J.R., and Strayer, D.S. (2010). Efficient CNS gene delivery by intravenous injection. Nat Methods *7*, 905-907.

89. Alvarez-Erviti, L., Seow, Y., Yin, H., Betts, C., Lakhal, S., and Wood, M.J. (2011). Delivery of siRNA to the mouse brain by systemic injection of targeted exosomes. Nat Biotechnol *29*, 341-345.

90. Froemming, M.K., and Sames, D. (2007). Harnessing Functional Plasticity of Enzymes: A Fluorogenic Probe for Imaging 17β-HSD10 Dehydrogenase, an Enzyme Involved in Alzheimer's and Parkinson's Diseases. Journal of the American Chemical Society *129*, 14518-14522.

91. Horton, K.L., Stewart, K.M., Fonseca, S.B., Guo, Q., and Kelley, S.O. (2008). Mitochondria-penetrating peptides. Chem. Biol. *15*, 375-382.

92. Azzolin, L., Antolini, N., Calderan, A., Ruzza, P., Sciacovelli, M., Marin, O., Mammi, S., Bernardi, P., and Rasola, A. (2011). Antamanide, a derivative of Amanita

phalloides, is a novel inhibitor of the mitochondrial permeability transition pore. PLoS One *6*, e16280.

93. Schulz, M.N., and Hubbard, R.E. (2009). Recent progress in fragment-based lead discovery. Curr Opin Pharmacol *9*, 615-621.

94. Congreve, M., Chessari, G., Tisi, D., and Woodhead, A.J. (2008). Recent developments in fragment-based drug discovery. J Med Chem *51*, 3661-3680.

95. Carr, R.A., Congreve, M., Murray, C.W., and Rees, D.C. (2005). Fragment-based lead discovery: leads by design. Drug Discov Today *10*, 987-992.

96. Ciulli, A., and Abell, C. (2007). Fragment-based approaches to enzyme inhibition. Curr Opin Biotechnol *18*, 489-496.

Figure 1: Working Hypothesis. Interaction of ABAD with Aβ enhances generation/accumulation of free radicals and impairs mitochondrial respiratory function. This leads to synaptic dysfunction and aggravates cognitive dysfunction.

Figure 2: Synaptic dysfunction caused by the ABAD-Aβ interaction. Binding of Aβ affects the enzymatic function of ABAD, thereby causing unfavorable changes in lipid metabolism and mitochondrial respiration. This ultimately leads to increased reactive oxygen species (ROS) production and impaired calcium (Ca^{2+}) retention and provokes the up-regulation of peroxiredoxin-2 (Prx-2) and endophilin-1 (Ep-1). 1) Prx-2 is able to degrade ROS but its function can be affected by elevated Ca^{2+} leading to its phosphorylation and inactivation and the accumulation of ROS. 2) Ep-1 plays a role in glutamatergic (glut) synaptic transmission by functioning in synaptic vesicle endocytosis, which is directly regulated by Ca^{2+} binding to Ep-1 [80]. Ep-1 can also be involved in 3) JNK-activation as well as 4) signaling events in the post-synapse leading to dendritogenesis. The correct balance of all of these events in the synapse, which is disturbed by the ABAD-Aβ interaction, is of crucial importance for synaptic plasticity and memory formation.

Figure 3: The ABAD decoy peptide approach. Left: Levels of Aβ are elevated in the AD mouse model (and the human AD brain), increasing its binding to loop D in ABAD. Endophilin-1 and peroxiredoxin-2 expression levels are increased in the AD mouse model as a result of the ABAD-Aβ interaction, which also causes neuronal cellular stress (increased ROS production, impaired metabolism, resulting in reduced plasma membrane integrity and LDH-release and apoptosis). Right: Administration of modified peptides based to the loop D amino acid sequence of ABAD are able to disrupt the ABAD-Aβ interaction in the AD mouse model *in vivo*, decrease the expression of endophilin-1 and peroxiredoxin-2 and restore cellular function and memory performance.

18

OMM

Mitochondrial respiration ↓

IMM

Matrix

Aβ

ABAD

ABAD

Free radicals ↑

Mitochondrial dysfunction

OMM: Outer mitochondrial membrane
IMM: Inner mitochondrial membrane
Aβ: Amyloid beta
ABAD: Amyloid-binding alcohol dehydrogenase

Presynapse

Postsynapse

Synaptic dysfunction

p-c-Jun

Ep-1

p-JNK

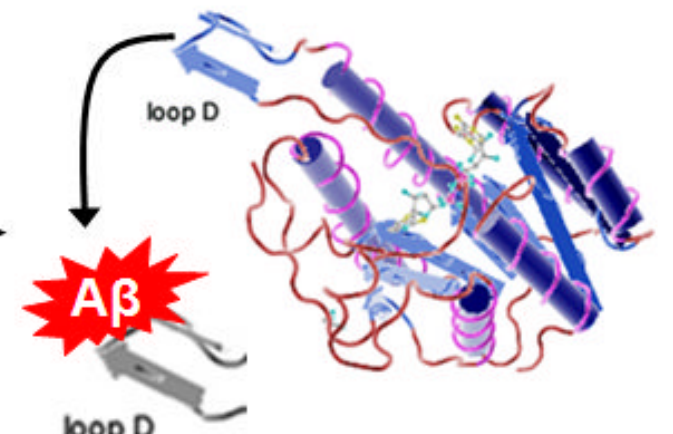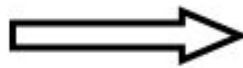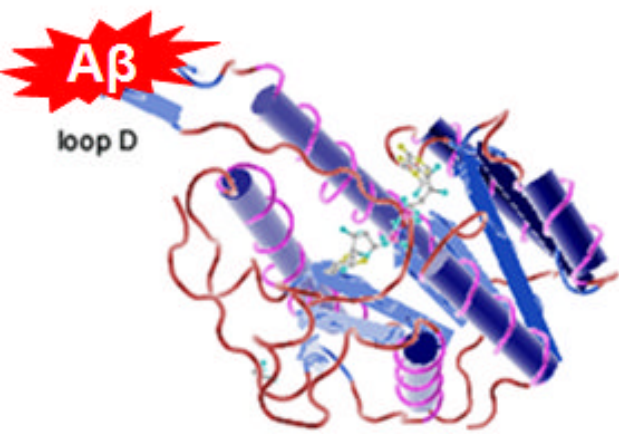ABAD Aβ

Prx-2

Cognitive dysfunction
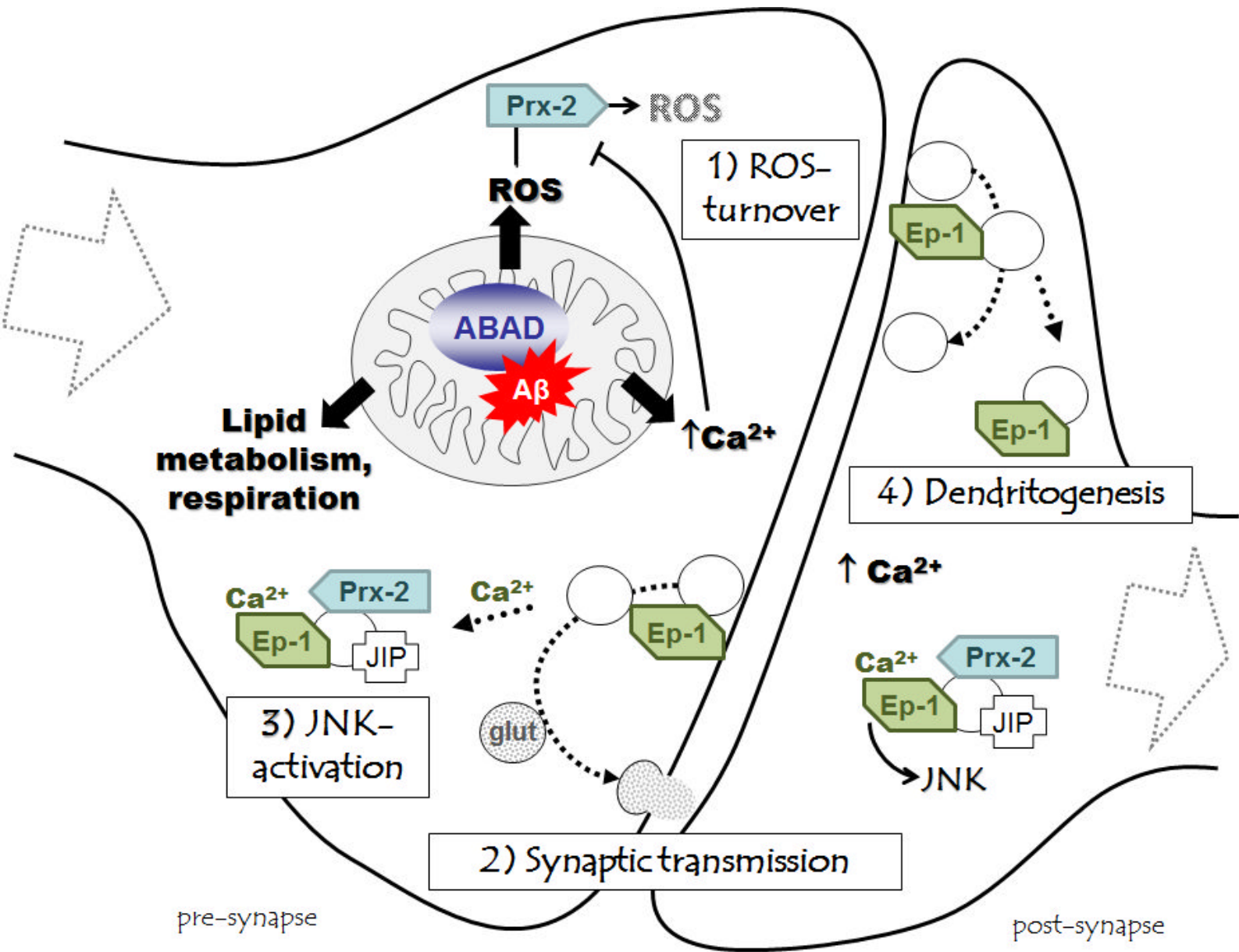
AD mouse model

Impaired memory performance

AD mouse model + decoy peptide

Improved memory performance

Aβ

loop D

Aβ

loop D

loop D

AD biomarkers:
- Endophilin-1
- Peroxiredoxin-2

Neuronal dysfunction:
- Reactive oxygen species
- LDH-release
- Apoptosis

AD biomarkers:
- Endophilin-1
- Peroxiredoxin-2

Neuronal dysfunction:
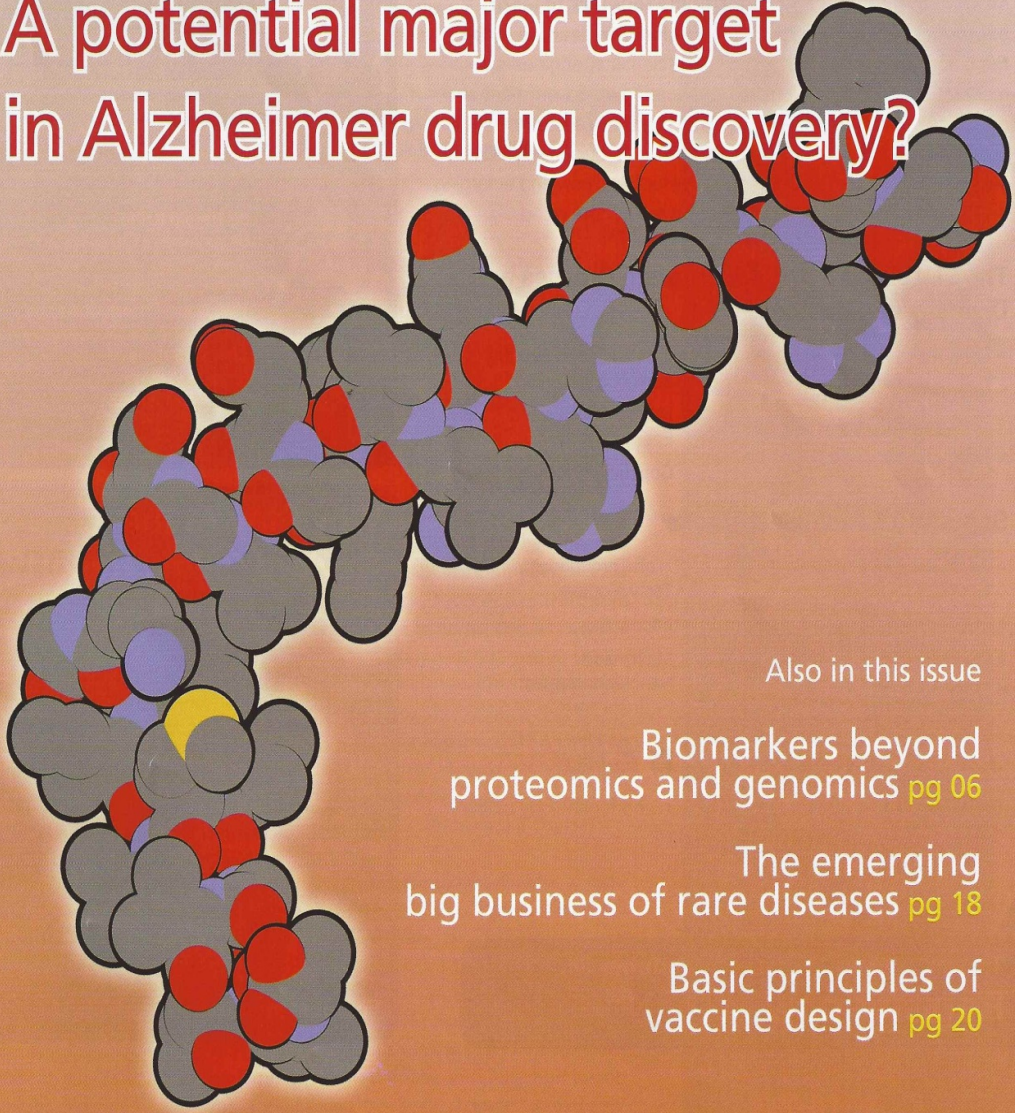- Reactive oxygen species
- LDH-release
- Apoptosis

BIO TECH

international

THE EUROPEAN MAGAZINE FOR THE LIFE SCIENCES INDUSTRY

A potential major target in Alzheimer drug discovery?

Also in this issue

Biomarkers beyond proteomics and genomics pg 06

The emerging big business of rare diseases pg 18

Basic principles of vaccine design pg 20

Weekly news updates on www.biotech-online.com

ABAD or a good approach to Alzheimer's disease drug discovery?

by Laura Aitken and Prof. Frank Gunn-Moore

The prevalence of Alzheimer's disease (AD) cases has been on a rapid increase for generations, however, we still find ourselves without the elusive cure for this disease. Due to the complexity of this disease, to try and describe every trial or therapeutic route that researchers are using to target AD would result in an article far larger than this magazine would allow. Therefore, we aim to highlight a few of the current Aβ drug targets and therapeutic approaches in the field and in particular focus on a protein- protein interaction, which could prove to be a major drug target in AD drug discovery. Also in this article we suggest that there may never be one "quick fix" therapy and that a combination of treatments may be needed to cure this debilitating disease.

Current treatments

There are commercial drugs available, (acetyl-cholinesterase inhibitors and NMDA receptor antagonists) which will help to alleviate some of the symptoms for a limited time and ultimately act to stabilize the remaining neuronal networks and prolong neuronal function until their therapeutic effect diminishes and drug tolerance occurs. Other commonly available drugs may be prescribed to help the patients deal with depression, anxiety, psychosis and other symptoms associated with AD. As with many other diseases, there have also been observations made that suggest a healthy diet and active lifestyle can slow down the progression of this disease.

Current Immunotherapy Strategies

Currently the most common approach for developing new treatments for AD involves tackling the formation or clearance of the amyloid-beta peptide (Aβ) and/or hyper-phosphorylated tau. More specifically using immunotherapy as a way of clearing these proteins. Using immunotherapy as a treatment for AD is not a new phenomenon, in fact it was first hypothesized over 13 years ago. Initial studies used transgenic mice which were immunized with the toxic Aβ42. These studies showed that immunization with Aβ42 mice essentially prevented amyloid deposition; astrocytosis was dramatically reduced, and there was also a reduction in Aβ-induced inflammatory response [1]. Aβ42 immunization also appeared to arrest the progression of amyloidosis in older transgenic mice. Overall it was shown that the direct Aβ immunization appeared to increase the clearance of amyloid plaques, and it was therefore suggested that this could be an effective therapeutic for AD. This direct immunization with synthetic intact Aβ42 stimulates T-cell, B-cell and microglial immune responses, and was an approach used by many groups, and because this immunotherapy approach had proved to be so effective in reducing amyloid plaques in AD mice model brains and also improving cognitive function, it was taken further into clinical trials. One trial, AN1792, from Elan Pharmaceuticals appeared successful in phase I, however the phase II trial of Aβ42 peptide vaccine was halted because of T cell-mediated meningoencephalitis in 6% of its patients.

Another possible therapeutic immunology approach involves the passive administration of monoclonal antibodies directed against Aβ. These antibodies can be targeted to Aβ disorders because they are considered conformational diseases, due to the amyloid formation triggering conformational changes in a specific peptide or protein, resulting in its mis-folding. Amyloid conformation- specific antibodies that recognize specific amyloid species, e.g., fibrils or oligomers, from many types of amyloid proteins have been produced and characterized. An example of this type of immunotherapy is Bapineuzumab IV, a monoclonal antibody that can target Aβ and has been used in investigational therapy studies for the treatment of mild-to-moderate AD. Recently, phase III clinical trials using this antibody have been halted by Pfizer as the therapeutic affects (at the highest dose) did not improve cognitive function performance when

→

compared to patients receiving the placebo drug.

Although the Aβ immunotherapy approach has proved to be somewhat frustrating due to a lack of clarity on where the broken down amyloid is sequestered, there are many continuing approaches into utilising this field. One such example of a useful tool that has come from an immunology study, is the use of carbon-11-labelled Pittsburgh compound B (^{11}C-PiB) PET, a marker of cortical fibrillar Aβ load *in vivo*, which was used to investigate whether Bapineuzumab would reduce cortical fibrillar Aβ load in patients with AD. This study showed that treatment with Bapineuzumab for 78 weeks reduced cortical ^{11}C-PiB retention compared with both baseline and placebo, therefore concluding that ^{11}C-PiB PET seems to be a useful tool in assessing the effects of potential AD treatments on cortical fibrillar Aβ load *in vivo*.

Overall, the use of vaccine strategies to treat AD may still hold promise. Both active and passive immunization strategies reduced AD-like pathology and restored cognitive deficits in transgenic mice. Although they have been relatively unsuccessful to date, the knowledge gained from studies using A[11] immunotherapy will allow the optimization of new-generation vaccines and the development of new tools to study this disease. If the side effects and therapeutic affect can be maximized then an Aβ vaccination could provide the first definitive treatment for AD.

In the meantime, what other drug strategies are there?

Protecting specific sensitive targets
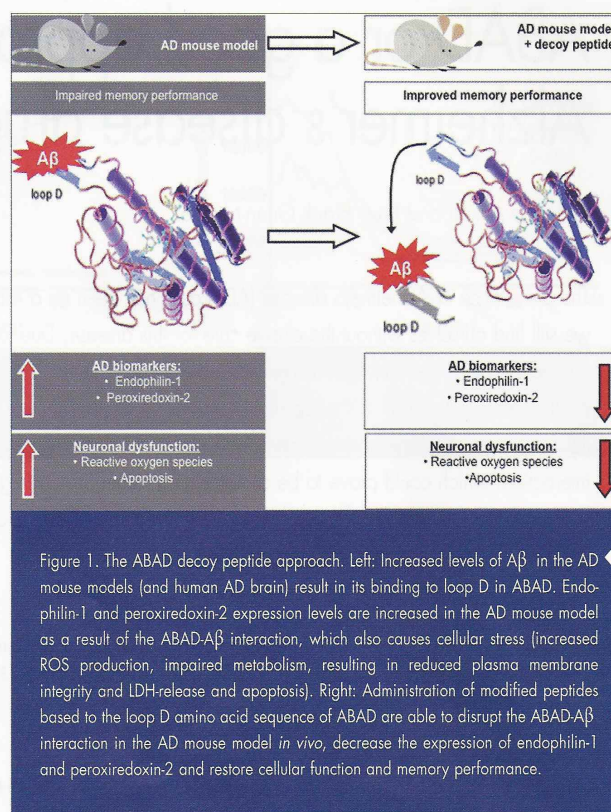The concept that we also need to protect specific sensitive targets within the cell should also be considered.

Figure 1. The ABAD decoy peptide approach. Left: Increased levels of Aβ in the AD mouse models (and human AD brain) result in its binding to loop D in ABAD. Endophilin-1 and peroxiredoxin-2 expression levels are increased in the AD mouse model as a result of the ABAD-Aβ interaction, which also causes cellular stress (increased ROS production, impaired metabolism, resulting in reduced plasma membrane integrity and LDH-release and apoptosis). Right: Administration of modified peptides based to the loop D amino acid sequence of ABAD are able to disrupt the ABAD-Aβ interaction in the AD mouse model *in vivo*, decrease the expression of endophilin-1 and peroxiredoxin-2 and restore cellular function and memory performance.

In particular, the focus of our own research is the role of protecting the function of a specific mitochondrial protein, amyloid binding alcohol dehydrogenase (ABAD). Mitochondrial dysfunction is a well-recognized fact in the progression of AD, though until recently the mechanisms involved could only be loosely labelled as changes in metabolism. The discovery that Aβ can be present and can accumulate within the mitochondria and specifically bind to ABAD has opened up a new area of AD research.

The ABAD-Aβ interaction as a drug target in AD
ABAD was first identified in 1997 via a yeast two hybrid screen for Aβ binding molecules, and is now the most characterized Aβ binding molecule having been characterized using a variety of techniques ranging from biophysical approaches (NMR, SPR) through to immunoprecipitation experiments from both AD transgenic mice and human AD brains. ABAD has been shown to be able to catalyse, with the help of its co-factor NAD^+/NADH, the reduction of aldehydes and ketones and oxidation of alcohols for energy production utilizing different substrates. It has been challenging to pinpoint the exact *in vivo* substrates of ABAD in the brain, though our recent work suggests that there are indeed subtle changes in lipid metabolism in response to altered ABAD activity in cells.

ABAD activity can be manipulated in two ways, under conditions of stress (it increases) or in the presence of Aβ (it decreases). With regard

to the latter, the change in activity due to the binding of Aβ to ABAD has been previously presented as a rather digital response, that is, as Aβ binds to ABAD it switches its activity off with respect to a number of simple substrates. However, recent data suggests that this rather digital view may be an over simplification. Moreover, studies have now identified further consequences of Aβ binding to ABAD in living organisms. Specifically, there are a number of genes that are switched on and appear to be controlled by the binding of Aβ to ABAD. Examples include the antioxidant protein peroxiredoxin-II and the presynaptic endocytic protein endophilin-1 (also referred to as endophilin A1) (2,3), both of which have also been found to be up-regulated in the human AD brain. The ability to control the expression of an array of other proteins could suggest that it

is not a simple question of switching off ABAD activity, but potentially that the binding of Aβ to ABAD causes the enzyme to change its ability to utilize certain substrates, which in turn would directly or indirectly affect other proteins. This evidence would then suggest that the ABAD-Aβ interaction might be considered a potential drug target in AD.

The most convincing data that this interaction was significant came from the ability of a peptide based on the sequence of ABAD to which Aβ binds, to work as a decoy *in vivo*. Initial experiments showed that modifying the decoy peptide by addition of peptide sequences from the cell membrane transduction domain of the human immunodeficiency virus-1 Tat protein, enabled the ABAD decoy peptides to cross cell membranes and prevent Aβ toxicity in neuronal

cultures [4]. By adding a mitochondrial targeting sequence to the decoy peptide, this facilitated its localization in mitochondria, after intraperitoneal injection, and allowed it to be transported through the blood brain barrier. It was then possible to show in 6-month old transgenic animals expressing elevated levels of ABAD and Aβ, that the observed increases in the expression levels of peroxiredoxin-II and endophilin-1, could be reversed [2,3]. Even more significant was the finding that using the same approach, it was possible to reverse the behavioural changes in these animals as well [5]. Another important aspect of these studies was, that the reversal of behavioural changes could be achieved by both purified peptide injected intraperitoneally and also in a transgenic animal model expressing the ABAD region 92-120. These findings are summarised in figure 1.

→

How do we target the ABAD-Aβ interaction?

ABAD is a sensitive site in AD that can be protected from its interaction with Aβ, which could be beneficial in AD treatment. Classically, protein-protein interactions have been avoided as therapeutic targets because of perceived difficulties in developing a compound. To overcome the perceived problems, then it is necessary to be creative. For example, crossing the blood brain barrier is a perennial problem when dealing with small molecules; however, the studies above have shown that intraperitoneally-injected peptides are capable of crossing the blood brain barrier and targeting the correct site in animal models. Other recent work using retroviruses have also shown to have the same capability. Another recent breakthrough has been the use of targeted exosomes, again injected intravenously, which allowed biological relevant compounds (in this case siRNA) encapsulated in these membranes, to be successfully delivered into the brain. Therefore there may be new horizons for getting compounds across the blood brain barrier.

Our research in academia focuses on the development of small molecules as drugs against the ABAD-Aβ interaction. For example, we are investigating a series of analogues based on the immunosuppressant drug frentizole. Frentizole was identified by an ELISA-based screening assay, as a novel inhibitor of the ABAD-Aβ interaction, and was subsequently modified with the production of a novel benzothiazole urea, resulting in a 30-fold improvement in potency. Being an immunosuppressant it resulted in un-wanted side effects when it entered clinical trials; however, this approach indicated that it might be possible to develop pharmacologically active and medically useful compounds targeting ABAD. We have also utilised fragment-based drug discovery as an approach for designing new drugs for against this interaction. Using two screening technologies thermal shift analysis and saturated transfer difference NMR spectroscopy we have identified compounds with millimolar affinity for the target. Using two methods, grouping compounds, for example using structure activity relation (SAR) analysis, or alternatively combining fragments (in order to effectively sample the available chemical space) we hope to improve affinities for the target.

Overall although the ABAD-Aβ interaction is not a classical site for drug therapy, the biology dictates that this interaction may be a future target. At the very least, it has been shown that it is possible to identify not just new drug targets but also novel biological pathways and events that occur in neurodegenerative diseases such as AD.

> "...it might be possible to develop pharmacologically active and medically useful compounds targeting ABAD."

Conclusion

In this brief review we have highlighted some of the major strategies for Aβ drug discovery in AD. More specifically we have shown that we believe that there will never be a one drug cures all method for AD. Instead treatments for this debilitating disease could be broken down into three categories: The formation or clearance of Aβ and/or hyper-phosphorylated tau, the support and stabilization of the remaining neuronal networks and the protection of specific sensitive targets. In regards to the latter, we believe that drugs targeting the ABAD-Aβ interaction may play a huge role in the treatment of AD.

References

1. Schenk D, Barbour R, Dunn W, Gordon G, Grajeda H, Guido T, Hu K, Huang J, Johnson-Wood K, Khan K et al. Immunization with amyloid-beta attenuates Alzheimer-disease-like pathology in the PDAPP mouse. Nature 1999; 400: 173-177.

2. Ren Y, Xu HW, Davey F, Taylor M, Aiton J, Coote P, Fang F, Yao J, Chen D, Chen JX et al. Endophilin I Expression Is Increased in the Brains of Alzheimer Disease Patients. Journal of Biological Chemistry 2008; 283: 5685-5691.

3. Yao J, Taylor M, Davey F, Ren Y, Aiton J, Coote P, Fang F, Chen JX, Yan SD, Gunn-Moore FJ. Interaction of amyloid binding alcohol dehydrogenase/Abeta mediates up-regulation of peroxiredoxin II in the brains of Alzheimer's disease patients and a transgenic Alzheimer's disease mouse model. Mol. Cell. Neurosci 2007; 35: 377–382.

4. Lustbader JW, Cirilli M, Lin C, Xu HW, Takuma K, Wang N, Caspersen C, Chen X, Pollak S, Chaney M et al. ABAD Directly Links Aß to Mitochondrial Toxicity in Alzheimer's Disease. Science 2004; 304: 448-452.

5. Yao J, Du H, Yan S, Fang F, Wang C, Lue L-F, Guo L, Chen D, Stern DM, Gunn Moore FJ et al. Inhibition of Amyloid-β (Aβ) Peptide-Binding Alcohol Dehydrogenase-Aβ Interaction Reduces Aβ Accumulation and Improves Mitochondrial Function in a Mouse Model of Alzheimer's Disease. The Journal of Neuroscience 2011; 31: 2313-2320.

The authors

Laura Aitken, BSc Hons and Frank Gunn-Moore* PhD, BSc

University of St Andrews
School of Biology
Medical and Biological Sciences
Building
North Haugh
St Andrews, KY16 9TF, UK

*Corresponding author
e-mail: fjg1@st-andrews.ac.uk